UNIVERSAL
LIBRARY

OU_154611

UNIVERSAL
LIBRARY

OSMANIA UNIVERSITY LIBRARY

Call No. 539.7/F918P Accession No. 34

Author Frisch - O. R.

Title Progress in nuclear physics

This book should be returned on or before the date last marked below.

PROGRESS SERIES

NUCLEAR PHYSICS

Volume 2

PROGRESS IN NUCLEAR PHYSICS

2

Editor
O. R. FRISCH, O.B.E., F.R.S.
Cavendish Laboratory, Cambridge

LONDON
PERGAMON PRESS LTD
1952

Published in Great Britain by Pergamon Press 2, 3 & 5, Studio Place, London S. W. 1
Printed in Germany by Universitätsdruckerei H. Stürtz AG., Würzburg

CONTENTS

PAGE

FOREWORD vii

ACKNOWLEDGEMENTS viii

1 THE ELECTRON OPTICAL PROPERTIES OF MAGNETIC BETA RAY SPECTROMETERS 1
N. F. Verster
Institute for Nuclear Research, Zeeman Laboratory, Amsterdam

2 NUCLEAR PARAMAGNETIC RESONANCE 21
R. V. Pound
Lyman Laboratory, Harvard University, Cambridge, Mass.

3 LUMINESCENT MATERIALS FOR SCINTILLATION COUNTERS 51
G. F. J. Garlick
Department of Physics, University of Birmingham

4 THE NEUTRON-PROTON INTERACTION 89
G. L. Squires
Atomic Energy Research Establishment, Harwell

5 FISSION 120
W. J. Whitehouse
Atomic Energy Research Establishment, Harwell

6 THE LOW-LYING EXCITED STATES OF LIGHT NUCLEI 174
W. E. Burcham
Department of Physics, University of Birmingham

7 THE NUCLEAR SHELL MODEL 235
B. H. Flowers
Atomic Energy Research Establishment, Harwell

8 IONISATION BY FAST PARTICLES 271
T. E. Cranshaw
Atomic Energy Research Establishment, Harwell

NAME INDEX 285

SUBJECT INDEX 294

EXTRACT FROM THE FOREWORD TO VOL. I

NUCLEAR PHYSICS has firmly established itself as a separate branch of physical science, and indeed within its field segregation is taking place: some researchers specialize in the construction of accelerating machines, some in the design of detecting equipment, others in the mathematical interpretation of results. This specialization we may regret, but we cannot prevent it. The best we can do is to minimize its ill effects by making it easier for the physicist to obtain information outside his special field.

This volume is intended to help both the nuclear physicist in finding information in fields adjacent to his own, and the other scientist in getting an introduction to some technique in nuclear physics which he may wish to use for his own purpose. It is planned that a similar volume will appear every year.

O. R. FRISCH

ACKNOWLEDGEMENTS

The editor and publishers wish to thank the many authors, editors and publishers concerned for permission to reproduce the following illustrations from the sources named:

Australian Journal of Science:
Fig. 9 (cont. by W. E. BURCHAM)

Atomics:
Fig. 50 (cont. by W. J. WHITEHOUSE)

Canadian Journal of Research:
Fig. 16 (cont. by W. E. BURCHAM)
Figs. 3, 9 and 11b (cont. by W. J. WHITEHOUSE)

Dan. mat. fys. medd.:
Fig. 12 (cont. by N. F. VERSTER)
Fig. 16 (cont. by W. J. WHITEHOUSE)

Ionisation Chambers and Counters by D. H. WILKINSON (Cambridge University Press):
Fig. 1 (cont. by T. E. CRANSHAW)

Nature, London:
Fig. 22 (cont. by W. E. BURCHAM)
Fig. 25 (cont. by W. J. WHITEHOUSE)

Philosophical Magazine:
Fig. 5 (cont. by W. E. BURCHAM)
Fig. 20 (cont. by W. J. WHITEHOUSE)

Philosophical Transactions of the Royal Society:
Fig. 26 (cont. by W. J. WHITEHOUSE)

Proceedings of the Physical Society:
Fig. 6 (cont. by W. E. BURCHAM)
Fig. 4 (cont. by B. H. FLOWERS)

Proceedings of the Royal Society, series A:
Figs. 7, 13 and 20 (cont. by W. E. BURCHAM)

Physical Review:
Figs. 3, 8, 9, 11, 12, 14, 15, 17, 21 and 23 (cont. by W. E. BURCHAM)
Figs. 5–7 (cont. by B. H. FLOWERS)
Figs. 7 and 8 (cont. by G. L. SQUIRES)
Figs. 1, 2, 4, 5a, 7, 10, 11a, 13, 17, 19, 22–24, 27 and 29–31
(cont. by W. J. WHITEHOUSE)

Radiochemical Studies of the Fission Products, vol. 3: Ed. by C. D. Coryell and N. Sugarman (McGraw-Hill Book Co.):
Fig. 8 (cont. by W. J. WHITEHOUSE)

THE ELECTRON OPTICAL PROPERTIES OF MAGNETIC BETA RAY SPECTROMETERS

N. F. Verster

Introduction

The design of beta ray spectrometers has been greatly improved during the last years and a material increase in both luminosity and resolving power has resulted. It seems worth while to compare the results achieved until now and to make an electronoptical analysis of the most important types of spectrometers. Only those types will be discussed in which the electrons are focused by rotationally symmetric magnetic fields. These fields can be used to focus electrons in two entirely different ways (Fig. 1). In the first case the electron trajectories are about normal to the direction of the magnetic field and the Lorentz force resulting from this movement deflects and focuses the electrons. Depending on the direction of the field either positive or negative electrons are deflected in the right direction. Instruments, based on this principle, will be called *prismatic beta ray spectrometers*. In the other case the electron trajectories make only a small angle with the axis of symmetry of the magnetic field. Due to the Lorentz force the velocity of the electrons gets a component normal to the axis and to the original direction and the Lorentz force caused by this new component directs the electrons back to the axis. If the direction of the magnetic field is changed the electrons rotate in the opposite direction,

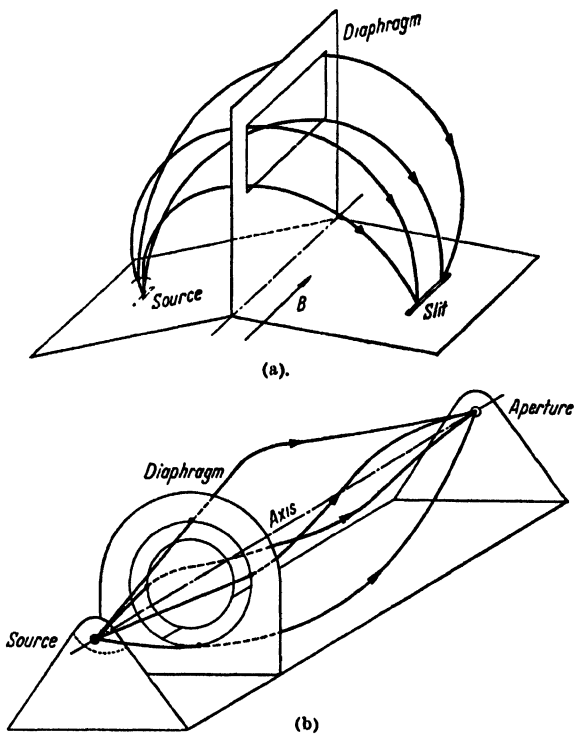


Fig. 1. (a) Electron trajectories in a prismatic spectrometer. (b) Electron trajectories in a spectrometer of the lens type.

but the second mentioned LORENTZ force does not change its direction. For this reason the radial movement is independent of the sign of the charge of the electrons, and a separation of both types of electrons is only possible if the transmission depends on the angular movement. Instruments of this kind are called *lens type beta ray spectrometers*.

A complete electronoptical analysis of the focusing of electrons by rotationally symmetric magnetic fields of otherwise arbitrary shape is very complicated, mainly because the electron path is described by non-linear second order differential equations. Approximate solutions can be obtained by using a suitably chosen series expansion.

Spectrometers of both types can be constructed using a homogeneous magnetic field. In this case an analysis of the focusing mechanism is very simple. As these instruments show many properties of spectrometers using an inhomogeneous magnetic field they will be discussed to some extent. The derivation and solution of the ray path equations valid for inhomogeneous fields is outlined in the appendix. Although non-relativistic mechanics are used the equations (after elimination of the time variable) are valid for any value of the electron energy if the relativistic value $m_0 v\,(1-v^2/c^2)^{-\frac{1}{2}}$ is taken for the electron momentum p. This is so because the LORENTZ force is normal to the velocity and so does not change the energy of the electron.

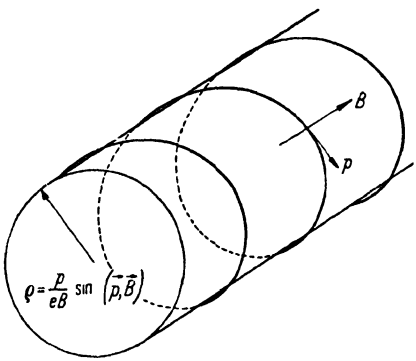


Fig. 2. Helical trajectory of an electron in a homogeneous magnetic field.

An electron, moving in a homogeneous magnetic field will describe a helix (Fig. 2). The motion in the direction of the field is linear, while the motion normal to this direction is circular with a radius $r = (p/eB)\sin(\boldsymbol{p},\boldsymbol{B})$ or $Br = (p/e)\sin(\boldsymbol{p},\boldsymbol{B})$ B being the value of the magnetic induction (in Gauss) and e the charge of the electron (in E.M.U.).

If the electron moves normal to the field direction, we see that the product of magnetic induction and radius of curvature is equal to the ratio of the momentum and the charge. For this reason a quantity $(B\varrho)$ (magnetic rigidity) can be defined by $(B\varrho) = p/e$ while it is also possible to express the momentum in electron gauss centimeters in the same way, as the energy can be expressed in electron volts.

We then have

$$r = \frac{(B\varrho)}{B}\sin(\boldsymbol{p},\boldsymbol{B})\,. \tag{1}$$

The following relations exist between the kinetic energy and the momentum

$$E = \left[\sqrt{\left(\frac{p}{1{\cdot}7044\ \text{keG cm}}\right)^2+1}-1\right]\times 0{\cdot}5110\ \text{Mev}$$

$$p = \sqrt{\frac{E}{1\ \text{Mev}}+\frac{E^2}{1{\cdot}0220\ (\text{Mev})^2}}\times 3{\cdot}372\ \text{keG cm}\,.$$

Simpler relations hold between η defined by $\eta = p/m_0\, e$ and ε defined by $\varepsilon = w/m_0c^2$, w being the total relativistic energy.

We get

$$\varepsilon^2 = \eta^2 + 1$$

and

$$E = 0{\cdot}5110\,(\varepsilon - 1)\,\text{Mev}$$

$$p = 1{\cdot}7044\,\eta\ \text{keG cm}.$$

As the momentum of electrons is proportional to the radius of curvature of their trajectories as well as to the value of the magnetic induction, a spectrum can be explored either by measuring the intensity of the electrons at different places in a constant field or by keeping the position of the detector fixed but varying the value of the induction. The first method can only be applied with success in a prismatic spectrometer with a homogeneous field (semi-circular spectrometer). A large part of the spectrum can be registered simultaneously on a photographic plate. In the second case a Geiger counter is usually used as detector. The spectrum has to be measured point by point. The latter method has many advantages, for instance, the possibility of improving the focusing action of the field by the use of a suitable chosen inhomogeneous field shape. If the magnetic induction is proportional to the current through the magnet coil a measurement of this current directly yields the momentum of the detected electrons after calibration in one point. If an iron yoke is used, in general, the induction is no longer proportional to the current and will depend on its history so that a direct measurement of the magnetic field becomes necessary. The iron yoke must be designed in such a way that the field shape does not change when the value of the induction is changed.

The Semi-Circular Spectrometer

In a prismatic spectrometer, using a homogeneous magnetic field, the electron trajectories are circular and focusing takes place after 180°. Such an instrument is called a semi-circular spectrometer. It has been developed by Rutherford and Robinson[1] in 1913. A large number of these instruments has been described, using either photographic plates or Geiger counters as detectors. They are well suited for absolute measurements of the momentum[2]. They are generally designed to yield a high resolution, the transmission is however very low. The electron optical properties can be derived in a simple way (Fig. 3), as follows:

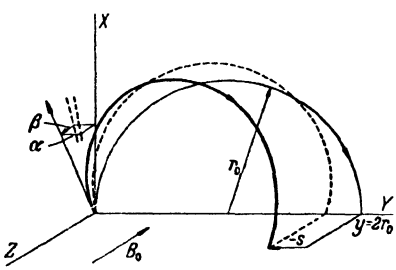


Fig. 3. Coordinates used in the description of the semicircular spectrometer.

Assume a magnetic field B_0 in the z direction. An electron, leaving the origin under an angle α with the xz plane and an angle β with the xy plane will, according to eq.(1) describe a helix with a radius $r = \frac{(B\varrho)}{B_0}\cos\beta$. For not too large values of β the angle between the projection of this helix on the

xy plane and the x axes is equal to α. This helix intersects then the yz plane in a point $y = 2\frac{(B\varrho)}{B_0}\cos\alpha\cos\beta$, $z = \pi\frac{(B\varrho)}{B_0}\sin\beta$. Electrons with a momentum p_0 leaving the origin under small angles α and β are thus focused in the yz plane on the line $y = 2r_0$, r_0 being given by $p_0 = eB_0r_0$. Electrons with a momentum p equal to $p_0(1+\Delta)$ and starting under somewhat larger angles will strike the yz plane at a distance s from this line, s being expressed by

$$\frac{s}{r_0} = -(\alpha^2+\beta^2) + 2\Delta\,. \tag{2}$$

The first term represents the spherical aberration, the second one the chromatic aberration or dispersion. The shape and intensity of the image on a photographic plate placed in the yz plane can be calculated by this equation. The intensity distribution across the image of a point source is given in Fig. 4. To estimate the properties of the instrument in case the electrons are detected by a Geiger counter, the aberration expression (2) is better used as

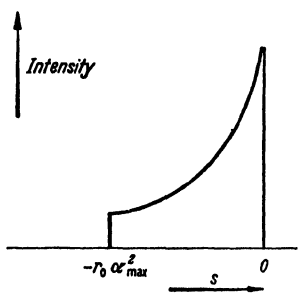


Fig. 4. Intensity distribution along the image of a point source as formed in a semi-circular spectrometer.

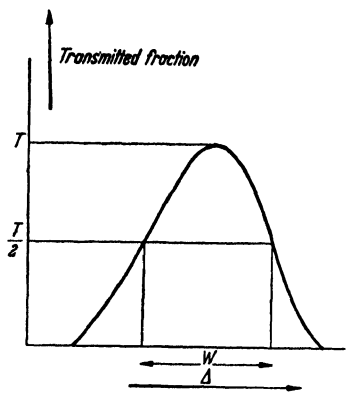


Fig. 5. General shape of a transmission curve (line profile).

$$\Delta = \frac{(\alpha^2+\beta^2)}{2} + \frac{s}{2r_0}\,.$$

The variation in Δ due to the first term depends on the luminosity, while the influence of the second term is determined by the source and slit widths.

From the limitation of α, β and s it is possible to calculate for any value of Δ the fraction of all electrons with a momentum corresponding to this value of Δ reaching the Geiger counter. The maximum fraction is called the transmission T. The line width W is measured at half this value (Fig. 5). The resulting curve (the transmission curve) represents the momentum distribution of the electrons entering the counter for a constant value of the magnetic induction B as well as the line shape obtained for monokinetic electrons by varying B.

In order to compare the types of instruments to be described we will introduce some quality factors in the following way: Assume that the dimension of the exit opening is equal to the image of the source. The transmission

is then entirely determined by the exit angles, while the total variation in Δ is equal to twice the contribution of the source dimension (d) and twice the contribution of the spherical aberration. This last term will be either proportional to the transmission or to the square of the transmission in the different types of spectrometers.

We will assume that the line width W is equal to one half of the maximum variation in Δ. A spectrometer can be characterised by one of the following formula:

$$W = S_1 T + \frac{d}{D} \tag{3a}$$

or

$$W = S_2 T^2 + \frac{d}{D} \tag{3b}$$

the factors S_1 and S_2 will be called the spherical aberration factors and D will be called the dispersion factor.

In the case of a semicircular spectrometer we have $D = 2r_0$. A circular baffle limiting α and β to $\alpha^2 + \beta^2 \leq \gamma^2$ will yield a transmission of $\pi\gamma^2/4\pi = \frac{1}{4}\gamma^2$ and a maximum variation in Δ equal to $\frac{1}{2}\gamma^2$. The line width is in this case proportional to the transmission corresponding to eq.(3a) with $S_1 = 2$. The maximum value of β is in general limited however by the length of the exit slit to a very low value. In order to obtain a reasonable transmission the value of α has to be increased so that $\alpha_{\max} \gg \beta_{\max}$. It is clear that this limitation of α and β is less favourable with respect to the ratio of line width and transmission.

The transmission is equal ro $\alpha_{\max} \times \beta_{\max}/\pi$ and the maximum variation in Δ is given by $\alpha^2_{\max}/2$. This corresponds to eq.(3b) with $S_2 = \pi^2/2\beta^2_{\max}$.

In many applications the surface activity of the source is given rather than the total activity. The effective area, defined as the product of source area and transmission is then a good measure of the luminosity. The optimum source width d for a semicircular spectrometer with $\alpha \gg \beta$ can be calculated as $d = 2DS_2T^2$. The performance of a spectrometer with $r_0 = 20$ cm and a length of the source and exit slit of 1·2 cm is shown in Fig. 15 and Fig. 16. The transmission is calculated for a point source, the effective area for the value of the source width given above.

The semi-circular spectrometer has been greatly improved by the use of an inhomogeneous magnetic field in two ways. First the influence of α on the spherical aberration has been eliminated so that larger values of α can be used and secondly it has been possible to obtain axial focusing so that a more favourable limitation of α and β is possible. As in this case also the spherical aberration is reduced, resulting in a further decrease in S, and the dispersion is increased the latter method has yielded very good results.

Prismatic Spectrometers with an Inhomogeneous Field

Using cylindrical coordinates r, φ, z with the reduced coordinates $\varrho = \frac{r - r_0}{r_0}$ and $\zeta = z/r_0$ the focusing of electrons leaving the point $\zeta = \zeta_0$ of the line source $\varphi = 0$, $\varrho = 0$ with a momentum $p = e B_0 r_0(1 + \Delta)$ under exit angles α and β will be studied in some detail. The radial displacement in the focal

plane will be denoted by s. As the exit slit is parallel to the axis the axial displacement is of minor importance. The magnetic field is rotationally symmetric around the z-axis and symmetric with respect to the median plane $z = 0$. This last condition has to be understood as a symmetry of the vector potential. The induction is then antisymmetric due to its pseudo vector character. Under these symmetry conditions an adequate description of the entire field distribution is furnished by the value of the magnetic induction $B(\varrho)$ in the median plane due to the field equations div $\boldsymbol{B} = 0$, curl $\boldsymbol{B} = 0$. $B(\varrho)$ can be expanded in the series

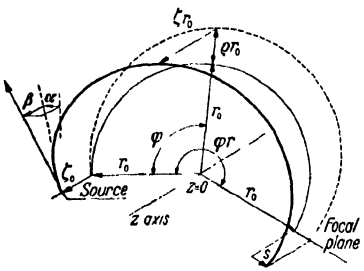


Fig. 6. Coordinates used in the description of a prismatic spectrometer.

$$B(\varrho) = B_0(1 + k\varrho + l\varrho^2 + m\varrho^3 + \cdots). \quad (4)$$

A systematic analysis of the focusing properties can be made by studying the influence of the successive terms in this series. The first term B_0 determines the momentum of the electrons following the circular trajectory $r = r_0$ viz. $p = e B_0 r_0$. The next coefficient k governs the behaviour of electrons moving at a small distance from this circle. If the electrons start at $\varphi = 0$, $\varrho = 0, \zeta = 0$ they are radially focused at $\varphi_r = \pi(1 + k)^{-\frac{1}{2}}$, $\varrho = 0$ while they are focused axially at $\varphi_a = \pi(-k)^{-\frac{1}{2}}$, $\varrho = 0$. The radial dispersion is given by $s/r_0 = 2\Delta/(1 + k)$. The dispersion factor D is thus equal to $2r_0/1 + k$. To calculate the trajectories of electrons travelling at a greater distance from the circle $\varrho = 0, \zeta = 0$ the value of l has to be taken into account. The solution of the equation of motion then yields the required expression for $s = s(\Delta, \alpha, \beta, \zeta_0)$. In the case of a semicircular spectrometer the magnetic field is characterized by $k = 0$, corresponding to radial focusing after 180° and no axial focusing.

The aberrations are in this case given by

$$\Delta = \frac{\alpha^2[3 + 4l]}{6} + \frac{\beta^2[1 + (\pi^2 - 4)\,l]}{2} - l\,\zeta_0^2 - \pi\,l\,\zeta_0\beta + \frac{s}{2r_0}. \quad (5)$$

In the case of a homogeneous field spectrometer ($l = 0$) we find $\Delta = \frac{(\alpha^2 + \beta^2)}{2} + \frac{s}{2r_0}$ in agreement with (2). The radial spherical aberration can be eliminated by choosing $l = -\frac{3}{4}$. We then obtain[3]

$$\Delta = 2{\cdot}70\,\beta^2 + 0{\cdot}75\,\zeta_0^2 + 2{\cdot}35\,\zeta_0\beta + \frac{s}{2r_0}. \quad (6)$$

The focusing angles φ_r and φ_a remain 180° and infinity respectively. The dispersion remains also unchanged.

The aberration expression shows that the radial spherical aberration has been eliminated at the expense of a large increase in axial aberration while also terms depending on ζ_0^2 and $\zeta_0\,\beta$ are introduced.

By using a special method to solve the ray path equation, BEIDUK and KONOPINSKI[3] have also calculated the values of the next terms in the series

expansion of $B(\varrho)$ required to eliminate the radial aberration to a high order. The required field is given by

$$B(\varrho) = B_0(1 - \tfrac{3}{4}\varrho^2 + \tfrac{7}{8}\varrho^2 - \tfrac{9}{16}\varrho^4 + \tfrac{51}{320}\varrho^5 \cdots). \tag{7}$$

LANGER and COOK[4] have described a shaped field spectrometer in which this magnetic field is used. The radius r_0 of the principal ray path has the large value of 40 cm. The total variation in α equals 32°. Using a source of 4 mm width a line width W of 0·5% by a transmission T of about 0·1% is obtained.

Although this represents a very successful improvement of the homogeneous field spectrometer, still better results have been obtained by chosing a more favourable value of the coefficient k. The most favourable value seems to be $k = -\frac{1}{2}$. In this case both radial and axial focusing take place after $\pi\sqrt{2}$ radian = 255°. The aberration is described by

$$\Delta = \frac{\alpha^2(8l-1)}{6} + \frac{\beta^2(3-8l)}{6} + \frac{\zeta_0^2(3-4l)}{12} + \frac{s}{4r_0}. \tag{8}$$

The term depending on $\zeta_0\beta$ has vanished and as a result of the axial focusing the influence of the ζ_0^2 depending term can be eliminated by using a curved exit slit. The dispersion in twice as great as for a corresponding 180° spectrometer. For $l = \frac{1}{8}$ the radial aberration will vanish, the axial aberration then being equal to $\Delta = \beta^2/3 + \cdots$ while for $l = \frac{3}{8}$ the axial aberration vanishes, the radial aberration being $\Delta = \alpha^2/3 + \cdots$. If one choses $l = \frac{1}{4}$ the aberration expression gets the shape $\Delta = (\alpha^2 + \beta^2)/6 + \zeta_0^2/6 + s/4r_0$.

A circular diaphragm limiting α and β to $\alpha^2 + \beta^2 \leq 4T$ will in this case yield best results[5] and can be realised in practice as β is no longer limited by the height of the exit slit. The spherical aberration constant S_1 in this case gets the value of $\frac{2}{3}$. Under similar conditions a homogeneous field spectrometer yields $S_1 = 2$, so a gain of a factor 3 is obtained while for a spectrometer without axial focusing this favourable limitation of α and β can only be realised for extremely low values of the transmission. It is also possible to use $l = \frac{1}{8}$ and eliminate the radial spherical aberration to a high order by a suitable choice of the coefficients m etc., but this has as yet not been done. The required field shape is given by[6]

$$B(\varrho) = B_0(1 - \tfrac{1}{2}\varrho + \tfrac{1}{8}\varrho^2 + \tfrac{1}{16}\varrho^3 - \tfrac{31}{256}\varrho^4 + \cdots). \tag{9}$$

The properties of the double focusing spectrometer have been amply discussed by SIEGBAHN and SVARTHOLM[7, 8, 9] and by SHULL and DENNISON[10].

SIEGBAHN and SVARTHOLM[7, 8] describe a small scale spectrometer with a mean radius of curvature of 12·5 cm. Over a region of 2·6 cm the field shape is proportional to $r^{-\frac{1}{2}}$, corresponding to $k = -\frac{1}{2}$, $l = \frac{3}{8}$. A line width W 0·6% by a transmission T of 0·15% is obtained. Recently HEDGRAN *et al*[31] have described a large instrument with a mean radius of curvature of 50 cm and a polegap of 28 cm. The value of l is $\frac{3}{8}$, so that a high value of β can be used. The linewidth and transmission are varied by shutters only limiting the radial exit angle α, while β remains 0·2 radian. A maximum transmission of 1% can be obtained. Using a source of 5 mm width a line width of 0·9% is then obtained.

The resolving power can be substantially increased by reducing the transmission.

SHULL[11] describes a double focussing spectrometer with a mean radius of curvature of 17 cm. The value of l is $\frac{1}{3}$. By a square baffle both α and β are limited to $\pm 0{\cdot}1$ radian. A line width W of 0·33% by a transmission T of 0·32% can be achieved.

KURIE *et al.*[12] have built an instrument with $r_0 = 24$ cm yielding a transmission of 0·2% by a line width of 0·33%. The value of l lies between $\frac{1}{3}$ and $\frac{1}{4}$.

The double focusing spectrometer with $l = \frac{1}{4}$ and a circular limitation of α and β can be described by $W = S_1 T + d/D$ with the values $S_1 = \frac{8}{3}$ and $D = 4r_0$. The shaped field 180° spectrometer can be characterized by $W = S_2 T^2 + d/D$ with $S_2 = 2{\cdot}70\,\pi^2/\alpha_{max}^2$ and $D = 2r_0$, if we assume that the radial spherical aberration is completely eliminated for $\alpha \leq \alpha_{max}$. The value of T is however limited by the maximum value of β, accepted by the exit slit. In the corresponding case of a double focusing spectrometer using the field shape given by (10) we find $S_2 = \pi^2/3\alpha_{max}^2$ and $D = 4r_0$.

In Fig. 15 and 16 the theoretical performance of these types is represented for the following dimensions:

$r_0 = 20$ cm, length of the source and exit slit 1·2 cm and for the first and last type $\alpha_{max} = 0{\cdot}3$ radian.

The transmission has been calculated for zero source dimensions while the effective area has been calculated for an optimum source dimension.

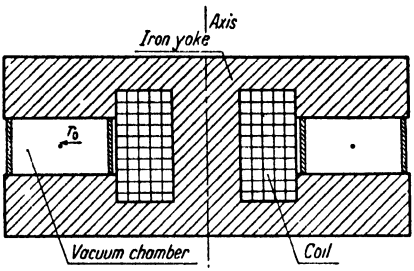


Fig. 7. Common design of a magnet for a prismatic spectrometer.

Design of the magnet

Although an iron free magnet has the advantage of a direct proportionality between the current through the coils and the momentum of the electrons, the use of an iron yoke is for most applications more favourable as the required number of ampere turns is greatly reduced. The required field shape can be obtained by a suitable shape of the pole faces. This is generally determined experimentally. Fig. 7 shows a common design of the magnet for a prismatic spectrometer.

The beta ray spectrometer of KOFOED-HANSEN

A prismatic spectrometer of an entirely different and promising design has recently been built by KOFOED-HANSEN *et al.*[32]. A schematic illustration of this instrument is given in Fig. 8. The source and counter are placed on the axis and the lines of force describe circles around the axis. Between the flat pole faces the field strength is inversely proportional to the radial distance. The focusing is governed by the shape of the boundary curve of the pole pieces and the large degree of freedom in this shape allows an essentially exact

focusing of electrons starting in widely different directions. Exit angles between 50° and 150° are used. Two-directional focusing takes place due to the axial symmetry of the instrument (neglecting the effect of the fringing field). A transmission of 12% by a resolution of 2% has been obtained with a source diameter of 5 mm.

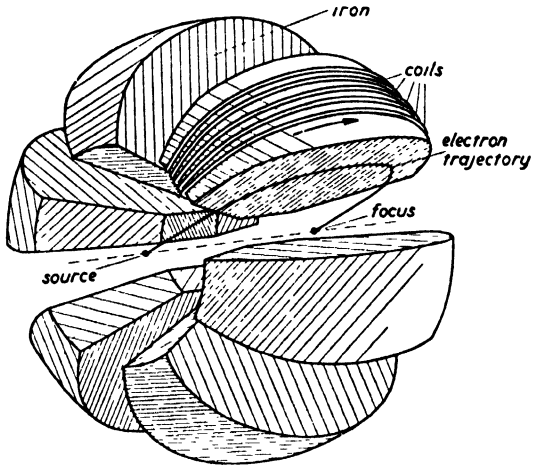


Fig. 8. A schematic illustration of the spectrometer of KOFOED-HANSEN *et al* [32], utilising 6 gaps of opening angle 30°.

BETA RAY SPECTROMETERS OF THE LENS TYPE

The electron optical design of lens type beta ray spectrometer has been greatly improved during the last years. The results have been obtained, however, in a somewhat different way as compared with the development of the semicircular spectrometer. In the latter case the original instrument uses a homogeneous field while the field shape for the improved types, namely the shaped field 180° spectrometer and the double focusing spectrometer, can be calculated exactly by theoretical methods. This results from the fact that the focusing quality is completely determined by the first few coefficients from the series development of the magnetic induction $B(\varrho)$ (4). The properties of a magnetic lens on the other hand depends on the value of $B(z)$ along the axis so that a systematic analysis is no longer possible as instead of a few coefficients an entire function is of importance. It will be shown, however, that the lens can be characterised by a few constants. The value of these constants can be estimated from a rough knowledge of the field shape. The question of optimum design is still very complicated. As lenses of high quality require more copper and power than a low quality thin lens, and as a spectrometer can be improved as well by increasing the quality of the lens as by increasing its dimensions, the optimum lens design depends also on economical considerations.

Lens type spectrometers with a homogeneous field are not essentially different from those with an inhomogeneous field while the simplicity of the ray path equation makes it possible to obtain some fundamental properties in a simple way (Fig. 9).

An electron, leaving the z-axis at $z = 0$, will describe a helix. The time τ required for one revolution of an electron with a momentum p if given by $\tau = 2\pi m/eB$. After one revolution the electron will cross the axis again at the point $x = (2\pi p/eB)\cos\alpha$. The radial part of the movement is sinusoidal and is given by

$$r = 2\frac{(B\varrho)}{B}\sin\alpha\sin\left[z\frac{B}{2B\varrho\cos\alpha}\right] \tag{10}$$

where $(B\varrho)$ is equal to p/e.

The momentum of the electrons focused at $z = l$ for small values of α has the value of $p_0 = e(B\varrho)_0 = eB \times l/2\pi$. Electrons with a momentum $p_0(1+\Delta)$

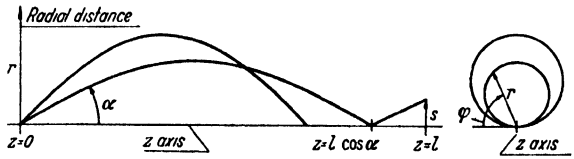


Fig. 9. Electron trajectories in a lens type spectrometer with a homogeneous field.

and starting under somewhat larger exit angles will strike the focal plane at a distance s from the axis, s being represented by

$$s = \Delta\alpha l - \alpha^3 l/2\,. \tag{11}$$

This expression is analogous to the expressions obtained for prismatic spectrometers (eq. 2, 5 and 8). The first term represents the dispersion, the second one the spherical aberration. It is clear that the centre of the lens cannot be used as the dispersion is proportional to α.

The ray path equation, describing the trajectory in a rotationally symmetrical field of otherwise arbitrary shape can be expanded in powers of r. The first term yields $\frac{d^2r}{dz^2} - r \times B^2(z)/4(B\varrho)^2 = 0$, $B(z)$ being the value of the magnetic induction along the axis. The value of $B(z)$ describes the entire field shape due to the field equations div $\boldsymbol{B} = 0$, curl $\boldsymbol{B} = 0$.

The momentum p_0 of the electrons focused at $z = l$ for small values of α is determined by the boundary conditions $r(0) = r(l) = 0$. The next term in the series expansion allows a calculation of the spherical aberration. The dispersion is calculated in a similar manner[13]. The aberration expression gets the shape

$$s = \Delta\alpha C_1 - \alpha^3 C_2 \quad \text{or} \quad \Delta = \alpha^2\frac{C_2}{C_1} + \frac{s}{\alpha C_1}\,. \tag{12}$$

The value of C_1 and C_2 can be calculated from $B(z)$ and the electron trajectory for small values of α. Both constants have the dimension of a length and are of the same order as the instrumental length l. A circular source of diameter d is placed on the axis at $z = 0$ and an exit aperture is placed at $z = l$. The exit angle is limited by an annular diaphragm to $\alpha_0 + \delta\alpha < \alpha < \alpha_0 + \delta\alpha$. The transmission is equal to $4\pi\alpha_0\,\delta\alpha/4\pi = \alpha_0\,\delta\alpha$, and the maximum variation in Δ due to the spherical aberration is equal to $4C_2/C_1\alpha_0\delta\alpha$ (Fig. 10). This corresponds to a linear relation between spherical aberration and transmission as represented

by eq.(3a). The factors S_1 and D are given by $S_1 = 4C_2/C_1$, $D = \alpha_0 C_1$. These expressions are only true for a lens with a magnification of 1. Otherwise the expressions become more complex, but we will limit ourselves to the simpler case of unit magnification. In this case D is almost independent on the field shape and instrumental length and is approximately given by $D = 3{\cdot}5\, r_{max}$. The value of C_2/C_1, however, depends strongly on the field shape. For a homogeneous field eq.(11) yields $C_2/C_1 = \frac{1}{2}$. Thin lenses, which require less ampere turns yield much higher values, for example 3. Suitably chosen concave fields will yield values somewhat lower than $\frac{1}{2}$ [14]. The field shape necessary to reduce C_2/C_1 to zero, as calculated by GLASER[15] cannot be realized in practice. It will be shown that the influence of the spherical aberration can be reduced, however, by a different design of the instrument.

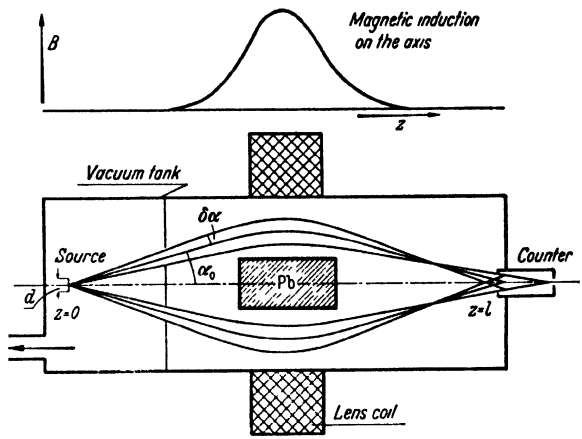


Fig 10. Schematic design of a thin lens spectrometer.

The theoretical performance for a lens type spectrometer, characterized by $l = 100$ cm, $r_{max} = 10$ cm and $C_1/C_2 = 1{\cdot}5$ is shown in Fig. 15 and Fig. 16.

A great number of lens type beta ray spectrometer has been described in the literature. One of the first successful instruments has been described by DEUTSCH, ELLIOT and EVANS[16]. A short lens is used. The value of C_2/C_1 is about 3·5 if the entire lens coil is used. The instrumental length $l = 100$ cm and the maximum radius is about 6 cm. The transmission can be varied, according to the required resolution. The following results are obtained:

a) source diameter $(d) = 0{\cdot}5$ cm, $T = 0{\cdot}8\%$, $W = 6\%$

b) source diameter $(d) = 0{\cdot}4$ cm, $T = 0{\cdot}13\%$, $W = 1{\cdot}7\%$.

QUADE and HALLIDAY[17] describe a spectrometer with a lens consisting of four separate coils. The coils are placed in such a way that the spherical aberration is minimum, determined experimentally with an electron gun. In this way a value of 1·2 for C_2/C_1 is obtained. The instrumental length is 95·5 cm, the maximum radius 10 cm. The authors describe only an adjustment for high resolution using a source of 0·3 cm radius, yielding a transmission of 0·12% by a line width of 0·78%.

K. SIEGBAHN[14] has described a lens spectrometer with a magnetic field shaped to reduce the spherical aberration to a high degree (Fig.11). The instrumental length is about 50 cm, the maximum radius 6 cm. A value of 1·4 for S_1 [eq. (3a)] corresponding to $C_2/C_1 = 0{\cdot}35$ follows from the published

data on line width and transmission. By a line width of 6·8% a transmission of 3·5% can be obtained[18].

From these examples it is clear that although the design of lens spectrometers offers the possibility of a high transmission as compared with the semicircular spectrometer, this increase of the luminosity is accompanied by a similar increase of the line width. The dispersion of both types of instruments is of the same order, depending, of course, on the dimensions. It will be shown that the influence of the spherical aberration in a lens spectrometer can be reduced, resulting in an instrument well suited for good resolution at high luminosity. In this case, however, the source dimension has to be reduced simultaneously, and the source area being proportional to the square of the source diameter, the effective area will be small. Prismatic spectrometers are more favourable in this respect as the source area is proportional to the source width and the source height has only little influence on the resolution.

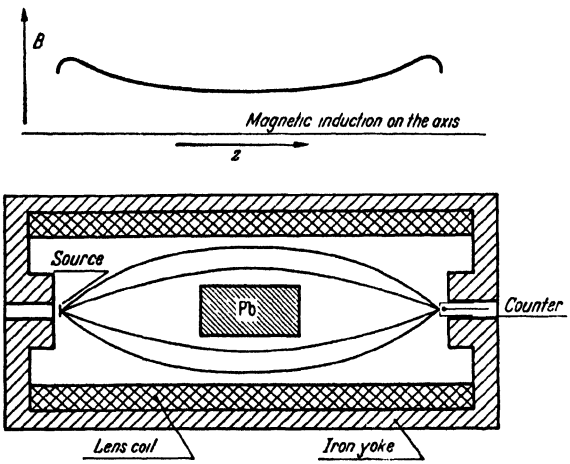


Fig. 11. Lens type spectrometer of SIEGBAHN, using a field shape yielding low spherical aberration.

Lens type spectrometers with annular focusing

It will be clear from Fig. 12 that an annular slit placed at $z = l-d$ can be made much narrower than a circular aperture placed at $z = l$.

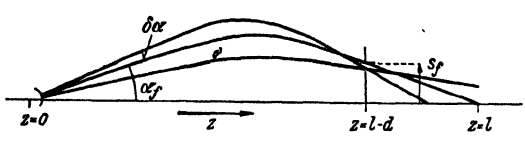


Fig. 12. Coordinates of the annular focus.

This can be quantitatively treated using the aberration expression (12). The focusing properties in the plane $z = (l-d)$ are also described by $\Delta = s/\alpha\, C_1 + \alpha^2\, C_2/C_1$. The values of C_1 and C_2 do not differ materially from those calculated for $z = l$, provided the value of d is not too large. The value of the momentum, corresponding to $\Delta = 0$ will of course have changed. A so-called ring focus will be present if $\partial\Delta/\partial\alpha = 0$ yielding $\alpha_f^3 = s_f/2\,C_2$. If this trajectory passes through the centre of the counter window we have $d = s_f/\alpha_f = 2\,C_2\,\alpha_f^2$. The index f denotes the coordinates of the ring focus. A series expansion of the aberration expression yields

$$\Delta - \Delta_f = (\alpha - \alpha_f)^2 \frac{3C_2}{C_1} - \frac{(s-s_f)}{\alpha_f C_1}. \qquad (13)$$

This expression shows that the dispersion has remained unchanged but that, for not too high values of the transmission, the influence of the spherical aberration has been greatly reduced. The performance can be described by eq.(3b): $W = S_2 T^2 + d/D$,[19] with $S_2 = 3\, C_2/\alpha_f^2\, C_1$ and $D = \alpha_f\, C_1$.

A high value of α_f is very favourable, but for too high values the treatment given here is no longer valid. In the case of a homogeneous field one finds an optimum value of 45° [20, 21]. If however, economic considerations are taken into account, the optimum value of α_f becomes about 22° [21].

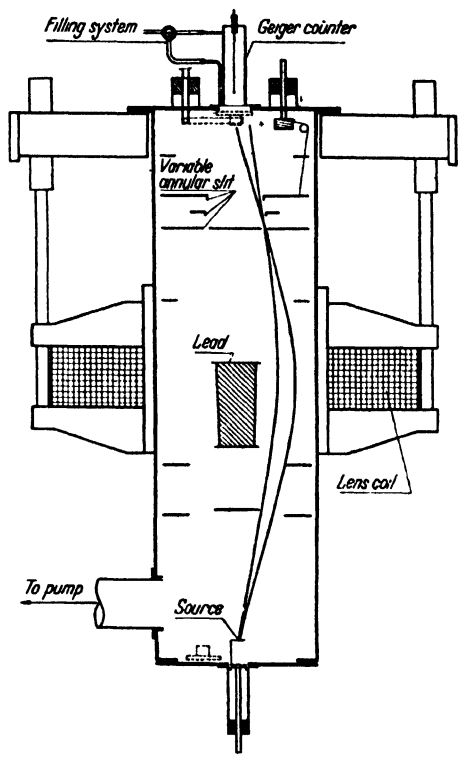


Fig. 13. The Amsterdam lens type spectrometer, using annular focusing.

Sometimes the diameter of the counter window will determine the optimum value of α_f. From eq. (12) it follows that the required diameter of the counter window is equal to $6 C_2\, \alpha_f T$.

A high value of α_f will thus reduce the maximum transmission obtainable. If we consider a spectrometer with $l = 100$ cm, $C_1 = 130$ cm, $C_2 = 195$ cm ($C_2/C_1 = 1{\cdot}5$) and $\alpha_f = 0{\cdot}27$ radian corresponding to $r_{max} = 10$ cm, we find that a counter window of 3·6 cm diameter will limit the transmission to 1·14%.

The theoretical performance of this instrument is shown in Fig. 14 and Fig. 15.

The use of a ring focus has, apart from the increased resolution, the advantage that the line area is independent of a small eccentricity in the focal plane, so that an imperfect compensation of stray magnetic fields will not disturb the shape of the low energy part of a beta ray spectrum. Lens spectrometers with a central aperture are extremely sensitive in this respect.

An extensive discussion of the properties of a homogeneous field spectrometer (solenoid spectrometer) with annular focusing has been given by DUMOND [20] and by PERSICO [21]. A detailed analysis is possible in this case as the ray path can be calculated exactly. Their results are also shown in Fig. 15 and Fig. 16.

The solenoid spectrometer described by WITCHER [22] in 1940 uses a ring focus. A line width of 5% by a source diameter of 2 cm and a transmission of 1% is obtained.

By using the calculations of PERSICO the performance of this spectrometer has recently been improved [29].

SCHMIDT *et al.*[23] describe a solenoid spectrometer designed in accordance with the results of DUMOND and PERSICO. The maximum transmission is 5%. At a transmission of 3% a line width of 0·95% was found.

The source area is, however, extremely small as the required source diameter is given as $r_{max}/170$.

A spectrometer using a magnetic field shaped for low spherical aberration has been built by ZÜNTI[24]. A line width of 1·3% by a source diameter of 0·3 cm and a transmission of 2·7% is obtained.

HORNYAK *et al.*[30] have made a spectrometer with a lens of medium thickness and free of iron. The transmission is estimated as 0·5%, the line width is 1·5%.

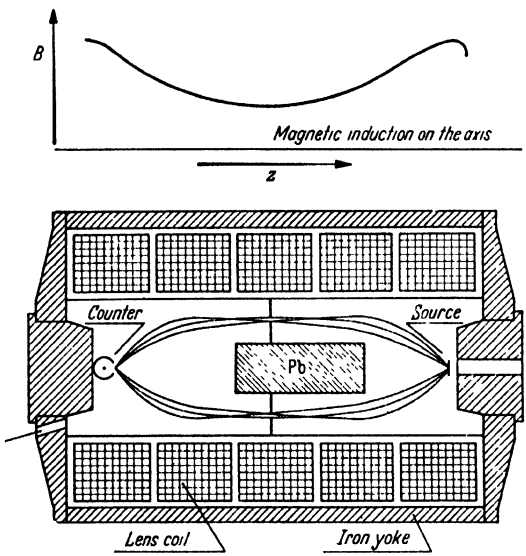


Fig. 14. Design of the intermediate image spectrometer of SLÄTIS and SIEGBAHN.

The author[13] has built a spectrometer (Fig. 13) with a thin lens, C_2/C_1 being about 2. The instrumental length is 100 cm. By a transmission of 1% and a source diameter of 0·3 cm a line width of 1·3% is obtained. The diameter of the counter window (3·6 cm) has limited the transmission to this value.

The intermediate image spectrometer

SIEGBAHN and SLÄTIS[25] have recently described a very interesting type of lens spectrometer (Fig. 14). The magnetic field and the trajectories are symmetric with respect to the plane $z = l/2$. The electrons, passing through the slit in this plane, are again focused on the axis at $z = l$. BOTHE[26] has independently given an extensive treatment of the properties of such an instrument using two thin lenses.

It can be shown that the field shape has to obey certain conditions in order to yield a symmetric ring focus. A homogeneous field, for example, will not give rise to trajectories as shown in Fig. 13.

Two symmetrically placed thin lenses at a distance of more than $l/4$ from the symmetry plane on the other hand, fulfil the conditions for an intermediate image spectrometer, if only third order aberration is taken into account. The field shape used by SIEGBAHN and SLÄTIS is, however, more favourable as a lower spherical aberration is obtained.

The behaviour at the intermediate image is described by an aberration expression of the same kind as (13):

$$\Delta - \Delta_f = A_1(\alpha - \alpha_f)^2 + A_2(s - s_f). \qquad (14)$$

For the second focus we obtain a more complicated expression of the following kind:

$$s = -A_3(\Delta-\Delta_f)^2 + A_4(\alpha-\alpha_f)(\Delta-\Delta_f) - A_5(\alpha-\alpha_f)^3 .$$

The influence of the spherical aberration on the size of the image becomes negligible, but the dispersion is very small. For this reason no important contribution to the resolution from the aperture in this second focal plane is to be expected.

The second focus has, however, the advantage that a small counter can be used and that scattered electrons will not be able to pass both the annular slit at $z = l/2$ and the aperture in the second focal plane $z = l$. This kind of instrument is well suited for extreme high transmission. The design is more complicated than that of most other kinds of spectrometers.

The spectrometer described by SIEGBAHN and SLÄTIS gives a transmission of 8% by a line width of 4% and a source diameter of 0·5 cm.

The performance of this type of spectrometer, estimated from (14) and the data of SIEGBAHN and SLÄTIS, has also been represented in Fig. 15 and Fig. 16.

The general shape of the aberration expression for the second focus has been obtained from the fact that two types of solutions of the boundary problem $r(0) = r(l) = 0$ exist in the neighbourhood of the principal solution, characterized by $\Delta = \Delta_f$, $\alpha = \alpha_f$, *viz.* a symmetric trajectory and an unsymmetric trajectory. The existence of this last solution is the characteristic feature of the intermediate image spectrometer.

A high value of the exit angle is very favourable and can be used because of the existence of the second focus. The third order perturbation method, which can be used to calculate the coefficients, occurring in the aberration expression, is therefore of little value for these instruments.

RICHARDSON has attacked the electron-optical problem by chosing a field shape, described in the entire r, z-space by an analytic function, and solving numerically the exact ray path eq. (A 4). As the magnetic field has to obey the field equations, the choice of a mathematically simple and physically suitable field shape is rather restricted. RICHARDSON[33] uses a field characterized by lines of force describing confocal elipsoids, while the source and the counter are placed on the axis between the foci of these elipsoids. A general insight in the focusing properties is obtained from an optical analogon by observing that the magnetic field can be replaced by a medium with a refractive index proportional to $(1-(A/B\varrho)^2)^{\frac{1}{2}}$. This field proves useful for an intermediate image spectrometer with exit angles of almost 90°.

Two pole pieces 16 cm apart and with an experimentally determined profile furnish the required magnetic field shape.

Using a source of 1 mm diameter and a transmission of 2·5%, a line width of 1·35% has been obtained.

COMPARISON OF THE DIFFERENT TYPES

Each of the two kinds of spectrometers described in the preceding pages, the prismatic and the lens type, can be subdivided in two groups depending on the relation between transmission T and line width W, according to the

eq.(3a) and (3b). These equations, together with the values of S_1 or S_2 directly yield the transmission as a function of the line width. In order to calculate the effective area F, defined as the product of the source area and the transmission, it is necessary, however, to distinguish between the prismatic and the lens type. In the first case F is given by

$$F = h \times d \times T \tag{15a}$$

h being the length of the source (the axial dimension) while d is the width of the source (the radial dimension). The influence of h on the resolving power is neglected in eq.(3a) and (3b).

In the case of lens type spectrometers F is given by

$$F = \tfrac{1}{4}\pi d^2 T \tag{15b}$$

d being the diameter of the source.

In Table 1 we have given for the different combinations of eq.(3) and (15) the value of d required to yield a maximum effective area by a constant line width. The table also gives the effective area and the transmission as a function of the lens width.

Table 1

Class	*Focusing properties*	*eq.*	*Effective area*	*eq.*	*Optimum d*	*Transmission T (point source)*	*Effective area F*
I	$W = S_1 T + d/D$	(3a)	hdT	(15a)	DS_1T	W/S_1	$0{\cdot}25\, hDW^2/S_1$
II	$W = S_2 T^2 + d/D$	(3b)	hdT	(15a)	$2DS_2T^2$	$W/S_2^{\frac{1}{2}}$	$0{\cdot}38\, hDW^{\frac{3}{2}}/S^{\frac{1}{2}}$
III	$W = S_1 T + d/D$	(3a)	$\frac{1}{4}\pi d^2 T$	(15b)	$2DS_1T$	W/S_1	$0{\cdot}12\, D^2W^3/S_1$
IV	$W = S_2 T^2 + d/D$	(3b)	$\frac{1}{4}\pi d^2 T$	(15b)	$4DS_2T^2$	$W/S_2^{\frac{1}{2}}$	$0{\cdot}22\, D^2W^{\frac{3}{2}}/S^{\frac{1}{2}}$

In Table 2 we have given the values of the constants for the different kinds of prismatic spectrometers described. As dimensions are chosen: mean radius of curvature (r_0) = 20 cm, length of the source and exit slit (h) = 1·2 cm, polegap = 5 cm, limiting β in the case of the double focusing spectrometers. For the types with high order elimination of the radial spherical aberration we have assumed that this elimination is complete for $\alpha \leq 0{\cdot}3$ radian.

Table 2

No	*Type*	*Field shape*	*Class (Table 1)*	*S*	*D cm*	*T*	*F*
1	Semi circular . .	$B = B_0$	II	$5{\cdot}4 \times 10^4$	40	$4{\cdot}3 \times 10^{-3} W^{\frac{1}{2}}$	$0{\cdot}08\, W^{\frac{3}{2}}$
2	Shaped field. . .	eq. (7)	II	300	40	$5{\cdot}8 \times 10^{-2} W^{\frac{1}{2}}$	$1{\cdot}08\, W^{\frac{3}{2}}$
3	Double focusing .	$B = B_0 \times (1 - \frac{1}{2}\varrho + \frac{1}{4}\varrho^2)$	I	0·67	80	$1{\cdot}5\, W$	$36\, W^2$
4	Double focusing .	eq. (10)	II	36	80	$0{\cdot}17\, W^{\frac{1}{2}}$	$6{\cdot}14\, W^{\frac{3}{2}}$

Table 3 gives the quantitative results for lens type spectrometers with the following properties: lens constants C_1 = 130 cm and C_2 = 195 cm, corresponding to $C_2/C_1 = 1{\cdot}5$. Exit angle 0·27 radian corresponding to r_{max} = 10 cm;

diameter of the counter window 3·6 cm. The table also gives the result for a solenoid spectrometer with 45° exit angle and $r_{max} = 10$ cm as calculated by DUMOND[20]. In this case too a counter window of 3·6 cm has been assumed.

Table 3

No	Type	Class (Table 1)	S	D cm	T	F cm²
5	Medium lens, central focus	III	6	35	$0{\cdot}17\,W$	$24\,W^2$
6	Medium lens, annular focus.	IV	62	35	$0{\cdot}13\,W^{\frac{1}{2}}$	$35\,W^{\frac{1}{2}}$
7	Solenoid, annular focus; calculated by DUMOND				$0{\cdot}45\,W^{\frac{1}{2}}$	$170\,W^{\frac{1}{2}}$

The results of Table 2 and Table 3 are graphically represented in Fig. 15 and Fig. 16. The values for the intermediate image spectrometer (No. 9)

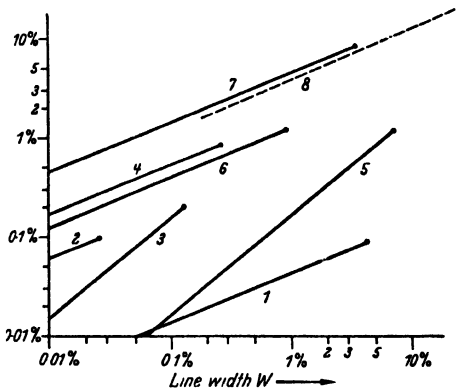


Fig. 15. Transmission versus line width for the different spectrometers described. The numbers refer to Tables 2 and 3.

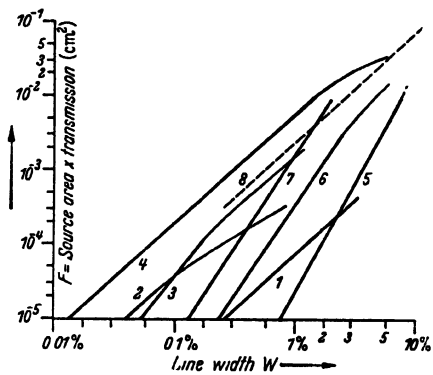


Fig 16 Effective area versus line width for the different spectrometers described. The numbers refer to Tables 2 and 3.

are estimated from (14) and the data of SIEGBAHN and SLÄTIS. The thin parts of the lines represent the regions were the transmission has its maximum value and the source dimension is larger than the optimum value given in Table 1.

It should be noted that these graphs are calculated from the simple formulae given in the text so that the exact values will in general deviate somewhat from the values given here.

APPENDIX

THE MOTION OF AN ELECTRON IN A ROTATIONALLY SYMMETRIC MAGNETIC FIELD

I. Analytical description of the magnetic field

The magnetic field can be described by the vector potential A obeying the equation curl curl $A = 0$. Due to the axial symmetry both A_r and A_z vanish; the remaining component A_φ will be denoted by A. In the case of a prismatic spectrometer the electrons move near the circle $r = r_0$, $z = 0$ and A is symmetric with respect to the median plane $z = 0$. A series expansion of A in this

region can then be derived from the value of $B_z(r, 0)$, which can in turn be expanded in a series. Introducing $\varrho = (r - r_0)/r_0$ and $\zeta = z/r_0$ we have $B(\varrho, 0) = B_0(1 + k\varrho + l\varrho^2 + \cdots)$. The series expansion of A has the shape

$$\left.\begin{aligned} A(\varrho, \zeta) = B_0 r_0 \Big(\varrho + \frac{k-1}{2}\varrho^2 + \frac{2l-k+3}{6}\varrho^3 + \cdots \\ - \frac{k}{2}\zeta^2 - l\varrho\zeta^2 - \cdots\Big). \end{aligned}\right\} \tag{A1}$$

In the median plane rA has the simpler shape

$$rA = B_0 r_0^2 \Big(\varrho + \frac{k+1}{2}\varrho^2 + \frac{l+k}{3}\varrho^3 + \frac{m+l}{4}\varrho^4 + \cdots\Big). \tag{A2}$$

In the case of a lens type spectrometer the electrons move near the axis. A series expansion of A can in this region be derived from the value of B_z on the axis yielding[37]

$$A = \sum_0^\infty (-1)^n \frac{B(z)^{(2n)}}{n!\,(n+1)!} \times \frac{r^{2n+1}}{2^{2n+1}} = B(z)\frac{r}{2} - \frac{d^2B(z)}{dz^2}\frac{r^3}{16} + \cdots. \tag{A3}$$

II. The equation of motion

The equation of motion can be derived from the Lagrangian

$$L = \tfrac{1}{2} m v^2 + e(v \cdot A) = \tfrac{1}{2} m \dot{r}^2 + \tfrac{1}{2} m r^2 \dot{\varphi}^2 + \tfrac{1}{2} m \dot{z}^2 + e r \dot{\varphi} A .$$

After some reduction the Lagrangian equations get the shape

$$\left.\begin{aligned} r\dot{\varphi} &= v D \\ \ddot{r} &= -v^2 D \frac{\partial D}{\partial r} \\ \ddot{z} &= -v^2 D \frac{\partial D}{\partial z} \end{aligned}\right\} \tag{A4}$$

with $D = C/r - eA/p$. C is the ratio of the total angular momentum and the linear momentum p. e is the electronic charge. In the case of lens type spectrometers the value of C may in general be put equal to zero; in the case of prismatic spectrometers the value of C depends on the initial conditions and can be calculated by means of the first equation from (A4).

By choosing φ as independent variable (A4) is transformed to[9]

$$\left.\begin{aligned} -D r'' &= r^2 \frac{\partial D}{\partial r} + r'^2\Big(\frac{\partial D}{\partial r} - \frac{D}{r}\Big) + r' z' \frac{\partial D}{\partial z} \\ -D z'' &= r^2 \frac{\partial D}{\partial z} + r' z'\Big(\frac{\partial D}{\partial r} - \frac{D}{r}\Big) + z'^2 \frac{\partial D}{\partial z} . \end{aligned}\right\} \tag{A5}$$

If the electrons move in the median plane $z = 0$, the first equation of (A4) together with the geometrical equation $(r\dot{\varphi})^2 + \dot{r}^2 = v^2$ yields[3]

$$r'^2 = r^2\Big(\frac{1}{D^2} - 1\Big) \quad \text{or} \quad \frac{d\varphi}{dr} = \frac{D}{r(1-D^2)^{\frac{1}{2}}}. \tag{A6}$$

If on the other hand z is chosen as independent variable one obtains[13, 28]

$$\left.\begin{aligned} \varphi' &= -\frac{D(1+r'^2)^{\frac{1}{2}}}{(1-D^2)^{\frac{1}{2}} r} \\ r'' &= \frac{D(1+r'^2)\left(\frac{\partial D}{\partial r} - r'\frac{\partial D}{\partial z}\right)}{(1-D^2)} . \end{aligned}\right\} \tag{A7}$$

III. Method of solution

The first two terms of a series expansion of (A5) in powers of ϱ and ζ yield the following equations for electrons with a momentum equal to $-eB_0 r_0(1+\Delta)$ and starting at $\varphi = 0$, $\varrho = 0$, $\zeta = \zeta_0$ under exit angles α and β

$$\left.\begin{aligned} \varrho'' + (1+k)\varrho &= l\zeta^2 - \frac{(1+3k+2l)\varrho^2}{2} + \varrho'^2 + \Delta - \frac{(\alpha^2+\beta^2-k\zeta_0^2}{2} \\ \zeta'' - k\zeta &= 2(l+k)\varrho\zeta + \varrho'\zeta' + k\Delta\zeta . \end{aligned}\right\} \tag{A8}$$

These equations can be solved by customary perturbation methods yielding the aberration and dispersion.

The derivation and solution of these equations have been described by SVARTHOLM[9].

BEIDUK and KONOPINSKI have used eq. (A6) with the series expansion (A2) in order to determine the required field shape for high order elimination of the radial aberration in a 180° prismatic spectrometer.

The author[6] has calculated this field shape for any value of the coefficient k from eq. (5) by substituting a FOURIER series as solution.

A series expansion of (A7) in powers of r yields as first two terms for electrons with a momentum $e(B\varrho)$

$$\left.\begin{aligned} r'' + \frac{B^2 r}{(B\varrho)^2} &= -r^3\left(\frac{B^4}{16(B\varrho)^4} - \frac{BB''}{8(B\varrho)^2}\right) + r^2 r' \frac{BB'}{4(B\varrho)^2} - r r'^2 \frac{B^2}{4(B\varrho)^2} \\ \varphi' + \frac{B}{2(B\varrho)} &= -r^2\left(\frac{B^3}{8(B\varrho)^3} - \frac{B''}{16(B\varrho)}\right) - r'^2 \frac{B}{4(B\varrho)} . \end{aligned}\right\} \tag{A9}$$

The solution of the first of these two equations yielding spherical aberration and dispersion has been discussed by the author[13].

BIBLIOGRAPHY

[1] RUTHERFORD, E. and ROBINSON, H.; *Phil. Mag.* 26 (1913) 717.
[2] SIEGBAHN, K.; *Arkiv f. mat. astr. o. phys.* 30A (1944) No. 20.
[3] BEIDUK, F. M. and KONOPINSKI, F. J.; *Rev. Sci. Instrum.* 19 (1948) 594.
[4] LANGER, L. M. and SHARP COOK, C. S.; *Rev. Sci. Instrum.* 19 (1948) 257.
[5] ROSENBLUM, E. S.; *Phys. Rev.* 72 (1947) 731.
[6] VERSTER, N. F.; *Physica* 16 (1950) 815.
[7] SIEGBAHN, K. and SVARTHOLM, N.; *Nature, Lond.* 157 (1946) 872.
[8] SVARTHOLM, N. and SIEGBAHN, K.; *Arkiv f. mat. astr. o. fysik*, 33A (1946) No. 21.
[9] SVARTHOLM, N.; *Arkiv f. mat. astr. o. fysik*, 33A (1946) No. 24.
[10] SHULL, F. B. and DENNISON, O. M.; *Phys. Rev.* 71 (1947) 681; 72 (1947) 731.
[11] SHULL, F. B.; *Phys. Rev.* 74 (1948) 917.
[12] KURIE, F. N. D., OSABA, J. S. and SLACK, L.; *Rev. Sci. Instrum.* 19 (1948) 771.

[13] VERSTER, N. F.; *Appl. Sci. Research* B1 (1950) 363.
[14] SIEGBAHN, K.; *Phil. Mag.* 37 (1946) 162.
[15] GLASER, W.; *Z. Physik* 116 (1940) 19.
[16] DEUTSCH, M., ELLIOT, L. G. and EVANS, R. D.; *Rev. Sci. Instrum.* 15 (1944) 178.
[17] QUADE, E. A. and HALLIDAY, D.; *Rev. Sci. Instrum.* 19 (1948) 234.
[18] SLÄTIS, H.; *Arkiv f. mat. Astr. o. Fysik* 35A (1948) No. 3.
[19] FRANKEL, S.; *Phys. Rev.* 73 (1948) 804.
[20] DUMOND, J. W.; *Rev. Sci. Instrum.* 20 (1949) 160 and 616.
[21] PERSICO, E.; *Rev. Sci. Instrum.* 20 (1949) 191.
[22] WITCHER, C. M.; *Phys. Rev.*, 60 (1941) 31.
[23] SCHMIDT, F. H., KEISTER, G. L., MEYER, D. I. and GROSS, W. E.; *Bull. Amer. Phys. Soc.* 26 (1951) No. 1 (I 8).
[24] ZÜNTI, W.; *Helv. Phys. Acta* 21 (1948) 179.
[25] SIEGBAHN, K. and SLÄTIS, H.; *Arkiv f. Fysik* 1 (1949) No. 17.
[26] BOTHE, W.; *Naturwissenschaften* 37 (1950) 41.
[27] BUSCH, H.; *Ann. Phys.* 81 (1926) 974.
[28] ZWORYKIN, V. K., MORTON, G. A., RAMBERG, E. G., HILLIER, J. and VANCE A. W.; *Electrons optics and the electron microscope*, 1st ed., p. 504, New York, 1945.
[29] WU, C-S.; *Rev. mod. Phys.* 22 (1950) 386.
[30] HORNYAK, W. F., LAURITSEN, T. and RASMUSSEN, V. K.; *Phys. Rev.* 76 (1949) 731.
[31] HEDGRAN, A., SIEGBAHN, K. and SVARTHOLM, N.; *Proc. Phys. Soc.* A 63 (1950) 960.
[32] KOFOED-HANSEN, O., LINDHARD, J. and NIELSEN, O. B.; *K. Danske Vidensk. Selsk. Mat. Fys. Medd.* 25 (1950) No. 16.
[33] RICHARDSON, H. O. W.; *Phil. Mag.* 40 (1949) 233; *Proc. Phys. Soc.* A64 (1951) 163.

NUCLEAR PARAMAGNETIC RESONANCE

R. V. Pound

Introduction

Nuclei composed of odd numbers of either protons, neutrons, or both, possess non-vanishing angular momenta and associated magnetic moments. About two-thirds of the stable nuclear species fall into these classes. Studies of hyperfine structures of atomic spectra have provided a large amount of data on these moments. The elegant techniques developed by Rabi and his collaborators, using atomic and molecular beams, have greatly increased the amount and the precision of such data. More recently, data on a large fraction of the nuclei have been forthcoming from the, in some ways, even more precise methods of nuclear paramagnetic resonance[1] and nuclear induction[2], originated almost simultaneously by Purcell, Torrey, and Pound and by Bloch, Hansen, and Packard, respectively, in late 1945. In addition to the lengthening of the lists of accurately known values of nuclear magnetic moments, experimental studies of these resonances have shown the power of the method for the observation of certain properties of the matter in which the nuclei are immersed. As well as being interesting in themselves, many effects dependent on these properties have strong influences on the nature of nuclear resonance signals and on the amount of information about nuclear properties they can provide.

In the absence of electronic paramagnetism, ordinary matter, whether solid, liquid, or gaseous, should show a slight paramagnetism as a result of the magnetic dipole moments of its constituent nuclei. Such matter, if magnetized isothermally, should have a magnetic susceptibility very accurately in accord with Curie's law with χ_0 given by

$$\chi_0 = N \frac{\mu^2}{I^2} \frac{I(I+1)}{3kT}, \tag{1}$$

for a material containing only one species of magnetic nuclei. Here N is the number of such nuclei per unit volume, μ is the maximum component of magnetic moment of a nucleus along a given direction, I, the maximum component of angular momentum along that direction (measured in units of $h/2\pi$), k, Boltzmann's constant, and T the absolute temperature. Because the magnitudes of nuclear magnetic-dipole moments are only about 10^{-3} times that of an electron, the resulting paramagnetic susceptibilities would be only about 10^{-6} times as large as those of electronic origin, at the same temperatures. However, by utilizing the resonance method, the presence of such small induced magnetic polarization is rendered easily detectable in a manner which allows very accurate determination of the nuclear gyromagnetic ratio μ/I.

Two alternative, rather different, descriptions of the phenomenon of nuclear resonance have become customary. Under similar conditions both descriptions give the same results, but it is simpler to visualize some effects using one model and others with the other. Acquaintance with both is thus worthwhile but the present article will base the discussions on the quasi-optical description in terms of quantum mechanical energy levels and the transitions induced between them by applied radio-frequency fields. The model of BLOCH[3], based on the classical dynamics of the net magnetic moment vector under the influence of applied fields, will only be used to assist in the explanation of some transient effects.

BASIC THEORY

The $2I+1$ fold degeneracy of an isolated nucleus of spin I is removed by the interaction of the magnetic moment of the nucleus with a magnetic field H_z, taken as directed along the z-direction. Thus, the energy levels are given by

$$W_m = -m\mu H_z/I,$$

where m, the component of I along the z-direction, ranges from I to $-I$. In a liquid or solid there are of the order of 10^{21} such nuclei per unit volume with a certain amount of mutual interaction. Rigorously, one should use a much more complex description of the entire interacting system but the essential features of the system are revealed by considering each nucleus to occupy one of its $2I+1$ levels, independently. At the instant of application of the field, on the average, equal numbers of nuclei must be found in each state because there has been no net polarization of the system in the absence of the applied field. The isothermal nuclear paramagnetism of eq.(1) results if the populations of the energy levels become altered by an achievement of thermal equilibrium between the spin system and the lattice. Mechanisms for such spin-lattice coupling will be discussed later but, if such an equilibrium is achieved, the ratios of adjacent upper to lower energy level populations become, in accord with a BOLTZMANN distribution, $\exp(-\mu H_z/I\,kT)$. At room temperatures and with fields as high as 20,000 gauss this factor differs from unity by only about one part in 10^5. The presence of nuclear moments in matter is only detectable if this small difference in populations exists.

In experiments on nuclear paramagnetic resonance, an oscillatory r-f magnetic field is applied at right angles to the z-direction. Such a field can be considered as composed of two oppositely rotating fields, and the component rotating in a sense determined by the sign of the nuclear magnetic moment (the sense of precession of a classical top with a collinear magnetic moment and angular momentum) will induce transitions where m, the magnetic quantum numbers, change by plus and minus one with equal probabilities. From standard radiation theory, the magnetic dipole transition probability is given by,

$$W_{m\to m'} = (8\pi^3/3h^2)\,|(m\,|M|\,m')|^2\,\varrho_\nu \qquad (2)$$

where M is the magnetic moment operator, and ϱ_ν is the energy density per unit frequency range in an isotropic, unpolarized radiation field. Under the

conditions of interest at present the applied radiation is at a single frequency and the levels (as will be shown later) have relatively greater width. This situation may be described by $g(\nu)$, a shape function for the observed resonant absorption line, so normalized that

$$\int_0^\infty g(\nu)\, d\nu = 1 . \tag{3}$$

The effective relationship between the actual applied r-f field and the isotropic, unpolarized radiation field of eq. (2) can be expressed as

$$\varrho_\nu = 3H_1^2\, g(\nu)/4\pi$$

where H_1 is the amplitude of the circularly polarized component of the appropriate sense, equal to one-half the amplitude of the oscillatory field. From these relationships one obtains the required transition probability,

$$W_{m\to(m-1)} = \tfrac{1}{4}\gamma^2 H_1^2\, g(\nu)\,(I+m)\,(I-m+1) \tag{4}$$

where γ is used for $2\pi\mu/I\,h$ and the well known matrix elements of the magnetic dipole have been introduced. The transition probability $W_{(m-1)\to m}$ is identical and it is only the tendency of the spin system to assume, through a spin-lattice interaction, a thermal distribution that a net absorption of energy from the r-f field results. In equilibrium at temperature T, since at ordinary values of T and H_z the energy differences are so small compared to kT, the difference between the population of level m and the next higher level, $m-1$, is to a good approximation

$$N_m - N_{m-1} = N\,h\nu/(2I+1)\,kT .$$

Each upward transition of this surplus results in an absorption of energy $h\nu = h\gamma H_z/2\pi$, with the upward and downward transitions of the remaining bulk of the spins giving no net effect. The power absorbed in the sample per unit volume is

$$P_a = \gamma^2 H_1^2 N (h\nu)^2 I(I+1)\, g(\nu)/6\,kT , \tag{6}$$

where the transitions have been summed over $m = I$ to $m = -I+1$.

The presence of this absorption causes a reduction in the Q-factor of a circuit supplying the oscillatory magnetic field. A resonance is detectable by observation of the decrease in Q, or in shunt resistance of a shunt resonant circuit, accompanying the adjustment of its resonant frequency, or of the static field H_z, to the correct value. Because the Q-factor is the ratio of energy stored to energy dissipated per radian, contributing elements of dissipation may be treated separately as inverse Q's. These give additively a net inverse of the Q of the circuit. In this sense then, the inverse Q for the nuclear absorption is

$$1/Q = P_a/\nu H_1^2 = \gamma^2 \hbar^2 N I(I+1)\,\nu\, g(\nu)/6kT . \tag{6}$$

The inverse Q can be shown to be $4\pi\chi''$, where χ'' is an imaginary component of a complex magnetic susceptibility. Thus χ'' may be written

$$\chi'' = \frac{\pi}{2}\left[\frac{N\gamma^2\hbar^2 I(I+1}{3kT}\right]\nu\, g(\nu) = \frac{\pi}{2}\,\chi_0 \nu\, g(\nu) \tag{7}$$

with $\hbar$ equal to $h/2\pi$ and χ_0 given by eq.(1). As in all resonant absorption, a dispersion must accompany the effect, with the appropriate accompanying frequency dependence in the real part of the magnetic susceptibility χ'. This dispersion can be shown to give rise to an equally detectable effect, observable as a detuning of the resonant circuit.

In computing the absorption coefficient, it has been assumed that the thermal distribution and the corresponding lower level surpluses exist in the steady state in the presence of the r-f signal field. This can only be so if the spin-lattice coupling mechanism is capable of removing excess energy from the spin system to the lattice at an appropriate rate. It is conventional to describe the heat contact between the spin system and its surroundings in terms of a spin-lattice relaxation time T_1. If there are only two levels, as for I of $\frac{1}{2}$, it is found that the approach to equilibrium can be described by an exponential law. In differential form, if n is the surplus in the lower level at time t, and n_0 is the equilibrium surplus at temperature T

$$\frac{dn}{dt} = \left(\frac{1}{T_1}\right)(n_0 - n).$$

Application of the r-f signal competes to give

$$\frac{dn}{dt} = \left(\frac{1}{T_1}\right)(n_0 - n) - 2n W_{\frac{1}{2}\to -\frac{1}{2}}.$$

In the steady state, dn/dt is zero, and

$$n/n_0 = [1 + \tfrac{1}{2}\gamma^2 H_1^2 T_1 g(\nu)]^{-1}. \tag{8}$$

In the event the second term is not negligible, the susceptibility drops from its value for infinitesimal H_1 and, therefore, the effect saturates. Under certain conditions the same factor can describe the behaviour of the absorption coefficient of systems of nuclei of higher spin. It is convenient to define a second time, $T_2 = \frac{1}{2}\, g(\nu)_{\max}$ making the saturation factor $[1 + \gamma^2 H_1^2 T_1 T_2]^{-1}$ at maximum absorption. The T_2 is a measure of the inverse of the line breadth in the absence of broadening resulting from inhomogeneity of H_z. Its exact relationship to the width between half-maximum absorption points depends on the actual line shape. A quantity T_2^* is sometimes used to identify the experimentally observed quantity; this may be smaller because of inhomogeneity of H_z than the similar quantity, T_2, characteristic of the sample itself.

In the model of BLOCH[3], the same effects are described by analysis of the dynamics of the net magnetic and angular momenta when subjected to the static and r-f magnetic fields. In thermal equilibrium, these collinear vectors lie along the static field in the z-direction. The details of the dynamics depend strongly on the rates of change of variables involved, but in general the influence of the applied r—f field is to pull the magnetic moment vector out of parallelism with the z-direction. If left free in such a condition, it will precess about the z-direction with the frequency $\nu = \gamma H_z/2\pi$. It is clear, according to this picture, that all effects are equally observable as an oscillatory magnetic moment along any direction in the x, y plane. If the reaction on the

coil providing H_1 itself is observed, the effect may be a reactance or a resistance, depending on the phase of the precessing magnetic moment relative to H_1. BLOCH and his collaborators in the nuclear induction technique[3] take advantage of the reality of the rotating magnetic moment by coupling to it with a coil with its axis at right angles to both the strong field and to the axis of the coil providing H_1. This arrangement provides useful decoupling from the driving signal. In this picture the time T_1 refers to a rate of recovery of the z-component to its equilibrium value and the time T_2 to that of the x and y components to their equilibrium null values. This model is especially useful for the interpretation of "transient" effects.

The motion of the net magnetic moment is easily understood if a system of coordinates rotating in the sense of the precession is introduced. The precession frequency relative to a system rotating about the z axis is reduced to $(\gamma H_z/2\pi) - (\omega/2\pi)$ where ω is the angular velocity of the rotating system. Thus, relative to such coordinates, the effective field strength in the z-direction is $(H_z - \omega/\gamma)$. If the rotating system is chosen to have the frequency of H_1, the resulting motion of the net magnetic moment will be simply a precession about the fixed field which is the resultant of H_1 and the effective field along z. Such precession is altered by the effects characterized by the time constants T_1 and T_2 or T_2^*. As an example, if ω is exactly γH_z, and the system is initially in equilibrium with no r-f field applied, at the instant of switching on H_1, the magnetic moment must begin to precess in the plane of z, y', if x' is taken along H_1. If H_1 is sufficiently strong, several cycles of this precession can occur, but after a time of the order of T_2^* the effect is damped out. Thus, a fixed pick-up coil would receive as a transient effect an induced voltage at the frequency $\omega/2\pi$, amplitude modulated at the frequency $\gamma H_1/2\pi$. This effect has been utilized by TORREY[4] as a means of measuring T_1 and T_2. Another pulse technique, most easily understood through the rotating coordinate model, has been devised by HAHN[5].

DETECTION TECHNIQUES

The theoretical ease of detection of nuclear paramagnetic resonance varies widely with factors characteristic of the sample—the values of γ, I, N_0, T_1 and T_2. The first successful experiments[1] observed direct static unbalance of a bridge of which one arm contained the absorption cell, when the value of H_z was set to a critical value. Greatly improved sensitivity was achieved by the use of a modulation technique whereby effects directly coherent with the modulation of the field are emphasized.

It is possible to estimate the detectability of a signal of this sort, relative to inherent noise. Modulation of the field (or of frequency) results in a time dependent absorption which, in turn, modulates the power available from the coil containing the sample, whether it be the driving coil itself or a crossed coil. Evidence of the absorption is carried by the resulting modulation side bands and, for detection, these must possess power at least of the order of magnitude of the power of thermal agitation noise available in an appropriate bandwidth

in the same source. At infinitesimal levels of H_1, ($\gamma^2 H_1^2 T_1 T_2 \ll 1$), the available signal power is proportional to the driving power, but as the level of the latter is increased, the saturation effect sets in. For observation of absorption, the available signal is maximized for $\gamma^2 H_1^2 T_1 T_2 \sim 1$ and for dispersion it approaches an identical maximum level asymptotically as the driving level is increased. In both cases the resulting ratio of signal power to that of noise is given by the formula

$$\frac{P_s}{P_n} = \frac{V_c Q_0 (A\zeta)^2 \hbar^4 N^2 \gamma^2 \nu_0^3 T_2^* [I(I+1)]^2}{2304 (kT)^2 (BF) T_1}. \tag{9}$$

In this formula, V_c is the volume of the coil, Q_0 its Q factor, A a modulation coefficient of order of 0·5, ζ is a filling factor measuring the fraction of the magnetic energy of the coil stored in the volume of the sample, ν_0 is the frequency of resonance, B is the equivalent noise bandwidth, F the noise figure of the amplifying apparatus and 2304 is $2^8 \times 3^2$. The other quantities are already defined. The noise figure measures the ratio of the output noise power of the instrument to that which would ideally be present if only amplified noise originating in the resistance of the coil were present, and has an ideal minimum of unity. The frequency ν_0 is limited by the magnetic field available. Using an empirical relation relating the Q of a coil to its volume and frequency $Q_0 = 0{\cdot}037\, \nu_0^{\frac{1}{2}} V_c^{\frac{1}{2}}$, one can write the amplitude ratio of signal to noise as

$$\left.\begin{aligned} A_s/A_n \approx 1{\cdot}62 \times 10^{-4} V_c^{\frac{1}{2}} \zeta A \hbar^2 N \gamma^{\frac{11}{4}} H_0^{\frac{7}{4}} T_2^{*\frac{1}{2}} \times \\ \times I(I+1) (kT)^{-\frac{3}{2}} (BF)^{-\frac{1}{2}} T_1^{-\frac{1}{2}}. \end{aligned}\right\} \tag{10}$$

The care necessary to obtain adequate sensitivity varies considerably with the nature of the sample, as can be verified by putting typical values into eq.(10). For $I = \frac{1}{2}$ and M = one nuclear magneton, about 10^{18} nuclei are required to give $A_s/A_n = 1$, with $V_c = 1$ cm^3, $H_0 = 15{,}000$ gauss and $B = 1$ cycle per sec at room temperature, under the optimum condition, $T_2^* = T_1$.

Considerable attention must be paid to the magnet, the source of H_0. Because many line breadths are naturally small, the field homogeneity must be small if only to avoid diminishing T_2^*. Magnets with gaps having diameters about four or more times their lengths are usually used. Rim shims or slight conical depressions in the pole pieces are used to decrease radial dependence of the field strength. The sample dimensions are usually less than $\frac{1}{10}$ of the pole diameters. High field stability is required, especially if narrowband-widths and thus long observation times are necessary, and battery supplies are often used for the magnet current. Alternatively, electronic current regulation and sometimes automatic field regulation derived from a nuclear resonance signal itself, is used[6]. Permanent magnets have been used with considerable success. Unfortunately, they are found to have drifts, apparently with temperature, amounting to parts in 10^4 under typical conditions.

Apparatus of four principal types is being used in present studies of the resonance effect itself, each having some relative merits. The first of these, used extensively at Harvard[7,8,9] for relaxation time studies, is outlined in

Fig. 1. The sample is contained in the coil in the strong field and this coil is resonated with capacity at a given frequency. This circuit and an identical "dummy" one form two sides of a bridge in which a balance, to nearly null, of transmission of signal generator output to the amplifier input is achieved by a phase inversion provided by an extra half-wavelength of coaxial line in one side. Loading of the circuits by the generator is avoided by weak capacitive coupling to the terminating resistance at the ends of the input lines from the generator. The output coupling is chosen to provide the amplifier

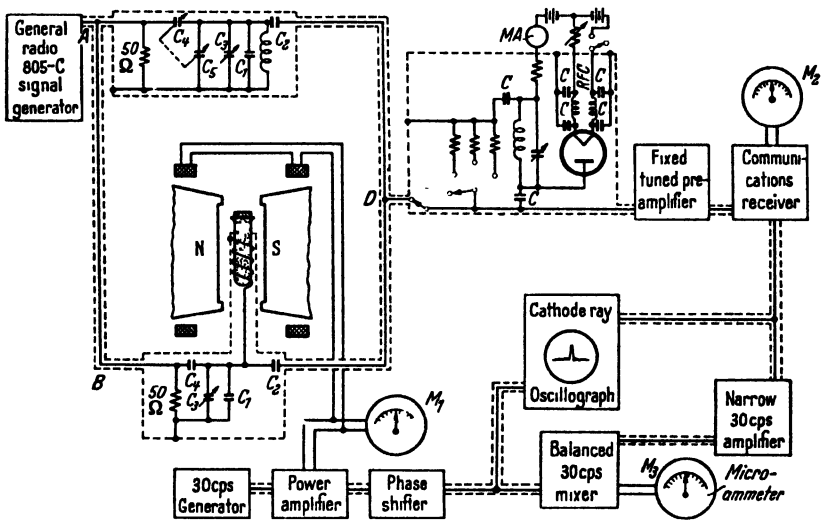


Fig. 1. A block diagram of a "bridge" circuit. The output point D is nearly a voltage node because of the extra half-wavelength of line AB, in one side. Detection is either by the oscillograph or by the narrow-band system on the meter. A circuit used for noise-figure measurements, with a temperature-limited diode, is shown at the input to the r-f amplifier.

with a source resistance resulting in minimum noise figure. A circuit for measurement of this noise figure with the help of a temperature limited diode is shown in the diagram at the input to the amplifier. The main part of the amplifier is a superheterodyne communications receiver. The preamplifier is used to improve the noise figure. For intense lines, the field is swept by an amount several times the line breadth and the output of the receiver is connected to vertical deflection circuits of a cathode ray oscillograph, horizontally swept at the modulation frequency. The line is thereby displayed directly and moves across the screen as the field strength is slowly varied. For weaker lines, and for more quantitative observation of properties of lines, a field modulation less than the line breadth is used and the receiver output is fed to a highly selective amplifier passing only the modulation frequency. This in turn feeds a mixer or phase sensitive detector[10], mixing with the modulation frequency, and thus producing a d-c current recorded by a meter. In this scheme the r-f noise bandwidth is just twice (for two sidebands) the equivalent noise bandwidth of the meter, or of the RC circuit feeding it, and often is as small as 0·01 cps. A derivative of the line shape with respect to field is observed.

In principle, there is no necessity for the decoupling of the receiver from the generator, provided by the bridge. Direct detection of the voltage across the single tuned circuit, supplied from a high impedance source, is all that should be required. In practice, it is difficult to produce a detector of sufficiently low inherent noise to allow detection at the level of the noise inherent in the input circuit itself. Amplification before detection, without balancing out the driving signal, is difficult because the voltage soon overloads the amplifier. In addition, the noise introduced as modulation on the driving signal itself usually would contribute very dominant excess noise if it were not balanced out before amplification.

The bridge is never run fully balanced, an unbalance signal always feeding into the amplifier as a carrier. The modulation of this, resulting from a resonance signal, is fractionally very small and, thus, the detector of the receiver actually behaves as a mixer, converting the side bands linearly to audio frequency. The resonance signal can be derived from either the absorption or the dispersion or any mixture of the two depending on the phase of the unbalance signal. If the bridge is unbalanced principally in phase, dispersion is displayed; if unbalanced in amplitude, absorption is displayed.

Bridges of various other designs have been used to advantage. An awkward feature of the bridge described is the use of a half-wavelength cable for phase inversion on one side. An input transformer having a symmetrical push-pull output and a wide band of useful frequencies would considerably simplify operation with quickly variable frequency[4]. Twin T circuits have certain virtues in this application[11, 12].

Saturation effects of the absorption are observed by changing the level of the signal generator and altering the gain of the receiver to maintain a fixed level at its detector. Thus the amplitude of the resonance signal is a measure of the fractional absorption and is constant at levels of driving signal below saturation. It then drops off as $\gamma^2 H_1^2 T_1 T_2$ becomes of the order of unity and greater. Direct observation of the growth of the absorption is possible, for sufficiently long T_1, if short observations of the resonance can be made at intervals, with H_1 low enough not to disturb the spin system.

The scheme of detection originated by BLOCH and his collaborators[13] utilized separated driving and pick-up coils placed at right angles to one another and to the field. In other respects the technique is like that above with the crossed coils giving geometrically the effect of a bridge. It is usually necessary to supplement the balance obtained by use of trimming devices, either compensating electrical circuits or geometrical adjustments, and in this way a very stable belance can be achieved. This facilitates the use of larger driving fields. Balance in amplitude is usually used, leaving the system sensitive to the dispersive component which does not decrease in excessive r-f fields. In searching for unknown resonances, the lines can be broadened by large H_1 without sacrificing amplitude. There is then no need to search in level of H_1 and in modulation field amplitude as well as in H_z, as is necessary in the absorption method without previous clues. This arrangement also provides information on the sign of γ given by the sense of the dispersive signal, as the resonance

is traversed from a given direction. This is most conveniently utilized by comparison with a nucleus of known sign under the same conditions of balance because otherwise it is necessary to know the phase of the unbalance of the "bridge".

The other two methods of detection use the circuit containing the sample as the frequency determining circuit of an oscillator, in the one case running in a steady state and in the other as a quenched or superregenerative oscillator. Many variations are possible on both of these methods, almost any oscillating circuit being applicable to a certain degree. For the most favourable cases (for instance, the resonance of protons in paraffin oil) an oscillator of the simplest sort is adequate. Again a field modulation is used and the level of oscillation dips as the resonance is traversed in the modulation cycle. The plate circuit of the oscillator may be used directly as a detector of this dip, and the signal there treated exactly as in the bridge circuit, feeding either to an oscilloscope or, via selective amplifiers and phase sensitive detector, to a meter. The effective amplification, but not necessarily the signal-to-noise ratio, of such a device is a maximum at the threshold of oscillation, as with a regenerative detector.

A special, flexible, circuit with control of its oscillation level has been developed[14,15,16]. For constancy of characteristics and the achievement of a minimum noise figure, separate detection is employed, isolated by a buffer amplifier. The *d-c* detected level is used as a feedback with a long time constant to maintain a predetermined oscillation level over a frequency range of about 2:1, achieved through variation of the tuning capacity. Various coils allow operation from 35 Mc/sec downwards. Its principal advantages are that search in frequency at fixed field is easy and that it responds entirely to the absorption component. Dispersion can be detected as frequency modulation, of course. Thus, difficult calibrations of field are avoided and line shapes can be recorded, using a recording milliammeter in conjunction with the phase-sensitive detector. A clock motor drive of the tuning condenser provides continuous slow scanning for search use. Investigation of the noise figure of such a system has shown it to be as small as 2 at low frequencies and low levels of oscillation and poorer at high levels and high frequencies. Thus, this circuit is as sensitive as any other for detection of resonances of a certain range of $\gamma^2 T_1 T_2$. It is at a disadvantage if conditions are such that $\gamma^2 T_1 T_2$ is very small, and difficulty in achieving very low levels of oscillation also limits its usefulness in conditions at the other extreme. A block diagram of this system is given in Fig. 2 and a circuit of the oscillator unit as developed by WATKINS[16] in Fig. 3. It is necessary, for stable operation with the narrow band phase sensitive detector, to minimize the direct pick-up of field modulation by the *r-f* coil. A coil, supplied with current at the modulation frequency, of adjustable phase and amplitude, is added to balance out such pick-up and is shown in the block diagram. A calibrator circuit that provides an artificial signal through use of modulated electronic resistance, used for intensity measurement is also shown. A circuit of this type, in conjunction with oscilloscopic presentation, makes a very simple and precise

device for magnetic field calibrations, using, for instance, a proton resonance. It has been operated down to about 200 gauss with sample volumes less than 1 cm^3.

The super-regenerative system is similar except that the oscillator does not run in a steady state but is turned on and off by a quench voltage. The rise of oscillation on each cycle is influenced by the presence of a nuclear resonance signal. The oscillatory magnetic moment in the coil, induced by the last pulse, persists and greatly assists the start of oscillation on the next quench cycle, provided that the time between is not long compared with T_2^*.

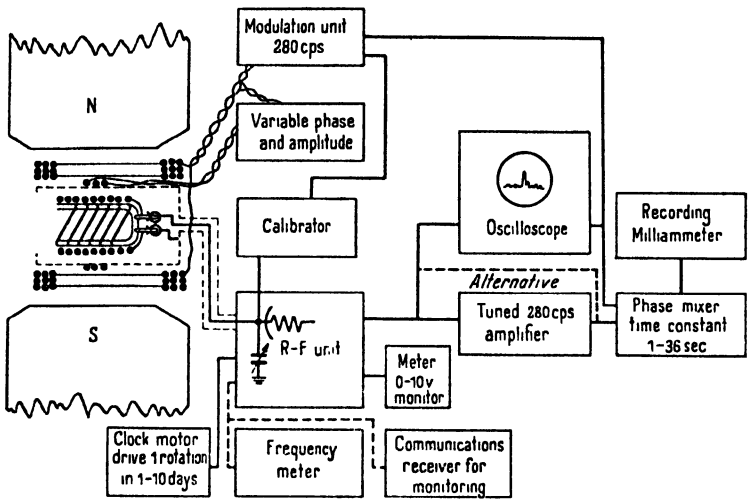


Fig. 2. A block diagram of the oscillating spectrograph. With display on the cathode-ray oscilloscope and manual tuning, such a system is convenient for measuring magnetic fields to high precision through the proton resonance in, for example, paraffin oil.

This technique has been widely applied by D. WILLIAMS and collaborators[17] to the measurement of g-factors. It has an advantage in that the applied signal, H_1, can be large, at the peak of oscillation, but that the detection is at the threshold of oscillation where the noise figure is a minimum. It is therefore best suited, compared with the steady state oscillator, to conditions of small $\gamma^2 T_1 T_2$. It suffers from having a complex response resulting from the many component spectrum of the pulsed oscillator and is thus not well suited to either precise frequency measurements or to line shape studies.

In addition to these methods, some novel pulse techniques, to be mentioned later, have been developed, notably that of TORREY[4] and the spin echoes method of HAHN[5].

SPECTRA IN LIQUIDS

The principal source of broadening measured by $g(\nu)$ or T_2 is the dipole-dipole coupling. Crudely, the magnitude of the actual field H_z acting on a given nucleus in a condensed phase of matter is increased or decreased according to the contributions of the dipolar fields of neighbouring nuclei. On the average,

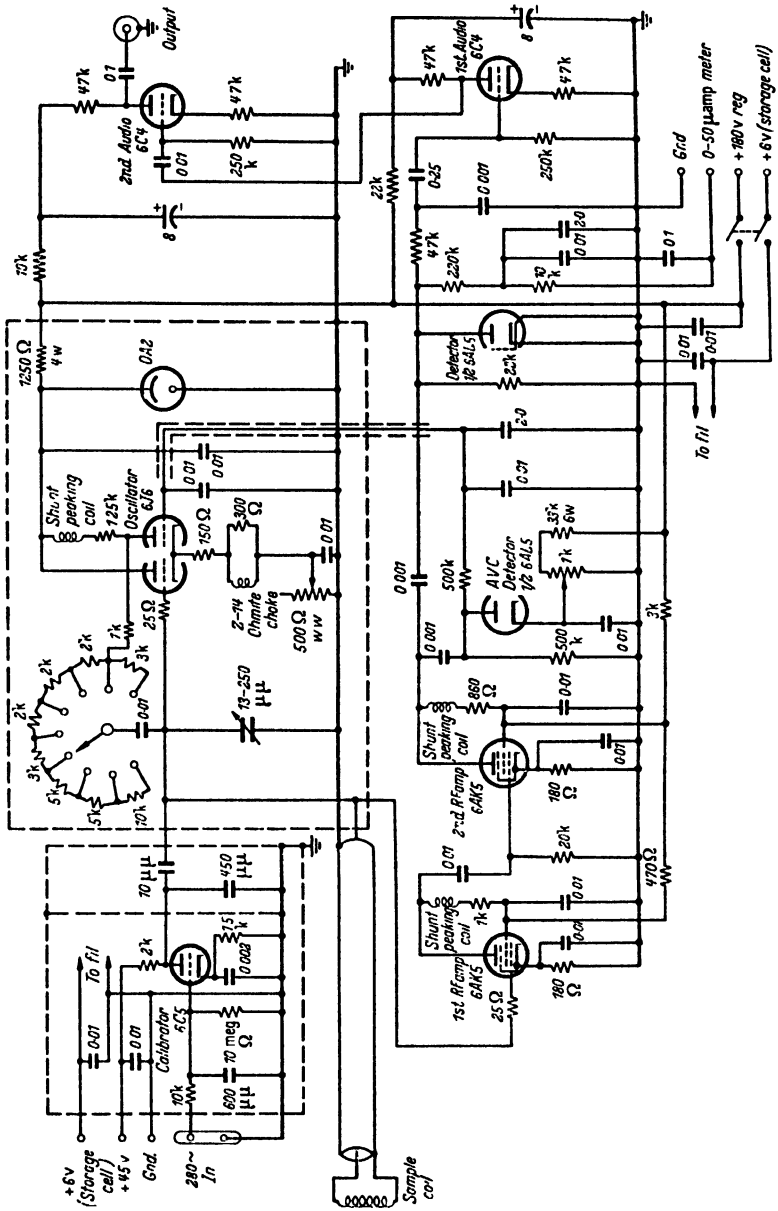


Fig. 3. A circuit diagram of an oscillator unit recently developed for use as a spectrograph. A calibrator, useful for relative intensity and saturation measurements, is shown. In use, this is supplied with a signal at the modulation frequency and produces a deflection of the recording meter. This oscillator can be operated from about 35 mcs downwards and has minimum noise figure if the largest feedback resistor for which oscillation occurs is used.

because of the very small degree of net polarization, the contribution is nearly zero but it is distributed in a random way and can be expected therefore to spread out the resonance from a discrete one to one covering a range of fields

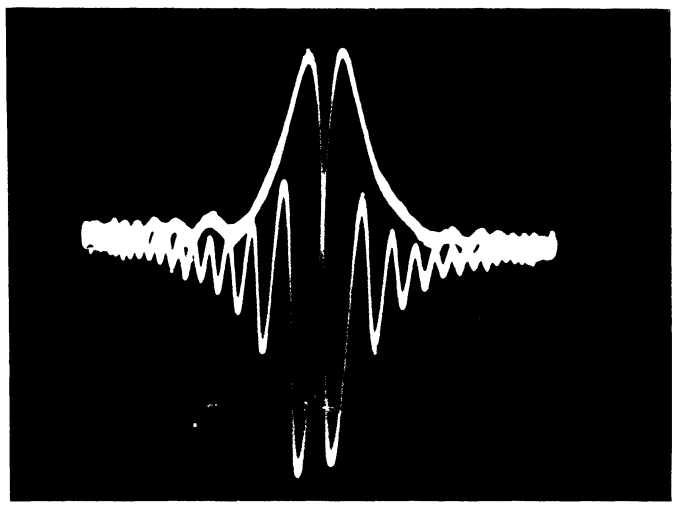


Fig. 4. A reproduction of the transient effect known as the "wiggles". This pattern is characteristic of the proton resonances in liquids of low viscosity with ordinary modulation frequencies. (T_2 is not much shorter than the period of the modulation.)

(To face page 32)

passes on but the x, y component of magnetic moment is sustained for a time roughly equal to T_2^*, which could be as long as T_2 in a perfectly homogeneous field and, thus, could be several seconds in water. If there were no r-f carrier present in the receiving apparatus, the response would be a rise with a fairly long tail on the after side which, with a sinusoidal sweep, is on the right for one sweep through resonance and on the left for the next. The presence of a carrier results in alternate constructive and destructive interference of the picked up nuclear signal, which has the instantaneous precession frequency determined by the net field, and the fixed carrier frequency. This interpretation can be strengthened by observing that the period of the wiggles grows shorter away from resonance. Further, an asymmetry, with emphasis of the wiggles after the sweep in one sense, can be introduced by detuning the receiver in the sense of the frequency emitted at that time in the cycle. A quantitative study involving the solution of equations for the dynamics of the magnetic moment vector under the appropriate conditions has been given by JACOBSOHN and WANGNESS[18]. An important result for precision measurements is that the full pattern must have perfect symmetry, either even or odd depending upon whether the system responds to absorption or dispersion.

From the considerations explaining narrowed lines it was possible to propose and confirm a mechanism accounting quantitatively for not only T_2 but also for the spin-lattice relaxation time T_1 in liquid, gaseous and certain kinds of solid samples. In a water molecule tumbling in accord with thermal agitation it is evident that the local magnetic field is not only effectively averaged but that it contains radio frequency components. The magnetic field at one proton due to its neighbor is a randomly fluctuating quantity and has r-f components in a continuous spectrum from zero frequency up to well above the frequency characteristic of the tumbling motion itself, $1/\tau_c$ where τ_c is the correlation time of the random motion. Subject to certain usually justifiable assumptions about the nature of the random process, the square of the local magnetic field can be shown to have a spectrum such that the intensity of frequency components in frequency interval $\Delta\nu$ at frequency ν is given by a relation of the form

$$H^2(\nu)\,\Delta\nu = \overline{4\,|H^2(t)|}\;\frac{\tau_c}{1+4\pi^2\nu^2\tau_c^2}\,\Delta\nu. \tag{11}$$

The constant $\overline{|H^2(t)|}$ is independent of the correlation time and the frequency and measures the time average of the square of the local field, and is of the order of μ^2/r^6. This r-f local field is capable of causing transitions of the nuclear spin and, because the motion giving rise to the spectrum is thermal in origin, such transitions can produce thermal equilibrium between the spin system and the thermal motion. To avoid going into a detailed picture of the system including all degrees of freedom, it is conventional to say that such transitions are more probably downward than upward by the factor $\exp(h\nu/kT)$. The calculated transition probability W from such a source is then related to the relaxation time T_1 by

$$T_1 = 1/2W \tag{12}$$

where W is given by

$$W \approx \frac{\mu^2}{4\hbar^2} H^2(\nu_0) \tag{13}$$

derived from (2) and neglecting the factor dependent on I and m and with ν_0 as the resonant frequency. In this way an expression results for the relaxation time

$$T_1 = \frac{\hbar^2}{\mu^2} \frac{1 + 4\pi^2 \nu_0^2 \tau_c^2}{\tau_c} \frac{1}{\overline{|(H^2(t)|}} . \tag{14}$$

A more exact and more detailed picture differs quantitatively in that (a) all neighbours need be taken into account; (b) various neighbours may have differing correlation times; and (c) a more detailed calculation shows that transitions in which both nuclei of an interacting pair may make transitions together and thus a spectral density at $2\nu_0$ plays a role. Nevertheless, considering only a single correlation time, a relation

$$\frac{1}{T_1} = C_1 \left[\frac{\tau_c}{1 + 4\pi^2 \nu_0^2 \tau_c^2} + \frac{2\tau_c}{1 + 16\pi^2 \nu_0^2 \tau_c^2} \right] \tag{15}$$

results, where C_1 is dependent on the time averaged surroundings but not on frequency or τ_c.

The line breadth in the frozen, rigid lattice would be, as mentioned, of the order of magnitude of μ/r^3 in gauss. A theoretically more tractable problem than that of calculating the breadth between half-peak absorption points is that of calculating a "mean squared breadth". This so-called second moment may be defined as $\langle \Delta\nu^2 \rangle_{av} = \int_0^\infty (\nu - \nu_0)^2 g(\nu)\, d\nu$. VAN VLECK[19] has calculated this for a rigid lattice with the result

$$\left(\frac{1}{2\pi T_2''} \right)^2 \equiv \langle \Delta\nu^2 \rangle_{av} \equiv \frac{9}{4} \left(\frac{\mu}{I} \right)^4 \frac{1}{\hbar^2} \left[\frac{I(I+1)}{3} \right] \sum_{j \neq i} (1 - 3\cos^2 \theta_{ij})^2 r_{ij}^{-6} . \tag{16}$$

The θ_{ij} is the angle between $\vec{r}_{ij}$, a position vector representing the j-th nucleus relative to the i-th, and the direction of the applied field. Except for the factor 9/4 this is the result one would calculate from the model based on the dispersion of local fields. In addition to that mechanism there is a broadening from a shortening of lifetime of a nucleus in a given state, m, from the fact that a neighbouringpair can make transitions in opposite senses, conserving energy, but their individual phases are interrupted. A simple estimate of line breadth from this cause also gives μ/r^3 gauss and VAN VLECK's calculation takes account of both processes. For non-identical nuclei only the dispersion of local static fields can have an effect since paired transitions cannot occur with conservation of energy.

In the non-rigid lattice the breadth is always less than in the rigid. Its calculation depends again on the spectral density of the randomly fluctuating local field but in the region of zero frequency instead of ν_0, and it can be shown that for $\tau_c \gg T_2''$, the value of T_2 is very nearly equal to T_2'', defined by eq.(16). For $\tau_c \ll 1/\omega_0$, T_2 is very nearly equal to T_1. A graphical representation in Fig.5 illustrates the behaviour of both T_1 and T_2 as functions of τ_c

according to this simplified model. The relative scales are fixed by a particular choice of C_1 of eq. (15). Two sets of curves are given, one solid and one dashed, for two operating frequencies, ν_0. It will be noted that the line breadth starts to decrease from that of the rigid lattice at $\tau_c = T_2''/\sqrt{2}$ independently of ν_0. On the other hand, T_1 is a minimum at $\tau_c = 1/2\pi\sqrt{2}\,\nu_0$. This can be explained by realizing that, whereas the integrated spectral density of the local field over all frequencies is independent of τ_c, the component at a given ν_0 may decrease or increase with τ_c, according to whether the flat part of the spectrum extends above ν_0 or not.

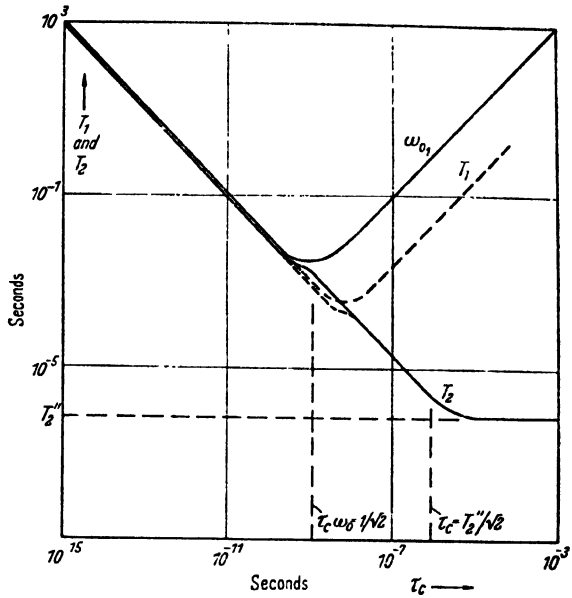


Fig. 5. The dependence of T_1 and T_2 on correlation time τ_c, assuming all interactions to have the same correlation time. Two values of the resonance frequency have been assumed, the higher giving the solid curves and the lower the dashed. The scale of ordinates depends on the value of T_2'' assumed.

Experimental confirmation of these relationships is good. As an example, the proton resonance in glycerin, which shows an enormous range of viscosity with temperature, and so of τ_c, has been found to behave as in Fig. 6. Exact agreement cannot be expected because the model of the surroundings of a proton is too simplified. The theory predicts a relaxation time for the protons in water of 3·4 sec and experiment shows about 2 sec, an adequate agreement. An experimentally easily observable change of T_2 is that of the protons in paraffin wax initially melted and observed as it sets.

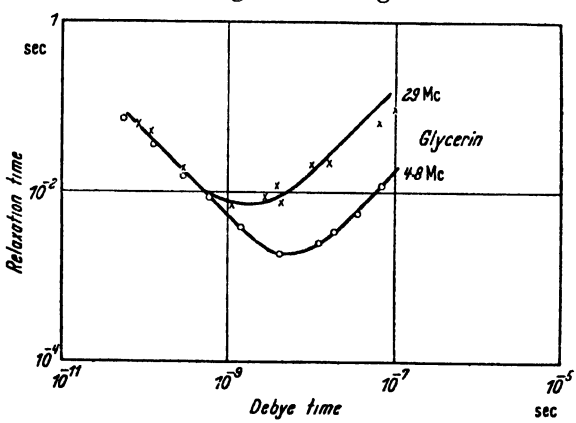


Fig. 6. The relaxation time T_1 and the line-width parameter T_2 of the protons in glycerin plotted against the ratio of viscosity to absolute temperature.

Aqueous solutions of salts provide useful samples of a large class of nuclei. Relaxation times in these, in the absence of nuclear electric quadrupole effects, might be considerably longer than that

of protons in water because of less close approach to the water protons and because of generally smaller g-factors than that of the proton. Shortened relaxation time can be achieved by the addition to the solution of paramagnetic ions, such as Mn^{++}, so intensifying the local field spectral intensity. An estimate of T_1 based on an analogous argument to the above leads to

$$(1/T_1) = 3g^2 \eta N_{ION} \mu_{eff}^2 / 5kT \qquad (17)$$

where g is the nuclear μ/I, η is the viscosity in poises, N_{ION} is the number of paramagnetic ions per cm^3, and μ_{eff} is the effective magnetic moment of the ions. In reaching this result, it is necessary to make assumptions about the diffusion coefficient of the ions and the radius of nearest approach. Experimentally, in their effect on the proton resonance the proportionality of $1/T_1$ to N_{ION} is confirmed and values of μ_{eff} calculated from the equation, using measured values of η, are reasonably close to directly measured values of μ for these ions. In concentrated solutions of other ions of which the nuclear resonance is desired, complexes frequently seem to form reducing the effectiveness of the paramagnetic ions. Observation of the resonance of the nuclei of the paramagnetic ions themselves would not seem to be easy because of the broadening from the enormous fluctuating electronic field. A large electronic contribution to the average field would also be present at the position of such nuclei.

Nuclear resonance has been observed in a few gases at high pressures[20,11]. For example, the proton resonance has been observed in gaseous hydrogen at about ten atmospheres of pressure. The mechanisms determining T_1 and T_2 are very similar to those in water except that the molecular reorientations occur in intermolecular collision. In addition to the spin-spin interaction within a molecule, there is a comparable interaction between the nuclear moments and the molecular magnetic field. Both of these are averaged out, leaving narrow lines, because at the high pressures necessary to achieve a detectable density, the mean time between collisions is very short compared to T_2. It is, in fact, very short compared to $1/\nu_0$ and, since it is further shortened by an increase of pressure, T_2 and T_1 increase with increasing pressure. Thus the curious effect of "pressure-narrowing" results. At ten atmospheres and 300° K, the protons in H_2 have $T_1 \sim 0{\cdot}015$ sec.

Noble gases, such as He^3, have practically negligible relaxation from direct collisions. ANDERSON[11] has been able to catalyze the relaxation in He^3 at 20 atmospheres by addition of an equal pressure of paramagnetic O_2.

SPIN ECHOES

A novel scheme developed by HAHN[5] allows observation of T_2 almost independent of field inhomogeneity. Pulsed r-f signals of high amplitude and short duration are utilized. In one variation, a first pulse is applied for such a time that the net magnetic moment precesses just 90°, to the x, y plane. The precession frequencies, because of inhomogeneity, are different in different parts of the sample so that, after the pulse, the oscillatory x and y components of magnetic moment disappear in the time T_2^*. In a coordinate system rotating

with the precession frequency in the median field, some parts lag and others lead the average, smearing the magnetic moment out over the x', y 'plane. Application of a second pulse twice as long as the first at any time τ after the first has the effect of flipping over the whole magnetization in the x', y' plane and parts which led now lag the median and vice-versa. These parts are still in the same fields as before and they all therefore recoalesce on the median at a time τ after the second pulse, reproducing, for a time about T_2^*, an oscillatory moment picked up as an echo in a receiver connected to the coil. By variation of τ, it is possible to observe the decay of the echo, and so of the x, y component, from other causes than inhomogeneity, revealing the real effect of T_2. Observation of modulation on the echo envelope led to the suggestion of distinct frequencies for protons in different environments in complex molecules.

Measurements of Nuclear g-Factors

The resonant frequencies of a very large number of stable nuclei have been measured, mostly in liquids and aqueous solutions. Considering the question of detectability, it will be seen that the available signal-to-noise ratio of eq.(10) is a maximum for $T_1 = T_2^*$, realizing that $T_1 \gtrsim T_2^*$, in general. Non-viscous solutions and liquids can provide this condition, as shown above, and thus lend themselves most readily to investigation of g-factors. It will be seen that, in principle, the value of T_1 and T_2^* are unimportant but in practice several limitations occur. First, for large T_1, an impossibly homogeneous field is required to avoid adding to the breadth and so shortening T_2^*. On the other hand, if T_1 is very short, a very large value of H_1 is required to obtain the optimum signal-to-noise ratio and then it is difficult to maintain the receiver noise figure F at a low value. Making T_1 and consequently T_2, unnecessarily short also reduces the available precision because of broadening. In many liquid samples of $I > \frac{1}{2}$ this already exists because of the electric quadrupole effect to be described later.

By use of crossed receiving and transmitting coils, the workers at Stanford have included determinations of signs of g-factors[21]. From intensity observations information is gained on spins because, for a given g-value, all other factors being constant, the intensity is proportional to $I(I+1)$, as is apparent from eq.(10) or eq.(16). Difficulties in measurements of absolute intensities and of exact values for $g(\nu)$ in many cases introduce uncertainty in values obtained for spins by this means.

With sufficient care, relative values of g-factors can be determined to as many as seven significant figures, as for instance has been done for the proton-deuteron ratio[22, 23]. By confining measurements to frequency ratios, all determinations can be referred back to the absolute determination of the g-factor of the proton[24].

Although the experimental frequency ratios can be, for many nuclei, determined with extreme precision there is some uncertainty of the actual nuclear g-factors in most cases. The magnetic field at the nucleus is not exactly that applied to the sample and the small difference is a property of

the atomic or molecular state of the surroundings of the nucleus. The field at the nucleus is decreased by the diamagnetic effect of the surrounding electrons and this shift for free atoms has been computed by LAMB[25] using a FERMI-THOMAS model for the atoms. He finds the shift in field ΔH, given by

$$\Delta H = -0{\cdot}319 \times 10^{-4} Z^{\frac{3}{2}} H_0. \tag{18}$$

Here Z is the nuclear charge and the effect is most serious for heavy nuclei. Recently, computations for the shift based on HARTREE and HARTREE-FOCK wave functions for several representative atoms have been made by DICKINSON[26], with results different from but near to those given by LAMB's formula. The applicability of these relations to ions in solution and particularly to molecules and complexes is obviously subject to question. Experimentally it has been discovered that different solutions containing, for instance, fluorine in different chemical combinations such as HF, BeF_2 and KF, give frequencies differing by as much as parts in 10^4 ([27, 28, 29]). Such effects are rather large to result from differences in diamagnetism and may arise from induced paramagnetism in the event of low lying excited electronic states. So long as such shifts cannot be accurately predicted, nuclear g-factors cannot be claimed to be known nearly so accurately as the frequency ratio measurements would allow. Ratios of g-factors of isotopes of the same element are not obscured by such effects.

In other than the free atomic state, the diamagnetic shift is known accurately only for the hydrogen molecule. RAMSEY[30] has given the formal procedure for calculating diamagnetic shifts in molecules and has been able to evaluate the shift in hydrogen molecules for which accurate values of pertinent molecular constants are available from numerical evaluation from the COOLIDGE-JAMES wave functions and from resonance studies in molecular hydrogen in beams. His result is a diamagnetic correction for $\Delta H = -2{\cdot}68 \times 10^{-5} H_0$. Application of LAMB's formula for atomic hydrogen leads to $\Delta H = -3{\cdot}19 \times 10^{-5} H_0$ and is thus a bit off, as would be expected. Experimental studies[31, 32] of proton resonances in water, hydrogen gas, and paraffin oil, among others, reveal diamagnetic shifts relative to hydrogen, on the order of a part in 10^6, allowing comparison of other g-factors to the protons in these samples to be corrected to values relative to the absolute g-factor of the proton, via RAMSEY's diamagnetic correction.

Work of HAHN, using the method of spin-echoes indicated that in some liquid samples there might be several differing shifts corresponding to protons bound in non-equivalent positions in a molecule. Using an extremely homogeneous field and slow sweeping technique, ARNOLD, DHARMATTI, and PACKARD[33] have resolved such lines finding, for example, three lines spaced 0·018 gauss apart for the three differing proton situations in ethyl alcohol, the OH, the CH_2 and the CH_3 groups. These lines themselves show even finer structures under higher resolution[34].

Also contributing to the difficulty of making accurate measurements of g-factors in liquids is the discovery that the behaviour of paramagnetic ions

added to solutions to shorten T_1 is not so simple as one might suppose. DICKINSON[35] measured shifts accompanying addition of such ions as a function of concentration and of sample shape and did not confirm the expected shifts calculated from paramagnetic susceptibility and the demagnetization factors determined by the sample shapes. An explanation, suggested by BLOEMBERGEN and DICKINSON[35, 26] is based on the idea that the paramagnetic ion, in collision with the ion containing the nucleus being studied, is perturbed by the electric field in such a way that its effective electronic g-factor depends on the orientation of the vector joining the two ions relative to the field direction.

A relatively up-to-date table containing nuclear moment data collected from paramagnetic resonance and induction experiments as well as from microwave spectroscopy, optical spectroscopy and molecular and atomic beams has been compiled by MACK[36]. This gives extensive references to the papers describing the experiments concerned. The bibliography of the present article contains only a few papers specifically concerned with g-factor determinations, chosen as examples of the techniques[37, 38, 39, 40, 41, 42].

The almost exclusive application of the method to stable nuclei, with the exception of I^{129} ([39]) is related to the fact that such a large number of nuclei (of the order of 10^{18}) are required for detection, under typical conditions. Improvements by large factors are not readily achieved.

MAGNETIC INTERACTION IN SOLIDS

In a rigid crystal lattice the two mechanisms of broadening discussed above and leading to the second moment eq.(16) are present. Lines are therefore much broader than in many liquids and the line breadth may be a function of the direction of the applied magnetic field relative to the crystal axes in single crystals. Such an effect has been observed in the F^{19} resonance in CaF_2[43] and careful measurements of the second moment show the theoretical prediction to be born out[19]. That such an effect should occur can be understood if it is realized that a very large part of the second moment is contributed by the six nearest neighbors in the simple cubic lattice of fluorine. If the field is chosen along a 111, or body diagonal, direction these neighbours all fall at such angles that $(3\cos^2\theta - 1)$ is zero and their contribution vanishes. The peak intensity is thus a maximum at that orientation.

On the other hand, the situation with respect to relaxation time T_1 is not easily understood. The mechanism of the liquid model no longer applies and a mechanism involving the elastic waves of the lattice excited by thermal agitation must be sought. A theory based on the modulations introduced in the dipole-dipole coupling by such acoustic waves, originally applied to relaxation of electronically paramagnetic crystals by WALLER[44], can be adapted to this case. Two mechanisms are considered. First, one has transitions induced from the vibrations of the lattice at frequency ν_0. This effect is very small owing to the low values of ν_0 compared to the main frequencies of vibration and to the smallness of lattice constant compared to the acoustic wavelength. It leads to values of T_1 of the order of magnitude of 10^{14} seconds at room tem-

peratures. The other mechanism involves absorption of lattice phonons of frequency ν' and re-emission at ν'', where $|\nu' - \nu''| = \nu_0$, a process that can result because of the essential non-linearity of the dipole-dipole interaction which varies as r^{-3}. Because this process involves participation of all lattice frequencies, it is far stronger than the direct process at ordinary temperatures and relaxation times of the order of magnitude of hours are predicted.

Relaxation times in crystals, like the CaF_2 cited above, are found usually to be a few seconds, and thus much shorter than the prediction. Furthermore, they are found to be considerably less temperature sensitive than the theory would suggest, with the observation by ROLLIN of a relaxation time of a few seconds in LiF at 1·5° K [45]. An explanation of such shortened values of T_1 is given by the theory of paramagnetic impurities put forward by ROLLIN and HATTON [46, 47, 48] and by BLOEMBERGEN [49]. According to this, a very small concentration of electronically paramagnetic impurities can bring about very rapid relaxation of the nuclear spins inside small spheres around each impurity, wherein the local field spectrum at ν_0 will be strong from strong relaxation of the impurity itself. Energy diffuses from the bulk of the spins to these locations by a random-walk process with a step corresponding to a mutual flip of a pair of interacting spins. BLOEMBERGEN'S tests with crystals containing controlled impurities gave reasonable agreement with such an hypothesis. An impurity content of as little as one part in 10^6 is sufficient to dominate over the mechanisms of WALLER'S theory. Colour centres produced by X-rays [50] and by pile irradiation [48] can have similar effects.

Some crystals have structures in which a pair or a small group of nuclei are considerably nearer to one another than they are to the remaining nuclei. As a result of this, certain structures can appear on the resonance line. For instance, hydrated crystals such as gypsum, $CaSO_4 \cdot 2H_2O$, possess pairs of protons in each water molecule, with two non-equivalent orientations of such molecules in the unit cell. The near neighbour of each proton contributes a component of field along the z-direction of $\pm \frac{\mu}{r_{ij}^3}(3\cos^2\theta - 1)$ with the plus or the minus sign determined by the state of the neighbour $m = \pm \frac{1}{2}$. The angle θ is the angle between the vector direction, $\vec{r}_{ij}$, joining the two protons and the z-direction (the direction of the field). Thus, in a single crystal the proton resonance of each water molecule is doubled with a splitting dependent on the orientation of the crystal in the field. Actually this is a case where, like the line breadth calculation, the situation is not sufficiently well described by the model. A quantum mechanical calculation treating the two protons of one molecule as a coupled system of spin unity, with the dipole-dipole interaction treated as a perturbation, shows that the splitting is equivalent to a field of $\pm 3\mu(3\cos^2 - 1)/2r^3$. With this, excellent agreement with the proton-proton distances in water in the gaseous state is found and accurate determination of the directions of proton-proton lines is possible [51]. Fig. 7 taken from [51] shows the experimental derivatives of the absorption lines for several angles together with absorption lines calculated from them. There are four peaks at most orientations, two per orientation of water molecule in the unit cell.

Even in the powder form, where the distribution of orientation of microcrystals is uniform, some evidence of structure remains and conclusions about crystal or molecular structure can be drawn. This technique has been applied to a number of substances[52]. The problem of theoretical interpretation becomes more severe as the number of particles in the group goes up. Calculations for a triangular configuration of three spins have been made by ANDREW and BERSOHN[53]. Some structure can remain if rotation of the group

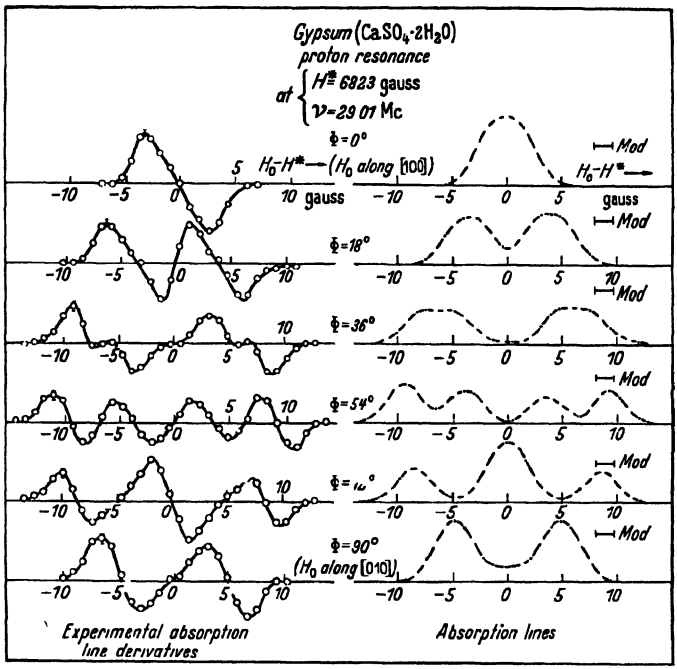


Fig 7. Experimentally determined absorption curve derivatives and absorption curves computed from them for the proton resonance in a single crystal of gypsum. The various curves correspond to various values of the angle φ between the direction of the field H_0 and the (100) direction, with the field always in the (001) plane.

about fixed axes relative to the group occurs and, thus, otherwise difficult to obtain information about internal states and configurations is provided. In certain cases changes of structure or of breadth occur as temperature is varied, with stationary groups at low temperature going over into free or hindered rotations at high temperatures[54, 55, 56, 57]. It should be remarked that the temperature of such line shape transition is not the same as that of an accompanying anomaly in the specific heat because the line shape begins to change when the average life time of a given orientation becomes shorter than T_2''. This, in the ammonium halides, is about 100° C below the associated specific heat anomalies. The line breadth change is not abrupt but covers a range of several degrees of temperature. A complex spectrum has been worked out by ANDREW[58], assuming rotation only about certain axes, to account for an observed multiplet structure in the antimony resonance in an aqueous solution of SbF_6^- ions[37].

HATTON and ROLLIN[43] have observed an interesting line shape transition in the proton resonance of solid hydrogen near 1° K. The line changes from a single one to two symmetrically displaced peaks as the temperature is reduced from 1·7° K to 1° K with all three lines showing at intermediate temperatures. The effect is thought to be associated with the splitting of the molecular rotational states of orthohydrogen (the only component contributing to the resonance) by crystalline electric fields. The structure would only appear at temperatures low enough to provide the required lifetime of a given molecular state.

More detailed information on internal motion of such groups in crystals can be obtained by studies of spin-lattice relaxation times. In these cases the relaxation mechanism is similar to that in liquids. Because T_1 is a measure of the local field spectrum at ν_0, its value gives information at all temperatures rather than just in the small range of temperature of the line width transition. Studies by SACHS and TURNER, reported by PURCELL[59], of the proton resonance in ammonium halides are consistent with the view that the line width change occurs when the tetrahedral ions jump to new equivalent orientations in a time on the average of the order to T_2''. The rate inferred from correlating relaxation times with curves like Fig. 5 increases with increasing temperature in accord with an exponential excitation function. This technique has been applied by NEWMAN to several other crystals[60].

In some crystals, nuclei can serve, via resonance, to measure net internal fields at various lattice sites due to electronic magnetic moments at other ions. BLOEMBERGEN[61] observed at low temperatures ten separate proton resonances in single crystals of $CuSO_4 \cdot 5H_2O$ corresponding to different net contributions of the cupric ions and the neighbouring protons to the field at the positions of the ten non-equivalent protons in the unit cell. The splittings increased as the temperature was decreased owing to the increasing net polarization of the cupric ions, and the center of gravity shifted accordingly. Such observations were greatly facilitated by the presence in $CuSO_4 \cdot 5H_2O$ of a strong exchange interaction between the cupric ions. This reduces the intensity of the local field spectrum at ν_0 and consequently reduces the broadening of the proton resonance by the cupric ions. Similar observations have been made by POULIS[62] and he has also confirmed the existence of anti-ferromagnetism at low temperatures in this way in $CuCl_2 \cdot 2H_2O$[63].

Resonance of nuclei can be observed in metals and, in fact, a sensitive apparatus will normally record the resonance of Cu^{63} and Cu^{65} in the wire of its own coil. Because of the small skin depth of the *r-f* field, finely powdered samples are best and observations of relaxation times T_1[64, 46] confirm the theoretical estimates[65] based on coupling via the thermally excited conduction electrons. The relaxation times are found to be proportional to inverse temperature and to be of the order of seconds at 1° K. Metals seem to be the most promising for attempts to achieve spin lattice equilibrium at temperatures far below 1° K, in the absence of considerable electronic paramagnetism in the same sample.

It has been discovered[66] that the resonance in metals is shifted, for the same applied field, to higher frequencies than that of the same nucleus in a non-conducting salt, by amounts of the order of one part in a thousand. This at first puzzling result may be explained as due to the paramagnetism of the conduction electron[67, 68]. It is a much larger shift than the bulk paramagnetic effect because the electron wave functions have high densities in the vicinity of the ions compared with their average density. It can be seen that such a shift should not be strongly temperature dependent because only the thermally excited electrons, above the FERMI energy, contribute. This number decreases with temperature but the degree of polarization per electron in a given field increases as the inverse temperature.

Crystals of high purity can show relaxation times of minutes or even hours at room temperature but there is no case where such relaxation times have been demonstrated to be determined by the mechanism of WALLER. Pure single crystals of LiF have been found to have a value of T_1 for the Li^7 resonance of five minutes and this discovery made possible some interesting associated experiments[50]. It was found, for instance, that, if the crystal was allowed to achieve thermal equilibrium in a strong field, the crystal could be quickly removed and reinserted in any orientation with no loss in intensity of the Li^7 resonance. When it was held outside the field for several seconds, the intensity on reinsertion was found to be reduced and in this way the spin-lattice relaxation time in a negligible field was determined to be 15 sec. If, while the crystal was held external to the field, it was subjected to a *r-f* field in the range from 0 to 200 kcs it was found that the loss of intensity on reinsertion could be greatly increased. By a study of the dependence of this effect on the low frequency, an absorption spectrum for the nuclear spin system in negligible static fields was observed[69]. In small applied fields the spectrum so determined showed evidence of components corresponding to the g factors of both Li^7 and F^{19}. The peak of the rather broad absorption, in negligible fields, at about 50 kcs corresponds roughly to the frequency resulting from the internuclear fields of several gauss in the crystal.

In an attempt to discover the conditions determining the sense of the magnetic moment vector relative to the direction of the strong field when the crystal was quickly removed and reinserted, several experiments were performed[70]. An operation that resulted in a reversed magnetic moment in the crystal upon remagnetization was devised. The magnetization subsequently decayed through a null value back to the equilibrium magnitude and direction with the exponential time constant of 5 min characteristic of the spin-lattice coupling. The reversal was accomplished by holding the crystal, originally in equilibrium in the strong (6500 gauss) magnet, in a field of about 100 gauss. A condenser was discharged through a coil and resistance in such a way that the 100-gauss field reversed in about 0·2 μsec and decayed back to its original direction in about 1 millisec. The whole operation outside the strong test field was performed in about 2 sec. The reversed magnetization is evidenced by the presence of a radiation line instead of the normal absorption line. This would result with an inverted distribution over the energy levels.

The spin system just after re-insertion in the strong field may be described by a BOLTZMANN distribution with a negative value of the absolute temperature. Closer examination of the conditions of the experiment suggests that the spin system, to the extent that it is isolated from the lattice, is actually in an equilibrium state because the spin-spin coupling is very strong. In fact, just before re-insertion in the strong field the crystal was taken through the negligible earth's field in which the states must be described by spin-spin coupling only. Thus, except in the first reversal, the spin system follows changes in field magnitude and direction adiabatically. Simple removal of the crystal from a strong field to a negligible one results in adiabatic demagnetization to a spin temperature of about 1° K, the reversal and return to the negligible field results apparently in a spin temperature of about —1° K and the remagnetization results in a spin temperature of —300° K. The decay is to higher magnitudes of negative temperature, through infinite and down to the lattice temperature. No passing through absolute zero is implied and the system at negative temperature is, in fact, hotter, not colder, than any system at positive temperature. Only systems with a limited number of energy levels can be brought into such a condition and it results from putting into the system more energy than results in equal populations of the levels. It is important to realize that the relatively strong interaction among the elements of the system, as compared to that between the spin-system and lattice, produce rapid equilibrium internal to the system, justifying the use of the term temperature. Transient reversals can easily be produced in liquid samples, for instance, but they could not be said to fully justify a description in terms of temperature because T_1 and T_2 are so nearly equal.

ELECTRIC QUADRUPOLE EFFECTS

Nuclei of spin greater than $\frac{1}{2}$ can, and usually do, possess electric quadrupole moments. As a result, the energy of nuclear orientation is not completely described by the magnetic effects. Electrostatic potentials of lower than cubic symmetry interact with such nuclei and this can have profound effects on the nuclear paramagnetic resonances. The studies of nuclear resonances in solids described above have been confined to nuclei of spin $\frac{1}{2}$, such as the proton and F^{19}, or to cubic crystals, for this reason.

In aqueous solutions and in molecular liquids the Brownian motion leads to a strong averaging out of the electric quadrupole interaction, just as it does of the dipole-dipole magnetic interaction. The time averaged interaction is, however, much stronger than that of the magnetic and for a given correlation time it therefore is the principle contributant to T_1 and T_2. Even in D_2O, the value of T_1 observed for the deuteron is shorter than that of the protons in H_2O under similar conditions, instead of longer as should result from the smaller g-factor of the deuteron[8]. In heavier nuclei having larger electric quadrupole moments, like those of Br^- and I^- ions in solution[71, 41], the lines are considerably broadened by the shortness of T_1 and T_2. By this means it was possible, for instance, to correlate the g-factors and quadrupole moments of the two equally abundant bromine isotopes.

A theory of relaxation time in liquids would follow analogous lines to that using only the magnetic effects. Unfortunately quantitative results are difficult to interpret because they involve the complex characteristics of concentrated solutions. These depend strongly on concentration and temperature.

In a rigid crystal of lower than cubic symmetry the electric quadrupole interaction leads to strong splitting of a resonance line. For an isolated nucleus in a strong magnetic field the energy levels, including the electric quadrupole effect as a first order perturbation, become

$$W_m = -(m\mu H_z/I) + \frac{eQ}{4I(2I-1)}\cdot[3m^2 - I(I+1)]\,\frac{\partial^2 V}{\partial z^2} \qquad (19)$$

where Q is the conventionally defined scalar measuring the nuclear electric quadrupole moment and V is the electrostatic potential at the position of the nucleus, arising from all charge external to it. The value of $\partial^2 V/\partial z^2$ is a function of direction relative to the crystal axes. As a result, powdered specimens, with microcrystals randomly oriented, show very smeared out spectra if non-cubic. For odd half-integral I, the $m = \frac{1}{2} \rightarrow m = -\frac{1}{2}$ transition, because of the symmetry in m, should be unaffected by the quadrupole coupling, according to eq.(19). If the coupling is moderately strong, the first order perturbation of eq.(19) is not a sufficiently accurate description and in the second and higher even orders, this transition is also smeared out. As a consequence, nuclear resonances in powders, if moderate electric quadrupole coupling exists, are almost unobservable. Considerable spreading is observable even in the Li^7 resonance in Li_2CO_3, for instance[72], where the nuclear quadrupole moment is relatively small.

In single crystals there is a unique value or several such values of $\partial^2 V/\partial z^2$ determined in part by the orientation of the crystal with respect to the field. Thus the spectra may be split into $2I$ components, or several sets of such components if there are non-equivalent lattice sites, the spacing of the components depending on the orientation of the crystal. The resonance of Na^{23} with spin $\frac{3}{2}$ in $NaNO_3$, for instance, shows the three lines reproduced in Fig. 8. In this case, because the crystal has an axis of trigonal symmetry through the Na positions, the value of $\partial^2 V/\partial z^2$ must go as $\frac{1}{2}(3\cos^2\theta - 1)$, where θ is the angle between the z-direction (that of the magnetic field) and the crystal axis. Observation of the splitting as a function of angle fully confirms this, except for a very small departure requiring higher order terms in the theory. In this case the maximum central-satellite splitting was 167 kc/sec, with a centre frequency of 7·18 Mc/sec.

The spectrum of Al^{27}, with spin of $\frac{5}{2}$, in single crystals of Al_2O_3 shows the anticipated five-line structure with a centre-to-far-satellite maximum splitting of 720 kc/sec. Here there was a considerable second order contribution causing the central line to change with angle (the $m = \frac{1}{2}$ to $-\frac{1}{2}$ transition). Perfect agreement between the experimental dependence and theory was obtained[72].

It is apparent that useful information can be obtained from these spectra. This technique has been utilized by SCHUSTER and PAKE[73] to determine the spin of Be^9 as $\frac{3}{2}$ from the spectrum in a chrysoberyl crystal. It is useful for determination of accurate values of the ratios of electric quadrupole moments

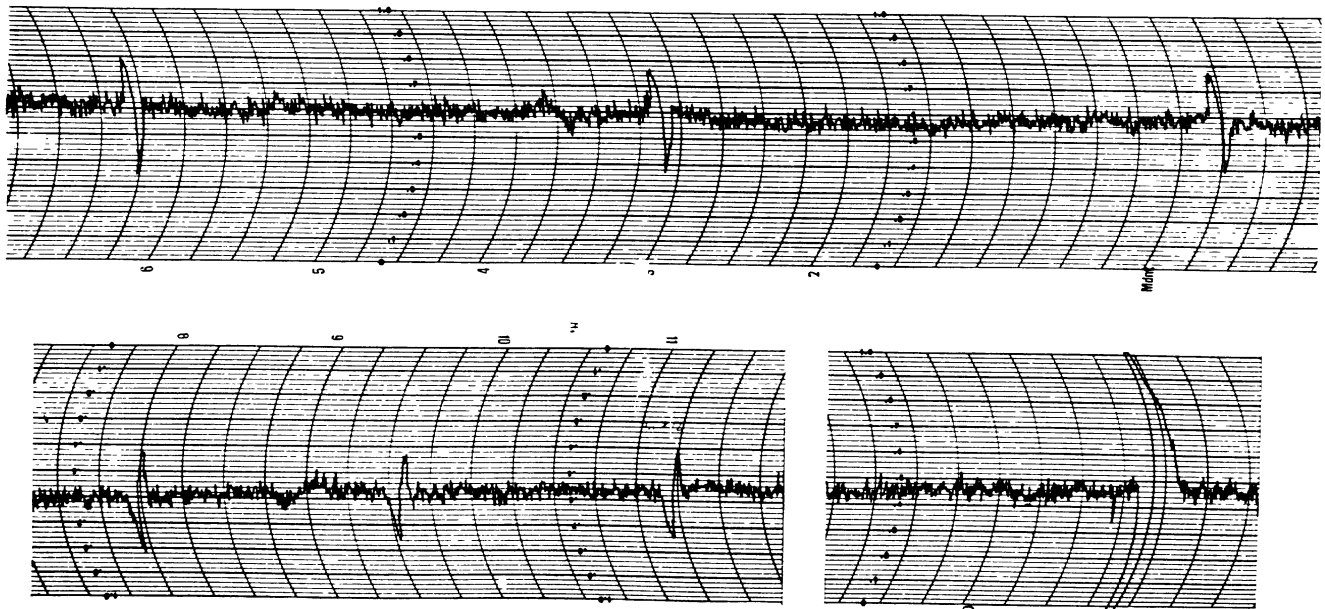


Fig. 8. An r-f spectrogram of the resonance of Na^{23} in a single crystal of $NaNO_3$. In the upper record, the trigonal crystal axis was along H_0, in the lower left it was at 90° to H_0, and in the lower right at 54°. The electric quadrupole splitting causes a separation between components of 167 kcs at 0°, and a small asymmetry explained by carrying the perturbation calculation to higher orders is noticeable at 54°. A broad resonance from the Cu^{63} in the wire of the r-f coil is apparent to the left (high frequency side) of the central line in two of the runs.

(To face page 15)

FARADAY effect and would not give rise to coupling to a crossed coil, as with the purely magnetic resonances, because no magnetic polarization of the nuclei is present.

Observation of these spectra should be possible with techniques similar to that used for nuclear paramagnetic resonance. It is complicated by the fact that the apparatus must scan in frequency and for that reason the self-oscillating schemes have mainly been used, particularly the superregenerative technique. The latter is relatively suitable because it is found at ordinary temperatures that T_1 and T_2 are short and, for the best signal-to-noise ratio, rather large r-f field strengths are useful. Single crystals are not required for detection of the pure quadrupole spectra.

The first zero field resonances to be found in the solid state were those of Cl^{35} and Cl^{37} by DEHMELT and KRUGER[75] in $trans_{12}$ dichlorethylene, cooled in liquid air, in the region of 30 Mc/sec, using a superregenerative scheme. The ratio of the frequencies gives an accurate measure of the ratio of the quadrupole moments. Their results have been improved by later measurements on several compounds containing co-valently bonded Cl^{77}. Shortly later DEHMELT[78] observed lines of several iodine compounds resulting from the two transitions, $\pm\frac{5}{2} \rightarrow \pm\frac{3}{2}$ and $\pm\frac{3}{2} \rightarrow \pm\frac{1}{2}$ of I^{127} with a spin of $\frac{5}{2}$. Some of these compounds, including I_2 and SnI_4, were observed at room temperature. The two frequencies in each compound are in the ratio of nearly 2:1 and the departure from 2:1 can be shown to be a measure of the deviation of the electrostatic potential from axial symmetry The frequencies of the lower line fell between 200 and 450 Mc/sec, depending on the compound, and the line breadths between 10 and 100 kc/sec. The frequencies themselves usually increase with decreasing temperature, as a consequence, presumably, of the damping out of vibrations of the molecules

The line breadths seem to be greater than can be attributed to dipole-dipole interactions. A study of the temperature dependence of the frequencies and breadths of the resonance in I_2 down to liquid helium temperatures reveals broadening with decreasing temperature[79]. Apparently, crystalline strains are responsible, producing an effect analogous to that of an inhomogeneous magnetic field, as evidenced by the dependence of breadth at low temperature on the state of compression of the polycrystalline sample. The relaxation time of the two lines was found to differ being, at 4° K, about 20 sec for the high frequency line and 5 min for the low. The large line breadths make the detection of the resonance much more difficult than would be expected if magnetic dipole-dipole coupling determined the breadths.

The existence of a pure electric quadrupole coupling of such a magnitude is the basis of one of the methods proposed to attain spatial alignment of nuclei at low temperature[80]. Predominant population of the $\pm\frac{5}{2}$ state results if the spins can be brought into thermal equilibrium at temperatures such that $kT < h\nu$. Relatively simple single crystals are required to give the direction of quantization spatial significance. Such alignment would facilitate the study of the angular distribution of radioactive decay. The principal problem presented is that of achieving the thermal equilibrium.

References

[1] Purcell, E. M., Torrey, H. C. and Pound, R. V.; Resonance Absorption by Nuclear Magnetic Moments in a Solid, *Phys. Rev.* 69 (1946) 37.

[2] Bloch, F., Hansen, W. W. and Packard, M. E.; Nuclear Induction, *Phys. Rev.* 69 (1946) 127.

[3] Bloch, F.; Nuclear Induction, *Phys. Rev.* 70 (1946) 460.

[4] Torrey, H. C.; Transient Nutations in Nuclear Magnetic Resonance, *Phys. Rev.* 76 (1949) 1059.

[5] Hahn, E. L.; Spin Echoes, *Phys. Rev.* 80 (1950) 580.

[6] Packard, M. E.; A. Proton-Controlled Magnetic Field Regulator, *Rev. Sci. Instrum.* 19 (1948) 435.

[7] Bloembergen, N., Purcell, E. M. and Pound, R. V.; Nuclear Magnetic Relaxation, *Nature, Lond.* 160 (1947) 475.

[8] Bloembergen, N., Purcell, E. M. and Pound, R. V.; Relaxation Effects in Nuclear Magnetic Resonance Absorption, *Phys. Rev.* 73 (1948) 679.

[9] Bloembergen, N.; *Nuclear Magnetic Relaxation*, Martinus Nijhoff, The Hague 1948.

[10] Schuster, N. A.; A Phase-Sensitive Detector Circuit Having High Balance Stability. *Rev. Sci. Instrum.* 22 (1951) 254.

[11] Anderson, H. L.; Precise Measurement of the Gyromagnetic Ratio of He^3, *Phys. Rev.* 76 (1949) 1460.

[12] Grivet, P., Soutif, M. et Buyle, M.; Un pont à haute frèquence simplifié pour l'observation de la resonance magnétique nucléaire, *C. R. Acad. Sci. Paris* 229 (1949) 113.

[13] Bloch, F., Hansen, W. W. and Packard, M.; The Nuclear Induction Experiment, *Phys. Rev.* 70 (1946) 474.

[14] Pound, R. V.; A Radiofrequency Spectrometer for the Detection of Resonance Absorption by Nuclear Moments. *Phys. Rev.* 72 (1947) 527.

[15] Pound, R. V. and Knight, W. D.; A Radiofrequency Spectrograph and Simple Magnetic-Field Meter, *Rev. Sci. Instrum.* 21 (1950) 219.

[16] Watkins, G. D. and Pound, R. V.; An Improved *R-f* Spectrometer; *g*-Factor Ratios Li^7/Li^6 and Cl^{35}/Cl^{37}, *Phys. Rev.* 82 (1951) 343.

[17] Zimmerman, J. R. and Williams, D.; Determination of Nuclear Gyromagnetic Ratios I, *Phys. Rev.* 76 (1949) 350, and 76 (1949) 638.

[18] Jacobsohn, B. A. and Wangness, R. K.; Shapes of Nuclear Induction Signals, *Phys. Rev.* 73 (1948) 942.

[19] Van Vleck, J. H.; The Dipolar Broadening of Magnetic Resonance Lines in Crystals, *Phys. Rev.* 74 (1948) 1168.

[20] Purcell, E. M.,Pound, R. V. and Bloembergen, N.; Nuclear Magnetic Resonance Absorption in Hydrogen Gas, *Phys. Rev.* 70 (1946) 986.

[21] Proctor, W. G.; On the Magnetic Moments of Tl^{203}, Tl^{205}, Sn^{115}, Sn^{119}, Cd^{111}, Cd^{113}, and Pb^{207}, *Phys. Rev.* 79 (1950) 35.

[22] Lindström, G.; An Experimental Investigation of the Nuclear Magnetic Moments of D^2 and H^1, *Phys. Rev.* 78 (1950) 817.

[23] Smaller, B., Yasaitis, E. and Anderson, H. L.; Magnetic Moment of the Deuteron, *Phys. Rev.* 81 (1951) 896.

[24] Thomas, H. A., Driscoll, R. L. and Hipple, J. A.; Measurement of the Proton Moment in Absolute Units, *Phys. Rev.* 78 (1950) 787.

[25] Lamb, W. E.; Internal Diamagnetic Fields, *Phys. Rev.* 60 (1941) 817.

[26] Dickinson, W. C.; The Time Average Magnetic Field at the Nucleus in Nuclear Magnetic Resonance Experiments, *Phys. Rev.* 81 (1951) 717.

[27] Dickinson, W. C.; Dependence of the F^{19} Nuclear Resonance Position on Chemical Compound, *Phys. Rev.* 77 (1950) 736.

[28] Proctor, W. G. and Yu, F. C.; The Dependence of a Nuclear Magnetic Resonance Frequency Upon Chemical Compound, *Phys. Rev.* 77 (1950) 717.

[29] GUTOWSKY, H. S. and HOFFMAN, C. J.; Chemical Shifts in the Magnetic Resonance of F^{19}, *Phys. Rev.* 80 (1950) 110.
[30] RAMSEY, N. F.; Magnetic Shielding of Nuclei in Molecules, *Phys. Rev.* 78 (1950) 699.
[31] THOMAS, H. A.; The Diamagnetic Correction for Prs in Water and Motonineral Oil, *Phys. Rev.* 80 (1950) 901.
[32] GUTOWSKY, H. S. and MCCLURE, R. E.; Magnetic Shielding of the Proton Resonance in H_2, H_2O and Mineral Oil, *Phys. Rev.* 81 (1951) 276.
[33] ARNOLD, J. T., DHARMATTI, S. S. and PACKARD, M. E.; Chemical Effects on Nuclear Induction Signals from Organic Compounds, *J. Chem. Phys.* 19 (1951) 507.
[34] PACKARD, M. E. and ARNOLD, J. T.; A Fine Structure in Nuclear Induction Signals from Ethyl Alcohol. *Bull. Amer. Phys. Soc.* 26 (1951) 19.
[35] BLOEMBERGEN, N. and DICKINSON, W. C.; On the Shift of the Nuclear Magnetic Resonance in Paramagnetic Solutions, *Phys. Rev.* 79 (1950) 179.
[36] MACK, J. E.; A Table of Nuclear Moments, January 1950, *Rev. Mod. Phys.* 22 (1950) 64.
[37] PROCTOR, W. G. and WU, F. C.; On the Nuclear Magnetic Moments of Several Stable Isotopes, *Phys. Rev.* 81 (1951) 20.
[38] CHAMBERS, W. H. and WILLIAMS, D.; Nuclear Gyromagnetic Ratios II, *Phys. Rev.* 76 (1949) 638.
[39] WALCHLI, H., LIVINGSTON, R. and HEBERT, G.; The Nuclear Magnetic Moment of I^{129}, *Phys. Rev.* 82 (1951) 97.
[40] POUND, R. V.; The Magnetic Moment of Cu^{63} and Cu^{65}, *Phys. Rev.* 73 (1948) 523.
[41] POUND, R. V.; On the Nuclear Magnetic Moments of I^{127}, Ga^{69}, Ga^{71}, and P^{31}, *Phys. Rev.* 73 (1948) 1112, and 74 (1948) 228.
[42] ALDER, F. and YU, F. C.; On the Spin and Magnetic Moment of O^{17}, *Phys. Rev.* 81 (1951) 1067.
[43] PURCELL, E. M., BLOEMBERGEN, N. and POUND, R. V.; Resonance Absorption by Nuclear Magnetic Moments in a Single Crystal of CaF_2, *Phys. Rev.* 70 (1946) 988.
[44] WALLER, I.; Über die Magnetisierung von paramagnetischen Kristallen in Wechselfeldern, *Z. Phys.* 79 (1932) 370.
[45] ROLLIN, B. V., HATTON, J., COOKE, A. H. and BENZIE, R. J.; Nuclear Magnetic Resonance at Low Temperature, *Nature, Lond.* 160 (1947) 436.
[46] HATTON, J. and ROLLIN, B. V.; Nuclear Magnetic Resonance at Low Temperatures. Proc. Roy. Soc. *A.* 199 (1949) 222.
[47] DARBY, F. J. and ROLLIN, B. V.; Nuclear Magnetic Relaxation in Solids, *Nature, Lond.* 164 (1949) 66.
[48] ROLLIN, B. V. and HATTON, J.; Nuclear Paramagnetism at Low Temperatures, *Phys. Rev.* 74 (1948) 346.
[49] BLOEMBERGEN, N.; On the Interaction of Nuclear Spins in a Crystalline Lattice, *Physica* 15 (1949) 386.
[50] POUND, R. V.; Nuclear Spin Relaxation Times in Single Crystals of LiF, *Phys. Rev.* 81 (1951) 156.
[51] PAKE, G. E.; Nuclear Resonance Absorption in Hydrated Crystals. Fine Structure of the Proton Line, *J. Chem. Phys.* 16 (1948) 327.
[52] GUTOWSKY, H. S., KISTIAKOWSKY, G. B., PAKE, G. E. and PURCELL, E. M.; Structural Investigations by Means of Nuclear Magnetism I, *J. Chem. Phys.* 17 (1949) 972.
[53] ANDREW, E. R. and BERSOHN, R.; Nuclear Magnetic Resonance Line Shape for a Triangular Configuration of Nuclei, *J. Chem. Phys.* 18 (1950) 159.
[54] GUTOWSKY, H. S. and PAKE, G. E.; Nuclear Magnetism in Studies of Molecular Structure and Rotation in Solids. Ammonium Salts, *J. Chem. Phys.* 16 (1948) 1164.
[55] GUTOWSKY, H. S. and PAKE, G. E.; Structural Investigations by Means of Nuclear Magnetism II, Hindered Rotation in Solids, *J. Chem. Phys.* 18 (1950) 162.
[56] ANDREW, E. R.; Molecular Motion in Certain Hydrocarbons, *J. Chem. Phys.* 18 (1950) 607.
[57] ANDREW, E. R.; Nuclear Resonance in Solid Hydrocarbons, *Physica* 17 (1951) 607.
[58] ANDREW, E. R.; Nuclear Magnetic Resonance Absorption in $NaSbF_6$, *Phys. Rev.* 82 (1951) 443.

[59] PURCELL, E. M.; Nuclear Resonance in Crystals, *Physica* 17 (1951) 282.
[60] NEWMAN, ROGER; Proton Nuclear Magnetic Resonance Studies in KH_2PO_4, KH_4AsO_4, $NH_4H_2PO_4$, and $NH_4H_2AsO_4$, *J. Chem. Phys.* 18 (1950) 669.
[61] BLOEMBERGEN, N.; Fine Structure of the Magnetic Resonance Line of Protons in $CuSO_4 \cdot 5H_2O$, *Physica* 16 (1950) 95.
[62] POULIS, N. J.; Decomposition of the Proton Magnetic Resonance Line in Paramagnetic Crystals, *Physica* 17 (1951) 392.
[63] POULIS, N. J., HANDEL, J. VAN DEN, UBBINK, J., POULIS, J. A. and GORTER, C. J.; On Antiferromagnetism in a Single Crystal, *Phys. Rev.* 82 (1951) 552.
[64] BLOEMBERGEN, N.; Nuclear Magnetic Relaxation in Metallic Copper, *Physica* 15 (1949) 588.
[65] HEITLER, W. and TELLER, E.; Time Effects in the Magnetic Cooling Method I, *Proc. Roy. Soc. A.* 155 (1936) 629.
[66] KNIGHT, W. D.; Nuclear Magnetic Resonance Shift in Metals, *Phys. Rev.* 76 (1949) 1259.
[67] TOWNES, C. H., HERRING, C. and KNIGHT, W. D.; The Effect of Electronic Paramagnetism in Nuclear Resonance Frequencies in Metals, *Phys. Rev.* 77 (1950) 852.
[68] KOHN, W. and BLOEMBERGEN, N.; Remarks on the Nuclear Resonance Shift in Metallic Lithium, *Phys. Rev.* 80 (1950) 913.
[69] RAMSEY, N. F. and POUND, R. V.; Nuclear Audiofrequency Spectroscopy by Resonant Heating of the Nuclear Spin System, *Phys. Rev.* 81 (1951) 278.
[70] PURCELL, E. M. and POUND, R. V.; A Nuclear Spin System at Negative Temperature, *Phys. Rev.* 81 (1951) 279.
[71] POUND, R. V.; The Nuclear Magnetic Moments of Bromine, *Phys. Rev.* 72 (1947) 1273.
[72] POUND, R. V.; Nuclear Electric Quadrupole Interactions in Crystals, *Phys. Rev.* 79 (1950) 685.
[73] SCHUSTER, N. A. and PAKE, G. E.; The Spin of Be^9, *Phys. Rev.* 81 (1951) 886.
[74] SCHUSTER, N. A. and PAKE, G. E.; The Electric Quadrupole Moment of Li^6, *Phys. Rev.* 81 (1951) 157.
[75] BECKER, G. and KRÜGER, H.; Über das Verhaltnis der Kern-Quadrupolmomente der Cu-Isotope, *Naturwiss.* 38 (1951) 122.
[76] DEHMELT, H. G. and KRÜGER, H.; Kernquadrupolfrequenzen in festem Dichloräthylen, *Naturwiss.* 37 (1950) 111.
[77] LIVINGSTON, R.; The Quadrupole Moment Ratio of Cl^{35} and Cl^{37} from Pure Quadrupole Spectra, *Phys. Rev.* 82 (1951) 289.
[78] DEHMELT, H.; Kernquadrupolfrequenzen in kristallinen Jodverbindungen, *Naturwiss.* 37 (1950) 398.
[79] POUND, R. V.; Nuclear Electric Quadrupole Splitting in Crystalline I_2, *Phys. Rev.* 82 (1951) 343(A).
[80] POUND, R. V.; On the Spatial Alignment of Nuclei, *Phys. Rev.* 76 (1949) 1410.

LUMINESCENT MATERIALS FOR SCINTILLATION COUNTERS

G. F. J. Garlick

CONTENTS

1. *General Introduction* 51
(a) Short historical survey 51
(b) Desirable characteristics of luminescent materials 53
(c) The photomultiplier characteristics 54

2. *Classes of luminescent materials for scintillation counters.* 54
(a) Inorganic crystals 55
(b) Organic crystals 58
(c) Organic liquids and plastics 61

3. *The production of large crystals for scintillation counters* 63
(a) Growth of cadmium and zinc sulphide crystals 63
(b) Synthetic halide crystals 64
(c) Tungstate and sapphire crystals 65
(d) Growth of hydrocarbon crystals 67

4. *Energy measurements with scintillation counters* 67
(a) Response of scintillators to different radiations 67
(b) Detection of charge dparticles 68
(c) Detection of neutrons 70
(d) Detection of cosmic ray particles 71
(e) Detection of fission fragments 72
(f) Measurement of gamma ray energies 72
(g) X-ray measurements 75
(h) Miscellaneous 75

5. *Fundamental mechanisms in scintillation crystals.* 76
(a) Inorganic crystals 76
(b) Luminescence processes in organic molecules 81

1. GENERAL INTRODUCTION

(a) *Short historical survey*

The scintillation counter has now become a familiar instrument for the detection of nuclear radiation in all fields of nuclear research. Its essential features are a luminescent solid or liquid which emits scintillations when bombarded by the radiation to be detected, and a photoelectric multiplier tube which picks up the scintillations and provides pulses of voltage at its output. These pulses can be counted and analysed by conventional techniques. Some of the chief advantages of this type of detector over other types, such as the GEIGER-

MULLER counter are the high sensitivity to gamma rays, the very rapid response time and the high resolution which is very advantageous for coincidence measurements. Our present intention is to review the development, characteristics and uses of the luminescent materials employed in the scintillation counter. We shall also consider the fundamental mechanisms of excitation and light emission in these substances, in particular the striking differences between these mechanisms for inorganic and organic crystals and liquids.

As is well known, one of the earliest methods for the detection of alpha particles from naturally radioactive substances was the spinthariscope in which the visible scintillations from a zinc sulphide phosphor screen due to particle bombardment were observed visually. This instrument, which is first associated with the name of CROOKES, was used extensively by RUTHERFORD in his early experiments. The first published attempt to use a scintillating phosphor with a photoelectric multiplier appears to be that of BLAU and DREYFUSS[1] in 1945. They used a screen of microcrystalline zinc sulphide. The first observations of individual particles by means of the photoelectric detection of the scintillations produced seem to have been made by CURRAN and BAKER[1a] but their work remained classified until 1947. The first published accounts were by KALLMANN and his co-workers in Berlin[2] and by COLTMAN and MARSHALL[3] in the U.S.A in 1945. A little while later BROSER and KALLMANN[4] reported the successful use of naphthalene crystals as beta and gamma ray detectors. They employed the crystals in conjunction with a photomultiplier having a caesium cathode. In the same year DEUTSCH[5] reported the use of naphthalene for gamma ray detection in conjunction with an R.C.A. 931 A type photomultiplier having an antimony-caesium cathode. He confirmed KALLMANN's claim that the intrinsic efficiency of the naphthalene crystals for gamma ray detection (1 Mev energy) was of the order of 10% and that by cooling the photomultiplier to reduce its thermionic noise, 100% counting of the gamma rays falling on the crystals could be achieved. In 1948 BELL[6] showed that anthracene crystals used with antimony-caesium surfaced photomultipliers gave much larger output pulses from the multiplier than naphthalene. This was followed by an exhaustive search for better crystals for scintillation detectors and in that same year two conferences provided full discussions of progress and possibilities in the use of scintillation counters, one at Rochester, U.S.A. and the other at Birmingham, England. In 1948 also HOFSTADTER[7] developed the thallium activated alkali iodides as gamma ray detectors and reported much higher, absolute counting efficiency values than those for the hydrocarbons, presumably due to the higher density of the halides. Later the use of a non-crystalline solid, namely polystyrene, as a detector with very fast response time was reported[8]. Since then the use of liquid and plastic materials in scintillation detectors has become quite common where a large volume of detector is necessary, as in cosmic ray studies. The notable advance in liquid detectors was made by REYNOLDS'[9] discovery of the high efficiency of solutions of p-terphenyl in xylene. Quite recently even better performance has been claimed for plastics in which a small amount of a suitable luminescent material has been incorporated during polymerisation[10].

Several reviews of the development of scintillation counters have already appeared. The first was that of JORDAN and BELL[11] while others due to PRINGLE[12] and to HANLE[13] have appeared more recently. The latter has provided an up to date list of over one hundred and fifty references to the subject.

(b) *Desirable characteristics of luminescent materials*

Arising out of accumulated experience in the use of scintillation counters, it is now possible to specify many of the desirable characteristics which a luminescent solid or liquid should possess if it is to be used as an efficient radiation detector. They may be summarised as follows.

(i) The luminescent material must have a high efficiency for conversion of the energy of the incident radiation or particles into that of the emitted luminescence.

(ii) The spectrum of the emitted light must match as closely as possible the spectral response of the cathode of the photomultiplier with which it is used. It is desirable that the photocathode spectral response should lie in the blue-violet or ultraviolet regions since response to the red is linked with a high value of the thermionic emission of the cathode. A compromise is usually necessary and at the end of the introduction we discuss the available photosurfaces.

(iii) It is essential that the luminescent materials should be transparent to their own luminescence emission.

(iv) It is desirable that the luminescent substance can be obtained as a large optically homogeneous mass, either as a single crystal without flaws, or in solution (solid or liquid). It should also be possible to mould or machine the material to any convenient shape.

(v) An important quantity is the refractive index of the luminescent solid or liquid. In the case of many inorganic phorphors used in counters the value of the index is rather high (about 2) and difficulty is experienced in getting the emitted light out of the ~~the~~ solid.

(vi) The material should have a high stopping power for the radiation to be detected. This involves not only consideration of its density but of the particular mechanism of energy conversion. For example, hydrogenous materials are more favourable when fast neutrons are to be detected. We discuss these problems later.

(vii) One of the most important factors in the choice of a luminescent material for counting is the rise and decay of the luminescence during and after excitation. It is desirable that both rise and decay should occur in as short a time as possible.

(viii) The luminescent detector must be as stable as possible both under the conditions of the experiment, that is, particular atmosphere or vacuum conditions, and also under prolonged exposure to the radiation being detected. We shall consider later stability in relation to the fundamental mechanisms of interaction of the primary radiation with the material.

(c) *The photomultiplier characteristics*

It is useful to spend a little time in discussing the characteristics of the photomultiplier used to detect the scintillations emitted by the phosphor detector since the efficient analysis of the nuclear radiation depends on a correct matching of the multiplier and the phosphor. First of all we consider the spectral response and sensitivity of the primary photocathode of the multiplier. In Fig. 1 are given the spectral response curves of photosurfaces in use in multipliers for scintillation counters[14]. It is seen that the caesium surface has peaks of response in the ultra violet and in the red regions of the spectrum,

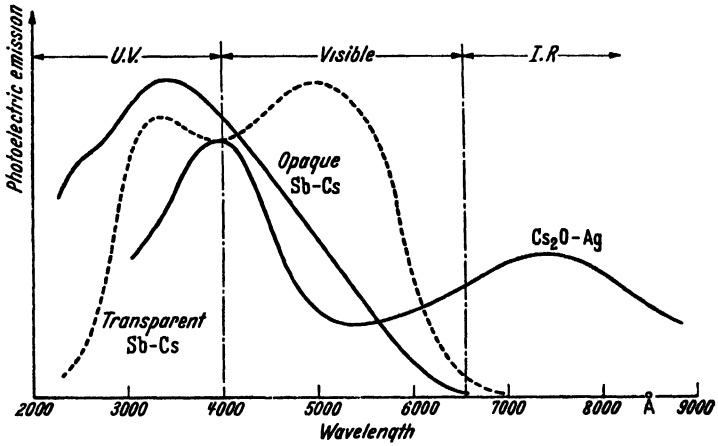


Fig. 1. Spectral response of different photomultiplier cathodes (units arbitrary for each surface) Sensitivities (photometric and absolute) Cs_2O-Ag: 10–60 μA/lumen, max 2–3 mamp./watt (I. R.). Sb-Cs opaque 30–100 μA/lumen., max. 65 mamp./watt (blue). Sb-Cs transparent. 10–40 μA/lumen., max. 30 mamp./watt (blue).
N.B. At maximum sensitivity the Sb-Cs opaque cathode has a quantum efficiency of approx. 20%.

whereas the antimony-caesium surface has a peak in the blue region. KALLMANN[2] used the former type of multiplier in his early experiments (with cooling) which accounts for the apparently good response of naphthalene crystals which are not so useful when antimony-caesium surfaces are employed. There is also a considerable difference between the absolute efficiency of these two surfaces as shown by the values included in the diagram caption of Fig. 1.

When using the photomultiplier as a detector of scintillations the statistical fluctuations in the number of photoelectrons produced per scintillation become important. In many applications of the counter to energy measurement of alpha particles and protons the individual scintillations only release about 400 or 500 electrons at the photosurface. This means that a spread in magnitude of the output pulses of as much as 10% in the optimum case has to be tolerated. We shall mention this consideration later in discussing the use of crystals as proportional counters.

2. Classes of Luminescent Materials for Scintillation Counters

For convenience we may classify the luminescent solids and liquids as follows: (a) Inorganic crystals. (b) Organic crystals. (c) Organic liquids and plastics.

The distinction between inorganic and organic crystals is not a very important one to the user of scintillation counters but it happens that two important features distinguish these groups, namely, the differences in density and in decay time of the luminescence.

(a) *Inorganic crystals*

(i) *Zinc and cadmium sulphides*

These materials are very well known as suitable for cathode ray tube screens and a large amount of fundamental and applied research has been concentrated on them in the past[15,16,17,18,19]. Screens of copper activated zinc sulphide phosphors were used in the early spinthariscopes. These phosphors are prepared by special heat treatment of very pure raw materials and in most cases a deliberate addition of a specific impurity such as copper or silver (usually about 0·01%)

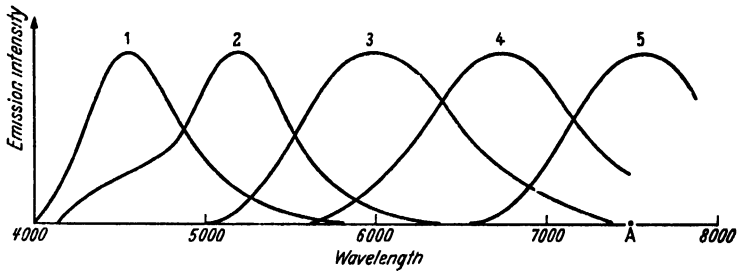


Fig. 2. Cathodoluminescence spectra of sulphide phosphors. 1. Zns-Ag; 2. Zns-Cu; 3. ZnS (40%) Cds (60%) Ag; 4. ZnS (20%) Cds (80%) Ag; 5. Cds-Ag. All Ag und Cu concentrations 0 01%.

is made. Zinc and cadmium sulphides form a mixed crystal system when fired together and the luminescence emission spectrum, as well as other important properties like after-glow, depends on the relative proportions of the sulphides. When made at temperatures above 1025° C zinc sulphide assumes a hexagonal crystal lattice. Below this temperature the cubic habit (diamond or blende type) can be obtained by suitable flux treatment. In this case it is possible to obtain flat plate-like crystals with dimensions a considerable fraction of a millimetre. The spectra of various typical specimens of zinc, cadmium and zinc-cadmium sulphide phosphors are given in Fig. 2 for cathode ray excitation of the materials[20].

Comparison of Figs. 1 and 2 shows that the emission of silver activated zinc sulphide matches the spectral response of the antimony-caesium cathode while the cadmium sulphide emission matches that of the caesium cathode. The latter combination has been extensively used by KALLMANN and his co-workers as discussed later. Silver activated zinc sulphide represents the most efficient phosphor available for conversion of particle energy into luminescence. KALLMANN[21] gives the intrinsic conversion efficiency of the ZnS-Ag phosphor as about 20% while for cathode ray excitation and using aluminium backing for the phosphor screen an efficiency of 25% has been claimed[22]. However, while zinc and cadmium sulphides possess this high efficiency it is difficult to obtain them in the form of large single crystals. FRERICHS has made cadmium sulphide,

yrcstals up to 2 cm in length (see Section 3) and a recent verbal communication from BROSER and WARMINSKY reports success in making good single crystals of luminescent zinc sulphide. STUDER *et coll.*[23] have succeeded in making thin transparent layers of zinc sulphide on glass and REYNOLDS and CZYZAK[24] have reported production of non-luminescent crystals of zinc sulphide several millimetres in length. Further disadvantages of zinc and cadmium sulphides are their slow response and decay times which are effectively greater than 100 μsecs, and their high refractive indices (Table 1).

(ii) *Alkali halide and alkaline earth halide phosphors*

The luminescence characteristics of large crystals of the alkali halides activated by thallium impurity have been the subject of many studies during the past two decades (see ref. 18, Chap. III). These halides are relatively easily grown from the melt as large single crystals. Those of most interest for scintillation counters are the iodides of sodium and potassium activated by thallium[7], and pure lithium fluoride. Fluorite (calcium fluoride) has also been employed in scintillation counters. The sodium and potassium iodides containing thallium have relatively broad emission bands at about 4100 Å and so match the antimony caesium cathode. Since potassium iodide contains the K^{40} isotope it is naturally radioactive and so has an undesirable background emission as well as a rather long decay time (*i.e.* > 10 μsecs) Sodium iodide has a much shorter decay time (0·25 μsec) and no self activity but is extremely hygroscopic and must be sealed into containers unless used in vacuo. Both iodides have densities of about 3·6 while their refractive indices are about 1·7. Data have also been given for thallium activated caesium and lithium iodides[25] which have densities of 4·5 and 4·06 respectively and decay times longer than 1 μsec. In recent months KALLMANN and FURST[26] have reported success using silver activated sodium chloride crystals (emission in the ultra violet region 2350–2600 Å and 3200–4500 Å), with a 1P28 type multiplier (silica envelope). MANDEVILLE, *et coll.*[27] have found that an efficient scintillation counter results when silver activated sodium chloride crystals are combined with photosensitive G-M. counters. An absolute efficiency of 15% is claimed for excitation by Po. α-particles and the decay time of luminescence is estimated to be about 0·2 μsec. They have examined a large number of materials for use in this type of counter but none of these surpass the sodium chloride crystals.

FARMER, MOORE and GOODMAN[28] have used pure synthetic lithium fluoride crystalls in scintillation counters and report a decay time of about 1 μsec and intrinsic efficiencies of 9·5, 11 and 1·6% for thermal neutrons, polonium alpha particles and Co^{60} γ rays respectively. The characteristics of pure calcium fluoride crystals have been investigated by MCINTYRE[29]. The decay time of ts luminescence is 0·15 μsec.

i(iii) *Tungstate phosphors*

The tungstates of zinc, cadmium, magnesium, calcium etc. all show luminescence after heating in the pure state to a high temperature. Fig. 3 gives the cathodoluminescence spectra of some of these phosphors[20]. Scheelite, *i.e.*, natural calcium tungstate shows similar characteristics to the synthetic phosphor

but is found in some localities, notably Kern County, California as large transparent crystals. Its blue luminescence emission is a reasonable match to the antimony caesium photocathode and it has been found quite efficient for detection of α, β and γ rays[30, 31]. It can be obtained in large crystal form by the Verneuil method (see Section 3) and has a density of 6·1 and refractive index of 1·92. The chief drawback is its decay time with half life of 3 μsecs. (It is quite stable in air or in vacuo.) It has been investigated as a detector for low

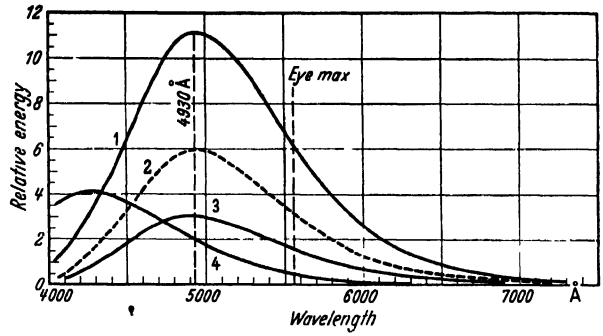


Fig. 3. Cathodoluminescence spectra of some "Unactivated" tungstate phosphors 1. $MgWO_4$; 2. $CdWO_4$; 3. $ZnWO_4$; 4. $CaWO_4$.

energy electrons[32] (500 ev) having for these an absolute conversion efficiency of 5×10^{-2}%.

(iv) *Lead activated barium sulphate*

Barium sulphate containing lead as impurity and prepared by heat treatment is a white microcrystalline powder which emits a blue luminescence when excited by particles, X-rays or gamma rays. It was developed for X-ray intensifying screens[33]. There are no reports so far of large synthetic crystals of this phosphor being prepared. Natural barytes, even that from deposits known to contain lead, does not show any appreciable luminescence (writer's investigations). The powder-form, synthetic phosphor, is quite efficient for particle and γ ray excitation, its density is 4·5, its refractive index 1·64 and its luminescence decay time a little less than a microsecond. As shown in Section 3 below it may be possible to prepare it as large crystals.

(v) *Zinc oxide phosphors*

When suitably prepared by heating in a controlled reducing atmosphere at 1000° C zinc oxide shows a green luminescence emission and responds to particle or gamma ray excitation with a decay time of about 1 μsec[20]. It is not as efficient as silver activated zinc sulphide and so far no large single crystals are available.

(vi) *Miscellaneous*

Some specimens of blue luminescent diamonds examined in the writer's laboratory have been found to give scintillations under alpha particle or gamma ray bombardment but no exhaustive investigations have yet been made. A

serious disadvantage in using diamonds would be their high refractive index of 2·42. Moon[31] has investigated a number of different natural and synthetic crystals for their scintillation efficiency under γ ray excitation and his results are given briefly in Table 2. Amongst those giving "excellent" response we may note synthetic sapphire which is available as large transparent crystals with a density of 4 g/cc and a refractive index of 1·77.

Two other inorganic substances have been investigated recently by the author. One is cadmium iodide activated by lead (see also ref. [31a]) which seems to be very efficient for α, β and γ rays has a green-yellow emission and has a decay time in the microsecond region. It might prove a useful detector for slow neutrons due to its high cadmium content. It can be grown as a single crystal from water or acetone solutions. The other material was well known in earlier days as a fluorescent screen for X rays. It is barium platino-cyanide $BaPt(CN)_4 \cdot 4H_2O$ and can be obtained as large crystals by crystallisation from aqueous solution. It has a decay time of 2·5 μsec and is a very efficient γ ray detector.

(b) *Organic crystals*

In this section we shall consider in detail only those substances that are reasonably efficient as scintillation counters. Discussion of the fundamental processes involved in their excitation and emission is given in Section 4. The distinctive

Table 1—Characteristics of luminescent materials for scintillation counters

Material	*Form*	*Density (g/cc)*	*Refr. index*	*Emission bands (Å)*	*Intrinsic efficiency (%)*				*Decay time (μsec)*
					αp	β	n	γ	
ZnS-Ag	powd.	4·1	2·4	4500	20	20	—	13·5	>10
CdS-Ag	crys.	4·8	2·5	7600	23	23	—	23·0	>10
NaI-Tl	crys.	3·7	1·7	4100	20	20	—	20	0·25
NaCl-Ag	crys.	2·2	1·5	2600	15	10	—	10	0·20
KI-Tl	crys.	3·2	1·65	4000	5	5	—	5	>10
CsI-Tl	crys.	4·5	1·75	white	—	15	—	—	>1
LiI-Tl	crys.	4·1	1·95	blue-gr.	—	10	—	—	>1
LiF	crys.	2·3	1·39	—	11		9·5	1·6	1
CaF_2	crys.	3·2	1·41	—	—	—	—	—	0·15
$CaWO_4$	crys.	6·1	1·9	4300	1·5	—	—	—	3
$BaSO_4$-Pb	powd.	4·5	1·65	blue	2·0	—	—	—	<1
ZnO	powd.	5·5	2·0	5000	2·0	—	—	—	1
Al_2O_3	crys.	4·0	1·8	3000	—	—	—	good	—
Naphthalene	crys.	1·15	1·6	3850	0·3	—	—	5–10	0·06
Anthracene	crys.	1·25	—	4450	1·5	—	—	10	0·03
Phenanthren	crys.	1·03	1·7	4500	0·6	—	—	10	0·008
Dibenzyl	crys.	1·0	—	3500–4000	—	—	—	6	0·016
Stilbene	crys.	1·16	—	4000–4200	0·8	—	—	6	0·008
Tolane	crys.	1·0	—	—	—	—	—	—	0·04
Terphenyl	crys.	1·23	—	3200–4000	—	—	—	10	0·012
Terphenyl in xylene	sol.	0·86	1·5	3200–4000	—	—	—	5–10	0·002
Diphenylbutadiene in plastic		—	1·5	—	—	—	—	5–10	0·006

N.B. Position of emission bands only approximate.

Table 2

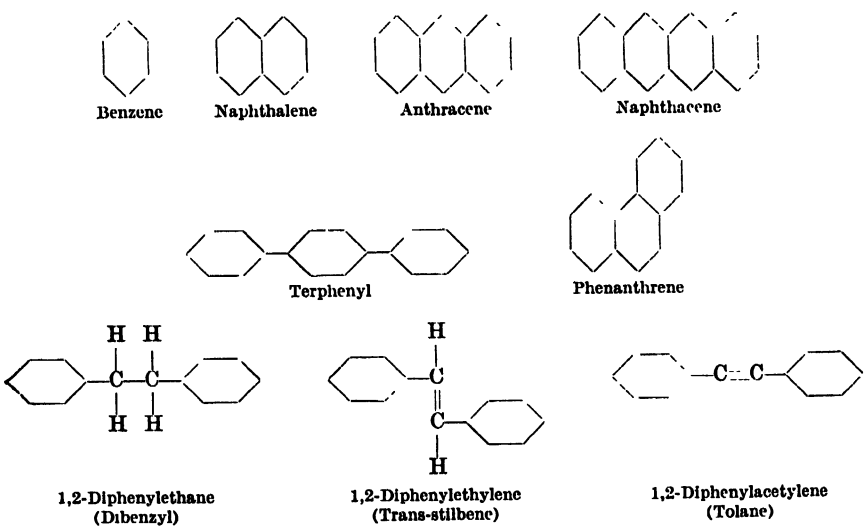
I. Excellent response	II. Fair response
$CaWO_4$ (Scheelite)	$PbCO_3$ (cerusite)
CaF_2 (synthetic and natural fluorite)	Phenatite
$LiAlSi_2O_4$ (Spodumene)	Apatite (pale yellow)
Al_2O_3 (synthetic sapphire)	$CaB_2Si_2O_8$ (danburite)
LiF (synthetic	
III. Medium response	IV. Weak response
$M_5SO_4KCl3H_2O$ (Kainite)	$SrSO_4$ (celestite)
Topaz	Tourmaline (pink)
$Be_3Al_2Si_6O_{18}$ (beryl)	$CaSo_42H_2O$ (gypsum)
$CaCO_3$ (calcite)	$CaBSiO_4(OH)$ (datolite)
Sulfur	Maple syrup sugar crystal
	Halite (NaCl)
	NaCl (artificial)
V. No response	
SiO_2 (clear quartz)	$KAlSi_3O_8$ (orthoclase)
$CaCO_3$ (aragonite)	$KMg_2Al_2Si_3O_{10}(OH)_2$ (phologopite)
Al_2O_3+Cr (artificial ruby)	$KAl_3Si_3O_{10}(OH)_2$ (muscovite)
	KCl (artificial)

feature of organic crystals compared with those of inorganic nature is the shortness of their luminescence decay times.

(i) *Naphthalene crystals*

In Table 3 we give the structural formula of naphthalene and other organic materials used in scintillation counters. Naphthalene was first used by KALLMANN for the detection of γ rays[4]. He found that the purity of his crystals was

Table 3



an important factor in determining their efficiency as counters. With good crystals he claimed an absolute efficiency for γ ray detection of about 5–10%. This value was later confirmed by DEUTSCH[5] using an R.C.A. 1P21 multiplier. Fig. 4 shows the luminescence emission spectrum of naphthalene. It is evident that the emission will be a reasonable match to the caesium surfaced photomultiplier used by KALLMANN but much less suitable for use with the antimony-caesium surfaced multipliers in common use in the U.S.A. and in this country. Naphthalene is very easily grown as large single crystals of several inches in dimensions, its melting point being 80° C. Initial purification can be achieved by steam distillation or by recrystallisation techniques.

(ii) *Naphthalene containing anthracene*

It is known from the work of BOWEN *et coll*[34, 35] that if naphthalene contains a fraction of a percent of anthracene its luminescence emission is predominantly that of anthracene when excited by radiation absorbed in the host lattice. A similar phenomenon is observed for naphthacene as impurity in anthracene and for pentacene as impurity in naphthacene. An efficient mode of energy transport exists between the absorption sites in the matrix lattice and the emitting molecules. We shall discuss this mechanism later. From the practical viewpoint this process enables naphthalene crystals containing anthracene to be used efficiently with antimony-caesium surfaced photomultipliers since the emission is in the anthracene bands shown in Fig. 4. The output pulse magnitudes from the photomultiplier using such crystals with ~1% anthracene content are two or three times those when pure naphthalene is used and usually about ½ those from pure anthracene crystals[36].

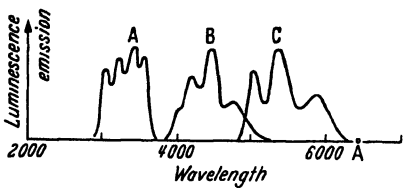


Fig. 4. Luminescence spectra of hydrocarbons. *A* Naphthalene; *B* Anthracene; *C* Naphthacene.

(iii) *Pure anthracene*

As stated in Section 1, BELL[6] found anthracene to be much more efficient than naphthalene in conjunction with 1P21 and 5819 type photomultipliers because of its spectral match. Since this discovery anthracene crystals have been extensively used for γ ray detection. For similar reasons to those stated in para. (ii) above, anthracene must be obtained in a very pure state in order to give its own luminescence emission when excited. The initial purification can be made by repeated co-distillation of the material with ethylene glycol[37] with subsequent separation by washing with water and careful drying. Anthracene is easily oxidised when heated and so single crystals have to be made under vacuum or inert atmosphere conditions by the method described in Section 3.

(iv) *Dibenzyl, stilbene and tolane*

These three compounds form a related structural series as shown in Table 3 and are more lucidly called diphenyl ethane, diphenyl ethylene and diphenyl acetylene respectively. It was found by several different workers[38, 39, 40]

that their efficiency as scintillation counters increased from dibenzyl to tolane the latter being reported to give six times the pulse magnitude characteristic of stilbene[38], the latter being superior to anthracene. These measurements were for gamma ray excitation. These crystals are also noted as a group for their very short luminescence decay time which is about 0·006 μsec[41, 42, 43]. The temperature dependence of the decay time of stilbene has been measured by POST and SHIRER[43]. It only changes from 0·0044 μsec at −196° C to 0·006 μsec at room temperature while anthracene shows a much greater change from 0·01 μsec to 0·023 μsec over the same temperature range. Reference to Table 1 will show the comparative features of these and the other related hydrocarbons.

(v) *Terphenyl*

Terphenyl or diphenyl benzene (see Table 3) has been investigated in crystalline form and compares very favourably with stilbene as regards its efficiency and decay time (Table 1). Terphenyl forms very rugged crystals, according to HOFSTADTER[41], compared with other materials. It has, however, come into prominence as a suitable "activator" solute for liquid solutions used in scintillation counters [see Section (c)].

(vi) *Phenanthrene*

Phenanthrene is closely allied to anthracene in its characteristics. GITTINGS[39] has given results using this material in conjunction with 1P21 and 1P28 photomultipliers.

(vii) *Miscellaneous organic materials*

In recent articles the scintillation characteristics of many different organic compounds have been given. In 1950 HOFSTADTER[44] listed many materials giving their emission and light yield for particles. Amongst them and not noted above are pyrene, chrysene, acenaphthene, quaterphenyl, fluoranthene and fluorene. SCHILLINGER *et coll.*[45] have reported that chrysene is as good as anthracene but their comparisons were made for small chrysene crystals obtained by slow cooling of toluene solutions. COLLINGE and ROBBINS[46] have investigated the response of many of the above crystals to alpha particles. In this respect anthracene is superior to stilbene, chrysene and anthracene in naphthalene while such materials as phenanthrene, pyrene, fluorene, dibenzyl, fluoranthene and diphenyl are much poorer.

(c) *Organic liquids and plastics*

(i) *Liquid solutions*

In 1950 REYNOLDS and his collaborators[9]* investigated various solutions of hydrocarbons such as naphthalene and anthracene in benzene, *p*-terphenyl in benzene, dibenzyl in ether, terphenyl in xylene, some pure solvents and melted dibenzyl. Their results indicated that while pure liquids were not efficient as scintillators dilute solutions of some hydrocarbons possessed excellent response

* Earlier experiments on total fluorescence yield of solutions were made by AGENO, CHIOZZOTTO and QUERZOLI [see Phys. Rev. 79 (1950) 720].

to gamma rays. Two of the most efficient systems were terphenyl in benzene at 60° C and terphenyl in xylene at room temperature. The optimum concentrations were found to be:

(i) 2 g *p*-terphenyl in 100 cc benzene at 60° C.

(ii) 0·5 g *p*-terphenyl in 100 cc xylene at 20° C.

N.B. Difficulty is experienced in obtaining sulphur-free xylene which is essential for good counting solutions. However, sulphur free toluene is readily obtained and gives comparable performance with p-terphenyl as solute.

The efficiencies of these solutions were the same as that of a naphthalene crystals for Co^{60} gamma rays. Other measurements[47] give their scintillation pulse magnitudes as 0·4 of those for anthracene when a 5819 type multiplier

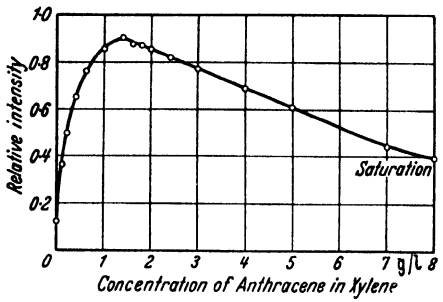


Fig. 5. Variation of scintillation efficiency of xylene with concentration of anthracene solute.

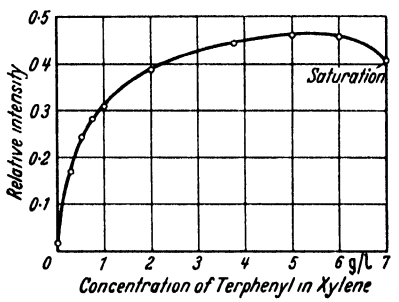


Fig. 6 Variation of scintillation efficiency of xylene with concentration of terphenyl solute.

is used. Other studies in the same year due to KALLMANN[48] showed that solutions of carbazole, phenanthren or fluorene in toluene or xylene responded to particle or γ ray excitation and that this response was sometimes improved by addition of paraffin to the solutions. These studies show the need for extremely high standards of purity of the materials used. Luminescence processes in solutions are very easily quenched by the presence of very minute amounts of contaminants.

In recent papers KALLMANN and FURST[49], have made a systematic study of liquid solutions as counters and have given full discussion of the mechanisms involved which we discuss later. In their first paper they study the variation of counting efficiency with concentration of solute and with concentration of a second solvent. Some of their results are given in Figs. 5 and 6 for anthracene in xylene and terphenyl in xylene. Adding 2·5 cc/litre of paraffin to a solution of 8 g/l of anthracene in xylene causes its efficiency for γ rays to increase by a factor of two whereas the addition of paraffin oil to a much more efficient system such as terphenyl in xylene always has a deleterious effect. Further experiments on mixed solvents and also solutes are described in a second paper by these authors. These studies are discussed in a later section.

The decay time of luminescence in terphenyl-xylene solutions has been investigated by POST[50]. For the saturated solution the rise of luminescence takes about 2×10^{-9} secs while the mean decay time is estimated to be $6\text{–}10 \times 10^{-9}$ secs. Spectral emission measurements and pulse height comparisans have

been made by HARRISON and REYNOLDS[51]. The emission for terphenyl is in bands between 3200 and 4000 Å with a maximum in the region of 3600 Å. The efficiency of the saturated solution of terphenyl in xylene is only 35% that of an anthracene crystal when a glass envelope, 1P21 photomultiplier is used but is 65% of the value for anthracene when an ultra violet sensitive 1P28 multiplier is used. The response of these liquids to various particles and to radiation are discussed in Section 4.

(ii) *Plastics*

MACINTYRE[8] investigated the response of polystyrene as a scintillation counter and gave the rise time luminescence as about 4×10^{-9} secs. Since then the incorporation of fluorescent molecules into plastics has resulted in much more efficient systems. SCHORR and TORNEY[52] investigated various methods of incorporating the fluorescent molecules such as mixing into the melt and addition during polymerisation with and without catalysts. Of these the incorporation of terphenyl in polystyrene during polymerisation with 1% benzoil peroxide present as catalyst yielded the best product. We give in Table 4 results for studies of the response for specimens of these materials 5 mm thick to various types of radiation when used with different photomultipliers[53]. The efficiencies are expressed as ratio of output pulse magnitudes for a stilbene crystal to that of the plastic.

More recently KOSKI[54] has investigated plastics such as lucite (*perspex*), paraplex and polystyrene containing anthracene. Whilst lucite and paraplex give poor results a solution of 2% anthracene or stilbene in polystyrene gives a product with a scintillation efficiency for Co^{60} rays equivalent to that of a single crystal of the solute molecules, but with slight differences in emission spectra. PICHAT and KOECHLIN[55] have reported studies on polystyrene containing tetraphenyl-butadiene a 2% solution, the solute being mixed in before polymerisation is more efficient that solutions of terphenyl in xylene. They found that from 1% solid solution up to pure tetraphenyl-butadiene the mean intensity of the scintillations increases as the logarithm of the solute concentration.

3. THE PRODUCTION OF LARGE CRYSTALS FOR SCINTILLATION COUNTERS

Many of the present day methods for growing large single crystals have been described in a recent book by BUCKLEY[56] together with current theories of crystal growth and habit. In this section we shall be concerned with methods applicable to the various types of luminescent crystals described in the previous section. In all these methods BUCKLEY's words are applicable ' It should be remembered that in the preparation of large clear crystals, the touch of the artist is about as important as the application of established scientific principles." In almost all of the methods crystallisation occurs from the melt but the first method below and two or three later ones are exceptions.

(a) *Growth of cadmium and zinc sulphide crystals*

We first describe the method developed by FRERICHS[57]. A diagram of his apparatus is given in Fig. 7. Cadmium metal contained in a small porcelain boat is placed in the cylindrical silica muffle of a furnace *F*. A stream of

hydrogen enters at one end of the muffle and a stream of hydrogen sulphide near to the boat. The gases pass out and are safely burnt or conducted away at the other end of the muffle. The muffle is heated by the furnace to 800 or 1000° C and then allowed to cool slowly. The gas stream reacts with the cadmium and at a certain stage of the cooling crystals of cadmium sulphide grow on the wall of the muffle. Their dimensions, limited by the size of muffle, are usually 2×10 or $20 \times 0{\cdot}1$–$0{\cdot}2$ mm and the best are flat and clear. They have the hexagonal structure. The method has been applied recently to produce single crystals of luminescent zinc sulphide (verbal comm. from I. BROSER).

Another method for production of zinc sulphide crystals is described by REYNOLDS and CZYZAK[24]. Crystals were grown by heating zinc sulphide

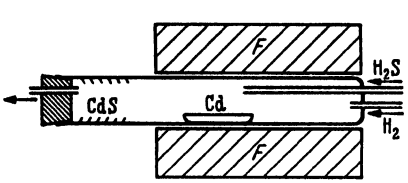


Fig. 7.

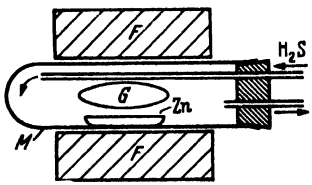


Fig. 8.

Fig. 7. FRERICH's apparatus for growing CdS crystals.

Fig. 8. Apparatus for deposition of ZnS films on glass. *F* furnace; *G* glass disc; *M* glass tube; *Zn* zinc in porcelain boat.

precipitate in an atmosphere of hydrogen sulphide in sealed tubes at 1150° C. The sizes obtained were $2 \times 2 \times 10$ mm and some specimens showed a blue luminescence.

STUDER, CUSANO and YOUNG[23] describe methods of depositing transparent, luminescent layers of zinc sulphide on glass. Their first arrangement is shown in Fig. 8. A stream of H_2S vapour (to be completed) passes through a glass tube held in a furnace at 400–600° C. The tube contains a small boat of zinc and above it a well cleaned glass disc. An appropriate activator impurity salt is mixed with the zinc. Zinc sulphide is formed and deposits on the glass disc as a transparent luminescent layer. Thicknesses up to 1 μ have been obtained in this way. In the second method these workers evaporate layers of zinc fluoride on to glass discs and then transform them to zinc sulphide layers by heating in a stream of hydrogen sulphide at 500° C. These films only have about half the luminescence efficiency of those made by the first method.

(b) *Synthetic halide crystals*

Large crystals of many of the alkali halides have been available commercially for a long time. One of the methods used was described by KYROPOLOUS as early as 1926[58]. It is applicable to thallium activated sodium and potassium iodides. Its essential features are shown in Fig. 9. A furnace contains a platinum crucible in which the halide is melted. Dipping into the melt is a platinum tipped rod which is hollow and is cooled by an internal air stream. Crystals grow on the cooled rod and this is then raised from the melt as shown

(b) so that only one of the seed crystals remains in contact with the melt. By control of the furnace temperature a much larger crystal is grown on this seed crystal. For very large crystals the seed crystal is clamped to the cooling rod by a set screw arrangement. MENZIES and SKINNER[59] have developed a similar method for larger crystals. After growth the cooling process must be slowed up to ensure proper annealing of the crystals formed.

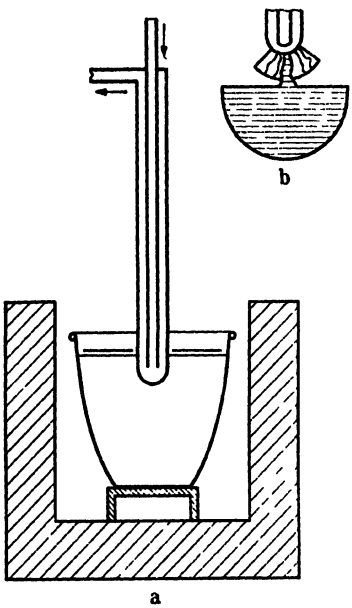


Fig. 9. (a) Method of KYROPOULOS; (b) Arrangement for seeding melt (KYROPOULOS).

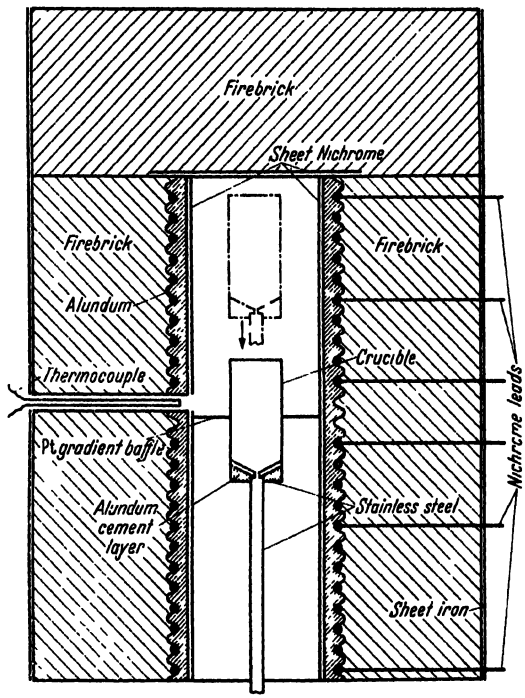


Fig. 10. STOCKBARGER's arrangement for LiF crystals grown at atmospheric pressure.

A somewhat different method for halide crystals has been developed by STOCKBARGER[60] as illustrated by Fig. 10 for growing lithium fluoride and also calcium fluoride crystals. The furnace is in two parts with a temperature baffle between the two. The upper one is at a higher temperature than the lower one and the temperature gradient at the baffle is quite sharp. The platinum crucible containing the melt is slowly lowered from the upper furnace compartment into the lower the temperature falling through the melting point between the two. The crucible has a conical bottom and beneath, a metal supporting rod. By this method crystals of fluorite several inches in diameter and as many long have been obtained.

(c) *Tungstate and sapphire crystals*

In 1902 VERNEUIL[61] disclosed a method of producing large crystals of sapphire and ruby which is used commercially at the present time. A sketch of the apparatus is shown in Fig. 11. The essential procedure is to feed a fine stream

of the powdered material to be synthesised into a crystal into an inverted oxyhydrogen blow pipe which plays on an alumina rod and builds the crystal on it. The powder is shaken at controlled intervals through a fine sieve *B* and is carried by the oxygen stream into the burner *N*, the hydrogen entering at lower place (*P*). The blow pipe nozzle terminates in a furnace chamber

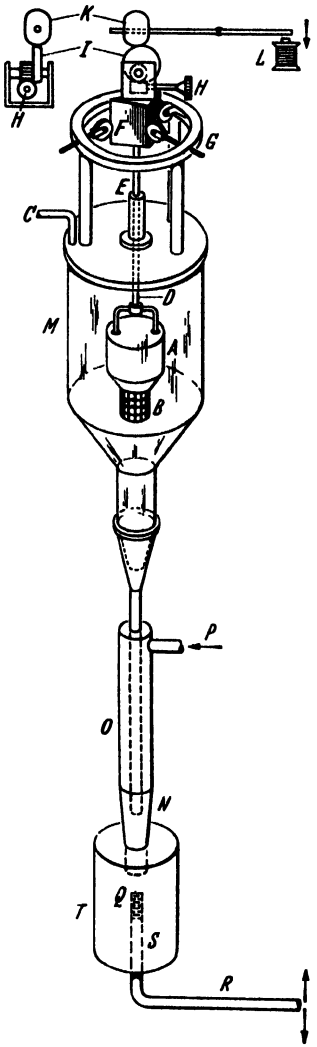


Fig. 11. VERNEUIL's apparatus for growth of large corundum crystals.

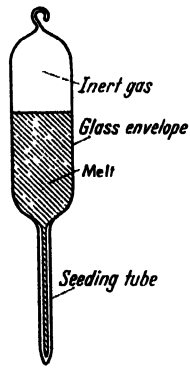


Fig. 12. Glass vessel used in STOCKBARGER type furnace for growing hydrocarbon crystals.

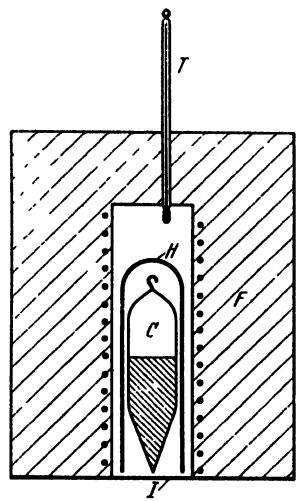


Fig 13. ZERFOSS method for growing hydrocarbon crystals[62]. *F* furnace; *H* "heat shield"; *I* poor insulation layer; *T* thermometer; *C* crystal vessel.

T in which is mounted vertically a sintered alumina rod. A cone of the sintered powder builds up on the rod and its tip approaches the hottest part of the flame. Here it melts and spreads out the, incoming powder building up a spherical surface. The alumina rod is gradually lowered and a boule of crystal builds up.

This method has been applied to the growing of synthetic scheelite crystals many cm long which have identical scintillation characteristics to the natural mineral[62]. The method might be tried for the production of synthetic crystals of lead activated barium sulphate.

(d) *Growth of hydrocarbon crystals*

Two different methods for production of large crystals of such organic solids as naphthalene, anthracene and stilbene have proved successful[37, 63]. One of them is a simple adaptation of the STOCKBARGER method already described. The material is sealed off in a glass vessel of cross section as shown in Fig. 12. The long capillary at the bottom is used to provide initial seeding of the melt by initially lowering it into the bottom half of the STOCKBARGER furnace. The vessel is lowered at a rate of about 2 inches per day. Glass tubes through the whole furnace act as guides. Large clear crystals several cm in diameter and 5–10 cm long have been made by this process.

Some workers[62] have used a rather different furnace and a fixed vessel for the melt as shown in Fig. 13. The furnace is arranged with a poor thermal insulation as its base so that a temperature gradient exists along its vertical direction. The temperature is taken well above the melting point and then the whole is slowly cooled. Obviously crystal growth begins from the bottom as before. This method avoids the lowering system of the above method but apparently gives similar crystal products.

The second method is essentially based on a method developed by STÖBER[63] for crystals having a unique crystallographic axis and anisotropic properties and has been successfully used at A.E.R.E., Harwell, and by the writer for large naphthalene crystals. A thermostated oil bath has beakers of naphthalene suspended in it so that when the latter is melted its surface is at the same level as the oil surface. The bath is then slowly cooled through the melting point of the naphthalene and a single crystal grows downwards from the surface of the melt. A glass rod annulus supported at a few millimetres below the surface and of diameter just less than that of the inside of the beaker serves to support the crystal when formed since it would tend to sink. The heat flow is in the opposite direction to that in STÖBER'S original method where the bottom of the melt is cooled.

4. ENERGY MEASUREMENTS WITH SCINTILLATION COUNTERS

(a) *Response of scintillators to different radiations*

One of the possible uses for scintillation counters is the proportional counting of particles and high energy radiation. Provided that the radiation incident on the detector is completely absorbed, a scintillation light output proportional to or having a simple relation to the absorbed energy is expected. The organic crystals show significant deviations from such proportional response as shown below. In this section we consider the response of crystals to particles and to X-rays and gamma rays and indicate some of the practical success obtained in using these crystals as energy spectrometers.

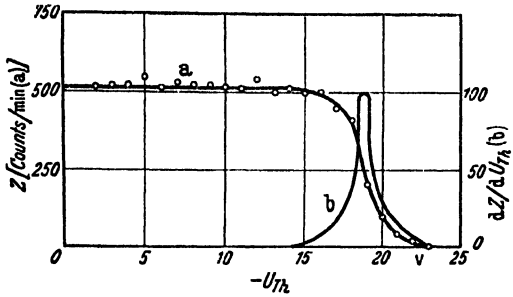


Fig. 14. (a) Relation between number of counts Z and grid bias U_{Th}; (b) distribution of pulse size for α-particles of given energy.

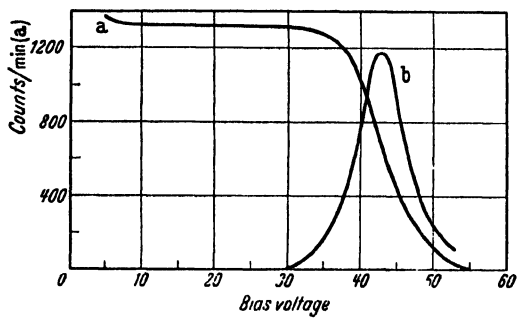


Fig. 15. (a) Bias curve for scintillations from transparent fragment of scheelite for 4·5-Mev particles; (b) differentiated bias curve.

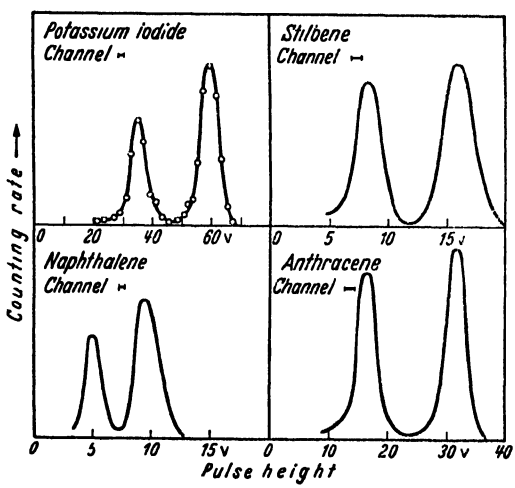


Fig. 16. Pulse-height distributions in single crystals of α-particles from thorium C+C'.

(b) *Detection of charged particles*

The first demonstration of the scintillation counter as a proportional detector for alpha particles was given by KALLMAN[64] using a cadmium sulphide crystal. Fig. 14 shows his "integral" and "differential" bias curves for the crystal bombarded by alpha particles from polonium. Fig. 15 gives similar results obtained by bombardment of a small single crystal of scheelite by 5 Mev alpha particles[65]. Following this, "differential" bias curves showing pulse size distributions for scintillations due to homogeneous alpha particles bombarding different crystals were given by HARDING, FLOWERS and EPPSTEIN[66]. Their results are given in Fig. 16 for sodium iodide activated by thallium, anthracene, stilbene and naphthalene crystals. The spread in the pulse distributions shown by these curves is known from later experiments in the writers, laboratory to be due almost entirely to statistical fluctuations in the photomultiplier. The latter are due to the fact that for the above curves only about 400 photoelectrons are produced at the multiplier cathode per scintillation giving a statistical deviation in the pulse output size of 10%. The curves of Fig. 16 emphasize the lack of linear response to heavy particles shown by organic crystals. Similar departures from linearity are shown by organic liquids and plastics. The cause appears to be the density of ionisation and the effect has been studied by several workers[67–72].

TAYLOR *et coll.*[71] have investigated the response of crystals to different particles and particle energies and their results for anthracene are given in Fig. 17. Similar curves are obtained for other organic crystals while thallium activated sodium iodide gives linear response over a very wide energy range as shown by Fig 18. Since the non-linear effects are dependent on ionisation density they are not so noticeable, except at relatively low energies, when electrons excite the organic crystals. Fig. 19 gives curves for different crystals using electrons of energies up to 600 kev[72]. The non-linear response is only noticeable for anthracene and stilbene when the electron energy is less than 100 kev whereas it is noticeable for alpha particle excitation up to energies of 10 Mev. Response of crystals to electrons has also been investigated by HOFSTADTER *et coll.*[73], by KOLLER and ALDEN[74] for thin evaporated layers of luminescent zinc sulphide and by HOPKINS[75] for anthracene crystals. Fig. 20 shows the pulse size distributions obtained by FRANZEN, PEELLE and SHERR[69] using scintillation counters to detect protons of 16·4 Mev energy. Because of the larger particle energy and consequently greater scintillation intensity the curves

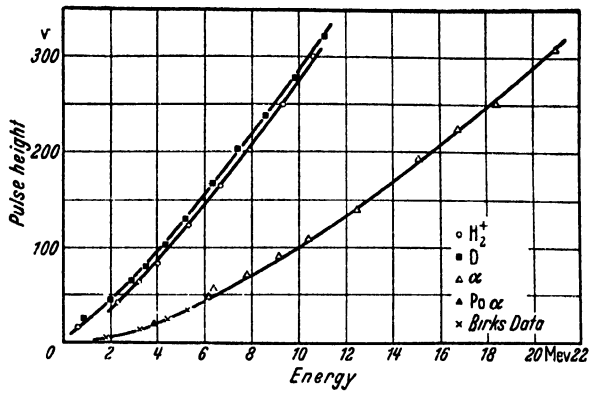


Fig 17. Response of anthracene to molecular hydrogen ions, deuterons, and alpha-particles. Note that the molecular hydrogen ions are detected as two protons entering the crystals simultaneously.

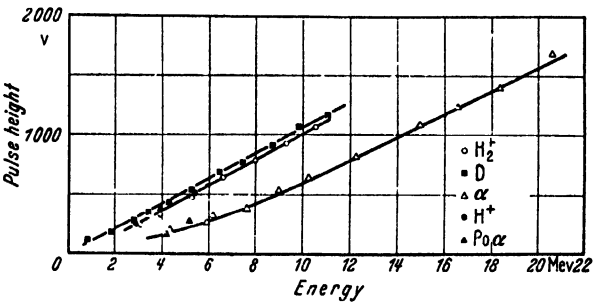


Fig 18. Response of thallium activated sodium iodide to molecular hydrogen ions, deuterons, and alpha-particles The arbitrary pulse-height scale is the same as in Figs. 17 and 19.

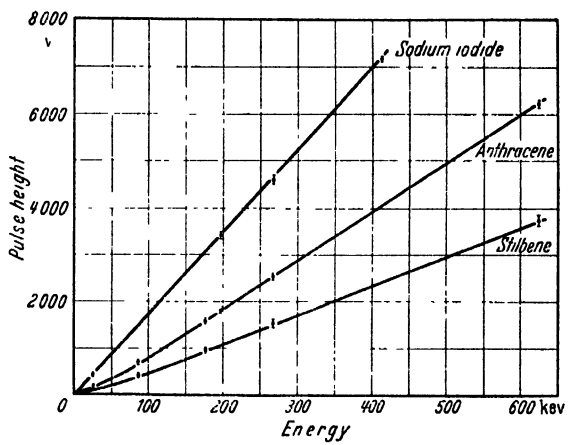


Fig.19. Response of anthracene, stilbene, and sodium iodide to electrons.

are much sharper than those of previous figures. The pulse distributions obtainable for monoenergetic electrons from a β-ray spectrometer are shown in Fig. 21 for an anthracene crystal. KOLLER and ALDEN[74], studying the response of evaporated zinc sulphide layers to electrons over an energy range of 2–40 kv find a linear relation between electron energy and light output provided that the range of the primary electrons is less than the layer thickness. It is of theoretical interest that they find 90% of the electron energy to be expended in a layer whose thickness equals half the range.

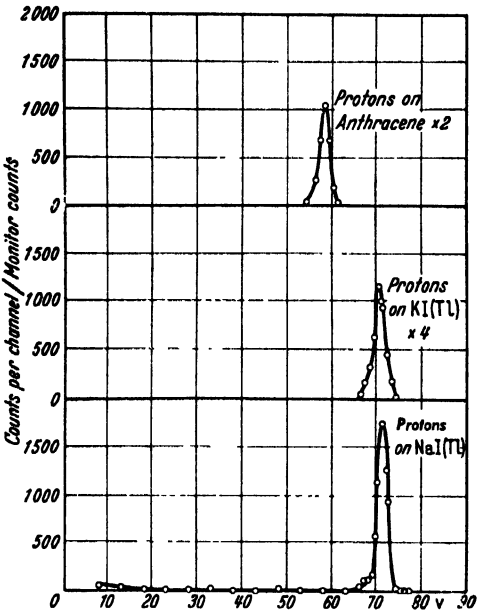


Fig. 20. Pulse distributions for 16 4-Mev protons bombarding various crystals.

(c) *Detection of neutrons*

Both crystalline and liquid scintillators have been applied to neutron detection. In 1948 BELL[6] reported that anthracene exposed to neutrons from a PoBe source gave scintillation pulses twice the magnitude of those from Co^{60} gamma rays. He used a 1 cm thick crystal and estimated that 10% of the neutrons incident on the crystal were counted. Using lithium fluoride FARMER, MOORE and GOODMAN[28] obtained counting efficiencies of about 10% for thermal neutrons. HARDING[76] has used anthracene and a suspension of thallium activated potassium iodide in α-bromonaphthalene for fast neutron detection. The latter not only provides a hydrogenous medium in which "knock-on" protons are produced but also has the same refractive index as the phosphor particles. This enables the emitted light to be efficiently collected system. Bias curves for equal fluxes of fast neutrons (2·5 Mev) and for gamma rays (2·62 Mev) are given in Fig. 22.

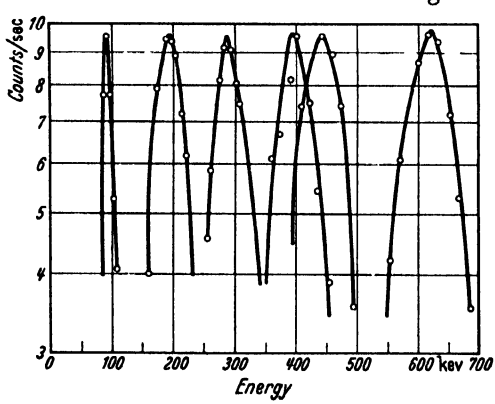


Fig. 21. Pulse distributions for monoenergetic electrons bombarding anthracene.

Other workers have used scintillating liquids as neutron detectors[77]. Fig. 23 gives bias curves for fast neutrons of different energies exciting a terphenyl-xylene solution in a 1 in. × 1¼ in. diam. glass cell. Also included

for 14 Mev neutrons is the theoretical curve assuming one isotropically distributed collision per neutron entering the solution. Counting efficiencies of 5–10% are obtained for this arrangement. The use of longer cells does not

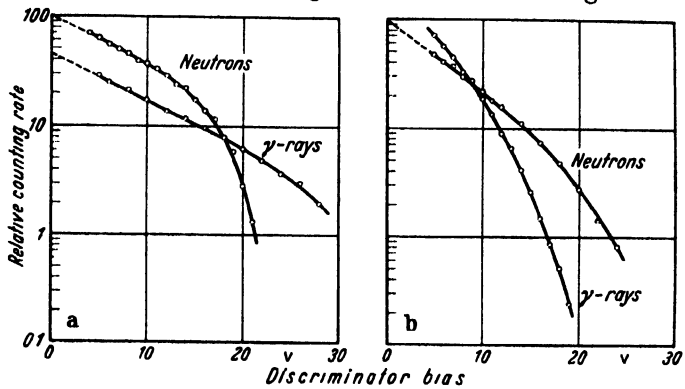


Fig. 22. (a) Relative counting-rates in anthracene for equal fluxes of 2·5-Mev neutrons and 2·62-Mev γ-rays. (b) Relative counting-rates in potassium iodide activated with thallium + α-bromonaphthalene for equal fluxes of 2·5-Mev neutrons and 2·62-Mev γ-rays.

seem to have any advantage. The chief disadvantage of the scintillation counter for neutrons is its disproportionately high sensitivity to γ rays. HARDINGS' arrangement using potassium iodide dispersed in α-bromonaphthalene appears to possess the best discrimination against gamma rays as shown by comparison of Figs. 22(a) and 22(b). Reference may also be made to other reports not considered here which are concerned with the detection of neutrons by scintillation counters[78–82].

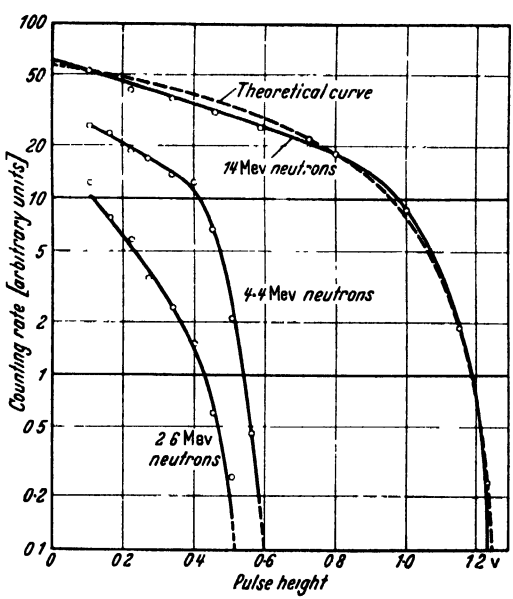


Fig. 23. Bias curves for neutrons of different energies bombarding terphenyl-in-xylene solution.

(d) *Detection of cosmic ray particles*

The application of scintillation counters to cosmic ray detection demands the use of large volumes of detector. Crystals of naphthalene activated by anthracene have been grown for this purpose up to 8 in. diameter and ½ in. thick[83]. To collect the light efficiently the crystal was mounted in an integrating hemisphere of special design. Other workers[84] have investigated various phosphors for cosmic ray detection and relative pulse sizes for single cosmic rays entering the phosphor layers (11 cm diam. × 0·5 cm

thick) are given in Table 5 [84]. Measurements of the pulse heights for μ-mesons exciting an anthracene crystal (1¼ in. × 1¼ in. diam.) have been made by ROSER and BOWEN[85] for energy ranges 29–48 and 48–170 Mev. Proportional response of the crystal to μ-mesons over these ranges is indicated by the results with deviations of less than 5%.

KRAUSHAAR, THOMAS and HENRI have detected π–μ meson decay using a scintillation counter[86] while the pulse distribution for cosmic rays in anthracene at 30,000 feet has been measured by REIFFEL, STONE and REST[87]. A solution of pyrene in xylene has been successfully used by NEY and THON[86].

(e) *Detection of fission fragments*

Fission fragments should be easily detected by the scintillation counter. BROSER and KALLMANN[89] have used a ZnS-Ag phosphor and have obtained pulses 3× those for uranium α particles but with detection efficiencies of only 3% for the 60–90 Mev fragments from U^{238}.

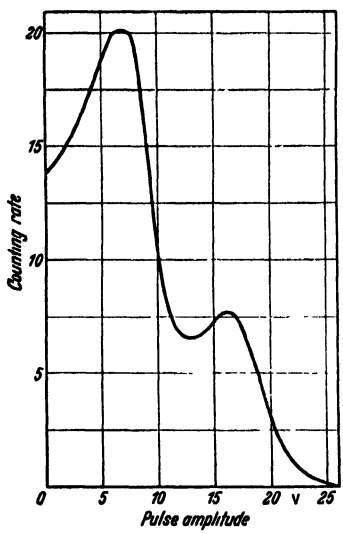


Fig. 24. Distribution of pulses from a well-collimated source of Na^{24} γ-rays showing the resolution of the 1·4- and 2·8-Mev γ-rays.

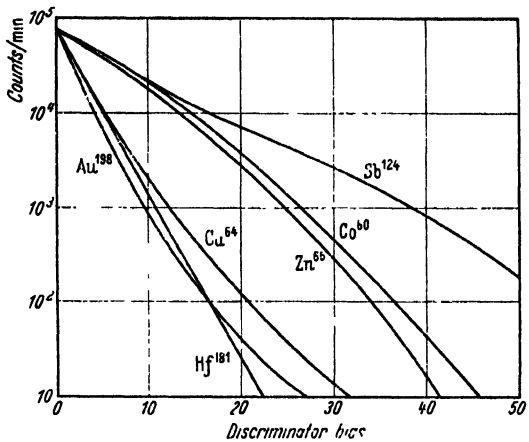


Fig 25. Integral bias curves for gamma rays of different energies. Curves plotted to correspond to the same number of secondaries produced in the phosphor in each case (from HOLMES, 1949).

(f) *Measurement of gamma ray energies*

Many investigations of nuclear decay and emission involving detection of gamma rays have now been made using the scintillation counter. In this section we shall only make reference to the studies which indicate the best methods of using such counters for gamma ray spectroscopy. When gamma rays enter the scintillating medium they may lose their energy by three different processes as follows:

(i) by Compton encounters;

(ii) by photoelectric conversion;

(iii) by pair production.

(i) *Compton encounters*

In Compton encounters the gamma ray only loses part of its energy in a single collision and unless the scintillating crystal or liquid has large volume the gamma ray energy will not be completely absorbed in it. The theoretical aspects of such encounters in a scintillator have been considered by SEITZ and MUELLER[90]. To use Compton encounters as an indication of gamma ray energies large crystals of naphthalene activated with anthracene have been used by CAVANAGH[91] and his pulse distribution for well collimated gamma rays from Na^{24} is shown in Fig. 24. Where it is essential to combine energy resolution with short resolving times this method would seem desirable. The use of smaller crystals is a disadvantage when the radiation includes gamma rays of different energies but for homogeneous gamma rays the smaller crystals, in which only one Compton encounter is likely, are quite useful. Fig. 25 shows plots of log (counting rate) vs. discriminator bias for different gamma ray sources. Approximately straight lines are obtained at the higher discriminator settings whose slopes are proportional to the gamma ray energy.

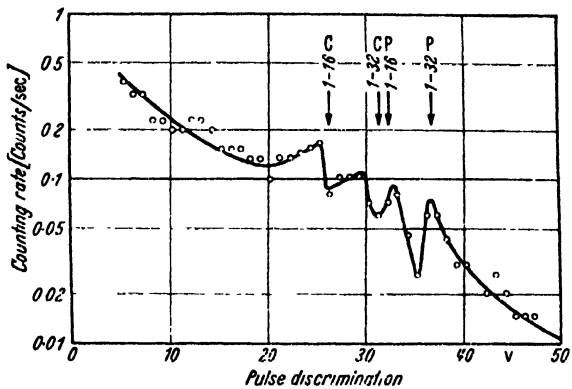


Fig. 26. Differential counting-rates in calcium tungstate with 1 mC of cobalt-60 at 1 m. Photomultiplier voltage 1,080; amplifier gain 1,600; mass of crystal 0·1244 gm, resolving time 200 μsec.

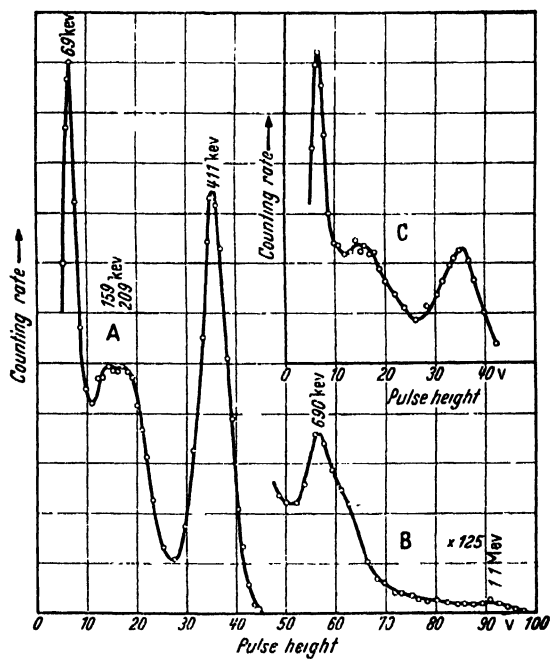


Fig. 27. Scintillation spectrometer pulse-height distribution for the gamma rays from neutron-activated gold. *A* Lower energy gamma rays and X-ray; *B* counting rate scale × 125 to show new high energy components; *C* relative distribution of *A* after 11 half-lives of Au^{198}.

HOFSTADTER and MCINTYRE[92] have used two NaI-Tl crystals in a coincidence system in order to obtain energy discrimination using Compton encounters. The primary gamma rays are scattered by one crystal and those scattered

at a definite angle, *i.e.* which have lost a definite energy, are detected by a second crystal. By counting coincidences very high energy resolution can be obtained but at the expense of counting efficiency.

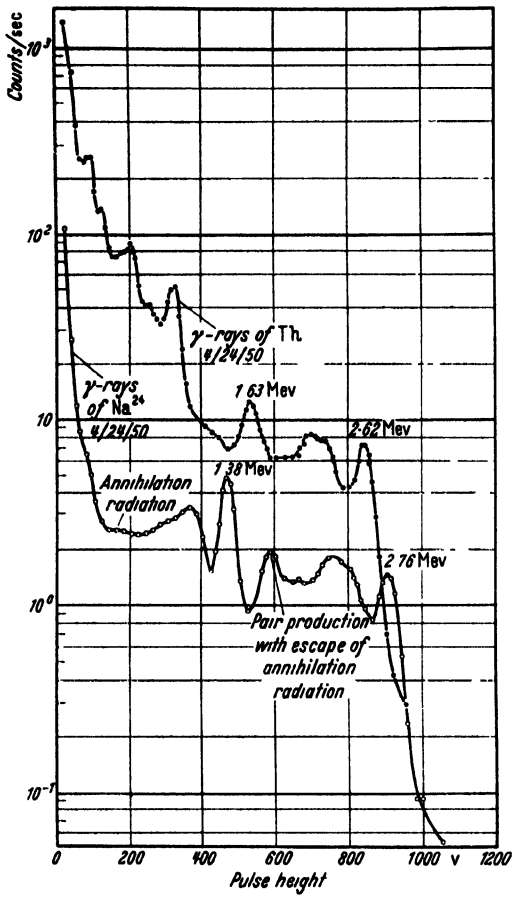


Fig. 28. Pulse distribution for thorium and Na^{24} rays bombarding NaI-Tl crystal showing pair production peaks etc.

(ii) *Photoelectric conversion*

When gamma ray energies of less than 1 Mev are to be measured the photoelectric conversion process may be utilised. The probability of this process increases as the gamma ray energy decreases and with the increase of elements of high atomic number in the scintillator. For this reason the relatively dense crystals of thallium activated sodium iodide and calcium tungstate are suitable although the long decay time of luminescence in the latter is a serious disadvantage. Since the gamma ray energy is lost completely in the process and if the photoelectrons remain in the crystal the system should behave proportionally. To avoid too much background due to Compton encounters a "thin" crystal is used. Fig. 26 shows the pulse distributions obtained by BELCHER[93] for a scheelite crystal (0·124 gm) for Co^{60} gamma rays. The letters *C* and *P* indicate peaks due to Compton and photoelectric encounters respectively. BELCHER reports poorer resolution for a potassium iodide crystal, to be expected since its density is only about one half that of scheelite. Fig. 27 shows the pulse distribution for gamma rays from neutron activated Au^{198} obtained with a 1 cm cube of NaI-Tl crystal as detector[94].

(iii) *Pair production*

As we have seen the Compton encounter is the predominant process in organic crystals at medium gamma ray energies, (~1 Mev). To measure lower energies it is usual to use inorganic crystals and utilise the photoelectric effect. At energies above 1 Mev pair production will occur and since the gamma ray energy is completely absorbed in this process it affords a means of measuring energies above this limit. When the positron is annihilated the two photons (0·511 Mev) may escape from the crystal but if they are absorbed then they

give rise to a peak in the measured distribution. Fig. 28 shows the distribution for the gamma rays of Na^{24} and of thorium and its products as obtained by BELL[95] using a NaI-Tl crystal. The 2·62 Mev gamma ray of ThC'' gives three peaks, one at 2·62 Mev being due to photoelectric conversion, with absorption of the X-ray from the iodine and to pair production with complete absorption of both annihilation photons. The low peak is for pair production with escape of both photons produced by annihilation. Between these two peaks a multiple peak occurs which seems due to pair production with capture of one photon plus a distribution due to Compton encounters. A similar but somewhat more complicated distribution is given for the gamma ray emission of Na^{24}.

When energies exceed 7 Mev the lower pair production peak is predominant, and this method of detection might be useful for detection and energy measurement in this region.

(g) *X-ray measurements*

As an example of the use of scintillation counters for X-ray detection we may cite the work of WEST, MEYERHOF and HOFSTADTER[73] (although KALLMANN was able to detect X-rays in his early experiments). The above workers used small crystals of thallium activated sodium iodide backed with a thin aluminium reflector and investigated the response to X-rays from 5–80 kev energy. They found that 100% counting could be achieved over this range and from 50–80% counting for 2 kev X-rays. Fig. 29 shows their pulse distributions obtained from 8 kev and from 2 kev X-rays respectively and also that from the photomultiplier noise. Statistical spread in pulse size is of course much larger in these low energy regions than in those for gamma rays shown in Fig. 27.

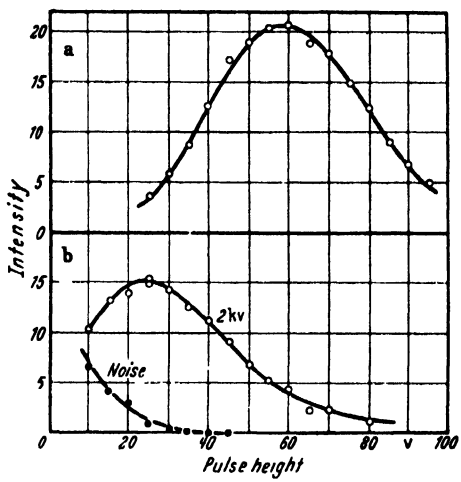


Fig. 29 (a) Pulse height distribution due to 8-kev fluorescent X-rays from Cu (1 5-volt channel width). (b) Pulse height distribution due to 2-kev X-rays and due to photo-multiplier noise.

Powder type phosphors such as ZnS-Ag or $BaSO_4$-Pb function efficiently as X-ray detectors but are obviously not suitable for X-ray energy measurement.

(h) *Miscellaneous*

In this section we consider two important factors in the use of the scintillation counter that arise in the luminescent detector. The first is the transmission of emitted light from the crystal, liquid or plastic to the photomultiplier cathode. When crystals have high refractive indices the critical angle is small and it is difficult to get the light out of the crystal. To minimise this difficulty the crystal is attached to the multiplier window or to light piping of *perspex* or quartz by a medium of intermediate refractive index. In using media such

as paraffin, canada balsam etc. care has to be taken that they do not absorb the emitted light. The problem of light collection from crystals has been considered by SHURCLIFF and JONES[94].

A further point to be considered when using scintillators is the presence of multiple counting. This can arise from amplifier characteristics but it may also be due to the relation of these to the decay time of the luminescent material. Since the decay is a random process (see next section), when a small number of luminescence centres are excited then the intensity of a scintillation decreases with time as shown in Fig. 30 for a scheelite crystal[96]. If the amplifier time constant is too short compared with the decay time of the luminescence then a photon or groups of photons emitted later in the decay may register as an additional count. This and other problems have been investigated recently by BELCHER[97].

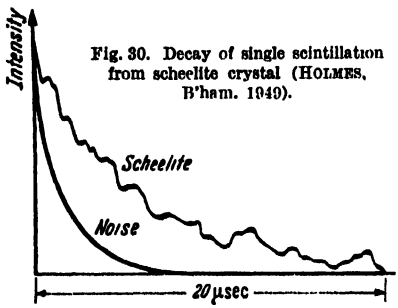


Fig. 30. Decay of single scintillation from scheelite crystal (HOLMES, B'ham. 1949).

5. FUNDAMENTAL MECHANISMS IN SCINTILLATION CRYSTALS

(a) *Inorganic crystals*

(i) *Conditions for luminescence emission*

When energy is absorbed by a solid it may be dissipated in the following ways:

(a) All the energy may be used to increase the thermal vibrations of the constituent atoms.

(b) Some energy may be used in photochemical changes.

(c) Photoelectrons may be emitted.

(d) The energy may be re-radiated as luminescence.

(e) In some cases, particularly when heavy particles bombard solids, energy is partly used in disordering the structure of the solid.

Here we are first of all concerned with the atomic conditions which give rise to emission of the absorbed energy as luminescence and secondly with the other modes of energy loss which obviously affect the intrinsic luminescence efficiency. To obtain luminescence it is generally accepted that a solid must contain atomic or molecular groups in which electronic transitions take place (with resulting luminescence emission) which are protected from interactions with the surrounding material. Such systems are usually called luminescence centres. The potential configurations of such centres have been suggested by VON HIPPEL[98] and by SEITZ[99] and are based on the known configurations for diatomic and simple polyatomic molecules. BOWEN[100] discusses their application to the study of luminescence in organic molecules. Fig. 31 shows the potential energy of a normal and excited luminescence centre plotted against some configurational co-ordinate x; in the case of a diatomic molecule x is the

separation of the atomic nuclei. All electronic transitions are represented by vertical lines. In the normal state the transition AA^1, absorption of a photon, raises the electron to the excited state this being followed by a fall of the electron to the minimum of the state and consequent thermal dissipation of excess energy. Luminescence is due to the return transition BB^1 and further thermal loss of energy occurs to reach the state A. Unless the minima are in a vertical line the luminescence quantum will always be less than that absorbed and so although the quantum efficiency can reach unity the absolute energy conversion efficiency will in general be less than unity. If the two curves come close together as shown then at sufficiently high temperatures the excited

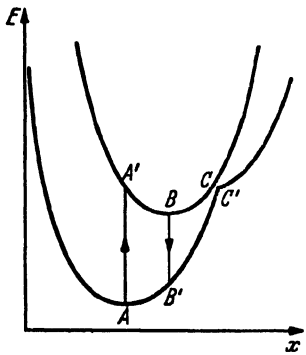


Fig. 31. Potential energy configurations for a luminescence centre.

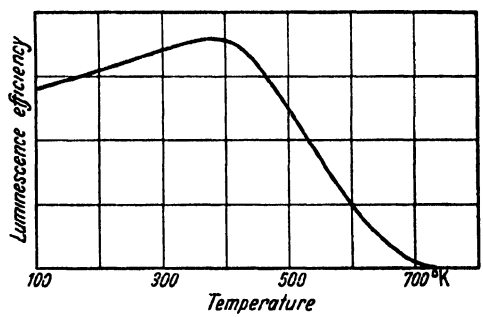


Fig 32. Luminescence efficiency vs. temperature for Mn^{++} centres in ZnS phosphor. Excitation by 4358 A radiation.

centre return to its normal state by a series of vibrational interactions with its surroundings, following the path CC^1B^1A. In this case no luminescence occurs. Thus we may expect the luminescence efficiency to depend on the relative probabilities of electronic transitions or vibrational transitions. If the first process has a probability α and the second a probability β [where $\beta =$ const. $\exp(-E/kT)$], E being the energy difference between B and C of Fig. 31 then the luminescence efficiency η follows the relation:

$$\eta = \frac{\alpha}{\alpha + \gamma \exp(-E/kT)}$$

γ being another constant. Fig. 32 shows the experimentally obtained curve of efficiency vs. temperature for excitation of the luminescent centres formed by Mn^{++} ions as impurity in zinc sulphide[18].

The structure of the luminescence centres in inorganic crystals used in scintillation counters is of the greatest interest here. In the zinc and cadmium sulphides the silver impurity ions form these centres when combined in a complex with halogen ions included in preparation[101]. The detailed structure of these centres is not known as yet. In thallium activated alkali halides investigations by SEITZ[102] indicate that pairs of thallous ions form the emitting centres. In calcium tungstate and in zinc oxide the excess of one constituent gives rise to suitable centres[103]. Excess WO_4 ions form centres in scheelite and excess Zn atoms in zinc oxide. In pure lithium and calcium fluorides and

sapphire it is not certain what the luminescence centres are but in blue luminescent diamonds it is thought that the emission occurs at sites in the lattice where a carbon atom is missing[104].

(ii) *Energy transfer in crystal phosphors*

In using phosphors as scintillators we are never concerned with absorption and emission processes entirely confined to the luminescence centres. The exciting radiation is absorbed in the bulk material and considerable ionisation occurs. Since phosphors show conversion efficiencies for alpha particles of the order of 20% we have to enquire how the energy absorbed is transferred from the matrix lattice atoms to the specific centres where emission occurs. To do this we make use of the modern picture of the energy states of electrons in crystal lattices which was originally developed by BLOCH[105] and specifically applied to phosphors by RIEHL and SCHÖN[106] and by JOHNSON[107]. This model has since been modified by several workers to explain the more detailed characteristics of phosphors. In an isolated atom the electron energy states are sharp and discrete but when atoms are arranged in close proximity on a perfect crystal lattice their mutual interaction perturbs the electron states which split into many levels forming sets of quasi continuous energy bands which extend throughout the crystal lattice. The bands are broader and the gaps between them narrower for outer electrons since these are most perturbed. The final processes involved in luminescence are essentially confined to the valence or outer electrons and in Fig. 33 we give the energy band system for these electrons in insulating crystal. For such crystals the highest occupied energy band is completely filled the next band of allowed energies above being empty. Defects and impurity atoms or excess lattice constituents give rise to rather more discrete levels which are also localised at the defect or impurity atom in the lattice. Fig. 33 includes such levels showing how the energy states of a luminescence centre lie in the normally forbidden region between the filled and empty energy bands. Defects and sometimes impurity atoms can give rise to levels for electrons just below the empty band which play a part in phosphorescence and in thermal dissipation of the absorbed energy since they can trap electrons which have been raised into the empty band above. The process of excitation of the crystal by high energy particles can be described thus in terms of such a model.

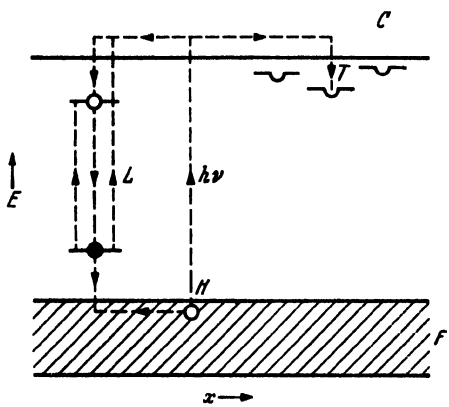


FIG 33. Energy-level scheme for an impurity-activated crystalline phosphor. *C* conduction band; *F* filled band; *H* positive hole; *L* luminescence centre; *T* electron traps.

The bombarding particle produces a large number of ionised particles along its track by exciting them from lattice atoms or ions. Most of these electrons

will come from energy levels below that of the valence electron band. After these electrons have produced further ionisation and the resulting secondary electrons have continued the cascade process a stage is reached where numbers of electrons of relatively small energies remain in the empty band of Fig. 33 and the levels below the valence band have been reoccupied. Vacancies in the valence band behave like positively charged electrons in an applied field and so are known as "positive holes". These holes capture electrons from the ground states of the luminescence emission centres and also from filled trapping levels[108]. Then electrons in the empty conduction band can combine with empty luminescence centres or be captured in trapping states. Both processes provide a means for the electrons to return to their normal ground states but the combination with luminescence centres results in emission of the electron energy in its transition to the ground state whereas transitions of trapped electrons to combine with positive holes in the valence band will be non-radiative at ordinary temperature. This is because the trapping centres are not protected from thermal interaction with the matrix lattice. It is fairly obvious that provided a particle or gamma ray is completely stopped by the crystal, the luminescence efficiency will depend on the relative numbers of luminescence centres and non-radiative centres and on their respective capture cross sections for electrons as well as on the intrinsic conversion efficiency for the luminescence centres themselves as discussed above.

As yet no detailed studies are available to show whether the quantitative theory of non-radiative transitions in traps or defects proposed by SCHÖN[108] is valid. However, we shall discuss below some relevant results in the consideration of phosphor deterioration under bombardment. The above description gives a brief outline of the mechanism of energy transfer in inorganic crystals in which the transport is effected both by excited electrons and their vacancies or positive holes. We now have to consider the time effects involved in these mechanisms which affect the practical application of these inorganic crystals.

(iii) *Rise and decay of luminescence*

The rise and decay of luminescence emission in inorganic phosphor crystals will depend on the time delay between absorption of the exciting radiation and the transfer of the energy to the luminescence centres and also on the probability of radiative transitions within the luminescence centres themselves. Studies of the dependence of the latter process on temperature and thus on non-radiative energy degradation have been made by KRÖGER *et coll.*[109] We have seen that the temperature dependence of emission is dependent on the non-radiative transitions within the centre. The decay of luminescence is also affected. If the transition probability for luminescence is p then it easy to show that the emission I decays according to the relation:

$$I = I_0 \exp(-pt)$$

where I_0 is the initial intensity and I that at time t; when non-radiative transitions are included it can be shown that this relation becomes:

$$I = I_0 \exp[-(p + p')t]$$

where p' is the probability of non-radiative transition and is given by $p' = \exp(-E/kT)$ above. Thus as the temperature is increased a value is reached at which the rate of decay of luminescence p' increases rapidly and the luminescence efficiency decreases rapidly with temperature.

Such a dependence of decay rate and efficiency on temperature is shown by tungstate phosphors and the initial decay of thallium activated alkali halides but in the case of zinc and cadmium sulphide crystals the decay rate and efficiency are much more influenced by the time delay between absorption of energy and the capture of electrons in luminescence centres. Such electrons may first be captured in the trapping states shown in Fig. 33 and then escape by thermal activation to combine with empty luminescence centres. A quantitative study of this process has been made by many different workers during the last decade and reference should be made to literature concerned with it [18, 110, 111, 16]. The probability of the non-radiative transition of trapped electrons to the valence band will also affect the delay time and so the resulting decay of luminescence is of complex form and has a marked dependence on temperature. It is very rarely of exponential form but usually hyperbolic of the form:

$$I = I_0(1 + pt)^{-n}$$

where p and n are constants. The distribution of trapping states in depth below the conduction band will determine the length of afterglow of a phosphor[110] and it is the trapping processes that cause the relatively long afterglows of the sulphide phosphors and also the long afterglow of thallium activated potassium iodide compared with that of thallium activated sodium iodide.

(iv) *Response and stability of inorganic crystals*

The transport of energy in inorganic crystals usually involves the motion of charged particles as described above, but in organic crystals, as we shall see below, the presence of charged particles *i.e.* of high ionisation densities is detrimental to the resonance transfer process which takes place. Thus as shown above in Section 4, densely ionising particles give rise to a non linear energy response in organic crystals but in the inorganic crystals the intensity of the scintillations is propotional to the energy absorbed and there is in general no difference between the intrinsic efficiencies for alpha particles and gamma ray excitation. We would expect this since the transfer process itself involves ionised electrons.

In using crystals for scintillation counters we are always concerned with their stability under bombardment. Inorganic crystals are most affected by the heavier particles. A theoretical paper by SEITZ[112] considers the relative effects of different particles in disordering a crystal lattice compared with the ionisation produced. We shall not consider his arguments here but it is clear that the mass of the particle in relation to its charge will affect the amount of energy lost in non-ionising collisions with the lattice. Neutrons will thus be most effective in disordering a lattice. The result of this disordering is to produce more defects or trapping states in which non-radiative transitions to the ground state can take place. Thus prolonged bombardment of a phosphor

crystal will not only destroy the luminescence centres by direct collisions but will decrease the efficiency of energy transfer to the centres by disordering of the matrix lattice. BROSER and WARMINSKY[112] have recently published studies of the effect of alpha particle bombardment on the luminescence efficiency of cadmium sulphide crystals. The decrease in efficiency with alpha particle dosage is not of the same form for luminescence due to alpha particle and ultra violet light. They offer a quantitative theoretical treatment of the different effects of bombardment when these different excitants are used which is based on the SCHÖN model of trapping states functioning as non-radiative centres[108]. It would be useful to have further extensive studies of these deterioration processes in relation to the state of lattice disorder since results might point the way to the production of crystals with much higher conversion efficiencies.

(b) *Luminescence processes in organic molecules*

(i) *Conditions for luminescence in organic molecules*

In this section we are concerned with the processes occurring in organic solids and liquids used for scintillation counters. First of all it is useful to consider the conditions necessary for luminescence to occur at all. Energy absorbed by a molecule may appear as luminescence but it may be dissipated in other ways such as by thermal degradation, collisional transfer to another molecule, molecular dissociation or photochemical change. Space does not permit of an extensive discussion of these processes here and the reader is referred to other literature for this. An excellent and component survey of fluorescence in organic molecules in relation to these other processes has been given by BOWEN[100]. It was thought for a long time that condensed ring structures were favourable to luminescence in organic molecules but factors such as the arrangement of conjugated double bonds seem to be more important. A good example of the latter factor is seen in the series, dibenzyl, stilbene, tolane[38]. Again it is possible to state in a general way that electron attracting groups in a molecule decrease the likelihood of luminescence. An excellent example of this is the decrease in fluorescence yield from ultra-violet excitation in the series fluorescein[114], (yield 80%) tetrabromofluorescein (20%), tetra-iodo-fluorescein (20%) the increasing polarisability of the substituted halogen causing increased localisation of the π electrons of the ring systems. Another general condition for luminescence is that when a molecule is excited there should not be too much coupling between the electronic and vibrational states of the molecule or more simply that excitation does not cause any marked change in the structure and stability of the molecule. The simplest molecules to satisfy those conditions are those of the homologous series benzene, naphthalene anthracene, etc. (see Table 3). All these molecules have common features namely the presence of conjugated double bonds and ring systems of non-localised electron orbitals. Increase in the number of rings alters the energy states of these electrons and thus the emission spectra as shown above by Fig. 4. The presence of electron attracting substitution groups (such as NO_2 or halogens) in the rings will decrease the luminescence efficiency while other groups will either

enhance the efficiency or leave it unaltered. This point is illustrated by the high luminescence efficiencies of such systems as dibenzyl, stilbene and tolane[38]. In solid or liquid solution the luminescence efficiency of such molecules will be markedly affected by other solute molecules having high polarisability. Hence the need for careful purification of materials for scintillation crystals or liquids.

(ii) *The decay of luminescence*

We have already seen that the organic scintillators are characterised by short decay times. In cases where the decay is not markedly affected by temperature, it is characteristic of a normal electronic transition depending on the mean life time of the excited state of the particular molecule. Thus the luminescence decay follows the exponential form given above. It can be deduced from the breadth of the absorption bands of the molecule. The effective decay rate may, however, be altered by a delay in the transfer of energy from its absorption site to the luminescent molecule as discussed below.

(iii) *Energy transfer processes in organic crystals and liquids*

In experiments carried out by BOWEN and his collaborators[34, 35] it was found that the luminescence of naphthalene crystals containing anthracene impurity excited by ultra violet light was predominantly that due to the anthracene molecules even at very small concentrations of the latter. This phenomenon had been first observed by BOWEN[34] in anthracene containing naphthacene impurity. When such crystals are dissolved in benzene the effect disappears and the luminescence of each constituent appears in proportion to its concentration. Fig. 34 shows the results obtained by BOWEN, MICKIEWICZ and SMITH[35] for different crystal systems. Similar effects are observed in naphthalene containing anthracene when γ ray excitation is used as we have seen. Now excitation by ultra violet or by gamma radiation involves absorption by the matrix crystal and by the impurity molecules. If the molar concentration of anthracene is only 0·1% then it absorbs only 0·1% of the total energy. However, the observed luminescence emission is mainly characteristic of the anthracene molecules and of very much greater intensity than would arise from absorption in these molecules alone. We must therefore postulate an efficient mechanism for transfer of the absorbed energy from lattice absorption sites to the fluorescent impurity molecules. BOWEN[34] has suggested that an "exciton" transfer occurs from one molecule of the lattice to another until the "exciton" is trapped at an impurity molecule where its energy can be converted into a luminescence photon. In such a process there is no charge transport as in transfer processes in inorganic crystals. In fact the presence of free electrons may be deleterious since the resulting ionised molecules will also trap the energy and dissipate it non-radiatively. BOWEN assumes that for exciton transfer and trapping the fluorescent impurity molecules must be capable of electronic transitions with lower quantum energy than those of the lattice molecules. Thus after light absorption several different processes may occur to dissipate the absorbed energy. First of all the matrix constituents

themselves may emit luminescence or they may act as quenchers, dissipating the energy thermally. Secondly exciton transfer of the energy through the matrix to the impurity molecules may occur. If the latter are of suitable type and concentration the energy may emitted as luminescence. Some impurities

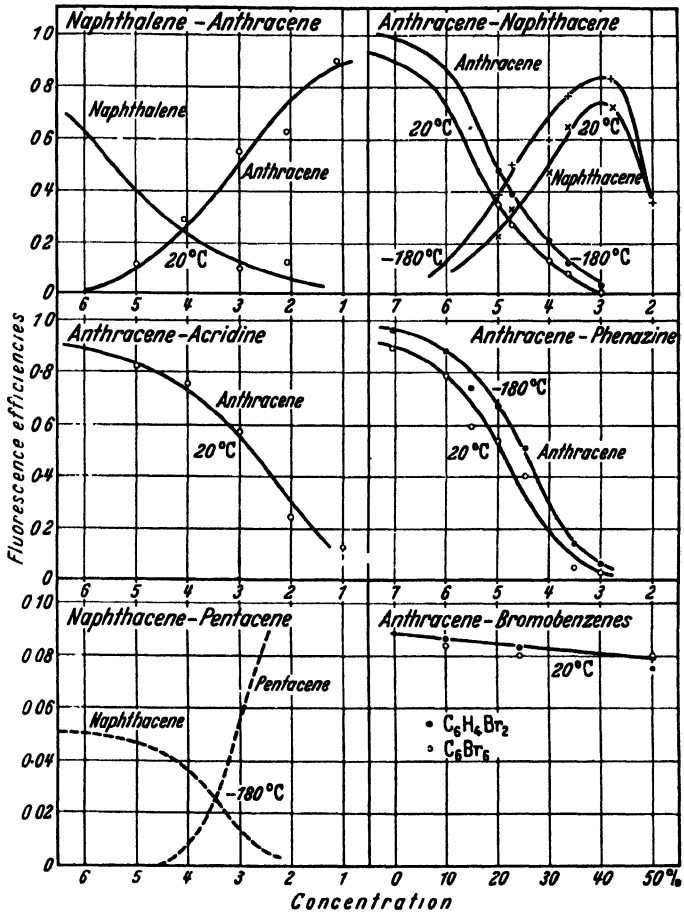


Fig. 34. Fluorescence efficiences of solid solutions of hydrocarbons.

may trap the energy and dissipate it non-radiatively or the fluorescent impurity may be present in too high a concentration so that interaction between its molecules occurs and results in quenching effects.These processes have been considered by BOWEN *et coll.*[35] and later for solutions of fluorescent molecules in organic liquids by KALLMANN and FURST[49]. From measurements of absorption band areas the "life time" of the exciton process in anthracene crystals has been estimated to be about 10^{-8} secs and it does not seem to increase markedly the interval between absorption and re-radiation of energy. In a pure crystal the exciton is presumably trapped finally at mosaic boundaries, crystal flaws and surfaces.

Since, as we have seen, liquid solutions such as terphenyl in xylene have efficiencies for γ ray counting of the same order as for crystals, the luminescence being characteristic of the solute which is present in small concentration, we must assume a similar energy transfer process to that in crystals. In a comprehensive paper in 1950 KALLMANN and FURST[49] gave results of experiments on many different fluorescent solutions and also an extensive theoretical discussion. We shall attempt to give some of the relevant points from their paper. They find that the scintillation efficiency of pure solvents such as benzene, ether, hexane, paraffin, toluene and xylene is very small. This is because of the high probability of an excited molecule meeting an unexcited one and the consequent quenching of the emission (termed concentration quenching).

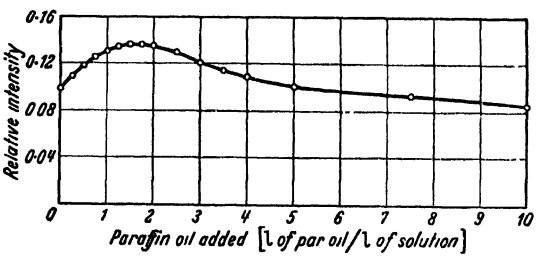


Fig. 35. Effect of adding paraffin oil to saturated solution of carbazole in xylene.

If impurity molecules are present then, as in the crystalline state, they may trap the energy before quenching can occur. Of course there is still the possibility of quenching due to collision of the excited solute molecule with a solvent molecule or another unexcited solute molecule (internal quenching). Quenching may also occur due to radiationless electron transitions from excited states of the solute molecule to its ground state. Another fact to be borne in mind in attempting a theoretical explanation of the solution characteristics is the effect of a second solvent or second solute constituent as described in Section 2. For example, dilution of solutions of carbazole or anthracene in xylene by adding a considerable amount of paraffin oil does not affect the light output under a given excitation to any extent (as shown by Fig. 35). It is possible that the action of the paraffin is to reduce the effective concentration of anthracene molecules and so reduce internal quenching due to their interaction. This reduction offsets the effect of diluting the xylene which would decrease the probability of resonance transfer from solvent to solute. Since with terphenyl the internal quenching is much smaller than with anthracene, the addition of paraffin to xylene solutions will have a deleterious effect on the counting efficiency.

The probability that solute molecules will trap excitons will depend on their concentration and so we would expect that for small concentrations the luminescence efficiency in the solute emission bands would increase proportionally with the solute concentration. This is found to be so in the case of liquid solutions. Interaction of solute molecules, and resultant quenching causes a saturation effect at higher concentrations as shown in Fig. 34.

(iv) *The response of organic materials to different exciting particles or radiation*

We have seen that organic crystals and liquids are far less efficient for detection of heavy particles than for electrons or γ rays. This difference can be given

a qualitative explanation in terms of the density of ionisation. Such particles as protons and alpha particles have relatively high specific ionisations when compared with beta particles of equivalent energy. The presence of ionised molecules in crystalline or liquid solutions will hinder the exciton transfer process between solvent and solute molecules. This deleterious effect will obviously depend on the density of ionization. An interesting investigation[70] referred to in Section 4 can be considered again here. If the differential light output dL/dE for heavy particles and for electrons (L is light output, E the particle energy) is plotted against the energy loss per unit path in the medium dE/dx (the latter is known for protons and for electrons) then for anthracene curves are obtained as in Fig. 36. These curves do not join when extrapolated,

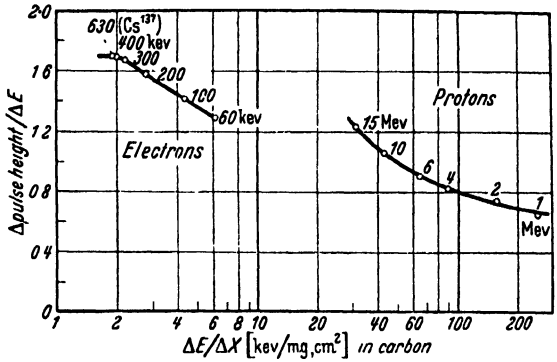


Fig 36 Differential light output obtained as a function of the differential energy loss. The electron and proton data were normalized to the light output caused by the 624-kev Cs^{137} electron.

which indicates that the ionisation density does not have a simple effect on the energy transfer process. An alternative and perhaps more fundamental treatment of results is to plot the specific luminescence dL/dx against dE/dx the specific energy loss. More exhaustive experiments are indicated in this respect on crystalline and liquid solutions. In the case of solutions of luminescent molecules in plastics similar transfer processes to the above must exist. Quenching by collision is not ruled out for solvent and solute molecules since there is still a great degree of freedom for molecules in these solids as shown by measurements of polarisation of fluorescence[115].

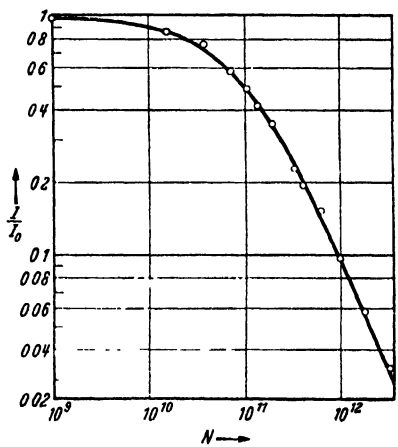


Fig. 37. Theoretical curve and experimental points for deterioration of anthracene crystal under particle bombardment. (I luminescence intensity at dosage of N particles; I_0 initial intensity.)

(v) *Deterioration processes in organic systems*

Particle or radiation bombardment of crystals or solutions will always cause some disruption of the constituent molecules and increase of disorder in the system, particular in crystals. These changes will decrease the counting efficiency since they will obstruct the energy transfer processes. So far no extensive quantitative investigations of deterioration of organic crystals have been made. Studies of the fall in luminescence of anthracene under prolonged

exposure to α-particles have been made recently by BIRKS[67] in Glasgow. His theoretical curve and experimental points for the fall in intensity with exposure is given in Fig. 37. The general form of this curve which is hyperbolic is explained as follows. If N alpha particles have bombarded the crystal by the time they have destroyed $q_0 - q$ molecules, q being the number undestroyed per cc, and q_0 the initial number per cc and each alpha particle has a probability α of destroying a molecule it encounters, then the relation between q and N is given by:

$$-\frac{dq}{dN} = \frac{\alpha q^2}{q_0}$$

which by integration gives

$$q = q_0(1 + \alpha N)^{-1}.$$

Since the scintillation intensity depends on the number of molecules still emitting it will decrease as q. This seems to be the case experimentally. Simultaneous study of the change in ultraviolet excited luminescence with particle dosage would have furnished valuable information from a theoretical viewpoint.

REFERENCES

[1] BLAU, M. and DREYFUSS, B.; *Rev. Sci. Instrum.* 16 (1945) 245.
[1a] CURRAN, S. C. and BAKER, W.; *Rad. Lab. Rep. Berkeley*, 7-6-16, Nov. 17, 1944.
[2] BROSER, I. and KALLMANN, H.; *Z. Naturforsch.* 2a (1947) 439.
[3] COLTMAN, J. W. and MARSHALL, F. H.; *Nucleonics* 1 (1947) 58.
[4] BROSER, I. and KALLMAN, H.; *Z. Naturforsch.* 28 (1947) 642.
[5] DEUTSCH, M.; M. I. T. report 1947.
[6] BELL, P. R.; *Phys. Rev.* 73 (1948) 1405.
[7] HOFSTADTER, R.; *Phys. Rev.* 74 (1948) 100, 628; *ibid* 75 (1949) 796.
[8] MCINTYRE, W. J.; *Phys. Rev.* 75 (1949) 1290.
[9] REYNOLDS, G. T. and SALVINI, G.; *Phys. Rev.* 78 (1950) 488.
[10] KOSKI, W. S.; *Phys. Rev.* 82 (1951) 317.
[11] JORDAN, W. H. and BELL, P. R.; *Nucleonics* 4 (1949) 30.
[12] PRINGLE, R. W.; *Nature, Lond.* 166 (1950) 11.
[13] HANLE, W.; *Naturwiss.* 38 (1951) 176.
[14] ZWORYKIN, V. K. and RAMBERG, E. G.; *Photoelectricity*, John Wiley, New York 1949.
[15] KROGER, F. A.; *Some aspects of the Luminescence of Solids*, Elsevier, Holland 1949.
[16] LEVERENZ, H. W.; *Luminescence of Solids*, John Wiley, New York 1950.
[17] PRINGSHEIM, P.; *Fluorescence and Phosphorescence*, Interscience Pub., New York 1949.
[18] GARLICK, G. F. J.; *Luminescent Materials*, Oxford, Univ. Press 1949.
[19] — *Cathodoluminescence*, Review in *Advances in Electronics, vol. II*, Academic Press Inc. (Publishers), New York 1950.
[20] LEVERENZ, H. W.; RCA Report. 25481 (Wash. 1946).
[21] BROSER, I., KALLMANN, H. and MARTINS, U. M.; *Z. Naturforsch.* 4a (1949) 204.
[22] LONGINI, R. L.; *Phys. Rev.* 75 (1949) 335.
[23] STUDER, F. J., CUSANO, D. A., and YOUNG, A. H.; *J. Opt. Soc. Amer.* 41 (1951) 559.
[24] REYNOLDS, D. C. and CZYZAK, S. J.; *Phys. Rev.* 79 (1950) 543.
[25] *Nucleonics* May (1950) 72.
[26] KALLMANN, H. and FURST, M.; *Phys. Rev.* 82 (1951) 964.
[27] MANDEVILLE, C. E. *et coll.*; *Phys. Rev.* 79 (1950) 1010; 80 (1950) 299, 300; 81 (1951) 163.
[28] FARMER, E. C., MOORE, H. B., and GOODMAN, C.; *Phys. Rev.* 76 (1949) 454.
[29] MCINTYRE, W. J.; *Phys. Rev.* 75 (1949) 1439.
[30] GARLICK, G. F. J. and FATEHALLY, R.; *Phys. Rev.* 75 (1949 1445.

[31] Moon, R. J.; *Phys. Rev.* 73 (1948) 1210.
[31a] *C. R. Acad. Sci. Paris* 233 (1951) 1023.
[32] Rall, W. and Wilkinson, R. G.; *Phys. Rev.* (1950) 77.
[33] Renwick, F. F. and Tasker, H. S.; Brit. Pat., 540, 252 (1940).
[34] Bowen, E. J. and Mikiewicz, E.; *Nature, Lond.* 159 (1947) 706.
[35] — – and Smith, F. W.; *Proc. Phys. Soc.* A. 62 (1949) 26.
[36] Birks, J. B.; *Proc. Phys. Soc.* A. 63 (1950) 1044.
[37] Teazel, C. E. and Smith, C. D.; *Rev. Sci. Instrum.* 19 (1948) 817.
[38] Koski, W. S. and Thomas, C. O.; *Phys. Rev.* 76 (1949) 308; 79 (1950) 217.
[39] Gittings, H. T. *et coll.*; *Phys. Rev.* 75 (1949) 205.
[40] Ravilious, C. F., Elliot, J. O. and Liebson, S. M.; *Phys. Rev.* 77 (1950) 851.
[41] Hofstadter, R., Liebson, S. H. and Elliot, J. O.; *Phys. Rev.* 78 (1950) 81.
[42] Lunby, A.; *Phys. Rev.* 81 (1951) 324.
[43] Post, R. F. and Shirer, N. S.; *Phys. Rev.* 78 (1950) 80.
[44] Hofstadter, R.; *Nucleonics* May (1950) 71.
[45] Schillinger, E. J., Waldman, B. and Miller, W. C.; *Phys. Rev.* 75 (1949) 900.
[46] Collinge, B. and Robbins, E. J.; *Nature, Lond.* 166 (1950) 1109.
[47] Reynolds, G. T. and Harrison, F. B.; *Phys. Rev.* 80 (1950) 129.
[48] Kallmann, H.; *Phys. Rev.* 78 (1950) 621.
[49] — and Furst, M.; *Phys. Rev.* 79 (1950) 857; 81 (1951) 853.
[50] Post, R. F.; *Phys. Rev.* 79 (1950) 735.
[51] Harrison, F. B. and Reynolds, G. T.; *Phys. Rev.* 79 (1950) 732.
[52] Schorr, M. G. and Torney, F. L.; *Phys. Rev.* 80 (1950) 474.
[53] - and Farmer, E. C.; *Phys. Rev.* 81 (1951) 891.
[54] Koski, W. S.; *Phys. Rev.* 82 (1951) 317.
[55] Pichat, L. and Koechlin, V.; *J. Chim. Phys.* 48 (1951) 225.
[56] Buckley, H. E.; *Crystal Growth*, John Wiley, New York 1951.
[57] Frerichs, R.; *Phys. Rev.* 72 (1947) 594.
[58] Kyropoulos, S.; *Z. anorg. Chem.* 154 (1926) 308; *Z. Phys.* 63 (1930) 849.
[59] Menzies, A. C. and Skinner, J.; *Faraday Soc. Disc.* (1949) 306.
[60] Stockbarger, D. C.; *Rev. Sci. Instr.* 7 (1936) 133; *Faraday Soc. Disc.* 294 (1949) 299.
[61] Verneuil, A.; *Compt. Rend.* 135 (1902) 791; *Ann. chim. phys.* 8 ser, 3 (1904) 20.
[62] Zerfoss, S., Johnson, L. R. and Imber, O.; *Rev. Sci. Instrum.* 21 (1950) 294.
[63] Stober, F.; *Z. Krist.* 61 (1925) 299.
[64] Kallmann, H.; *Research* 2 (1949) 62.
[65] Garlick, G. F. J. and Fatehally, R. A.; 75 (1949) 1446.
[66] Harding, G. N., Flowers, B. H., Eppstein, J. S.; *Nature, Lond.* 163 (1949–50) 990.
[67] Birks, J. B.; *Proc. Phys. Soc.* A. 63 (1950) 1294.
[68] Michaelis, E. G.; *Helv. Phys. Acta* 23 (1950) Sup. 3. 155.
[69] Franzen, W., Peelle, R. W. and Sherr, R.; *Phys. Rev.* 79 (1950) 742.
[70] Frey, H. B., Grim, W. M., Preston, W. M. and Gray, T. S.; *Phys. Rev.* 82 (1950) 372.
[71] Taylor, C. J., Remley, M. E., Jentschke, W. K. and Kruger, P. G.; *Phys. Rev.* 83 (1951) 169.
[72] Jentschke, W. K., Eby, F. S., Taylor, C. J., Remley, M. E. and Kruger, P. G.; *Phys. Rev.* 83 (1951) 170.
[73] West, H. I., Meyerhof, W. E. and Hofstadter, R.; *Phys. Rev.* 81 (1951) 141.
[74] Koller, L. R., and Alden, E. D.; *Phys. Rev.* 83 (1951) 684.
[75] Hopkins, J. I.; *Phys. Rev.* 79 (1950) 407; *Rev. Sci. Instr.* 22 (1951) 29.
[76] Harding, G. N.; *Nature, Lond.* 167 (1951) 437.
[77] Falk, C. E., Poss, H. L. and Yuan, L. C. L.; *Phys. Rev.* 83 (1951) 176.
[78] Moulton, W. G. and Sherwin, C. W.; *Rev. Sci. Instr.* 20 (1949) 766.
[79] Hofstadter, R. *et coll.*; *Phys. Rev.* 82 (1951) 749.
[80] Sun, K. H. and Shoupp, W. E.; *Rev. Sci. Instrum.* 21 (1950) 395.
[81] Frey, H. B.; *Rev. Sci. Instrum.* 21 (1950) 886.
[82] Neiler, J. H., Owen, G. E. and Allen, A. J.; *Phys. Rev.* 83 (1951) 242.
[83] Batchelor, R., Smith, J. W. and Blackmore, L.; *Nature, Lond.* 165 (1950) 688.

[84] MONTGOMERY, C. G. and MONTGOMERY, D. D.; *Phys. Rev.* 80 (1950) 757.
[85] ROSER, F. X. and BOWEN, TH; *Phys. Rev.* 82 (1951) 284.
[86] KRAUSHAAR, W. L., THOMAS, J. E. and HENRI, V. F.; *Phys. Rev.* 78 (1950) 486.
[87] REIFFEL, L., STONE, C. A. and REST, F. G.; *Phys. Rev.* 82 (1951) 121.
[88] NEY, E. P. and THON, D. M.; *Phys. Rev.* 81 (1951) 1068, 1069.
[89] BROSER, I. and KALLMANN, H.; *Ann. Phys. Lpz.* 4 (1948) 85.
[90] SEITZ, F. and MUELLER, D. W.; *Phys. Rev.* 78 (1950) 605.
[91] CAVANAGH, P. E.; *Phys. Rev.* 82 (1951) 791.
[92] HOFSTADTER, R. and MCINTYRE, J. A.; *Phys. Rev.* 78 (1950) 619.
[93] BELCHER, E. H.; *Nature, Lond.* 166 (1950) 826.
[94] PRINGLE, R. W. and STANDIL, S.; *Phys. Rev.* 80 (1950) 762.
[95] BELL, P. R.; *Science* 112 (1950) 7.
[96] SHURCLIFF, W. A. and JONES, R. C.; *J. Opt. Soc. Amer.* 39 (1949) 912.
[97] BELCHER, E. H.; *Nature, Lond.* 166 (1950) 742.
[98] HIPPEL, A. VON; *Z. Phys.* 101 (1936) 680.
[99] SEITZ, F.; *Trans. Faraday Soc.* 35 (1939) 74.
[100] BOWEN, E. J.; *Quart. Rev. Chem. Soc.* 1 (1947) 1.
[101] KRÖGER, F. A. and HELLINGMAN, J. E.; *Electrochem. Soc.* 93 (1948) 157; *ibid* 95 (1949) 68.
[102] SEITZ, F.; *J. Chem. Phys.* 6 (1938) 150.
[103] RANDALL, J. T.; *Trans. Faraday Soc.* 35 (1939) 2.
[104] BULL, C. B. and GARLICK, G. F. J.; *Proc. Phys. Soc.* A. 63 (1950) 1283.
[105] BLOCH, F.; *Z. Phys.* 52 (1928) 555.
[106] RECHL, N. and SCHON, M.; *Z. Phys.* 114 (1939) 682.
[107] JOHNSON, R. P.; *J. Opt. Soc. Amer.* 29 (1939) 387.
[108] SCHON, M.; *Z. Naturforsch.* 6a (1951) 251.
[109] KROGER, F. A. *et coll.*; *Physica* 14 (1948) 81.
[110] RANDALL, J. T. and WILKINS, M. H. F.; *Proc. Roy. Soc.* A. 184 (1945) 366.
[111] *Luminescent Materials* (a symposium). John Wiley, New York 1948.
[112] SEITZ, F.; *Discuss. Faraday Soc.* No. 5 (1949) 271.
[113] BROSER, I. and WARMINSKY, R.; *Z. Naturforsch.* 6a (1951) 85.
[114] WAWILOV, S.; *Z. Phys.* 22 (1924) 266.
[115] PRINGSHEIM, P. and VOGELS, H.; *J. Phys. et le Rad.* 8 (1937) 121.

THE NEUTRON-PROTON INTERACTION

G. L. Squires

I. Introduction 89
II. Effective range theory 91
III. Neutron-proton scattering 99
IV. Photo-disintegration of the deuteron 105
V. Comparison of the proton-proton and neutron-proton forces 114
VI. High energy data and tensor forces 116
VII. Summary 117

I. Introduction

Our knowledge of the neutron-proton interaction comes in the main from two sources, the scattering of neutrons by protons and the properties of the deuteron.

For neutron-proton scattering at energies below about 4 Mev, the de Broglie wavelength, λ, of the centre of mass motion, is large compared to the range of the nuclear forces. Hence the nuclear interaction is effective only for states of zero orbital angular momentum, the S states. Experimentally it is observed that the states of higher orbital angular momentum remain undisturbed up to about 10 Mev.

The effect of the nuclear forces is to shift the phase of the asymptotic form of the S wave. The scattering cross-section in the centre of mass system is given by

$$\sigma = \frac{4\pi}{k^2} \sin^2 \delta \qquad (1)$$

where δ is the phase shift and $k = 2\pi/\lambda$.

δ is a function of E, the energy of the incident neutron. The precise nature of the function depends on the detailed form of the interaction potential i.e. on its shape, range and depth. Thus a possible method of analysing the low energy (below 10 Mev) scattering data is to assume an explicit potential, compute the theoretical cross-sections and compare them with the experimental values. Such a comparison involves much computation and it turns out that the present experimental results are not sufficiently accurate to distinguish between such differently shaped potentials as the square well and the Yukawa well.

In view of this it has long been felt that a less detailed theoretical approach might be more profitable. Breit and his collaborators[1] showed, in the case of proton-proton scattering, that two parameters only are determined by the low energy data. Therefore since all the wells usually assumed may be specified by two parameters—width and depth, say—any reasonably shaped potential can, by suitably choosing its width and depth, be made

to give the observed cross-sections. Without using a specific interaction potential, LANDAU and SMORODINSKY[2] gave a semi-empirical formula for the phase shift as a function of energy for p–p and n–p scattering. Later, SCHWINGER[3] using a variational method obtained their results rigorously.

The present paper gives an account of this theory which is sometimes known as the effective range theory. We do not adopt SCHWINGER's approach but instead follow BETHE[4] who has obtained SCHWINGER's results by simpler methods.

In the effective range theory the relation between the phase shift and the energy is expressed as an expansion of the quantity $k \cot \delta$ in terms of k^2 i.e. in terms of the energy since this is proportional to k^2.

$$k \cot \delta = -\frac{1}{a} + \frac{1}{2} r_0 k^2 - T k^4 + \cdots . \tag{2}$$

The merit of this expansion lies in the fact that for energies below 10 Mev the term in k^4 and higher order terms are negligible, and so the relation between δ and k is determined by two parameters, a and r_0. It can be seen that both quantities have the dimensions of length. a is known as the scattering length and r_0 as the effective range.

The approximate relation

$$k \cot \delta = -\frac{1}{a} + \frac{1}{2} r_0 k^2 \tag{3}$$

is known as the shape-independent formula.

Any potential well that is specified by two parameters and that satisfies one very mild condition can be made to give the observed values of a and r_0. The condition is that the well must be such that the value of T and the coefficients of higher order terms in k^2 are small. This restriction precludes well shapes with very long tails but these are in any case ruled out by WIGNER's original argument based on the binding energies of H^2, H^3 and He^4.

For any particular well shape we can choose its width and depth—these terms will be defined precisely later—to give the observed values of a and r_0. The value of T, which depends upon the shape of the well, can then be calculated. It might therefore be thought that measurements made at higher energies when the $T k^4$ term becomes appreciable would distinguish between different well shapes. However, this is not so because from 15–25 Mev the S wave shift is almost 90° i.e. $\cot \delta \approx 0$. The cross-section is given in general by

$$\sigma = \frac{4\pi}{k^2} \sin^2 \delta = \frac{4\pi}{k^2 + k^2 \cot^2 \delta}$$

and when $\cot \delta \approx 0$, the $k^2 \cot^2 \delta$ term, which contains the shape dependent parameter, is small compared with the k^2 term. In this energy range measurements of the scattering cross-section just give the wavelength of the neutron. At higher energies the scattering becomes very complicated. Scattering for waves other than S waves begins to occur and effects due to tensor forces become appreciable.

We see then that we are restricted to energies below about 15 Mev, and within this range, unless the cross-sections and energies are measured very accurately, no information on potential shape can be obtained.

The neutron-proton system has two S states corresponding to spin one (triplet interaction) and spin zero (singlet interaction). The scattering cross-section is therefore given by

$$\sigma_n = \frac{4\pi}{k^2}\left(\frac{3}{4}\sin^2\delta_t + \frac{1}{4}\sin^2\delta_s\right) \tag{4}$$

where δ_t and δ_s are the respective phase shifts of the triplet and singlet states. Both δ_t and δ_s may be written in the form of (2), each with its own set of coefficients.

The values of a_t and a_s are obtained from very low energy (less than 10 ev) scattering experiments. At such energies the k^2 term in (2) is negligible. The binding energy of the deuteron together with a_t gives r_{0t} for, as we show later, the three quantities are simply related.

There is no bound state of the deuteron with spin zero; hence r_{0s} cannot be obtained in the same way. It can, however, be found by measuring σ_n. Eqns. (3) and (4) show that σ_n is a known function of a_t, a_s, r_{0t} and r_{0s}. Thus since a_t, a_s and r_{0t} are known, r_{0s} may be calculated.

BETHE and LONGMIRE[5] have applied the effective range theory to the photodisintegration of the deuteron. An account of their analysis is given in Sect. IV. It is shown that the photoelectric disintegration of the deuteron provides another means of estimating r_{0t}, while the capture of slow neutrons by protons—the process inverse to photodisintegration—gives another value for r_{0s}.

A brief account of low energy proton-proton scattering is given in Sect. V. The effective range and scattering length of the p–p potential are compared with the corresponding quantities in the n–p singlet interaction. (The PAULI exclusion principle precludes a triplet interaction for protons in the S state.)

Tensor forces have been ignored throughout Sect. II to V which deal only with low energy data. A summary of the results of high energy scattering experiments is given in Sect. VI, together with an indication of how tensor forces modify the results obtained in the previous sections.

In presenting the effective range theory in this article the author has drawn largely upon the papers of BETHE[4], BETHE and LONGMIRE[5], and BLATT and JACKSON[6]. The reader is referred to these papers for more detailed arguments and calculations.

II. EFFECTIVE RANGE THEORY

1. *Definition of scattering length, a, and effective range, r_0*

Consider a neutron and a proton interacting under the influence of a spherically symmetric potential $U(r)$.

We employ the following notation.

E_1 = energy of the neutron in the laboratory system. In this system the proton is at rest and the neutron moves with velocity v_1.

M = mass of proton = mass of neutron
μ = reduced mass of the system = $M/2$
k_1 = wave number of the motion in the centre of mass system
$= \frac{\mu v_1}{\hbar} = \frac{2\pi}{\lambda_1}$
$V(r) = \frac{M}{\hbar^2} U(r)$.

The wave equation of the motion in the centre of mass system is

$$\nabla^2 f_1 + k_1^2 f_1 - V f_1 = 0. \tag{5}$$

f_1 can be expanded in terms of LEGENDRE polynomials[7].

$$f_1 = \sum_{l=0}^{l=\infty} \frac{u_1^{(l)}(r)}{r} P^{(l)}(\cos\theta) \tag{6}$$

where $u_1^{(0)}$ satisfies

$$\frac{d^2 u_1}{dr^2} + k_1^2 u_1 - V u_1 = 0. \tag{7}$$

We have dropped the superscript (0) that shows u_1 is an S wave function, because all the scattering that we deal with in this paper is due to S waves. The subscript will be used to distinguish different energies.

For a second energy, E_2,

$$u_2'' + k_2^2 u_2 - V u_2 = 0. \tag{8}$$

Multiply (7) by u_2 and (8) by u_1. Subtract and integrate. This gives

$$\left[u_2 u_1' - u_1 u_2'\right]_0^R = (k_2^2 - k_1^2) \int_0^R u_1 u_2 \, dr \tag{9}$$

where R is arbitrary.

We now introduce a function ψ_1 which represents the asymptotic behaviour of u_1 outside the range of the nuclear forces. This function satisfies (7) with V put equal to zero and may be written in the form

$$\psi_1 = \frac{\sin(k_1 r + \delta_1)}{\sin\delta_1}. \tag{10}$$

It is convenient to normalise ψ_1 so that it equals unity at $r = 0$ — hence the factor $1/\sin\delta_1$. The normalisation of ψ_1 determines that of u_1 since u_1 tends to ψ_1 at large r. δ_1 is the phase shift of the S wave at energy E_1, relative to the corresponding wave when V is everywhere zero.

ψ_1 and ψ_2 satisfy

$$\left[\psi_2 \psi_1' - \psi_1 \psi_2'\right]_0^R = (k_2^2 - k_1^2) \int_0^R \psi_1 \psi_2 \, dr. \tag{11}$$

Subtract (9) from (11) and let R be large compared with the range of $V(r)$.

Consider the left hand side. At the upper limit R, $u_1 = \psi_1$ and $u_2 = \psi_2$ and therefore the contribution at this limit is zero. At the lower limit $u_1 = u_2 = 0$ for otherwise the wave functions f_1 and f_2 would be infinite at the origin.

On the right hand side the upper limit of integration may be extended to infinity, again because $u = \psi$ for large r.

We thus have

$$(\psi_1 \psi_2' - \psi_2 \psi_1')_{r=0} = (k_2^2 - k_1^2) \int_0^\infty (\psi_1 \psi_2 - u_1 u_2)\, dr \tag{12}$$

which with the aid of (10) becomes

$$k_2 \cot \delta_2 - k_1 \cot \delta_1 = (k_2^2 - k_1^2) \int_0^\infty (\psi_1 \psi_2 - u_1 u_2)\, dr\,. \tag{13}$$

We define a function ϱ of the energies E_1, E_2 by

$$\varrho(E_1 E_2) = 2 \int_0^\infty (\psi_1 \psi_2 - u_1 u_2)\, dr\,. \tag{14}$$

As k tends to zero, $k \cot \delta$ tends to a constant which is denoted by $-\alpha$. Putting $k_1 = 0$ in (13) and dropping the subscript 2, we have

$$k \cot \delta = -\alpha + \tfrac{1}{2} k^2 \varrho(0, E)\,. \tag{15}$$

This relation is exact.

Consider the integral $\int_0^\infty (\psi_1 \psi_2 - u_1 u_2)\, dr$. The integrand will be different from zero only within the range of the nuclear forces, but within this range $k^2 \ll V$ and the functions u and ψ are thus only slightly dependent on energy. Therefore $\varrho(0, E)$ is approximately equal to $\varrho(0, 0)$.

The quantity $\varrho(0, 0)$ is a constant of the potential and is independent of the energy of the system. It is denoted by r_0 and known as the effective range, a rather misleading name because, as we shall see later, r_0 depends not only on the range but also on the depth of the potential.

$$\varrho(0, 0) = r_0 = 2 \int_0^\infty (\psi_0^2 - u_0^2)\, dr\,. \tag{16}$$

We show later that

$$\varrho(0, E) - r_0 = 0(k^2 r_0^3)\,. \tag{17}$$

(15) may therefore be rewritten

$$k \cot \delta = -\alpha + \tfrac{1}{2} r_0 k^2 + 0(k^4)\,. \tag{18}$$

The reciprocal of α is denoted by a and, like ϱ, has the dimensions of length. It is identical with the FERMI scattering length[8] as we now show.

FERMI originally defined his scattering length, a_F, in the following way. Consider a uniform beam of slow neutrons being scattered by a nucleus at the origin. Since only the S wave is disturbed the scattered wave is spherically symmetrical and at large distances from the nucleus the wave function may be written $e^{ikz} - \frac{a_F}{r} e^{ikr}$. The first term represents the incident wave and the second the scattered wave. The scattering cross-section is given by

$$\sigma = 4\pi a_F^2\,. \tag{19}$$

But σ is also given by

$$\sigma = \frac{4\pi}{k^2}\sin^2\delta = \frac{4\pi}{k^2 + k^2\cot^2\delta}. \tag{20}$$

At zero energy $k\cot\delta = -\alpha = -\frac{1}{a}$ and we have

$$\sigma = 4\pi a^2. \tag{21}$$

Thus a and a_F are equal numerically. The equality of sign follows from equation (10) with $k = 0$.

2. *Definition of intrinsic range and well-depth parameter*

Let $U(r)$ be any arbitrary potential function.

All potentials of the form $\eta V(r/\xi)$, where η and ξ are independent of r, are said to have the same shape. η is a measure of the depth of the well and ξ is a measure of its range.

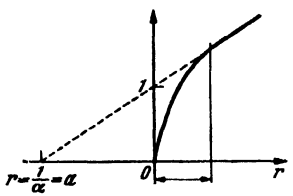


Fig. 1.

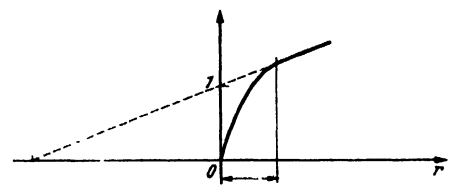


Fig. 2.

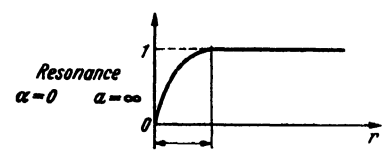


Fig. 3.

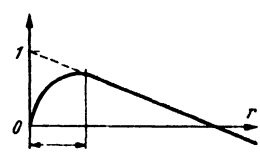


Fig. 4.

Fig. 1–4. Zero energy wave functions. u_0 ——; ψ_0 - - -, Range of forces indicated by ←→.

It has been pointed out that the effective range depends on both the depth and range of the potential. It is therefore convenient to define a new range parameter, known as the intrinsic range, which is independent of the depth of the well.

Consider the neutron-proton system at zero energy. When k is zero (10) becomes

$$\psi_0 = 1 + kr\cot\delta = 1 - \alpha r. \tag{22}$$

Thus ψ_0 is a straight line intercepting the r axis at $r = 1/\alpha = a$.

Fig. 1 shows u_0 and ψ_0 for a given potential $U(r)$. In the case illustrated α is negative. Now let us multiply U by a constant $\eta > 1$. Within the range of the nuclear forces the curvature of u_0 will increase and thus α will increase algebraically (Fig. 2). If we steadily increase η, α will continue to increase, pass through zero (Fig. 3), and become positive (Fig. 4).

Denote the potential for which α is zero by $U^{(R)}(r)$ and the corresponding u_0 by $u_0^{(R)}$. $\psi_0^{(R)} = 1$. $U^{(R)}$ is known as a resonance potential because the scattering cross-section for zero energy neutrons, given in general by

$$\sigma = \frac{4\pi}{\alpha^2},$$

is infinite for this potential.

The intrinsic range of the original potential is defined to be the effective range of $U^{(R)}(r)$. It is denoted by b. Thus

$$r_0^{(R)} \equiv b = 2\int_0^\infty [1 - (u_0^{(R)})^2]\, dr. \tag{23}$$

It is clear from this definition of b that all potentials of the form

$$\text{constant} \times U(r)$$

have the same intrinsic range.

There is an infinite set of values of η for which α is zero. $U^{(R)}$ is obtained from the lowest value. The wave functions for the next lowest value are shown in Fig. 5.

The quantity s, given by

$$U(r) = s\, U^{(R)}(r), \tag{24}$$

is known as the well depth parameter

Further insight into the significance of the resonance potential may be obtained by considering the wave functions of the system for energies other than zero.

When the energy is small and positive, ψ behaves as a sine function of long wavelength. For all positive values of the energy, ψ can be fitted smoothly to u whatever the value of s.

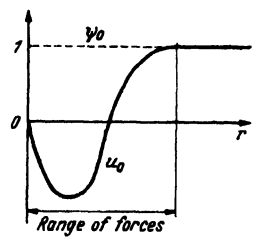


Fig 5. Zero energy wave functions at second resonance. u_0 ——; ψ_0 – –.

For negative energies ψ is a function of the form $e^{-\gamma r}$ and thus has a negative slope. If the potential is deeper than the resonance potential ($s > 1$, $\alpha > 0$), ψ can be fitted smoothly to u for one value of γ only. But it can be seen from Figs. 1–3 that whatever the value of γ, no fit is possible when $s \lesssim 1$ ($\alpha \lesssim 0$).

To sum up

$U > U^{(R)}$	$s > 1$	$a > 0$	$\delta_0 = \pi$	One bound state occurs
$U < U^{(R)}$	$s < 1$	$a < 0$	$\delta_0 = 0$	No bound state possible

It has been assumed that s is not sufficiently large for u to possess nodes within the range of the potential. This is correct for neutron-proton scattering but may not be so when neutrons interact with complex nuclei. In such cases more than one bound state may be possible and, even though s is greater than unity, a may be negative.

3. *Analytic form of potentials*

The four well shapes most commonly assumed in the theory of the neutron-proton interaction are

(1) Square well

$$\left.\begin{aligned} -U &= W_S \qquad r < l_S \\ &= 0 \qquad r > l_S \end{aligned}\right\} \tag{25 S}$$

(2) Gaussian well

$$-U = W_G \exp\left(-\frac{r^2}{l_G^2}\right) \tag{25 G}$$

(3) Exponential well

$$-U = W_E \exp\left(-\frac{r}{l_E}\right) \tag{25 E}$$

(4) YUKAWA well

$$-U = \frac{l_Y W_Y}{r} \exp\left(-\frac{r}{l_Y}\right). \tag{25 Y}$$

It may be pointed out that of these four potentials the YUKAWA well is the only one that has a theoretical basis. The other three are chosen for mathematical convenience.

The length l_Y, in the YUKAWA well, is related to the meson mass, μ_t, by[9]

$$\mu_t = \frac{\hbar}{c\, l_Y}$$

i.e.

$$\frac{\text{mass of meson}}{\text{mass of electron}} = \frac{\lambda_{\text{Compton}}}{l_Y}. \tag{26}$$

BLATT and JACKSON[6] have given figures relating b and l for these four wells. They are

Square

$$b = l_S \tag{27 S}$$

Gaussian

$$b = 1{\cdot}4355\, l_G \tag{27 G}$$

Exponential

$$b = 3{\cdot}5412\, l_E \tag{27 E}$$

YUKAWA

$$b = 2{\cdot}1196\, l_Y. \tag{27 Y}$$

We can readily show that $b = l_S$ for the square well, for when $k = 0$ equation (7) becomes

$$u'' + \frac{M}{\hbar^2} W_S u = 0 \qquad r < l_S, \tag{28}$$

the permissible solution of which is

$$u = \sin \sqrt{M W_S}\, \frac{r}{\hbar}. \tag{29}$$

When $W_S = W_S^{(R)}$, its value at resonance, the slope of u at $r = l_S$ is zero. Therefore

$$W_S^{(R)} = \frac{1}{M}\left(\frac{\pi\hbar}{2 l_S}\right)^2$$

and

$$b = 2\int_0^\infty \left[1 - (u^{(R)})^2\right] dr = l_S.$$

4. *Relation between α, r_0, s and b*

We write

$$u_0(r) = \psi_0(r) - g(r) = 1 - \alpha r - g(r). \tag{30}$$

Fig. 3 shows that $g^{(R)}(r)$ is never negative. Then

$$r_0 = 2\int_0^\infty (\psi_0^2 - u_0^2)\,dr = 2\int_0^\infty (2g - g^2 - 2\alpha r g)\,dr. \tag{31}$$

Let us start with a potential which has $s = 1\,(\alpha = 0)$

$$r_0 = b = 2\int_0^\infty (2g^{(R)} - [g^{(R)}]^2)\,dr. \tag{32}$$

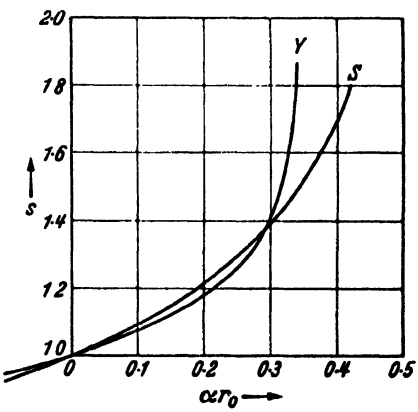


Fig. 6. s vs. αr_0 plotted from the formulae given in Table 5 of BLATT and JACKSON[6]. The curves for the Gaussian and exponential potentials have been omitted to avoid confusion

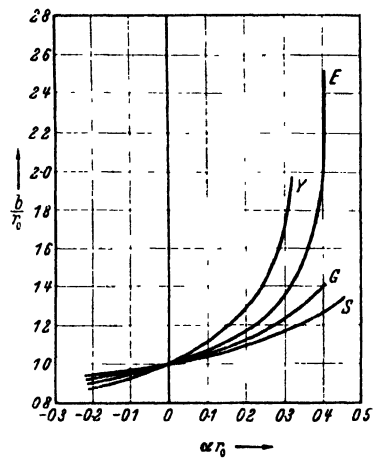


Fig. 7. $\frac{b}{r_0}$ vs. αr_0 from Fig 6 of BLATT and JACKSON[6]. S = Square, G = Gaussian, E = Exponential; Y = YUKAWA.

Increase s. α becomes positive but to a first approximation g does not change from $g^{(R)}$. Therefore

$$r_0 \approx b - 4\alpha\int_0^\infty r g^{(R)}(r)\,dr. \tag{33}$$

Thus the effective range decreases as the well depth increases. The longer the tail of the well, the farther does $g^{(R)}$ extend and since $g^{(R)}$ is multiplied by r in the integral, bigger values of r are weighted more heavily. Therefore for two wells with the same intrinsic range and (positive) scattering length, the effective range will be smaller for the one with the longer tail.

BLATT and JACKSON[6] give curves and formulae relating α and r_0 with s and b. Figs. 6 and 7 show s and b/r_0 as functions of (αr_0).

It must be emphasized that b is never observed directly, and so the fact that the relation between b and r_0 depends on the potential shape does not help to select any particular shape. The quantities given by experiment are α and r_0. A potential shape is then selected and the values of b and s which the observed values of α and r_0 imply for that shape, are obtained from curves or formulae.

5. *Variation of* $\varrho(0, E)$ *with* E

The variation of $\varrho(0, E)$ with energy provides the terms of order k^4 and higher in (18). We do not consider this variation in detail but merely give BETHE's argument showing that the k^4 term in (2) is small.

Expand ψ in terms of k. From (10)

$$\left.\begin{aligned}\psi &= \cos kr + \cot\delta \sin kr \\ &= 1 - \tfrac{1}{2}k^2r^2 + rk\cot\delta - \tfrac{1}{6}r^3k^3\cot\delta + 0\,(k^4r^4).\end{aligned}\right\} \tag{34}$$

Insert for $k\cot\delta$ the expression given in (3)

$$\psi = 1 - \alpha r + \tfrac{1}{2}k^2 r(r_0 - r) + \tfrac{1}{6}k^2\alpha r^3 + 0\,(k^4r^4). \tag{35}$$

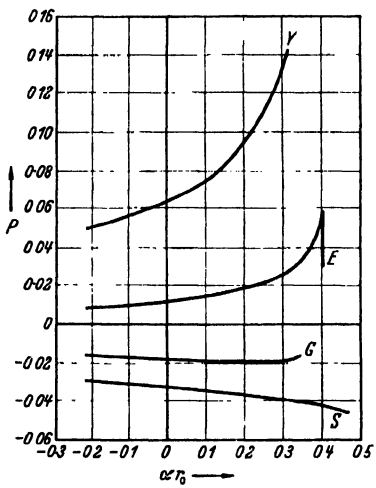


Fig. 8. P vs. αr_0 from Fig. 10 of BLATT and JACKSON[6].

It is convenient to write ψ in the form

$$\psi = \psi_0 + k^2\chi_1 + k^4\chi_2 + \cdots. \tag{36}$$

Then

$$\chi_1 = \tfrac{1}{2}r(r_0 - r) + \tfrac{1}{6}\alpha r^3. \tag{37}$$

This function is zero at $r = 0$ and again at a value of r which, if $\frac{1}{3}\alpha r_0 \ll 1$, is close to r_0. For values of r of the order of r_0 i.e. within the range of the nuclear forces, χ_1 is small and is some small fraction of r_0^2.

By analogy with (36) we write

$$u = u_0 + k^2 v_1 + k^4 v_2 + \cdots. \tag{38}$$

Then

$$\left.\begin{aligned}&\tfrac{1}{2}\varrho(0, E) - \tfrac{1}{2}\varrho(0, 0) \\ &\quad = \int_0^\infty [\psi_0(\psi - \psi_0) - u_0(u - u_0)]\,dr\end{aligned}\right\} \tag{39}$$

$$= k^2\int_0^\infty (\psi_0\chi_1 - u_0 v_1)\,dr + 0(k^4). \tag{40}$$

v_1, like χ_1, is small within the range of the nuclear forces for it is zero at $r = 0$ and must approach χ_1 when the nuclear forces become negligible. Outside the range of the nuclear forces the integrand is zero. Therefore the integral in (40) is small compared to r_0^3.

From (2) (15) and (40)

$$\int_0^\infty (\psi_0\chi_1 - u_0 v_1)\,dr = T. \tag{41}$$

BLATT and JACKSON, setting

$$T \equiv Pr_0^3, \tag{42}$$

have calculated P for various potentials. Their graphs showing the relation between P and αr_0 are reproduced in Fig. 8.

Neglecting terms $0(k^4)$ in (40), we have

$$\varrho(0, E) = r_0 - 2Pr_0^3k^2 \tag{43}$$

which may be generalised with the aid of (14) and (15) to

$$\varrho(E_1E_2) = r_0 - 2Pr_0^3(k_1^2 + k_2^2). \tag{44}$$

6. *The binding energy of the deuteron*

The deuteron binding energy, ε, gives a useful relation between the triplet scattering length a_t and the triplet range function $\varrho_t(0, -\varepsilon)$

Consider eq. (12) when $E_1 = 0$ and $E_2 = -\varepsilon$. The functions u_2 and ψ_2 become u_0 and ψ_0 corresponding to the ground state of the deuteron.

where γ is defined by

$$\psi_0 = e^{-\gamma r} \tag{45}$$

$$\varepsilon = \frac{\hbar^2 \gamma^2}{M} . \tag{46}$$

$$\psi_2'(0) = -\gamma \quad \text{and} \quad k_2^2 = -\gamma^2 .$$

Therefore eq. (12) becomes

$$-\gamma + \alpha_t = -\gamma^2 \int_0^\infty (\psi_0 \psi_0 - u_0 u_0)\, dr$$

$$\frac{1}{a_t} = \gamma - \frac{1}{2}\gamma^2 \varrho_t(0, -\varepsilon) \tag{47}$$

$$\approx \gamma - \frac{1}{2}\gamma^2 r_{0t} . \tag{48}$$

The function $\varrho_t(0, -\varepsilon)$ will be denoted simply by ϱ_t.

ε is known with great accuracy. The value adopted in this paper is that obtained by MOBLEY and LAUBENSTEIN[10]. They determined the threshold energy for photodisintegration using X-rays from an electrostatic generator and found

$$\left.\begin{aligned} \varepsilon &= 2{\cdot}226\,(1 + \varepsilon_1)\,\text{Mev} \\ \varepsilon_1 &= \pm\, 0{\cdot}0015 . \end{aligned}\right\} \tag{49}$$

This value agrees well with other accurate measurements of ε. BELL and ELLIOT[11] measured the energy of the γ rays emitted in the capture of slow neutrons by protons and found

$$\varepsilon = (2{\cdot}230 \pm 0{\cdot}007)\ \text{Mev} .$$

A third estimate is provided by mass determinations. The results[12, 13]

$$n - H = (0{\cdot}782 \pm 0{\cdot}002)\ \text{Mev}$$

$$2H - D = (1{\cdot}442 \pm 0{\cdot}005)\ \text{Mev}$$

give

$$\varepsilon = (2{\cdot}224 \pm 0{\cdot}006)\ \text{Mev} .$$

The value of γ obtained from (49) is

$$\gamma = (2{\cdot}317 + 1{\cdot}16\,\varepsilon_1) \times 10^{12}\ \text{cm}^{-1} . \tag{50}$$

III. NEUTRON-PROTON SCATTERING

1. *Measurement of a_t and a_s*

(a) *Free proton cross-section*

For slow neutrons the k^2 term in (3) may be neglected and the scattering cross-section is given by

$$\sigma_f = 3\pi a_t^2 + \pi a_s^2 . \tag{51}$$

σ_f, known as the free proton cross-section, is measured by scattering neutrons in hydrogen or a hydrogen compound, at energies sufficiently low for the k^2 term in (3) to be negligible but sufficiently high for the scattering protons to be effectively free. The most accurate measurement that has so far been made is that of MELKONIAN[14] who used neutrons in the energy range 0·8 to 15 ev. He obtained a value

$$\left.\begin{aligned} \sigma_f &= 20{\cdot}36\,(1+\varepsilon_2)\text{ barns} \\ \varepsilon_2 &= \pm\,0{\cdot}005\,. \end{aligned}\right\} \tag{52}$$

(b) *Coherent scattering amplitude*

The quantity

$$f = 2\,(\tfrac{3}{4}\,a_t + \tfrac{1}{4}\,a_s)$$

is called the coherent scattering amplitude. In order to measure f, neutrons of thermal and subthermal energies must be used. The DE BROGLIE wavelength of such neutrons is of the order of interatomic distances. Interference effects may thus be observed and these permit a determination of the coherent scattering amplitude[8].

Three different experiments have been devised to measure f. The most accurate appears to be that of HUGHES, BURGY and RINGO[15]. They reflected neutrons from a liquid hydrocarbon mirror and measured the angle of total reflection. This gives the refractive index of the hydrocarbon which in turn gives the mean scattering length of the nuclei in the mirror. The carbon scattering length is known from other experiments. Thus f may be calculated. The value obtained is

$$\left.\begin{aligned} f &= -\,3{\cdot}78\,(1+\varepsilon_3)\times 10^{-13}\text{ cm} \\ \varepsilon_3 &= \pm\,0{\cdot}005\,. \end{aligned}\right\} \tag{53}$$

The scattering of slow neutrons by parahydrogen also gives a value for f. The theory shows that the elastic cross-section for a parahydrogen molecule in its ground state is given by

$$\sigma_{\text{para}} = k_{00}\,(3\,a_t + a_s)^2 \tag{54}$$

where k_{00} is a numerical coefficient that depends on the temperature of the hydrogen and the energy of the neutrons. SUTTON *et al.*[16] have measured f in this way and find

$$f = -\,(3{\cdot}95 \pm 0{\cdot}15)\times 10^{-13}\text{ cm}\,.$$

A serious drawback to this experiment arises from the fact that the scattering cross-section of orthohydrogen is about 30 times that of parahydrogen. Thus the presence of a small unknown quantity of orthohydrogen will considerably increase the apparent value of σ_{para}. The experiment is being repeated by SQUIRES and STEWART[17]. Preliminary measurements indicate $f = -\,(3{\cdot}73 \pm 0{\cdot}06)\times 10^{-13}$ cm.

A third estimate of f is provided by the experiments of SHULL *et al.*[18]. By measuring the neutron diffraction patterns of sodium hydride crystals, they find

$$f = -\,(3{\cdot}96 \pm 0{\cdot}2)\times 10^{-13}\text{ cm}\,.$$

In view of the large experimental errors, the agreement between the results of SUTTON and SHULL must be considered fortuitous. HUGHES' value of f is used in calculations in this article.

From (52) and (53) we obtain

$$a_t = (0{\cdot}538 + 0{\cdot}37\,\varepsilon_2 - 0{\cdot}21\,\varepsilon_3) \times 10^{-12}\,\text{cm} \tag{55}$$

$$a_s = -(2{\cdot}369 + 1{\cdot}11\,\varepsilon_2 + 0{\cdot}14\,\varepsilon_3) \times 10^{-12}\,\text{cm}. \tag{56}$$

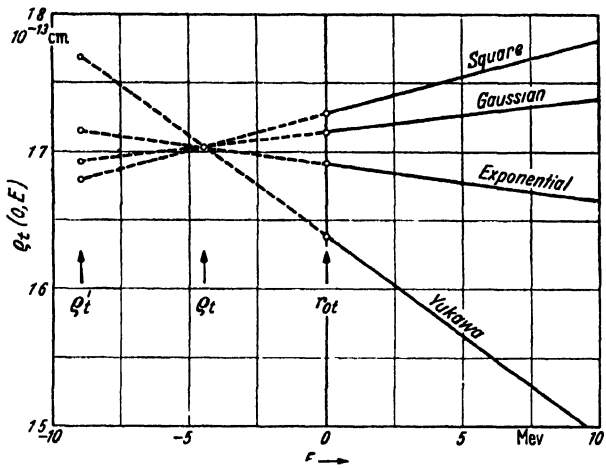


Fig. 9. $\varrho_t(0, E)$ vs E. The lines are based on the values of a_t and ϱ_t given in eqns. (55) and (57) respectively.

2. *Determination of the triplet effective range*

Inserting the experimental values of γ (50) and a_t (55) in eq. (47) we find

$$\varrho_t = (1{\cdot}704 + 2{\cdot}6\,\varepsilon_1 + 4{\cdot}83\,\varepsilon_2 - 2{\cdot}68\,\varepsilon_3) \times 10^{-13}\,\text{cm}. \tag{57}$$

The error in ϱ_t is

$0{\cdot}004 \times 10^{-13}$ cm from the deuteron binding energy

$0{\cdot}024 \times 10^{-13}$ cm from the free proton cross-section

$0{\cdot}015 \times 10^{-13}$ cm from the coherent scattering amplitude.

As these errors are independent the total error in ϱ_t is $0{\cdot}03 \times 10^{-13}$ cm or 1·7%.

Starting from ϱ_t we can calculate r_{0t}, the triplet effective range. If we employ what may be termed simple effective range theory, and neglect terms in k^4 and of higher order in eq. (15), r_{0t} is equal to ϱ_t. If however the term in k^4 is retained we have from (43)

$$\varrho_t = r_{0t} + 2\gamma^2 P r_0^3. \tag{58}$$

P can be obtained from Fig. 8. Although P is given as a function of r_0 and not of ϱ_t in this figure, an iterative method rapidly gives an accurate value for P and r_{0t}, Knowing r_{0t} and a_t, we can obtain s and b at once from Figs. 6 and 7. The results are given in Table 1.

Table 1—Parameters of the triplet potential implied by $\varrho_t \equiv \varrho_t(0, -\varepsilon) = 1{\cdot}704 \times 10^{-13}$ *cm and* $a_t = 5{\cdot}38 \times 10^{-13}$ *cm*

Potential shape	P	r_{0t} in 10^{-13} cm	ϱ'_t in 10^{-13} cm	s	b in 10^{-13} cm	W in Mev (see eq. (25))	l in 10^{-13} cm (see eq. (25))
Square	−0 040	1 726	1·682	1 44	2 04	35·3	2 04
Gaussian	−0 018	1·713	1 694	1 43	2 15	70 9	1 50
Exponential	+0 030	1 688	1 719	1·42	2 35	193 0	0·66
YUKAWA	+0·138	1 638	1·768	1 42	2 91	52 3	1 38

The value of the intrinsic range, b, for the YUKAWA well gives for the meson mass

$$\mu_t = (281 \pm 10)\, m_e \tag{59}$$

where m_e is the mass of the electron. This may be compared with the experimental value for the mass of the π meson, $(276 \pm 2)\, m_e$[19].

Eq. (43) is plotted in Fig. 9 for the four potential shapes, using the values of P and r_{0t} given in Table 1.

3. *n–p scattering at energies up to 6 Mev*

From eqs. (4) and (15) we have the exact relations

$$\sigma_n = \frac{3}{4}\sigma_t + \frac{1}{4}\sigma_s \tag{61}$$

$$\sigma_t = 4\pi\left\{k^2 + \left[-\frac{1}{a_t} + \frac{1}{2}k^2\varrho_t(0, E)\right]^2\right\}^{-1} \tag{62}$$

$$\sigma_s = 4\pi\left\{k^2 + \left[-\frac{1}{a_s} + \frac{1}{2}k^2\varrho_s(0, E)\right]^2\right\}^{-1} = 4\pi\,(k^2 + k^2\cot^2\delta_s)^{-1}. \tag{63}$$

σ_t and σ_s are the triplet and singlet scattering cross-sections.

If we neglect terms in k^4, (62) becomes

$$\sigma_t = 4\pi\left\{k^2 + \left(-\frac{1}{a_t} + \frac{1}{2}k^2 r_{0t}\right)^2\right\}^{-1} \tag{64}$$

which, with the aid of (48), may be written

$$\begin{aligned}\sigma_t &= 4\pi\left\{k^2 + \left[-\gamma + \frac{1}{2}(\gamma^2 + k^2)\, r_{0t}\right]^2\right\}^{-1} \\ &= \frac{4\pi}{k^2 + \gamma^2}\left\{1 - \gamma r_{0t} + \frac{1}{4}r_{0t}^2(\gamma^2 + k^2)\right\}^{-1}.\end{aligned} \tag{65}$$

Neglecting further the term in r_{0t}^2, we have

$$\sigma_t \approx \frac{4\pi}{k^2 + \gamma^2}\,\frac{1}{1 - \gamma r_{0t}} \tag{66}$$

which shows that to a first approximation the effect of the finite range of the nuclear forces is to multiply the zero range cross-section by the energy independent factor $(1 - \gamma r_{0t})^{-1}$, a result pointed out by BETHE and BACHER[20].

The analysis of n–p scattering data is complicated by the mixture of triplet and singlet scattering. If, adopting the simple effective range theory, we put $\varrho_t(0, E) = r_{0t} = 1{\cdot}704 \times 10^{-13}$ cm all the quantities on the right hand side of (62) are known. Thus $\frac{3}{4}\sigma_t$ may be calculated and subtracted from the measured scattering cross-section to give $\frac{1}{4}\sigma_s$. $k \cot \delta_s$ may then be plotted against k^2, and r_{0s} obtained from the slope of the best line.

Scattering experiments with neutrons of energies from 35 kev to 6 Mev have been carried out by BAILEY *et al.*[21], D. H. FRISCH[22] and LAMPI, FREIER and WILLIAMS[23]. Those of the last are the most accurate and their results are given in Fig. 10. The two curves shown in this figure represent theoretical cross-sections based on the following values

$$a_t = 5{\cdot}38 \times 10^{-13} \text{ cm}$$
$$a_s = -23{\cdot}69 \times 10^{-13} \text{ cm}$$
$$r_{0t} = 1{\cdot}704 \times 10^{-13} \text{ cm}$$
$$r_{0s} = 0{,}3 \times 10^{-13} \text{ cm}.$$

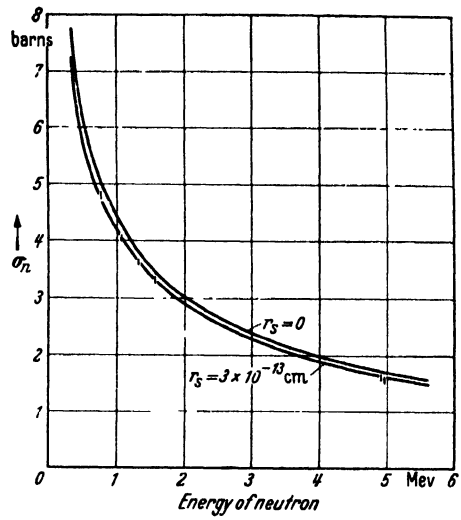


Fig 10. Theoretical $n - p$ scattering cross-sections based on

$a_t = 5{\cdot}38 \times 10^{-13}$ cm
$a_s = -23{\cdot}69 \times 10^{-13}$ cm
$r_{0t} = 1{\cdot}704 \times 10^{-13}$ cm
$r_{0s} = 0{,}3 \times 10^{-13}$ cm.

The experimental points shown are those of LAMPI, FREIER and WILLIAMS[23].

It can be seen that a large change in the singlet effective range does not have much effect on the total cross-section and so the latter must be measured very accurately to give r_{0s}. At 5 Mev the errors in σ_n and E contribute about equally to the error in r_{0s}. At this energy an error of 1% in both σ_n and E results in an error of about 20% in r_{0s}. This assumes that r_{0t} is known exactly. An uncertainty of $0{\cdot}1 \times 10^{-13}$ cm in r_{0t} leads to an uncertainty of $0{\cdot}3 \times 10^{-13}$ cm in σ_{0s}.

Fig. 11 shows $k \cot \delta_s$ plotted against k^2 for the results of LAMPI *et al.* The best line that has the value $0{\cdot}422 \times 10^{12}$ cm^{-1} $\left(= -\frac{1}{a_s}\right)$ when $k^2 = 0$, gives

$$r_{0s} = (2{\cdot}5 \pm 0{\cdot}5) \times 10^{-13} \text{ cm}. \tag{67}$$

The results of BAILEY *et al.* have been analysed in a similar manner and, though the value obtained for r_{0s} is somewhat lower than that of LAMPI, the two values are consistent with their errors.

So far we have only used the first two terms in the expansion of $k \cot \delta$. A more detailed analysis can be made by taking into account the third term in the expansion. $\varrho_t(0, E)$ is obtained from eq. (43) (Fig. 9). The plot of

$k \cot \delta_s$ against k^2 will then depend upon the potential shape. It must be remembered that the best fit will not be given by the shape for which the points lie closest to a straight line. If the square well is the "best" shape, the $k \cot \delta_s v\, k^2$ points will be concave upwards for the square well plot (P is negative for a square well).

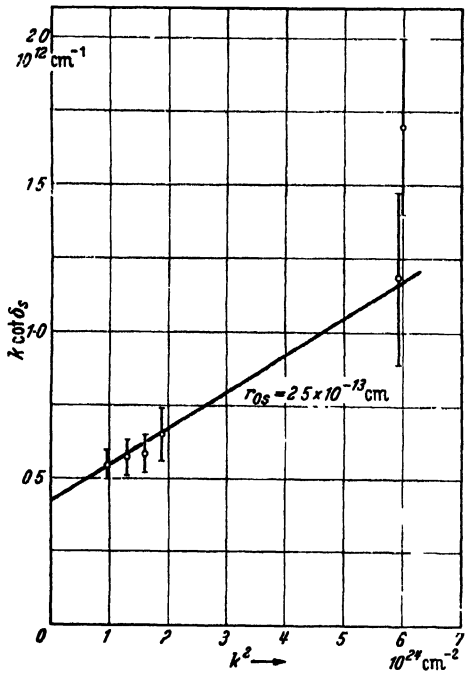


Fig. 11. $k \cot \delta_s$ plotted against k^2 for the results of LAMPI, FREIER and WILLIAMS[23].

However it is clear from the original simple analysis that the experimental results are not sufficiently accurate for any one shape to give a better fit than the others. Moreover the accuracy would have to be increased by a factor of at least three in order to distinguish between a square and a YUKAWA well. It might therefore be thought that the more accurate calculation was unnecessary at the present stage. This would be so if the scattering data were our only source of information on the neutron-proton interaction. But we have other information, in particular that provided by the capture of slow neutrons by protons. It turns out —see Sect. IV. 3—that the value of the singlet effective range calculated from that process depends upon the shape of the well and that it is larger for a long-tailed than for a short-tailed well. In the case of n–p scattering the reverse is true. This can be seen from Table 2 where the results of the more accurate analysis are given. SALPETER[21] has pointed out that the combination of these results gives a much more sensitive means of distinguishing potential shapes than that provided by the scattering data alone. For each potential shape the value of r_{0s} is calculated both from the scattering and from the capture data, and the shape for which the two values are in closest agreement is observed. The results of this procedure are discussed in the section on the capture data.

Table 2—Values of r_{0s} implied by the n–p scattering results of LAMPI, FREIER *and* WILLIAMS[23] *when the P term in the expansion of $k \cot \delta$ is taken into account. The error in each r_{0s} and b_s is $\pm 0{\cdot}5 \times 10^{-13}$ cm.*

Potential shape	r_{0s} *in* 10^{-13} *cm*	b_s *in* 10^{-13} *cm*
Square	$2{\cdot}5_5$	2·5
Gaussian	2·5	2·4
Exponential	2·5	$2{\cdot}3_5$
YUKAWA	2·4	2·2

IV. Photo-Disintegration of the Deuteron

1. *Photoelectric effect: theory*

The cross-section for the disintegration of the deuteron, due to its interaction with the electric field of a γ ray quantum, is proportional to M_{el}^2 where

$$M_{\mathrm{el}} = \int_0^\infty r\, w_g\, w_f\, dr\,. \tag{68}$$

w_g and w_f are the normalised radial eigenfunctions of the initial and final states respectively.

The initial state is the ground state of the deuteron. w_g is therefore proportional to u_g, the constant of proportionality N_g being fixed by the normalisation equation

$$\int_0^\infty w_g^2\, dr = 1\,. \tag{69}$$

The final state must be a P state, otherwise M_{el} is zero. w_f is given by[25]

$$w_f = -\frac{\sin(kr+\delta_P)}{kr} - \cos(kr+\delta_P)\,. \tag{70}$$

δ_P is the phase shift. Let the energy of the final state i.e. the sum of the kinetic energies of the neutron and proton, be E. If the wavelength, $\lambda = \hbar/\sqrt{ME}$, is large compared with the range of the nuclear forces, the neutron and proton are effectively free in the final state, and the wave function may be replaced by that for a free particle. The latter is obtained from (70) by putting $\delta_P = 0$. It behaves as r^2 for small r and therefore the contribution of small r to the integral is small. Thus at moderate energies (below 5 Mev) the error involved in replacing w_g by its asymptotic form, Φ_g, is negligible.

Now

$$\Phi_g = c\, e^{-\gamma r}$$

where c is a constant which is determined by the normalisation of u_g. Suppose that instead of inserting Φ_g in M_{el}, we insert $\Phi_g' = c'\, e^{-\gamma r}$ where

$$\int (\Phi_g')^2\, dr = 1\,. \tag{71}$$

This is the procedure adopted by Bethe and Peierls[26] and leads to the well-known result

$$\sigma_{e0} = \frac{8\pi}{3}\,\frac{e^2\hbar}{Mc}\,\frac{\varepsilon^{\frac{1}{2}}E^{\frac{3}{2}}}{(\varepsilon+E)^3}\,. \tag{72}$$

σ_{e0} would be the correct cross-section if the range of the forces were zero; for then $w_g = \Phi_g'$ for all r and normalising Φ_g' by (71) would ensure the normalisation of w_g. But for a finite force range the function w_g' corresponding to Φ_g' does not satisfy (69). It is only in this way, i.e. through the normalisation

of the ground state wave function, that the range of the forces enters into the photoelectric cross-section.

To obtain σ_e, the photoelectric cross-section, we simply multiply σ_{e0} by $(w_g/w_g')^2$.

Since

$$\int w_g^2\,dr = \int (\Phi_g')^2\,dr = 1$$

and

$$\int [(\Phi_g')^2 - (w_g')^2]\,dr = 2\gamma \int (\psi_g^2 - u_g^2)\,dr = \gamma\,\varrho_t(-\varepsilon, -\varepsilon),$$

we have

$$\frac{\sigma_{e0}}{\sigma_e} = \frac{\int (w_g')^2\,dr}{\int (w_g)^2\,dr} = \int (\Phi')^2\,dr - \int [(\Phi')^2 - (w_g')^2]\,dr = 1 - \gamma\,\varrho_t(-\varepsilon, -\varepsilon).$$

Put

$$\varrho_t' \equiv \varrho_t(-\varepsilon, -\varepsilon).$$

Then

$$\sigma_e = \frac{\sigma_{e0}}{1 - \gamma\,\varrho_t'}. \tag{73}$$

2. *Photomagnetic effect: theory*

The magnetic field of a γ ray can also bring about the disintegration of the deuteron. The final state of the process is a ^1S state and the dissociated nucleons are therefore distributed isotropically in the centre of mass system. This is to be contrasted with the photoelectric effect where the final state is a P state and the nucleons have a $\sin^2\theta$ distribution. (θ is the angle in the centre of mass system between the incident γ ray and the neutron—or proton.)

The majority of the magnetic dipole transitions are due to the ordinary magnetic dipole moment of the deuteron but some transitions are brought about by the so-called exchange currents. We define a function $\varepsilon_5(E)$ by

$$\sigma_m'(E) = \sigma_m(E)\,[1 - \varepsilon_5(E)]. \tag{74}$$

σ_m is the magnetic disintegration cross-section and σ_m' is the cross-section calculated on the assumption of zero exchange current effect. As before E is the energy of the final state.

The exchange contribution to the photomagnetic effect is discussed below. Meanwhile we shall confine our attention to σ_m'. It is convenient to write σ_m' in the form

$$\sigma_m'(E) = S(E)\,\sigma_{m0}(E) \tag{75}$$

where $\sigma_{m0}(E)$ is the cross-section for nuclear forces of zero range. The matrix element for the ordinary magnetic dipole transition from the ground state to a ^1S state of energy E is proportional to

$$M_m = N_g N_s \int_0^\infty u_g\,u_s\,dr. \tag{76}$$

$N_g\,u_g$ and $N_s\,u_s$ are the normalised radial eigenfunctions of the initial and final states respectively.

The asymptotic forms of u_g and u_s are

and
$$\left.\begin{aligned} \psi_g &= e^{-\gamma r} \\ \psi_s &= \frac{\sin(kr+\delta_s)}{\sin\delta_s} \end{aligned}\right\} \qquad (77)$$
$$k^2 = \frac{ME}{\hbar^2}.$$

δ_s is the phase shift for the singlet state of energy E and, if terms in k^4 are neglected, satisfies

$$k\cot\delta_s = -\alpha_s + \tfrac{1}{2}k^2 r_{0s}. \qquad (78)$$

We define a zero range phase shift δ_{s0} by

$$k\cot\delta_{s0} = -\alpha_s \qquad (79)$$

and denote the corresponding ψ_s by ψ_{s0}. The final state is unbound and the normalising factor is

$$N_s = \frac{\sin\delta_s}{k}. \qquad (80)$$

Denote the zero range values of N_g and N_s by N_{g0} and N_{s0} respectively. M_{m0} the zero range value of M_m is given by

$$M_{m0} = N_{g0}N_{s0}\int_0^\infty \psi_g\,\psi_{s0}\,dr \qquad (81)$$

Thus since σ'_m is proportional to M_m^2,

$$S(E) = \left(\frac{N_g}{N_{g0}}\right)^2\left(\frac{N_s}{N_{s0}}\right)^2\left(\frac{\int u_g u_s\,dr}{\int\psi_g\psi_{s0}\,dr}\right)^2. \qquad (82)$$

Let us compare the three factors on the right hand side of (82) with their counterparts in the photoelectric effect. The first factor is the same for both processes and we have seen that it introduces the effective range of the triplet interaction. The second factor is unity for the electric case if, as we assumed, the final state is free. It is to be expected that in the magnetic case this factor will depend on the effective range of the singlet interaction. At low energies, the third factor is very close to unity for the electric process but this is not true in the magnetic case. BETHE and LONGMIRE[5] show that to a first approximation it depends on the sum of the singlet and triplet effective ranges. If the calculation is taken to greater accuracy this term depends on the well shape in a rather complicated manner.

As before

$$\left(\frac{N_g}{N_{g0}}\right)^2 = \frac{1}{1-\gamma\varrho'_t}. \qquad (83)$$

Eq. (78) and (80) give

$$N_s^2 = \left[k^2 + (-\alpha_s + \tfrac{1}{2}r_{0s}k^2)^2\right]^{-1}$$

whence

$$\left(\frac{N_s}{N_{s0}}\right)^2 = \left[1 + \frac{\frac{1}{4}r_{0s}^2k^4 - \alpha_s r_{0s}k^2}{k^2+\alpha_s^2}\right]^{-1}. \qquad (84)$$

Put

$$D = \int_0^\infty (\psi_g \psi_s - u_g u_s)\, dr. \tag{85}$$

Then, since

$$\int \psi_g \psi_s\, dr = \frac{\gamma + k \cot \delta_s}{\gamma^2 + k^2},$$

$$\int u_g u_s\, dr = \frac{\gamma - \alpha_s - \gamma^2 D + k^2 (\tfrac{1}{2} r_{0s} - D)}{\gamma^2 + k^2}. \tag{86}$$

Eq. (83) (84) and (86) give the required range factor

$$S(E) = \left[1 - \gamma \varrho_t'\right]^{-1} \left[1 + \frac{\tfrac{1}{4} r_{0s}^2 k^4 - \alpha_s r_{0s} k^2}{k^2 + \alpha_s^2}\right]^{-1} \left[1 + \frac{k^2 (\tfrac{1}{2} r_{0s} - D) - \gamma^2 D}{\gamma - \alpha_s}\right]^2. \tag{87}$$

BETHE and LONGMIRE show that

$$D = \tfrac{1}{4} (r_{0t} + r_{0s}) \tag{88}$$

is a fairly good approximation for several potential shapes. The substitution of this expression for D in (87) gives

$$S(E) = 1 + \frac{1}{2} \left(\frac{\gamma^2 - 2\alpha_s \gamma - k^2}{\gamma - \alpha_s}\right) (r_{0t} - r_{0s}) - \frac{\alpha_s^2 (k^2 + \alpha_s \gamma)}{(\gamma - \alpha_s)(k^2 + \alpha_s^2)} r_{0s} + 0\,(r_0^2). \tag{89}$$

At zero energy the coefficient of the term $(r_{0t} - r_{0s})$ is about four times the coefficient of the following term. Thus the photomagnetic effect provides an approximate method of estimating the difference between the effective ranges for the triplet and singlet interaction.

The expression for the zero range cross-section is[27]

$$\sigma_{m0} = \frac{2\pi e^2 \hbar}{3 M^2 c^3} (\mu_p - \mu_n)^2 \frac{k \gamma (\gamma - \alpha_s)^2}{(k^2 + \gamma^2)(k^2 + \alpha_s^2)}. \tag{90}$$

μ_p and μ_n are the magnetic moments of the proton and neutron respectively in units of the proton magneton. It is assumed that these moments are unchanged when the proton and neutron are bound in the deuteron.

We now return to the effects of exchange currents on the photomagnetic process. It was first pointed out by SIEGERT[28] that the existence of charge exchange forces between nucleons implies that electric currents must flow in the space between them. These exchange currents react with an electromagnetic field and modify the properties of nuclei in two ways. Apart from their effect on the photomagnetic cross-section they may give a contribution to the magnetic moment of a nucleus. SACHS[29] has shown that this contribution is antisymmetric for the interchange of neutrons and protons and thus vanishes for a self-conjugate nucleus such as the deuteron. However, the exchange currents do give rise to magnetic dipole transitions in the deuteron. AUSTERN and SACHS[30] have attempted to calculate this effect by relating it to the experimental values of the exchange magnetic moments of H^3 and He^3 in their ground states. For an exact calculation a specific meson theory is needed but a rough estimate may be obtained without this, and it is found that at zero disintegration energy the exchange contribution to the cross-section is about 4%.

$$\varepsilon_5(0) = 0{\cdot}04. \tag{91}$$

We shall use this value in our calculations. Moreover we shall assume that, for disintegration energies small compared with the deuteron binding energy, ε_5 remains constant.

By analogy with (75) we write

$$\sigma_m(E) = R(E)\,\sigma_{m0}(E) \tag{92}$$

where

$$R = \frac{S}{1-\varepsilon_5}. \tag{93}$$

3. *Capture of slow neutrons by protons*

(a) *Theory*

The capture of slow neutrons by protons is the inverse process to the photo-disintegration of the deuteron at energies just above the threshold. Since at these energies the electric cross-section is proportional to $E^{\frac{1}{2}}$ while the magnetic cross-section is proportional to $E^{\frac{1}{2}}$ the latter is predominant.

Thus the range factor for slow neutron capture is the range factor for the magnetic disintegration evaluated at zero energy. Let σ_H be the capture cross-section and σ_{H0} its value for zero range of forces. The expression for σ_{H0} is[27]

$$\sigma_{H0}\,v = \frac{2\pi e^2\hbar^4}{M^5c^5}(\gamma-\alpha_s)^2\frac{\gamma^3}{\alpha_s^2}(\mu_p-\mu_n)^2 \tag{94}$$

where v is the relative velocity of neutron and proton.

$$\left.\begin{aligned}\sigma_H &= R(0)\,\sigma_{H0}\\ &= \frac{1}{1-\varepsilon_5}\,\frac{1}{1-\gamma\varrho_t'}(\gamma-\alpha_s-\gamma^2D)^2\frac{2\pi e^2\hbar^4\gamma^3}{M^5c^5\alpha_s^2}(\mu_p-\mu_n)^2.\end{aligned}\right\} \tag{95}$$

(b) *Experiment*

For the experimental value of the capture cross-section we take[12]

$$\sigma_H = (0{\cdot}328 \pm 0{\cdot}013)\ \text{barns}^*. \tag{96}$$

This value is for neutrons with a velocity of 2200 m/sec and gives

$$\left.\begin{aligned}\sigma_H\,v &= 7{\cdot}22(1+\varepsilon_4)\times 10^{-20}\ \text{cm}^3/\text{sec}\\ \varepsilon_4 &= \pm 0{\cdot}04.\end{aligned}\right\} \tag{97}$$

Of the quantities in eq. (95) all except D are now known. MACK[31] gives $\mu_p-\mu_n = 4{\cdot}705$. ε_5 is obtained from (91) and ϱ_t' from Table 1. Thus D is determined. Its value depends on the potential shape since ϱ_t'—obtained from ϱ_t—depends on the shape also.

Instead of using the simple formula of BETHE and LONGMIRE (88) to determine r_{0s} from D we use a more accurate expression due to SALPETER[24]. The results thus obtained for D and r_{0s} are shown in Table 3.

The experimental error of the capture cross-section and the uncertainty in the exchange contribution lead to an error of $0{\cdot}5\times10^{-13}$ cm in r_{0s}. The

* The error has been increased over that given in reference[12]. There is still much uncertainty concerning σ_H, a recent result obtained at Oak Ridge giving a value as high as 0·35 barns.

Table 3—Values of D and r_{0s} obtained from the n–p capture cross-section $\sigma_H v = 7{\cdot}22 \times 10^{-20}$ cm³/sec.

The fraction of this cross-section due to exchange moments is assumed to be 0·04

Potential shape	*D in 10^{-13} cm*	*r_{0s} in 10^{-13} cm*
Square	1·00	2·4
Exponential	1·03	2·5
YUKAWA	1·07	2·6

error due to the deuteron binding energy, the free proton cross-section and the coherent n–p scattering amplitude amounts only to $0{\cdot}2 \times 10^{-13}$ cms It is therefore very desirable that the capture cross-section should be known to better accuracy. The usual method of determining σ_H is to measure σ_B/σ_H. The inaccuracy of σ_H lies about equally in this ratio and in σ_B, the boron absorption cross-section.

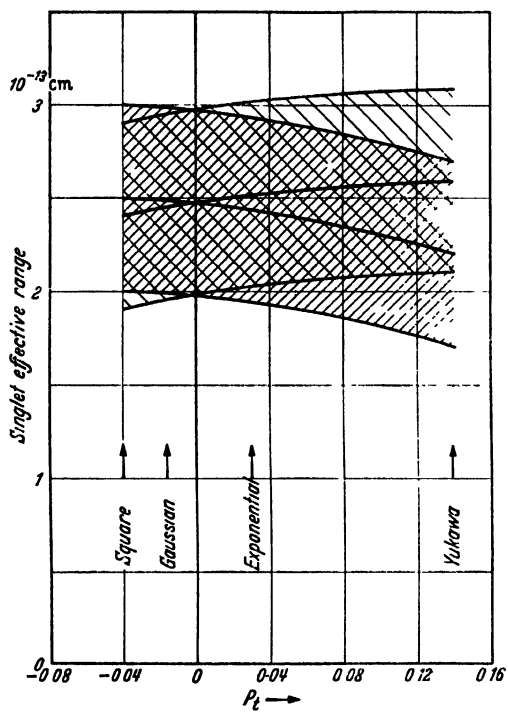


Fig. 12. Singlet effective range for different potential shapes obtained from the capture cross-section and $n-p$ scattering data.

Region permitted by the capture cross-section.
Region permitted by $n-p$ scattering data.

The values of r_{0s} given in Table 3 are plotted in Fig. 12 together with the values obtained from the scattering data and it can be seen that the two sets of values are consistent. It can also be seen that the present values of r_{0s} and the uncertainties involved are such that it is not possible to rule out any range of values for P between those for a square and a YUKAWA well.

4. *Photo-disintegration: comparison with experiment*

Many experiments have been performed to measure the photo-disintegration of the deuteron at energies close to the threshold. Measurements of the total disintegration cross-section, $\sigma_T = \sigma_e + \sigma_m$, and of the ratio σ_m/σ_e have been made at three γ ray energies. These are

2·507 Mev (Ga^{72}), 2·615 Mev (ThC″) and 2·757 Mev (Na^{24}).

σ_m/σ_e is found by measuring the angular distribution of the dissociated nucleons. If the number of protons, say, ejected into unit solid angle at an angle θ is

$$n(\theta) = a + b \sin \theta , \tag{98}$$

then

$$\frac{\sigma_m}{\sigma_e} = \frac{3a}{2b} . \tag{99}$$

The most accurate measurements of σ_m/σ_e are those of BISHOP, BEGHIAN and HALBAN[32]. Their results are given in Table 4. The values for σ_T that appear in the Table are the weighted means of results given in references[33-35].

Table 4—Experimental values for the total photodisintegration cross-section[33-35] *and for the ratio of the magnetic to the electric cross-section*[32]

γ ray	Ga^{72}	ThC''	Na^{24}
E_γ in Mev	2·507	2·615	2·757
E in Mev	0·281	0·389	0·531
σ_T in 10^{-28} cm^2	11·7±1 0	13·9±0·6	15·8±1·2
$\sigma_m\ \sigma_e$	0·600±0·02	0·360±0·008	0·247±0·007

σ_m/σ_e has also been measured by WOODWARD and HALPERN[36] at other energies. An electrostatic generator was used to produce a continuous γ ray spectrum up to an energy of 3·2 Mev. A γ energy was selected by ensuring that only those photo-protons with a certain range, and hence a certain energy, were counted. The results are included in Fig. 15.

The theoretical photoelectric cross-section is readily calculated. On substituting the values of the constants in (72) we obtain

$$\sigma_{e0} = 3{\cdot}782 \times 10^{-26} \frac{E^{\frac{3}{2}}}{E_\gamma^4} \text{ cm}^2 . \tag{100}$$

E and E_γ, the energy of the γ ray, are in Mev. The values for ϱ_t' (eq. 73) are taken from Table 1.

The resulting values of σ_e are listed in Table 5.

Table 5—Theoretical photoelectric and photomagnetic cross-sections in 10^{-28} cm^2

E_γ in Mev	2 507		2 615		2 757	
	σ_e	σ_m	σ_e	σ_m	σ_e	σ_m
Square	5·86	4·27	8·41	3·67	11·44	3·11
Exponential . .	5·94	4·27	8·53	3·67	11·60	3·11
YUKAWA . . .	6·06	4·23	8·69	3·66	11·83	3·10
Experimental .	7·3±0·6	4·4±0·4	10·2±0·5	3·7±0·2	12·7±1·0	3·1±0·2

The range factor for the photomagnetic process, $R(E)$, is given by (87) and (93). If it is assumed that ε_5 does not depend on the energy—which is

probably true at low energies—a considerable simplification can be effected by writing

$$R(E) = R(0)\left[\left\{1 + \frac{\frac{1}{4} r_{0s}^2 k^4 - \alpha_s r_{0s} k^2}{k^2 + \alpha_s^2}\right\}^{-1}\left\{1 + \frac{k^2(\frac{1}{2} r_{0s} - D)}{\gamma - \alpha_s - \gamma^2 D}\right\}^2\right]. \qquad (101)$$

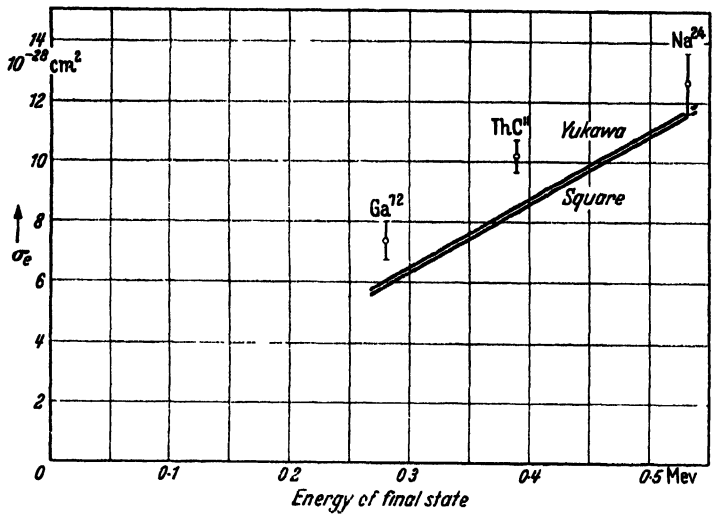


Fig. 13. Photoelectric cross-sections given by effective range theory together with the experimental values.

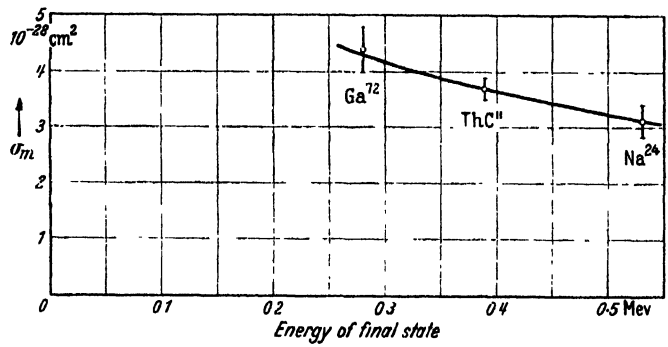


Fig. 14. Photomagnetic cross-sections given by effective range theory together with the experimental values.

The advantage of expressing $R(E)$ in this way is that the quantity in square brackets is very close to unity and does not depend very much on the values inserted for r_{0s} and D; while the quantity $R(0)$ is given directly by the ratio of the measured value of the capture cross-section to the theoretical zero-range cross-section (94). Thus we do not need to know the numerical value of ε_5. Furthermore, all the well shapes will give closely similar values for $R(E)$. The reason that our treatment of the scattering data and of the photoelectric effect gives different results for different potential shapes is the presence of the $\frac{1}{1-\gamma\varrho_t'}$, term. By expressing the photomagnetic range

factor as $R(0)$ times an energy term, we eliminate the factor $\frac{1}{1-\gamma a_t'}$. It is included in $R(0)$.

Inserting values in the right hand side of (94) gives

$$\sigma_{H0} v = 6{\cdot}534 \times 10^{-20} \text{ cm}^3/\text{sec}. \tag{102}$$

From (97) and (102) we obtain

$$R(0) = 1{\cdot}104. \tag{103}$$

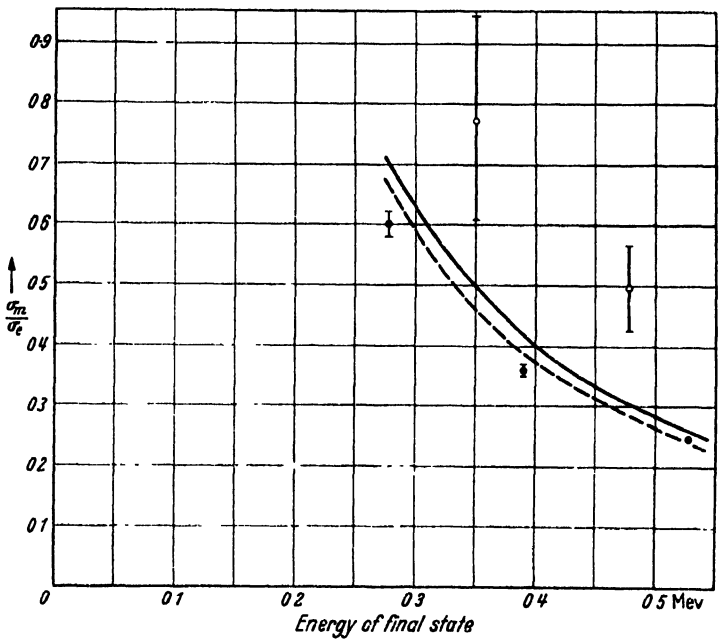


Fig. 15 Ratio of photomagnetic to photoelectric cross-sections plotted against energy of final state.
——— effective range theory;
- - - - calculations of HANSSON and HULTHÉN,
BISHOP, BEGHIAN and HALBAN [32];
WOODWARD and HALPERN [36].

The expression in square brackets in eq. (101) has been evaluated by substituting for r_{0s} and D the values given in Table 3. Multiplication of the results by 1·104 gives $R(E)$. On inserting the values of the constants in the expression for σ_{m0} (90), we find

$$\sigma_{m0} = 6{\cdot}936 \times 10^{-28} \frac{E^{\frac{1}{2}}}{E_\gamma (E + 0{\cdot}0739)} \text{ cm}^2 \tag{104}$$

where E and E_γ are in Mev.

Thus σ_m may be calculated. The final results are given in Table 5.

In Figs. 13, 14 and 15 the experimental values of σ_e, σ_m and σ_m/σ_e are shown together with the predictions of the effective range theory.

It can be seen that the photoelectric cross-sections predicted by the effective range theory are too small. We may consider the experimental

results in a different way and regard them as a direct measurement of the quantity, ϱ_t'. The value of ϱ_t' obtained from the results in Table 4 is

$$\varrho_t' = (2{\cdot}11 \pm 0{\cdot}12) \times 10^{-13}\,\text{cm}.$$

WILKINSON[37] has measured the total photodisintegration cross-section at six γ-ray energies from 4·45 to 17·6 Mev. At these energies the photomagnetic cross-section is relatively small, and even a crude estimate of its magnitude suffices to determine the photoelectric cross-section from the total cross-section. Replacing the wave function u_q in the matrix element M_{el}, by its asymptotic form ψ_q causes an appreciable error at high energies. To allow for the error, the expression for σ_e given in (73) is multiplied by a correction factor. This factor depends on the shape of the well and, at a given energy, is larger for a long tailed than for a short tailed well.

The results obtained by WILKINSON are

$$\varrho_t' = (1{\cdot}73 \pm 0{\cdot}09) \times 10^{-13}\,\text{cm for a square well}$$

and

$$\varrho_t' = (1{\cdot}79 \pm 0{\cdot}09) \times 10^{-13}\,\text{cm for a YUKAWA well.}$$

The values of ϱ_t' given in Table 1 are consistent with those found by WILKINSON, but not with the value given by the photodisintegration experiments at low energies. The values of ϱ_t' listed in Table 1 are obtained from eq. (57) and (44) and are based on the assumption that the function $\varrho_t(E_1, E_2)$ varies linearly with energy; in other words, that the term in k^6 in eq. (2) is negligible. If further experiments confirm the discrepancy between the values of ϱ_t' given directly by the photoelectric cross-section and those obtained from eq. (57) and (44), the effective range theory may have to take account of higher terms in the expansion of $k \cot \delta$, in which case its usefulness will be considerably reduced.

Calculations by NAGEL[38] indicate that, for a YUKAWA-type well, the variation of the function $\varrho(0, E)$ with energy is significantly non-linear. However, the series for $k \cot \delta$ converges more slowly for a long tailed than for a short tailed well, and it may still be true that the departure of $\varrho(0, E)$ from linearity is negligible for a well with a short tail.

HANSSON and HULTHÉN[39] have calculated the photoelectric and photomagnetic cross-sections directly, using accurate approximations for the neutron-proton wave functions. The latest values of HULTHÉN and NAGEL[38] interpolated to a meson mass of 285 m_e and a deuteron binding energy of 2·226 Mev, are shown in Fig. 15. It can be seen that these values are in better agreement with the results of BISHOP, BEGHIAN and HALBAN[32] than are the values given by the effective range theory.

V. COMPARISON OF THE PROTON-PROTON AND NEUTRON-PROTON FORCE

A detailed account of low energy proton-proton scattering has been given by JACKSON and BLATT[40]. The equation analogous to (2) for the p–p interaction is (equations 1.1 and 1.2 of reference[40])

$$K = -\frac{\pi \cot \delta}{\exp(2\pi\eta) - 1} + h(\eta) = \frac{\hbar^2}{Me^2}\left(-\frac{1}{a} + \frac{1}{2} r_0 k^2 - P r_0^3 k^4 + \ldots\right) \quad (105)$$

where

$$\eta = \frac{e^2}{\hbar v}$$

$$h(\eta) = -\log\eta - 0{\cdot}5772\ldots + \eta^2 \sum_{n=1}^{\infty} \frac{1}{n(n^2+\eta^2)} .$$

v is the relative velocity of the protons. δ is the nuclear phase shift.

The COULOMB force is an added complication in p-p scattering. On the other hand the fact that the ^3S state is forbidden means that the cross-section at a given energy is determined by one phase shift only.

The constants a and r_0 in eq. (105) are obtained by plotting the experimental values values of K against the energy. As with n–p scattering the present data are not sufficiently accurate to distinguish between any of the commonly assumed potentials. JACKSON and BLATT find that the values of a and r_0 that give the best fit to the data at energies below 3·5 Mev are

$$\left.\begin{aligned} a &= -(7{\cdot}67 \pm 0{\cdot}05)\times 10^{-13}\ \text{cm} \\ r_0 &= (2{\cdot}65 \pm 0{\cdot}07)\times 10^{-13}\ \text{cm} . \end{aligned}\right\} \qquad (106)$$

The "best" values of a and r_0 depend somewhat on the value assumed for P. The values in (106) correspond to $P = 0$.

The constant a changes appreciably when the Coulomb field is switched off, but the effective range r_0 and higher coefficients in (105) are almost unchanged.

Eq. (106) shows that the effective range of the p–p nuclear interaction lies within the present experimental limits of the effective range of the n–p singlet interaction (Fig. 12), but these limits are so wide that the comparison is not very significant*.

The scattering lengths of the two interactions however are known with some accuracy. Their values are given in Table 6.

Table 6. n–p and p–p scattering lengths (in 10^{-12} cm)

Shape of nuclear potential	$-a_s$	$-a_p$	$-a'_s$	$-a'_p$
Square.	2·369±0·006	1·643±0·035	2·289±0·007	1·696±0·035
YUKAWA. . . .		1·832±0·035	2·064±0·014	2·213±0·070

The value of a_p, the proton-proton scattering length in the absence of the Coulomb field, depends on the shape assumed for the nuclear force. We see that the n–p singlet scattering length a_s has a larger negative value than a_p. indicating that, if the shape and range are the same, the n–p potential is deeper than the p–p potential for the ^1S state.

However it has been pointed out by SCHWINGER[41] that even if the specifically nuclear n–p and p–p forces are the same, a difference in the depth of the wells is to be expected. This arises from magnetic forces, such as the dipole-dipole interaction, between the nucleons. Owing to the difference in sign between the magnetic moments of the proton and the neutron, the magnetic

* *Note added in proof:* An accurate measurement of the n-p scattering cross-section at 14 Mev has been carried out by POSS *et al* [*Phys. Rev.* 87 (1952) 11, 21]. The results, analysed by SNOW, indicate a singlet effective range of $(2\ 22 \pm 0\ 24)\times 10^{-13}$ cm for a square well and $(2{\cdot}11 \pm 0{\cdot}40)\times 10^{-13}$ cm for a YUKAWA well. The values of r_0, given in the summary have been adjusted to take account of these values.

dipole interaction is attractive in the n–p ^1S state and repulsive in the p–p ^1S state. Thus its effect is to make the n–p force appear slightly stronger than the p–p force.

The effect of the magnetic forces on the scattering length depends on the shape of the nuclear potential. SCHWINGER has calculated the hypothetical scattering lengths a' that would result if the magnetic forces were zero. The results in Table 6 show that a'_p is numerically smaller than a'_s by $(26 \pm 2)\%$ for a square well, but numerically larger by $(7 \pm 4)\%$ for a YUKAWA well. We may therefore conclude that charge independence does not hold if the nucleons have a square well interaction but is consistent with present low energy data if the potential has a fairly long tail.

In the ^1S state, the n–p and p–p interactions are close to resonance, *i.e.* the well depth parameter is almost unity and the scattering length is large compared with the range of the nuclear forces. This means that a small change in the depth of the well gives rise to a large change in the scattering length. A difference of 1% in scattering length corresponds to less than 0·1% in well depth.

VI. HIGH ENERGY DATA AND TENSOR FORCES

1. *Scattering experiments at high energies*

We have confined ourselves so far to the results of experiments at low energy. These experiments give information only about the S states. At higher energies scattering occurs in states of higher orbital momentum and experiments at such energies provide information on the exchange nature of the nuclear forces.

n–p scattering experiments have been carried out at energies up to 280 Mev[42-46]. The results of HADLEY *et al.*[42] at 40 and 90 Mev, indicate that the differential cross-section is almost symmetrical about 90° in the centre of mass system. Exact symmetry would indicate zero interaction in states of odd orbital momentum, i.e. that the n–p potential was half-ordinary and half-exchange. CHRISTIAN and HART[47] have calculated from the degree of asymmetry observed by HADLEY *et al.* that the P state force is about $(10 \pm 10)\%$ of the S state force, and is repulsive.

In the calculation of the photoelectric cross-section it was assumed that the final state of the dissociated nucleons, a P state, was free. BETHE and LONGMIRE[5] show that the effect of a 10% repulsive P state interaction is to reduce the low energy cross-section by about 0·2%.

Although the four potential shapes, square, Gaussian, exponential and YUKAWA, give equally good fits to the low energy data, this is not so for the high energy results. CHRISTIAN and HART[47] conclude from their analysis of the 40 and 90 Mev data that these cannot be explained on the basis of a square or Gaussian well. Of the two long-tailed potentials, the YUKAWA is superior for predicting the variation of the differential cross-section with angle, but the exponential gives better values for the total cross-section. Both shapes give total cross-sections that are too high, the discrepancy for the YUKAWA well amounting to about 25% at 90 Mev.

p–p differential scattering cross-sections have been measured at energies up to 345 Mev[48-53]. Unlike n–p scattering which ceases to be isotropic at about 20 Mev, p–p scattering is observed to be almost isotropic (apart from small angle COULOMB scattering) up to the highest energies at which measurements have been made. The experimental values at 240 Mev and above are however larger than the theoretical maximum for S state scattering alone. To explain the p–p results, CHRISTIAN and NOYES[54] postulate a tensor interaction of high singularity for states of odd parity. This is contrary to the charge independence hypothesis for, as stated above, the interaction in the odd states of the neutron-proton system is small.

Other theories have been put forward which attempt to explain the p–p scattering results while still retaining charge independence. JASTROW[55] has suggested a singlet potential which becomes repulsive at small distances. CASE and PAIS[56] use a velocity-dependent spin-orbit force. At the moment there appears little to choose between the different theories. Further experiments are necessary, for some discrepancy exists in the p–p results above 75 Mev. The cross-sections obtained at Berkeley are significantly lower than the others.

2. *Effect of tensor forces on low energy results*

The effect of tensor forces was neglected throughout Sect. II to V. It was originally shown by RARITA and SCHWINGER[57] that tensor forces contribute little to the scattering at low energy. Their conclusions, based on a square well potential, have been confirmed by CHRISTIAN and HART[47] for more general potential shapes. CHRISTIAN[58] has calculated that the effect of a tensor force is to lower the value of the effective range by a few per cent. The anisotropy of the low energy scattering caused by the tensor forces is less than 1% which is quite beyond detection with present experimental techniques.

BETHE and LONGMIRE[5] have calculated the effect of tensor forces on the photo-disintegration of the deuteron. They conclude that the effect is very small in the electric case. The transitions $^3D_1 \rightarrow {}^3P$ form a negligible fraction of the total electric dipole transitions. The tensor forces do cause a change in the shape of the wave function u at small values of r but, as we have seen, the value of this function close to the origin has almost no effect on the cross-section.

In the magnetic case the inclusion of tensor forces causes a small change in D. This results in a decrease of about $0{\cdot}1 \times 10^{-13}$ cm in the value of r_{0s} obtained from the capture cross-section. The effect of transitions $^3D \rightarrow {}^1D$ is negligible.

VII. SUMMARY

1. The experimental data at low energies are not at the moment sufficiently accurate to distinguish the shape of the neutron-proton potential for either the triplet or singlet interaction.

2. The values of the triplet scattering length and the deuteron binding energy lead to

$$\varrho_t = (1{\cdot}704 \pm 0{\cdot}030) \times 10^{-13}\ \text{cm}$$

from which we may deduce

Potential shape	*Triplet effective range in 10^{-13} cm*	*Triplet intrinsic range in 10^{-13} cm*
Square	1·73±0·03	2·04±0·03
YUKAWA	1·64±0·03	2·91±0·03

3. The value of the singlet effective range deduced from scattering data is consistent with that given by the absorption cross-section.

$$r_{0s} = (2{\cdot}35 \pm 0{\cdot}4) \times 10^{-13}\ \text{cm}.$$

This value of r_{0s} together with that of the singlet scattering length gives

Potential shape	*Singlet intrinsic range in 10^{-13} cm*
Square	2·3±0·4
YUKAWA	2·1±0·4

4. Comparison of the singlet scattering lengths of the specifically nuclear n-p and p-p interactions indicates that charge independence does not hold if the potential has a square shape. But for a potential with a tail slightly shorter than that of the YUKAWA, the two scattering lengths are in good agreement.

5. The low energy cross-sections for the photoelectric disintegration of the deuteron which the effective range theory predicts are somewhat low. The more exact theory of HANSSON and HULTHÉN is in better agreement with the experimental values of σ_m/σ_e.

The author wishes to thank Dr. WILKINSON and Dr. HUGHES for sending him copies of their papers in advance of publication. He is further indebted to Dr. WILKINSON for extremely helpful discussions.

REFERENCES

[1] BREIT, G., CONDON, E. U. and PRESENT, R. D.; *Phys. Rev.* 50 (1936) 825 and BREIT, G., THAXTON H. M. and EISENBUD, L.; *Phys. Rev.* 55 (1939) 1018.
[2] LANDAU, L. and SMORODINSKY, J.; *J. Phys. U.S.S.R.* 8 (1944) 154. SMORODINSKY, J.; J. *Phys. U.S.S.R.* 8 (1944) 219.
[3] SCHWINGER, J.; *Phys. Rev.* 72 (1947) 742A.
[4] BETHE, H. A.; *Phys. Rev.* 76 (1949) 38.
[5] BETHE, H. A. and LONGMIRE, C.; *Phys. Rev.* 77 (1950) 647.
[6] BLATT, J. M. and JACKSON, J. D.; *Phys. Rev.* 76 (1949) 18.
[7] MOTT, N. F. and MASSEY, H. S. W.; *Theory of Atomic Collisions*, Ch. II, Oxford University Press.
[8] FERMI, E. and MARSHALL, L.; *Phys. Rev.* 71 (1947) 666.

[9] FERMI, E.; *Nuclear Physics*, revised ed., p. 135. Chicago Univ. Press.
[10] MOBLEY, R. C. and LAUBENSTEIN, R. A.; *Phys. Rev.* 80 (1950) 309.
[11] BELL, R. E. and ELLIOT, L. G.; *Phys. Rev.* 79 (1950) 282.
[12] HORNYAK, W. F., LAURITSEN, T., MORRISON, P. and FOWLER, W. A.; *Rev. Mod. Phys.* 22 (1950) 291.
[13] ROBERTS, T. R. and NIER, A. O.; *Phys. Rev.* 77 (1950) 746.
[14] MELKONIAN, E.; *Phys. Rev.* 76 (1949) 1744.
[15] HUGHES, D. J., RINGO, G. R. and BURGY, M. T.; *Phys. Rev.* 77 (1950) 291; 84 (1951) 1160.
[16] SUTTON, R. B. *et al.*; *Phys. Rev.* 72 (1947) 1147.
[17] SQUIRES, G. L. and STEWART, A. T.; Unpublished.
[18] SHULL, C. G., WOLLAN, E. O., MORTON, G. A. and DAVIDSON, W. L.; *Phys. Rev.* 73 (1948) 842.
[19] BIRNBAUM, W., SMITH, F. M. and BARKAS, W. H.; *Phys. Rev.* 83 (1951) 895 A.
[20] BETHE, H. A. and BACHER, R. F.; *Rev. Mod. Phys.* 8 (1936) 82.
[21] BAILEY, C. L. *et al.*; *Phys. Rev.* 70 (1946) 583.
[22] FRISCH, D. H.; *Phys. Rev.* 70 (1946) 589.
[23] LAMPI, E. E., FREIER, G. D. and WILLIAMS, J. H.; *Phys. Rev.* 80 (1950) 853.
[24] SALPETER, E. E.; *Phys. Rev.* 82 (1951) 60.
[25] Reference [9], p. 176.
[26] BETHE, H. A. and PEIERLS, R.; *Proc. Roy. Soc.* A 148 (1935) 146.
[27] BETHE, H. A.; *Elementary Nuclear Theory*, Ch. XI. Chapman and Hall, Ltd.
[28] SIEGERT, A. J. F.; *Phys. Rev.* 52 (1937) 787.
[29] SACHS, R. G.; *Phys. Rev.* 74 (1948) 433.
[30] AUSTERN, N. and SACHS, R. G.; *Phys. Rev.* 81 (1951) 710.
[31] MACK, J. E.; *Rev. Mod. Phys.* 22 (1950) 64.
[32] BISHOP, G. R., BEGHIAN, L. E. and HALBAN, H.; *Phys. Rev.* 83 (1951) 1052.
[33] BISHOP, G. R., *et al.*; *Phys. Rev.* 80 (1950) 211.
[34] SNELL, A. H., BARKER, E. C. and STERNBERG, R. L.; *Phys. Rev.* 80 (1950) 637.
[35] SHINOHARA *et al.*; *J. Phys. Soc.* (Japan) 4 (1949) 77.
[36] WOODWARD, W. M. and HALPERN, I.; *Phys. Rev.* 76 (1949) 107.
[37] BARNES, C. A., CARVER J. H., STAFFORD, G. H. and WILKINSON, D. H.; *Phys. Rev.* 86 (1952) 359. WILKINSON, D. H.; *Phys. Rev.* 86 (1952) 373.
[38] NAGEL, B.; Private communication.
[39] HANSSON, I. F. E. and HULTHÉN, L.; *Phys. Rev.* 76 (1949) 1163. HANSSON, I. F. E.; *Phys. Rev.* 79 (1950) 909. See also reference 32.
[40] JACKSON, J. D. and BLATT, J. M.; *Rev. Mod. Phys.* 22 (1950) 77.
[41] SCHWINGER, J.; *Phys. Rev.* 78 (1950) 135.
[42] HADLEY, J. *et al.*; *Phys. Rev.* 75 (1949) 351.
[43] HILDEBRAND, R. H. and LEITH, C. E.; *Phys. Rev.* 80 (1950) 842.
[44] TAYLOR, A. E., PICKAVANCE, T. G., CASSELS, J. M. and RANDLE, T. C.; *Phil. Mag.* 42 (1951) 328.
[45] DEJUREN, J. and MOYER, B. J.; *Phys. Rev.* 81 (1951) 919.
[46] FOX, R. *et al.*; *Phys. Rev.* 80 (1950) 23.
[47] CHRISTIAN, R. S. and HART, E. W.; *Phys. Rev.* 77 (1950) 441.
[48] PANOFSKY, W. K. H. and FILLMORE, F. L.; *Phys. Rev.* 79 (1950) 57.
[49] CORK, B., JOHNSTON, L. and RICHMAN, C.; *Phys. Rev.* 79 (1950) 71.
[50] BIRGE, R. W., KRUSE, U. E. and RAMSEY, N. F.; *Phys. Rev.* 83 (1951) 274.
[51] CHAMBERLAIN, O., SEGRÈ, E. and WIEGAND, C.; *Phys. Rev.* 83 (1951) 923.
[52] CASSELS, J. M., PICKAVANCE, T. G. and STAFFORD, G. H.; *Proc. Roy. Soc.* A 214 (1952) 262.
[53] OXLEY, C. L. and SCHAMBERGER, R. D.; *Phys. Rev.* 85 (1952) 416.
[54] CHRISTIAN, R. S. and NOYES, H. P.; *Phys. Rev.* 79 (1950) 85.
[55] JASTROW, R.; *Phys. Rev.* 81 (1951) 165.
[56] CASE, K. M. and PAIS, A.; *Phys. Rev.* 80 (1950) 203.
[57] RARITA, W. and SCHWINGER, J.; *Phys. Rev.* 59 (1941) 436.
[58] CHRISTIAN, R. S.; *Phys. Rev.* 75 (1949) 1675.

NUCLEAR FISSION

W. J. Whitehouse

1. Introduction 120
(1.1) Historical 120
(1.2) A summary of some theoretical work 123
(1.3) Experimental techniques 126
2. Fission cross-sections and thresholds 128
(2.1) Neutron cross-sections and thresholds 128
(2.2) Cross-sections for fission by charged particles 130
(2.3) Photofission cross-sections and thresholds 131
3. The distribution in mass, energy and charge of the fragments from binary fission 133
(3.1) The mass distribution 133
(3.2) The energy distribution 135
(3.3) The velocity distribution 139
(3.4) The relationship between the mass ratio and the energy ratio 140
(3.5) The distribution of nuclear charge in fission 141
4. The ranges of the fission fragments 144
5. Emission of neutrons and γ-rays in fission 148
6. Angular correlations between the directions of emission of neutrons and γ-rays, and that of the fragments 151
7. Spontaneous fission 152
(7.1) Experimental conditions 152
(7.2) Spontaneous fission rates 153
(7.3) Neutron and γ-ray emission in spontaneous fission. 154
(7.4) The mass and energy distribution of the fragments in spontaneous fission 155
(7.5) Similarity between spontaneous and induced fission 156
8. Fission and the shell model of the nucleus 157
9. The emission of light nuclei during fission 158
(9.1) The discovery of the particles 158
(9.2) The long-range particles 159
(9.3) The short-range particles 161
10. Fission into three or more parts of comparable size 163
11. The characteristics of very high energy fission 164
12. Miscellaneous experiments 167
(12.1) Fission by π^--mesons 167
(12.2) The possibility of fission following the capture of μ^--mesons 168
(12.3) The apparent emission of a meson in fission 168
(12.4) A search for the hypothetical negative proton in fission 169
(12.5) A search for the hypothetical di-neutron in fission 169
(12.6) The time required for fission 169

1. Introduction

(1.1) *Historical*

The dramatic connection between the discovery and exploitation of fission and the course of recent history does not concern us here, except in so far as it has affected the trend of research and the publication of results.

After a short period of intense and fruitful international activity (TURNER[1] refers to more than one hundred papers in his review article of January 1940), the whole subject became "classified" and virtually disappeared from the literature. It is true that a few valuable papers were published during the war, especially by German workers, but most of the important advances were being made in secret. Soon after the end of the war the slow process of "de-classification" began, and the accumulated knowledge began to appear, interspersed between the reports of contemporary researches. Nearly all the restrictions upon publication have now been removed. Their last effects may be apparent in a few of the succeeding pages, sometimes as the absence of one of a group of associated constants, sometimes when a result is quoted without discussion or experimental details. It seems, however, that nearly all the known facts about the actual process of fission have been made public, and that the present is therefore an appropriate time for a review of progress.

It may perhaps be useful to recapitulate the most important experimentally determined facts of fission in the form of a highly condensed summary of the first portion of TURNER's paper. The contemporary account which he gives is, in fact, still worth reading for the fascinating picture of research in progress which it presents, and we shall in any case ask the reader to refer to it for most of the references to the early work.

The experiments which led to the discovery of fission were carried out by FERMI and his collaborators in an attempt to prepare transuranic elements, of atomic number greater than 92, by the process of neutron capture followed by β-decay. Such processes do in fact exist and we may anticipate by quoting the best known of them in its modern form

$$U_{92}^{238} + n \rightarrow U_{92}^{239} \xrightarrow{\beta} Np_{93}^{239} \xrightarrow{\beta} Pu_{94}^{239}$$

However, the number of artificial radioactive periods found in Rome, Berlin and Paris was much greater than anticipated, and it proved to be unexpectedly difficult to fit them into a scheme consistent with the properties of the heavy and transuranic elements.

In addition to the apparent transuranic elements, there were four which were supposed to be β-active isotopes of radium, because they were precipitated along with barium, and their four daughters, which were supposed to be isotopes of actinium, because they were precipitated along with lanthanum. However, HAHN and STRASSMANN were driven, after exhaustive chemical tests, to conclude that one of these pairs consisted of isotopes of barium and lanthanum—they are now known to be the fission products Ba^{140} (half life 12·8 days) and La^{140} (half life 40 hours). HAHN and STRASSMANN therefore suggested that the uranium nucleus could, after capturing a neutron, split into two approximately equal fragments, and they proceeded to identify other elements of medium atomic weight among the products of the neutron irradiation of uranium, including isotopes of the rare gases krypton and xenon.

It was immediately realised by MEITNER and FRISCH that a great amount of energy would be released in the process (for which they coined the name fission) because the combined masses of the two fragments would be less than that of the parent nucleus, by an amount corresponding to about 200 Mev. They concluded therefore that the two fragments would fly apart with great velocity, and would be able to ionise a gas. FRISCH was the first to observe the large pulses of ionisation, and this was immediately confirmed by many other experiments. The recoil of the fragments was also demonstrated by JOLIOT, by MEITNER and FRISCH, and by BRETSCHER and COOK, who collected the radioactive fission products on various surfaces close to the uranium compound layer in which they originated.

JENTSCHKE and PRANKL showed that the pulses of ionisation could be divided into two groups with mean energies of about 60 and 100 Mev, indicating that the nucleus tended to split into two unequal parts. This asymetry in fission was later confirmed both by the chemical identification of the products and by measurement of the ranges of the fragments. Cloud chamber photographs of the fission fragments show this very clearly.

The primary fission fragments were expected to have a large excess of neutrons over their stable isobars ($_{54}Xe^{140}$ and $_{38}Sr^{99}$ were suggested as a possible pair) and to decay to the stable forms by a series of β-emissions. This was in fact observed and used to identify the products. The great neutron excess led several groups of observers to look for neutrons emitted at the instant of fission. Such neutrons were found by HALBAN, JOLIOT and KOWARSKI, and by ANDERSON, FERMI and HANSTEIN, and were proved to be of high energy by DODÉ, HALBAN, JOLIOT and KOWARSKI. ROBERTS, MEYER and WANG demonstrated that a small fraction of the neutrons, the so-called delayed neutrons, continued to come from the uranium after the cessation of the neutron bombardment, and this was explained as neutron emission from highly excited states formed by the β-decay of certain fission products.

The earliest experiments were all on fission initiated by the capture of neutrons. It was rapidly shown, however, that fission of the heaviest elements could be initiated by fast protons, deuterons and other particles, and by γ-rays. Later, following a theoretical prediction, spontaneous fission was observed experimentally by FLEROV and PETRZHAK, in which the nucleus divides from the ground state without the intervention of any external agency.

The term fission embraces a number of associated processes. The commonest and most systematically studied of these is binary fission, in which the nucleus divides into two fragments of comparable size. However, in a minority of cases, nuclei of low atomic weight are emitted in addition to the main fragments, at the instant of fission, and rare processes occur in which the nucleus divides into three or more large fragments. The fission of very highly excited nuclei differs in important respects from that of the less highly excited, in particular in being accompanied by the emission of a number of particles. The only experimental criterion which we can commonly apply,

in order to be able to say that a fission has occurred, is that a heavily ionising particle has been emitted, and there does not seem to be any logical dividing line between the processes which we describe as fission and those which we describe as spallation or star-formation.

In this article we shall be concerned primarily with the actual fission of the nucleus, but this can only be studied experimentally through measurements on the fragments which are emitted. Most of the report is based upon a bibliography[2] of the literature published since 1946, and as far as possible the account has been biassed in favour of papers which have appeared during the last three years.

(1.2) *A summary of some theoretical work*

Although we shall be primarily concerned with experimental researches, it may be useful to recapitulate, very briefly, some of the contributions to the theory of fission[3]. The most valuable results were first obtained from the liquid drop model of the nucleus, originally used in this connection by MEITNER and FRISCH[4], and developed by BOHR and WHEELER[5], FRENKEL[6, 7], PRESENT, REINES and KNIPP[8, 8a] and others. These papers all depend upon the calculation of the total energy of an electrically charged drop which is distorted. They seek to determine the critical shape, beyond which the drop cannot be distorted without splitting into two, and the critical energy which must be given to the drop in order to cause it to assume an unstable form.

Owing to the fact that the critical shape of the drop is often very far from spherical, the early calculations, which were based upon expansions in powers of the parameters describing the deformation, were not sufficiently accurate. The calculations which FRANKEL and METROPOLIS[9] carried out on the Eniac machine did not suffer from these purely mathematical approximations; but the results were pretty much the same. The critical energies for fission are given in the same form as by BOHR and WHEELER, i.e.

$$E_f = E_0^S \xi \tag{1}$$

where E_0^S is the surface energy of the undeformed drop, and $\xi = f\{(Z^2/A)/(Z^2/A)_{\text{lim}}\}$. Here (Z^2/A) and $(Z^2/A)_{\text{lim}}$ are the so-called fission parameters for the nucleus in question, and for a hypothetical heavy nucleus which is just unstable to fission as a result of infinitesimally small disturbances*. The values for ξ calculated by FRANKEL and METROPOLIS are shown in Table 1.

Table 1—*Values of the function used for determining the fission threshold*

$x = (Z^2/A)/(Z^2/A)_{\text{lim}}$	0·9	0·81	0·77	0·74	0·65
ξ	0·0007	0·0050	0·009,	0·0136	0·0400

The calculated values of the fission thresholds of the isotopes in the neighbourhood of uranium are shown in Fig. 1. In deriving these thresholds

* $(Z^2/A)_{\text{lim}}$ has the value 45, when calculated from the constants of the semi-empirical binding energy formula. From other arguments, based upon the estimated fission thresholds of the uranium isotopes, its value is given as 47·8.

it has been assumed that $x = 0{\cdot}74$ and $E_0^S = 538$ Mev for the compound nucleus of U^{239}. These are purely hydrodynamical thresholds, which do not include the effects of zero-point oscillations (estimated by BOHR and WHEELER to reduce the fission threshold by about 0·4 Mev) or of barrier penetration. They would therefore be expected to be somewhat above the experimental photofission thresholds of the isotopes in question. The calculated critical shapes of the drops are shown in Fig. 2. FRANKEL and METROPOLIS confirm the original calculations when they find that symmetrical fission is the most probable.

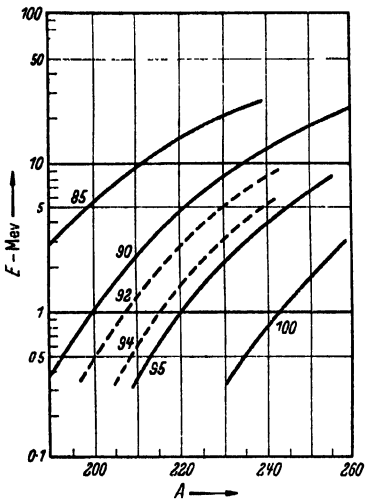


Fig. 1. Fission thresholds for the nuclei near uranium, calculated from the liquid drop model. Quantum-mechanical effects not included. (From FRANKEL & METROPOLIS[9].)

Spontaneous fission was originally predicted by BOHR and WHEELER, as a result of barrier penetration, analogous to that

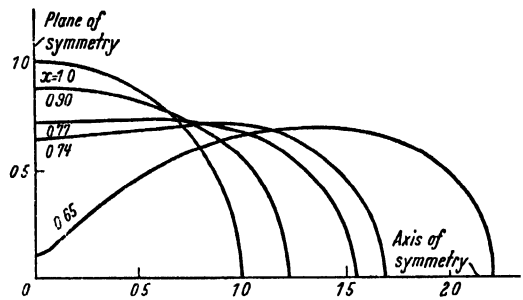


Fig. 2. Critical shapes of droplets for various values of $x = (Z^2/A)/(Z^2/A)_{\text{lim}}$.
(From FRANKEL & METROPOLIS[9].)

encountered in the theory of α-decay. They used the following very approximate formula to estimate the penetrability of the barrier

$$P \propto \exp\left[-(2ME_f)^{\frac{1}{2}}\alpha/\hbar\right] \qquad (2)$$

where M is the mass of the nucleus, and α, which is analogous to the barrier thickness, is of the order of the sum of the radii of the two fragments. FRANKEL and METROPOLIS have made a much more detailed calculation of the Gamow penetrability of the fission barrier of U^{238}. They find, however, that the result is so sensitive to small changes in the nuclear radius or surface energy that it is fruitless to attempt to compare the result with experiment*.

The predominance of asymmetrical fission was not explained by the original liquid drop theory, as formulated by BOHR and WHEELER, and refined by FRANKEL and METROPOLIS. FRENKEL[7] attempted to do this by assuming that penetration through the barrier was responsible, and applying a formula based upon the reduced mass $M_1M_2/(M_1+M_2)$ of the fragments. This implies, in effect, writing $4M_1M_2/(M_1+M_2)$ for M in equation 2, where M_1 and M_2 are the masses of the fragments. The reduced mass favours

* For $x = 0{\cdot}74$ the calculated mean life for spontaneous fission is 10^{16} years, and for $x = 0{\cdot}75$ it is 10^{17} years.

asymmetrical fission, but the corresponding barrier height $E_f(M_1, M_2)$ is higher. The observed asymmetry is supposed to result from these two opposing effects.

The question now arises, how the observed asymmetry in fast neutron fission can result from barrier penetration, when the excitation energy of the nucleus is above the fission threshold. FRENKEL explains this by considering the time required for the drop to attain a condition in which fission is possible. At first the energy of the drop is distributed freely among all the possible modes of vibration, but fission into two comparable parts cannot take place unless the fundamental mode of vibration, and one or two of the lowest harmonics, have large amplitudes. FRENKEL assumes that it takes a considerable time for the energy to become concentrated in these lower

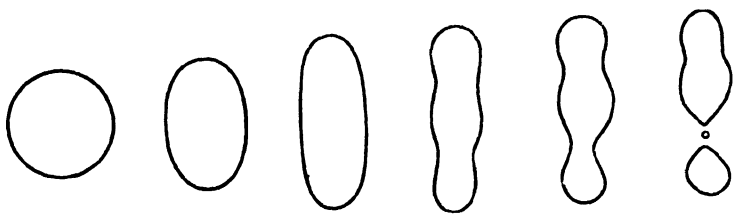


Fig. 2.1.

modes, so that the relevant part of the excitation energy, that which causes fission, rises quite slowly. As it approaches the top of the barrier the "tunnel effect" comes into play, and asymmetric fission occurs. The quantitative results of this theory do not appear to have been published.

A number of methods of reconciling the asymmetry of fission with the liquid drop model have been proposed[10-13], in which the properties of the "nuclear fluid", such as compressibility, inertia, polarisability, or inhomogeneity, are invoked.

(*Note by the Editor.* Various proposed explanations of the fission assymmetry were discussed at Physics Conferences, but do not appear to have been printed. In one of them which was related to me by J. A. WHEELER, it is assumed that the nucleus becomes very elongated and finally develops two constrictions (see Fig. 2.1); eventually one of these constrictions breaks, leading to two unequal fragments. According to this idea the heavier fragment would to be created in a much more deformed state and hence with much higher excitation; that would seem to contradict the result (§ 6) that more neutrons are emitted from the light fragment. Another explanation suggests that the nucleus at the critical shape—near which it might be expected to stay for a fairly long time—is unstable with respect to flow of matter from one half into the other; a small initial asymmetry, such as may be caused by zero point oscillation, might be sufficiently magnified by this instability to account for the observed assymmetries.)

An equally important defect of the liquid drop model is that the calculated fission thresholds, as shown in Fig. 1, are not in accordance with the experimental facts (§ 2.3). It is not merely that the numerical value for any particular isotope is wrong, for that might be remedied by changing the constants in the calculation, but that the measured variation between the photofission thresholds of the lightest and heaviest isotopes is much less than predicted. Further the calculations predict a lower photofission

threshold for U^{235} than for U^{238}, in accordance with the values of (Z^2/A), whereas the experiments place the isotopes in the opposite order. Similar considerations apply to the spontaneous fission rates (§ 7), which have been incorrectly deduced from the liquid drop model by several authors. It is difficult to see how any purely hydrodynamical theory can deal with these isotopic effects.

Another theory which may be useful in explaining the phenomena of fission is the shell model of the nucleus, proposed by MAYER[14] and others. This accounts for especially stable configurations of 2, 8, 20, 28, 50, 82 and 126 neutrons or protons in the nucleus and is well correlated with a number of nuclear properties. In particular the stability at the "magic numbers" leads to departures from the smooth curves of the masses of the nuclei, of the order of several Mev. and is also connected with irregularities in the nuclear radius. We shall refer later (§ 8) to the proposal by MEITNER[15] to explain the asymmetry of fission, and to other cases in which the shell model has been invoked. In its present state the shell model gives a number of interesting hints and suggests useful analogies, but it does not seem to be in a form which allows quantitative predictions to be made about the fission process.

(1.3) *Experimental techniques*

It is interesting to reflect that fission, though essentially a physical phenomenon, was discovered by a chemist, and to observe that a considerable proportion of the evidence presented in the following sections was obtained by chemical means. It would not be proper to attempt any description of the advances in Radiochemistry which have made possible these contributions to our understanding of fission. Advances in the techniques of Nuclear Physics, which have a direct bearing on this problem may, however, be enumerated.

The most important of these is probably the preparation of separated isotopes, or of isotopic mixtures enriched in particular components, and particularly the preparation of pure specimens of the transuranic elements. The availability of intense neutron beams from piles, and of high energy particles and γ-rays has also led to many new experiments.

The detection of the charged particles emitted in fission has been affected by the great improvements which have been made in ionisation chambers. The first of these is the use of electron collection in certain very pure gases, including hydrogen, nitrogen, boron trifluoride and the noble gases. The electrons are collected in times of the order of microseconds, compared with the milliseconds required for gaseous ions. These chambers, together with improved electronic apparatus, have made it possible to amass much more experimental information, resulting in better statistical accuracy. By their use the effect of background radiation is greatly diminished, and, in coincidence experiments, the random counting rate is reduced. Another advance was the introduction by FRISCH of the grid into the ionisation chamber, which makes the pulse due to the collection of electrons proportional to the amount of ionisation. The publication of the electrostatic theory of

the grid chamber, by BUNEMANN, CRANSHAW and HARVEY[16] has had a great effect upon the quality of experiments in which this instrument has been used.

We have no space to describe the manifold varieties of the ionisation chamber as it is used in investigating fission, and shall be content with two

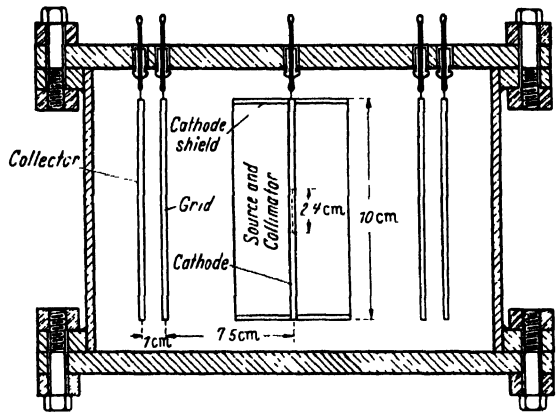


Fig. 3. Double gridded ionisation chamber. (From BRUNTON & HANNA[58].)

examples. Fig. 3 shows a double, back to back, ionisation chamber used by BRUNTON, HANNA and THOMPSON[58, 60] for measuring the ionisation due to associated pairs of fission fragments (§ 3.2). When pulsed sources, especially of high energy X-rays are used to induce fission, it may be necessary to

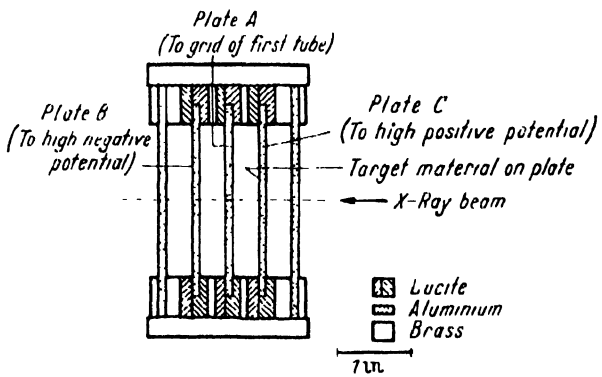


Fig. 4. Differential ionisation chamber for detection of fission pulses in the presence of intense X-radiation (From BALDWIN & KLAIBER[39])

use a differential ionisation chamber, or the sudden pulse of ionisation from the source may mask that from the fission fragment. The original version of this chamber, by BALDWIN and KLAIBER[39] is illustrated in Fig. 4. The ionisation of the X-rays affects both halves of the chamber equally, and the effects can be balanced out. The fission fragment causes ionisation in only half of the chamber and is therefore detectable.

Scintillators with photomultipliers will detect fission fragments, and were used for this purpose in the direct measurements of the fragment

velocities (§ 3.3). The rapid response was especially valuable in this experiment. Unfortunately the pulse of light from the comparatively slow, heavy fragment is not proportional to its energy. For instance, in ZnS, a fission fragment releases only about one-seventh as much light, compared to its energy, as does an α-particle[17]. For this reason the scintillation counter is useless for work on the energy spectrum of the fission fragments, and it suffers from grave disadvantages when it is necessary to detect the fragments against a strong background of α-particles. Scintillation counters have, of course, greatly improved the efficiency of detection of the γ-rays from fission (§ 6). Organic scintillators can also be used for detecting fast neutrons, but do not discriminate well between these particles and a background of γ-rays.

The new photographic plate techniques[18] have contributed very considerably to the study of the fission process, especially to the investigation of the light nuclei which are occasionally emitted during fission (§ 9), and to the first observations of fission into three or more fragments (§ 10).

2. Fission Cross-Sections and Thresholds

Much experimental work has been carried out on the determination of fission cross-sections and thresholds, but it is not proposed to devote any space to a detailed description of the methods which have been used. This section will be little more than a list of those results which have been published in the open literature. All cross-sections will be given in "barns" (1 barn $= 10^{-24}$cm^2).

(2.1) *Neutron cross-sections and thresholds*

(a) *Thermal fission cross-sections*

In May 1952 the official figures given in Table 2 were released as nuclear data forlow power research reactors[19], without any indication of the experimental methods by which they had been obtained.

Table 2—Slow neutron fission cross-sections of uranium. (For neutrons having a Maxwellian distribution of velocities, with a most probable value of 2200 m/sec)

Cross-section (barns)	U^{235}	U^{238}	*Natural uranium*	Pu^{239}
Fission . . .	549	0	3·92	664
Capture . . .	101	2·80	3·5	361
Scattering . .	8·2	8·2	8·2	—

The average value of the fission cross-section for natural uranium, by neutrons above the U^{238} fission threshold, is given as 0·29 barns.

The thermal neutron cross-section for natural uranium has been measured by Facchini and Gatti[20], who obtained a value of $3{\cdot}97 \pm 0{\cdot}12$. They used a gridded ionisation chamber to compare the number of fissions in uranium with the number of disintegrations in lithium, in a standard neutron flux provided by a Ra-α-Be source. The ratio of the cross-sections of lithium and boron was taken as $0{\cdot}0948 \pm 0{\cdot}0013$ (Fenning, Graham and Seligman[21]), and the cross-section of boron as 703 barns (Fermi, Marshal and Marshal[22]).

BISWAS and PATRO[23] carried out a very similar experiment, but used proportional counters to compare the number of fissions from a film of U_3O_8 with the number of disintegrations in a boron counter. They quote $\sigma(f)$ for thermal neutrons on U^{235} as 526 ± 10 barns, but since they used a value of 732 barns for the thermal cross-section of boron, their value is not really in good agreement with the others quoted above.

The thermal neutron cross-sections for the following isotopes have also been published.

*Table 3—Thermal neutron fission cross-sections**

Isotope	$\sigma(f)$ *(barns)*	*Ref.*	*Isotope*	$\sigma(f)$ *(barns)*	*Ref.*
Ac^{227}	<2	24	Pu^{238}	<20	28
Ra^{223}	<100	24	Am^{241}	3·0	28
Ra^{226}	$<1 \times 10^{-4}$	25	Am^{242}	~ 2500	28
Ra^{228}	<2	24	Am^{243}	<25	28
U^{233}	~ 500	26	Cm^{242}	<5	28
Np^{237}	0·019**	27			

(b) *Fission thresholds*

As was shown by BOHR and WHEELER, some of the nuclides among the elements near uranium are not expected to undergo fission with thermal neutrons, because the binding energies of the captured neutrons are not large enough to excite the compound nucleus to a level above the fission barrier. The typical graph of the fission cross-section of such a nucleus would therefore be expected

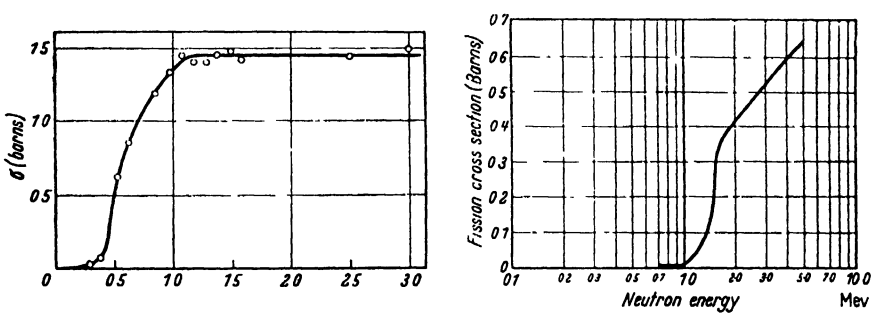


Fig. 5. (a) Fast neutron cross-section for the fission of Np^{237}.
(b) Fast neutron cross-section for the fission of U^{238}. (a) from KLEMA[30]; (b) from *Atomics* 2 (1951) 15.

to rise rapidly with energy. Once the fission barrier had been surmounted the cross-section would have a relatively steady value, provided the relative probabilities of fission and of other processes remained the same. The graph of the fission cross-section of Np^{237} has the expected form[30] (Fig. 5a). The cross-section for U^{238} however is anomalous[19] (Fig. 5b).

* STREET, GHIORSO and THOMPSON[28a] give the following cross-sections for slow neutron fission; Am^{242} ~ 6000 barns, $Am^{242m} \sim 2000$ barns, $Am^{243} < 40$ barns. CUNNINGHAM and GHIORSO[28b] give $3{\cdot}0 \pm 0{\cdot}2$ barns for the thermal neutron fission cross-section of Am^{241}.

** For a Maxwellian distribution of neutrons at 293° K.

Values for the fast neutron thresholds of several isotopes are quoted, without comment or explanation, by FELD *et al.*[31] and are shown in Table 4.

The fast fission thresholds for Th^{232} and U^{238} were measured by SHOUPP and HILL[32] using neutrons from the Li(p, n) reaction. They give values of $1{\cdot}1 \pm 0{\cdot}05$ for Th^{232} and $1{\cdot}0 \pm 0{\cdot}1$ for U^{238}.

Table 4—Thresholds for fast fission by neutrons

Nucleus	Bi^{209}	Th^{232}	Pa^{231}	U^{238}	Np^{237}
Threshold (Mev)	60	1	0·5	1	0·5

(c) *Fission by very energetic neutrons*

KELLY and WIEGAND[33] using a compensating ion chamber similar to that of BALDWIN and KLAIBER (Fig. 4), but filled with argon, measured the fission yields, relative to thorium, from a number of elements bombarded by 84 Mev neutrons. They also bombarded samples of lead of different isotopic composition and calculated the yields from the pure isotopes. Their results are shown in Table 5.

Table 5—Relative fission yields with 84 Mev neutrons
(KELLY and WIEGAND)

Element or isotope	Bi	Pb	Pb^{206}	Pb^{207}	Pb^{208}	Tl	Hg	Au	Pt
Relative Fission Yield	0·019	0·0055	0·0070 $\pm$0·0005	0·0101 $\pm$0·002	0·0028 $\pm$0·0003	0·0032	0·0023	0·0020	0·0009

The fission cross-sections of uranium and thorium for 90 Mev neutrons have been measured by JUNGERMAN, KELLEY, WIEGAND and WRIGHT and are quoted as 1·4 and 1·0 barns by JUNGERMAN and WRIGHT[136].

(2.2) *Cross-sections for fission by charged particles*

The fission cross-section for 200 Mev deuterons on bismuth has been shown by chemical means to be 0·2 barns[135], and for 380 Mev α-particles on U^{238} to be about 2 barns[134].

The fission excitation functions of deuterons and α-particles of 19 and 38 Mev respectively on uranium and thorium were measured by JUNGERMAN and WRIGHT[34]. The recoil fragments were collected on aluminium foils, and the number of fissions which had occurred was estimated from the observed β-activity. A calibration was attempted against the thermal neutron fission from one of the foils in a known neutron flux. This calibration was later shown to be erroneous by a factor of 1·5–1·7, owing to the different distribution of fission fragments in low-energy and high-energy fission.

In a much more complete investigation JUNGERMAN[35] employed a double, compensating ionisation chamber (§ 1·3) to observe the ionisation of the fission fragments from U^{238}, U^{235}, Th^{232}, Bi^{209} and Au^{197}, when bombarded by deuterons up to 200 Mev and α-particles up to 400 Mev. The values near the thresholds,

which occur at about 8 Mev for deuterons and about 21 Mev for α-particles were measured especially carefully.

Some of JUNGERMAN's results are given in a slightly simplified form in Fig. 6. The statistical spread of the observations, which was often considerable is omitted from this figure. In the curves for U^{238} and Th^{232} the initial rising portions are functions of the penetrability of the Coulomb barrier by the charged particle, and are found to be in good agreement with the calculations of WEISSKOPF, assuming a nuclear radius of $1{\cdot}48\,A^{\frac{1}{3}} \times 10^{-13}$ cm. At higher energies the fission cross-section is below the theoretical value, presumably because of the competition of other reactions. The other two nuclei investigated by JUNGERMAN do not undergo fission unless a very large energy of excitation is suppllied to the nucleus, and the threshold is therefore so high as to be virtually unaffected by the Coulomb barrier. The cross-sections at the upper limits of the energies agree within experimental error with those obtained by chemical means, and quoted above.

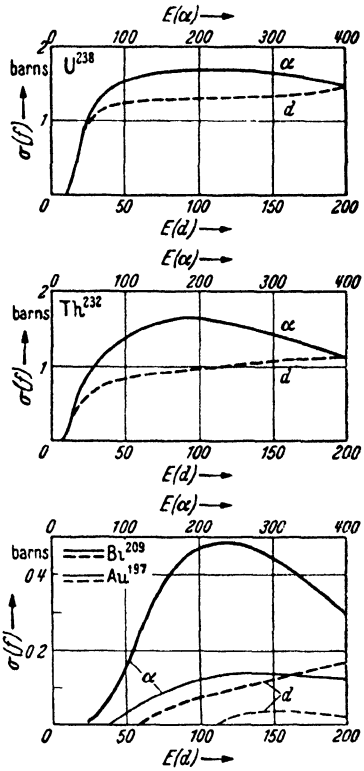


Fig. 6. Fission excitation functions for α-particles and deuterons.

An approximate estimate of the cross-section for fission of uranium by carbon ions has been made by J. M. HOLLANDER[35a]. The experimental figure, given as a result of analysis for active silver, strontium and barium, is ~0·1 barns. As an explanation of this small value it is suggested that the majority of the carbon ions suffer RUTHERFORD scattering before they can enter the uranium nucleus. Owing to the high electrostatic potential barrier the compound nuclei (Cf^{247} and Cf^{250}) cannot be formed with excitation energies less than ~60 Mev. The fission is therefore expected to be of the high energy type discussed in § 11, but the experimental evidence is as yet insufficient to confirm this.

(2.3) *Photofission cross-sections and thresholds*

Photofission was first observed experimentally using mono-energetic γ-rays from nuclear reactions, particularly the 6·3 Mev line from the $F^{19}(p, \gamma)$ reaction and the 17·5 Mev line from the $Li(p, \gamma)$ reaction. Some of the results of the experiments are collected in Table 6.

X-rays of higher energies are produced in the form of a continuous Bremsstrahlung spectrum from machines such as betatrons or synchrotrons. The

Table 6—Photofission cross-sections for monoenergetic γ-rays (barns)

Isotope	Energy of γ-ray (Mev)	
	6·3	17·5
U^{238}	0·0035±0·0010[36] 0·0022[38]	0·046±0·015[37] 0·0167[38] (~0·005)[39]
Th^{232}	0·0017±0·0005[36]	0·0072[38]

quantities which are reasonably easy to measure are fission rate and the maximum energy of the γ-radiation. The spectrum of the radiation and its intensity

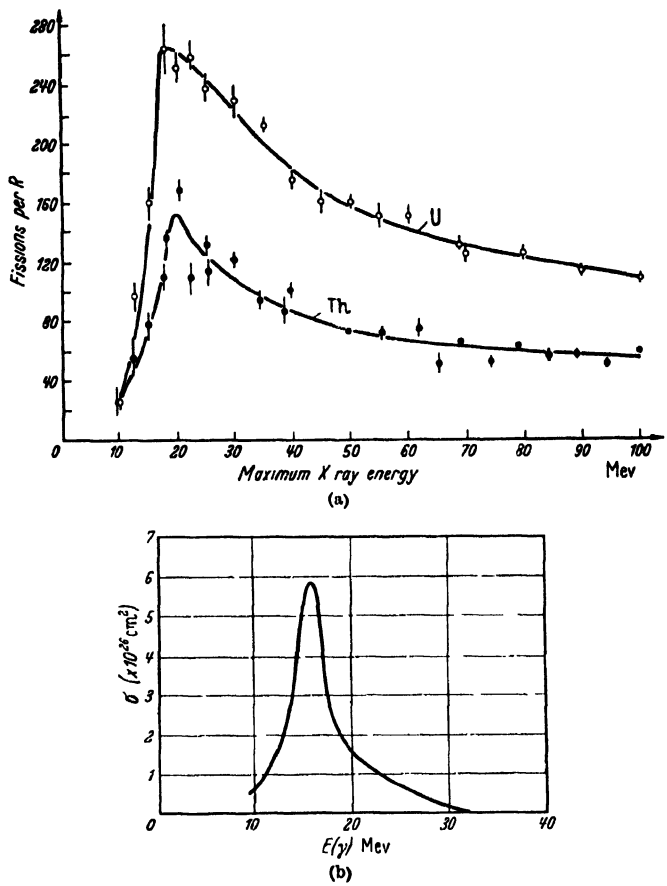


Fig. 7. (a) Photofission yields for uranium and thorium for bremsstrahlung.
(b) Cross-section for photofission of uranium. Because of approximations made in the calculation this curve must be considered of only qualitative significance. (From BALDWIN & KLAIBER[39])

are not usually so well known. The last quantity is often quoted in terms of röntgen units, but the measurement of the intensities of such high energy X-rays is difficult, and the results of different observers do not always agree.

BALDWIN and KLAIBER[39] observed photofission in uranium and thorium with X-rays of maximum energies up to 100 Mev, using the ionisation chamber shown in Fig. 4. They obtained the yield curves shown in Fig. 7a, the shape of which indicates a maximum for the cross-section at about 17 Mev (see Fig. 7b). This result appears to be confirmed by OGLE and MCELHINNEY[40].

GOWARD *et al.*[41] found a value for

$$\int_0^{23} \sigma \, dE = 1{\cdot}5 \pm 0{\cdot}3 \text{ Mev. barn}$$

for uranium, which is about 4·5 times that found by BALDWIN and KLAIBER.

MCELHINNEY and OGLE[42] have compared the photofission of several elements to that of U^{238}, using the radioactivity of the fission fragments as a means of detection. The maximum energy of the X-ray spectrum was varied from 12·4 to 21·7 Mev, and appeared to have little effect on the ratios. The results are shown in Table 7.

Table 7—Photofission relative to uranium
(From MCELHINNEY and OGLE[42])

Fission product activity per atom relative to U^{238}				
Pu^{239}/U^{238}	U^{235}/U^{238}	U^{233}/U^{238}	Th^{232}/U^{238}	Io^{130}/U^{238}
2·51	1·49	2·49	0·257	0·847

The threshold values for photofission were measured by KOCH, MCELHINNEY and GASTEIGER[43] using a differential ionisation chamber of the type mentioned in § 1·3.

These figures are interesting, since they might be expected to give a direct measurement of the barrier height against spontaneous fission, and also to

Table 8—Photofission thresholds

Isotope	Th^{232}	U^{238}	U^{236}	U^{235}	Pu^{239}
Measured Photofission . Threshold . .	5·40 ±0·22	5·18 ±0·27	5·08 ±0·15	5·31 ±0·25	5·31 ±0·27

check the calculations of the liquid drop model. They are quite incompatible with the values calculated by FRANKEL and METROPOLIS[9] as is shown in § 1.2.

They are, as WAY[44] points out, compatible with the neutron-binding energies of the isotopes and with the decay energies of the radioactive bodies.

3. THE DISTRIBUTION IN MASS, ENERGY AND CHARGE OF THE FRAGMENTS FROM BINARY FISSION

(3.1) *The mass distribution*

The heavy nucleus which undergoes fission contains a greater ratio of neutrons to protons than do the medium weight nuclei into which it splits. The initial fission products are therefore unstable, even after the emission of prompt neutrons. As is well known, they attain stability by a series of β-decay processes, during which the mass of the individual nuclei remains constant. Radiochemical

investigations of such β-decay chains are therefore a most suitable method of exploring the mass distributions, for, in general, it is possible to find the yield of any given mass by a measurement of the abundance of one fairly long-lived isotope near to the end of the chain. It is true that a percentage of the products emit delayed neutrons (§ 5) a process which causes some transfer from one mass number to another, but this effect is small, and can be allowed for.

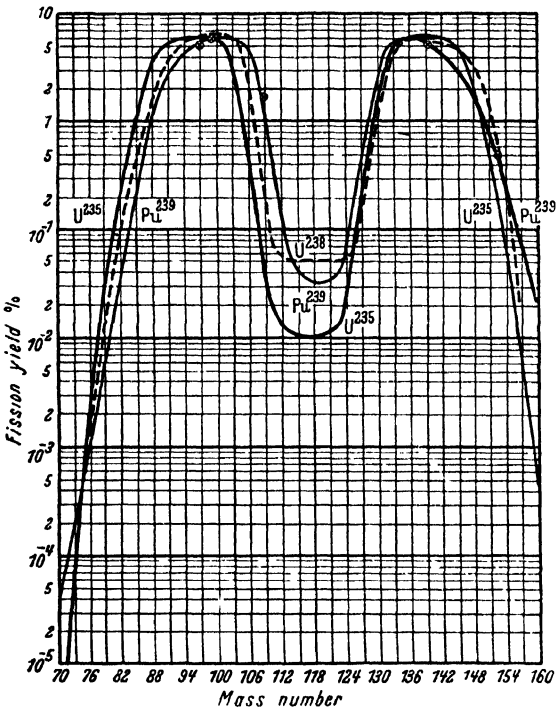


Fig. 8. Mass yield curves for thermal neutron fission of U^{233} and U^{235}, Pu^{239} and fast neutron fission of U^{238}. (From CORYELL & SUGARMAN[47].)

Our general knowledge of the mass distribution of the products from neutron fission of U^{233}, U^{235}, U^{238} and Pu^{239} was obtained predominantly by such radiochemical methods, and is the work of a large number of chemists[46-51]. The evidence has been summarised by WAY and DISMUKE[45]. The curves, of Fig. 8, representing the results of the American groups of workers, are reproduced from STEINBERG and FREEDMAN[49]*. A fission product may result directly from the fission process, or may be formed by the decay of one or more ancestors, which were themselves original products. The term *direct* or *independent* yield is used for the former process. The *chain yield* or *mass yield* is the sum of all the independent yields along the decay chain.

The curves of Fig. 8 ought to be symmetrical about a value $(A+1-\nu)/2$, where A is the mass number of the original nucleus, and ν is the number of prompt neutrons emitted; and so they are, within experimental error. However it is noticeable that the spread about the central minimum is not the same in the three curves. The three peaks representing the heavy fragments are almost exactly superimposed, while the peaks representing the light fragment are quite widely separated. This behaviour is discussed in § 8. The areas under the curves should each be equal to 200%, since two fragments are formed in each fission. STEINBERG's[48] values for the integrated yields are given in Table 9.

The deviations from the expected values may well be due to experimental errors in the radiochemical assays, which depend upon quantitative β-counting, a technique which is not always reliable to within a few percent.

* See also TURKEVITCH and NIDAY[49a] for the mass yields from the fission of Th^{232} by pile neutrons.

The mass spectrometer was used by THODE and GRAHAM[52] to measure the relative mass yields of the chains which end in the stable isotopes Kr^{83}, Kr^{84}, Kr^{86} and Xe^{131}, Xe^{132}, Xe^{134} and Xe^{136}. They also discovered a long lived isotope Kr^{85}, and later MACNAMARA, COLLINS and THODE[53] investigated the yield and half-life of Xe^{133}. By these experiments divergences from the smoothed yield curve were found*, which are given in Table 10.

Table 9—Integrated chemical mass yields in thermal fission

Target nucleus	Sum of fission yields, %		
	Light group	*Heavy group*	*Total*
U^{233}	90·2	86·9	177·1
U^{235}	97·3	97·1	184·4
Pu^{239}	96·7	88·1	184·8

INGHRAM, HESS and REYNOLDS[54] found discrepancies between the smooth yield curve and mass spectrometer results for isotopes of caesium, even after they had corrected for fractionation of the isotopes from the target. INGHRAM, HAYDEN and HESS[55] investigated a number of chains ending in isotopes of

Table 10—Fission yields from mass spectrometer determination, compared with the smooth chemical yield curve (MACNAMARA *et al.*[53])

Mass chain. .	131	132	133	134	135	136	137	138
Mass spec. . .	2·8	4·2	5·0	5·5	5·9	6·1	6·2	6·2
Chem. yield. .	2·8	4·2	6·3	7·4	—	6·1	—	—

Nd, Sm, Eu and Gd, with mass numbers between 143 and 160. They were forced, by conditions resulting from the method of chemical separation of the rare earths, to fit together the measurements for the different elements in a rather arbitrary manner. In this way they obtain a smooth yield curve which diverges in a regular manner from the chemical yield curve**.

These authors point out that it is possible, in principle, to investigate the entire yield curve with the mass spectrometer, using a special technique of isotope dilution[56]. If in addition the depletion of U^{235} were measured, absolute yields would be obtainable.

(3.2) *The energy distribution*

The commonest method of measuring the kinetic energy of the fragments is by the ionisation which they produce in a gas. This always involves some assumption concerning the energy w, required to produce an ion pair in the gas concerned.

$$E_I = \overline{w}(E, M)\, I \tag{3}$$

where E_I is the fragment energy, measured by ionisation methods, I is the number of ion pairs, and $\overline{w}(E, M)$ is the average value of w over the path of a fragment of mass number M with an initial energy E.

* A hypothesis to account for these divergences from the smooth curve is referred to in § 8. Interesting results, obtained by the mass spectrometer, on the fission products from spontaneous fission are quoted in § 7.

** See also GLENDENIN, STEINBERG, INGHRAM, and HESS[56a].

These measurements of the energy are related to those of the mass by the laws of conservation of energy and momentum, which give

$$M_L E_L = M_H E_H \tag{4}$$

where M_L, M_H are the mass numbers of the light and heavy fragments, and E_L, E_H their kinetic energies. In stating this equation in so simple a form the effect of the prompt neutrons has been neglected. Most of these prompt neutrons must be presumed to be emitted at, or immediately after the instant of fission, before the fragments have travelled any appreciable distance*. The emission of a single prompt neutron in a random direction from a moving fragment of mass number M_F, would reduce the average kinetic energy very nearly in the ratio $(M_F-1)/M_F$. This is the same error as is found in the chemical mass distribution, and is less than the experimental uncertainties. However, prompt neutrons emitted in the forward direction would decrease the observed kinetic energy of the fragments, and those emitted in the backward direction would increase it. The isotropic emission of prompt neutrons from the moving fragments would, therefore, introduce a spread into the observed energy distribution. To a first approximation this is $\pm 2(E_F E_n/M_F)^{\frac{1}{2}}$, where E_F, M_F are the kinetic energy and mass number of the fragment, and E_n is the kinetic energy of the neutron.

New measurements of the ionisation of paired fission fragments have been made by BRUNTON and HANNA[57, 58] for the slow neutron fission of U^{233} and U^{235}, and by BRUNTON and THOMPSON[59, 60] for Pu^{239}. These experiments made use of the high thermal neutron flux from the Chalk River pile and of modern electronic techniques to increase the statistical accuracy, and they supersede the similar investigations of FLAMMERSFELD, JENSEN and GENTNER[61], JENTSCHKE[62] and DEUTSCH and RAMSAY[63]**.

The double ionisation chamber shown in Fig. 3 was used. The source was contained in a thin collodion film and mounted on one side of a collimator consisting of a plate with closely spaced holes. Only fragments whose direction was within 45° of the normal were counted, and losses due to oblique passage through the source, and to escape of electrons in the fringing field, were reduced. Only coincident pulses in the two chambers were accepted, so that the collimation applied to one chamber was automatically extended to the other. Careful precautions were taken to ensure that the best conditions prevailed with respect to the purity and composition of the Argon-CO_2 mixture in the chamber, the potentials of the various electrodes, and the linearity and resolving times of the electronic apparatus.

The pulses from the uncollimated chamber were passed through an electronic "gate", which selected pulses within a given range of energies, which was usually 5 Mev wide. The coincident pulses from the collimated chamber were passed into a 30-channel pulse analyser, which measured their energy distribution. When the gate was wide open the familiar double-humped curve (Fig. 9)

* See § 5 for evidence of delays of the order of 10^{-8} sec in the case of a small proportion of the so-called prompt neutrons.

** FOWLER and ROSEN[64] investigated the energies of single fission fragments by an ionisation method.

was obtained. By first setting the gate at the low energy end of the spectrum, and moving it up in steps of 5 Mev the details of the distribution can be investigated.

The electronic apparatus was calibrated by feeding pulses into the chamber amplifiers through two identical small condensers of capacity C. If V is the voltage of the pulse it will produce a current pulse equal to the collection in the chamber of a charge of VC coulombs. Thus an absolute calibration is possible in principle; in practice, however, the apparatus was calibrated against the known energies of the α-particles (4·823 Mev for U^{233}, 4·396 Mev for U^{235} and 5·159 Mev for Pu^{239}). For this reason any difference between the value of w for α-particles and for fission fragments will affect the result. Corrections are necessary for absorption in the source, and for ionisation losses in the collimator. Some of the results are quoted before these corrections are applied, and some after, so that a little care is required to avoid confusion.

The results are discussed very thoroughly in the two longer papers[58, 60] mentioned above. Space limits us to the discussion of a typical selection. The general behaviour of the three isotopes is compared in Table 11.

The distribution of the energies of the fission fragments is most fully shown by contour diagrams, one of which is reproduced in Fig. 10. From this it can be seen:

(a) The kinetic energy evolved by the fission of a single nucleus varies very greatly, from about 120 Mev to about 180 Mev, and even with a given mass ratio the kinetic energy varies by as much as 50 Mev. This variation has been attributed to variations in the number and energies of the prompt neutrons, or to the primary charge distribution.

(b) The kinetic energy of the fragments is not a maximum for symmetrical

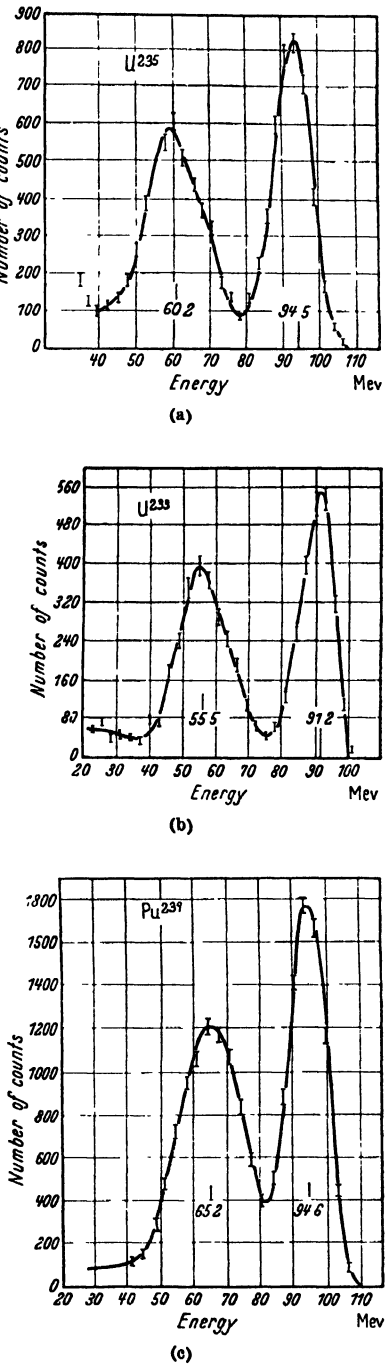


Fig. 9(a), (b) and (c). Energy spectrum of fission fragments. (From BRUNTON *et al.*[58, 60].)

Table 11—Comparison of fissile nuclides

	U^{233}	U^{235}	Pu^{239}
Most probable energy of light fragment Mev	93·0	94·5	94·6
Most probable energy of heavy fragment Mev	56·6	60·2	65·2
Ratio of most probable energies	1·64	1·57	1·45
Width* of high energy peak Mev	14	12	14
Width* of low energy peak Mev	22	20	24
Width* of total energy curve	22	25	27
Width* of total energy curve for most probable mass ratio (from contour diagrams)	20	20	22
Mass ratio for most probable total energy	1·26	1·23	1·20

* At half maximum.

fission. In Fig. 11 the most probable value of the energy is plotted against the mass ratio. (See also the results of KATCOFF, MISKEL and STANLEY § 4).

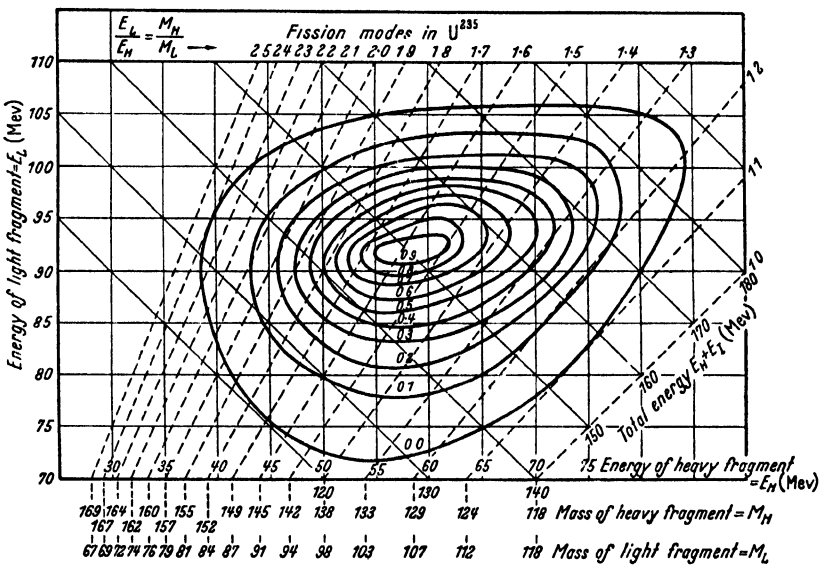


Fig. 10. Contour diagram showing the fission modes of U^{235}. (Uncorrected for absorption in source, and collimator losses.) (BRUNTON & HANNA[57].)

(c) The most probable mode of fission of U^{235} has a total energy E_I of 156 Mev. This result is compared with those obtained by other methods in § 3.4.

(d) A heavy fragment of *lower* than average energy tends to be paired with a light fragment of *lower* than average energy. Since the sum of the masses of the two fragments is almost constant, an unusually large heavy fragment is always paired with an unusually small light fragment. Thus the double-humped energy distribution curve is not even approximately an inversion of the double-humped mass-distribution curve.

These experiments do not appear to add any new general conclusions to those drawn from earlier experiments, but they extend the work to new isotopes and with greater accuracy. Comparison of the contour diagrams for Pu^{239}, U^{235}, U^{233} reveals differences in detail, which the present theories of fission seem to be quite incapable of explaining.

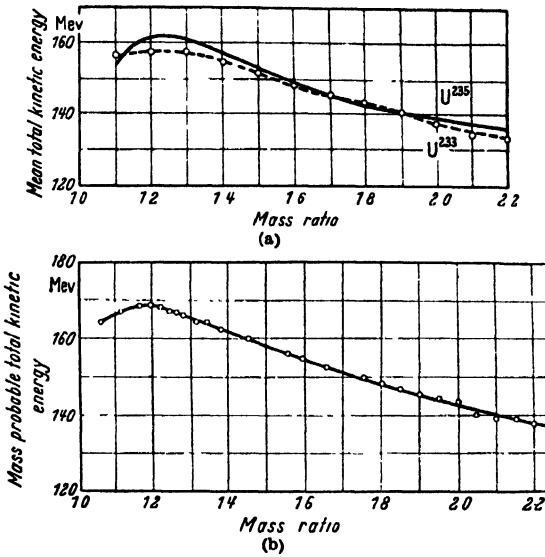


Fig. 11. Variation of the most probable total kinetic energy of the fragments with mass ratio. (a) U^{233} and U^{235}, (b) Pu^{239}.

(3.3)

The velocity distribution

The velocity distribution of the fission fragments is being investigated by LEACHMAN[65], by a direct method. A thin foil bearing a film of U^{233}, U^{235} or Pu^{239} is irradiated by thermal neutrons, and pairs of fragments are detected by

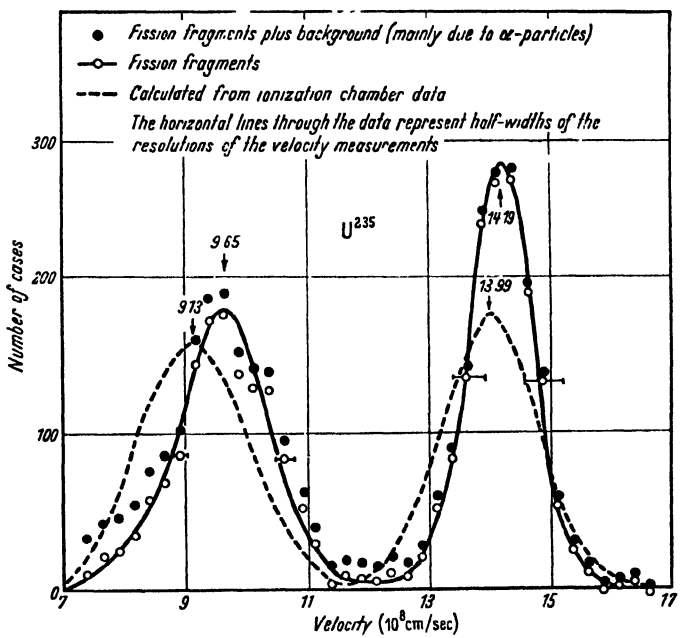


Fig. 12. Velocity distribution of fission fragments.

scintillation detectors. One fragment travels only about 1 cm before striking a detector, while the other travels about 350 cm along an evacuated tube.

The pulses from the two detectors are displayed upon the screen of a fast cathode ray tube and photographed. The velocity of the fragment can be obtained from the distance apart of the two peaks.

These experiments are not published but preliminary results*, shown in Fig. 12, indicate that the velocity calculated from BRUNTON and HANNA's energy measurements is less than that measured directly**. This, as will be shown in the next section can be attributed to a difference between the value of w for α-particles and for fission fragments.

(3.4) *The relationship between the mass ratio and the energy ratio*

Measurements of the ratio of the kinetic energies of pairs of fragments, and of the mass ratios, do not appear at first sight to be in good agreement with each other. This is shown by a series of diagrams in the papers of BRUNTON *et al.*[58,60],

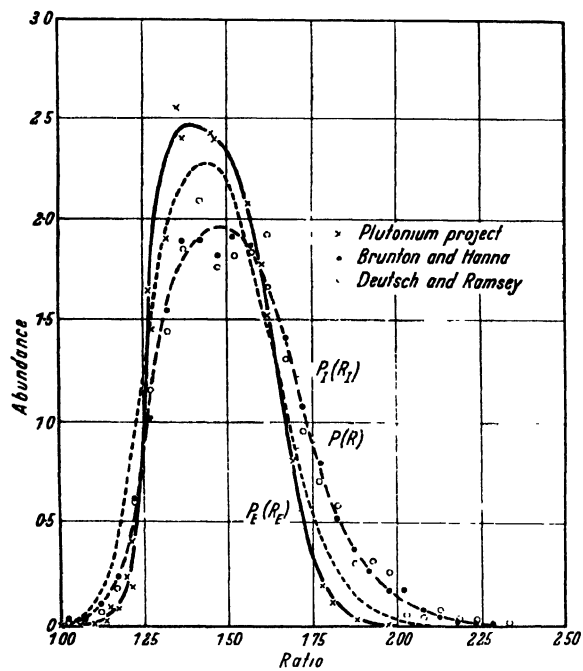


Fig. 13. Distributions of the ratios of the energies of the fragments in the slow neutron fission of U^{235}. $P_I(R_I)$ from ionisation measurements; $P_E(R_E)$ calculated from the chemical yields; $P(R)$ calculated from $P_E(R_E)$. (LEACHMAN[65])

and equally clearly in a diagram due to LEACHMAN[65], which is reproduced as Fig. 13. The distribution obtained from the chemical mass ratio, by application of eq. (4), $P_E(R_E)$ in Fig. 13, is narrower than that obtained from ionisation measurements, $P_I(R_I)$. The latter comes from an equation similar to eq. (3), using the value of w appropriate to α-particles.

* Kindly sent by Dr LEACHMAN.

** Neither curve in Fig. 12 has been corrected for foil losses which amount to about 1 Mev in each case; and the two curves are therefore comparable with each other.

LEACHMAN attributes part of the divergence between the two distributions to dispersion in the ionisation measurements. Such dispersion is partly instrumental, and partly a genuine deviation of the fragment energy from the mean, due to the emission of prompt neutrons. The curve $P(R)$ (Fig. 13) is calculated from $P_E(R_E)$, making reasonable assumptions about the dispersion in fragment energy.

There is still a considerable discrepancy between the distributions $P(R)$ and $P_I(R_I)$. LEACHMAN has shown that this discrepancy can be made to disappear by reasonable assumptions about the ionising powers of the fragments. The two distributions can in fact be reconciled with each other if the ratio w_I/w_H, (i.e. of the energies which the average light and heavy fragments respectively dissipate in producing one ion pair), falls from 1, for symmetrical fission to about 0·9 when the ratio of the fragment masses is 2:1.

The velocity measurements described in § 3.3 indicate, according to LEACHMAN, that the values of w for the most probable light and heavy fragments exceed that for an α-particle by about 1·06 and 1·11 respectively. On this basis BRUNTON and HANNA's value of 156 Mev for the most probable kinetic energy released in fission is increased by 12·4 Mev. This brings it into better agreement with HENDERSON's[66] calorimetric value, of 165 ± 8 Mev.

The errors in all these calculations linking the mass, ionisation, and calorimetric measurements are still rather large, but it is clear that there is no reason to suspect any unexplainable discrepancy between the various experiments. Several hypotheses have been advanced in the past to account for the supposed differences, for instance that all the prompt neutrons are emitted from one of the fragments*. It now appears that there is no significant difference between the different measurements of the distributions of the fragments, and that hypotheses about the fission process itself cannot expect any support from experiments of the accuracy at present feasible.

(3.5) *The distribution of nuclear charge in fission*

There does not appear to be any direct physical method for determining the nuclear charge of a primary fission fragment. Both of the two fragments formed in fission carry away a large proportion of their orbital electrons with them. The residual charge on each of the fragments is in fact only about 20e, and this is rapidly decreased as the velocity of the fragment is reduced[78]. For this reason physical measurements, such as those depending upon the curvature in a magnetic field, do not give results which are directly related to the atomic number of the fragment.

Such experimental evidence as exists concerning the division of nuclear charge in fission is therefore almost entirely chemical, and involves attempts to measure the primary fission yields. Before summarising this evidence we shall mention certain postulates which have been put forward to forecast the division of charge. In this connection we shall use the symbol Z_A to represent the most stable charge for a given mass number and Z_P for the most probable charge of the primary fission product.

* See footnote on p 151.

(a) *The postulate of unchanged charge distribution* follows from the simplest form of the liquid drop model, and assumes that the charge divides in the same ratio as the mass. Thus the most probable charge Z_P of all the primary fragments from U^{235}, should be $92A/233{\cdot}5$ where A is the mass-number of the fragment. This postulate predicts longer average disintegration chains for the heavy fragment than for the light.

(b) *The postulate of minimum potential energy* put forward by WAY and WIGNER[45, 67] depends upon the supposition that during the nuclear agitation which precedes fission the charges rearrange themselves in such a way as to

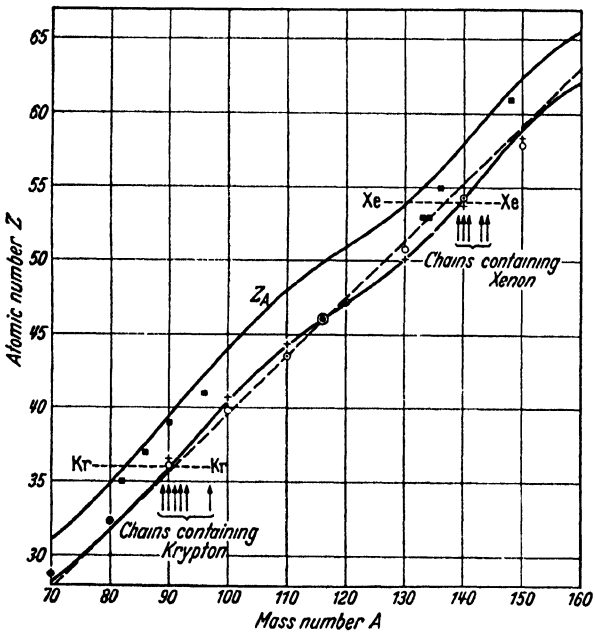


Fig. 14. The most probable charges of primary fission products from U^{235}.

Z_A —— Stability curve
Z_P - - - Based on postulate of unchanged charge distribution
Z_P + Based on postulate of minimum potential energy
Z_P ⊙ Based on PRESENT'S theory of non-uniform charge distribution
Z_P —— Based on postulate of equal chain-length
■ Isotopes for which independent yields are known

make the potential energy a minimum. This energy consists of the binding energy of the fragments and of the electrostatic energy due to their mutual repulsion. The former is calculated from the semi-empirical formula, using BOHR and WHEELER'S values for the constants, and the latter from the energy of two charged spheres in contact.

(c) PRESENT'S *theory of unequal charge distribution* is calculated, for spherical fragments in contact, on the basis of a general model in which the distribution of charge in the nucleus is not uniform[68]. The mutual repulsion of the protons causes them to spread outwards towards the surface of the nucleus, and results in the smaller fragment of an asymmetric fission having a greater ratio of charge to mass than the larger.

(d) *The postulate of equal chain lengths*, or of equal charge displacement, was put forward on purely empirical grounds by GLENDENIN, CORYELL and EDWARDS[69]. According to this postulate the value of $Z_P - Z_A$ is constant for all values of A.

The predictions of the various postulates are shown diagramatically in Fig. 14, the numerical values for which were obtained from GLENDENIN[70].

The chemical evidence comes chiefly from three sources. First there are the independent yields of *shielded isotopes*, Br^{82}, Rb^{86} and Cs^{136}. These yields can be measured with comparative ease because stable isobars exist, which prevent the formation of the shielded isotope by decay from other members of the chain. Secondly, there are the results of experiments in which the fissile material in solution is exposed to a neutron flux while an inert gas is passed through the solution. Those fission products which are noble gases, Kr and Xe, are swept out of the solution, and it is therefore possible to estimate the proportion of the chain yield which precedes and includes the noble gases. The chains to which this type of experiment applies are indicated in Fig. 14, from which it will be apparent that the higher the mass number of the chain the earlier it is interrupted by the rare gas sweeping experiment, and the smaller the swept yield will be. Finally there are a few instances in which the independent yields can be determined directly, after a short irradiation. The effects of prior members of the chain must be corrected for, from the known half-lives and yields. The method is especially suitable for nuclides whose immediate predecessors in the chain have long half-lives.

Table 12—Independent yields of some primary fission products. [The yield is from $U^{235}(n, f)$ unless otherwise stated]

Isotope	*Independent yield, %*	*Reference*
Br^{82}	$(4{\cdot}1 \pm 0{\cdot}5) \times 10^{-5}$	71
Rb^{86}	$3{\cdot}1 \times 10^{-5}$	70
	$2{\cdot}3 \times 10^{-5}$	71
Rb^{86} (from Pu)	$1{\cdot}3 \times 10^{-4}$	71
Y^{90}	$< 2{\cdot}8 \times 10^{-3}$	71
I^{133}	0·5	72
I^{134}	0·9	72
Nb^{96}	$5{\cdot}7 \times 10^{-4}$	71
Cs^{136}	$6{\cdot}2 \times 10^{-3}$	70
	$5{\cdot}7 \times 10^{-3}$	71
Cs^{136} (from Pu)	$8{\cdot}9 \times 10^{-2}$	70
	$1{\cdot}9 \times 10^{-2}$	71
Pm^{148}	10^{-4}	71

It is not desirable here to attempt to criticise the chemical experiments, or to indicate the detailed arguments used. We shall therefore be content to present some recent data on the independent yields in Table 12.

The evidence of these independent yields is quite inadequate for the purpose of determining exactly the distribution of nuclear charge, for the isotopes concerned (see Fig. 14) are all on one side of the region where the most abundant primary fission products are supposed to be formed, and are scattered over a wide range of mass numbers. It is usual to arrange the data by assuming that the distribution of direct yields is symmetrical about the line of Z_P, and that its width is independent of A. It is then possible to see which of the four postulates referred to above gives the most self-consistent curve. Diagrams of this type have been prepared by GLENDENIN[70], both for the independent yields and for gas-sweeping experiments. The example shown in Fig. 15 was prepared by COOK[71]. The fourth postulate, of equal chain lengths, is usually considered to give the best account of the observations, and is at the same time the simplest*.

* Further discussion will be found in the reports by GLENDENIN[70], and WAY and DISMUKE[46].

The chemical evidence, as will be seen from Fig. 15 points to the existence of fission chains with about six members. The independent yields appear to fall away very steeply on each side of the centre of the chain, in contrast to the wide distribution in the mass of the products.

BRUNTON[73] has attempted to relate the spread in the measured energy of the primary fission fragments (§ 3.2) to the distribution of charge in fission. The energy spread may be attributed either to fluctuations in the numbers and energies of the prompt neutrons, or to variations in the atomic numbers of the primary fragments, and hence to their binding energies. BRUNTON examined the consequences of the assumption that the entire spread is due to variations in Z, although, as he points out, it is more probable that the correct answer lies between the two extremes. Using reasonable values for the binding energies and kinetic energies of the prompt neutrons, and for the energies of the prompt γ-rays, and employing the semi-empirical binding energy formula in a form due to FEENBERG[74], he calculates the charge distributions. The result is in direct contradiction to the chemical evidence which has been summarised above. For instance the conjugate pair of fragments $A_L = 95$, $A_H = 141$ exhibits two separate maxima, according to BRUNTON, for the most probable charge. These are at $Z_L = 35$, $Z_H = 57$, and $Z_L = 41$, $Z_H = 51$, in contrast to the single maximum near $Z_L = 38$, $Z_H = 54$, predicted by the chemical evidence. The theoretical results of BRUNTON are inherently less probable than the indications of the chemical yields. They would, in any case, have to be modified if LEACHMAN's value (§ 3.4) for the total kinetic energy of the fragments were adopted.

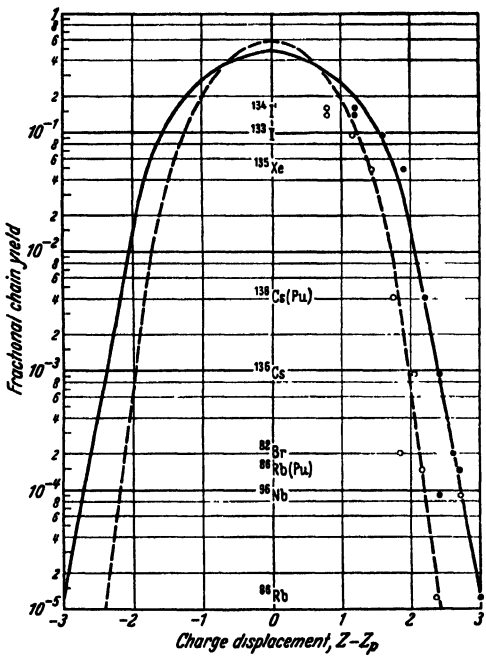


Fig 15. (Supplied by G.B.COOK) Independent fission yields fitted to the postulates of GLENDENIN (•) and of PRESENT (○).

4. THE RANGES OF THE FISSION FRAGMENTS

The ranges and other properties of the fission fragments might be more properly discussed under the heading of the Passage of Charged Particles through Matter[75, 77] than in an article on the fission process. A knowledge of the ranges is however so often required in experiments on fission that it will be convenient to summarise some of the experimental results.

It was shown theoretically, particularly by BOHR[76, 77], that the range may be divided into two parts over which the mechanisms of energy loss are quite different. In the first part of the range the fragment is very highly ionised, and the loss of energy takes place mainly through excitation and ionisation of the atoms of the medium*. The total charge of the fragment is determined by a process of capture and loss of electrons, equlibrium being set up when the most loosely bound orbital electrons of the fragment have velocities comparable with the translational velocity of the fragment through the medium. The fragments each start with effective charges of about 22 e, where e is the electronic charge[78, 79] but as they lose velocity their effective charge is reduced, and consequently their ionising power also decreases. Eventually the fragment becomes almost completely neutralised and the rate of loss of energy is very small, even though, due to their large masses, the fragments still possess energies of several Mev. During the last part of the range the fragments are supposed to lose energy by nuclear collisions, in which energy is imparted to the stopping atom as a whole.

The equation governing the velocity decrease with range of the fragment, derived on classical grounds by BOHR is

$$\frac{dv}{dR} = 2\pi N \frac{(z_1^*)^2 e^4}{m_1 \mu v^3} L_e + 2\pi N \frac{z_1^2 z_2^2}{m_1 m_2 v^3} L_\nu \qquad (5)$$

where N is the number of stopping atoms per cc; $z_1 e$, $z_2 e$, m_1, m_2 are the charges and masses of the fragment and the stopping atom respectively; $z_1^* e$ is the effective charge of the fragment in ionic collisions; μ and e are the mass and charge of the electron; L_e is the logarithmic term in electronic stopping formula, which is approximately proportional to v for heavy substances; L_ν is the logarithmic term in the nuclear stopping formula, which can be taken as constant.

The first term on the right hand side is dominant when $v > v_0 = 2\pi e^2/h$, the velocity of an electron in the first BOHR orbit of the hydrogen atom. Since $z_1^* \propto v/v_0$ and $L_e \propto v$ we see that the rate of loss of velocity at the beginning of the range is approximately constant. In the latter part of the range when $v < v_0$, the second term is dominant and the rate of loss of velocity is proportional to $1/v^3$.

As a result of these two processes the curves for the energy loss along the range are as shown in Fig. 16a and b, which are due to LASSEN. The initial comparatively steep fall in the curve corresponds to the period during which the energy is mainly lost by ionisation. This portion of the range can be extrapolated to give an extrapolated fission range R_F, which can be readily calculated[76] in terms of the range R_α of an α-particle of the same initial velocity v_i:

$$R_F/R_\alpha = 5(m_1/z_1^3)(v_0/v_i)^2. \qquad (6)$$

This extrapolated range is particularly useful in calculating the initial energy loss of the fragment.

* There are however some direct collisions with the atoms of the stopping material, and these account for the short branch tracks observed in cloud chamber photographs.

The second small maximum in the curve representing the rate of energy loss is due to the effect of nuclear collisions. The experimental results are in good

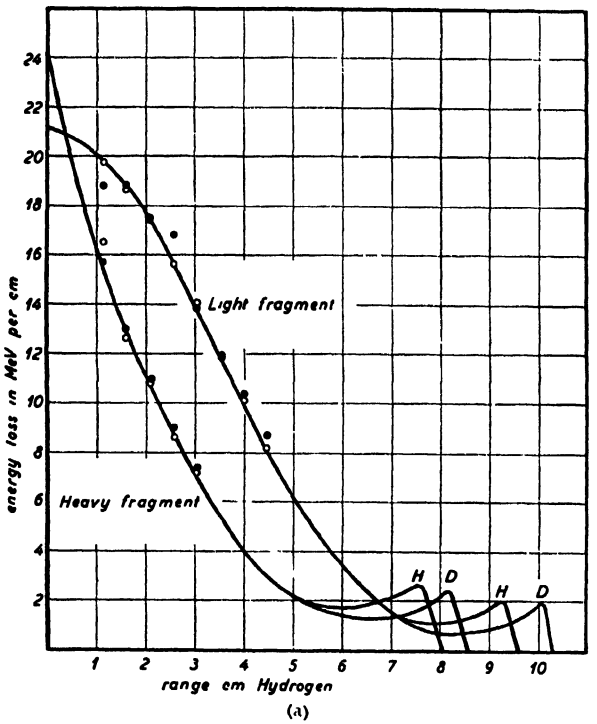


Fig. 16(a) and (b). Energy loss of fission fragments along their range. (LASSEN[78].)

general agreement with the theoretical predictions. In particular the path travelled by the fragment during this last part of the range increases as the

mass number of the stopping material is decreased. The behaviour of hydrogen however is unique owing to its abnormally small value of m/z.

Experimental values for the ranges of the fragments in air have been published by BØGGILD, MINNHAGEN and NIELSEN[80], who made the measurements by means of a cloud chamber, in which only small corrections are necessary for the stopping power of the gas. Their values for the mean ranges are given in Table 13.

Table 13—Ranges of fission fragments in various gases (mm)

	(Ref [80]) Mean range in air	Delayed neutron emitters: Br^{87} and I^{137} (Ref. [85])				
		H_2	D_2	He	air	A
Light fragment . .	25·4	96·0	99·5	137	23·8	25·2
Heavy fragment .	19·5	76·0	80·0	116	18·7	18·6
(Total range) . . .	44·9					

Note· The delayed neutron emitters are listed here as Br^{87} and I^{137}, since these are the isotopes which actually travel through the gas.

In previous experiments BØGGILD, ARRØE and SIGURGEIRSSON[81] had investigated the fragment ranges in D_2, H_2, He, A and Xe. CAMPBELL, GOOD and STRAUSER[85] have measured the ranges of two delayed neutron emitters and their values are included in table 13.

KATCOFF, MISKEL and STANLEY[82] made direct measurements of the mean and extrapolated ranges of plutonium fission fragments of twenty known masses. The collimated fragments passed along a tube containing a known pressure of air and were stopped in a series of thin laquer films. These were analysed radiochemically for individual fission fragments, and the activities plotted against the distance travelled. Fig. 17 shows the extrapolated ranges plotted against the mass number of the fragment*. The straggling of the fragments can also be estimated by this means; it is about 5%, which is in reasonable agreement with theoretical predictions.

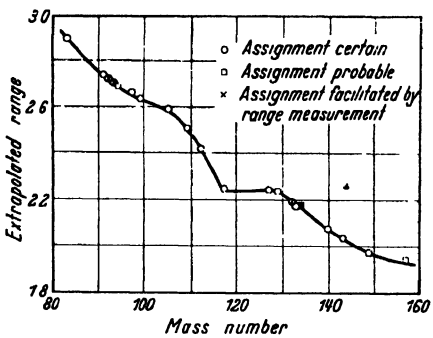


Fig. 17. Extrapolated range in air (760 mm 15° C) of Pu fission fragments, as a function of mass (KATCOFF, MISKEL & STANLEY [82].)

SEGRÈ and WIEGAND[83] and SUZOR[84] have investigated the ranges of the fragments from U^{235} in collodion, cellulose acetate, aluminium, copper, silver and gold, by different methods. The first used both ionisation chambers, and also the method of measuring the activity on catcher foils. SUZOR used a chemical method in which the activities of Te^{132}, Mo^{99} and Zr^{97} were measured in a

* The two broad peaks on the curve can be interpreted as indicating that the kinetic energy of fission is a maximum when the mass-ratio of the fragments is 1·2.

series of thin foils. In both cases the ranges were compared with those of Po α-particles (4·66 Mev). Both experiments show that the stopping powers of all the substances, except those containing hydrogen, are nearly equal to the values for α-particles of 4·5–4·6 Mev (see Table 14). This fact can therefore be used to make approximate calculations of the range in any material.

Table 14—Relative mass stopping power (μ) and atomic stopping power (s) for various substances

Substance	*4·66 Mev α-particle*	*Fission fragments*	
		SEGRE *and* WIEGAND	SUZOR
Collodion	$\mu = 1{\cdot}38$	$\mu = 1{\cdot}70$	
Cellulose acetate			$\mu = 1{\cdot}60 \pm 0{\cdot}03$
Al	$\mu = s = 1$	$\mu = s = 1$	$\mu = s = 1$
Cu	$\mu = 0{\cdot}69$ $s = 1{\cdot}62$	$\mu = 0{\cdot}66$ $s = 1{\cdot}52$	$\mu = 0{\cdot}59 \pm 0{\cdot}01$ $s = 1{\cdot}39$
Ag	$\mu = 0{\cdot}51$ $s = 2{\cdot}04$	$\mu = 0{\cdot}55$ $s = 2{\cdot}20$	$\mu = 0{\cdot}52 \pm 0{\cdot}01$ $s = 2{\cdot}08$
Au	$\mu = 0{\cdot}36$ $s = 2{\cdot}62$	$\mu = 0{\cdot}34$ $s = 2{\cdot}48$	$\mu = 0{\cdot}35 \pm 0{\cdot}005$ $s = 2{\cdot}56$

The ranges of the fragments in photographic emulsions have been measured by a number of workers, some of whose results are further referred to in § 9. DEMERS[115] and VIGNERON[86] have measured the ranges of the separate fragments, for which it in necessary to mark the point of origin of the tracks. DEMERS accomplished this by means of a thin sandwich of uranium-bearing compound between two layers of emulsion. VIGNERON used small particles of an insoluble uranium compound embedded in the emulsion. Their results, which are not necessarily contradictory, since different emulsions were employed, are given in Table 15.

Table 15—Ranges of fission fragments in photographic emulsions

	DEMERS *(own emulsion)* μ	VIGNERON *(Ilford E_1)* μ
Heavy fragment . .	11·2	10·4
Light fragment . .	14·4	13·4
Total	25·5	23·8

5. EMISSION OF NEUTRONS AND γ-RAYS IN FISSION

The published data on the number of neutrons emitted in the slow neutron fission of U^{235}, and on their energy distribution, was summarised by BOYER and TITTLE[87] in 1949. In the official release[19] of May 1952 the average number of prompt neutrons (ν) emitted per thermal fission is stated to be $2{\cdot}5 \pm 0{\cdot}1$, and their energy is stated to be distributed according to the formula*

$$N(E)\,dE = \exp(-E)\sinh\sqrt{2E}\,dE. \qquad (7)$$

* The details of some of the experimental evidence have been received since this was written. See ref. 87a.

The value ν for fast fission of U^{238} is given as 2·55 and that for slow neutron of Pu^{239} as $3{\cdot}0 \pm 0{\cdot}1$.

The delayed neutrons from fission originate when one of the fission fragments is formed in so highly excited a state that neutron emission is possible. Since the latter process is practically instantaneous the neutron appears to have the period of the preceding β-decay. For instance Br^{87} decays to Kr^{87} which emits a neutron in a small percentage of cases. It is a common practice to refer to the former isotope as the delayed neutron emitter, but this is strictly speaking, inaccurate.

The delayed neutron emitters have been investigated by a number of workers. The physical methods used by all the experimenters are similar, and consist in irradiating a specimen of the fissile element for a convenient period,

Table 16—Delayed neutrons from thermal fission of U^{235}

Half life (seconds)	*Yield, relative to total neutron emission, %*	*Estimated energy (Kev)*	*Chemical identification*
55·6	0·025	250	Kr^{87} (Ref. [89])
22·0	0·166	560	Xe^{137} (Ref. [89])
4·51	0·213	430	Kr (Ref. [90])
1·52	0·241	620	
0·43	0·085	420	
(0·05)	(0·025)		
	Total 0·755		

and plotting a neutron decay curve, which is analysed into components. HUGHES, DABBS, CAHN and HALL[88] used a machine familiarly known as the "rabbit", a cartridge containing several grams of enriched uranium which could be impelled rapidly into the thermal column of a pile, by compressed carbon dioxide. After a suitable period of irradiation, depending upon the half-life of the delayed neutron period being studied, the cartridge was shot out of the thermal column into a paraffin block containing a BF_3 counter.

The total absolute yields of delayed neutrons were measured by a device known as the "guillotine", by which a neutron beam from the pile was allowed to fall on a piece of uranium metal and then suddenly interrupted. The delayed neutron activity could then be extrapolated back to the instant at which the beam was interrupted. The half-lives and yields obtained by HUGHES *et al.* for the five main delayed neutron emitters are given in Table 16, together with the chemical identification of some of the periods by other authors.

Investigations of the slow neutron fission[91] of Pu^{239} and the fast neutron fission[92, 93] of U^{238} and Th^{232} have shown that the five main activities all have the same half-lives as those from U^{235}, within experimental error. The total yield of delayed neutrons from Pu^{239} appears to be about half that from U^{235}. The total yield from fast neutron fission of U^{238} and Th^{232} appears to be 3–4 times that of U^{235}. There are variations in the relative yields of the separate periods, which may be related to the energy of the neutrons causing fission.

DE HOFFMAN, FELD and STEIN[94] irradiated U^{235} for a period of about 10 millisec in an apparatus known as the "dragon," which was built by FRISCH. This consisted of a hollow cylinder of active material (a mixture of U^{235} and a moderator) large enough to be nearly critical, through which a slug of active material was allowed to fall. While the slug was in the cylinder the chain reaction was capable of being maintained by prompt neutrons and provided an intense burst, lasting about 10 millisec and containing about 10^{14} neutrons. The slug and the cylinder both became active, and the decay in their neutron emission could be measured. Besides the five main periods listed in Table 16 there were indications of a 6 millisec period which appeared to contribute about 2% to the total number of delayed neutrons.

SNYDER and WILLIAMS[95] have investigated very short time delays in the "prompt" neutrons by a method depending upon the velocity of the fission fragment. A foil of uranium, enriched in U^{235}, was wrapped round a large, paraffin-lined, proportional counter which detected fast neutrons by proton recoils. This was enclosed by a cylindrical space about 3·5 cm across, which could either be evacuated or filled with propane gas. The whole apparatus was placed in a slow neutron flux. When the space was evacuated about half the fragments crossed it in a time of the order of 5×10^{-9} sec, and came to rest on the outer wall. Neutrons emitted from this position were counted with reduced efficiency because of the smaller solid angle subtended by the counter. When the space was filled with gas all the fragments were stopped near the counter, and neutrons emitted from them were counted with greater efficiency. It was in fact possible to detect a difference in the counting rate, in the two experiments, from which it was concluded that $3{\cdot}6 \pm 2{\cdot}8\%$ of the neutrons were emitted from the fragments after delays of at least 8×10^{-9} sec; this is partly accounted for by the known delayed neutrons.

The prompt γ-rays from fission have been investigated by KINSEY, HANNA and VAN PATTER[96] by means of coincidence measurements between a fission chamber and γ-sensitive Geiger-Müller counters. The resolving time was of the order of one microsecond, which defines the meaning of the word "prompt" in the experiment. The total energy of the γ-radiation emitted was found by calibrating the counters against standardised sources of Th C′ (2·62 Mev) and Co^{60} (1·1 and 1·3 Mev). The quantum energy of the radiation was estimated by finding the absorption coefficients for the secondary electrons produced in aluminium, and also by measuring the attenuation of the original radiation in lead. The experiments indicated that the total energy of γ-radiation is $4{\cdot}6 \pm 1{\cdot}0$ Mev per fission and that the average quantum energy is of the order of 2·5 Mev. There are indications of a soft component of about 500kev.

ROSE and WILSON have repeated these measurements in connection with their work on the angular distribution of the γ-radiation (§ 6). They find that the total γ-ray energy is $5{\cdot}2 \pm 0{\cdot}5$ Mev per fission. They conclude that about six "prompt" γ-rays are emitted per fission, with a wide distribution of energies, extending at least up to $2\frac{1}{2}$ Mev.

6. Angular Correlations Between the Directions of Emission of Neutrons and γ-Rays, and that of the Fragments

Experiments on the angular distributions of the prompt neutrons and γ-rays are difficult because detectors of these radiations have a comparatively low efficiency, and most of the results in this field are rather inconclusive.

Wilson[97] investigated the directional properties of the neutrons with respect to the fragments. The source was a U^{235} foil in a slow neutron beam. The fragments were detected by a simple parallel plate ionisation chamber, and were collimated within cones of about 5° semi-angle, by a perforated plate. The neutrons were detected by proton recoils in a group of paraffin-lined proportional counters, which could be moved with respect to the ionisation chamber, in order to measure the neutron intensity in different directions. Coincidences between the fission fragments and the neutrons were measured. The coincidence rate was very low, being about 1×10^{-4} of the fission rate.

The number of coincidences was about five times as great when the detector was in the line of the fragments as when it was at right angles. The statistical accuracy was not great enough to justify a plot of the angular distribution of the neutrons, but the results were consistent with the hypothesis of isotropic evaporation of the neutrons from the moving fragments.

De Benedetti, Francis, Preston and Bonner[98] have investigated the angular dependence of coincidences between fission neutrons, without any knowledge of the direction of the fragments, and their experiment is therefore complementary to Wilson's A beam of slow neutrons struck a foil bearing U^{235}. Two neutron-sensitive proportional counters situated in a plane through the foil, at right angles to the beam, could be rotated with respect to each other. The fast neutrons from the uranium foil passed along the axes of these counters, each of which contained 20 polythene films perpendicular to the wire. The sensitivity to Po-α-Be neutrons was about 1%, and the discrimination against γ-radiation was good. Coincidences between neutrons in the two counters were detected by a circuit having a resolving time of $0{\cdot}3\,\mu$ sec. The random coincidence rate was greater than the effect to be studied, but the resolving time could not be reduced because of delays in the firing of the proportional counters. The coincidence rate was measured with the counters at 30°, 60°, 90°, 135° and 180° to each other. It was approximately constant for angles between 0° and 90°, and increased by a factor of about 2 between 90° and 180°. If it is assumed that the directional effect is due to the emission of neutrons from the moving fragments, the experiment indicates that at least twice as many neutron pairs originate from opposite fragments as from the same fragment. The alternative is to assume that pairs of neutrons are emitted preferentially in opposite directions from the same fragment, which is inherently improbable*.

It is interesting to note that Peierls[99] has laid down certain criteria which must be obeyed by any distribution in energy of neutrons which are

* Fraser[98a] has published a preliminary report of experiments on the angular distribution of prompt neutrons from the slow neutron fission of Pu^{239}. The ratio of the neutrons emitted in the directions of the light and heavy fragments is $1{\cdot}72 \pm 0{\cdot}06$. It appears from these experiments that the light fragment emits about 30% more neutrons than the heavy.

emitted isotropically from the moving fragments, and that the energy distribution of eq.(7) appears to be consistent with these.

The angular distribution of the prompt γ-rays from the slow neutron fission of U^{235} has been investigated by ROSE and WILSON [100]. The source was a foil of U^{235} situated in a slow neutron beam. A proportional counter detected those fragments which were emitted in a cone of semi-angle approximately 20°. and the bias could be set so that it detected either both the fragments or only the light fragment. The coincident γ-rays were detected by a sodium iodide scintillation detector, which could be rotated with respect to the direction of the fission fragment. Small corrections were necessary for scattering of the γ-rays by the metal parts of the apparatus.

Significant variations in the coincidence rate were found as the angle between the γ-ray detector and the fragment was changed. In the first place there was a fairly sharp maximum when the γ-ray detector was behind the proportional counter. This was interpreted as being due to delayed γ-rays (half-life $\sim 0{\cdot}1$ μ-sec) emitted from fragments stopped in the counter. After this peak had been subtracted there were still variations of the order of 20% in the γ-ray intensity as a function of energy, which could be expressed by the expansion $(1 + a\cos\theta + b\cos^2\theta)$. The simplest interpretation of a $\cos\theta$ term of this magnitude is that the fragment which goes into the foil radiates after it has come to rest, while the other fragment radiates before it has slowed down appreciably. The sign of the $\cos^2\theta$ term means that rather more γ-rays are emitted in the line of the fission fragments than at right angles.

7. SPONTANEOUS FISSION

(7.1) *Experimental conditions*

Spontaneous fission, predicted theoretically by BOHR and WHEELER, was discovered experimentally, in uranium, by FLEROV and PETRZHAK[101], who showed that the phenomenon was very rare, and that it was not attributable to cosmic radiation, or to any known external cause.

There are two chief difficulties in experiments on this phenomenon, which are to some extent connected with each other. The first is due to the slow rate of spontaneous fission in all except a few of the transuranic nuclides. The second is due to the fact that the fissions must nearly always be measured against a heavy background of α-particles.

The majority of the experiments have been made with ionisation chambers, in which case the background of ionisation from the α-particles is a limiting factor. The pulses generated by single α-particles are five to ten times smaller than those of the least energetic fission fragment which it is desired to observe. Nevertheless if there is a finite chance of the fluctuation in the background of α-activity being as large as a fission pulse, the experiment is impossible. For this reason, even when the resolving time of the chamber and amplifier are reduced to a minimum, it is still impossible to observe fissions against a background of more than a few millicuries of α-particles. This, for instance, in the case of an α-emitter with a half life of about a year, represents only a few

micrograms of material*. Thus even though the spontaneous fission rate may be high, the actual counting rate may be very small, and long periods of observation may be necessary. For this reason it is, in many cases, impossible to do more than quote an upper limit for the spontaneous fission rate, indicating that no fissions have been observed during a certain period.

A very good method of reducing the effect of the α-particle background is to observe only the first part of the tracks[102], for the fission fragments ionise more heavily at the beginning of their ranges, and the α-particles at the ends of theirs.

Owing to the slow rate of counting it is necessary to have electronic apparatus in which no spurious pulses are generated. For this reason battery operated ionisation chambers and amplifiers are usually employed[103], and these are especially shielded from electrical disturbances. Mains driven apparatus, which is in many respects more convenient, can be used for the faster counting rates (down to about one count per day) if it is driven from a separate generator and if electrolytic condensers are not used in the early stages of the amplifiers[104]. It is also necessary in some cases to shield the fissile material against cosmic ray neutrons.

Photographic emulsions, loaded with the element to be investigated, have also been employed for the detection of spontaneous fission. When this technique is used it is necessary to prepare an image free from α-particle tracks. This can be done either by using an emulsion which is only sensitive to the heavy fission tracks, or by bleaching, or by the use of selective developers. Whichever method is used, all the detail of the fission tracks is lost[105]. The labour of searching for the rare fission events may be very great. The results obtained by this method have, in fact, nearly all been superseded by better experiments performed with ionisation chambers.

(7.2) *Spontaneous fission rates*

The spontaneous fission rates of nearly twenty nuclides have been measured by counting methods, most of them at the Los Alamos laboratory by SEGRÈ, CHAMBERLAIN, FARWELL, JUNGERMAN and WIEGAND. The results of these experiments, and those of several other workers have been summarised by SEGRE[103], and are included in the following table.

In Fig. 18 the spontaneous fission rates are plotted[106a, b], on a semi-logarithmic scale, against the parameter Z^2/A. It will be observed that, with the exception of U^{234}, all the points for the even-even isotopes lie upon a line of very low curvature. The exceptional behaviour of U^{234} is so striking as to suggest that further work upon it would be worth while. Experiments upon the even-odd and odd-even isotopes are more difficult because the spontaneous fission rates are so low, and the experimental results are correspondingly more scanty. The points for these isotopes do appear to lie upon two curves.

* In such cases α-particle counting may be the only practicable method of measuring the amount of material present, and the accuracy of the result depends upon a knowledge of the α-half life. Another method is to put the specimen in a known neutron flux, in which case it is necessary to know the fission cross-section.

Table 17—Spontaneous fission rates. (The estimated errors are those of the original authors)

Nuclide	*Fissions observed*	*Hours of observation*	*gm hr of observation*	*Fissions per gm per sec*	*Reference*
Ra^{226}	2			$\ll 0{\cdot}6$	106
Th^{230}	2	1326	1·45	$<3{\cdot}8\times10^{-4}$	103
Th^{232}	178	6300	1202	$4{\cdot}2\times10^{-5}$	103
Pa^{231}	11	2200	0·62	5×10^{-3}	103
U^{232}	3	950	5×10^{-5}	16	103
U^{233}	1	1050	1 35	$<2\times10^{-4}$	103
U^{234}	0	3370	$3{\cdot}4\times10^{-2}$	$<9\times10^{-3}$	103
U^{234}	0	313	$1{\cdot}25\times10^{-3}$	$<0{\cdot}4$	107
U^{235}			(see note * below)	$(3{\cdot}0\pm1{\cdot}7)\times10^{-4}$	103
U^{238}			(see note * below)	$(6{\cdot}90\pm0{\cdot}24)\times10^{-3}$	103
Np^{237}	6	1480	1·11	$<1{\cdot}4\times10^{-3}$	103
Np^{239}	0	146	$2{\cdot}5\times10^{-5}$	<11	103
Pu^{238}	144	833	19×10^{-6} **	$2{\cdot}14\times10^{3}$ **	103
Pu^{239}	12	10000	0·33	$1{\cdot}0\times10^{-2}$	103
Am^{241}	3	2700	$(1{\cdot}6\times10^{-5})$†	(46)†	103
Cm^{242}				$(7{\cdot}56\pm0{\cdot}2)\times10^{6}$	108

* The rates for U^{235} and U^{238} are calculated from the results of a number of experiments with mixtures of varying isotopic composition.

** Based upon a half-life for α-decay of 60 years. The current value is 90 years, and the spontaneous fission rate should be reduced in proportion.

† The half-life for α-decay is quoted in the original paper as 40 years, whereas the accepted values are 400–500 years. We have assumed that this is a misprint.

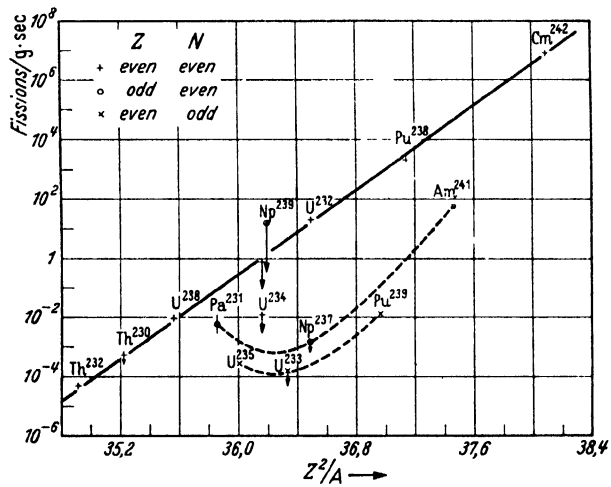


Fig. 18. Spontaneous fission rates as a function of Z^2/A. (A point with an arrow indicates an upper limit.)

(7.3) *Neutron and γ-ray emission in spontaneous fission*

The greater part of the work upon neutron emission in spontaneous fission has been summarised by SEGRÈ[103]. The neutrons were first detected by FERMI, by observations on the neutron density in a pile just below the critical size. According to SEGRÈ the best value is obtained from a similar experiment

in the Clinton pile, which gives for uranium (238) a value of $(1{\cdot}5 \pm 0{\cdot}15) \times 10^{-2}$ neutrons per gram per second. This is in good agreement with several independent observations made with BF_3 counters, of which work SEGRÈ gives a summary. More recently LITTLER[109] has made an experiment on the Gleep pile at Harwell, using, for comparison, a source calibrated by the sensitive "pile oscillator" method, and finds a value of $(1{\cdot}65 \pm 0{\cdot}1) \times 10^{-2}$ neutrons per second per gram of U^{238}. It should be pointed out that part of the charge of the Gleep pile is uranium oxide, so that if any $O(\alpha, n)$ reactions took place the apparent neutron emission would be increased. However, measurements on the neutron emission of oxygen when subjected to bombardment by polonium α-particles[110], show that this effect would be negligible. We may therefore take LITTLER's value for the neutron emission with SEGRÈ's for the spontaneous fission rate, from which we obtain the number of neutrons per fission

$$(U^{238}) = 2{\cdot}4 \pm 0{\cdot}2.$$

The emission of neutrons from thorium was measured by POSE[111]. This measurement is considerably more difficult than the corresponding experiment with uranium, and is probably in error, because the result is $0{\cdot}24 \times 10^{-3}$ neutrons per gram per second (according to SEGRÈ's recalculation of the results) leading to $\nu(Th^{232}) = 5{\cdot}7$, which seems higher than is probable.

BARCLAY, GALBRAITH and WHITEHOUSE[111a] give a ratio of the neutron emissions from the spontaneous fission of natural uranium and thorium of $(153 \pm 10\%)$. Using LITTLER's value for the neutron emission of uranium we obtain a value of about $1{\cdot}08 \times 10^{-4}$ neutrons per gram per second from thorium. Combining this with SEGRÈ's value for the spontaneous fission rate we obtain $\nu(Th^{232}) = 2{\cdot}6 \pm 0{\cdot}3$.

There is no quantitative information about the prompt γ-rays from spontaneous fission, but they have often been observed, and appear to have about the same energy and relative intensity as those from neutron-induced fission.

(7.4) *The mass and energy distribution of the fragments from spontaneous fission*

Some very interesting results have been obtained by MACNAMARA and THODE[112], by means of mass spectrographic analysis of the rare gases in uranium minerals, which give information about the mass distribution of the fission products from spontaneous fission. Their curve, which is reproduced in Fig. 19, indicates that the distribution is very similar to that from neutron-induced fission. Since there is the strongest evidence for assuming that the curve is symmetrical, the justification for the dotted parts of the curve is stronger than might be supposed at first sight. MACNAMARA and THODE's results do not give any information about the central minimum of the yield curve, and it would be interesting to know whether this is deeper than for neutron-induced fission.

A direct comparison between the energy distribution of the fragments from spontaneous fission of U^{238} and from neutron-induced fission of U^{235} has been made by WHITEHOUSE and GALBRAITH[104]. The experiment was made in a large

gridded ion chamber, using about 60 mg of natural uranium spread over about 675 sq.cm. This thickness was necessary to obtain a spontaneous fission counting rate of about 0·6 per hour. The spontaneous fissions were observed with the chamber shielded from cosmic ray neutrons, and the neutron-induced fissions were observed, under identical conditions, by bringing up a neutron source. Both energy distributions were slightly, but equally, distorted owing to the thickness of the uranium film. The results are shown in Fig. 20, from which it will be seen that there is no significant difference between the two distributions.

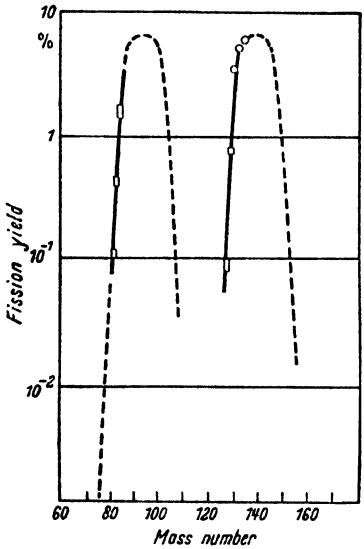


Fig. 19. Mass fission yield from spontaneous fission of U^{238}. (MacNamara & Thode[112].)

A similar experiment on Cm^{242} by Hanna, Harvey, Moss and Tunnicliffe[108] also yielded two peaks, with maxima at about 95 and 65 Mev, but the statistical accuracy was less than in the preceding measurements.

(7.5) *Similarity between spontaneous and induced fission*

It was at one time thought that the asymmetry of neutron-induced fission might be related to the excitation of the nucleus, and that spontaneous fission might be expected to be symmetrical. This hypothesis is excluded by the experiments mentioned above. Experiments on spontaneous fission are naturally less accurate than those on induced fission, but they appear to indicate, unanimously, that the two processes are closely similar if not identical.

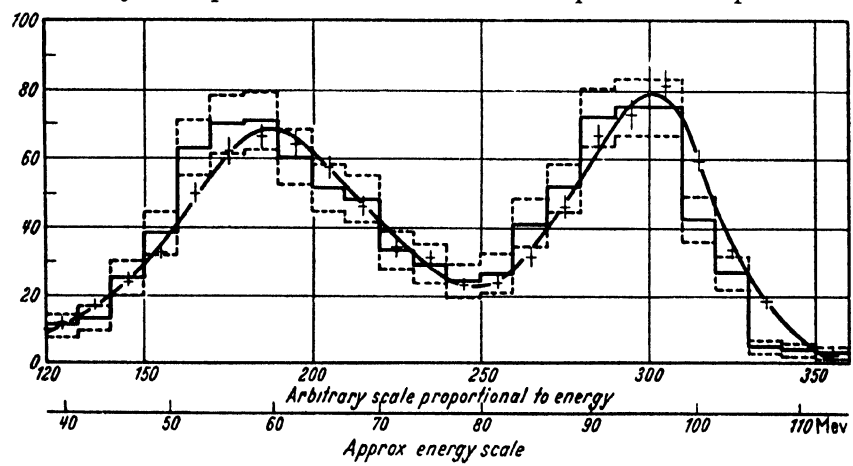


Fig. 20. Comparison of the energy distributions of the fragments from spontaneous fission (histogram) and from neutron-induced fission continuous line. (Whitehouse & Galbraith[104].)

The measurements of spontaneous fission rates emphasise the inadequacies of the liquid drop theory of fission, and of simple ideas of barrier penetration. These offer no explanation of those wide divergences in behaviour between neighbouring isotopes, which appear to be connected with the exact numbers of neutrons and protons in the nucleus.

8. Fission and the Shell Model of the Nucleus

It was pointed out briefly by Mayer[14], and independently and in more detail by Meitner[15], that the asymmetry of fission might have some connection with the shell model of the nucleus; if more than 132 neutrons are available, fragments would tend to form with shells of 50 and 82 neutrons respectively. Meitner especially stresses the fact that fission of bismuth by fast particles is predominantly symmetrical; this she attributes to the fact that in this case there are not enough neutrons. It had been suggested that the difference lies in the high energy of the particles needed to cause bismuth fission; however it is likely that a number of neutrons are evaporated first, and that the ultimate fission process occurs with little energy to spare, just as in the slow neutron fission of uranium. On the other hand, it appears somewhat doubtful to what extent neutron shells can be assumed to be effective in the highly excited and badly deformed nascent fragments. It had long appeared to be anomalous that symmetrical fission, for which the ordinary semi-empirical binding energy formulae predict a maximum total release of energy, should be approximately 600 times less probable with slow neutrons, than fission into fragments with a mass ratio of about 3:2. However the specially stable configurations of 50 and 82 neutrons or protons, which are among those postulated for the shell model, are expected to influence both the binding energies and the radii of nuclei. Irregularities of binding energy of several Mev are in fact indicated by mass spectrometer measurements, which are, however, not yet completely reliable in the regions of interest. Variations of energy in the neighbourhood of the shells containing 126 protons and neutrons can be deduced from the α-particle energies[113]. These might be sufficient to make asymmetric fission energetically more favourable[3].

The qualitative connection between the shell model and the mass yield curve is illustrated in Fig. 21, in which the most probable distribution of primary fission products is shown. This distribution is obtained from the mass yield curve (Fig. 8), making allowance for the prompt neutrons, and estimating the lengths of the decay chains from Glendenin's postulate of equal charge displacement (§ 3.5). The limits indicated on the figure are rather arbitrarily chosen at the points where the fission yields are 1%.

Let us visualise a very broad statistical distribution in mass of the primary fission products, constrained by the tendency to complete the 50 and 82 shells, where possible. The lower limit in mass of the heavy group of fragments is set by both the $Z = 50$ and $N = 82$ shells, and the sharp dip in the yield curve at about $A = 132$ can be attributed to this. The lower limit of mass of the light fragment can be attributed to the tendency to complete the $N = 50$ shell, and since only one "magic number" is operating, the slope of the

yield curve might be expected to be less steep. When we consider that the yield curve must be symmetrical, we see that a plausible (but no more than plausible!) explanation has been given for all its main features.

The variation of the mass yield curve with the mass number of the nucleus which is undergoing fission (Fig. 8) can also be understood in a qualitative manner by consideration of Fig. 21. The lower slope of the peak representing the heavy fragment, being associated with two magic numbers, remains very nearly the same for all three isotopes. In order to preserve symmetry the peak for the light fragment is obliged to move upwards if the mass of the original fissile nucleus is increased. The further this peak moves from the $N = 50$ magic number the less steep will we expect the two outer portions of the yield curve to be. This also seems to be in accordance with the experimental evidence.

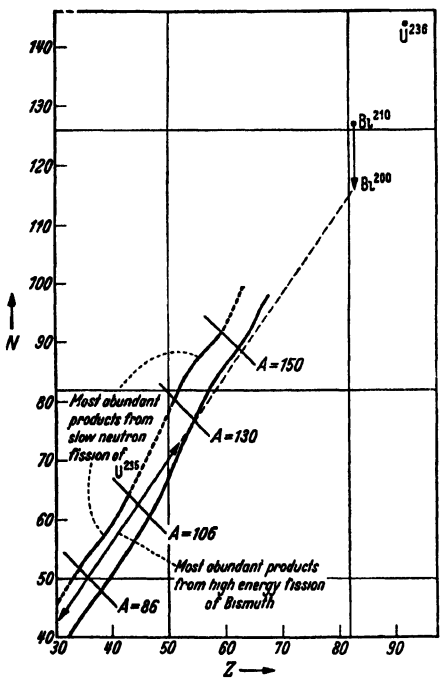


Fig. 21. Primary products from high energy and low energy fission.

The shell model has also been invoked to explain the delayed neutrons in fission. We observe first that the two delayed neutron emitters which have been identified with the greatest certainty (Kr^{87}, $Z = 36$, $N = 51$ and Xe^{137}, $Z = 54$, $N = 83$) both have just one more neutron than the stable shell. The last neutron might therefore be expected to be particularly loosely bound, and in general, nuclei with 51 or 83 neutrons might form the majority of the delayed neutron emitters.

GLENDENIN[70] has suggested that delayed neutron emitters of this type might be responsible for the irregularities in the mass yield curve discovered by THODE and GRAHAM, and discussed in § 3.1. His explanation is discussed by WAY and DISMUKE[45] and also by MACNAMARA, COLLINS and THODE[53]*. It gives a qualitative explanation of the anomalous fission yields, but the more quantitative estimations do not fit the observed data very well.

9. The Emission of Light Nuclei During Fission

(9.1) *The discovery of the particles*

The emission of light nuclei of long range in the fission of uranium was noticed by ALVAREZ (quoted by FARWELL, SEGRÈ and WIEGAND[114]), and was investigated by several groups of workers in the United States[114, 116], and Canada[115],

* See also GLENDENIN, STEINBERG, INGHRAM and HESS[53a], in which evidence is given for a preferential tendency to form the masses 133–136, and the complementary masses 98–100, in the primary fission process. This is supposed to be connected with the 82 neutron shell.

but the results were not published until after the war. Independently GREEN and LIVESEY[117], and TSIEN, CHASTEL, HO and VIGNERON[118] observed the particles. CASSELS, DAINTY, FEATHER and GREEN[119] first showed the presence of a more abundant group of short-range particles. Both these groups have now been extensively investigated both by the photographic plate technique and by counting methods. There are still, however, some points of disagreement between the various groups of workers, which will become apparent in the succeeding paragraphs.

(9.2) *The long-range particles*

FARWELL, SEGRÈ and WIEGAND[114], using a coincidence arrangement and a double ionisation chamber, found light particles with ranges up to 23 cm of air, and measured the frequency of their occurrence (Table 18). By measurements of ionisation they showed that the particles were probably α-particles, and this agrees with the majority of measurements of grain density in photographic emulsions [115, 116, 117, 120, 122]. TSIEN[121] however found masses varying from 2 to 9.

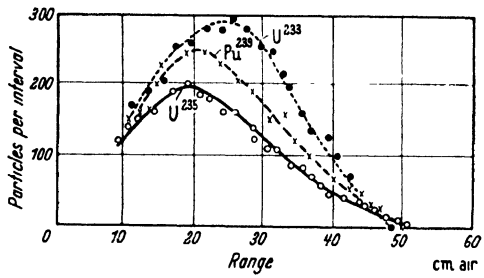


Fig. 22. Range distributions of long range particles emitted in fission. (ALLEN & DEWAN[127].)

A careful investigation in photographic emulsions of both the long and short range groups was published by GREEN and LIVESEY[122], and TITTERTON[123] has studied the tracks of 600,000 fission events. The results of these Herculean labours have not as yet been published in full, and it is not possible to do justice to them in this account. Evidence for the emission of long range particles in the photo-fission of Th and U, by Bremsstrahlung with a maximum energy of 23 Mev, has been presented by TITTERTON and GOWARD[124] and TITTERTON and BRINCKLEY[125].

TSIEN and his associates found that the long range particles were not emitted in the fast fission of thorium and uranium, with neutrons produced by 6·7 Mev deuterons on beryllium. This result appears to be contradicted by TITTERTON[126] who found 8 long range particles among 12,000 fissions in uranium, and 8 among 14,000 fissions in thorium, using 2·5 Mev neutrons in each case.

ALLEN and DEWAN[127] have made a careful study of the long range particles emitted in the slow neutron fission of U^{233}, U^{235} and Pu^{239}, using counting methods dependent upon two different arrangements of proportional counters, and upon a double ionisation chamber. They confirm much of the previous work, but with greater statistical accuracy. They find, by comparison of range and energy distributions, that all the particles are α-particles, and, in particular, that no protons are emitted. The range distribution is continuous, and extends to 50 cm of air, with a broad maximum near 20 cm (Fig. 22). The energy

distribution of the particles from U^{235} is fairly symmetrical about 15 Mev, with a maximum about 26 Mev (Fig. 23).

The energy distribution of the fission fragments coincident with the long-range α-particles was compared directly with that resulting from normal binary fission, and the usual two peaks were found, (Fig. 24), the ratio of the energies of the light and heavy fragments being the same in each case. How-

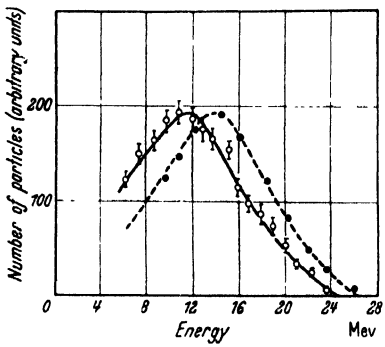


Fig. 23

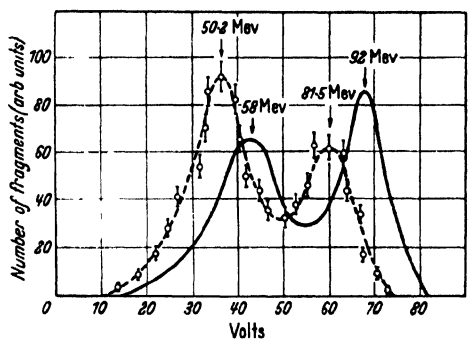


Fig. 24

Fig. 23. Energy distribution of long-range particles emitted in the fission of U^{235}. The broken line shows the distribution after correction for absorption in the aluminium foil which was introduced to stop the fission fragments and natural α-particles. The full circles indicate the values predicted from the range measurements. (ALLEN & DEWAN[127].)

Fig. 24. Energy distribution of fission fragments. The broken curve represents fragments in coincidence with long-range α-particles. The solid curve is the normal distribution taken under identical conditions. The reduced size of the high energy peak is an instrumental effect. (ALLEN & DEWAN[127])

ever, when a long range α-particle is emitted, the kinetic energy of the two heavy fragments is reduced, so that the total kinetic energy is approximately the same as in binary fission.

ALLEN and DEWAN's estimates of the frequency of emission of long-range α-particles is not in agreement with other experiments (Table 18).

The reason for this disagreement is not clear, but as suggested by ALLEN and DEWAN it may be due to a different energy distribution in the neutrons

Table 18—Rate of occurrence of long range α-particles emitted in fission

Observers	*Nuclide*		*Type of neutron*
ALLEN and DEWAN . .	Pu^{239}	1 in 445 ± 35	Pile
ALLEN and DEWAN . .	U^{235}	1 in 550 ± 30	Thermal
		1 in 505 ± 50	Pile
ALLEN and DEWAN . .	U^{233}	1 in 405 ± 30	Pile
TITTERTON	U^{235}	1 in 422 ± 50	Pile
GREEN and LIVESEY .	U^{235}	1 in 300	Cyclotron produced and slowed down
FARWELL, SEGRE and WIEGAND	Pu^{239}	1 in 500	Cyclotron produced and slowed down
FARWELL, SEGRE and WIEGAND	U^{235}	1 in 250	Cyclotron produced and slowed down
DEMERS.	U^{235}	1 in 250	Ra-α-Be slowed down
MARSHALL.	U^{235}	1 in 230	Thermal from pile

causing the fission. The sources of the neutrons used in the experiments are indicated in the last column of Table 18, from which it will be obvious that there is no very obvious correlation between them and the frequency of occurrence of α-particles.

The angular distribution of the long range particles was not studied by ALLEN and DEWAN, but has been investigated several times. TITTERTON[123] has probably collected the greatest number of observations, and his results are accordingly given in Fig. 25. The most probable angle of the light particle with the direction of the two main fragments is not quite a right angle, but is inclined towards the track of the lighter, or more energetic fragment. This is in accordance with the hypothesis that the three particles are formed simultaneously, with low kinetic energy, and then fly apart under the influence of their mutual electrostatic repulsions. TSIEN[121] has made a detailed analysis of this process, using a simplified model consisting of spheres in contact, and has shown that the time required for the particles to separate and attain nearly their full velocity would be less than 10^{-20} sec*.

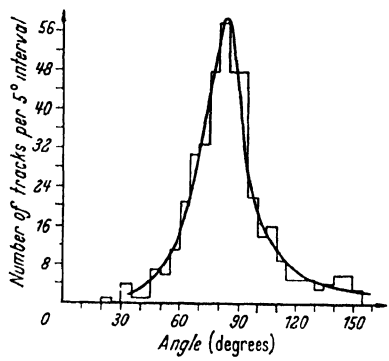


Fig. 25. Angular distribution of light, long-range particles emitted in the slow neutron fission of uranium. (TITTERTON[123].)

There is no detailed and generally accepted explanation of the formation of the long-range particles. FEATHER[128] suggested that the α-particle is emitted from a highly excited fragment whose mass is in one of the regions of α-instability ($Z \sim 40$ and $Z \sim 60$). The very high state of excitation of the fragment is invoked to explain the emission of the α-particle within so short a time. According to this view the ratio of the masses of the main fragments, in coincidence with the α-particles, should be rather larger than that which is observed, but not sufficiently so to be directly contradicted by the experimental evidence.

An alternative view is that the α-particle is emitted during the actual process of fission. It has been compared to the "plateau droplet" which is often seen to form in the division of ordinary liquid drops. As the two main fragments moved further apart, an α-particle in the neck of the dumb-bell would be accelerated by electrostatic forces, in the manner described by TSIEN.

(9.3) *The short-range particles*

The existence of short range particles emitted in the fission process was first shown by CASSELS *et al.*[119] in an arrangement of two counters at right angles, one of which detected a fission fragment and the other the particle. It is difficult to distinguish between a short-range particle emitted in fission and the

* DEMERS, with his "sandwich" technique, by which the origin of the fission fragments is located in the emulsion, has shown experimentally that the α-particle is emitted within 10^{-14} sec.

recoil of a light atom struck by the fragment. GREEN and LIVESEY[122] however found, in uranium loaded emulsions, that there were more short tracks branching from the main track of the fragments near the centre than could be accounted for by recoils from the moving fragments. They concluded that genuine emission of light particles with a range up to 8 mm of air occurred in about 1 % of fissions, and that the particles were emitted preferentially at right angles to the main fission track, though with a broader distribution than the long range particles. (See Fig. 26.)

TSIEN[121] and his collaborators observed light particles of about the same abundance, but gave 3 cm air equivalent as the maximum range. Since, however, none of these workers distinguished between the kind of particle emitted in the two cases, the definition of the upper limit of the short-range particles may perhaps be regarded as arbitrary.

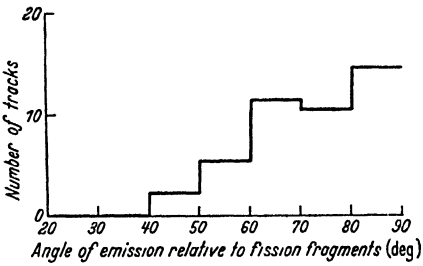


Fig. 26. Angular distribution of short-range light particles. (GREEN & LIVESEY[122].)

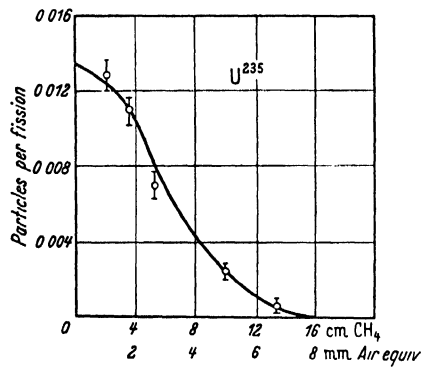


Fig. 27. Ranges of short-range particles from U^{235}. (ALLEN & DEWAN[129].)

MARSHALL[120] concluded that the short tracks observed by GREEN and LIVESEY were all recoil atoms, but this does not appear to be confirmed by later work with proportional counters.

ALLEN and DEWAN[129] working with two windowless proportional counters, a geometrical arrangement similar to that of CASSELS *et al.*, studied the ranges and specific ionisations of the short range particles emitted in the slow neutron fission of U^{233} and U^{235}. They were able to show that the particles were not recoil atoms from the material in the foil or the gas in the counter. Neither were they fission fragments scattered back from the source. In order to find the total abundance of the particles they had to use the angular distribution of GREEN and LIVESEY, since their observations were confined to one angle. Their results for U^{235} indicate that short range particles are emitted with a frequency of 1 in 76 ± 8 fissions, and with a maximum range of 8 mm air equivalent (Fig. 27). The maximum specific ionisation of the particles is at least ten times as great as for α-particles. For U^{233} they obtained an abundance of 1 in 72 ± 6 fissions and a maximum range of 7·4 mm of air.

ALLEN and DEWAN were not able to determine the masses of the particles from their observations*. Photographic plate evidence is against masses

* The figure 12 ± 1 attributed to them by TITTERTON and BRINCKLEY is a misquotation. If it is assumed that the maximum initial specific ionization corresponds to the maximum range, then an estimated mass of 13 ± 4 is obtained. There is little justification for this assumption.

greater than 12, while the measurements of specific ionisation suggest that the particles are heavier than α-particles. It seems clear, however, that the processes of emission of the short and long range particles are quite different.

GOWARD, TITTERTON and WILKINS[130] have reported an event, observed in photographic emulsion, in which it appears probable that a Be^8 nucleus is emitted during fission, which immediately breaks up into two α-particles.

10. FISSION INTO THREE OR MORE PARTS OF COMPARABLE SIZE

The possibility of true ternary fission into three parts of comparable size was foreseen on theoretical grounds by BOHR and WHEELER[5], and by PRESENT and KNIPP[8, 131]. From the mass differences it can be shown that the total energy released in ternary fission should be greater than in binary fission, but the process was nevertheless expected to be rare.

A phenomenon resembling fission into three or into four approximately equal parts has been observed by TSEIN and his associates[121] and by DEMERS[115]. TSEIN *et al.* claim these events as genuine ternary and quarternary fissions. TITTERTON[123], however, claims that the similar events observed by him are explicable on the hypothesis that the additional tracks are due to silver or bromine atoms from the emulsion, recoiling after having been struck by the fission fragments.

The frequency of tripartition of U^{235} has been investigated by ROSEN and HUDSON[132] in a triple pulse ionisation chamber, which was so arranged that if one fragment from a normal binary fission entered the part of the chamber designated II, the other fragment could enter either I or III but not both. A coincidence was not recorded unless at least 40 Mev was released simultaneously in all three portions of the chamber.

Because the phenomenon of tripartition is so rare fast counting rates had to be used in order to obtain statistically significant results, and there was a comparatively high probability of two binary fissions occuring within the resolving time of the apparatus. The confusion between these pairs of binary fissions and a true triple fission can be reduced by rejecting all events in which more than 100 Mev is released in part II of the chamber. After all these precautions the probability of two separate binary fissions being observed was high compared to that of a ternary fission. However a linear function could be found, connecting the triple and single counting rates, which by extrapolation to zero gave the rate of true ternary fissions. By this rather indirect method ROSEN and HUDSON obtained a rate for tripartition into three approximately equal parts of $6{\cdot}7 \pm 3{\cdot}0$ per 10^6 binary fissions.

We have seen that the emission of light nuclei of short range is a comparatively common event, occurring in more than 1 % of fissions, that the emission of long range α-particles is comparatively uncommon, and that true ternary or quaternary fission is extremely rare. It is improbable that the processes leading to the two groups of light particles are at all similar. It may be, however, that the emission of the short range light particles is essentially the same as ternary fission. If penetration of the Coulomb barrier plays any part in ternary fission, the discrimination in favour of the escape of a particle of small mass would be very great.

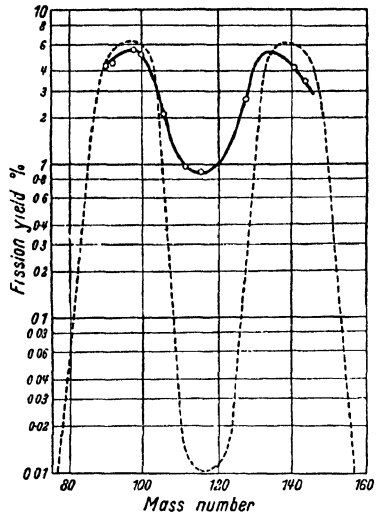


Fig. 28. Fission yields from U^{235} with 14 Mev neutrons compared with the thermal yield.

11. The Characteristics of Very High Energy Fission

Fission produced by very energetic particles, which cause a very high degree of excitation in the nucleus, has certain characteristics of its own. The phenomenon was reported by Perlman, Goeckermann, Templeton and Howland[133] who observed the presence of fission products in all the elements from bismuth to tantalum after bombardment with very fast neutrons, protons or deuterons. The fission of uranium by 380 Mev α-particles has been studied by O'Connor and Seaborg[134] and of bismuth and lead with 190 Mev deuterons by Goeckermann and Perlman[135], using quantitative chemical methods to study the fission product yields. Jungerman and Wright[136] have investigated the fission of U^{238}, U^{235}, Th^{232} and Bi^{209} by 90 Mev and 45 Mev neutrons, using a gridded ionisation chamber to measure the fragment energies. Newton[137] has investigated the fission of Th^{232} with 34 Mev

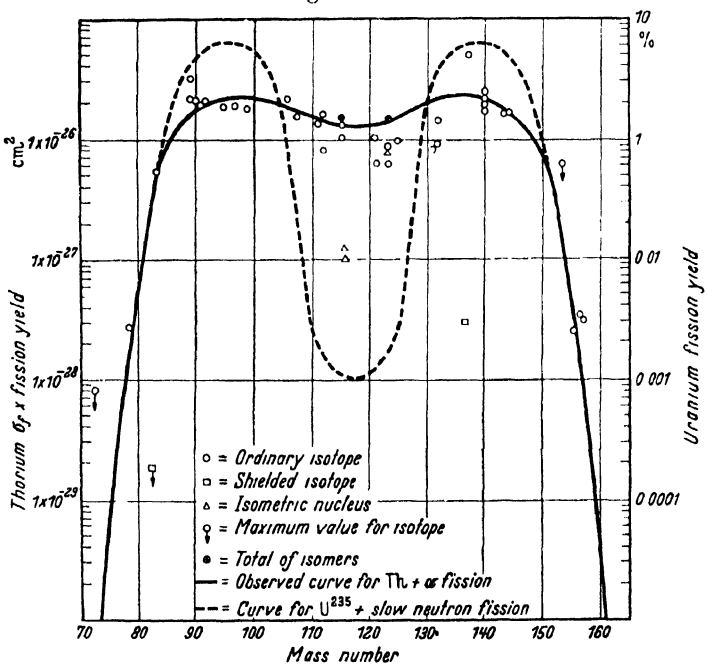


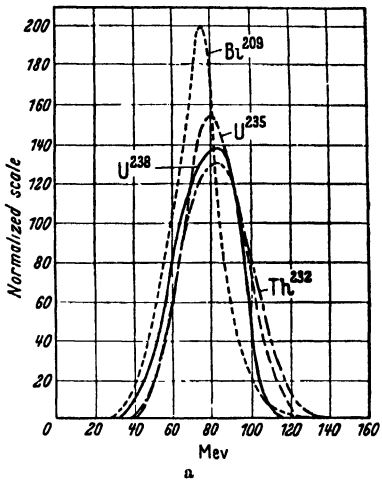
Fig. 29. Fission yield of thorium with 38 Mev helium ions, compared to that with slow neutrons. (Newton[137].)

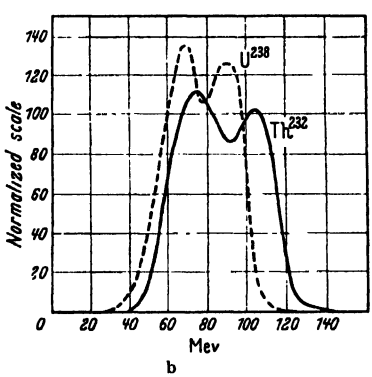
α-particles using chemical methods to detect the mass yield of the products. In addition there have been a number of experiments with neutrons up to

about 15 Mev*, so that the transition between low energy and high energy fission has been quite thoroughly explored.

The first characteristic of high energy fission is that symmetrical cleavage of the nucleus is predominant. As the total excitation energy of the prompt neutron is increased, the central depression in the mass yield curve is seen to fill up, and a single-peaked curve is obtained. Fig. 28 shows the yield from the fission of U^{235} with 14 Mev neutrons[138], compared with that from thermal neutron fission. Fig. 29 shows NEWTON's chemical yield curve for the fission of Th^{232} by α-particles of 38 Mev. This curve is directly comparable with the preceding, because the compound nucleus U^{236} is the same in each case.

Fig. 30a and b shows some of JUNGERMAN and WRIGHT's curves for the fission of various nuclides by neutrons with most probable energies of 90 Mev and 45 Mev





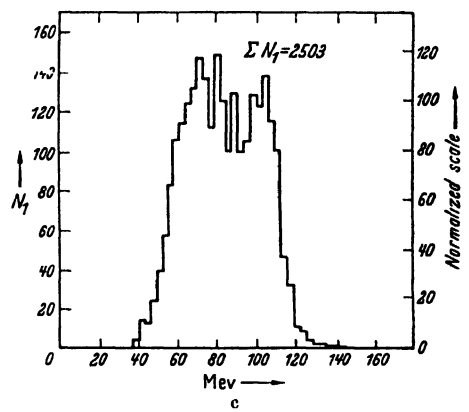


Fig 30(a). Probable fragment energy distributions for 90 Mev neutrons on U^{238}, U^{235}, Th^{232} and Bi^{209}.
(b) Probable fragment energy distributions for 45 Mev neutrons on U^{238} and Th^{232}.
(c) Single fragment distributions, 45 Mev neutrons on Th^{232}. (From JUNGERMAN & WRIGHT[136].)

and Fig. 30c shows one of the histograms on which the curves are based, in order to enable the reader to estimate the statistical accuracy of the experiment.

Fig. 31 is GOECKERMANN and PERLMAN's chemically determined mass distribution for the fission of bismuth with 190 Mev deuterons. This curve shows no sign of a double peak, and the average mass number of the products is about $A = 100$.

The fission products formed at these high energies are noticeably different from those obtained in slow neutron fission. The β-decay chains are all short,

* See for instance FRIEDLAND[137a] on the fission of U^{235} by 2,5 and 14 Mev neutrons.

and many stable isotopes are formed as primary products. Further, the lighter fragments tend to emit β^--particles, but the heavier fragments may be neutron-deficient and decay by β^+-emission or orbital electron capture.

These facts can all be explained in the following manner. It is supposed that the first stage, after the excitation of the nucleus, is the evaporation of a number of neutrons. The evaporation of charged particles from nuclei of such high atomic numbers is relatively improbable. Finally a stage is reached at which the nucleus, which is still rather highly excited, becomes unstable owing to the increase in the "fission parameter" Z^2/A. Fission then occurs very rapidly without allowing time for any re-arrangement of the nucleons, so that the charge and mass divide in the same proportions. This is in contrast to fission at low energies, in which the Postulate of Unchanged Charge Distribution (§ 3.5) does not appear to hold.

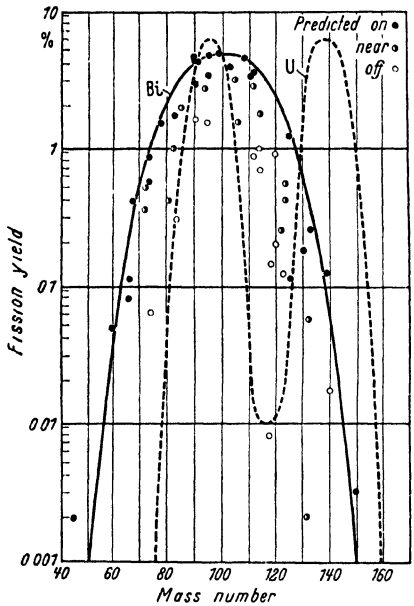


Fig. 31. Yields for products of the irradiation of bismuth with 190 Mev deuterons. (From GOECKERMAN & PERLMAN[138].)

The process is illustrated diagrammatically in Fig. 21 for the compound nucleus of Bi^{210}. Ten neutrons are supposed to be evaporated from this nucleus in the first stage, in order to account for the mean mass-number of the products. See YAMAGUCHI[139] for a theoretical discussion. As can be seen from the diagram the lighter primary products are above the stability line, and have a neutron excess, while the heavier are below it, and are neutron deficient. The value of Z^2/A for Bi^{199} is approximately the same as that for the naturally occurring uranium isotopes.

The hypothesis outlined above leads us to expect that the yield in high energy fission will decrease with the mass of the isotope which is bombarded, because the value of Z^2/A is less, and more neutrons have to be evaporated before fission can occur. This is in accordance with the experiments of GOECKERMANN and PERLMANN[135] who used deuterons to bombard two samples of lead, which had been enriched in Pb^{204} and Pb^{206}. The former gave greater fission yields of Mo^{99} for all deuteron energies, the ratio being 30:1 at 30 Mev and 3·5:1 at 100 Mev.

The same process can be used to explain the results of JUNGERMANN and WRIGHT on the kinetic energy of the fragments. It has long been realised that the kinetic energy of the fragments in ordinary asymmetric fission is very nearly equal to the electrostatic potential energy at the instant of fission, if for the purposes of calculation the fragments are treated as spheres in contact. Thus the kinetic energy in asymmetric fission would be

$$E_a = (Z_1 Z_2)\, e^2/r_0\, (A_1^{\frac{1}{3}} + A_2^{\frac{1}{3}})$$

where Z_1, Z_2 are the atomic numbers and A_1. A_2 the mass numbers of the fragments, and r_0 is approximately $1{\cdot}5 \times 10^{-13}$ cm. For high energy symmetric fission, with neutrons

$$E_s = (Ze/2)^2/2r_0\,((A-J+1)/2)^{\frac{1}{3}}$$

where Z and A are the atomic and mass number of the original nucleus, and J is the number of neutrons which evaporate. The ratio E_s/E_a is 0·88 for bismuth and uranium respectively according to JUNGERMANN and WRIGHT's calculation and $0{\cdot}94 \pm 0{\cdot}04$ by experiment.

BATZEL and SEABORG[140] have given reasons for supposing that medium weight elements undergo a process which might properly be called fission. They were investigating the spallation reactions of such elements and found that a number of relatively heavy radioactive products were formed. For instance Cl^{38} was produced from copper at a bombarding energy insufficient to account for a true spallation reaction such as $Cu^{63}(p, pn\,6\alpha)Cl^{38}$. However a reaction such as $Cu^{63} + p \rightarrow Cl^{38} + Al^{25} + n$ would have been energetically possible. They have also observed Na^{24} from Cu, $Se^{43, 44}$ from Br, Co^{61} from Ag, Na^{24} and $Ga^{66, 72}$ from Sn, and $Ga^{66, 72}$ from Ba. The recoil energies of the products also support the hypothesis of a process similar to fission. For instance Cr^{49}, formed from copper has a recoil energy of about 5 Mev even after allowance has been made for the recoil due to the impinging proton. This is easily explicable by a reaction such as $Cu^{63} + p \rightarrow Cr^{49} + C^{12} + 3\,n$. In a true spallation reaction, in which a number of lighter products were emitted, a very improbable degree of asymmetry would be required to explain the recoil of the Cr^{49} nucleus.

There appears, therefore, to be a more or less continuous series of reactions between the stars produced by cosmic rays and other energetic particles, and the familiar process of binary fission.

12. MISCELLANEOUS EXPERIMENTS

This section will be devoted to a short discussion of certain experiments which it has been difficult to classify elsewhere and which do not merit extended treatment.

(12.1) *Fission by π^--mesons*

Fissions have been observed in photographic plates, loaded with uranyl acetate, and exposed to slow π^--mesons in the Berkeley cyclotron[141]. According to theory, the meson is captured by a single proton within the nucleus, leading to the production of a neutron with an energy of the order of 100 Mev. Momentum is conserved by the recoil of one or more neighbouring nucleons. Thus we should expect fission of the uranium nucleus by π^--mesons to be of the same type as that initiated by high energy particles.

Twenty events were observed, this number being in agreement with the assumption that all uranium nuclei which capture a π^--meson undergo fission. The fission tracks were symmetrical about the point of entry of the meson, and were approximately the same length as those from neutron induced fissions.

Three of the events showed the emission of fast light particles, approximately at right angles to the line of the tracks of the main fragments. These tracks cannot be due to protons recoiling from the fission fragments and are probably explicable as recoil particles from the original fast neutron formed by capture of the meson.

Fission following π^--meson capture is thus, in all probability, almost exactly similar to very high energy fission induced by energetic particles, and Mrs. AL-SALEM's microphotographs appear to be the only visual records of this process which have been published.

(12.2) *The possibility of fission following the capture of μ^--mesons*

WHEELER[142] has forecast, on theoretical grounds, the possibility of fission occurring as a result of the capture of a μ^--meson by a heavy element. After it is captured the meson will occupy BOHR orbits near the heavy nucleus. The energy released in the $2s-1s$ transition in uranium is about 7 Mev*, and if this were imparted to the nucleus fission might occur. Quite distinct from this externally induced meson fission is the internally-induced fission which would be expected to follow the final capture of the meson by the nucleus. The meson reacts with one of the protons of the nucleus, producing a neutron and a neutral particle, probably a neutrino ($P+\mu^-\rightarrow N+\nu$). In this case most of the energy is carried away by the neutral particle, and the neutron receives a small fraction, the most probable value being of the order of 15 Mev[143]. It therefore seems extremely likely, according to this theory, that heavy nuclei such as uranium nuclei would undergo fission after capturing a μ^--meson.

Fission by μ^--mesons, if it exists would be very difficult to observe. GALBRAITH and WHITEHOUSE[144] have searched for fissions in uranium, in coincidence with penetrating charged cosmic ray particles. They found some fissions in coincidence with fast protons, but obtained no evidence of fissions in coincidence with μ^--mesons. The statistics of the experiment are, however, so poor that it is only possible to conclude that the probability of fission following capture of a μ^--meson is less than 0·3.

(12.3) *The apparent emission of a meson in fission*

An event was observed in one of the uranium loaded plates exposed at the Berkeley cyclotron, in which a 5 Mev meson and a fast proton were emitted from a nucleus undergoing fission. The energy released in fission is sufficient to make the production of a π-meson energetically possible, but the process is inherently improbable. However, as a result of this observation BRADNER and BOWKER[145] searched for π-mesons emitted during fission, with negative results. They infer that the original event was the direct production of a meson as the result of a very fast neutron striking a nucleon in uranium. The fission followed this event and was not directly associated with it.

* This is the figure for the normal nucleus; for the dumb-bell shaped nucleus predicted for the liquid drop theory of fission, the energy would, according to WHEELER, be reduced by 1 or 2 Mev.

(12.4) *A search for the hypothetical negative proton in fission*

The elusive negative proton has been sought for a number of years, especially by FEATHER[146]. One of the possible processes by which it might be formed is as the alternative to the emission by a fission fragment of a delayed neutron and a β-particle. If the negative and positive protons have the same mass the reaction is energetically possible. A number of possible modes of decay of the hypothetical particle were considered by SCOTT and TITTERTON[147] and it was concluded that its track would be visible at the end of the track of one of the fission fragments. Whether the track of the negative proton ended in a star or not, would depend upon its mode of decay.

In the course of various experiments $6{\cdot}5 \times 10^5$ fission tracks were observed in photographic emulsions, representing $1{\cdot}3 \times 10^6$ fragments, without any evidence of a negative proton. It is therefore concluded that the upper limit to the probability of the emission of a negative proton, as an alternative to a delayed neutron, is about 1 in 5×10^3.

(12.5) *A search for the hypothetical di-neutron in fission*

The expected properties of the hypothetical di-neutron have been discussed by several authors including FEATHER[148], who has suggested that it might be released in fission. A search for the di-neutron in a graphite pile was made by FENNING and HOLT[149] who irradiated bismuth and looked for the 2·16 minute α-activity of AcC^{211}, which might have been formed according to the proposed reaction $Bi^{209}(n^2, \gamma)AcC^{211}$. This experiment gave a negative result. In unfinished experiments FENNING is searching for He^6 formed by capture of the hypothetical di-neutron in He^4.

(12.6) *The time required for fission*

The time required for the fission process was investigated in 1939 by FEATHER by an ingenious method depending upon the recoil of the nucleus after being struck by a fast neutron[150]. He concluded that at least some of the fissions occurred within 5×10^{-13} sec. This experiment does not appear to have been repeated, with improved accuracy, during the intervening years.

WILSON[151] has carried out an experiment which is, in a sense, complementary to FEATHER's, which shows that practically all the fissions occur within 10^{-8} sec. He used a recoil method in a double ionisation chamber. If the uranium nucleus, struck by a fast neutron, had travelled through the gas of the chamber for longer than 10^{-8} sec before undergoing fission, their fragments would have been able to penetrate a grid, and coincidences in the two halves of the chamber would have been observed. WILSON was able to conclude that less than 1 in 5×10^5 fissions were delayed by this time.

REFERENCES

[1] TURNER, L. A.; *Rev. Mod. Phys.* 12 (1940) 1.
[2] A.E.R.E. Inf/Bib. 76 (1951).
[3] WICK, G. C.; *Brookhaven Conference Report* (BNL–C–9) 1949.
[4] MEITNER, L., and FRISCH, O. R.; *Nature, Lond.* 143 (1939) 239.

[5] BOHR, N. and WHEELER, J. A.; *Phys. Rev.* 55 (1939) 426.
[6] FRENKEL, J; *J. Phys. U.S.S.R.* 1 (1939) 125.
[7] — *ibid* 10 (1946) 533.
[8] PRESENT, R. D. and KNIPP, J. K.; *Phys. Rev.* 51 (1940) 75 and 1188.
[8a] — REINES, R. D. and KNIPP, J. K.; *ibid* 70 (1946) 557.
[9] FRANKEL, S. and METROPOLIS, N.; *Phys. Rev.* 72 (1947) 914.
[10] YASAKI, T. and MIYATAKE, O.; *Phys. Rev.* 79 (1950) 740, and 80 (1950) 754
[11] JUNGERMAN, J.; *Phys. Rev.* 80 (1950) 285.
[12] SWIATECKI, J.; *Phys. Rev.* 83 (1951) 178.
[13] HILL, D. L.; *Bull. Amer. Phys. Soc.* 26 (1951) (3) 45.
[14] MAYER, M. G.; *Phys. Rev.* 74 (1948) 235, *ibid* 78 (1950) 16.
[15] MEITNER, L.; *Nature, Lond.* 165 (1950) 561.
[16] BUNEMANN, O., CRANSHAW, T. E. and HARVEY, J. A.; *Can. J. Res.* A 27 (1949) 191.
[17] BROSER, I. and KALLMAN, H.; *Ann. Physik.* 4 (1948) 85.
[18] ROTBLAT, J.; *Progress in Nuclear Physics* I (1950) 37.
[19] *Nature, Lond.* 169 (1952) 871.
[20] FACHINI, U. and GATTI, E.; *Helv. Phys. Acta* 23 (1950) 556, and *Nuovo Cimento* 7 (1950) 589.
[21] FENNING, F., GRAHAM, G. and SELIGMAN, H.; *Can. J. Res.* 25 A (1947) 73.
[22] FERMI, E., MARSHAL, J. and MARSHAL, L.; *Phys. Rev.* 72 (1947) 193.
[23] BISWAS, S. and PATRO, A. P.; *Indian J. Phys.* 23 (1949) 97.
[24] PETERSON, S. and GHIORSO, A.; *National Nuclear Energy Series Div. IV*, Vol. 14 B, p. 1381.
[25] AMES, D. and GHIORSO, A.; *ibid* p. 1383.
[26] SEABORG, G. T., GOFMAN, J. W., STOUGHTON, R. W.; *ibid* p. 1426.
[27] GHIORSO, A., OSBORNE, D. W. and MAGNUSSON, L. B.; *ibid* p. 1639.
[28] HANNA, G. C., HARVEY, B. G., MOSS, N. and TUNNICLIFFE, P. R.; *Phys. Rev.* 81 (1951) 893.
[28a] STREET, K., GHIORSO, A. and THOMPSON, S. G.; *Phys. Rev.* 85 (1952) 135.
[28b] CUNNINGHAM, B. B. and GHIORSO, A.; *Phys. Rev.* 82 (1951) 558.
[29] KENNEDY, J. W., SEABORG, G. T., SEGRÈ, E., WAHL, A. C.; *Phys. Rev.* 70 (1946) 555.
[30] KLEMA, E. D.; *Phys. Rev.* 72 (1947) 88.
[31] FELD, B. T., FISHBACK, H., GOLDBERG, M. L., GOLDSTEIN, H. and WEISSKOPF, V. F.; NYO 636.
[32] SHOUPP, W. E. and HILL, J. E.; *Phys. Rev.* 75 (1949) 785.
[33] KELLY, E. L. and WIEGAND, C.; *Phys. Rev.* 73 (1948) 1135.
[34] JUNGERMAN, J. and WRIGHT, S. C.; *Phys. Rev.* 74 (1948) 150.
[35] — *Phys. Rev.* 79 (1950) 632.
[35a] HOLLANDER, J. M.; UCRL 1396.
[36] HAXBY, R. O., SHOUPP, W. E., STEVENS, W. E. and WELLS, W. H; *Phys. Rev.* 59 (1941) 57.
[37] CHARBONNIER, G., SCHERRER, P. and WÄFFLER, H.; *Helv. Phys. Acta* 22 (1949) 385.
[38] ARAKATSU, B., UEMURA, Y., SONODA, M., SHIMIZU, S., KIMURA, K. and MURAOKA, K.; *Proc. Phys.—Math. Soc. Jap.* 23 (1941) 440.
[39] BALDWIN, G. C. and KLAIBER, G. S.; *Phys. Rev.* 71 (1947) 3.
[40] OGLE, W. E. and MCELHINNEY, J.; *Phys. Rev.* 81 (1951) 344.
[41] GOWARD, F. K., JONES, E. J., WATSON, W. H. H. and LEES, D. J.; *Proc. Phys. Soc.* 64 A (1951) 96.
[42] MCELHINNEY, J. and OGLE, W. E.; *Phys. Rev.* 81 (1951) 342.
[43] KOCH, H. W., MCELHINNEY, J. and GASTEIGER, E. L.; *Phys. Rev.* 77 (1950) 329.
[44] WAY, K.; AECD 2752.
[45] — and DISMUKE, N.; Fission product yields (A summary of the facts) ORNL 280, 1949.
[46] Plutonium Project Report. *J. Amer. Chem. Soc.* 68 (1946) 2411. Reprinted in *Rev. Mod. Phys.* 18 (1946) 50.

[47] CORYELL, C. D. and SUGARMAN, N.; *Radiochemical Studies of the Fission Products* McGraw-Hill, 1951.
[48] STEINBERG, E. P., SEILER, J. A., GOLDSTEIN, A. and DUDLEY, A.; 1947, MDDC 1632.
[49] — and FREEDMAN, M. S.; *Radiochemical Studies of the Fission Products*, Vol. III, p. 1378, McGraw-Hill 1951.
[49a] TURKEVITCH, A. and NIDAY, J. B.; *Phys. Rev.* 84 (1951) 52.
[50] GRUMMIT, W. E. and WILKINSON, G.; *Nature, Lond.* 161 (1948) 520.
[51] YAFFE, L. and MACKINTOSH, C. E.; *Can. J. Res.* 25 B (1947) 371.
[52] THODE, H. G. and GRAHAM, R. L.; *Can. J. Res.* 25 A (1947) 1.
[53] MACNAMARA, J., COLLINS, C. B. and THODE, H. G.; *Phys. Rev.* 78 (1950) 129.
[54] INGHRAM, M. G., HESS, D. C. and REYNOLDS, J. H.; *Phys. Rev.* 76 (1949) 1717.
[55] — HAYDEN, R. J. and HESS, D. C.; *Phys. Rev.* 79 (1950) 271.
[56] HAYDEN, R. J., REYNOLDS, J. H. and INGHRAM, M. G.; *Phys. Rev.* 75 (1949) 1500.
[56a] GLENDENIN, L. E., STEINBERG, E. P., INGHRAM, M. G. and HESS, D. C.; *Phys. Rev.* 84 (1951) 860.
[57] BRUNTON, D. C. and HANNA, G. C.; *Phys. Rev.* 75 (1949) 990.
[58] — and — *Can. J. Res.* 28 A (1950) 190.
[59] — and THOMPSON, W. B.; *Phys. Rev.* 76 (1949) 848.
[60] — and — *Can. J. Res.* 28 A (1950) 498.
[61] FLAMMERSFELD, A., JENSEN, P. and GENTNER, W.; *Z. Phys.* 120 (1943) 450.
[62] JENTSCHKE, W.; *Z. Phys.* 120 (1943) 165.
[63] DEUTSCH, M. and RAMSAY, M.; MDDC 945, 1945.
[64] FOWLER, J. L. and ROSEN, L.; *Phys. Rev.* 72 (1947) 926.
[65] LEACHMAN, R. B.; *Phys. Rev.* 71 (1951) 235, and private communication.
[66] HENDERSON, M. C.; *Phys. Rev.* 58 (1940) 774.
[67] WAY, K. and WIGNER, E. P.; *Phys. Rev.* 73 (1948) 1318.
[68] PRESENT, R. D.; *Phys. Rev.* 72 (1947) 7.
[69] CORYELL, C. D., GLENDENIN, L. L. and EDWARDS, R. R.; *Phys. Rev.* 75 (1949) 335.
[70] GLENDENIN, L. E.; Office of Naval Research (U.S.A.) Technical Report No. 35, 1949.
[71] COOK, G. B.; Private communication.
[72] PAPPAS, A. C. and CORYELL, C. D.; *Phys. Rev.* 81 (1951) 329.
[73] BRUNTON, D. C.; *Phys. Rev.* 76 (1949) 1798.
[74] FEENBERG, E.; *Rev. Mod. Phys.* 19 (1947) 239.
[75] TAYLOR, A. E.; *Reports on Progress in Physics.* The Physical Society London. In press.
[76] BOHR, N.; *Phys. Rev.* 59 (1941) 270.
[77] — *Dan. Mat. fys. Med.* 18 (1948) (8).
[78] LASSEN, N. O.; *Dan. Mat.-fys. Med.* 25 (1949) (11).
[79] — *Phys. Rev.* 79 (1950) 1016.
[80] BØGGILD, J. K., MINNHAGEN, L. and NIELSEN, O. B.; *Phys. Rev.* 76 (1949) 988.
[81] — ARRØE, O. H. and SIGURGEIRSSON, T.; *Phys. Rev.* 71 (1947) 281.
[82] KATKOFF, S., MISKELL, J. A. and STANLEY, C. W.; *Phys. Rev.* 74 (1948) 631.
[83] SEGRÈ, E. and WIEGAND, C.; *Phys. Rev.* 70 (1946) 808.
[84] SUZOR, F.; *Ann. de Phys.* 4 (1949) 269.
[85] CAMPBELL, E. C., GOOD, W. M. and STRAUSER, W. A.; *Phys. Rev.* 75 (1945) 1292.
[86] VIGNERON, L.; *Compt. Rend.* 231 (1950) 1743.
[87] BOYER, K. and TITTLE, C. W.; *The Science and Engineering of Nuclear Power Vol. II*, Addison Wesley Press 1949.
[87a] NERESON, N., *Phys. Rev.* 85 (1952) 600; BONNER, T. W., AECD 3110; WATT, B. E., LADC 1156, HILL; D. L., CP 3800; BLOCH, F. and STAUB, H.; AECD 3158.
[88] HUGHES, D. J., DABBS, J., CAHN, A. and HALL, D.; *Phys. Rev.* 73 (1948) 111.
[89] SNELL, A. H. and MILLER, L. C.; *Phys. Rev.* 74 (1948) 1217.
SNELL *et al.*; *Phys. Rev.* 72 (1947) 541 and 545.

[90] SUGARMAN, N.; *J. Chem. Phys.* 15 (1947) 544.
[91] REDMAN, W. C. and SAXON, D.; *Phys. Rev.* 72 (1947) 570.
[92] CREVELING, L. G., HOOD, J. R. and POOL, M. L.; *Phys. Rev.* 76 (1949) 946.
[93] SUN, K. H., CHARPIE, R. A., PECJAK, F. A., JENNINGS, B., NECHAJ, J. F. and ALLEN, A. J.; *Phys. Rev.* 79 (1950) 3.
[94] HOFFMAN, F. DE, FELD, B. T. and STEIN, P. R.; *Phys. Rev.* 73 (1948) 636.
[95] SNYDER, T. M. and WILLIAMS, R. W.; *Phys. Rev.* 81 (1951) 171, and LADC 252.
[96] KINSEY, B. B., HANNA, G. C. and VAN PATTER, D.; *Can. J. Res.* 26 A (1948) 79.
[97] WILSON, R. R.; *Phys. Rev.* 72 (1947) 189.
[98] DE BENEDETTI, S., FRANCIS, J. E., PRESTON, W. M. and BONNER, J. W.; *Phys. Rev.* 74 (1948) 1645.
[98a] FRASER, J. S.; *Phys. Rev.* 85 (1952) 726.
[99] PEIERLS, R.; British Report BDDA–13.
[100] ROSE, B. and WILSON, A. R. W.; Private communication.
[101] PETRZHAK, K. A. and FLEROV, G. N.; *C.R. Acad. Sci. U.S.S.R.* 28 (1940) 500. *J. Gen. Phys.* 3 (1940) 275.
[102] PONTECORVO, B. and WEST, D.; Chalk River Report MP–200 (unpublished).
[103] SEGRE, E.; *Phys. Rev.* 86 (1952) 21.
[104] WHITEHOUSE, W. J. and GALBRAITH, W.; *Phil. Mag.* 41 (1950) 429.
[105] PERFILOV, N. A.; *J. Expt. Theor. Phys. U.S.S.R.* 17 (1947) 476. *J. Phys. U.S.S.R.* (3) (1947) 11.
[106] WEST, D.; Chalk River Report MP–18 Section II.
[106a] SEABORG, G. T.; *Phys. Rev.* 85 (1952) 157 and 757.
[106b] WHITEHOUSE, W. J. and GALBRAITH, W.; *Nature, Lond.* 169 (1942) 494.
[107] BRETSCHER, E., COOK, G. B., MARTIN, G. R. and POOLE, M. J.; BR–384.
[108] HANNA, G. C., HARVEY, B. G., MOSS, N. and TUNNICLIFFE, P. R.; *Phys. Rev.* 81 (1951) 466.
[109] LITTLER, D. J.; *Proc. Phys. Soc.* 65A (1952) 203.
[110] ROBERTS, J. H.; MDDC–731.
[111] POSE, H.; *Z. Phys.* 121 (1943) 293.
[111a] BARCLAY, F. R., GALBRAITH, W., and WHITEHOUSE, W. J.; *Proc. Phys. Soc.* 65 A (1952) 73.
[112] MACNAMARA, J. and THODE, H. G.; *Phys. Rev.* 80 (1950) 471.
[113] PRYCE, M. H. L.; *Proc. Phys. Soc.* 63 A (1950) 692.
[114] FARWELL, G., SEGRE, E. and WIEGAND, G.; *Phys. Rev.* 71 (1947) 327.
[115] DEMERS, P.; *Phys. Rev.* 70 (1946) 974. *Can. J. Res.* 25 A (1947) 223.
[116] WOLLAN, E. O., MOAK, C. D. and SAWYER, R. B.; *Phys. Rev.* 72 (1947) 447.
[117] GREEN, L. L. and LIVESEY, D. L.; *Proc. Int. Conf.* Cambridge July 1946.
[118] TSIEN, S. T., CHASTEL, R., HO, Z. W. and VIGNERON, L.; *Compt. Rend.* 223 (1946) 986.
[119] CASSELS, J. M., DAINTY, J., FEATHER, N. and GREEN, J. L.; *Proc. Roy. Soc.* 191 A (1947) 428.
[120] MARSHALL, L.; *Phys. Rev.* 75 (1949) 1339.
[121] TSIEN, S. T.; *J. de phys. et rad.* 9 (1948) 6.
[122] GREEN, L. L. and LIVESEY, D. L.; *Phil. Trans. Roy. Soc.* 241 A (1948) 323.
[123] TITTERTON, E. W.; *Proc. Harwell Conference* 1950. *Nature, Lond.* 168 (1951) 590.
[124] — and GOWARD, F. K.; *Phys. Rev.* 76 (1949) 142.
[125] — and BRINCKLEY, T. A.; *Phil. Mag.* 41 (1950) 500.
[126] — *Phys. Rev.* 83 (1951) 673.
[127] ALLEN, K. W. and DEWAN, J. T.; *Phys. Rev.* 80 (1950) 181.
[128] FEATHER, N.; *Nature, Lond.* 159 (1947) 607.
[129] ALLEN, K. W. and DEWAN, J. T.; *Phys. Rev.* 82 (1951) 527.
[130] GOWARD, F. K., TITTERTON, E. W. and WILKINS, J. J.; *Nature, Lond.* 164 (1949) 661.
[131] PRESENT, R. D.; *Phys. Rev.* 49 (1941) 466.
[132] ROSEN, L. and HUDSON, A. M.; *Phys. Rev.* 78 (1950) 533.

[133] PERLMAN, I., GOECKERMANN, R. H., TEMPLETON, D. H. and HOWLAND, J. J.; *Phys. Rev.* 72 (1947) 352.
[134] O'CONNOR, P. R. and SEABORG, G. T.; *Phys. Rev.* 74 (1948) 1189.
[135] GOECKERMANN, R. H. and PERLMAN, I.; *Phys. Rev.* 76 (1949) 628, and Brookhaven Conference Report BNL–C–9.
[136] JUNGERMAN, J. and WRIGHT, S. C.; *Phys. Rev.* 76 (1949) 1112.
[137] NEWTON, A. S.; *Phys. Rev.* 75 (1949) 17.
[137a] FRIEDLAND, S. S.; *Phys. Rev.* 84 (1951) 75.
[138] SPENCE, R. W.; *Proceedings of the Brookhaven Conference* BNL–C–9, 1949.
[139] YAMAGUCHI, Y.; *Prog. Theor. Phys.* 5 (1950) 143.
[140] BATZEL, R. E. and SEABORG, G. T.; *Phys. Rev.* 79 (1950) 528, and UCRL 1053.
[141] AL-SALEM, S. G.; *Phys. Rev.* 84 (1951) 254.
[142] WHEELER, J. A.; *Rev. Mod. Phys.* 21 (1949) 133.
[143] TIOMNO, J. and WHEELER, J. A.; *Rev. Mod. Phys.* 21 (1949) 153.
[144] GALBRAITH, W. and WHITEHOUSE, W. J.; Communications of the Dublin Institute for Advanced Studies, Series A, No. 9. In preparation. Also A.E.R.E. report N/R 987.
[145] BRADNER, H. and BOWKER, J. K.; *Phys. Rev.* 82 (1951) 265.
[146] FEATHER, N.; 1949, *Proceedings of the Edinburgh Conference.*
[147] SCOTT, J. M. C. and TITTERTON, E. W.; *Phil. Mag.* 41 (1950) 918.
[148] FEATHER, N.; *Nature, Lond.* 162 (1948) 213.
[149] FENNING, F. W. and HOLT, F. R.; *Nature, Lond.* 165 (1950) 722.
[150] FEATHER, N.; *Nature, Lond.* 143 (1939) 597.
[151] WILSON, R. R.; *Phys. Rev.* 72 (1947) 98.

THE LOW-LYING EXCITED STATES OF LIGHT NUCLEI

W. E. Burcham

CONTENTS

III. Introduction 174
III. The theoretical description of nuclear spectra 175
III. The width of nuclear levels 182
IV. Experimental methods for the study of excited states 184
(a) Energy release in transmutations produced by charged particles 184
(a.1) Particle accelerators 184
(a.2) Detection and analysis of particle groups 185
(a.3) Typical results 186
(b) Inelastic scattering of charged particles 189
(c) Transmutations produced by neutrons 190
(d) Elastic scattering of charged particles and neutrons 192
(e) The study of radiative transitions 194
(e.1) Radiative capture of protons 194
(e.2) Radiative capture of alpha-particles 197
(e.3) Radiative capture of neutrons 197
(e.4) Analysis of decay schemes 197
(e.4.1) Measurement of energy of gamma radiation and correlation with particle groups 199
(e.4.2) Determination of internal conversion coefficients 202
(e.4.3) Beta-decay 202
(f) Excitation by the photo-effect 204
(g) Angular distribution and angular correlation experiments 205
(h) Angular distributions in stripping processes 209
(i) Measurements of lifetime of nuclear states 210
(j) Summary of experimental methods for study of excited states of light nuclei 211
V. Experimental evidence 211
A. The odd isobars 213
B. The even isobars of mass $4n$ 220
C. The even isobars of mass $4n+2$ 227

I. INTRODUCTION

States of excitation are, after the charge and mass, among the most readily perceptible properties of nuclei. Experimental nuclear physics has always been intimately concerned with the identification and study of excited states, and there exists to-day a large body of tabulated information, of varying degrees of reliability, on these states. The obvious analogy between nuclear states and the excited states of atoms and molecules, with gamma radiation taking the place of light quanta, suggests the attractive possibility of predicting the existence and spacing of these nuclear levels in the way that wave mechanics predicts and describes atomic states. Up to the present this has unfortunately been impossible owing to the essentially different character of the forces

between nucleons from the long range Coulomb forces in the atom. The beauty of the wave mechanical treatment of simple atoms, and the power of the numerical methods which have been developed for the study of atomic wave functions are lacking in attempts to describe nuclear states theoretically. In the atomic case, there is no difficulty in principle, although there may be complication and inaccuracy in practical evaluation of term values, but with nuclei the difficulties are fundamental; we do not know what are the precise forces between nucleons, nor could we give exact solutions to the wave mechanical problem with such forces as we suspect that there must be. Yet some theory, however imperfect, is of great value to the experimental nuclear physicist, since it enables him to think of experiments in terms of a model which is probably not too far wrong, it helps him to avoid pitfalls and saves him much time in the planning of experiments, and finally, in its relevance to established experimental results, it plays at least a descriptive if not an explanatory part.

The present article is written primarily from an experimental point of view. It sets out to review the progress which has been recently made in methods of studying excited states, and to relate the results of recent experiments to such theoretical predictions as can be profitably discussed. For this type of discussion it is important that the experimental results should be accurate and that they should cover a wide range of energy of excitation. The last few years have brought important advances in both these respects, together with a clearer appreciation of the sort of information which can be obtained from a particular type of experiment.

The sharp, low lying states of light nuclei (of atomic number up to 10, say) have, on the whole, been most completely investigated, and the present article is mainly concerned with these, and particularly with those states of which a detailed study has been made. The main body of experimental information (up to August 1950) on the states of excitation of light nuclei is collected in the article by HORNYAK, LAURITSEN, MORRISON and FOWLER[1], (subsequently referred to as HLMF), which gives references to other similar surveys. General information on nuclear structure and properties is given in the well-known works by BETHE[2, 3, 4, 5], GAMOW and CRITCHFIELD[6], ROSENFELD[7], and MOTT and MASSEY[8], while for the particular subject of excited states of nuclei reference may be made to the monograph by DEVONS[9]*.

II. THE THEORETICAL DESCRIPTION OF NUCLEAR SPECTRA

It is possible to represent states of excitation of a nucleus in a formal manner as eigen-functions of the Hamiltonian operator describing the many interacting particles of the nucleus. The invariance properties of the Hamiltonian show that each state has a definite total angular momentum with quantum number J and a definite parity or symmetry which may be even (+) or odd (—). Calculation of the eigen-values of the system by the methods of quantum

* The author was privileged to see before publication an article by Professor T. LAURITSEN covering very much the same ground as the present one. This is appearing in Vol. I of the Annual Reviews of Nuclear Science, published by Annual Reviews Inc. Stanford, Ca. The form of the energy level diagrams in Section V was suggested by Professor LAURITSEN's article.

mechanics should give the energies of the ground state and excited states of the nucleus. Some such calculations have been made for the ground states of a few simple nuclei, using values for the interaction between nucleons which have been derived from detailed studies of the two- and three-body problem or from meson theory. No detailed prediction of excitation levels can however as yet be obtained by this method, and the direct approach to level spectra via nuclear forces has had to be discarded, at least temporarily, in favour of methods based either on the assumption of simplified interactions or on some particular nuclear model. It is difficult to find a mode of description which is suitable for all nuclei or even for different aspects of the behaviour of a particular nucleus, but each of the several simplifying assumptions co-ordinates some particular group of phenomena and provides some point of contact with experiment.

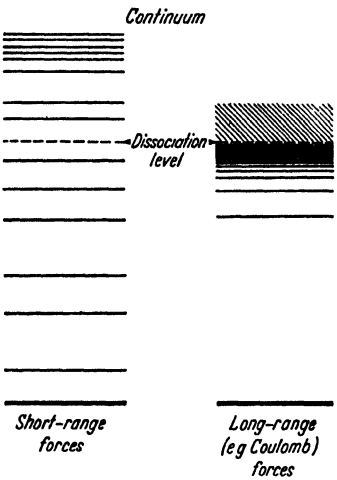


Fig. 1. Energy levels for short and long range forces (DEVONS[9], Fig. 1).

The most important characteristic of the forces between nucleons is their short range of action, of about 10^{-13} cm, which has a very marked effect on the type of level spectrum expected. In contrast to the Coulomb forces operating in the atom, nuclear forces lead to a level spectrum whose spacing does not tend to zero as the dissociation limit is approached. There is no essential difference between the bound levels below, and the virtual levels above, the dissociation limit (*cf.* Fig. 1), and nuclei have a finite number of bound levels.

From the different energy of the triplet and singlet states of the deuteron it follows that the force between neutrons and protons must be partly spin dependent, and it is clear that the force between two protons must include a Coulomb repulsion. These two factors must enter into the calculation of nuclear binding energies, but it is convenient in the first place to neglect them and to introduce them later as perturbations to the main nuclear forces, which are then taken to be independent of charge and spin.

The simplifying assumption of complete equality between the specifically nuclear (*np*), (*nn*) and (*pp*) forces between nucleons in the same state was made by WIGNER[10] in a general discussion of nuclear levels based on the symmetry properties of the nuclear system. The results of this treatment are summarised by WIGNER and FEENBERG[11]; it leads to the definition of a total isotopic spin quantum number T (formally analogous to the ordinary spin quantum number S), whose z-component is equal to half the difference between the number of neutrons and protons in the nucleus. The quantum number T classifies a set or multiplet of nuclear states of a certain binding energy. The $2T+1$ components of this multiplet are isobaric nuclei, each of which has a state, not necessarily the ground state, of the given binding energy. Parity and total angular momentum are the same for all the members of the multiplet.

The theory of WIGNER leads to the following important predictions, which are particularly useful in co-ordinating experimental results for light elements:

(a) *Odd isobars; mirror nuclei*

The difference in total energy between the ground states of the pairs of isobars with a neutron excess of ± 1, such as (He^5Li^5) (Li^7Be^7), should be accounted for solely by Coulomb repulsion, and the difference in mass between

Table 1—Energy difference between isobars due to Coulomb forces and neutron-proton mass difference

Nuclei		ΔE_{calc} (Mev)		ΔE_{obs} (Mev)*	
A. *Odd isobars* (mirror nuclei)					
H^3He^3		0·06		electron emitted (−0·018)	
He^5Li^5		0·62		α-unstable (0)	
Li^7Be^7		1·11		K-capture (0·88)	
Be^9B^9		1·54		α-unstable (1·09)	
$B^{11}C^{11}$		1·94		1·96	
$C^{13}N^{13}$		2·30		2·20	
$N^{15}O^{15}$		2·63		2·71	
$O^{17}F^{17}$		2·96		2·80	
$F^{19}Ne^{19}$		3·25		3·06	
$Ne^{21}Na^{21}$		3·57		3·6	
$Na^{23}Mg^{23}$		3·86		3·8	
B. *Even isobars*					
He^6Li^6	—	0·54	—	—	—
Li^8Be^8	Li^8B^8	1·02	2·65	—	2·0
$Be^{10}B^{10}$	$Be^{10}C^{10}$	1·43	3·44	—	3·55
$B^{12}C^{12}$	$B^{12}N^{12}$	1·84	4·19	—	4·20
$C^{14}N^{14}$	$C^{14}O^{14}$	2·22	4·94	—	4·95
$N^{16}O^{16}$	—	2·55	—	—	—
$O^{18}F^{18}$	—	2·89	—	—	—
$F^{20}Ne^{20}$	$F^{20}Na^{20}$	3·27	6·79	—	8·1
$Na^{24}Mg^{24}$	—	3·87	—	—	—

* The values of ΔE_{obs} are taken mainly from the diagrams in HLMF.

neutron and proton. This follows because of the equality assumed between (nn) and (pp) forces. There should be a similar correspondence between the excited states of these nuclei, and recent experimental evidence (see for example Li^7Be^7, $C^{13}N^{13}$, Section VA) bears this out. The observed and calculated energy differences for the ground states of the isobaric pairs discussed in Section VA are shown in Table 1; the calculated difference (for atomic masses) is obtained from the formula

$$\begin{aligned}\Delta E_{calc} &= \Delta E(\text{Coulomb}) - (n - H^1)\\ &= \frac{3}{5}\frac{e^2}{R}[Z(Z-1) - (Z-1)(Z-2)] - (n - H^1)\\ &= [0{\cdot}602(A-1)A^{-\frac{1}{3}} - 0{\cdot}78]\ \text{Mev}\end{aligned}$$

assuming that the nuclear radius is given by $R = 1{\cdot}42 \times 10^{-13} A^{\frac{1}{3}}$ cm where A is the mass number (ROSENFELD[7], p. 22). The value for $(n-H^1)$ is given by HLMF[1], p. 294. The observed energy differences are mainly taken from the energy level diagrams given by HLMF and should equal the observed upper limit of the positron spectrum from the nucleus (Z, A) together with the equivalent of two electron masses. The Table shows that the assumption of symmetric forces is well verified for all but the lightest nuclei, for which the simple Coulomb calculation is probably invalid; deviations which occur in the heavier nuclei are probably to be accounted for as a result of some specific alteration in the nuclear radius R.

The fact that the ground states of the mirror nuclei have the same wave-functions is also confirmed by the high probability of the β-transitions between them (see Section IVe, 4·3).

(b) *Even isobars of mass* $4n+2$

The even isobars of mass $4n+2$ can be grouped into triads of the type ($C^{14}N^{14}O^{14}$), the central member having equal numbers of neutrons and protons. The difference in total energy between C^{14} and O^{14} should be due to Coulomb repulsion, assuming again the equality of (nn) and (pp) forces and correcting for neutron-proton mass difference, and the pair of neutrons or protons extra to an assumed alpha particle core C^{12} would be expected, in accordance with the exclusion principle, to have anti-parallel spins. In N^{14} however, the two particles extra to the C^{12} core are a neutron and a proton; in that case parallel spins are permitted and indeed form a more tightly bound system, corresponding to the ground state of N^{14}, while an excited state of N^{14} in which the neutron and proton have anti-parallel spins should also exist. This state then belongs to the same T-multiplet as the ground states of C^{14} and O^{14} and has the same parity and angular momentum. It differs in binding energy from these states by a Coulomb term only, providing that the (nn), (pp) and (np) forces are all equal. Calculated energy differences between even isobars are also included in Table 1 for reference, together with observed values deduced from disintegration energies where possible.

The WIGNER theory does not provide quantitative estimates of the energy of excitation of nuclear levels. Further progress can be made by the adoption of some nuclear model, which must be consistent with the exclusion principle. For the purpose of describing light nuclei, the model which is immediately suggested is the *independent-particle model* in which each nucleon is assumed to move in an average potential field due to all the other nucleons. Solution of the wave equation for the nucleon with a particular assumed potential yields a set of eigen functions representing possible stationary states for the nucleon, each state being characterised, as in the atomic case, by a total energy and certain quantum numbers which depend on the type of potential chosen. If we consider a particular nucleus, these states correspond to possible energy levels with definite characteristics which may be observed experimentally; if we add successive nucleons to a given nucleus the states become filled in the order predicted by their energy values, and with a number of

nucleons determined by the exclusion principle. It is usual to assume an isotropic potential well, for which the levels are characterised by a principal quantum number n, equal to the total number of nodes in the wave function plus one, and an azimuthal quantum number $l(\leq n-1)$ which gives the orbital angular momentum of the state. States with $l = 0, 1, 2, 3 \ldots$ are described as s, p, d, $f \ldots$ states as in atomic spectroscopy and their parity is even or odd with l. If the potential well has steep sides and a flat bottom ("square well") the levels should be filled with successive nucleons in the order $(1s)^2$, $(2p)^6$, $(3d)^{10}$, $(2s)^2 \ldots$ although with some change in the well shape the $2s$ states may be made to fill before $3d$. The symbol $(2p)^6$ indicates 6 nucleons in states with principal quantum number 2 and azimuthal quantum number 1. For each l value there are $2l+1$ degenerate states with magnetic quantum number m such that $|m| \leq l$, and for each such state there are two possible spin directions so that $2(2l+1)$ states occur for both protons and neutrons. This model evidently predicts the formation of closed shells of nucleons containing 2, 8, 20 particles (grouping the $3d$ and $2s$ states together) and a discontinuity of nuclear properties such as binding energy and magnetic moment might be expected to occur with shell closure. The independent particle model has recently received much support from a study of such properties by MAYER[12], FEENBERG and HAMMACK[13] and NORDHEIM[14] (see the article on The Nuclear Shell Model by B. H. FLOWERS, in this volume).

A closed shell of nucleons, with quantum numbers n and l, has zero angular momentum and magnetic moment according to the independent particle model. The resultant angular momentum of an incomplete shell can be predicted if some specific assumption is made about the way in which the orbital and intrinsic spin momenta of the nucleons outside a closed shell combine. It is usually assumed that the RUSSELL-SAUNDERS coupling scheme applies to light nuclei; according to this the total orbital momentum and total intrinsic spin of the nucleons are first combined to give separate resultants, and these are then added vectorially to give the total angular momentum of the nuclear state. Thus for one neutron and one proton in the p-shell (Li^6), the complete nuclear wave function may be written down if spin dependent forces are neglected and the possible states are found to have orbital momenta 0, 2, 1 in order of increasing energy (BETHE[2]). The lowest states of such a nucleus are therefore characterised, in analogy with optical spectroscopy, by the symbols S, D, P. In this case the total intrinsic spin is 1 or 0 and each state may be a singlet or a triplet, *i.e.* ^1S, ^3S, ^1D, ^3D, ^1P, ^3P. Spin dependent central forces (HEISENBERG and BARTLETT forces) split the singlet from the triplet state and as it is clear from the spin of the deuteron that the triplet state is the lower, the ground state of Li^6 is of the type $^3S_1$ (where the suffix is the total angular momentum quantum number J). This type of description may of course be extended to nuclear states in general.

HEISENBERG and BARTLETT forces cause no splitting of energy levels if the resultant spin of either the neutrons or the protons in the nucleus is zero, as is usually the case in odd nuclei, such as Li^7 (^2P state). A further splitting

arises from the fact that the energy may differ according to the orientation of the spin vector with respect to the orbital moment (spin-orbit coupling). The ground state term of Li^7 splits for this reason into $^2P_{\frac{1}{2}}$ and $^2P_{\frac{3}{2}}$. The order of such spin-orbit doublets can be predicted if some assumption is made about the spin-orbit interaction. If this is assumed to be relativistic in origin, in which case it is comparatively weak, and certainly not strong enough to explain experimental results, it may be shown (ROSENFELD[7], p. 317) that the level of higher angular momentum lies lower (inverted doublet) when the orbital shell is less than half filled and higher (normal doublet) when the shell is more than half filled. The ground state and first excited state of Li^7 might therefore be expected to form an inverted doublet $^2P_{\frac{3}{2}, \frac{1}{2}}$.

The value of the independent particle model is that it gives, at least formally, a way of obtaining the complete nuclear wave function from the wave functions of the constituent nucleons. It predicts that two nuclei have the same level spectrum if gaps in the shell (e.g. $2p$-shell) of one correspond to occupied states in the same shell of the other; thus Li^6 and N^{14} should have similar spectra. Furthermore, the parity of the ground state follows directly from the configuration: while the s- or d-shell is closing the parity is always even, but while the p-shell is closing the parity is even or odd with the number of nucleons. In Section V of this article, experimental results will be compared as far as possible with the predictions of the independent particle model with weak spin-orbit coupling. Experiments usually suggest values for the total angular momentum and parity of a nuclear state, which is therefore often designated $(J+)$ or $(J-)$; with the assumption of the independent particle model assignments of spin and orbital quantum numbers may be made. Numerical calculations for the binding energy of the ground and low excited states of light nuclei may be carried out if particular potentials are assumed. This has been done for the nuclei up to oxygen by FEENBERG and WIGNER[15], FEENBERG and PHILLIPS[16] and ROSE and BETHE[17].

Strong spin-orbit forces have recently been proposed by HAXEL, JENSEN and SUESS[18] and by MAYER[19] to account for the marked nuclear shell structure among the odd nuclei throughout the periodic table. This leads to a coupling scheme in which the total angular momenta of nucleons in incomplete shells are added (jj coupling) rather than the resultant spins and orbital momenta separately. It is doubtful whether extreme jj coupling is effective in light nuclei, though strong non-central effects are certainly required to explain some anomalies in observed ground state spins (e.g. B^{10}).

Among other nuclear models which have been proposed, one of the most useful for a discussion of the properties of light nuclei is the *alpha particle model*. This was developed to describe nuclei of mass number $4n$ and equal numbers of neutrons and protons in which it may be assumed that the constituent nucleons are grouped into alpha-particles, containing most of the binding energy of the nucleus. The interactions between the alpha-particles may then be described by the methods developed for the study of polyatomic

molecules. (WHEELER[21], HAFSTAD and TELLER[22].) The model is particularly useful in predicting the symmetry properties of the ground and excited states of light nuclei owing to the limits imposed by the BOSE statistics for alpha-particles on the nuclear wave-function. The wave-function must not permit one alpha-particle to be distinguished from another, and since a rotation of a structure such as tetrahedron or equilateral triangle through a particular angle, e.g. $2\pi/f$ may cause alpha-particles to exchange places, the wave-function may only have an angular dependence of the type $\cos n f \theta$. In this way the angular momenta of the low rotational states of Be^8, C^{12}, O^{16} have been successfully predicted as shown in Fig.2, taken from the paper by HAFSTAD and TELLER[22]. The model predicts vibrational motion, and the total energy of a given state is in general equal to the sum of rotational and vibrational energies. Nuclei with mass number $4n \pm 1$ have also been discussed in terms of this model by HAFSTAD and TELLER[22].

Certain nuclei such as He^5, Be^9, C^{13}, O^{17} and their mirror isobars have one nucleon outside a tightly bound closed shell. In such cases low-lying states of the odd nucleon moving in the field of the core may be found in addition to those predicted by nuclear shell models. These are known as "single particle levels".

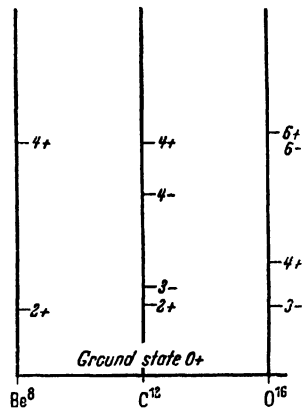


Fig. 2. Rotational states of alpha-particle nuclei (from HAFSTAD and TELLER[22]).

Both the independent particle model and the alpha-particle model are at variance with the fact that there is strong interaction between neighbouring nucleons. The success of the BOHR theory in describing the interaction of slow neutrons with nuclei is based on the assumption of rapid and complete transference of energy throughout the nucleus, regarded as a closely packed assembly of strongly coupled particles. The difference between the independent particle and strong coupling theories of the nucleus has recently been discussed by WEISSKOPF[23], who points out that the two theories really apply to different aspects of nuclear phenomena, the former to low lying, well separated states and the latter to states of considerably greater excitation. Thus it seems impossible to dispense with either theory, since each co-ordinates a distinct and different set of phenomena.

Some attention has also been devoted to rigid body models in which either the whole or part of the nucleus rotates about a central axis and the angular momentum of rotation is quantised (GUGGENHEIMER[24], PREISWERK[25]). Many known levels are predicted very closely by these models but the number of cases in which independent confirmation of the assumed quantum numbers has been obtained is small.

For heavy nuclei, and for light nuclei at high excitations, the number of levels per unit energy range becomes very large and the total width of the energy levels also increases, so that there is much overlapping, and the concept of individual levels loses its meaning. Statistical methods have been developed

to describe this situation, and have met with some success in predicting the behaviour of heavy nuclei; they are however not relevant to the present article.

III. The Width of Nuclear Levels

The considerations of Section II suggest reasons for the existence of some of the low lying states of light nuclei, and predict values of angular momentum and parity for these states. They do not, however, show how the levels are excited or how they lose their energy of excitation, and to describe these processes a theory of nuclear reactions is required.

Excited nuclei may lose their energy of excitation in a number of ways. If the energy is insufficient to cause dissociation of the nucleus into particles, the level is said to be bound and its energy can only be lost by a radiative process, as in the case of a vacant electronic state in an atom. If, however, particles can be emitted the level is described as virtual and the nucleus will break up, unless the particle emission is strongly retarded by a Coulomb barrier, or forbidden by a selection rule. The probability of electromagnetic transition in any system is governed by the ratio $(R/\lambda\!\!\!^{-})^2$ where R is the size of the radiating system and λ the wave-length radiated; the probability of radiative transitions decreases by this factor for successive orders of multipolarity. For an atom with $R = 5 \cdot 10^{-8}$ cm and a visible line of wave-length 5000° A this factor is $4 \cdot 10^{-5}$, so that electric dipole transitions, which are able to carry away one unit of angular momentum, are by far the most probable and higher order transitions are only rarely observed. Nuclei, however, have a special charge and mass symmetry which may make them unlikely to emit dipole radiation, and moreover the $(R/\lambda\!\!\!^{-})^2$ factor is much larger, about $10^{-2}-10^{-3}$, so that "forbidden" transitions are quite frequent, and magnetic dipole, electric quadrupole, and even octupole transitions are observed.

The probability of de-excitation of a level is represented formally by an exponential, time dependent term in the eigen-function of the state, which means that the energy is not sharply defined, but that the level has a certain width Γ, and a certain lifetime τ related to the width by the uncertainty principle $\Gamma\tau \simeq \hbar$. The true width of a level is sometimes measurable experimentally, but owing to the smallnes of $\hbar$ the level width and lifetime have not been measured independently for any level so far. In the case of virtual levels the emission of particles of various types from a nucleus contributes to the probability of decay and the total width is increased and must be expressed as a sum of partial widths Γ_p, Γ_q ... which cover all possible modes of decay including radiation.

The excitation of virtual states of a compound nucleus is an essential part of the Bohr theory of nuclear reactions, and the partial level widths describe the probabilities of emission of the corresponding types of particle from the compound states. If the energy levels at the excitation produced are well separated, the cross section for a nuclear reaction of the type $A(p, q)B$ may be described by the one-level formula developed by Breit and Wigner and others, which may be written

$$\sigma_{pq} = \frac{\lambda\!\!\!^{-2}}{4\pi} \cdot \omega \cdot \frac{\Gamma_p \Gamma_q}{(E - E_r)^2 + \frac{1}{4}\Gamma^2} \qquad (2)$$

where ω is a statistical factor*, $\Gamma = \Gamma_p + \Gamma_q + \cdots$ is the sum of the partial widths for all possible modes of de-excitation of the compound nucleus and λ is the wavelength of the incident particle in the centre-of-mass system. In this formula Γ_p and Γ_q, which are approximately equal to the level widths at resonance, contain energy dependent factors that allow for the coupling of the wave function inside the nucleus to the wave describing the emitted particles. These factors may be separated out by writing, following WIGNER[26]

$$\Gamma_p = 2\gamma_p^2 k_p T_{pl}$$

where p refers to the particle considered, k_p is its wave number and T_{pl} is the Coulomb and centrifugal barrier penetration factor for a particle p captured or emitted with orbital angular momentum l. γ_p^2 is called the reduced width, and may be deduced from experimentally observed widths by correcting for the energy dependent factors. These factors may be calculated from the formulae given by BETHE[3]; they have been calculated more exactly for protons and a number of light nuclei by CHRISTY and LATTER[27], and for the reactions of light nuclei in general by BLOCH *et al.*[28].

The reduced width is theoretically proportional to the level spacing at the excitation energy of the level considered, and experimental evidence on the whole supports this, although data are not yet sufficiently extensive to provide a stringent test. The reduced width for the emission of a particle from a particular level is unlikely to exceed the "WIGNER limit" of $\frac{3}{2}\frac{\hbar^2}{MR}$ where M is the reduced mass of the particle and R is the nuclear radius; this upper limit provides a useful check on angular momentum assignments to fit experimental results, since the l-value chosen must not give too great a reduced width. Widths about equal to the WIGNER limit are usually found for single particle levels. Dispersion theory also shows that in addition to a reduced width γ^2, each level has a characteristic level shift Δ which is proportional to γ^2 (WIGNER and EISENBUD[20]). Experimentally this level shift is included in the observed resonance energy E_r and cannot be extracted from it, but differences in Δ due to different reduced widths may be responsible for the displacement of corresponding levels in some mirror nuclei (see C^{13} N^{13}, O^{17} F^{17}, Section VA).

To summarise, the main properties of nuclear states accessible to the experimentalist are those of any quasi-stationary quantum mechanical state, namely energy of excitation above the ground state, lifetime or width, (and partial widths in the case of competitive modes of break up of virtual states), total angular momentum and parity. Properties such as electric quadrupole moment and magnetic moment have not yet been measured for excited states of light nuclei. In the following section the experimental methods which give information on these properties are examined, and recent developments in their techniques described.

* If s is the spin of the incident particle, j is the spin of the bombarded nucleus and J the angular momentum of the compound state, then $\omega = \frac{2J+1}{(2s+1)(2j+1)}$. This is sometimes useful in estimating values of J.

IV. Experimental Methods for the Study of Excited States

(a) *Energy release in transmutations produced by charged particles*

The simplest, and historically the earliest, method of establishing the existence of excited states is through a study of the particle groups emitted in nuclear transmutations, usually of the two-body type, releasing energy Q and represented by

$$A + p \rightarrow B + q + Q. \tag{3}$$

Experiments of this type were first made by Rutherford and Chadwick and their pupils for the (α, p) reactions and it was early recognised that the protons emitted showed a group structure, which could be interpreted as due to excited states of the residual nucleus B. The excitation energies were obtained as differences between the maximum Q-value observed and the other Q-values. The reaction was found to proceed most readily when the reacting products came together with certain definite energies now known as resonance energies. Precisely similar measurements are still being made, but the use of natural alpha-particles as bombarding particles has been almost superseded by that of artificially accelerated protons, deuterons, tritons and alpha-particles, and magnetic analysis has replaced range determination as the most important method of energy measurement. The increased precision of energy level determination which is now possible arises in approximately equal degree from the use of particle accelerators and from improved methods of detection. The combined precision of the determination of energy releases, from which the positions of excited states are deduced, can now be of the order of a few kev. This is small compared with the level spacing of light nuclei well into the region of virtual levels, but is still very large compared with the widths of bound levels.

(a.1) *Particle accelerators*

The main types of particle accelerator used in the study of excited states are the cascade generator, first applied by Cockcroft and Walton, the electrostatic generator, and the cyclotron. A description of recent developments in these machines has been given by Fortescue[29] and by Pickavance[30]. The two former types of equipment have been particularly useful in the study of light elements whose Coulomb barriers can be penetrated with appreciable probability by particles of 1 2 Mev energy. The operating voltage of an electrostatic generator can be controlled electronically to about 0·1 %, and a beam of greater homogeneity can be obtained by passing the "rough" beam from the accelerator through either a stable magnetic field with an energy selecting slit (Burcham and Devons[31], Bennett *et al.*[28]) or an electrostatic analyser (Fowler, Lauritsen and Lauritsen[33], Warren, Powell and Herb[34]). In this way an energy resolution of 0·01 to 0·02 % has been obtained with beam intensities of about 1 μA per kev width at 1 Mev; such conditions have permitted a direct study of the width of virtual levels at excitations of about 10 Mev above the ground state (Bender, Shoemaker and Powell[35]). In measurements of energy releases, this high precision in the definition of the

bombarding voltage is unnecessary, since the calculated energy release often contains the bombarding energy as a small correction only.

The cyclotron has recently been adapted by a number of workers to give beams of particles of homogeneity suitable for the study of bound levels by scattering and transmutation processes. By use of an auxiliary deflecting and focussing magnet (CURTIS *et al.*[36], RHODERICK[37]) a cyclotron can be made to provide a beam of 10 Mev deuterons of about 0·5 μA and ¼ in. in diameter at about 15 feet from the cyclotron. BURROWS, POWELL and ROTBLAT[38] have used the fringing field of a 37 in. cyclotron and a slit system to select a beam of 8 Mev deuterons with an energy spread of less than 1%. A magnetically focussed beam of 15·5 Mev deuterons has been used by the workers at the M.I.T. (BOYER *et al.*[39]) to study the ground state energy differences and excited states of a large number of nuclei throughout the periodic table.

(a.2) *Detection and analysis of particle groups*

The early method of analysis of charged particle groups by absorption, and detection by means of a proportional counter or a simple or differential ionisation chamber has been used recently by a number of workers (ALLAN and WILKINSON[40], HEYDENBURG and INGLIS[41], FRENCH and TREACY[42]), and is capable of an accuracy of about 50 kev in energies of 5 Mev. Direct recording of particle tracks in photographic plates has been used, following the early work by POWELL and his collaborators, by LATTES, FOWLER and CUER[43], and by ROTBLAT[44]. Increased precision can be obtained by the use of magnetic analysis, following the method used by RUTHERFORD, WYNN-WILLIAMS, LEWIS and BOWDEN[45] for determining the velocities of alpha-particles from naturally radioactive substances, and large magnets have recently been constructed and applied to artificial transmutation problems in a number of laboratories (BUECHNER *et al.*[46], SNYDER *et al.*[47], COLLINS, MCKENZIE and RAMM[48], KLEMA and PHILLIPS[49]). In some cases the determination of energy is made by comparing the observed momentum of the unknown group with that of the alpha-particles from polonium or RaC, the velocity of the alpha-particles from RaC, which has been measured by BRIGGS[50] with a precision of 4 parts in 10^5, being taken as standard. In the measurements made by COLLINS, MCKENZIE and RAMM[48] and by KLEMA and PHILLIPS[49] the magnetic field used to deflect the alpha-particles is determined with a precision of about 1 part in 10^5 by means of the nuclear resonance phenomenon, using the very accurately known gyromagnetic ratio of the proton (THOMAS, DRISCOLL and HIPPLE[51]). In all cases the use of such high precision analysis requires considerable attention to definition of beam energy, to target contamination and deterioration, and to geometrical arrangement; moreover the calculation of energy releases must be put into relativistic form. The accuracy of the best measurements reaches 0·07% for energy releases greater than about 3 Mev The limitations on size which are necessary to take advantage of the resolution made available by magnets of radius about 40 cm and the limitation on available beam current densities make the yield of particles rather small. This can be compensated for either by the use of a double focussing magnet

(SIEGBAHN and SVARTHOLM[52], SNYDER *et al.*[47]), or by making use of the integrating properties of the photographic plate as a detector (BUECHNER *et al.*[46]). A large solid angle can also be obtained by means of a spherical electrostatic analyser of the type developed and used by BROWNE *et al*[53].

The photographic plate (BUECHNER *et al.*[46]) has advantages as a detector of magnetically analysed particles when the object of the experiment is the measurement of energy releases for a fixed bombarding energy. Both proportional counters (COLLINS, MCKENZIE and RAMM[48]) and scintillation screens with a photomultiplier (BURCHAM and FREEMAN[54]) have also been used and are more convenient for the study of excitation functions, and for rapid checks on target deterioration.

For experiments in which precise measurement of energy is less important than a study of the relative intensity of a number of particle groups under different conditions of bombarding energy or angle of observation, increasing use is being made of pulse size analysis. The reaction products are allowed to enter a proportional counter, in which they stop, through a slit system, and the resulting distribution of pulse sizes is recorded by a multi-channel pulse analyser. A recently developed 120 channel instrument of this type (HUTCHINSON and SCARROTT[55]) is able to accept and analyse impulses at the rate of 1000 per sec, and the use of this technique will materially shorten many investigations. The method combines the advantages of an integrating property with the flexibility of counting techniques and is likely to be largely used in the future

When the emitted particle in reaction (3) is a neutron, the energy spectrum is most conveniently found by observing recoil proton tracks in a photographic emulsion. This method was developed by POWELL and others, and by using concentrated emulsions (POWELL *et al.*[56]) a precision of 50–100 kev in the measurement of neutron energies up to about 10 Mev can be achieved. Recently a time of flight method has been used for the detection of neutron groups whose emission leaves the residual nucleus in an excited state (JAMES and TREACY[57]).

(a.3) *Typical results*

The work of MALM and BUECHNER[58] on the $N^{14}(d\alpha)C^{12}$ and $N^{15}(d\alpha)C^{13}$ reactions is a good example of recent high precision studies of bound states by the transmutation method. Thin targets of tantalum nitride were bombarded with deuterons of energy 1·420 Mev from an electrostatic generator, and a magnetic analysis of the alpha-particle groups emitted by the targets was made. The protons were recorded in photographic plates after traversing the magnetic field, and their energy was found from the $H\varrho$ measurements which were related by fluxmeter observations to the $H\varrho$ for polonium alpha-particles. A typical specimen of their results is shown in Fig. 3, in which the number of tracks per unit area is plotted as a function of $H\varrho$; the precision of the method is well illustrated by the sharpness of the peaks. One contamination peak appears in this figure, and, as in all experiments of this type, this and similar peaks must be identified by comparison with runs made with other targets or by the

availability of exact data on other reactions. (The importance of exact information is well known to any experimenter who has been compelled to ascribe, one by one, the results of his work to unsuspected contaminants!) The final result is that there are groups in the $N^{14}(d\alpha)$ reaction corresponding to energy releases of $13{\cdot}575 \pm 0{\cdot}012$, $9{\cdot}137 \pm 0{\cdot}006$ and $3{\cdot}955 \pm 0{\cdot}003$ Mev, and in the $N^{15}(d\alpha)$ reaction of $7{\cdot}681 \pm 0{\cdot}006$, $4{\cdot}598 \pm 0{\cdot}004$ and $4{\cdot}004 \pm 0{\cdot}003$ Mev which correspond to the ground state and the two lowest excited states of C^{12} and C^{13} as shown in Fig. 3.

The use of the photographic emulsion technique for a study of excited states is well illustrated in Fig. 4, which is a histogram obtained by BURROWS[59]

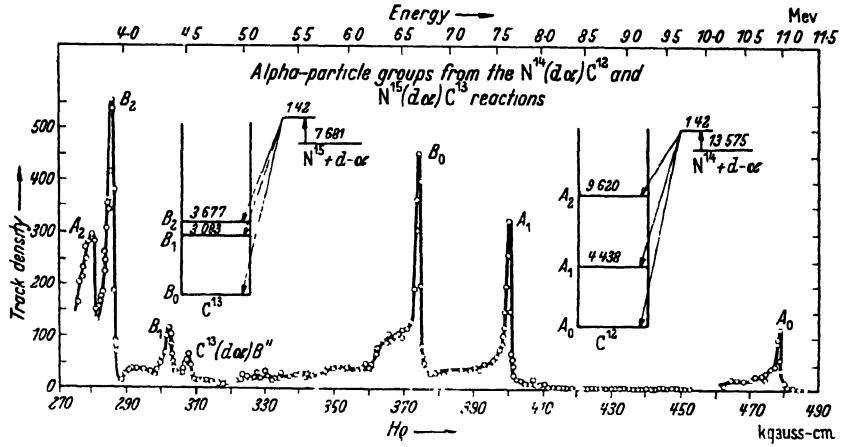


Fig. 3 Magnetic analysis of alpha-particle groups from tantalum nitride target bombarded by 1·42 Mev deuterons (MALM and BUECHNER[55]).

of the track lengths of charged particles from oxygen bombarded by 7·7 Mev deuterons. Groups 1, 2, 3, 5, 6 and 7 are due to protons emitted in the reaction $O^{16}(dp)O^{17}$. The use of high bombarding energies, gaseous targets and photographic plate detection allows a considerable extension of the energy range over which level spectra can be studied.

A large number of reactions of the light elements of the (dp), $(d\alpha)$ and $(p\alpha)$ type, with both positive and negative energy releases, have been studied in the last few years by these and similar methods (*cf.* STRAIT *et al.*[60], HARVEY[61], BURROWS, POWELL and ROTBLAT[38]). In most cases the reactions studied were of the non-resonant type and the bombarding energy was chosen either to be as high as possible, or for convenience in analysing the results, particularly in order to avoid possible coincidences between groups of particles from different elements. The results of this work give most valuable accurate information on the locations of the lower bound levels of light nuclei, as well as on nuclear masses, in terms of the standards used.

The study of virtual levels, unstable with respect to particle emission, by means of an electrostatic generator or cascade generator, combined with a magnetic spectrograph, is illustrated by the work of CHAO, TOLLESTRUP, FOWLER and LAURITSEN[62] and of FREEMAN[63] on the $F^{19}(p\alpha, \gamma)O^{16}$ reaction. In this

reaction and in others of the same type the yield of alpha-particles shows sharp resonances for certain definite energies of the incident proton. The energy release for the reaction was found by $H\varrho$ determinations with the magnetic spectrograph, and the yield of alpha-particles, separated from scattered protons by the magnetic analysis, was followed as the proton energy was varied; typical results are shown in Fig. 5. The sharp levels, at an excitation energy of about 12 Mev above the ground state of the Ne^{20} nucleus formed in the reaction, are clearly shown: in this case the possibility of alpha-particle emission in addition to proton re-emission so broadens the levels that their true width (3–10 kev) can be determined with the resolution available (0·03% up to 1500 kev bombarding proton energy[62]). Determination of the solid angle of the magnetic spectrograph, and studies of the angular distribution of the particles enables absolute yields of alpha particles per proton to be found. This information is

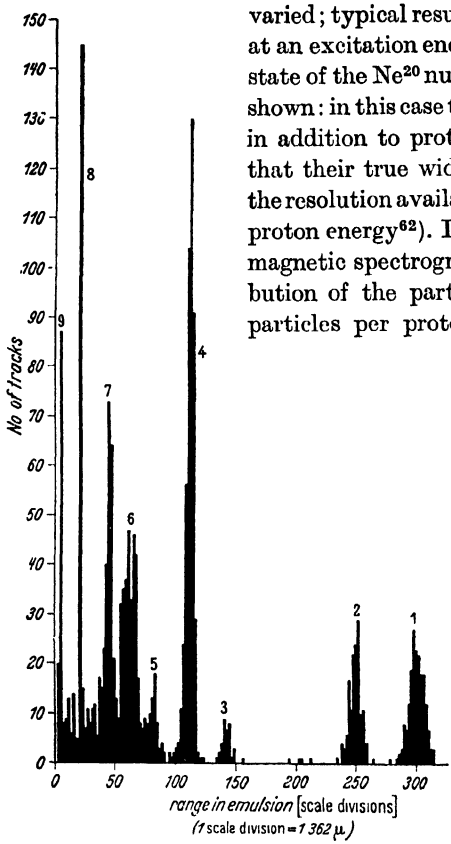


Fig. 4. Histogram of scattering and disintegration products of oxygen bombarded by 7·7 Mev deuterons (BURROWS[58]).

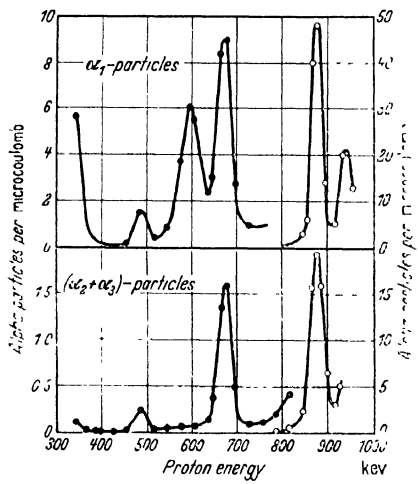


Fig. 5. Excitation functions of alpha-particle groups from fluorine bombarded by protons (FREEMAN[63]).

important since determinations of the cross section for a nuclear reaction at resonance may enable partial level widths to be estimated (*cf.* Section IVd, IVe.1).

Moreover, nuclear reactions are reversible and comparison of the cross sections for the inverse processes (pq), (qp) gives in agreement with the principle of detailed balancing,

$$\frac{\sigma_{pq}}{\sigma_{qp}} = \left(\frac{\lambda_p}{\lambda_q}\right)^2 \frac{\omega_p}{\omega_q}$$

(*cf.* SHOUPP, JENNINGS and SUN[64]) which might in certain cases enable the spin of a nucleus to be deduced from known spins of the other nuclei taking part in the reaction.

A typical example of the study of excited states by the (dn) reaction is the work of GIBSON[65] on the neutron spectrum from the $B^{11}(dn)$ reaction. Fig. 6 shows the results obtained; energy levels in C^{12} at $4{\cdot}47 \pm 0{\cdot}10$ and $9{\cdot}72 \pm 0{\cdot}15$ Mev were deduced.

In all nuclear transmutation studies the use of separated isotopic targets is of the greatest value in the interpretation of results and is in some cases essential. Separated stable isotopes of most elements are now available from

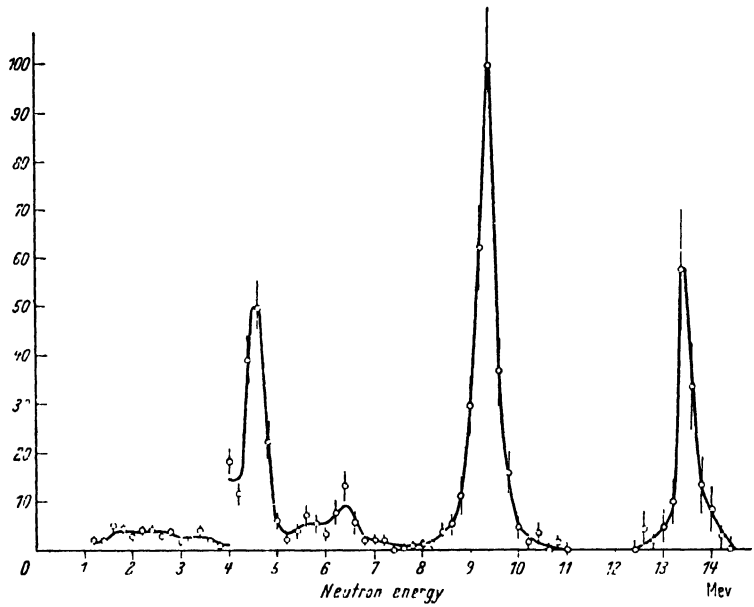


Fig. 6. Neutron spectrum from $B^{11}(dn)$ reaction (GIBSON[65]).

the Atomic Energy Research Establishment, Harwell (ALLEN[66]) and from the Atomic Energy Commission (U.S.A.) and they have been used extensively.

(b) *Inelastic scattering of charged particles*

Inelastic scattering is a particular case of a transmutation in which the emitted particle is similar to the incident particle *i.e.*

$$\left.\begin{aligned} A + p &\rightarrow A^* + p' \\ A^* &\rightarrow A + \gamma. \end{aligned}\right\} \tag{4}$$

In the centre of mass system the incident particle loses an energy equal to that necessary to excite the bombarded nucleus, which subsequently loses this energy in the form of γ-radiation. The process is analogous to the FRANCK-HERTZ experiment in atomic physics, and may be detected by the observation either of radiation or of retarded particles. The importance of the method lies in the fact that it yields information on the bound levels of the bombarded nucleus, as well as, in some cases, resonance energies of the

compound state (see, for example, B^{10}, Section VC). Unfortunately, the energy release in the process is necessarily negative and the number of levels which can be studied depends on the bombarding energy available. For this reason work of this nature has chiefly been carried out with cyclotron beams, although in a few cases the energies reached by electrostatic generators have been sufficient to excite the lowest levels (see Li^7 Section V).

Experiments have been made using protons (FULBRIGHT and BUSH[67]), deuterons (GREENLEES, KEMPTON and RHODERICK[68], and alpha-particles

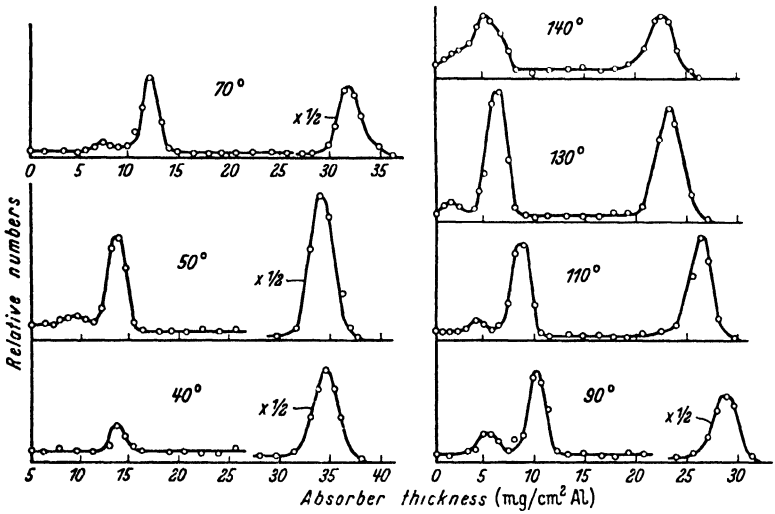


Fig. 7. Spectra of protons scattered from magnesium (E_p = 4 73 Mev) showing inelastically scattered group (RHODERICK[37]).

(SIEGBAHN and SLÄTIS[69]). Typical results are those of RHODERICK[37] who studied the lowest states of Mg^{24} and found an energy distribution of protons scattered from this element as shown in Fig. 7. The main inelastically scattered group arises from a 1·38 Mev level in Mg^{24}. The scope of such observations has been extended to higher deuteron energies by the M.I.T. cyclotron group[70].

(c) *Transmutations produced by neutrons*

Neutron induced reactions of type (3) have been studied since 1934, but in all the early experiments the main source of neutrons was the radon-beryllium mixture which gives a nearly continuous distribution of neutron energies up to a maximum. Homogeneous sources of neutrons can however be obtained from charged particle reactions, and a discussion of suitable reactions is given by HANSON, TASCHEK and WILLIAMS[71]. One of the most flexible sources of neutrons, which is both homogeneous and variable in energy from small energies upwards, is that using the (pn) reaction in Li^7:

$$Li^7 + H^1 \rightarrow Be^7 + n - 1{\cdot}647 \text{ Mev.} \qquad (5)$$

This reaction has a threshold at a proton energy 1·882 Mev and for proton energies above the threshold the neutron energy in a given direction can easily

be calculated. This source has the slight disadvantage that there is a 434 kev excited state in Be^7, which results in the production of a second group of neutrons when the incident proton energy exceeds 2·378 Mev (WILLARD and PRESTON[72]) but this shadow group is of low intensity and has not seriously affected any measurements which have recently been made using the Li(*pn*) source. The main group of neutrons produced by the $Li^7(pn)$ reaction is of homogeneity determined only by the homogeneity of the proton beam and the thickness of the lithium target, and with proper care, and the use of a stabilised electrostatic generator, a resolution of about 5 kev over an energy range limited only by the operational "ceiling" of the accelerator can be achieved.

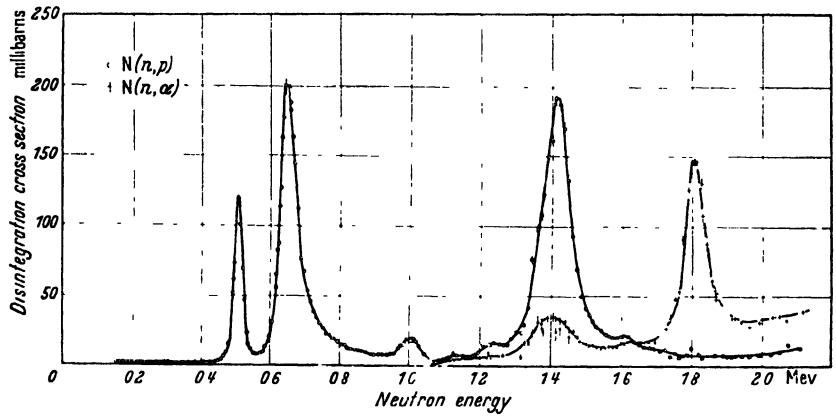


Fig. 8. Excitation functions for $N^{14}(np)$ and $N^{14}(n\alpha)$ reactions (JOHNSON and BARSHALL[74]).

Fast neutrons have not been much used for the study of bound levels by the transmutation method, although a few such results have been published (BLEULER and ROSSEL[73]). This is due to the low intensity of available sources of fast neutrons of energy high enough to excite bound levels. A number of virtual levels have however been studied by means of the (*np*) and (*nα*) reactions, and the results of JOHNSON and BARSCHALL[74] for nitrogen given in Fig. 8 show clearly the precision obtainable by use of the $Li^7(pn)$ neutron source. The neutrons were allowed to interact with nitrogen in a cylindrical ionisation chamber, and the yield of the reactions was found as a function of neutron energy. The energy release in the processes was found by passing the ionisation pulses to a calibrated pulse analyser; the use of ionisation chamber or proportional counter and pulse analyser has obvious advantages for the study of neutron induced reactions. The resonances indicate levels in the N^{15} nucleus which agree with those found in the inverse reaction $C^{14}(pn)$. Most of the information on virtual levels obtained by neutron bombardment has, however, come from measurements of total cross section of nuclei for both fast and slow neutrons; this is discussed in Section IV, d.

Very intense beams of slow neutrons are now available from reactors, but there are only a few nuclei with which transmutations other than capture can be observed with such neutrons. The reaction most thoroughly studied

is $B^{10}(n\alpha)Li^7$ (HANNA[75]) in which the excited state of Li^7 at 479 kev was observed using an ionisation chamber and pulse analyser technique. Radiative capture of slow neutrons and measurement of the energy of the subsequent gamma radiation gives accurate information on bound states of many nuclei and is discussed in Section IV, e.

(d) *Elastic scattering of charged particles and neutrons*

Elastic scattering of a particle by a nucleus, in which a compound state is formed, may be considered as a particular case of a transmutation, but it differs from the general type of rearrangement collision already considered for two reasons:

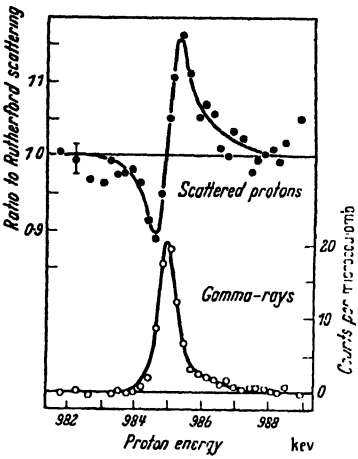


Fig. 9. Resonant scattering of protons by aluminium (BENDER *et al.*[77]).

(a) there is the possibility of interference betwen the waves describing the nucleons re-emitted by the compound nucleus and those scattered by the potential fields (Coulomb or nuclear) surrounding the nucleus, since the wave functions are coherent;

(b) in the particular case of identity between the incident and scattering nucleus the wave functions of the two particles in the system of the mass centre are also coherent and interference terms arise in the angular distribution for this reason.

If the compound system in a scattering process is formed with one of its resonance energies, the nuclear scattering has a maximum amplitude, and as the energy of the incident particle is varied through the resonance, the phase of the nuclear scattering relative to that of the potential scattering changes by π. This is revealed in observations of scattered intensity at a given angle by a curve of the dispersion type, the nature of the phenomenon being analogous to that of anomalous dispersion in optics. The possibility of the effect being experimentally observable depends of course on the ratio of the width of the energy level to the homogeneity of the particle beam. Resonant scattering of alpha-particles by a number of nuclei was investigated by DEVONS[76], who also discusses (DEVONS[9], p. 79) the conditions under which this phenomenon may most easily be observed. The resonant scattering of protons by aluminium has been demonstrated by BENDER *et al.*[77], who studied the variation of elastic scattering with proton energy near one of the gamma-ray resonances known from the $Al^{27}(p\gamma)Si^{28}$ reaction. Fig. 9 shows the variation of gamma-ray intensity and of the number of scattered protons per unit solid angle at 135°; the form of the curves agrees with that predicted by the BREIT-WIGNER theory, and indicates, under assumption of zero orbital momentum for the incident protons, a natural width of about 100 volts. This width is partly due to gamma-ray emission and partly due to proton re-emission, the latter being the main

contribution. The variation of cross-section at the resonance can be used to find the angular momentum of the virtual level concerned; a good example is provided by the work of GOLDHABER and WILLIAMSON[78] on the elastic scattering of protons by carbon which leads to assignments for the levels of N^{13}. Confirmation of such assignments is sometimes obtained from the experimentally determined level widths; comparison with the "WIGNER limit" (Section III) and the use of penetrability factors may suggest an orbital momentum for the incident charged particle.

The elastic scattering of neutrons is fully discussed by ADAIR[79] in his introduction to a collection of results on the neutron cross sections of the elements. The total cross section for removal of neutrons from a beam is due to

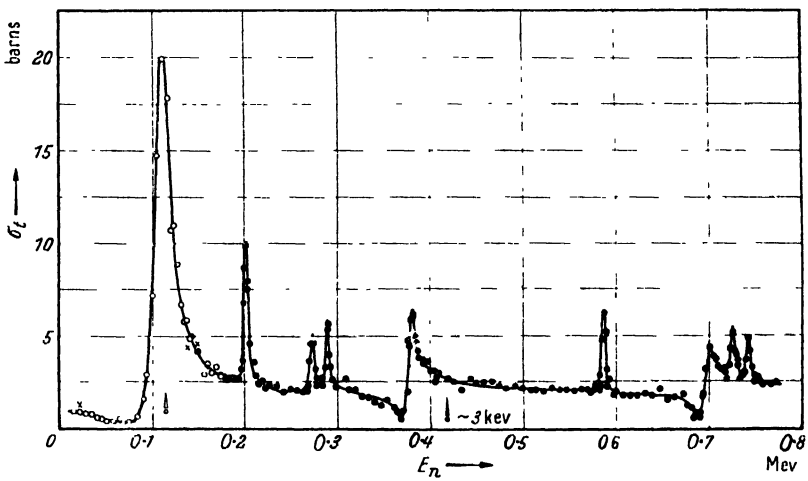


Fig. 10 Total cross section of sulphur for medium fast neutrons (ADAIR[79])

elastic scattering and absorption processes, and the elastic scattering shows resonances, and interference phenomena just as in the case of charged particles. Extremely fine definition of neutron energy is possible in the slow neutron region by means of velocity selectors of the pulsed cyclotron, pulsed linear accelerator (MERRISON and WIBLIN[80]), mechanical selector, or crystal spectrometer methods, the last two using the intense slow neutron beams from a reactor. A full discussion of most of these techniques is given by DEVONS[9]. The spacing of levels in the light nuclei in the region of excitation corresponding to the neutron binding energy of about 7 Mev is not close, and the slow neutron studies have revealed practically no levels for these elements since they extend only over about 1000 volts of energy. With monoenergetic neutrons from charged particle reactions, with energies between 50 and 1000 kev, the most probable interaction with light nuclei is elastic scattering, and Fig. 10 shows the collected results obtained by a number of workers for the total cross section of sulphur measured by a transmission method for this range of neutron energy. The peaks indicate virtual levels in the S^{33} nucleus; from the shape of the cross section curve near resonance, and the magnitude of the total cross

section, it may be possible to deduce the level width and spin of the compound state and from the Cevel width the orbital momentum of the incident neutron may be estimated. Examples of this method have recently been discussed by STAFFORD[80a] and by ADAIR[81]. Only centrifugal penetrability factors enter into neutron scattering processes and fast neutron widths are therefore greater than proton widths for low energy particles. The resonant scattering of low energy neutrons may be large in comparison with the potential scattering; this is evident by comparing the results for the total cross section of sulphur (Fig. 10) for the (*nn*) process with that for the (*pp*) scattering in aluminium previously shown (Fig. 9).

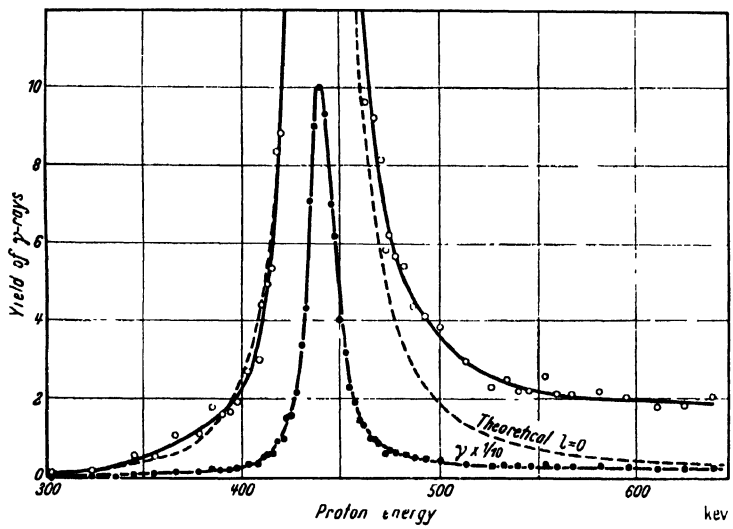


FIG. 11. The Li'(*pγ*) excitation function (BONNER and EVANS[84]).

(e) *The study of radiative transitions*

More detailed information on the virtual levels of light nuclei has been obtained by investigation of proton and neutron capture processes than by any other means. The study of the subsequent emission of gamma radiation both directly to the ground state, and by cascade to bound levels has proved comparable in fruitfulness with the investigation of the radioactive decay schemes of the heavy elements. An excellent summary of the experimental methods and results up to 1948 is given by FOWLER, LAURITSEN and LAURITSEN[82]. More recently a good deal of work on the radiation from bound excited states of residual nuclei has been carried out; this is discussed in Section IV, e. 4.

(e.1) *Radiative capture of protons*

The process

$$\begin{aligned} A + p &\rightarrow B^* \\ B^* &\rightarrow B + \gamma \end{aligned} \qquad (6)$$

(in which B is in general a stable, but sometimes a positron active nucleus) *i.e.* the capture of protons with the emission of gamma radiation, occurs for

the majority of light elements for proton energies below the (pn) threshold, where the main competitive process is elastic scattering. In some particular cases (*e.g.* B^{11}, N^{15}, F^{19} ...) alpha-particle emission competes; these processes will be disregarded for the present. The main characteristic of such capture reactions is the occurrence of sharp resonances in the intensity of gamma radiation as a function of proton energy. These are well displayed either as steps in the excitation function with a thick target, or as sharp peaks with a thin target. The natural width of the peaks is often determined by the re-emission of protons, which except for resonances at very low energies is always very

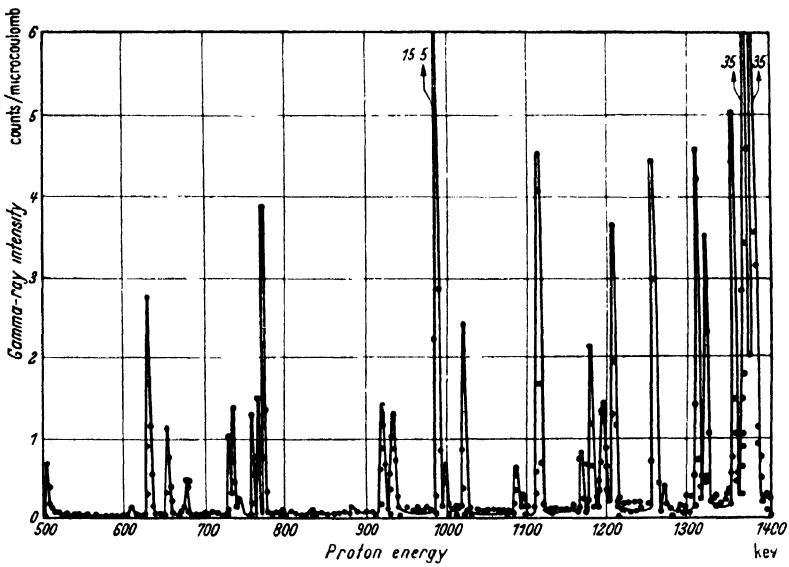


Fig. 12. The $Al^{27}(p\gamma)$ excitation function (BROSTROM, HUUS and TANGEN[85]).

much greater than the radiation width. In experiments the natural width is sometimes much less than the experimental width imposed by target thickness, and beam homogeneity, in which must be included DOPPLER motion of the target atoms. Examples of careful measurements of the real width of levels are to be found in the work of TANGEN[83], and of BONNER and EVANS[84]. Fig. 11 is taken from the work of BONNER and EVANS[84], and shows the well-known $Li^7(p\gamma)$ resonance at 441 kev; the homogeneity of the proton beam was about 300 volts and the observed width of 12 kev is the natural width of the level. Fig. 12 gives a picture of the type of level spectrum obtained for a nucleus at the upper end of the region of light nuclei, and shows how the level spacing has diminished from the values of a few hundred kev found for the lightest elements. The work is that of BROSTROM, HUUS and TANGEN[85] on the capture of protons by aluminium; in this work, despite the apparently high resolution the widths are still experimental, since the proton width is less than about 1 kev even at the highest bombarding energy used, owing to the high Coulomb barrier.

The analysis of such resonance curves gives the resonance energy E_r, and level width Γ directly when the level width is comparable with the experimental resolution. This will usually be so only when the proton width Γ_p is essentially equal to the total width Γ and very much greater than the radiation width Γ_γ. From the cross section at resonance the term $\omega\Gamma_\gamma$ can then be found, since if $E = E_r$ and $\Gamma \gg \Gamma_\gamma$ eq. (2) reduces to

$$\sigma_{res} = \frac{\lambda_r^2}{\pi}\omega\frac{\Gamma_\gamma}{\Gamma}. \tag{7}$$

If the level width is much less than the experimental resolution the yield integrated over the resonance is found, and from this, with knowledge of E_r and

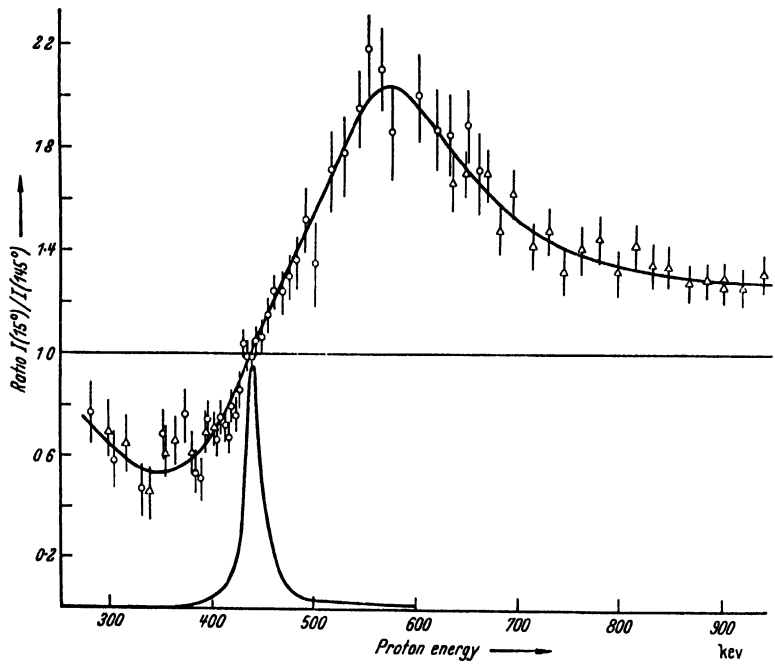


Fig. 13. Interference between resonant and non-resonant radiation in the $Li^7(p\gamma)$ reaction exhibited by variation of asymmetry of angular distribution with proton energy (DEVONS and HINE[86]).

of the stopping power of the target material, the term $\omega\frac{\Gamma_p\Gamma_\gamma}{\Gamma}$ may be found, which gives either $\omega\Gamma_p$ or $\omega\Gamma_\gamma$ according as Γ_p is very much less than or very much greater than Γ_γ. The observed magnitudes of Γ or Γ_p yield values of the reduced width when corrected for the energy dependent factors (Section III), and comparison with values of reduced width obtained in other reactions or with the Wigner limit may indicate probable l-values for the incident proton. This is useful in assigning spin and parity values for the compound state as in the analysis of elastic scattering resonances. The observed value of $\omega\Gamma_\gamma$ may be compared with the value expected for a gamma ray transition of given multipolarity (see Section IV, e. 4) which will also give information about

the momenta and symmetry properties of the states concerned. Examples of this process are discussed by FOWLER, LAURITSEN and LAURITSEN[82].

The shape of $(p\gamma)$ resonance curves has been shown to fit that predicted by the BREIT-WIGNER theory, when allowance is made for the variation of proton width with energy over the resonance. A particularly convincing demonstration of the validity of the dispersion formula comes from the work of DEVONS and HINE[86] on the $Li^7(p\gamma)$ reaction, in which there is interference between the radiation from the resonance level and coherent "background" radiation of low intensity and opposite parity (evident in Fig. 11 as an excess of intensity above the theoretical curve). The resulting asymmetry of the angular distribution (Fig. 13) can be observed over nearly 100 resonance widths from 200 to 1000 kev proton energy, and in addition to verifying the $\frac{1}{E_r - E}$ variation of amplitude given by the BREIT-WIGNER formula over this region, the experiment also shows the characteristic phase change of the wave-function as E passes through the resonance energy E_r.

The analysis of proton capture experiments is more complicated when competitive processes such as alpha-partic'e or neutron emission or inelastic scattering are possible. Detailed studies of cross section and angular distribution for the individual processes are generally necessary. A theoretical analysis of the $F^{19}(p\alpha)$ reactions by CHAO[87] illustrates the complexity of the problem.

Measurement of the energy of the capture gamma radiation is discussed in Section IV, e. 4.1.

(e.2) *Radiative capture of alpha-particles*

Observation of $(\alpha\gamma)$ reactions has been difficult until recently owing to the low intensity and poor resolution available with natural alpha-particle sources. The production of accelerated beams of He^+ ions, however, has already led to the observation of a number of resonance levels, and a considerable development in this field is likely in the immediate future. Interpretation of the results should be simpler because of the zero spin of the alpha-particle.

(e.3) *Radiative capture of neutrons*

This process, which is the main interaction of slow neutrons with heavy nuclei, has been observed for light nuclei and fast neutrons, but the cross sections are low, and with available intensities of fast neutron beams of controllable energy it seems difficult to undertake work on the capture gamma-rays analogous to those produced by proton capture.

The gamma radiation resulting from slow neutron capture in many nuclei including light nuclei has been extensively studied, and is discussed in Section IV, e. 4.1.

(e.4) *Analysis of decay schemes.*

Much precise information on the bound states of nuclei can be derived from a study of the energy and multipolarity of the gamma-radiation emitted from excited states. These may be:

(a) Bound states excited by inelastic processes (Section IV, a, b).

(b) Bound states excited by the β-decay of a radioactive nucleus, which itself may be produced by a nuclear transmutation or radiative capture process.

(c) Virtual states produced by a capture process.

In all cases the emitted gamma radiation arises as a result of a transition of a quantum mechanical system between two energy levels which may be regarded in a good approximation as stationary states. These levels have angular momentum and parity which must be conserved in the system (nucleus + radiation) and changes of these quantities in the radiating nucleus as a result of the transition must be impressed on the radiation field. If we adopt a semi-classical picture of the radiation process we may say that the radiation field arises from the time variation of the electric or magnetic moments of the radiating system. These moments are expressed quantum mechanically by integrals which in the case of electric moments have the form

$$M_{ab} = e \int \psi_b^* r^l \psi_a d\tau \tag{8}$$

where $\psi_a \psi_b$ are the wave-functions of the initial and final states of the nucleus and r is a position vector. When the wavelength of the emitted radiation is large compared with nuclear dimensions, the formula for the intensity of radiation may be expanded into a set of terms whose intensities fall off in the ratio $(R/\lambda)^2$ and which contain successively the electric dipole, quadrupole, and higher moments of the system for which $l = 1, 2, 3 \ldots$ Magnetic multipole moments of order l appear together with the electric moments of order $l + 1$. Evaluation of the angular parts of integrals M_{ab} using the wave-functions of given initial and final states leads to a selection rule for total angular momentum; this requires that vectorial combination of the initial and final angular momenta $\boldsymbol{J}_a$ and $\boldsymbol{J}_b$† shall give a resultant angular momentum $l\hbar$, which is carried away by the emitted photon. Symbolically, this requires that $J_a + J_b \geq l \geq |J_a - J_b|$. If either J_a or J_b is zero, then $l = J$; if both J_a and J_b are zero, radiation is absolutely forbidden, since no radiat ng charge or current distribution is then possible. Selection rules for parity are also easily derived for a multipole moment of order l from the requirement that the integrand in M_{ab} must be an even function if M_{ab} is not to vanish. The selection rules for radiative transitions are given in the following table:

Table 2—Selection rules for radiative transitions

	Electric multipoles	*Magnetic multipoles*
	$\Delta J = 0 \pm 1 \pm 2 \ldots$	
l even	no parity change	parity change
l odd	parity change	no parity change

Determination of the multipolarity of the quantum emitted in a radiative process helps in assigning quantum numbers J_a, J_b to the initial and final

† $\boldsymbol{J}_a$ is the vector related to the quantum number J_a by $|\boldsymbol{J}_a| = \frac{\hbar}{2\pi}\sqrt{J_a(J_a+1)}$.

states †. The multipolarity may be estimated from observed radiation widths for virtual states, with the assumption of reasonable values for the moments of the system (*cf.* FOWLER, LAURITSEN and LAURITSEN[82]), or from the lifetime of isomeric bound states in the heavier nuclei (SEGRÈ and HELMHOLZ[88]). It cannot be found by measurements on the properties of the radiation at any distance from the nucleus great compared with the wavelength of the radiation, since the gamma ray quantum is observed experimentally as a plane wave, but within the radiating atom processes of internal conversion occur which can be predicted theoretically; comparison with experiment then gives the multipolarity (Section IV e. 4·2).

The important evidence offered by angular correlation experiments is discussed in Section IV, g.

(e. 4.1) *Measurement of energy of gamma radiation and correlation with particle groups*—The methods of measuring energies of gamma radiation and of thereby establishing the level structure of a nucleus have recently been discussed by CAVANAGH[89], and will be only briefly listed here.

The *absorption method* is simple, and accurate for homogeneous radiations, providing care is taken with geometrical conditions, but it is almost useless when complex radiation is to be analysed. Probably the most generally useful method over the whole field of gamma ray energies is the determination of the energy of either the *photoelectrons*, or the *recoil Compton electrons* either by magnetic spectrographs (HORNYAK, LAURITSEN and RASMUSSEN[90]), or in an expansion chamber. The accuracy of this method is about 0·2%, *i.e.* not much worse than the accuracy of Q value determinations by heavy particle spectrographs, and the genetic connection between the emission of gamma radiation and the states indicated by heavy particle groups may be established with high accuracy. For the higher energy radiations, *pair spectrometry* is becoming increasingly important, but the sensitivity of a pair spectrometer is a rapidly falling function of quantum energy and the method is insufficient for a complete survey of the gamma ray spectrum of a nucleus. Gamma radiation of energy above 2·5 Mev may be detected and its energy determined by the *nuclear photoeffect* in deuterium. In this method deuterium is introduced into a photographic emulsion, either as an organic compound (MILLAR *et al.*[91]) or as heavy water (GIBSON *et al.*[92]) and the energy spectrum of photo-protons produced by exposure to gamma radiation is observed. Alternatively the energy distribution of the photo-protons produced in a proportional counter filled with deuterium is recorded by a multi-channel pulse analyser (CARVER and WILKINSON[93]). The latter method is probably the more accurate, but is of low sensitivity unless a high pressure deuterium chamber is used. Gamma radiation has also been studied quantitatively by means of other photo-nuclear reactions, notably $C^{12}(\gamma 3\alpha)$ (NABHOLZ, STOLL and WAFFLER[94]).

Low energy X- and gamma radiation emitted in nuclear processes may be studied by the proportional counter method developed by CURRAN, ANGUS and COCKROFT[95] and by PONTECORVO[96]. Increasing use is being made of

† One of these is usually known if the transition is to a ground state.

proportional scintillation spectrometry (JORDAN and BELL[97], HOFSTADTER and MCINTYRE[98], PRINGLE[99]) using both organic (naphthalene, anthracene) or inorganic phosphors. This method can combine high sensitivity and moderate energy discrimination with resolving times a short as 10^{-8} sec and has led to important advances, not only in the determination of the energy of gamma radiation but also in coincidence studies of decay schemes and angular correlation phenomena (BRADY and DEUTSCH[125]). Large counters using liquid scintillators such as a solution of terphenyl in benzene have also been developed and are extremely efficient detectors of both gamma radiation and fast neutrons (JAMES and TREACY[57]). High speed pulse analysers are particularly useful in scintillation spectrometry. A review of scintillation methods in nuclear physics is given in the article on Luminescent Materials for Scintillation Counters, by G. F. J. GARLICK in this volume.

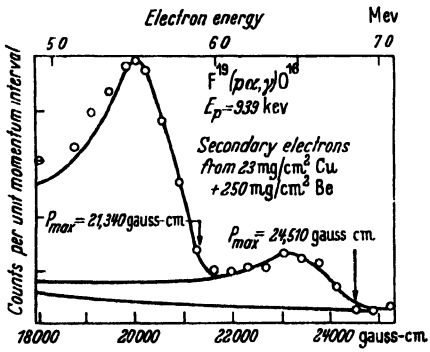


Fig. 14. Measurement of energy of gamma radiation from F^{19} $(p\alpha, \gamma)$ reaction by lens spectrometer (RASMUSSEN *et al.*[100]).

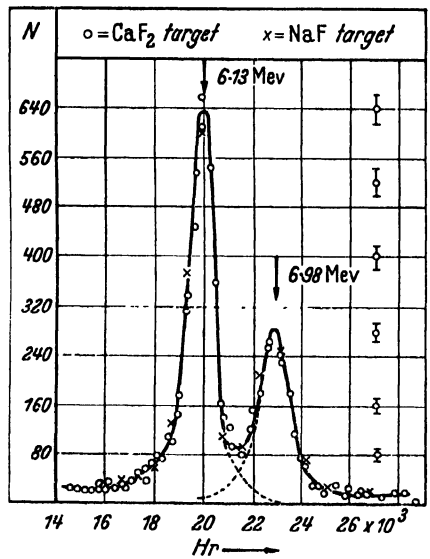


Fig 15. Measurement of energy of gamma radiation from F^{19} $(p\alpha, \gamma)$ reaction by pair spectrometer (WALKER and MCDANIEL[101]).

A typical investigation of the Compton recoil spectrum from nuclear gamma radiation is the work of RASMUSSEN *et al.*[100] on the excited states of the O^{16} nucleus, observed by means of the $F^{19}(p\alpha, \gamma)$ reaction. Fig. 14 shows the spectrum obtained with a lens spectrometer of resolution 2·5% in momentum; the energies of the gamma radiation deduced from this are $6{\cdot}151 \pm 0{\cdot}04$ and $7{\cdot}100 \pm 0{\cdot}06$, which are in excellent agreement with the level spectrum predicted from the corresponding alpha-particle groups (CHAO *et al.*[62]; FREEMAN[63]). The gamma radiation from the $F^{19}(p\alpha)$ reaction was also studied by WALKER and MCDANIEL[101] using a pair spectrometer of total resolution 6%; their results are shown in Fig. 15. Pair spectrometer studies of the gamma radiation from a number of proton capture reactions have been made by WALKER[102], and by RAE RUTHERGLEN and SMITH[103], who have also applied the method to the radiation from bound states excited in (dp) and (dn) reactions[170]. A very comprehensive series of measurements has been made by KINSEY[104] and his collaborators,

using the same method, on the gamma spectra resulting from slow neutron capture. Their results for silicon are shown in Fig. 16; they are in general agreement with the level scheme deduced from measurements of the corresponding (dp) reaction. In all such investigations the absolute and relative intensities of the radiation components may be used to estimate radiation widths which may be connected with the corresponding angular momentum and parity changes as discussed in Section IV e.4. It is clear

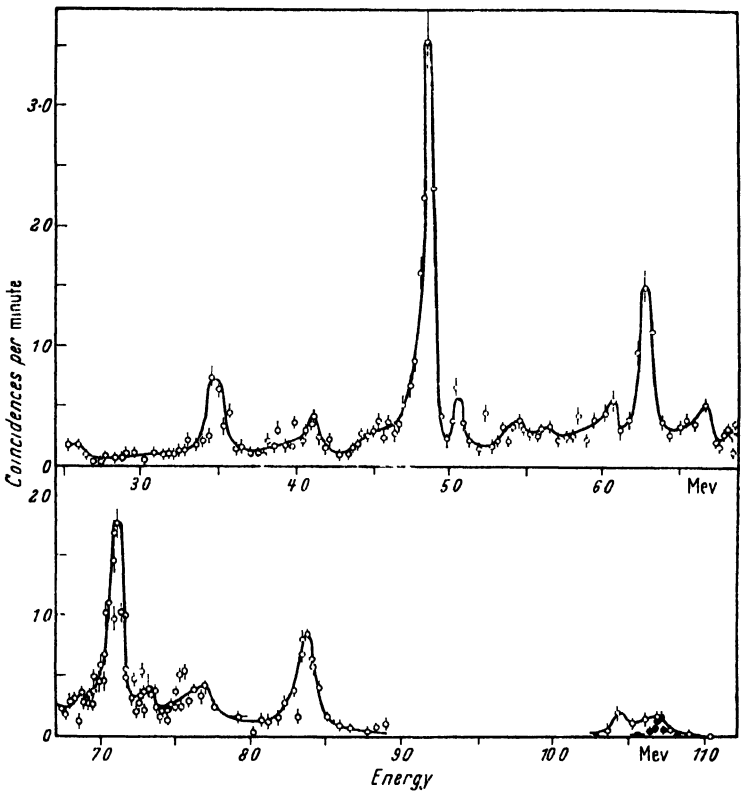


Fig 16 Measurement of energy of gamma radiation from neutron capture process in silicon by pair spectrometer (KINSEY *et al.*[104])

that the association of gamma radiation with groups of particles emitted in artificial transmutations is now nearly as satisfactory as that between the alpha-particle and gamma ray spectra of the natural radioactive elements. The close agreement that has been established in many cases gives considerable certainty to the level scheme. Confirmation of the connection between heavy particles and gamma radiation may be obtained from coincidence experiments (CURLING and NEWTON[105]). In this work the heavy particles were detected by means of thin anthracene screens which permit fast counting, and coincidence resolving times of about 15×10^{-9} secs were achieved. Under these conditions time-of-flight methods may be used both to measure the

energy of groups of particles associated with gamma radiation and to pick out a particular group of particles for the study of its associated radiation.

(e.4.2) *Determination of internal conversion coefficients*—The ejection of a K or L electron from the electronic structure of an atom as an alternative to the emission of a gamma ray quantum originating in the nucleus of the atom is a process whose probability depends on the multipolarity of the radiative transition. The ratio of the number of K electrons ejected to the number of L electrons, or the absolute probability of ejection of either may be observed experimentally and related theoretically to conversion coefficients calculated for the various multipole orders. This method, which has been much used in the determination of the multipolarity of isomeric transitions in heavy nuclei (SEGRÈ and HELMHOLZ[88]) fails unfortunately for light elements owing to the decreasing probability of conversion and to the rather small difference between the coefficients for differing multipoles.

There is, however, another type of internal conversion, practically independent of atomic number, and increasing in probability with energy, in which the quantum energy appears in the form of a positron-electron pair. The theory of this process, both for total cross section and electron-positron angular correlation has been worked out (ROSE[106], HORTON[107]), and shows that the angular correlation provides the most sensitive test for multipolarity. The absolute yield is about 10^{-3} pairs for a quantum of energy 6 Mev in a nucleus with $Z = 10$. Absolute yields are rather difficult to measure (RAE[108], MIMS *et al.*[109], DOUGHERTY *et al.*[110]), but the angular correlation has been checked for the pair emission in the reaction $F^{19}(p\,\alpha, \pi)\,O^{16}$ (DEVONS and LINDSEY[111]). In this particular reaction the pairs arise as a result of an electromagnetic transition between two states of zero spin and the same parity, for which gamma radiation is forbidden (*cf.* Section IV e.4).

(e.4.3) *Beta-decay*—Many light nuclei formed by transmutation processes decay into stable nuclei by the emission of β-particles, and in many cases the transition takes place to an excited state of the final nucleus as well as (or instead of), to its ground state. The theory of β-decay, which has recently been reviewed by SKYRME[112], is in some respects analogous to the radiation theory discussed in Section IV e.4. In particular the probability of β-decay, and thus the lifetime of β-emitters, depends on both the energy and angular momentum change in the transition, and determination of these quantities is therefore useful in assigning spin and parity to the states concerned. It is found that β-emitters may be classified empirically according to the value of the quantity ft (comparative half-life) where t is the half-life and f is an energy-dependent factor, which may be calculated from the upper limit of the β-spectrum (*cf.* FEENBERG and TRIGG[113]). The lowest ft values, of the order of 10^3, belong to *superallowed* transitions which take place between nuclei which have the same ground state wave-function such as the mirror nuclei (Li^7Be^7; $C^{13}N^{13}$ etc.). Rather higher ft values, of about 10^4 to 10^5, correspond to *allowed but unfavoured* transitions, in which there is still no parity change, but a change in wave-function (Li^8Be^8). Higher ft values correspond to

successively more *forbidden* transitions. Theoretically the difference between the different orders of forbiddenness is ascribed to a factor of the form R/λ_β entering into the probability of the β transition, but variations may also enter owing to particular configurations of the initial and final nuclei (FEENBERG and HAMMACK[13]).

The selection rules for changes of angular momentum and parity in β-decay depend on the mechanism assumed to represent the decay process. Two sets of rules, known as the FERMI selection rules and GAMOW-TELLER rules, cover the simplest types of interaction and are given in Table 3; the GAMOW-TELLER rules seem to agree the better with experimental facts except in the case of certain $O \rightarrow O$ transitions (see O[14]).

Table 3—Selection rules for β-decay

β-transition	*Fermi rules*		*Gamow-Teller rules*	
	Spin change	*Parity change*	*Spin change*	*Parity change*
Allowed	0	no	0 ± 1 except $0 \rightarrow 0$	no
1st forbidden	0 ± 1	yes	$0 \pm 1 \pm 2$	yes
2nd forbidden	$\pm 1 \pm 2$	no	$0 \rightarrow 0, \pm 2 \pm 3$	no

Assignment of a given β-transition, which may be a partial spectrum, to a particular class is not always unambiguous, since the *ft* values for the different classes of transition overlap, and reference must sometimes be made to the detailed shape of the spectrum (*cf.* WU[114]). Classifications of β-emitters have been published by KONOPINSKI[115], FEATHER and RICHARDSON[116], FEENBERG and HAMMACK[13], and a list of *ft* values by FEINGOLD[117], and the assignments of most transitions to allowed and forbidden categories have been discussed.

Complexity of a β spectrum, resulting from transitions to more than one state of the final nucleus, is shown by deviations of the Fermi plot of the experimental momentum distribution from a straight line. Further information on the nature of the decay scheme may be obtained from coincidence experiments (MITCHELL[118, 119]). β-γ coincidence counting shows whether or not a given β-transition is linked with the ground state of the final nucleus; γ-γ coincidences indicate complexity of the gamma ray spectrum. High precision in the spectrometer determinations of β and γ energies, coupled with coincidence measurements, usually enables the decay scheme to be settled unambiguously except, in certain cases, for the order of emission of gamma rays in cascade. Experimental methods for the study of β spectra and decay schemes have been reviewed by CAVANAGH[89]; the most important recent developments are the proportional counter method (CURRAN, ANGUS and COCKROFT[95]; PONTECORVO[96]) which is especially suitable for the investigation of β spectra with low end point energy, and the scintillation spectrometer using organic or inorganic phosphors (JORDAN and BELL[97]; PRINGLE[99]).

An example of this type of work is the analysis of the activity of Na^{24} by SIEGBAHN[120] who studied both β and γ ray spectra of this nucleus with a lens

spectrometer; the spectra obtained are shown in Fig. 17, from which there is evidence for a simple β-spectrum of upper limit 1·39 Mev and two γ-rays of energies 1·38 and 2·76 Mev. Coincidence counting methods, summarised by MITCHELL[119] confirm that there is a simple β spectrum followed by two gamma rays in cascade. The *ft* value for the β-transition places it in the first forbidden

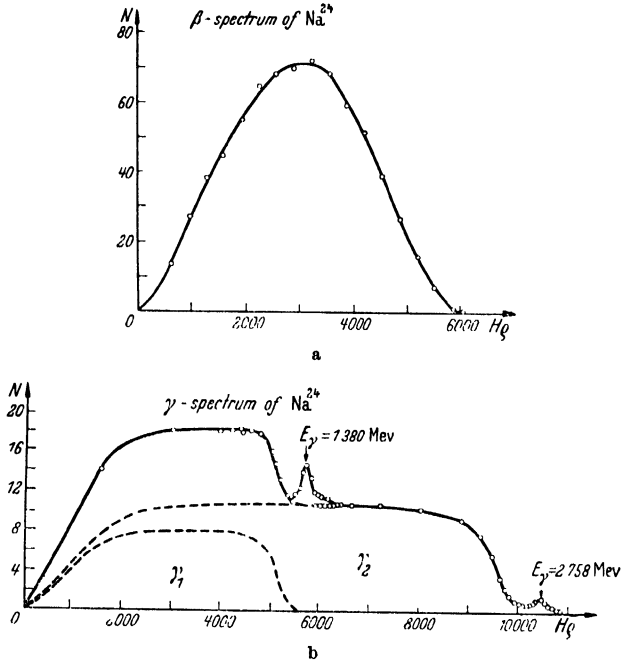


Fig. 17. β and γ spectra of Na^{24} (SIEGBAHN[120]).

class, and suggests that the transition $Na^{24} \rightarrow Mg^{24}$ has $\Delta J = 0, \pm 1$ (Yes) (KONOPINSKI[115]). The level structure of Mg^{24} resulting from these and other measurements is discussed later (Section V B).

(f) *Excitation by the photo-effect*

Nuclear photo-effects are often the inverse of a familiar capture reaction, *e.g.* $H^2(\gamma n)H^1$, and $H^1(n\gamma)H^2$. This type of reaction has not been much used for the study of the excited states of residual nuclei owing to the inflexibility of the available sources of homogeneous gamma radiation. The high intensity continuous sources of white X-radiation now available from synchrotrons and linear accelerators, and (of lower energy) from electrostatic generators, have however made possible the detection of direct excitation of bound levels in some cases in the heavier elements, where isomeric levels of long life exist. Continuous X-radiation has not yet been made sufficiently homogeneous, *e.g.* by crystal reflection, to enable it to excite bound levels (whose radiation width may be only about 0·1 volt) without also giving a large intensity of non-resonant Compton scattering. It is a general rule that nuclei cannot

absorb specifically the radiation which they emit, owing to recoil, but for heavy elements at least it is possible, by moving a radiating source at a speed of about 10^5 cm/sec to restore by means of the Doppler effect the energy lost in recoil (MOON[121]). In this way, resonant scattering of gamma radiation has been demonstrated, and from the cross section, the radiation width and hence the lifetime of the level may be deduced. It is possible that this, or an equivalent method, will ultimately be applied to the levels of light nuclei.

In particular cases the photo-effect may be used to study heavy particle reaction mechanisms; some knowledge of the bremsstrahlung spectrum must be assumed to give nuclear level shapes (GOWARD, TELEGDI and WILKINS[122]).

(g) *Angular distribution and angular correlation experiments*

The experimental and theoretical study of angular distributions and correlations in nuclear reactions has been responsible in the last five years for an important increase in our knowledge of the properties of the levels of light nuclei. It is convenient to divide discussion of these processes into those in which a compound state plays a part (two stage processes) and those such as stripping reactions and interactions of the very lightest nuclei in which direct transition between initial and final states is a sufficient description (one stage processes). We may represent processes of the first class as either

(a) a transmutation

$$A + p \rightarrow C \rightarrow B + q \tag{9}$$

or (b) a process in which an excited nucleus emits two radiations in rapid succession

$$\begin{aligned} D &\rightarrow C + p \\ C &\rightarrow B + q. \end{aligned} \tag{10}$$

These two cases are formally equivalent; each may be considered as a two-stage process proceeding through the compound nucleus C. The experimental information generally consists, in case (a), of the yield of q as a function of θ, the angle in the centre of mass system between the direction of emission of q and of incidence of p (angular distribution); in case (b) a study is made of the variation of the number of coincidences in a pair of suitable counters detecting the radiations p and q with the angle between their axes (angular correlation). Fig. 18 illustrates the difference between the two types of observation. Case (a) includes most of the straightforward angular distribution work which has been carried out for transmutations and involves only introducing the extra variable θ into the apparatus used for range measurements; typical arrangements are those of HEYDENBURG *et al.*[123] and of MARTIN *et al.*[124] for heavy charged particles and of DEVONS and HINE[86] for capture gamma radiation. Fig. 19 and 20 show some of the results of these workers. Case (b), where p and q are successive gamma-rays has been particularly studied by BRADY and DEUTSCH[125]; some of their results, obtained by using scintillation counters as detectors, are shown in Fig. 21. These suggest, when compared with theory, the sequence of spins 0-2-4 in the lowest levels of Mg^{24} (*cf.* section VB).

The importance of measurements such as those just described lies in the information which they give about the changes of angular momentum and parity in the reacting system. The theory necessary for the interpretation of the experimental results was first discussed, with particular reference to the case of successive gamma ray transitions, by HAMILTON[126] and by GOERTZEL[127] and generalisations to cover angular correlations between heavy particles and quanta in two stage processes have been made by YANG[128] and by FALKOFF and UHLENBECK[129]. Typical discussions of experimental results for processes of type (a) have been given by INGLIS[130, 131] for the $Li^7(p\alpha)He^4$ reaction and by CHAO[87] for $F^{19}(p\alpha, \gamma)O^{16}$. A review of the whole subject of angular correlations in two stage processes has been given by DEUTSCH[132].

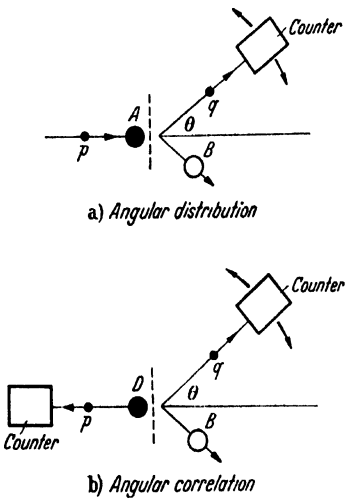


Fig. 18. Angular distribution and angular correlation experiments.

The essential features of these treatments may be summarised as follows: In processes of type (a) and (b) the capture or emission of particle p will form or leave the nucleus C in a superposition of states; for simplicity we consider the special case when only one state characterised by a total angular momentum quantum number J is formed. This state has, for any specified axis of quantisation (*e.g.* the direction of motion of p) $2J+1$ magnetic substates with quantum numbers J_z, as is well known in the case of the Zeeman splitting of optical spectral terms. If it happens that there is an equal probability of forming any of the substates of the state J, then the nuclei C concerned in the process are effectively isotropically distributed, and no correlation (isotropy) between the directions of p and q will be observed. In general however the magnetic substates are not formed with equal weight. To determine the probabilities, it is necessary to express the wave function describing the initial

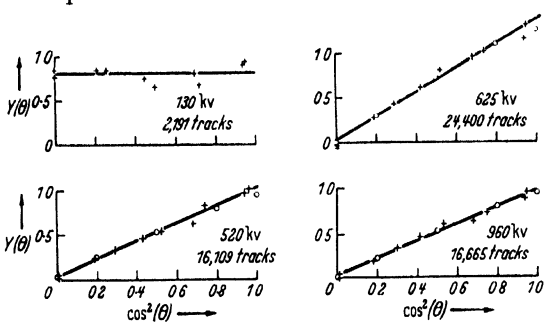


Fig. 19. Angular distribution of alpha-particles from reaction $Li^7(p\alpha)$ with respect to the direction of the incident protons (MARTIN *et al.*[134]).

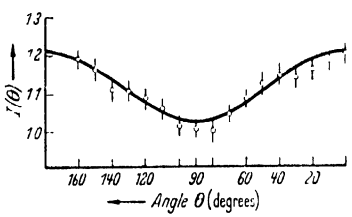


Fig. 20. Angular distribution of γ-radiation from $F^{19}(p\alpha, \gamma)O^{16}$ (DEVONS and HINE[88]).

system with its particular orbital and spin quantum numbers, in terms of eigenfunctions of the compound state of C with angular momentum quantum number J and substates J_z. The necessary transformation coefficients are given by CONDON and SHORTLEY[133]. The compound state (J, J_z) will have a finite lifetime before the emission of q and it is necessary for the interpretation of an angular correlation experiment for this lifetime to be much shorter than the time required for perturbing fields to destroy the orientation of the nuclei with respect to the chosen axis of quantisation. If this is so, then the wave function describing the emission of the radiation q from the nuclei C may be expressed in terms of the eigen-functions of the state J of C by transformation theory. If q is a charged particle the space wave function of the final state, for large distances of separation of B and q, can be resolved into a set of partial waves of orbital angular momentum quantum number l and z-component m. The angular dependence of the amplitude of these partial waves is given by $Y_l^m(\theta\varphi)$ and the corresponding intensity is proportional to $[Y_l^m(\theta\varphi)]^2$. If q is a photon, the eigenfunctions of the final state represent the classical radiation field described by Maxwell's equations and there are particular types of field for each l and m value (HEITLER[134]); the orbital angular momentum in the final system determines the multipole order of the quantum. A study of the angular correlation in either case may lead to angular momentum assignments.

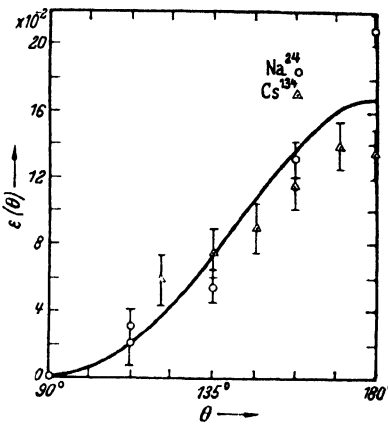


Fig. 21. Angular correlation of successive gamma rays from Na^{24} and Cs^{134} (BRADY and DEUTSCH[135]).

In most cases the problem of interpretation is complicated by the possibility of the emission of particles with more than one l value in a transition between two states. These radiations are coherent and their amplitudes must be added, with the assumption of arbitrary phase factors. Similar complexity results when the nucleus C is formed in a superposition of states of different J which is in general the case in an angular distribution experiment. Moreover the simple procedure that has been outlined applies only to cases in which the initial nuclei A (or D) are isotropically distributed. This is of course true if D is a radioactive element or if A is formed by capture of an s-wave particle, but the general case of the formation of A in a nuclear reaction and its subsequent decay is properly a three-stage process. Such processes have been discussed by BIEDENHARN, ARFKEN and ROSE[135].

The general formulae for angular correlations are complicated and will not be quoted here. They include resonance denominators from which the energy dependence of the angular correlations may be calculated, and in the case of charged particles, penetrability factors for different l-waves, together with other factors varying more slowly with energy which represent intrinsic

reaction probabilities. In many simple cases these factors may be disregarded and the theory of angular correlation then reduces to the linking together of three nuclear states with certain spin by the transformation coefficients for angular momenta. There are, however, a number of general results which are useful in analysing particle-particle or particle-quantum angular correlation patterns. Most of these also apply directly to correlation of successive quanta:

(1) *Axial symmetry*—The distribution of q is independent of azimuth about the direction of p since the initial configuration is an incoherent superposition of the states of spin of the two interacting particles.

(2) *Isotropy*—Angular distributions or correlations are isotropic when the incident wave, compound state or emitted wave has spherical symmetry, so that all sense of direction is lost. This is so if $l = 0$ for the incident or emitted particle, or $J = 0$ or $\frac{1}{2}$ for the compound state. The emission of a photon must carry at least one unit of angular momentum, as is shown by an evaluation of the moment of momentum of a spherical wave in the classical radiation field. However, superposition of a number of anisotropic patterns may also lead to isotropy.

(3) *Symmetry*—Anisotropic distributions may be either symmetric or asymmetric with respect to the origin of the radiation. If only one compound state is involved in the reaction, or if all the compound states involved have the same parity, the intensity distribution of emitted particles will be symmetrical under reflection in the origin and may be expressed in even powers of $\cos\theta$. Odd powers of $\cos\theta$ in heavy particle and quantum distributions can only result from interference between orbital wave-functions of opposite parity†. The parity of photon wave-functions is not determined by the angular momentum carried away, but the same result holds.

(4) *Energy dependence*—Variation of pattern with the energy of p usually indicates the effectiveness of more than one compound state.

(5) *Limitations on complexity of pattern*—One of the most useful general results is stated by YANG[128] as follows: "If only incoming waves of orbital angular momentum l contribute appreciably to the reaction, the angular distribution of the outgoing particles in the centre of mass system is an even polynomial of $\cos\theta$ with an exponent not higher than $2l$." This is true even if the compound state or outgoing waves have greater l values. If the outgoing wave has an orbital momentum $l' \leq l$, the complexity of the pattern is determined by l'. Multipole radiation of order l behaves in this respect as a particle with orbital angular momentum l; thus if in any process dipole radiation is emitted before or after another particle the correlation function cannot have terms higher than $\cos^2\theta$.

The angular correlation patterns observed with radiation are independent of the parity changes in the transitions, and therefore give no information as to whether the radiation is of magnetic or electric type. This may be ascertained by observing the polarisation direction correlation of the radiation,

† Odd powers of $\cos\theta$ also appear in relativistic problems such as electron-electron and electron-neutrino correlations (YANG[128]), in which orbital and spin momenta cannot be treated independently.

since for a given multipole, the electric vector for an electric transition is at right angles to that for a magnetic transition. Experiments of this type for successive gamma quanta have been made by METZGER and DEUTSCH[136].

One of the most successful applications of the theory of angular correlation to light nuclei is presented by the work of BARNES, FRENCH and DEVONS[137] and of ARNOLD[138] on the second excited state of oxygen at 6·13 Mev. This state is excited in the reaction

$$F^{19} + H^1 \rightarrow Ne^{20} \rightarrow O^{16*} + \alpha$$
$$O^{16*} \rightarrow O^{16} + \gamma \ (6{\cdot}13\ \text{Mev}).$$

The angular distribution of the alpha-particles with respect to the proton beam at the resonance energy of 340 kev is isotropic, and so is that of the gamma radiation, but the directional correlation of the gamma radiation with respect to the alpha-particles is markedly anisotropic; the actual experimental results are shown in Fig. 22. The distribution requires terms up to $\cos^6\theta$ for its expression, which indicates that the orbital momentum of the alpha-particle and the angular momentum of the O^{16*} nucleus must each be at least 3. If it is assumed that the compound state of Ne^{20} has $J = 1$ and that it is formed by s protons, so that these nuclei are isotropically distributed, the two stage theory can be applied and the observed pattern can be completely predicted. The radiative transition is octupole and polarisation experiments (FRENCH and NEWTON, private communication) show that the transition is electric, so that the 6·13 Mev state of O^{16} is of the type (3–). The assumed l-value for the alpha-particles then requires that the Ne^{20} level shall be of the type (1+), and since this state is formed by s-protons from F^{19}, the parity of F^{19} must be even, in agreement with the prediction of the independent particle model. It is evident that this experiment gives an unusual amount of valuable information.

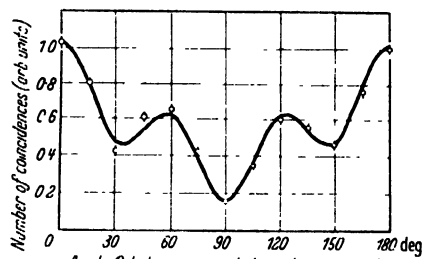


Fig 22. Angular correlation pattern for alpha-particles and gamma radiation in the reaction $F^{19}(p\alpha, \gamma)O^{16}$ (BARNES, FRENCH and DEVONS[137])

The general properties of $(\beta\text{-}\gamma)$ angular correlations have been listed by FALKOFF and UHLENBECK[129]. As might be expected, an allowed β-transition leads to no angular correlation (isotropy), and so also do forbidden transitions whose spectrum is of the allowed shape. Very few anisotropic patterns have been observed.

(h) *Angular distributions in stripping processes*

Nuclear reactions of the (dp) and (dn) type produced by high energy deuterons may be thought of as proceeding by a stripping process, in which either the neutron or proton of the incident deuteron enters the bombarded nucleus and is absorbed by it, leaving the other particle to carry off the balance of energy and momentum. No formation of a compound state is involved,

and asymmetry of the angular distributions mayin general be expected. Observations of (dp) reactions with 8 Mev deuterons show that the angular distribution of the emitted particle in such reactions is characterised by a very strong forward peak. Fig. 23 shows the results of BURROWS, GIBSON and ROTBLAT[139] for the $O^{16}(dp)O^{17}$ reaction using the photographic plate method of detection; the two curves correspond to the formation of O^{17} in its ground and first excited states. BUTLER[140] has shown that this forward peak is characteristic of the stripping process and that from the position of the maximum the spins and parities of the nuclear states concerned may be predicted.

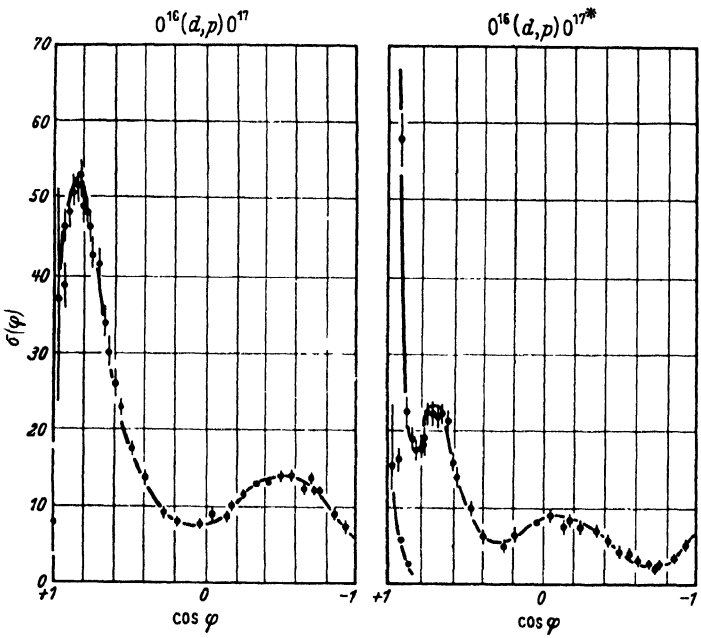


Fig. 23. $O^{16}(dp)$ angular distributions in centre-of-mass system; deuteron energy 8 Mev (BURROWS *et al.*[139]).

In the case of $O^{16}(dp)$ the results show that the neutron enters the O^{16} nucleus with orbital angular momentum 2 when it forms O^{17} in its ground state, and with no angular momentum when it forms O^{17} in its first excited state. The ground state of O^{17} should therefore be ($\frac{3}{2}$ or $\frac{5}{2}$, +) and the first excited state ($\frac{1}{2}$ +). It is obvious that this type of reaction gives the parity charge in a reaction directly, and the method will undoubtedly be exploited considerably in the future.

(i) *Measurements of the lifetime of nuclear states*

In heavy nuclei excited states of low excitation and high angular momenta may have very long lifetimes, and are known as isomeric states (SEGRÈ and HELMHOLZ[88]). The lifetimes of the bound excited states of light nuclei although also dependent on the angular momentum change, are very considerably shorter, although not so short as to make radiation widths directly

measurable at present. The lifetimes (or radiation widths) can be calculated on the assumption of particular nuclear models (*cf.* DEVONS[9], p. 101).

Measurements of lifetime of nuclear states of the light elements have been based on the Doppler effect and on recoil. If gamma radiation is emitted from a nucleus which is moving the spectrum will be broadened; if the nucleus is moving in a solid target the time after its formation before it is brought to rest can be calculated. In this way, ELLIOTT and BELL[141] showed by careful measurement of the energy spread of the gamma radiation from Li^{7*} formed in the $B^{10}(n\alpha)Li^{7*}$ reaction, that the excited state of Li^7 has a lifetime of $0{\cdot}75 \times 10^{-13}$ sec. The recoil method has been used by DEVONS, HEREWARD and LINDSEY[142] to measure the lifetime of the pair emitting state of O^{16}. The excited O^{16} in this experiment recoils after the emission of an alpha-particle in the reaction $F^{19}(p\alpha)O^{16*}$. A lifetime of 7×10^{-11} secs was established. The lifetime of Be^8 against alpha-particle break-up has been estimated by MILLAR and CAMERON[143], by observation of recoiling Be^8 nuclei in a photographic emulsion to be $(5{\cdot}3 \pm 1{\cdot}1)10^{-14}$ sec, but this value is probably an upper limit (WILKINS and GOWARD[144]). The delayed coincidence method of determining half lives (BUNYAN[145] *et al.*), which has been very fruitful in the study of isomeric transitions in heavy nuclei, has not yet been applied to light nuclei.

(j) *Summary of experimental methods available for study of excited states of light nuclei*

It is clear that practically every type of nuclear experiment yields some information on the properties of the levels of light nuclei. We may summarise the foregoing discussion as follows:

Position of level: Energy distributions of elastic and inelastic processes, including transmutation and scattering (IV, a, b, c, d, e). Resonance peaks or thresholds in excitation functions (IV, a, b, c, d, e).

Angular momentum: Angular distribution of reaction products (IV, g). Angular correlation of successive transitions (IV, g). Gamma ray multipolarity (internal pair formation) (IV, e, 4.2). β-transition probability (IV, e, 4.3). Total cross section (IV, d). Cross sections for inverse processes (IV, a.3).

Parity: Angular distribution of reaction products (IV, g). Gamma ray multipolarity (IV, e, 4·2). Polarisation-direction correlation (IV, g). β-transition probability (IV, e, 4·3).

Width, lifetime: Analysis of resonance curves (IV, e, 1). Resonant scattering of γ rays (IV, f). Doppler effect of gamma radiation (IV, i). Recoil method (IV, i).

V. EXPERIMENTAL EVIDENCE

Experiment has provided detailed information on the excitation energy and width of many nuclear levels, but the evidence for their spin and parity is usually much less definite. This makes it useless at present to attempt to draw up anything resembling an atomic term scheme for nuclei, and the classification of the observed levels of a particular nucleus is best based on excitation energy. The presentation adopted by HORNYAK, LAURITSEN, MORRISON and FOWLER[1] will be followed here, and their numerical values will be used unless later work (up to August 1951) has suggested modification. The main body of

references will also be found in their article; usually only the more recent work is quoted here.

The angular momentum, and (in the case of radioactive nuclei) the comparative half-life (*ft* value) of nuclei in their ground state are important in assigning properties to excited states, and the observed values for the nuclei discussed in this section are given in Table 4. Magnetic moments and electric quadrupole moments are useful in assigning quantum numbers to the ground state of some nuclei but have not been tabulated. The ground state character predicted by the independent particle model with weak spin-orbit coupling is also tabulated for reference. Where there is good evidence for a spin or parity assignment for an excited state from nuclear transmutation experiments the value is shown on the energy level diagram enclosed in brackets.

Table 4—Properties of light nuclei in their ground state

Nucleus	*Ground state (I P. model)* (a)	*Ground state spin* (b)	*ft* (c)	*Nucleus*	*Ground state (I P. model)* (a)	*Ground state spin* (b)	*ft* (c)
He^5	$^2P_{\frac{3}{2}}$, —	$(\frac{1}{2})$	α unstable	C^{14}	$^1S_0$, +	0	$9{\cdot}3\ 10^8$
Li^5	$^2P_{\frac{3}{2}}$, —	$(\frac{3}{2})$		N^{14}	$^3S_1$, +	1	
He^6	$^1S_0$, +	(0)	590	O^{14}	$^1S_0$, +	(0)	3000*
Li^6	$^3S_1$, +	1		N^{15}	$^2P_{\frac{1}{2}}$, —	$\frac{1}{2}$	
Li^7	$^2P_{\frac{3}{2}}$, —	$\frac{3}{2}$		O^{15}	$^2P_{\frac{1}{2}}$, —	$(\frac{1}{2})$	3700
Be^7	$^2P_{\frac{3}{2}}$, —	$(\frac{3}{2})$	2300 3600*	N^{16}	^3P, —	(2)	$6{\cdot}4\ 10^6$ $1{\cdot}2\ 10^{6}$* $4{\cdot}9\ 10^{4}$* $2{\cdot}9\ 10^{4}$*
Li^8	$^3P_2$, +		$4{\cdot}4\ 10^{5}$*				
Be^8	$^1S_0$, +	(0)		O^{16}	$^1S_0$, +	0	
B^8	$^3P_2$, +		$3{\cdot}2\ 10^{5}$*	O^{17}	$^2S_{\frac{1}{2}}$, +	$\frac{5}{2}$	
Be^9	$^2P_{\frac{3}{2}}$, —	$\frac{3}{2}$		F^{17}	$^2S_{\frac{1}{2}}$, +	$(\frac{5}{2})$	3240
B^9	$^2P_{\frac{3}{2}}$, —		α unstable	O^{18}	$^1S_0$, +	0	
Be^{10}	$^1S_0$, +	(0)	$7{\cdot}9\ 10^{13}$	F^{18}	$^3S_1$, +	(1)	4100
B^{10}	$^3S_1$, +	3		F^{19}	$^2S_{\frac{1}{2}}$, +	$\frac{1}{2}$	
C^{10}	$^1S_0$, +	(0)	2100*	Ne^{19}	$^2S_{\frac{1}{2}}$, +	$(\frac{1}{2})$	2000
B^{11}	$^2P_{\frac{3}{2}}$, —	$\frac{3}{2}$		F^{20}		(2)	$7 < 10^6$ 8×10^{4}*
C^{11}	$^2P_{\frac{3}{2}}$, —	$(\frac{3}{2})$	4300	Ne^{20}	$^1S_0$, +	(0)	
B^{12}	$^3P_0$, +	(1)	$1{\cdot}4\ 10^4$				
C^{12}	$^1S_0$, +	0		Na^{21}		4	$1{\cdot}22\ 10^{6}$* $5\ 10^{12}$*
N^{12}	$^3P_0$, +	(1)	$1{\cdot}7\ 10^4$				
C^{13}	$^2P_{\frac{1}{2}}$, —	$\frac{1}{2}$		Mg^{24}	$^1S_0$, +	(0)	
N^{13}	$^2P_{\frac{1}{2}}$, —	$(\frac{1}{2})$	4500				

(a) The ground state characters are taken from HLMF[1] or from ROSENFELD[7], except that the *d*-shell is assumed to start filling at A = 17.

(b) MACK [*Rev. Mod. Phys.* 22, (1950) 64] lists experimentally determined angular momenta. *J* values suggested by nuclear transmutation experiments or by β-decay are included in brackets

(c) HLMF Table 66; FEINGOLD[117].

* Transition to excited state of residual nucleus.

The division of the nuclei into odd and even isobars for the purpose of discussion is naturally suggested by the importance of Coulomb forces, and of Heisenberg forces respectively in these types of nuclei. Most of the odd isobars of low atomic number group into pairs of mirror nuclei, in which the numbers of neutrons and protons differs by ± 1. The sub-division of the even isobars into nuclei of mass number $4n$ and $4n+2$ has not much to justify it theoretically, but shows up some experimental regularities.

A. The odd isobars.

(i) H^3—He^3.

These are not known to have any excited states. The neutron-proton mass difference outweighs the Coulomb energy difference and H^3 is unstable against electron emission.

(ii) He^5—Li^5.

These nuclei have one nucleon in the p-shell and a pair of low states of the type $^2P_{\frac{3}{2},\frac{1}{2}}$ with a splitting due to spin-orbit interaction is expected, but the binding of the extra nucleon to the alpha-particle core is not strong enough to make either nucleus stable. The existence of the nuclei is revealed by results on the scattering of protons and neutrons by helium; and by transmutation experiments.

The results on the (nHe^4) scattering are collected by ADAIR[79] and show a single maximum in total cross section at a neutron energy of about 1·1 Mev. The latest work on the (pHe^4) scattering (FREIER, LAMPI, SLEATOR and WILLIAMS[146]) shows a maximum at backward angles in the differential cross section for protons of 2·2 Mev energy. Analysis of these results (CRITCHFIELD and DODDER[147], ADAIR[148, 149], GOLDSTEIN[150]) is not unambiguous but favours the conclusion that the doublet $P_{\frac{3}{2}}$–$P_{\frac{1}{2}}$ is inverted in both He^5 and Li^5 and that the nuclei are unstable in their ground state by about 1 and 2 Mev respectively with level widths of about 1 Mev. The $P_{\frac{1}{2}}$ state is also wide and is required to lie about 5 Mev higher in each nucleus; this splitting presumably measures the spin-orbit interaction. The He^5 levels are depressed by about 1 Mev with respect to those of Li^5 owing to the Coulomb energy difference and level shift Δ (Section III).

The reaction $Li^7(d\alpha)He^{5*}(n)He^4$† gives a group of alpha-particles corresponding to the formation of He^5 in its ground state, which appears from this reaction to be about 1 Mev wide. The angular correlation between the alpha-particles of this group and those resulting from the subsequent break-up of He^{5*} (lifetime about 10^{-21} sec) is anisotropic which eliminates the possibility of a pure $P_{\frac{3}{2}}$ ground state (FRENCH and TREACY[42]). He^5 is also formed in the reactions $He^4(dp)He^5$ and $T(tn)He^5$ (LELAND and AGNEW[151]) and in the latter reaction there is evidence for a 2·6 Mev excited state which could be the expected $P_{\frac{1}{2}}$ level. Li^5 is formed in both ground and excited states in the process $Li^6(\gamma n)Li^{5*}(p)He^4$ (TITTERTON and BRINKLEY[152]) Highly excited states of these nuclei are effective in the reactions $H^2(t\alpha)\,n$ and $H^2(He^3\alpha)H^1$.

† This abbreviation indicates $Li^7(d\alpha)He^5$ followed by $He^5 \rightarrow He^4 + n$, *i.e.* a two-stage process.

(iii) Li^7—Be^7

The two identical nucleons external to the alpha-particle shell in these nuclei are assumed to couple to give a spin zero. The remaining odd nucleon in the p shell should lead to a $^2P_{\frac{3}{2},\frac{1}{2}}$ doublet. The observed spin of $\frac{3}{2}$ for Li^7 shows that the doublet is inverted. The first excited state of Li^7 has been very firmly established at 479·0 ± 1 kev by observation of the reactions $Li^6(dp)$ $B^{10}(n\alpha)$, $Be^9(d\alpha)$, $Li^7(pp^1)$ and $Be^7(K)Li^7$, and a mirror state in Be^7 at 434·4 ± 4 kev excitation was observed recently by BROWN, SNYDER, FOWLER and LAURITSEN[153] in the reaction $B^{10}(p\alpha)$; it has also been found in the reactions $Li^7(pn)$ and $Li^6(dn)$. The assignment of spin $\frac{1}{2}$ to the first excited state of Li^7 is supported by observation of the angular distribution of the gamma radiation from the inelastic scattering of protons by Li^7 (isotropic for Ep up to 1 Mev) and by the angular correlation between the short range alpha-particles and subsequent gamma radiation in $B^{10}(n\alpha)$ (isotropic) and between short range protons and gamma radiation in $Li^6(dp)$ (isotropic) (NEWTON[154], THIRION[155], CLASS and HANNA[156]). The spin of the mirror state in Be^7 also could be $\frac{1}{2}$ from observation of the angular correlation between neutrons and gamma radiation (isotropic) in the reaction $Li^6(dn)$ (THIRION[157]). These assignments are in doubt chiefly because it is difficult with an excited state of spin $\frac{1}{2}$ to account for the branching ratio of 19/1 between short range and long range alpha-particles in the reaction $B^{10}(n\alpha)Li^{7*}(\gamma)Li^7$ with thermal neutrons. At higher energies however (BECHSEL *et al.*[158]), the ratio approaches the value $\frac{1}{2}$ predicted by the statistical weights of the final states on the assumption of an inverted doublet. The lifetime of the excited state of Li^7 is consistent with the emission of magnetic dipole or electric quadrupole radiation; the $^2P_{\frac{1}{2}} \rightarrow {}^2P_{\frac{3}{2}}$ transition of course takes place with no change in parity.

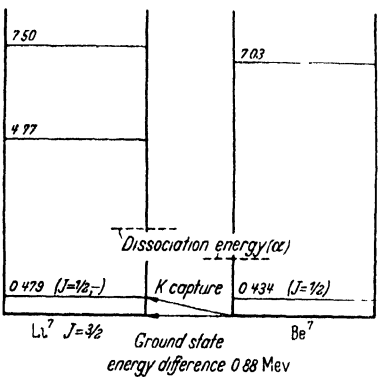


Fig. 24. Levels of mirror nuclei Li^7Be^7.

Be^7 decays into both the ground and 479 kev excited states of Li^7 by K-capture. The transitions are allowed and 10% of the disintegrations lead to the excited state (WILLIAMSON and RICHARDS[159]). This is in agreement with the theoretical ratio for transitions between a $P_{\frac{3}{2}}$ ground state of Be^7 and a $P_{\frac{1}{2}}$ excited state and $P_{\frac{3}{2}}$ ground state of Li^7, but the experimental branching ratio could also be fitted by the assumption of mixed P and D ground states.

The level schemes for Li^7 and Be^7 are compared in Fig. 24†. This shows a further state in Li^7 at 4·77 Mev found from the reactions $Li^7(pp')$, $Li^7(\alpha\alpha')$, $Li^7(dd')$ and $Be^9(d\alpha)$ (GOVE and HARVEY[160]), and another at 7·50 Mev found

† In this and other diagrams of the level schemes of the odd isobars the ground states are placed side by side; the actual energy difference is noted on the diagram. Experimental results for angular momenta and parity, usually tentative, are noted in brackets.

from $Be^9(d\alpha)$ only. The 4·77 Mev state could be the $^2P_{\frac{3}{2}}$ component of the spin-orbit doublet; the splitting would then be similar to that suggested for He^5. The higher state corresponds well with a 7·03 Mev state in Be^7 identified as a resonance in the reactions of Li^6 with protons (BASHKIN and RICHARDS[161]); the expected 4·8 Mev state in Be^7 has not yet been reported. The mirror nature of the two nuclei is well verified, the slight depression of the Be^7 levels relative to those of Li^7 being interpreted by INGLIS[162] and by MOTTELSON[163] as due partly to expansion of the Be^7 nucleus and partly to magnetic effects. This is consistent with the difference between the observed and calculated Coulomb energy difference (Table 1) which suggests a greater nuclear radius for Be^7.

Detailed theoretical discussions of the properties of this isobaric pair have been published by FEENBERG[164] and by INGLIS[162, 165] and a compilation of the relevant experimental information up to the end of 1950 is given in the paper of BROWN, SNYDER, FOWLER and LAURITSEN[153].

(iv) Be^9–B^9

These nuclei resemble the He^5–Li^5 isobars on the assumption that they may be considered as one nucleon external to an alpha-particle core. Be^9 is stable but the extra Coulomb repulsion in B^9 makes this nucleus unstable with respect to break-up into $(2\alpha + p)$. Be^9 has a narrow state at an excitation energy of 2·42 Mev, which, although it exceeds the dissociation limit by 0·7 Mev, is less than 7 kev wide. The state has been found in the $B^{11}(d\alpha)$ (VAN PATTER *et al.*[166]) and $Be^9(pp')$ (RHODERICK[37], BROWNE *et al.*[167]) reactions.

Further evidence on states of Be^9 may be inferred from the variation with energy of the cross section for the photo- and electro-disintegration of Be^9 and from the angular distribution of the resulting neutrons. GUTH and MULLIN[168] using a model in which a neutron is supposed loosely bound to a Be^8 core, and with the assumption of a $P_{\frac{3}{2}}$ ground state for Be^9, predict a bound $S_{\frac{1}{2}}$ state about 100 kev below the dissociation energy and a broad $D_{\frac{5}{2}}$ state at an excitation of about 4·2 Mev. No other evidence for these states has been found; and the known state at 2·42 Mev has not yet been shown to take part in the (γn) process. The $P_{\frac{1}{2}}$ component of the spin-orbit doublet has not been identified.

Little is known of B^9, which is produced in the reaction $Be^9(pn)$; there seem to be no levels up to 1·8 Mev.

(v) B^{11}–C^{11}

The level spectra of these nuclei are compared in Fig. 25, and clearly correspond quite well, with some depression of the C^{11} levels which may be due to expansion of this nucleus (*cf.* Be^7). The levels of B^{11} are determined by magnetic analysis of the proton groups in the $B^{10}(dp)$ reaction (VAN PATTER[169] *et al.*), and association of some of these groups with gamma radiation has been shown by CURLING and NEWTON[105] while some of the intercombination gamma ray energies have been measured with a pair spectrometer by RUTHERGLEN, RAE and SMITH[170]. The angular correlation between the protons emitted in the

formation of the 2·14 Mev state in the $B^{10}(dp)$ reaction and the subsequent gamma radiation is isotropic (THIRION[155]) suggesting spin ½ for thus state. The lower Q-values found in the (dp) experiments correspond to virtual levels in B^{11} unstable with respect to alpha-particle emission, and three of these levels have already been observed in the $Li^7(\alpha\gamma)B^{11}$ reaction (BENNETT, ROYS and TOPPEL[171]). A broad level at 11·6 Mev is deduced by fitting BREIT-WIGNER constants to the observed variation of cross section of the $B^{10}(n\alpha)$ reaction with neutron energy (MOTT and MASSEY[8], p. 325). The study of the levels of B^{11} well illustrates the application of the different techniques discussed in Section IV.

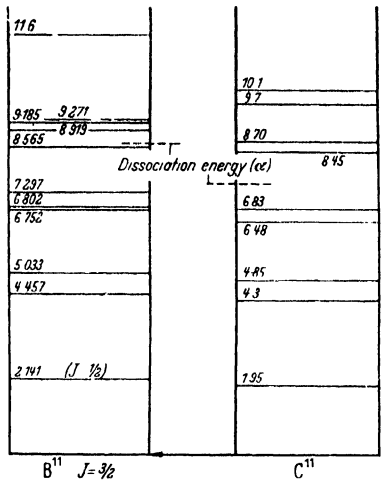


Fig. 25. Levels of mirror nuclei $B^{11}C^{11}$.

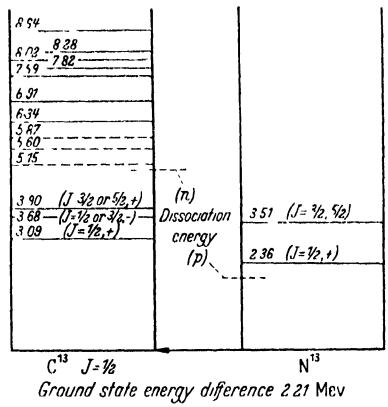


Fig. 26 Levels of mirror nuclei $C^{13}N^{13}$.

The C^{11} levels are obtained mainly from the $B^{10}(dn)$ reaction (JOHNSON[172]) using separated isotopes to distinguish the $B^{11}(dn)$ groups, and from the $B^{10}(p\alpha)$ and $B^{10}(p\gamma)$ reactions (WALKER[102]); gamma radiation from the 9·7 Mev state of C^{11} probably competes with low energy alpha-particle emission.

(vi) C^{13}—N^{13}

The independent particle model predicts a ground state of the type $^2P_{\frac{1}{2}}$ for these nuclei, and this is verified by observation for C^{13}.

Two low states of N^{13} have been found in the reactions $C^{12}(p\gamma)$, $C^{12}(dn)$ and $C^{12}(pp)$ (elastic scattering) (GOLDHABER and WILLIAMSON[78]). The first state, at 2·36 Mev is observed in all three reactions and has a width of 35 kev which suggests its formation by s-wave protons*. This agrees with the observed isotropy of the capture radiation from the level, while the radiation width of 0·63 ev estimated from the $(p\gamma)$ experiments fits with the assumption of electric dipole radiation. The level thus appears to be of $S_{\frac{1}{2}}$ character. The next level, at 3·51 Mev, is also found in all three reactions and has double the radiation width; the cross section at resonance in the $C^{12}(pp)$ reaction can be fitted by the assumption of close $P_{\frac{3}{2}}$ and $D_{\frac{3}{2}}$ levels. No other levels have been observed up to an excitation of nearly 6 Mev (by the (dn) reaction).

* Higher l values would give extremely high reduced widths in this reaction.

The mirror nucleus C^{13} has levels at 3·09 and 3·68 Mev which probably correspond to the 2·36 and 3·51 Mev levels in N^{13}. The reasons for the displacement have been discussed by THOMAS[173, 174] and by EHRMAN[175] in terms of the level shift Δ (Section III). The 3·09 Mev state in C^{13}, identified in $C^{12}(dp)$ (ROTBLAT[176]) and $N^{15}(d\alpha)$ emits gamma radiation of energy measured to be 3·083 Mev, whose pair internal conversion coefficient (THOMAS[177]) agrees with the value for electric dipole radiation, in analogy with that expected from the mirror state in N^{13}. The C^{13} state is also shown to be of type $(J = \frac{1}{2} +)$ by measurements of the angular distribution in the $C^{12}(dp)$ reaction (ROTBLAT[176]); both this and its mirror state are presumably single particle levels. After the 3·68 Mev state the (dp) reaction yields a very close level at 3·90 Mev and then no more certain levels until 6·34 Mev, which is in a region not investigated for N^{13}. The 3·68 and 3·90 Mev levels in C^{13} may correspond to the close doublet suggested for the 3·51 Mev level in N^{13}. There is some suggestion for levels in the 5–6 Mev region in C^{13} in both the $B^{10}(\alpha p)$ and $C^{12}(dp)$ reactions, but there seem to be none at this excitation in N^{13}, nor is there any evidence from neutron scattering by C^{12} that such levels in C^{13} exist. It is to be hoped that the availability of stronger artificial sources of alpha-particles will enable the (αp) experiments to be refined.

Fig. 26 compares the level systems of these two nuclei. A 0·8 Mev level in C^{13}, which has been reported from time to time, was not found in a careful investigation by BLUNDELL and ROTBLAT[178] using the (dp) reaction; nor is it apparent in the work of MALM and BUECHNER[58] on the $N^{15}(d\alpha)$ reaction.

(vii) N^{15}–O^{15}

These nuclei have 1 nucleon less than O^{16} and are expected according to the independent particle model to be $^2P_{\frac{1}{2}}$ in their ground state. The N^{15} spectrum is remarkable for the rather great excitation (5·28 Mev) of the lowest excited level and for the fact that this level is a member of a doublet of 30 kev spacing. The existence of this doublet was inferred from angular distribution measurements on an apparently homogeneous proton group in the (dp) reaction (POWELL, private communication) before it was demonstrated objectively by magnetic analysis (MALM and BUECHNER[179]). Energy measurements on the gamma radiation from the $(n\gamma)$ capture process in N^{14} (KINSEY, BARTHOLOMEW and WALKER[180]) agree well with the level system deduced from the (dp) reaction.

The O^{15} spectrum below the energy of 7·6 Mev has not been well studied owing to a lack of suitable reactions. The spectrum of gamma radiation from the $N^{14}(p\gamma)$ capture process (JOHNSON, MOAK and ROBINSON[180a]) fits in with levels at about 5, 6 and 7 Mev which correspond with those of the mirror nucleus. A level at 4·0 Mev in O^{15}, found in early work on the $N^{14}(dn)$ reaction, has been questioned (GIBSON and LIVESEY[181]); it would be difficult to fit into the mirror nucleus scheme. Both N^{15} and O^{15} have closely spaced levels above the dissociation energy. Those of the former have recently been studied by observation of resonances in the yield of the $N^{14}(np)$ and $N^{14}(n\alpha)$ reactions by STETTER and BOTHE[182] (*cf.* also Fig. 8). The decay of O^{15} to N^{15} is allowed.

(viii) O^{17}—F^{17}

If the filling of the $3d$-shell begins with these nuclei they should be of the type $(\frac{5}{2}+)$ in their ground state. This is supported by the observed spin of $\frac{5}{2}$ for O^{17} (ALDER and YU[188]). Confirmation of this latter value is obtained from the analysis by BUTLER[140] of the angular distribution of the proton groups from the $O^{16}(dp)$ reaction (BURROWS, GIBSON and ROTBLAT[139]) which indicates a ground state of $D_{\frac{3}{2}}$ or $D_{\frac{5}{2}}$, and an excited state at 873 kev which

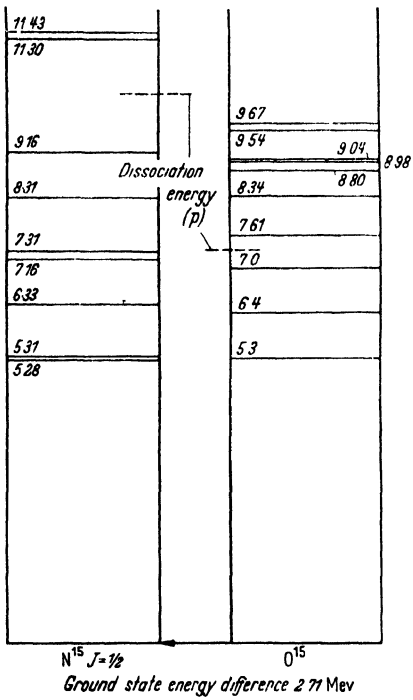


Fig. 27. Levels of mirror nuclei $N^{15}O^{15}$.

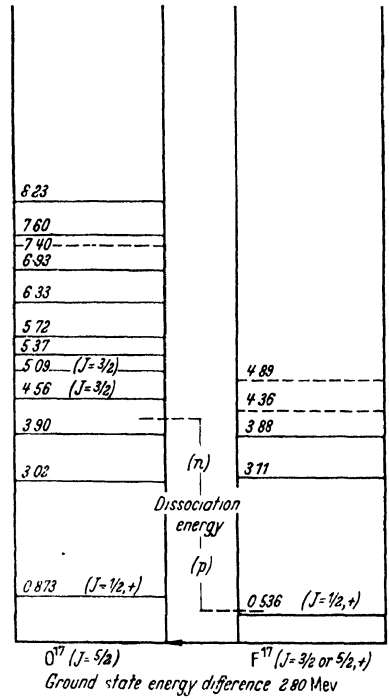


Fig. 28. Levels of mirror nuclei $O^{17}F^{17}$.

is $S_{\frac{1}{2}}$. Confirmation of spin $\frac{1}{2}$ for the first excited state of O^{17} is provided by the (isotropic) angular correlation between protons and gamma radiation in the $O^{16}(dp)$ reaction (THIRION[155]) and by the isotropic angular distribution of protons to the excited state in $N^{14}(\alpha p)$ (ROY[184]). An excited state of F^{17} at 536 kev has been observed in the reaction $O^{16}(dn)$ (AJZENBERG[185]) and the angular distribution of the neutron group corresponding to this state suggests a spin of $\frac{1}{2}$. The neutron group associated with the formation of F^{17} in its ground state has an angular distribution which does not disagree with a spin of $\frac{5}{2}$ for this state, so that the mirror properties of O^{17} and F^{17} are well verified. The β decay of F^{17} to the ground state of O^{17} is allowed (PEREZ-MENDEZ and LINDENFELD[186, 187]).

The rather complex level system of O^{17} has been established by magnetic and range analysis of the particle groups in the $O^{16}(dp)$ and $F^{19}(d\alpha)$ reactions. Measurements of the total cross section of O^{16} for fast neutrons (BOCKELMAN[188])

identify the spin of the 4·56 and 5·09 Mev levels as $\frac{3}{2}$. A number of analogous states in F^{17} (see Fig. 28) are known from the scattering and capture of protons by O^{16} (LAUBENSTEIN *et al.*[189]). The levels near 5 Mev in O^{17} and F^{17} probably include the $D_{\frac{3}{2}}$ component of the spin-orbit doublet.

(ix) F^{19}—Ne^{19}, Ne^{21}—Na^{21}, Na^{23}—Mg^{23}

For these nuclei the evidence on excited states rapidly becomes increasingly fragmentary, and is in many cases confined to work on the positron spectrum of the unstable nucleus and inelastic scattering of protons or deuterons by the stable nucleus. The mirror characteristics of the ground state are shown in Table 1.

(x) *Odd isobars with neutron excess + 3*

Production of the unstable electron emitters Li^9, C^{15}, N^{17} has recently been reported. There is no evidence on their excited states, but Li^9 and N^{17} decay into neutron-unstable states of Be^9 and O^{17} and C^{15} decays by an allowed (unfavoured) transition to the ground state of N^{15}. The nuclei O^{19}, Ne^{23} . . . are well-known β-emitters, sometimes decaying both to the ground and first excited state of the product nuclei with probabilities which enable tentative assignments of spin and parity to be made (*cf.* PEREZ-MENDEZ and BROWN[190]). The nuclei He^7, Be^{11}, B^{13} and F^{21} remain to be discovered.

(xi) *Summary*

Precise studies of reaction energies during the last few years have shown that the similarity between mirror nuclei extends to many of their excited states as well as to their ground states. This firmly supports the hypothesis of the equality of the (pp) and (nn) forces. It is probable that future work will exhibit still more similarities in the level spectra and that further confirmation of the identity between the spins of corresponding states will be forthcoming. This identity in the case of the ground states is well shown by the superallowed character of the β transitions, as represented by the particularly small and nearly constant ft values. The theory of mirror nuclei is so well verified that comparison of their binding energies is one of the best ways of finding the nuclear radius R, and in particular of determining the constant r_0 in the expression $R = r_0 A^{\frac{1}{3}}$, providing of course that the charge independence of nuclear forces is assumed.

There has been no great advance in our understanding of the magnitude of the level spacing. For "single particle" nuclei such as He^5, Be^9, C^{13}, O^{17} and their mirror isobars the doublet splitting is probably due to strong spin-orbit forces of the type assumed by MAYER in order to provide a (jj) coupling scheme for heavy nuclei; the magnitude of the splitting seems to be 4–5 Mev. The difference between the doublet separations of the stable and unstable odd isobars of neutron excess ± 1 can be accounted for, at least in the case of Li^7Be^7, by electrostatic and magnetic effects, and in some other cases by the level shift predicted by dispersion theory.

B. The even isobars of mass 4n

(i) He^4

The 1*s*-shell of neutrons and protons is completed at the alpha-particle, which has a maximum binding energy per nucleon, corresponding to saturation of the nuclear forces. It is unlikely that low excited states should exist owing to the compactness of the particle. The alpha-particle appears as residual nucleus in the transmutation $He^3(dp)He^4$ ($Q = 18{\cdot}5$ Mev) but no excited state lower than $20{\cdot}9 \pm 0{\cdot}4$ Mev above the ground state has been detected (ALLRED[191]). Gamma radiation of energy corresponding to a Q-value $19{\cdot}2 \pm 0{\cdot}6$ Mev has been observed from the reaction $H^3(p\gamma)He^4$ (ROCHLIN and MCDANIEL[192], ARGO *et al.*[193]). The angular distribution of the gamma radiation corresponds largely to a $^1P_1 - ^1S_0$ transition (electric dipole).

(ii) Li^8—Be^8—B^8

The Be^8 nucleus is unstable in its ground state and breaks up into two alpha particles with an energy release of 89 ± 5 kev. The reported lifetime of about $5 \cdot 10^{-14}$ sec (MILLAR and CAMERON[143]) is probably an upper limit (WILKINS and GOWARD[144]).

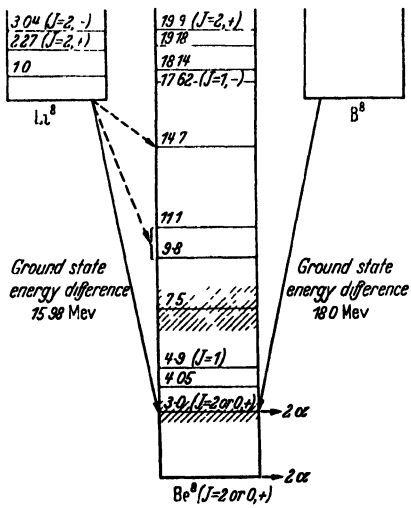


Fig. 29. Levels of nuclei $Li^8Be^8B^8$.

The excited states of Be^8 are shown in Fig. 29†. Some of the states, like the ground state, are unstable against break-up into two alpha-particles and these, in accordance with the requirements of BOSE statistics for alpha-particles, must be of even spin and parity. The broad level near 3 Mev of width about 1 Mev has been observed in the reactions $B^{11}(p\alpha)$, $B^{10}(d\alpha)$, $Li^7(dn)$, $Li^7(p\gamma)$, $C^{12}(\gamma\alpha)$, in the scattering of alpha-particles by helium, and in the β-decay of the Li^8 and B^8 isobars (BAXTER, BURCHAM and PAUL[194], LI and WHALING[195], ALVAREZ[196]) and is known to break up into alpha-particles. There is some uncertainty as to the properties of this level. WHEELER[197] suggested a spin 0 from his analysis of the $(\alpha\alpha)$ scattering and the angular distribution observed in the reaction $B^{11}(p\alpha)$ (DEE and GILBERT[198]) is not inconsistent with this. This spin value might be checked by observation of the angular correlation between the 14·8 Mev gamma radiation and the associated short range alpha-particles in the reaction $Li^7(p\gamma)$. The observations of STEARNS and MCDANIEL[199] on the angular distribution of the non-resonant gamma radiation in the $Li^7(p\gamma)$ reaction suggest a difference between the spins of the ground state and 3 Mev state of Be^8, which might mean a spin of 2 for the ground state. On the other hand, the angular distribution in the

† In this and other diagrams of the level schemes of the even nuclei, the unstable isobars are placed at the same level. Thus is equal to the decay energy of the electron-emitting isobar plus the correction ΔE from Table 1.

reaction $C^{12}(\gamma\alpha)$ (TELEGDI and ZUNTI[200]) favours spin 2 for the 3 Mev excited state which would be in agreement with the predictions of both the independent particle and alpha-particle model. The decay of Li^8 and B^8 to the ground state of Be^8 does not occur with appreciable intensity and must be at least one degree more forbidden than the allowed (unfavoured) transitions to the 3 Mev excited state, so that as it is likely from the independent particle model that Li^8 has a high spin (≥ 2) this evidence favours a high spin for the 3 Mev state. There is some evidence (BURCHAM and FREEMAN[201]) that the 3 Mev state observed in $Li^7(p\gamma)Be^{8*}$ is wider than that effective in other reactions and the possibility that the state is mixed is not excluded.

The other low lying states of Be^8, revealed by groups in particle reactions, seem to be mostly alpha unstable, and thus have even spin and parity, except for that at 4·9 Mev which emits gamma radiation, presumably because of odd spin or parity or both. Observations by THIRION[157] on the angular correlation between neutrons and gamma radiation in the $Li^7(dn)$ reaction suggest spin 1 for this state. An alpha emitting state at 7·9 Mev is indicated in the $C^{12}(\gamma\alpha)$ reaction.

Of the higher states, three in particular have been studied in detail, namely that at 17·62 Mev found as the 441 kev resonance in the $Li(p\gamma)$ reaction, that at 19·18 Mev showing as a resonance in the $Li^7(pn)$ reaction, and that at 19·9 Mev found in the $Li^7(p\alpha)$ reaction. The two former, together with another state at 18·14 Mev are noticed in the scattering of protons by lithium.

The 17·62 Mev state must be forbidden by either spin or parity rules to emit alpha-particles. From the angular distribution of the resonant gamma radiation (DEVONS and LINDSEY[202], STEARNS and MCDANIEL[199]), this state seems to be formed by s-wave protons and to be a (1−) state, although the observed cross section for elastic scattering of protons at the 441 kev resonance requires the assumption of p protons and indicates a (1+) state (COHEN[203]). The two sets of observations may be reconciled by the assumption that *both* the ground state and 3 Mev state of Be^8 have $J = 2$ (DEVONS and LINDSEY[202]).

The 19·9 Mev level is a broad state of even spin and parity, since it occurs in the $Li(p\alpha)$ reaction, and the assignment (2+) seems very likely. Electric quadrupole radiation competes with alpha-particle emission from this level and interferes, at a given proton energy, with the resonant dipole radiation of opposite parity from the 17·62 Mev state. The resulting pattern is that studied by DEVONS and HINE[86] (*cf.* Section IV, e.1). Difficulties still remain in this interpretation, particularly since the observed intensity of gamma radiation from the 19·9 Mev level requires a surprisingly large radiation width.

Levels in Li^8 are shown in the $Li^7(dp)$ reaction (GOVE and HARVEY[160]), and in the scattering of neutrons by lithium (ADAIR[81]). Analysis of the scattering cross sections suggests the spin and parity assignments shown for the two higher levels.

Calculation of the Coulomb energy difference and knowledge of the mass of Li^8 shows that the state of Be^8 analogous to the ground state of Li^8 and B^8 should be at an excitation of about 17 Mev. There is some

evidence for a state in this region from the observation of the production of slow neutrons in the reaction $Li^7(dn)$ at a deuteron energy of 2·1 Mev (TUCKER[204]).

(iii) B^{12}—C^{12}—N^{12} (Fig. 30)

The C^{12} spectrum presents many features of similarity with that of Be^8, although the ground state, expected to be $^1S_0$, is bound. The first excited state is well established at 4·44 Mev by observation of particle groups in the reactions $N^{15}(p\alpha)$, $N^{14}(d\alpha)$, $Be^9(\alpha n)$, $B^{11}(dn)$, $C^{12}(pp')$, $C^{12}(dd')$ and $B^{11}(p\gamma)$. It should be a $^1D_2$ state according to both the alpha particle and independent particle models, and this is consistent with recent observations of the angular correlation between the low energy neutrons and gamma radiation in the reaction $Be^9(\alpha n)C^{12*}(\gamma)C^{12}$, (JAMES and JONES privat communication). The energy of the gamma radiation checks with the difference in energy of the particle groups; measurements of its pair internal conversion coefficient should check that it is electric quadrupole. Decay of B^{12} takes place by allowed transitions mainly to the ground state of C^{12}, and weakly (5%) to the 4·44 Mev state (VENDRYES[206, 207]). N^{12} (ALVAREZ[196]) decays to the ground state of C^{12} by positron emission, and also to an alpha unstable level of C^{12} at about 12 Mev; there is some evidence (HORNYAK and LAURITSEN[208]) for decay of the mirror nucleus B^{12} to this level also, although the delayed alpha-particles have not been observed.

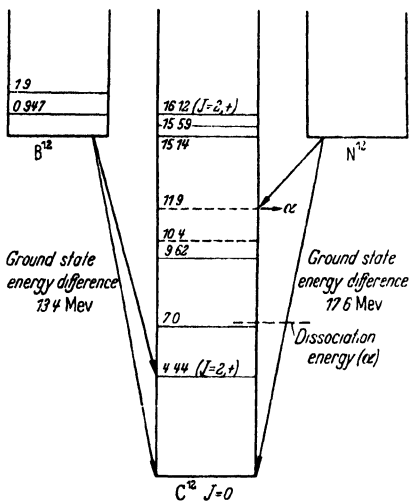


Fig. 30. Levels of nuclei $B^{11}C^{12}N^{12}$.

The level at 9·62 Mev is found in the reactions $N^{14}(d\alpha)$ and $B^{11}(dn)$, and the latter reaction also gives levels at 7·0, 10·4, 11·9, 15·14, 15·59 and 16·12 Mev. The levels above 15 Mev are much sharper than the others, which indicates that particle break-up is less probable in their case. The 16·12 Mev level is probably that which is observed as a 162 kev resonance in the $B^{11}(p\gamma)$ and $B^{11}(p\alpha)$ reactions; gamma radiation takes place both to the ground state and 4·44 Mev excited state in competition with alpha-particle emission and proton re-emission. There is also a "non resonant" emission of both alpha particles and gamma radiation which increases slowly with bombarding voltage. The homogeneous group of alpha-particles from the $B^{11}(p\alpha)Be^8$ reaction, corresponding to formation of Be^8 in its ground state has an anisotropic angular distribution with respect to the proton beam at the 162 kev resonance, but is isotropic for bombarding voltages above this (FRENCH and THOMSON, private communication). This suggests that two states of C^{12} are concerned in this reaction, the sharp state at 16·12 Mev, formed by p-wave protons,

and a much wider state of opposite parity at a considerably higher energy formed by s-protons and responsible for the "non resonant" alpha and gamma emission. Interference between the alpha-particle waves from these two states leads to an asymmetric angular distribution pattern which varies with proton energy in much the same way as the gamma radiation pattern in $Li^7(p\gamma)$ studied by DEVONS and HINE[86] (*cf.* Fig. 13). The 16·12 Mev state radiates strongly to the 4·44 Mev level and the angular distribution of the radiation is anisotropic; it is probably a (2 +) level. There is also a weaker radiation of about 16 Mev with an isotropic pattern which may come from a second level near 16 Mev (BIEDENHARN, ARFKEN and ROSE[135]).

Estimation of the Coulomb energy difference and knowledge of the binding energy of B^{12} places the state in C^{12} analogous to the ground states of B^{12} and N^{12} at about 15 Mev, near states which have actually been observed in the $B^{11}(dn)$ reaction. States of B^{12} have been observed in the $B^{11}(dp)$ and $Be^9(\alpha p)$ reactions.

(iv) N^{16}—O^{16}—F^{16}

The O^{16} nucleus may be thought of as a regular tetrahedron on the alpha-particle model; according to this pure rotational excited states with $J<3$ are not allowed, since it must be impossible to distinguish between the alpha-particles by a rotation through 120°. According to the independent particle model, the p-shell for neutrons and protons is completed at O^{16}, and the nucleus should have a spherically symmetrical wave function in its ground state ($^1S_0$). Nuclear properties show the regularities associated with shell closure, i.e. high binding energy, zero spin and magnetic moments, even parity; all of which are, however, also consequences of the alpha-particle model.

The low lying states of O^{16} have been studied in very great detail through the $F^{19}(p\alpha)$ reactions; the conclusions are summarised in Fig. 31. This reaction yields 4 groups of short range and 1 group of long range alpha-particles, all of which are resonant (see Ne^{20}). Emission of the short range alpha-particles leaves the nucleus O^{16} in excited states, three of which emit gamma radiation, and one of which decays by emission of positive and negative electron pairs. The excitation function for this pair production (DEVONS, HINE and LINDSEY[209], PHILLIPS and HEYDENBURG[210]) is the same as that for the long range alpha-particles, emission of which leaves O^{16} in its ground state. It seems from these observations that the ground state and 6·05 Mev excited state of O^{16} must both be (0 +) states, and studies of the angular correlation between the positive and negative electrons confirm this. The lifetime of the pair emitting state is $7{\cdot}10^{-11}$ sec (see Section IV, i) which agrees better with a model in which the excitation energy of the 6·05 Mev state is due to pure dilation of a liquid drop than with the alpha-particle model (DEVONS, HEREWARD and LINDSEY[142]).

The next excited state of O^{16} is a gamma ray emitting state at 6·13 Mev which is known to have $J=3$ and odd parity from angular correlation experiments both for intensity and polarisation (see Section IV, g).

Above this state are two further gamma emitting states at 6·91 and 7·11 Mev revealed by the appearance of other alpha-particle groups in the $F^{19}(p\alpha)$ reaction. The relative intensity of the two groups varies strongly from resonance to resonance; the variation is probably to be understood in terms of the orbital momenta of the alpha-particle groups emitted from the different resonance levels of Ne^{20}, but it has not been possible so far to give a quantitative picture of all the experimental facts. CHAO[87] has discussed the possibilities for the angular momentum of these levels and of the resonance levels in Ne^{20}, and angular correlation experiments at present in progress (SEED, private communication) may be expected to give further information.

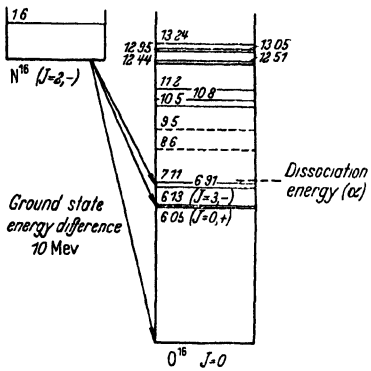


Fig. 31. Levels of nuclei $N^{16}O^{16}$.

The gamma radiation from the three low levels of oxygen has been thoroughly studied by RASMUSSEN *et al.*[100], (*cf.* Fig. 14) and the energies agree very closely with those predicted from the alpha-particle groups.

The 7·11 Mev level is near the dissociation limit of O^{16} into $C^{12}+He^4$ and levels above this have been studied by the reactions $C^{12}(\alpha\gamma)$, $C^{12}(\alpha\alpha)$, $N^{15}(dn)$ and $O^{16}(pp')$, but the results are not yet of great precision. More accurate information becomes available at an excitation of 12·44 Mev where resonances for the $N^{15}(p\alpha)$ reaction commence. This reaction reveals a situation very similar to that studied in the $F^{19}(p\alpha)$ reaction: gamma radiation associated with short range alpha particle groups is observed, and a long range alpha particle group leaving C^{12} in its ground state also appears. One of the levels in this region emits gamma radiation directly to the ground state of O^{16}. This level must be unable for reasons of spin or parity to break up into $C^{12}+He^4$, and its width will be determined by the proton width.

The decay of N^{16} proceeds to the ground state and some of the excited states of O^{16}; the resulting gamma radiation has been observed (MILLAR, BARTHOLOMEW and KINSEY[211]), and has components of 6·133 and 7·10 Mev in the ratio 12/1. The β-decay to the ground state and pair emitting state of O^{16} $(0+)$ is first forbidden, but to the 6·13 (3—) state and to the states near 7·0 Mev it is allowed according to the ft values. This suggests that the N^{16} ground state is of spin 2 and odd parity and that the 7·11 Mev level of O^{16} has odd parity, since this property does not change in an allowed transition.

Estimation of Coulomb energy difference puts the state analogous to N^{16} and F^{16} at 12–13 Mev in O^{16}, in which region several resonances are observed in $N^{15}(p\alpha)$. F^{16} is then calculated to be unstable with respect to proton emission, which explains why it has not been observed (ALVAREZ[196]).

(v) F^{20}—Ne^{20}—Na^{20}

The low levels of Ne^{20} are chiefly derived from expansion chamber and photographic plate determinations of the energy of the neutron groups from the

reaction $F^{19}(dn)$. Some of the associated gamma rays have been studied, but agreement in energy with the prediction from the particle groups is not good. The lowest state is established at 1·63 Mev by spectrometer studies of the F^{20} decay (LITTAUER[212]) which proceeds to this state via an allowed transition with a forbidden transition to the ground state. The 1·63 Mev state is also detected, though with not quite the same energy, in the $Ne^{20}(pp')$ $F^{19}(dn)$ and $F^{19}(p\gamma)$ (RAE, RUTHERGLEN and SMITH[103], CARVER and WILKINSON[93]) reactions. It is expected to be of type (2+) from the independent particle model (FEENBERG and HAMMACK[13]), and if so the ground state of F^{20} should be of even parity and of spin 2 or 3.

The states of Ne^{20} above 4·65 Mev should be alpha unstable, and an example of one such state at 9·7 Mev has been found by FRENCH, MEYER and TREACY[213]. The positron decay of Na^{20} (ALVAREZ[196]) also leads to alpha unstable states in this region; decay to the ground state appears to be forbidden as in the case of F^{20}.

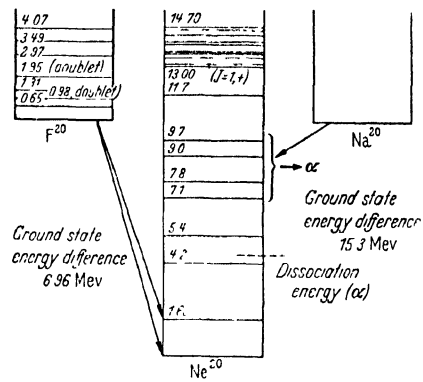


Fig. 32. Levels of nuclei $F^{20}Ne^{20}Na^{20}$.

The levels of Ne^{20} above 13·0 Mev have been very thoroughly studied by means of the $F^{19}(p\alpha)$ reactions (*cf.* Fig. 5). Resonances are found in the yield of (a) long range alpha-particles (HINE[214]), (b) short range alpha-particles leading to the pair emitting state of O^{16}, and in the associated pairs (PHILLIPS and HEYDENBURG[210]), (c) short range alpha-particles leading to the three low gamma emitting states of O^{16}, and (d) high energy capture radiation. The resonances (a) and (b) coincide, as is expected from the identical symmetry characteristics of the ground and pair emitting states of $O^{16}(0+)$, but differ from (c) and (d). The character of one of the resonances (c), for 340 kev proton energy is known to be (1+) from angular correlation experiments (see Section IV, g), and continuation of these experiments will probably lead to assignments for other levels. Capture radiation is observed at the 669 kev proton resonance, and proceeds to the 1·63 Mev excited state; the angular distribution is isotropic suggesting formation of the state by *s* protons. The yield of short range alpha-particles in the $F^{19}(p\alpha)$ reaction greatly exceeds that of the long range particles despite the opposite tendency expected owing to the Coulomb barrier. The reactions have been discussed in detail by CHAO[87].

The state in Ne^{20} analogous to the ground state of F^{20} is at about 10 Mev, in a region where the level system is poorly known. The F^{20} levels, found from the $F^{19}(dp)$ reaction (BUECHNER *et al.*[215]) are numerous, as are those of Ne^{20} at the comparable excitation, and show a number of close doublets.

(vi) Na^{24}—Mg^{24}

These nuclei show particularly clearly how information on nuclear states is obtained by a large number of different methods. The level structure is shown

in Figure 33. The levels of Na^{24} are known from the (dp) reaction (BUECHNER *et al.*[215]) and as in the case of F^{20}, are closely spaced and often of doublet structure. The state in Mg^{24} analogous to the ground state of Na^{24} would be at an excitation of about 9·5 Mev, a region in which the levels of Mg^{24} are poorly known. Above the proton binding energy of 11·74 Mev, however, a large number of sharp closely spaced levels are known from the $Na^{23}(p\gamma)$ (pp) and $(p\alpha)$ reactions (ALBURGER and HAFNER[216]).

The spin of Na^{24} has been found by an atomic beam method to be 4 (SMITH[217]). The ground state decays by what was long thought to be a simple first forbidden β spectrum (KONOPINSKI[115]) to a state of Mg^{24} at an excitation of 4·14 Mev, from which two gamma rays, of energies 2·76 and 1·38 Mev follow in cascade. The β and γ spectra were studied by SIEGBAHN[120] (*cf.* Section IV, e 4.3 and Fig. 17), and the cascade emission of gamma radiation was established by coincidence methods (MITCHELL[119]). The order of emission of the gamma radiation was settled by determination of the position of the low lying levels of Mg^{24} by inelastic scattering of protons (RHODERICK[37], *cf.* Fig. 7), deuterons (GREENLEES, KEMPTON and RHODERICK[68]), and neutrons (BEGHIAN, GRACE, PRESTON and HALBAN[218]), as well as from the (dn) reaction (MANDEVILLE[219]). Angular correlation between the direction of emission of the gamma rays suggested the sequence of spins 0–2–4 for the ground state (even-even nucleus), 1·38 Mev state and 4·14 Mev state of Mg^{24} (BRADY and DEUTSCH[125], *cf.* Section IV, g and Fig. 21, CHARPAK and SUZOR[220]). RAE[108], using a magnetic spectrometer, measured the pair internal conversion coefficient of the 2·76 Mev radiation and concluded that the radiation was electric dipole, which is incompatible with the quadrupole radiation required by the angular correlation experiment. MIMS *et al.*[109], however, using a different method, found a pair internal conversion coefficient agreeing well with theory for an electric quadrupole.

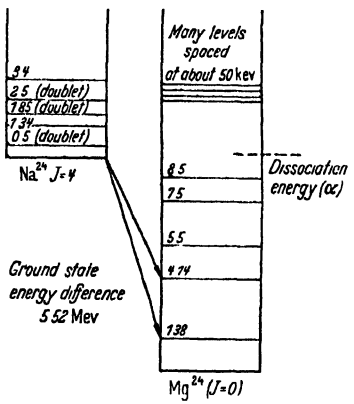


Fig. 33. Levels of nuclei $Na^{24}Mg^{24}$.

Recently, TURNER and CAVANAGH[221], by using a lens β spectrometer with scintillation detectors, have found a weak β spectrum linking the ground state of Na^{24} with the 4·14 Mev state of Mg^{24}, and also a gamma ray whose energy appeared to be nearly 4·14 Mev and which seemed to arise in a cross-over transition. This possibility was excluded by BEGHIAN, BISHOP and HALBAN[222] who found an energy of 3·7 Mev for the high energy radiation and suggested a new level in Mg^{24} for which there is at the moment no other evidence. They also found an upper limit of 1 in $2 \cdot 10^6$ disintegrations for any 4·14 Mev gamma ray. The ft values for the two β transitions are not in the ratio expected from the spins 2 and 4 for the levels of Mg^{24} but this may be due to uncertainties of the theory. Independent evidence on the parity of the ground state of Na^{24} would help to clarify this problem.

(vii) Al^{28}–Si^{28} *and heavier nuclei of mass number 4n*

The existing information is given by ALBURGER and HAFNER[216]. A very large number of levels above the proton binding energy is known in these nuclei from observations of resonances in the $(p\gamma)$, (pp) and $(p\alpha)$ reactions. Among numerous points of interest may be mentioned the observation of a 31 kev state in Al^{28} by magnetic analysis of protons emitted in the $Al^{27}(dp)$ reaction (ENGE *et al.*[223]). The gamma radiation from this state was observed by SMITH and ANDERSON[224] and appears, from the absence of internal conversion electrons, to be electric dipole.

(viii) *Summary*

The alpha-particle model is successful in predicting the symmetry properties of low rotational states, and it co-ordinates a group of nuclei of similar properties and particular stability. No satisfactory quantitative predictions of level spacing have been made.

C. The even isobars of mass 4n + 2

(i) He^6–Li^6

These nuclei are expected according to the independent particle model to be of the type $^1S_0$ and $^3S_1$ and each of even parity in their ground state. The ft value for the $He^6 \rightarrow Li^6$ β-decay is very low and suggests a super-allowed or mirror nucleus type of transition. Since it is almost certain that the spin must change by one in the transition, GAMOW-TELLER rules must be used. If correction is made for the Coulomb energy difference the difference in binding between He^6 and Li^6 is about 4 Mev, which may be regarded as the difference between the singlet and triplet states of a neutron and proton in the p-shell outside an alpha-particle core. The singlet state of Li^6 should therefore be at this excitation; in fact radiation at 3·0 Mev, apparently originating in Li^6, has been observed in the $Be^9(p\alpha)Li^{6*}$ reaction. A 3·0 Mev state would be unstable to break up into $H^2 + He^4$, although this could be prevented if the state were of zero spin and even parity as would be expected for the singlet level. Magnetic dipole radiation to the ground state would take place.

A 2·2 Mev level in Li^6 is observed in the $Li^6(pp')$ and $Li^7(d, t)$ reactions GOVE and HARVEY[160]) in the $Be^9(p\alpha)$ reaction (BROWNE *et al.*[167]), and in (α, d) scattering, and a 1·66 Mev level in He^6 in the $Li^7(t\alpha)$ reaction (PEPPER *et al.*[225]).

(ii) Be^{10}–B^{10}–C^{10}

The $^1S_0$ character predicted by the independent particle model for the ground states of B^{10} and C^{10} and $^3S_1$ for the ground state of B^{10} led to difficulties in interpreting the highly forbidden decay of Be^{10}. This was resolved by the measurement of a spin of 3 for B^{10} in its ground state, which is therefore probably of type $^3D_3$. The C^{10} decay, as shown in Fig. 34, takes place to a 0·72 Mev excited state of B^{10}, (probably with $J = 1$ as this transition is allowed) which is not accessible to Be^{10} owing to the lower energy of the transition.

The ground states of C^{10} and Be^{10} belong to a multiplet which should include a state of B^{10} at an excitation, calculated from the Coulomb term, n–p mass difference and mass of Be^{10}, of 2·0 Mev. The levels of B^{10} in this region are found from the $Be^9(dn)$ reaction (AJZENBERG[226]) and from spectrometer determinations of the gamma-ray energies; the better known levels are shown in the figure. The (dn) reaction also gives a group of levels in B^{10} between 4·79 and 8·88 Mev, some of these being observed as thresholds for slow neutron production. The reactions $Be^9(p\alpha)$, $Be^9(pd)$, $Be^9(pp)$ and $Be^9(p\gamma)$

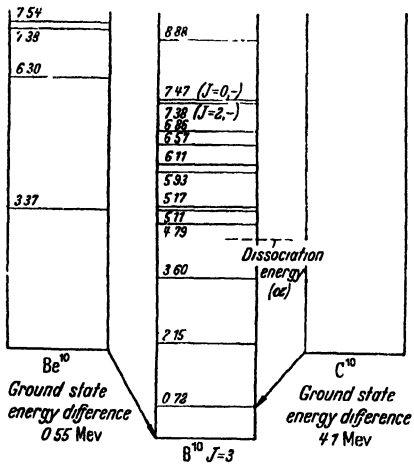


Fig. 34. Levels of nuclei $Be^{10}B^{10}C^{10}$.

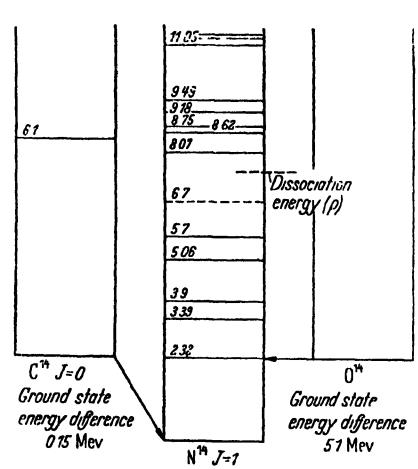


Fig. 35. Levels of nuclei $C^{14}N^{14}O^{14}$.

are resonant, and analysis of the proton scattering data and angular distributions of the particles has enabled assignments of spin to be made to the levels at 7·38 ($J=2-$) and 7·47 ($J=0-$) Mev. These values are consistent with electric dipole radiative transitions to the ground and first excited states of B^{10} respectively.

Be^{10} has relatively few levels compared with B^{10}; they are given by the $Be^9(dp)$ reaction, and by the scattering of neutrons by beryllium.

(iii) C^{14}—N^{14}—O^{14}

The independent particle model predicts that the spins of C^{14} and O^{14} should be zero, and that of N^{14} unity, and that each nucleus should be of even parity. This agrees with the measured spins of C^{14} and N^{14}. The C^{14}—N^{14} decay, however, has a ft value which indicates a second forbidden transition, which is surprising in view of the known spin change and of the fact that the spectrum has the allowed shape (WARSHAW[227]). The decay of O^{14} is allowed and takes place to a 2·32 Mev state in N^{14}. The energy of this state agrees well with that calculated for the analogue of the C^{14}—O^{14} ground states, and so should be of type ($J=0+$). This would make the O^{14}—N^{14} decay second forbidden according to GAMOW-TELLER rules. There is at present no satisfactory explanation of these facts, although GERJUOY[228] has suggested that the shell

model gives the parity of N^{14} incorrectly, and supports this by consideration of the relative intensities of the capture radiation components in $N^{14}(n\gamma)$. It is possible that the O^{14} decay is a case of mixed interactions and that the FERMI rules apply.

The 2·32 Mev level in N^{14} is also established by the $C^{13}(p\gamma)$ and $C^{13}(dn)$ reactions, and by spectrometer measurements of the gamma radiation in the bombardment of C^{13} by deuterons. The $C^{13}(p\gamma)$ reaction is resonant and the gamma radiation is isotropic, suggesting (0 or 1,—) for the resonant state at 8·07 Mev, and combination with the (1+) ground state by electric dipole radiation. The large radiation width in this reaction supports the prediction of the independent particle shell model that the parities of the C^{13} and N^{14} ground states are opposite. The intensity of the transition to the 2·32 Mev state is small, but not zero (CARVER and WILKINSON[93]).

A number of states in N^{14} between 2·32 and 8·07 Mev are found from the $C^{13}(dn)$ and $N^{14}(pp')$ reactions, and further levels are shown in the $C^{13}(p\gamma)$ capture process (SEAGRAVE, DAY and PERRY[229]). Above 11·05 Mev levels are found from resonances in the $C^{12}(dp)$ reactions; one of these has also been excited by the $C^{13}(pn)$ reaction (ADAMSON *et al.*[230]). A single state in C^{14} at 6·1 Mev has been found in the $C^{13}(dp)$ reaction (SPERDUTO *et al.*[231]).

(iv) O^{18}—F^{18}

The main information on the levels of these isobars is obtained from resonances in the reactions $O^{16}(dp)$ and $N^{14}(\alpha p)$ (ROY[184]) and from alpha-particle scattering in nitrogen. These are virtual levels; there is very little evidence on low states of F^{18} and none for states of O^{18}. The β-decay is theoretically, and experimentally, allowed; the Coulomb energy makes F^{18} unstable with respect to its isobar.

(v) Ne^{22}—Na^{22} *and heavier nuclei*

Na^{22} has a spin of 3 and decays by forbidden positron emission to an excited state of Ne^{22}, probably with spin 2. Excited states of Ne^{22} are known from the $F^{19}(\alpha p)$ reaction. In heavier $4n+2$ nuclei there is generally some information on levels from the proton capture, (αp) or (dn) reactions; the data are summarised by ALBURGER and HAFNER[216].

(vi) *Summary*

The odd-odd nuclei of equal neutron and proton number have a larger number of bound levels than their isobars with paired neutrons or neutron holes. Among the states of the $4n+2$ nuclei should be one whose excitation above the ground state might be expected to measure the spin dependent splitting in these nuclei. This is known to be 2·3 Mev in the deuteron and seems to be rather greater in Li^6. The evidence is not clear for $B^{10}N^{14}F^{18}$ and higher nuclei, but from the masses of the isobaric nuclei the splitting appears to be of the order of 2 Mev.

References

[1] Hornyak, W. F., Lauritsen, T., Morrison, P. and Fowler, W. A.; *Rev. Mod. Phys.* 22 (1950) 291.
[2] Bethe, H. A. and Bacher, R. F.; *ibid* 8 (1936) 82.
[3] Bethe, H. A.; *ibid* 9 (1937) 69.
[4] Livingston, M. S. and Bethe, H. A.; *ibid* 9 (1937) 245.
[5] Bethe, H. A.; *Elementary Nuclear Theory*, John Wiley, New York 1947.
[6] Gamow, G. and Critchfield, C. L.; *The Atomic Nucleus and Nuclear Energy Sources*, Oxford 1947.
[7] Rosenfeld, L.; *Nuclear Forces*, North Holland Publishing Co. Amsterdam 1948.
[8] Mott, N. F. and Massey, H. S. W.; *The Theory of Atomic Collisions*, Oxford 1949.
[9] Devons, S.; *Excited States of Nuclei*, Cambridge 1949.
[10] Wigner, E.; *Phys. Rev.* 51 (1937) 106 and 947.
[11] — and Feenberg, E.; *Reports on Progress in Physics* 8 (1941) 274.
[12] Mayer, M. G.; *Phys. Rev.* 74 (1948) 235.
[13] Feenberg, E. and Hammack, K. C.; *ibid* 75 (1949) 1877.
[14] Nordheim, L. W.; *ibid* 75 (1949) 1894.
[15] Feenberg, E. and Wigner, E.; *ibid* 51 (1937) 95.
[16] — and Phillips, M.; *ibid* 51 (1937) 600.
[17] Rose, M. E. and Bethe, H. A.; *ibid* 51 (1937) 205.
[18] Haxel, O., Jensen, J. H. D., and Suess, H. E.; *ibid* 75 (1948) 1766.
[19] Mayer, M. G.; *ibid* 78 (1950) 16.
[20] Wigner, E. and Eisenbud, L.; *ibid* 72 (1947) 29.
[21] Wheeler, J. A.; *ibid* 52 (1938) 108.
[22] Hafstad, L. R. and Teller, E.; *ibid* 54 (1938) 681.
[23] Weisskopf, V. E.; *Helv. Phys. Acta* 23 (1950) 187.
[24] Guggenheimer, K. M.; *Proc. Roy. Soc.* A. 181 (1942) 169.
[25] Preiswerk, P.; *Helv. Phys. Acta* 23 (1950) 7.
[26] Wigner, E.; *Amer. J. Phys.* 17 (1949) 99.
[27] Christy, R. F. and Latter, R.; *Rev. Mod. Phys.* 20 (1948) 185.
[28] Bloch, I. *et al.*; *ibid* 23 (1951) 147.
[29] Fortescue, R. L.; *Progress in Nuclear Physics I*, p. 21. London 1950.
[30] Pickavance, T. G.; *ibid* p. 1.
[31] Burcham, W. E. and Devons, S.; *Proc. Roy. Soc.* A. 173 (1939) 555.
[32] Bennett, W. E., Bonner, T. W., Mandeville, C. E. and Watt, B. E.; *Phys. Rev.* 70 (1946) 882.
[33] Fowler, W. A., Lauritsen, C. C. and Lauritsen, T.; *Rev. Sci. Instrum.* 18 (1947) 818.
[34] Warren, R. E., Powell, J. L. and Herb, R. G.; *ibid* 18 (1947) 559.
[35] Bender, R. S., Shoemaker, F. C. and Powell, J. L.; *Phys. Rev.* 71 (1947) 905.
[36] Curtis, B. R., Fowler, J. L. and Rosen, L.; *Rev. Sci. Instrum.* 20 (1949) 388.
[37] Rhoderick, E. H.; *Proc. Roy. Soc.* A. 201 (1950) 348.
[38] Burrows, H. B., Powell, C. F. and Rotblat, J.; *Proc. Roy. Soc.* A. 209 (1951) 461.
[39] Boyer, K., Gove, H. E., Harvey, J. A., Deutsch, M. and Livingston, M. S.; *Rev. Sci. Instrum.* 22 (1951) 310.
[40] Allan, H. R. and Wilkinson, C. A.; *Proc. Roy. Soc.* A. 194 (1948) 131.
[41] Heydenburg, N. P. and Inglis, D. R.; *Phys. Rev.* 73 (1948) 230.
[42] French, A. P. and Treacy, P. B.; *Proc. Phys. Soc.* A. 64 (1951) 452.
[43] Lattes, C. M. G., Fowler, P. H. and Cuer, P.; *ibid* 59 (1947) 883.
[44] Rotblat, J.; *Progress in Nuclear Physics I*, p. 37. London 1950.
[45] Rutherford, Lord, Wynn-Williams, C. E., Lewis, W. B. and Bowden, B. V.; *Proc. Roy. Soc.* A. 139 (1933) 617.
[46] Buechner, W. W., Strait, E. N., Stergiopoulos, C. G. and Sperduto, A.; *Phys. Rev.* 74 (1948) 1569.
[47] Snyder, C. W., Rubin, S., Fowler, W. A. and Lauritsen, C. C.; *Rev. Sci. Instrum.* 21 (1950) 852.

[48] COLLINS, E. R., MCKENZIE, C. D. and RAMM, C. A.; *Nature, Lond.* 167 (1951) 682.
[49] KLEMA, E. D. and PHILLIPS, G. C.
[50] BRIGGS, G. H.; *Proc. Roy. Soc.* A. 157 (1936) 183.
[51] THOMAS, H. A., DRISCOLL, R. L. and HIPPLE, J. A.; *Phys. Rev.* 78 (1950) 787.
[52] SIEGBAHN, K. and SVARTHOLM, N.; *Arkiv. f. Math. Astron. Fysik,* 33A, No. 21, 1946.
[53] BROWNE, C. P., CRAIG, D. S. and WILLIAMSON, R. M.; *Rev. Sci. Instrum.* 22 (1951) 952.
[54] BURCHAM, W. E. and FREEMAN, J. M.; *Phil. Mag.* 40 (1949) 807.
[55] HUTCHINSON, G. W. and SCARROTT, G. G.; *ibid* 42 (1951) 792.
[56] POWELL, C. F., OCCHIALINI, G. P. S., LIVESEY, D. L. and CHILTON, L. V.; *J. Sci. Instrum.* 23 (1946) 102.
[57] JAMES, D. B. and TREACY, P. B.; *Proc. Phys. Soc.* A. 64 (1951) 847.
[58] MALM, R. and BUECHNER, W. W.; *Phys. Rev.* 81 (1951) 519.
[59] BURROWS, H. B.; quoted by ROTBLAT[44].
[60] STRAIT, E. N., VAN PATTER, D. M., BUECHNER, W. W. and SPERDUTO, A.; *Phys. Rev.* 81 (1951) 747.
[61] HARVEY, J. A.; *ibid* 81 (1951) 353.
[62] CHAO, C. Y., TOLLESTRUP, A. V., FOWLER, W. A. and LAURITSEN, C. C.; *ibid* 79 (1950) 108.
[63] FREEMAN, J. M.; *Phil. Mag.* 41 (1950) 1225.
[64] SHOUPP, W. E., JENNINGS, B. and SUN, K. H.; *Phys. Rev.* 75 (1949) 1.
[65] GIBSON, W. M.; *Proc. Phys. Soc.* A. 62 (1949) 586.
[66] ALLEN, W. D. *Nature, Lond.* 168 (1951) 451.
[67] FULBRIGHT, H. W. and BUSH, R. R.; *Phys. Rev.* 74 (1948) 1323.
[68] GREENLEES, G. W., KEMPTON, A. E. and RHODERICK, E. H.; *Nature, Lond.* 164 (1949) 663.
[69] SIEGBAHN, K. and SLÄTIS, H.; *ibid* 159 (1947) 473.
[70] M. I. T. CYCLOTRON GROUP; M. I. T. Progress Report, July 1, 1950.
[71] HANSON, A. O., TASCHEK, P. F. and WILLIAMS, J. H.; *Rev. Mod. Phys.* 21 (1949) 635.
[72] WILLARD, H. B. and PRESTON, W. P.; *Phys. Rev.* 81 (1951) 480.
[73] BLEULER, E. and ROSSEL, J.; *Helv. Phys. Acta* 20 (1947) 445.
[74] JOHNSON, C. H. and BARSCHALL, H. H.; *Phys. Rev.* 80 (1950) 818.
[75] HANNA, G. C.; *ibid* 80 (1950) 530.
[76] DEVONS, S.; *Proc. Roy. Soc.* A. 172 (1939) 127.
[77] BENDER, R. S., SHOEMAKER, F. C., KAUFMAN, S. G. and BOURICIUS, G. M. B.; *Phys. Rev.* 76 (1949) 273.
[78] GOLDHABER, G. and WILLIAMSON, R. M.; *ibid* 82 (1951) 495.
[79] ADAIR, R. K.; *Rev. Mod. Phys.* 22 (1950) 249.
[80] MERRISON, A. W. and WIBLIN, E. R.; *Nature, Lond.* 167 (1951) 346.
[80a] STAFFORD, G. H.; *Proc. Phys. Soc.* A. 64 (1951) 388.
[81] ADAIR, R. K.; *Phys. Rev.* 79 (1950) 1018.
[82] FOWLER, W. A., LAURITSEN, C. C. and LAURITSEN, T.; *Rev. Mod. Phys.* 20 (1948) 236.
[83] TANGEN, R.; *Det. Kgl. Norsk. Vidensk. Selskab.* 1946 Nr. 1.
[84] BONNER, T. W. and EVANS, J. E.; *Phys. Rev.* 73 (1948) 666.
[85] BROSTROM, K. J., HUUS, T. and TANGEN, R.; *ibid* 71 (1947) 661.
[86] DEVONS, S. and HINE, M. G. N.; *Proc. Roy. Soc.* A. 199 (1949) 56.
[87] CHAO, C. Y.; *Phys. Rev.* 80 (1950) 1035.
[88] SEGRÈ, E. and HELMHOLZ, A. C.; *Rev. Mod. Phys.* 21 (1949) 271.
[89] CAVANAGH, P. E.; *Progress in Nuclear Physics I,* p. 140. London 1950.
[90] HORNYAK, W. F., LAURITSEN, T. and RASMUSSEN, V. K.; *Phys. Rev.* 76 (1949) 731.
[91] MILLAR, C. H., CAMERON, A. G. N. and GLICKSMAN, M.; *Can. J. Res.* A. 28 (1950) 475.
[92] GIBSON, W. M., GROTDAL, T., ORLIN, J. J. and TRUMPY, B.; *Phil. Mag.* 42 (1951) 555.
[93] CARVER, J. H. and WILKINSON, D. H.; *Proc. Phys. Soc.* A. 64 (1951) 199.
[94] NABHOLZ, H., STOLL, P. and WAFFLER, H.; *Phys. Rev.* 82 (1951) 963.

[95] CURRAN, S. C., ANGUS, J. and COCKROFT, A. L.; *Phil. Mag.* 40 (1949) 36.
[96] PONTECORVO, B.; *Helv. Phys. Acta* 23, Suppl. III (1950) 97.
[97] JORDAN, W. H. and BELL, P. R.; *Nucleonics* 5, No. 4 (1949) 30.
[98] HOFSTADTER, R. and MCINTYRE, J. A.; *Phys. Rev.* 79 (1950) 389.
[99] PRINGLE, R. W.; *Nature, Lond.* 166 (1950) 11.
[100] RASMUSSEN, V. K., HORNYAK, W. F., LAURITSEN, T. and LAURITSEN, C. C.; *Phys. Rev.* 77 (1950) 617.
[101] WALKER, R. L. and MCDANIEL, B. D.; *ibid* 74 (1948) 315.
[102] — *ibid* 79 (1950) 172.
[103] RAE, E. R., RUTHERGLEN, J. C. and SMITH, R. D.; *Proc. Phys. Soc.* A. 63 (1950) 775.
[104] KINSEY, B. B., BARTHOLOMEW, G. A. and WALKER, W. H.; *Phys. Rev.* 83 (1951) 519.
[105] CURLING, C. D. and NEWTON, J. O.; *Nature, Lond.* 166 (1950) 339.
[106] ROSE, M. E.; *Phys. Rev.* 76 (1949) 678.
[107] HORTON, G. K.; *Proc. Phys. Soc.* 60 (1948) 457.
[108] RAE, E. R.; *Phil. Mag.* 40 (1949) 1155.
[109] MIMS, H., HALBAN, H. and WILSON, R.; *Nature, Lond.* 166 (1950) 1027.
[110] DOUGHERTY, C. B., HORNYAK, W. F., LAURITSEN, T. and RASMUSSEN, V. K.; *Phys. Rev.* 74 (1948) 712.
[111] DEVONS, S. and LINDSEY, G. R.; *Nature, Lond.* 164 (1949) 539.
[112] SKYRME, T. H. R.; *Progress in Nuclear Physics I*, p. 115. London 1950.
[113] FEENBERG, E. and TRIGG, G. L.; *Rev. Mod. Phys.* 22 (1950) 399.
[114] WU, C. S.; *ibid* 22 (1950) 386.
[115] KONOPINSKI, E. J.; *ibid* 15 (1943) 209.
[116] FEATHER, N. and RICHARDSON, H. O. W.; *Proc. Phys. Soc.* 61 (1948) 452.
[117] FEINGOLD, A. M.; *Rev. Mod. Phys.* 23 (1951) 10.
[118] MITCHELL, A. C. G.; *ibid* 20 (1948) 296.
[119] — *ibid* 22 (36) 1950.
[120] SIEGBAHN, K.; *Phys. Rev.* 70 (1947) 127.
[121] MOON, P. B.; *Proc. Phys. Soc.* A. 64 (1951) 76.
[122] GOWARD, F. K., TELEGDI, V. and WILKINS, J. J.; *ibid* A. 63 (1950) 402.
[123] HEYDENBURG, N. P., HUDSON, C. M., INGLIS, D. R. and WHITEHEAD, W. D., *Phys. Rev.* 74 (1948) 405.
[124] MARTIN, L. H., BOWER, J. G., DUNBAR, D. N. F. and HIRST, F.; *Aust. J. Sci. Res.* A2 (1949) 25.
[125] BRADY, E. L. and DEUTSCH, M.; *Phys. Rev.* 78 (1950) 558.
[126] HAMILTON, D. R.; *Phys. Rev.* 58 (1940) 122.
[127] GOERTZEL, G.; *ibid* 70 (1946) 897.
[128] YANG, C. N.; *ibid* 74 (1948) 764.
[129] FALKOFF, D. L. and UHLENBECK, G. E.; *ibid* 79 (1950) 323 and 334.
[130] INGLIS, D. R.; *ibid* 74 (1948) 21.
[131] — *Proc. Harwell Nuclear Physics Conference*, Sept. 1950.
[132] DEUTSCH, M.; *Rep. on Prog. in Phys.* 14 (1951) 196.
[133] CONDON, E. U. and SHORTLEY, G. H.; *The Theory of Atomic Spectra*, pp. 75–77. Cambridge 1936.
[134] HEITLER, W.; *Proc. Camb. Phil. Soc.* 32 (1936) 112.
[135] BIEDENHARN, L. C., ARFKEN, G. B. and ROSE, M. E.; *Phys. Rev.* 83 (1951) 586.
[136] METZGER, F. and DEUTSCH, M.; *ibid* 78 (1950) 551.
[137] BARNES, C. A., FRENCH, A. P. and DEVONS, S.; *Nature, Lond.* 166 (1950) 145.
[138] ARNOLD, W. R.; *Phys. Rev.* 80 (1950) 34.
[139] BURROWS, H. B., GIBSON, W. M. and ROTBLAT, J.; *Phys. Rev.* 80 (1950) 1095.
[140] BUTLER, S. T.; *ibid* 80 (1950) 1095.
[141] ELLIOTT, L. G. and BELL, R. E.; *ibid* 76 (1949) 168.
[142] DEVONS, S., HEREWARD, H. G. and LINDSEY, G. R. *Nature, Lond.* 164 (1949) 586.
[143] MILLAR, C. H. and CAMERON, A. G. N.; *Phys. Rev.* 81 (1951) 316.
[144] WILKINS, J. J. and GOWARD, F. K.; *Proc. Phys. Soc.* A. 64 (1951) 849.

[145] BUNYAN, D. E., LUNDBY, A., WARD, A. H. and WALKER, D.; *Proc. Phys. Soc.* A 61 (1948) 300.
[146] FREIER, G. D., LAMPI, E., SLEATOR, W. and WILLIAMS, J. H.; *Phys. Rev.* 75 (1949) 1345.
[147] CRITCHFIELD, C. L. and DODDER, D. C.; *ibid* 76 (1949) 602.
[148] ADAIR, R. K.; *ibid* 81 (1951) 310.
[149] — *ibid* 82 (1951) 750.
[150] GOLDSTEIN, H.; *ibid* 79 (1950) 740.
[151] LELAND, W. T. and AGNEW, H. M.; *ibid* 82 (1951) 559.
[152] TITTERTON, E. W. and BRINKLEY, T. A.; *Proc. Phys. Soc.* A. 64 (1951) 212.
[153] BROWN, A. B., SNYDER, C. W., FOWLER, W. A. and LAURITSEN, C. C.; *Phys. Rev.* 82 (1951) 159.
[154] NEWTON, J. O.; *Proc. Phys. Soc.* A. 64 (1951) 938.
[155] THIRION, J.; *Compt. Rend.* 232 (1951) 2418.
[156] CLASS, C. M. and HANNA, S. S.; *Nature, Lond.* 168 (1951) 429.
[157] THIRION, J.; *Compt. Rend.* 233 (1951) 37.
[158] BECHSEL, H., HALG, W., HUBER, P. and STEBLER, A.; *Phys. Rev.* 81 (1951) 456.
[159] WILLIAMSON, R. M. and RICHARDS, H. T.; *ibid* 76 (1949) 614.
[160] GOVE, H. E. and HARVEY, J. A.; *ibid* 82 (1951) 658.
[161] BASHKIN, S. and RICHARDS, H. T.; *ibid* 84 (1951) 1124.
[162] INGLIS, D. R.; *ibid* 82 (1951) 181.
[163] MOTTELSON, B. R.; *ibid* 82 (1951) 287.
[164] FEENBERG, E.; *ibid* 81 (1951) 644.
[165] INGLIS, D. R.; *ibid* 81 (1951) 914.
[166] VAN PATTER, D. M. *et al.*; *ibid* 81 (1951) 233.
[167] BROWNE, C. P., WILLIAMSON, R. M., CRAIG, D. S. and DONAHUE, D. J.; *ibid* 83 (1951) 179.
[168] GUTH, E. and MULLIN, C. J.; *ibid* 76 (1949) 234.
[169] VAN PATTER, D. M., BUECHNER, W. W. and SPERDUTO, A.; *ibid* 82 (1951) 248.
[170] RUTHERGLEN, J. C., RAE, E. R. and SMITH, R. D.; *Proc. Phys. Soc.* A. 64 (1951) 906.
[171] BENNETT, W. E., ROYS, P. A. and TOPPEL, B. J.; *Phys. Rev.* 82 (1951) 20.
[172] JOHNSON, V. R.; *ibid* 81 (1951) 316.
[173] THOMAS, R. G.; *ibid* 80 (1950) 136.
[174] — *ibid* 81 (1951) 661.
[175] EHRMAN, J. B.; *ibid* 81 (1951) 412.
[176] ROTBLAT, J.; *Nature, Lond.* 167 (1951) 1027.
[177] THOMAS, R. G.; *Phys. Rev.* 80 (1950) 138.
[178] BLUNDELL, M. and ROTBLAT, J.; *ibid* 81 (1951) 144.
[179] MALM, R. and BUECHNER, W. W.; *ibid* 80 (1950) 771.
[180] KINSEY, B. B., BARTHOLOMEW, G. A. and WALKER, W. H.; *ibid* 77 (1950) 723.
[180a] JOHNSON, C. H., MOAK, C. D. and ROBINSON, G. P.; *ibid* 85 (1952) 727.
[181] GIBSON, W. M. and LIVESEY, D. L.; *Proc. Phys. Soc.* 60 (1948) 523.
[182] STETTER, W. and BOTHE, W.; *Zeits. für Nat.* 6a (1951) 61.
[183] ALDER, F. and YU, F. C.; *Phys. Rev.* 81 (1951) 1067.
[184] ROY, R. R.; *ibid* 82 (1951) 227.
[185] AJZENBERG, F.; *ibid* 83 (1951) 693.
[186] PEREZ-MENDEZ, V. and LINDENFELD, P.; *ibid* 80 (1950) 1097.
[187] — — *ibid* 83 (1951) 864.
[188] BOCKELMAN, C. K.; *ibid* 80 (1950) 1011.
[189] LAUBENSTEIN, R. A., LAUBENSTEIN, M. J. W., KOESTER, L. J and MOBLEY, R. C.; *ibid* 84 (1951) 12.
[190] PEREZ-MENDEZ, V. and BROWN, H.; *ibid* 78 (1950) 812.
[191] ALLRED, J. C.; *ibid* 77 (1950) 753.
[192] ROCHLIN, R. S. and MCDANIEL, B. D.; *ibid* 82 (1951) 298.
[193] ARGO, H. V. *et al.*; *ibid* 78 (1950) 691.
[194] BAXTER, A. S., BURCHAM, W. E. and PAUL, E. B.; *Phil. Mag.* 41 (1950) 937.

[195] LI, C. W. and WHALING, W.; *Phys. Rev.* 81 (1951) 661.
[196] ALVAREZ, L. W.; *ibid* 80 (1950) 519.
[197] WHEELER, J. A.; *ibid* 59 (1941) 27.
[198] DEE, P. I. and GILBERT, C. W.; *Proc. Roy. Soc.* A. 154 (1936) 279.
[199] STEARNS, M. B. and MCDANIEL, B. D.; *Phys. Rev.* 82 (1951) 450.
[200] TELEGDI, V. and ZUNTI, W.; *Helv. Phys. Acta* 23 (1950) 745.
[201] BURCHAM, W. E. and FREEMAN, J. M.; *Phil. Mag.* 41 (1950) 921.
[202] DEVONS, S. and LINDSEY, G. R.; *Proc. Phys. Soc.* A. 63 (1950) 1202.
[203] COHEN, E. R.; *Phys. Rev.* 75 (1949) 1463.
[204] TUCKER, E. B.; *ibid* 82 (1951) 299.
[205] VENDRYES, G.; *Compt. Rend.* 232 (1951) 1549.
[207] — *ibid* 233 (1951) 391.
[208] HORNYAK, W. F. and LAURITSEN, T.; *Phys. Rev.* 77 (1950) 160.
[209] DEVONS, S., HINE, M. G. N. and LINDSEY, G. R.; *Proc. Harwell. Nucl. Phys. Conf.* Sept. 1950, p. 32.
[210] PHILLIPS, G. C. and HEYDENBURG, N. P.; *Phys. Rev.* 83 (1951) 184.
[211] MILLAR, C. H., BARTHOLOMEW, G. A. and KINSEY, B. B.; *ibid* 81 (1951) 150.
[212] LITTAUER, R. M.; *Phil. Mag.* 41 (1950) 1214.
[213] FRENCH, A. P., MEYER, P. and TREACY, P. B.; *Proc. Phys. Soc.* A 63 (1950) 666.
[214] HINE, M. G. N.; *Thesis* Cambridge 1950.
[215] BUECHNER, W. W. *et al.*; *M. I. T. Progress Report*, Feb. 28, 1951.
[216] ALBURGER, D. E. and HAFNER, E. M.; *Rev. Mod. Phys.* 22 (1950) 373.
[217] SMITH, K. F.; *Nature, Lond.* 167 (1951) 942.
[218] BEGHIAN, L. E., GRACE, M. A., PRESTON, G. and HALBAN, H.; *Phys. Rev.* 77 (1950) 286.
[219] MANDEVILLE, C. E.; *ibid* 76 (1949) 436.
[220] CHARPAK, G. and SUZOR, F.; *Jour. de Phys.* 11 (1950) 633.
[221] TURNER, J. F. and CAVANAGH, P. E.; *Phil. Mag.* 42 (1951) 636.
[222] BEGHIAN, L. E., BISHOP, G. R. and HALBAN, H.; *Phys. Rev.* 83 (1951) 186.
[223] ENGE, H., BUECHNER, W. W., SPERDUTO, A. and VAN PATTER, D. M.; *ibid* 83 (1951) 31.
[224] SMITH, R. D. and ANDERSON, R. A.; *Nature, Lond.* 168 (1951) 429.
[225] PEPPER, T., ALLEN, K. W., ALMQVIST, E. and DEWAN, J. T.; *Phys. Rev.* 81 (1951) 315.
[226] AJZENBERG, F.; *ibid* 82 (1951) 43.
[227] WARSHAW, S. D.; *ibid* 80 (1950) 111.
[228] GERJUOY, E.; *ibid* 81 (1951) 62.
[229] SEAGRAVE, J. D., DAY, R. B. and PERRY, J. E.; *ibid* 81 (1951) 661.
[230] ADAMSON, R. E. *et al.*; *ibid* 80 (1950) 985.
[231] SPERDUTO, A., HOLLAND, S. S., VAN PATTER, D. M. and BUECHER, W. N.; *ibid* 80 (1950) 769.

THE NUCLEAR SHELL MODEL

B. H. Flowers

1. Introduction

Modern theories of the structure of the nucleus may fairly be said to have sprung from Chadwick's discovery of the neutron in 1932. In the same year, Bartlett[1, 2, 3] drew attention to the fact that the occurrence in nature of the lighter nuclei could be predicted in terms of the ordered addition of neutrons and protons. Starting with the α-particle, all known stable nuclei up to O^{16} may be obtained by repeating the addition sequence n, p, n, p; while from that point up to A^{36} the addition sequence becomes instead n, n, p, p, indicating that stability tends to favour neutrons over protons as one passes to heavier nuclei. The only exceptions to this rule are He^5 and Be^8, both of which are predicted as stable but are now well known to be unstable to heavy particle emission.

Bartlett's interpretation of these regularities drew upon an analogy with the structure of the extra-nuclear atom. He assumed that neutrons and protons formed "shells" containing $2(2l+1)$ particles of each kind, where $l\hbar$ is their orbital angular momentum; but of course, the ordering of these shells would be different from that found in atoms owing to the different forces involved. Thus the nuclei He^4, O^{16}, and A^{36}, for example, would correspond to the closing of the first s, p, and d shells, respectively.

These ideas were developed in particular by Elsasser[4, 5, 6] and by Guggenheimer[7, 8] in 1934. Elsasser observed that the nuclei He^4 and O^{16} are relatively strongly bound, as befitting closed shells, and postulated a system of energy levels for the individual nuclear particles which he derived in the first place from a uniform "spherical-well" potential common to all particles in the manner of a self-consistent field. Guggenheimer, studying the stability of nuclei as a function of their charge number, Z, and their neutron number, N, came to the conclusion that nuclear stability varies periodically in the sense of the periodic system of the elements. Plotting N against Z, he found that all the known stable nuclei lie along a rough curve or narrow band, which, however, shows marked discontinuities at certain points. Thus, Guggenheimer claimed discontinuities near $Z=20$, 36, 54, and 84, and at $N=50$ and 82, which he interpreted as due to closed shells. Neutron shells and proton shells appeared to be independent of each other. Extending this list of "magic numbers", Elsasser[5] found discontinuities at $N=2$, 8, 18, 32, 50, 60, and 126. These numbers he was further able to derive theoretically as occupation numbers of a spherical-well potential distorted by a central elevation, the so-called "wine-bottle potential".

It is of interest to note in passing that Elsasser, while postulating an overall potential for the nucleus, felt that a more realistic expression of

nuclear structure would demand that particles group themselves together in transient configurations, or sub-groups, which he pictured as forming and rapidly reforming under the influence of strong inter-particle forces. This idea of a "resonating-group structure" was later taken up and developed in some detail by WHEELER[9]. ELSASSER imagined the phenomenon of α-activity as due to a type of internal conversion in which an α-particle is formed by chance as one of these transient subgroups and is emitted before it breaks up again.

The model which began to develop was, then, an individual particle model in zeroth-approximation: each particle was assumed to move in an average potential field produced by the rest of the nucleus, but to be otherwise approximately independent of the detailed motion of all other particles. Under these circumstances, the appearance of the magic numbers may be attributed simply to the operation of the PAULI exclusion principle and to the requirements of the quantum theory as expressed by the angular momentum operators.

Considerable weight was given to the independent-particle picture by the discovery by SCHMIDT[10], and also independently by SCHÜLER[11], that the magnetic moments of nuclei could be represented approximately in a very simple manner. In SCHMIDT'S model it is recognised that the spin and magnetic moment of an even-even nucleus in its ground state are always zero, and it is assumed that in an odd mass nucleus the spin and magnetic moment are produced entirely by the motion of the odd particle, neutron or proton as the case may be. This being so, the magnetic moment can be calculated quite easily as a function of the spin; and it is found that the observed moments in most cases bear some relation to the values so calculated, as we shall see later.

The more detailed consequences of the application of the Pauli principle to the nuclei between helium and oxygen were considered by FEENBERG and WIGNER[12]. These authors performed a calculation, similar to that of SLATER (see COND. N and SHORTLEY[13]) in the atomic case, on the assumptions that nuclear forces are predominantly exchange forces, and that all these nuclei can be formed by successive additions of neutrons and protons to the first p-shell. Owing to the exchange nature of the forces, the symmetry properties of the wave-function with respect to permutation of particles are of decisive importance. Indeed, in contradistinction to the atomic case where terms are grouped more or less closely according to configurations, nuclear terms are grouped rather according to the symmetry character of the wave-function, regardless, to some measure, of the configurations from which they arise. This implies in addition that the interaction energies are comparable with the zero-order level spacings. The problem of nuclear symmetry was considered in detail in further papers by WIGNER[14, 15] using the methods of group theory; but we need not concern ourselves with this aspect at present. For calculations of total binding energy, the SLATER method, used in the manner of HARTREE and FOCK, was found to be extremely

poor. In view of the fact that the correlation energy, so important in the somewhat analogous electron theory of metals, is not properly taken into account, this is perhaps not surprising; nevertheless it was hoped that the ordering of terms could be correctly predicted for the light nuclei, and in particular their ground states. It was found that the spins of the nuclei Li^6 to O^{16} were indeed given correctly in this approximation, with the sole exception of B^{10}, then thought to have spin 1 as predicted by the theory, but now known to have spin 3. Moreover, the characteristic kinks in the mass defect curve in this region, long associated with a supposed α-particle structure, were obtained as a natural consequence of the PAULI principle and without prior assumptions regarding the existence of α-particles in the nucleus.

WIGNER'S symmetry theory was more general than an individual particle model; but in its later form as developed by WIGNER himself[15] (1937) and by BARKAS[16] (1939), it was able to shed some light on the shell theory. WIGNER found that the main bulk of the energy of a nuclear state could be expressed as the sum of two terms: the first of these was the product of a factor representing the symmetry character of the wave-function, and which accounted for most of the fluctuations in energy from nucleus to nucleus, with a factor which could plausibly be expected to vary smoothly with atomic weight; while the second term could be expected to vary smoothly except where a a radical change of structure occurred such as the commencement of a new shell. Comparison with the experimental values of the binding energies showed this to be so: in particular, the second term (WIGNER'S E_0) was found to suffer discontinuous changes in slope at atomic weight $A = 20$ and 40, but to vary almost linearly in between. This is in keeping with the idea that the d-shell is filling uniformly in this region.

Meanwhile, confronted with the striking phenomenon of resonant capture of neutrons, BOHR[17] in 1936 was putting forward the notions of the liquid drop nucleus which, as later formulated by BOHR and KALCKAR[18], BREIT and WIGNER[19], KAPUR and PEIERLS[20], and others, in the form of the dispersion theory, was to prove so successful in explaining many and varied nuclear processes. The essence of this theory, in complete antithesis to the individual particle model, was that all particles take part more or less equally in any nuclear event; nuclear levels are to be regarded as quantised states of the system as a whole and not as the excitation of single particles in an average nuclear field. It seems probable that it was largely on account of the evident success of the new ideas that the individual particle model lost what favour it had previously enjoyed. At all events, apart from a few isolated papers (e.g. HARKINS[21], suggesting the existence of further magic numbers and regularities, the individual particle model was to lie dormant for some ten years until MAYER[22] reopened serious discussion in 1948.

Since that date a vast quantity of evidence has been accumulated which establishes beyond reasonable doubt the existence of a set of magic numbers, and of some sort of periodic system for nuclei. There remain the fundamental

difficulties associated especially with the strong short-range interactions, the correlation energy, and the fact that there is no strong centre of force to act as overall potential as in the atomic case; nevertheless, there are several rival theories all of which attempt to correlate nuclear regularities in terms of the energy levels of single particles moving in an average nuclear field. After this brief historical introduction it is the purpose of the present review to summarise the evidence to date in support of the individual particle model, and to give some account of the various detailed interpretations which have been presented. It cannot be claimed that a complete list of references has been given, particularly to the experimental data*; but it is hoped that references are sufficiently representative to enable the reader to find without difficulty most of the information he may require.

2. Evidence for the Magic Numbers

In this section we shall consider some of the present-day evidence for the existence of closed shells in nuclei as indicated by the magic numbers. Each field of information will be considered under a separate heading for ease in further reference. However, the consideration of the magnetic moments and spins which, as Bartlett[2] pointed out, is of decisive importance to any shell model, deserves special study and will therefore be treated in a separate section. Similarly, evidence which also leads to an estimate of the energy discontinuities at the completion of closed shells will be dealt with in the next section. We shall be concerned principally with the magic numbers 20, 28, 50, 82, and 126, sufficient having already been said to suggest the special stability of configurations of 2 and 8 neutrons or protons.

Abundances of the elements

Assuming that closed shells represent particularly stable systems of nucleons, one might expect nuclei containing a magic number of neutrons or of protons, or both, to be especially abundant in nature. A table of the relative abundances of nuclei, compiled from data on the composition of the earth, sun, stars, and meteorites, has been published by Br wn[23]. If these figures are plotted against Z or N, pronounced peaks are seen, particularly at $O^{16}(N, Z=8)$. $Ca^{40}(N, Z=20)$, $Sn^{118}(Z=50)$; Sr^{88}, Y^{89}, $Zr^{90}(N=50)$; Ba^{138}, La^{139}, Ce^{140} $(N=82)$; and at $Pb^{208}(Z=82, N=126)$. There is also evidence that nuclei containing 40 neutrons or protons are unusually abundant. The trend of nuclear abundances has been strikingly demonstrated in a three-dimensional plot in the book by Gamow and Critchfield[24].

Number of stable isotopes

In Fig. 1 is shown a plot of the number of stable isotopes per element, as a function of Z. The lightest element to have more than two stable isotopes

* Many references to the experimental work regarding nuclear reactions are given in the article by Prof. Burcham in the present volume of *Progress in Nuclear Physics*. The present paper was written in September 1951, and it has not been possible to add more than a few references to work published since that date.

is O with $Z = 8$. The first with 4 isotopes is S, and it may be observed that the heaviest isotope of sulphur, S^{36}, has 20 neutrons. Five isotopes first occur at $Z = 20$; 7 appear with Mo, of which the lightest is Mo^{92} having 50 neutrons. Ten isotopes occur once only, namely in Sn with 50 protons.

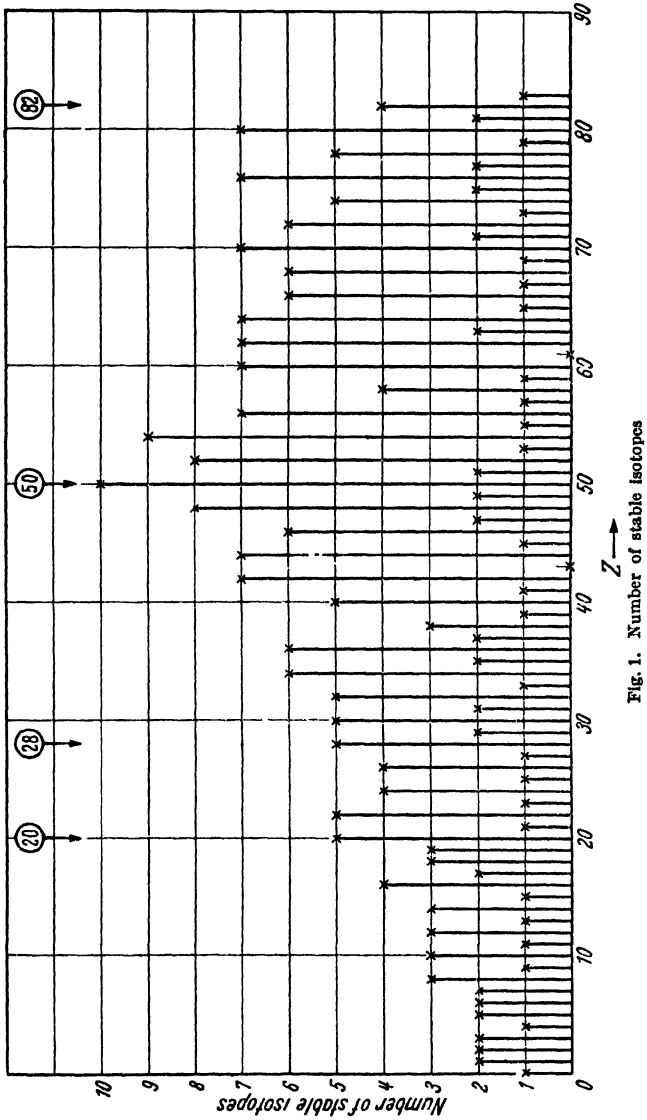


Fig. 1. Number of stable isotopes

Number of stable isotones

In Fig. 2 is shown a similar plot of the number of nuclei having a given number of neutrons: such nuclei have been called "isotones" by GUGGENHEIMER[7]. Five isotones occur only twice amongst the lighter elements, namely for

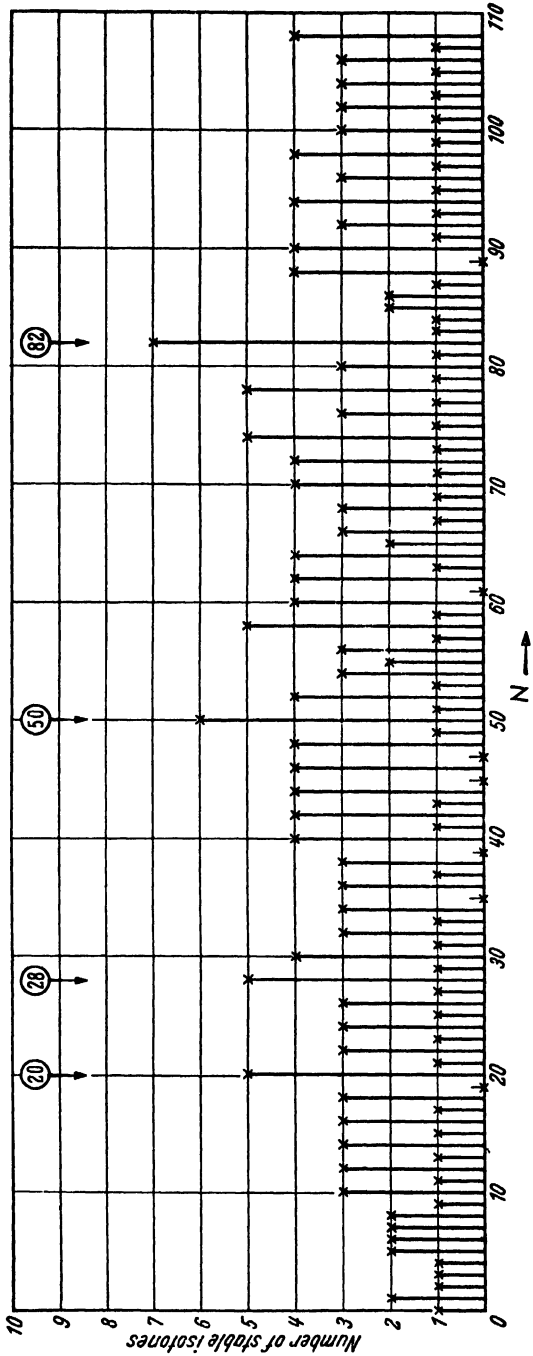


Fig. 2. Number of stable isotones.

20 and 28 neutrons. Six occur once only, for $N = 50$; similarly, seven occur only at $N = 82$. Four appear first for $N = 30$, of which Ni^{58} has 28 protons.

Width of the stability curve

A measure of the width of the region of stability of nuclei—the "Gamow valley"—is furnished by the quantity $\Delta N = N_{max} - N_{min}$, being the mass difference between the heaviest and lightest isotopes of a given element. The curve exhibits discontinuous changes in width. $\Delta N = 2$ first appears at $Z = 8$; $\Delta N = 4$ occurs amongst the light nuclei only for $N = 20$ and 28. $\Delta N = 8$ occurs first with Ca, $Z = 20$, and this abnormally high value is probably associated with the concurrence of $Z = 20$ with $N = 28$ at Ca^{48}. Several other cases of $\Delta N = 8$ exist, of which Kr^{86} and Mo^{92} have $N = 50$, while Ba^{138} and Nd^{142} have $N = 82$. $\Delta N = 12$ occurs twice: at Sn with $Z = 50$, and at Xe of which Xe^{136} has N = 82. A similar plot of ΔZ against N or Z yields further information of this nature.

Quadrupole moments

It has been pointed out by GORDY[25] that the quadrupole moments of nuclei are small or zero near to a magic number of neutrons or protons, and rise to maximum values at points corresponding to shells being about half to two-thirds filled. This may be understood if one regards the quadrupole moment as a measure

of the deviation of the nucleus from spherical symmetry: on a shell model such deviations would be most pronounced about halfway through the filling of a shell. We shall return to this question in a later section.

Fast neutron cross-sections

The absorption cross-sections for neutrons of a few Mev in energy of nuclei containing 50, 82, or 126 neutrons are unusually low, as the measurements of GRIFFITHS[26], MESCHERYAKOV[27], and HUGHES *et al.*[28], have shown. The

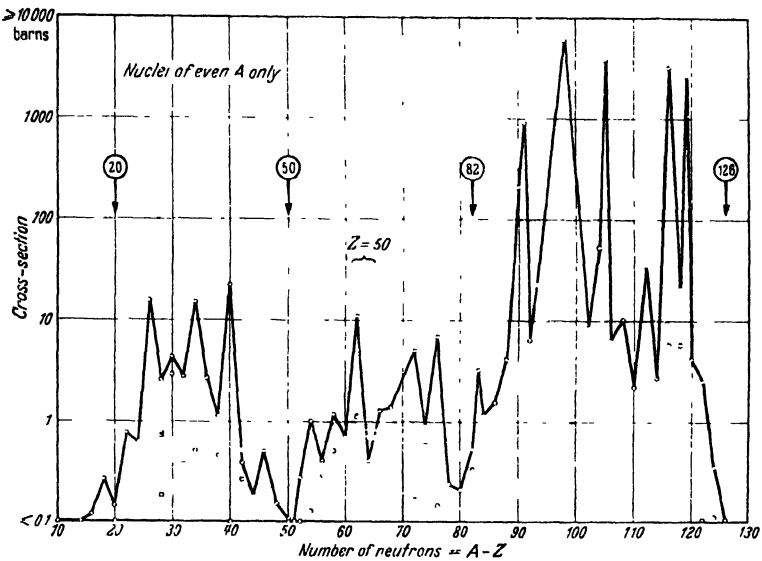


Fig. 3. Thermal neutron cross-sections.

general trend of cross-section is to increase with mass number: at sufficiently high energies one expects the cross-section to be proportional to the geometrical cross-section, or to $A^{\frac{2}{3}}$. While this is borne out in general, there are pronounced dips of the order of 10–30 times smaller than average in the neighbourhood of $Y^{89}(N=50)$, Ba^{138}, La^{139} and $Pr^{141}(N=82)$, $Bi^{209}(N=126)$, and $Pb^{208}(Z=82, N=126)$.

Thermal neutron cross-sections

Even the apparently chaotic fluctuations of the thermal neutron cross-sections can be made to show some semblance of shell structure. Fig. 3 is a plot, due to FLOWERS[29], of the isotopic cross-sections of nuclei of even A as a function of the number of neutrons. The zig-zag curve joins up the largest values of cross-section for given N where more than one such nucleus exists whose cross-section has been measured, a procedure which exaggerates the larger values and therefore tends if anything to mask the appearance of the characteristic low values associated with the magic numbers. The average behaviour of the curve is to rise from low values near the magic numbers

to high values almost half-way through the filling of a shell, as in the case of the quadrupole moments. A plot for nuclei of odd A shows a similar trend.

The asymmetry in fission

The probability of any particular mode of fission depends sensitively upon the energy available for the fragments to penetrate through the potential barrier. One might therefore expect, as discussed recently by MEITNER[29a], the most frequent modes to be those which lead to a minimum number of "loose" nucleons outside the closed shell (always supposing that one is entitled to apply the ideas of a shell model to processes involving such large changes in energy and high excitations of the fragment nuclei). U^{235}, for example, has 143 neutrons; and we find that the most probable modes are those which leave a small excess of neutrons over the closed shells of 50 and 82. It must be emphasized, however, that the interpretation of this phenomenon is by no means clear-cut; and SWIATECKI[30] has shown that hydrodynamical effects may be of considerable importance.

It is encouraging to find that Kr^{87} with 51 neutrons, and Xe^{137} with 83 neutrons, are both identified as delayed neutron emitters; for on a shell model the 51st and 83rd neutrons could be so loosely bound that evaporation following β-decay becomes feasible.

Missing stable isotopes

It is well known that no stable isotopes of Tc or Pm exist in nature, and these elements occur in the regions of 50 and 82 neutrons respectively. Moreover, if one restricts oneself to the odd mass nuclei, as emphasized by KOWARSKI[31], then A and Ce are also seen to exhibit the same anomaly, these being in the regions of 20 and 82 neutrons respectively. This evidence points to a sudden change in the stability limits at these numbers.

3. ESTIMATES OF THE ENERGY DISCONTINUITIES

In his original papers ELSASSER estimated the discontinuity in the binding energy of the last particle at $Z = 82$ and $N = 126$ to be about 1·6 Mev from considerations of the energy release in radioactive decay. A more detailed analysis by BERTHELOT[32] suggested a somewhat higher figure of about 2·4 Mev. This section will list some more recent data which confirm their figures, and which also suggest that a break of the same order of magnitude occurs at each of the magic numbers.

α-stability

The study of the energies of α-particles emitted in radioactive decay shows clearly the special stability associated with $Z = 82$ and $N = 126$; indeed, the occurrence of lead as the end-product of the three natural series is suggestive in itself. The situation is most clearly shown in a plot, due to GLÜCKAUF[33], of the energy contours of α-particle decay as functions of Z and N, which

we reproduce in Fig. 4. The addition of nucleons to a closed shell may be pictured as causing a decrease in α-stability, until a point is reached where there are sufficient loose nucleons to produce an interaction energy comparable to that existing within the closed shell. After this point is reached stability might be expected to regain its normal value until the shell is nearly filled. Considerations of the gradient of the energy contours leads to an estimate of the break in the binding energy of the last particle of about 2 Mev. GLÜCKAUF has applied similar methods to the binding energies of the lighter nuclei, as a result of which he finds discontinuities, again of about 2 Mev, in the neighbourhood of the magic numbers 8, 20, and 28.

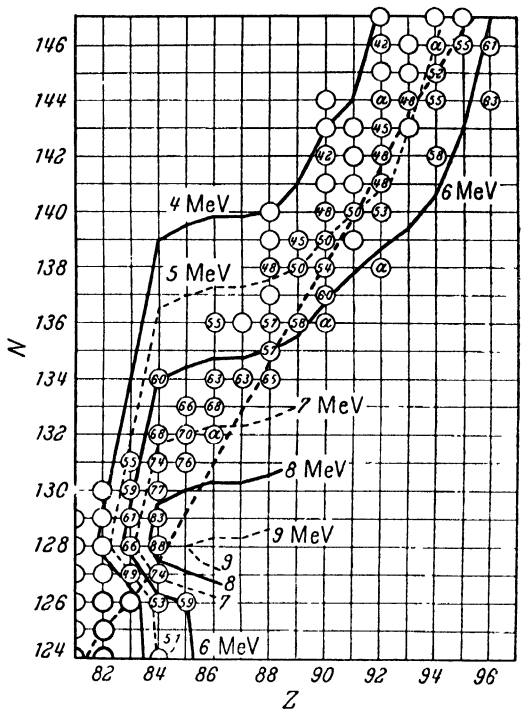


Fig. 4. α-particle energies of radioactive nuclei

The most recent complete analysis of α-particle energies has been made by PRYCE[34], who compares the observed energies with those calculated from the semi-empirical binding energy formula of WEIZSÄCKER (see BETHE and BACHER[35]). The existence of the natural α-emitter Sm^{152}, and the recent discovery of artificial α-emitters amongst the other rare earths by THOMPSON *et al.*[36], are presumably connected with the configuration of 82 neutrons. PRYCE'S calculations also refer to this region, but experimental data are not yet precise enough to make any comparison worthwhile.

Packing fraction curve

The stability of some of the magic number nuclei is strikingly shown by the study of nuclear masses. A curve of the packing fraction plotted against mass number has recently been published by DUCKWORTH *et al.*[37], our Fig. 5. which contains information gleaned mainly from mass spectrographic measurements, but also from the energies of γ-rays of neutron capture[38], and from reaction thresholds. This curve shows characteristic kinks at points corresponding to $N = 50$ and 126, and at $Z = 28$, 50, and 82. The low packing fraction of Si^{30} may readily be understood according to the level scheme proposed by JENSEN *et al.* and by MAYER, to be discussed presently; this scheme also predicts that 40 should be a "relatively magic" number, so that the break at Zr^{90} may be partly on account of the 40 proton configuration

in addition to the 50 neutrons. Similarly 32 is predicted to be relatively magic in this scheme, and Ni^{60} has in addition to 28 protons, 32 neutrons, which may partly account for the fact that it has the lowest packing fraction known. This last piece of information may be of importance in differentiating between the otherwise very similar schemes proposed by MAYER and by JENSEN and his co-workers.

Energy release in nuclear reactions

Further evidence regarding the discontinuities in binding energy may be obtained from the study of the Q-values of certain nuclear reactions. Of especial interest in this connection is the work of HARVEY[39], who measured the Q-values of the (d, p) reactions over a wide range of nuclei, particularly in the regions of the magic numbers, and so obtained the binding energy of the added neutron in the residual nucleus. Comparing these empirical values with the smooth ones given by the semi-empirical formula, he finds quite sharp breaks: a drop of 2·2 Mev occurs with 126 neutrons, and one of about the same magnitude at 50 neutrons; and similarly, there is a break at 82 neutrons, and probably also at 28 neutrons.

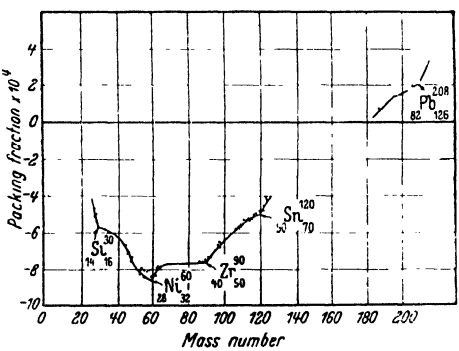


Fig. 5. Packing fraction.

β-stability

Finally, SUESS and JENSEN[40], in a detailed discussion, have recently considered the energy release in β-decay. Treating for this purpose β^--energies as positive and β^+-energies as negative, one may plot observed energies against neutron number. If all points which correspond to a given isotopic number $N-Z$ are now joined by a curve, it is found that discontinuities occur wherever the curve crosses a magic number, rising at neutron numbers or falling at proton numbers. The magnitude of these breaks is about 1 or 2 Mev. (The author is indebted to Prof. JENSEN for a prepublication copy of this work.)

Thus it appears fairly certain that there are energy discontinuities of about 2 Mev at least in the neighbourhood of the magic numbers 28, 50, 82, and 126. Since the average binding energy per particle in a nucleus is approximately 8 Mev, the effect in energy is one of some 25%. Remembering that the corresponding effect in atoms is about ten times as large, it is perhaps surprising that the nuclear shell structure is nevertheless so marked.

4. LEVEL SCHEMES

For all but the lightest nuclei the average density of nuclear matter is approximately constant. One would therefore expect that a reasonable zero-approximation to a self-consistent field would resemble a spherical well, having a

constant negative value for distances less than the nuclear radius and falling more or less abruptly to zero at the surface. For light nuclei this picture should be modified by allowing the edges of the well to become diffuse, to represent the large surface effect; so that in this region something resembling an oscillator potential is perhaps more realistic. (Since the lowest levels of each of these potentials are ordered identically—and these are the only levels of interest for light nuclei—this point is not, however, an important one.) In zero approximation one considers each particle as moving independently under the influence of this average potential, so that all one can hope

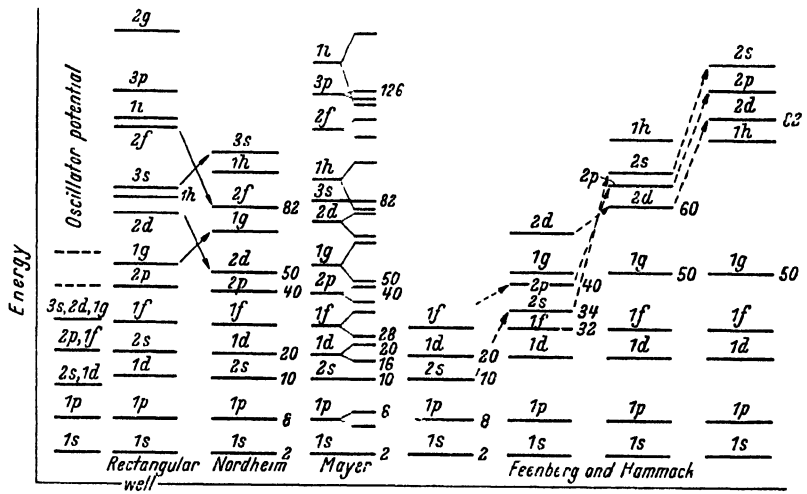


Fig. 6. Single particle level schemes.

to derive is some idea of the periodicities of nuclear structure which arise from the PAULI exclusion principle and from the ordering of the levels of each particle. A better approximation, in which the interactions between the particles is taken into account as a first-order perturbation, yields more information, insofar as one can assume knowledge of the nuclear forces, and enables one to make spin predictions and statements regarding the ordering of the levels of the complex system.

All the level schemes which have recently been proposed are basically related to the spherical well potential; the various schemes differ only in the manner in which this potential is distorted in order to bring the levels into accord with the observed magic numbers and with the spins and magnetic moments. The three main level schemes have been placed in convenient juxtaposition in a recent paper by FEENBERG[41], and we reproduce his diagram in Fig. 6.

The first column represents the levels of an isotropic harmonic oscillator potential; the second, those of a spherical well. The figures and letters attached to each level give the corresponding principal and azimuthal quantum numbers. Thus the notation nl denotes a state having l units of angular momentum and a radial wave-function with $n-1$ nodes, excepting nodes

at the origin in the case of s-states. Thus, in order of energy, the state nl is the nth state to appear with angular momentum $l\hbar$. It will be noted that this notation differs from that conventionally employed in atomic spectroscopy.

The third column contains the level scheme of NORDHEIM[42], as deduced from the observed spins and magnetic moments of the odd mass nuclei, and based upon the principle that the scheme should deviate as little as possible from that of the spherical well. Up to, and including, the $2p$ level the two schemes are in fact identical; for the main result of the NORDHEIM scheme is the raising of states of very high angular momentum, which might plausibly be produced in higher approximation by the interactions between particles. It may be observed that this result is in a sense in keeping with the ideas of a liquid drop nucleus which, strictly speaking, should have zero angular momentum in its ground state.

The fourth column shows the level scheme proposed by MAYER[43, 44], and independently, apart from rather minor differences, by HAXEL, JENSEN, and SUESS[45]. In this scheme, the basic levels are almost identically those of the spherical well; but it is assumed in addition that some form of strong spin-orbit interaction splits each level (except the s-levels) into two components corresponding to total angular momentum $j = l \pm \frac{1}{2}$, the larger j-value coming lower. It is further assumed, as would be reasonable for a coupling term of the form $\boldsymbol{\sigma} . \boldsymbol{L}$, that the spin-orbit splitting increases in importance with increasing l-values.

The remaining columns show the level scheme proposed by FEENBERG and HAMMACK[46], being a development of ELSASSER'S original proposals. Here the guiding principle is to take into account the changing shape of the overall potential as one passes to heavier nuclei. Thus the large surface effect of the lightest nuclei can be roughly represented by a spherical well with a central depression; while the Coulomb repulsion between the protons in a heavy nucleus can be represented by a spherical well with a central elevation. Both these potentials allow of simple approximate calculations. This level scheme is thus regarded as shifting in a consistent manner with atomic weight.

The closed shell configurations arising from these three schemes, together with the occupation numbers $2(2l+1)$ for each level, written in the usual spectroscopic way as powers, and the magic numbers which one obtains by summing the occupation numbers as each shell is successively filled, are given in Table 1. It may be seen that only the scheme of JENSEN-MAYER is able easily to account for the magic number 28. The observed magic numbers may be thought of in this scheme as undergoing a transition between those of the pure spherical well, given by

$$\sum_{i=0}^{n-1} (i+1)(i+2) = 2,\ 8,\ 20,\ 40,\ 70 \ldots \quad \text{for } n = 1,\ 2,\ 3 \ldots$$

and those for extreme spin-orbit coupling,

$$\sum_{i=0}^{n-1} (i+1)(i+2) + 2(n+\tfrac{1}{2}) + 1 = 6,\ 14,\ 28,\ 50,\ 82,\ 126 \ldots$$

Table 1—Closed shell configurations

Total numbers	NORDHEIM	JENSEN-MAYER	FEENBERG *and* HAMMACK	
			(light nuclei)	*(heavy nuclei)*
2	$(1s)^2$	$(1s)^2$	$(1s)^2$	$\left[\begin{matrix}(1s)^2\\(1p)^6\\(1d)^{10}\\(1f)^{14}\end{matrix}\right.$
8	$(1p)^6$	$(1p)^6$	$(1p)^6$	
	$(2s)^2$	$(2s)^2$	$(2s)^2$	
20	$(1d)^{10}$	$(1d)^{10}$	$(1d)^{10}$	
28	?	$(1f_{\frac{7}{2}})^8$	?	$\left.\begin{matrix}?\\\vdots\\\vdots\end{matrix}\right]$
	$(1f)^{14}$	$(1f_{\frac{5}{2}})^6$	$\left[\begin{matrix}(1f)^{14}\\\cdots\end{matrix}\right]$	
	$(2p)^6$	$(2p)^6$		
50	$(2d)^{10}$	$(1g_{\frac{9}{2}})^{10}$		$(1g)^{18}$
	$(1g)^{18}$	$(1g_{\frac{7}{2}})^8$		$(1h)^{22}$
	$\vdots$	$(2d)^{10}$		$\vdots$
	$\vdots$	$(3s)^2$		$\vdots$
82	$(2f)^{14}$	$(1h_{\frac{11}{2}})^{12}$		$(2d)^{10}$
		$(1h_{\frac{9}{2}})^{10}$		
	?	$(2f)^{14}$		?
		$(3p)^6$		
126		$(1i_{\frac{13}{2}})^{14}$		

Here the figures in italic type are the principal magic numbers, while the others are to be considered in this scheme as "relatively magic". For light nuclei the spin-orbit coupling (assumed to increase in importance with increasing l) is not yet sufficient to reproduce the full shell structure, while for middle weight nuclei it is still not strong enough to prevent the structure arising from the pure spherical well from intruding. Thus C^{12} with 6 neutrons and 6 protons should be especially stable, as it is; and also Si^{30} with 14 protons as mentioned previously. The number 32 would arise from the filling of the $2p_{\frac{3}{2}}$ level before the $1f_{\frac{7}{2}}$ level*; and the especial stability of Ni^{60} tends to support this view.

The objection may be brought, particularly against the NORDHEIM scheme, that the assignment of levels is from the theoretical point of view entirely arbitrary; and, as pointed out by Prof. PEIERLS, may even offend against a general theorem concerning the ordering of levels in a central potential. Moreover, as SWIATECKI[47] has shown in a refined calculation based upon the statistical model, the Coulomb repulsion of the protons in heavy nuclei is not nearly enough to bring about the central elevation required in the FEENBERG and HAMMACK theory; so that their level scheme, too, is open to the charge of arbitrariness. Certainly the electrostatic interaction must play some part; and the complete picture would probably require a combination of all three schemes, and others too. It may, however, be said that no level scheme should be accepted too literally: the suggested schemes are not necessarily the genuine levels of a single particle in a common potential, merely; but rather do they represent an average behaviour which takes into account empirically the interconfigurational mixing to be expected when levels appear in such close proximity. The mixing of configurations has often to

* See Fig. 8.

be taken into account in the theory of complex atomic spectra; *a fortiori* it may play an important part in nuclear spectroscopy.

On the whole, the weight of evidence seems to favour the JENSEN-MAYER scheme; and its comparitive lack of arbitrariness is an additional attraction. The great difficulty with this theory is that spin-orbit coupling of the required magnitude cannot at present be properly accounted for. It is about ten times too large to be due to relativistic effects. The axial-dipole coupling which is necessary to explain the quadrupole moment of the deuteron may be capable of giving a spin-orbit coupling (in second approximation) of the correct sign and magnitude, although this point is still doubtful*. Recently CASE and PAIS[48] have proposed a spin-orbit interaction of the form $\boldsymbol{\sigma} . \boldsymbol{L}$ to explain the high energy two-particle data. Using their form of interaction, HUGHES and LE COUTEUR[49] were able to show that an effect of about the correct order of magnitude could be obtained for the splitting of the levels of a single particle moving in the field of a spherically symmetric, spin-saturated, core of nucleons; but there is again some doubt regarding the sign of the splitting. As ROSENFELD[50] has emphasised, the only meson field theory which gives rise (in a weak coupling approximation) to the required sort of splitting is a vector meson field with both vector and tensor couplings to nucleons. Although π-mesons would seem to be pseudoscalar, there remains the possibility that the heavier mesons found in cosmic radiation may be responsible for these effects.

There is, however, further independent evidence, summarised by ROSENFELD[50, 51], that spin-orbit coupling terms must be present in the interaction; this evidence concerns the magnetic moments of H^3 and He^3, the apparent P-doublet of He^5 in the scattering of neutrons by He^4, and the lowest excited states of Li^7 and Be^7**. For these reasons, and for the sake of greater clarity, we shall confine our attention in what follows to the JENSEN-MAYER scheme.

5. SPINS AND MAGNETIC MOMENTS

It has already been said that in a zero-order approximation one cannot hope to derive any more than the bare periodicities in structure. The only exceptions to this rule are the nuclei consisting entirely of closed shells, in which case one can say immediately, on account of the PAULI principle, that the spin and therefore the magnetic moment are zero; and the nuclei consisting of closed shells plus or minus one particle, when one can say that the spin will be that of the loose particle, or of the "hole", $J = j$. In order to determine the spin values of more complex systems, it is necessary to go to the higher approximations, taking into consideration the forces of interaction.

Alternatively, one may short-circuit this procedure by the introduction of further basic assumptions. For the time being we shall follow this latter course; and in a later section we shall see to what extent the new assumptions may be justified in the higher approximations of the theory. Our assumptions

* See KEILSON[47a].

** See also the chapter by Prof. BURCHAM.

will be those which follow most naturally from the empirical data, namely those made in the SCHMIDT model for magnetic moments.

So far as is known, all even-even nuclei have zero spin; and it follows that they also have zero magnetic moment. On the other hand, SCHMIDT has shown that in the great majority of cases the magnetic moment of an odd-mass nucleus can approximately be said to arise from the motion of the odd particle. It is as if the presence of the added particle were to go unnoticed by the rest of the nucleus which continues to behave as a free even-even nucleus. In this picture we may regard the extent to which the observed magnetic moment deviates from the SCHMIDT value as a measure of the polarisation of the core by the odd particle.

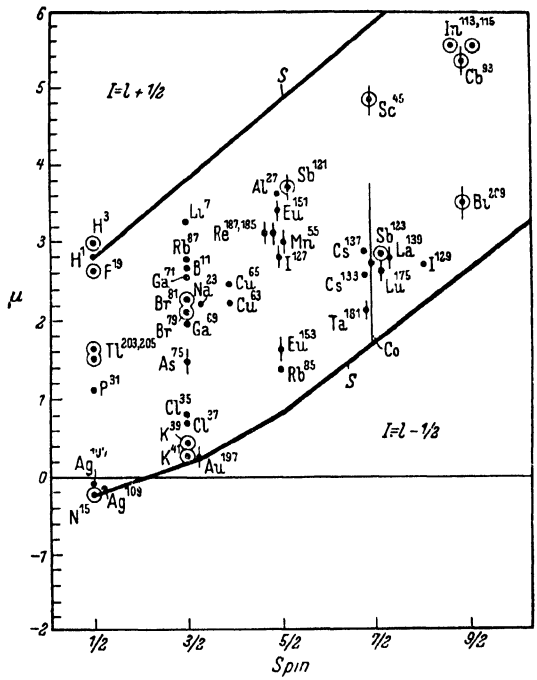


Fig. 7. Magnetic moments and SCHMIDT limits.

In this strictly one-particle model—as distinct from an individual particle model—the magnetic moment of a nucleus of total spin J may be written:

$$\mu = g_l l + g_s, \quad \text{for } J = l + \tfrac{1}{2},$$

$$\mu = g_l \frac{(l+1)(2l-1)}{2l+1} - g_s \frac{2l-1}{2l+1}, \quad \text{for } J = l - \tfrac{1}{2};$$

where the orbital g-factor $g_l = 1$ for a proton and 0 for a neutron, while the intrinsic moments are $g_s = 2{\cdot}79$ for a proton and $-1{\cdot}91$ for a neutron; and it is assumed that the odd particle moves in an orbit with angular momentum $l\hbar$.

The values calculated from these formulae are shown by the heavy lines in Fig. 7 together with the experimental points. The deviations are considerable as one might expect; but the points do at least seem to follow the trend of the SCHMIDT lines sufficiently, in most cases, for one to choose to which ideal value any measured point corresponds. The main result of this analysis is, then, to make possible the deduction of the orbital momentum of the odd particle from the measured spin and magnetic moment.

Particularly suggestive confirmation of this simple picture is afforded by the number of odd-mass nuclei, differing only in the addition of pairs of neutrons, that have identical spins and very nearly equal magnetic moments. These are shown in Table 2. Further confirmation of a more indirect nature is provided by the rather surprising feature that the deviations from the

Table 2—Spins and magnetic moments of nuclei differing by pairs of neutrons

Nucleus	*Spin*	*Magnetic moment*	*Nucleus*	*Spin*	*Magnetic moment*
Cl^{35}	$\frac{3}{2}$	0·8211	Te^{123}	$\frac{1}{2}$	?
Cl^{37}	$\frac{3}{2}$	0·6835	Te^{125}	$\frac{1}{2}$	?
K^{39}	$\frac{3}{2}$	0·392	I^{127}	$\frac{5}{2}$	2·8090
K^{41}	$\frac{3}{2}$	0·215	I^{129}	$\frac{1}{2}$	2·6173
Cu^{63}	$\frac{3}{2}$	2·2233	Xe^{129}	$\frac{1}{2}$	− 0·7726
Cu^{65}	$\frac{3}{2}$	2·3817	Xe^{131}	$\frac{3}{2}$	≈ + 0·8
Ga^{69}	$\frac{3}{2}$	2·016	Cs^{133}	$\frac{7}{2}$	2·5753
Ga^{71}	$\frac{3}{2}$	2·561	Cs^{135}	$\frac{7}{2}$	2·724
Br^{79}	$\frac{3}{2}$	2·108	Cs^{137}	$\frac{7}{2}$	2·837
Br^{81}	$\frac{3}{2}$	2·2668	Ba^{135}	$\frac{3}{2}$	0·837
Rb^{85}	$\frac{5}{2}$	1·3515	Ba^{137}	$\frac{3}{2}$	0·935
Rb^{87}	$\frac{3}{2}$	2·7471	Eu^{151}	$\frac{5}{2}$	3·4
Mo^{95}	$\frac{1}{2}$?	− 0·9098	Eu^{153}	$\frac{5}{2}$	1·5
Mo^{97}	$\frac{1}{2}$?	− 0·9289	Yb^{171}	$\frac{1}{2}$	0·45
Ag^{107}	$\frac{1}{2}$	− 0·086	Yb^{173}	$\frac{5}{2}$	− 0·65
Ag^{109}	$\frac{1}{2}$	− 0·160	Hf^{177}	$\frac{7}{2}$	?
Cd^{111}	$\frac{1}{2}$	− 0·5923	Hf^{179}	$\frac{9}{2}$	?
Cd^{113}	$\frac{1}{2}$	− 0·6196	Re^{185}	$\frac{5}{2}$	3·1433
In^{113}	$\frac{9}{2}$	5·4972	Re^{187}	$\frac{5}{2}$	3·1755
In^{115}	$\frac{9}{2}$	5·5088	Ir^{191}	$\frac{1}{2}$	?
Sn^{115}	$\frac{1}{2}$	0·9134	Ir^{193}	$\frac{3}{2}$	?
Sn^{117}	$\frac{1}{2}$	− 0·9951	Hg^{199}	$\frac{1}{2}$	0·4994
Sn^{119}	$\frac{1}{2}$	− 1·0411	Hg^{201}	$\frac{3}{2}$	− 0·607
Sb^{121}	$\frac{5}{2}$	3·3595	Tl^{203}	$\frac{1}{2}$	1·5962
Sb^{123}	$\frac{7}{2}$	2·5470	Tl^{205}	$\frac{1}{2}$	1·6118

ideal SCHMIDT values are no worse for nuclei having many particles outside closed shells than for those with only one loose particle. *A priori* one would expect the single-particle model to be a better approximation in the latter case.

In view of the effects of interconfigurational mixing, it is to be expected that pairs of levels within the same shell, which are such that spin-orbit coupling tends to bring them closer together, may often cross; and examples will be given to show that this takes place. Levels belonging to different shells, however, would not be expected to cross.

Furthermore, we should not be surprised if, for the heavier nuclei, proton levels occur in a slightly different order from neutron levels. For in the first place, the protons are more affected by the electrostatic repulsion which tends to favour higher angular momenta; and in the second place, owing to the large isotopic numbers of heavy nuclei, a given proton shell occurs later than its neutron counterpart, and so must be considered as existing in a slightly changed overall potential.

A further assumption[43] that, in the absence of a higher order calculation, must be made in order to account for the empirical data concerns the "pairing energy". It will be assumed that the interaction energy between pairs of particles in the same orbit is greater for orbits of larger angular momentum. Consequently the larger spin values appear less often than one would expect at first sight; and indeed spins of $\frac{11}{2}$ and $\frac{13}{2}$ corresponding to the h and i orbits are never found in the ground state, although there is strong evidence that they do occur in isomeric states (*q.v.*).

With this preamble we now proceed, closely following Mrs. MAYER[44] except where more recent data make necessary slight modifications, to a detailed discussion of the observed spins and magnetic moments of the odd-mass nuclei. It will be found that there are only three serious spin discrepancies, and in a later section it will be shown how it may be possible to account even for these; in addition there is one serious discrepancy amongst the magnetic moments.

For nuclei up to O^{16} there are no difficulties; and the level order $s_{\frac{1}{2}}$, $p_{\frac{3}{2}}$, $p_{\frac{1}{2}}$, is strictly adhered to. Thus H^3 and He^3 have spin $\frac{1}{2}$; Li^7, Be^9, and B^{11} have spin $\frac{3}{2}$; while C^{13} and N^{15} have again spin $\frac{1}{2}$ corresponding to the $p_{\frac{1}{2}}$ orbit.

The next shell opens with O^{17} which has been shown to have spin $\frac{5}{2}$, as should be. However, F^{19} with 9 protons has spin $\frac{1}{2}$, and according to the magnetic moment the odd particle requires an s orbit. This suggests that for such a light nucleus the spherical well potential is too steep: in the oscillator potential, the s and d levels coincide, so that this example cannot be regarded as a serious discrepancy*. We would expect the 9th and 10th protons in Na^{23} to pair up strongly in the $d_{\frac{5}{2}}$ orbit with zero resultant angular momentum, so that its configuration should be $(d_{\frac{5}{2}})^3$ or $(d_{\frac{5}{2}})^2 s_{\frac{1}{2}}$ and its spin correspondingly $\frac{5}{2}$ or $\frac{1}{2}$. Here we meet the first serious discrepancy, for the observed spin is $\frac{3}{2}$ and the magnetic moment indicates that the nucleus is in a P state. Beyond this point, the filling of the shell appears to be regular and to follow the order of levels of Fig. 8. Thus Mg^{25} and Al^{27} both have $d_{\frac{5}{2}}$ orbits, while P^{31} with 15 protons has spin $\frac{1}{2}$, indicating that the $d_{\frac{5}{2}}$ level is filled at 14 neutrons or protons and that this number may be regarded as relatively magic. S^{33}, S^{35}, Cl^{35}, Cl^{37}, K^{39}, and K^{41} should and do have spin $\frac{3}{2}$; and so the shell closes at 20.

The odd-mass nuclei with N or Z between 20 and 28 should all have spin $\frac{7}{2}$. There is only one exception: Mn^{55} with 25 protons is found to have spin $\frac{5}{2}$ and the magnetic moment indicates a D state. This constitutes the second spin discrepancy. At N or $Z = 28$ the $f_{\frac{7}{2}}$ level is full, and no spins of $\frac{7}{2}$ are again observed until the shell beginning at 51 neutrons is reached.

Beyond this point, and up to N or $Z = 37$, spins are all $\frac{3}{2}$ with the exception of Zn^{67} and Rb^{85} which have $f_{\frac{5}{2}}$ orbits. The interpretation is simply that the $f_{\frac{5}{2}}$ orbits fill preferentially in pairs (according to our assumption regarding

* The ground state of F^{17} is $\frac{5}{2}$ or $\frac{3}{2}$, even parity, and thus probably $d_{\frac{5}{2}}$; but the first excited state appears to be $s_{\frac{1}{2}}$ (see Prof. BURCHAM'S chapter). Similarly, BUTLER[80] has shown that the first excited state of O^{17} is $s_{\frac{1}{2}}$.

the pairing energy) the odd nucleon, except in these two cases, taking the nearby $p_{\frac{3}{2}}$ orbit. Y^{89} with 39 protons has spin $\frac{1}{2}$, as should be; and immediately after this the first spins of $\frac{9}{2}$ are found, namely Cb^{93} and Ge^{73}. In the subshell between 40 and 50 with one exception only spins of $\frac{1}{2}$ and $\frac{3}{2}$ are found; and once again the strong pairing forces may be invoked to account for the many

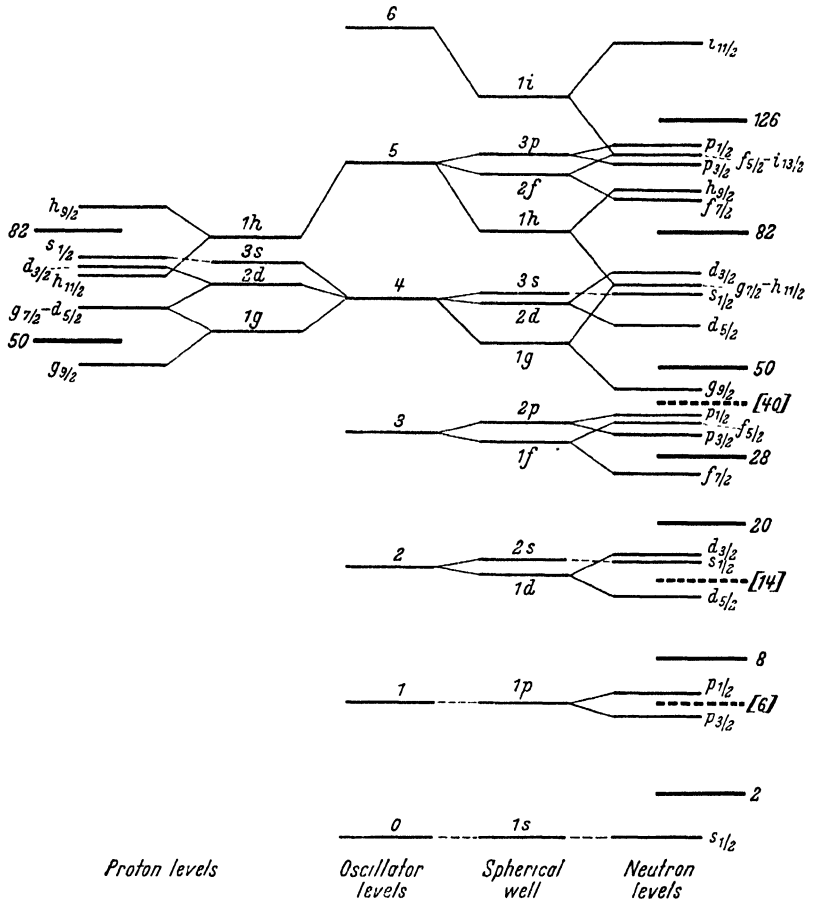


Fig. 8. JENSEN-MAYER level scheme.

values of $\frac{1}{2}$ that occur in this region. Se^{79}, however, with 45 neutrons has spin $\frac{7}{2}$, and therefore constitutes the third serious spin discrepancy. Apart from the the three spin exceptions mentioned above, we have encountered so far only two cases of neutrons and protons behaving differently: namely, the silver isotopes with 47 protons which have $p_{\frac{1}{2}}$ orbits, while Kr^{83} with 47 neutrons has $g_{\frac{9}{2}}$; and Tc^{99} with 43 protons is $g_{\frac{9}{2}}$, while Se^{77} with 43 neutrons is $p_{\frac{1}{2}}$.

In the shell between 50 and 82 neutrons or protons, no spins of $\frac{9}{2}$ should appear, nor are they found. The only serious discrepancy amongst the magnetic moments occurs in this region: it is Eu^{153} with 63 protons, which appears

to have a $f_{\frac{5}{2}}$ orbit instead of the expected $d_{\frac{5}{2}}$ for spin $\frac{5}{2}$. The $g_{\frac{7}{2}}$ and $d_{\frac{5}{2}}$ levels seem to be close together; from 50 up to 63 all spins are $\frac{5}{2}$ or $\frac{7}{2}$, arranged apparently arbitrarily. The isotopes of Mo may be exceptions, having spin $\frac{1}{2}$; but this point is not yet settled. From 63 up to 75 neutrons inclusive, all spins are $\frac{1}{2}$. This can most easily be understood with the ordering of levels given in Fig. 8, together with the usual assumption that pairing forces in both the $g_{\frac{7}{2}}$ and the $h_{\frac{11}{2}}$ levels are sufficient to depress them below the $s_{\frac{1}{2}}$ level. The neutron shell closes with the $d_{\frac{3}{2}}$ orbit, Ba^{135} and Ba^{137} with 79 and 81 neutrons, each having spin $\frac{3}{2}$.

The situation is somewhat different for the odd proton nuclei. From 51 to 63 protons inclusive, all spins are again $\frac{5}{2}$ or $\frac{7}{2}$. With the possible exception of Tm, having 69 protons, however, no spins of $\frac{1}{2}$ are encountered until 81 protons is reached, only the values $\frac{3}{2}$, $\frac{5}{2}$, and $\frac{7}{2}$ being found. There is some doubt about where the $h_{\frac{11}{2}}$ level is filling, but one would in any case expect it to fill in pairs. The shell ends at 81 protons with Tl^{203} and Tl^{205}, both of which have spin $\frac{1}{2}$. The electrostatic repulsion seems to have the predicted effect: relative to the neutron levels, the $g_{\frac{7}{2}}$ level is depressed and the $s_{\frac{1}{2}}$ level raised.

Too few spins are known in the following shell, 82 to 126, to enable any detailed discussion to be made. The neutron shell begins at Nd^{143} and Nd^{145}, with 83 and 85 neutrons respectively, and both these nuclei have spins of $\frac{7}{2}$; it ends with $p_{\frac{1}{2}}$ at Pb^{207} with 125 neutrons*. It is to be expected that $\frac{9}{2}$ spins will again appear in the region of neutron number 87 to 97, but no measurements seem to have been reported as yet. All that one can say about the proton shell is that it commences with an $h_{\frac{9}{2}}$ orbit, as indicated by Bi^{209}.

Nothing whatever can at present be said with any certainty about the neutron shell beyond 126.

6. Electric Quadrupole Moments

Having set up with the aid of the spins and magnetic moments a fairly detailed level scheme, it remains to be seen whether we can correlate it with further nuclear properties. The first property we shall consider is the electric quadrupole moment, for this will lead us to a better understanding of the magnetic moments. The regularities of the quadrupole moments have been studied recently by Rosenfeld[50].

Firstly, concerning the question of charge, it seems that there is no appreciable difference in behaviour between odd-proton nuclei and odd-neutron nuclei, both as regards sign and absolute magnitude. As Rosenfeld points out, this strongly suggests an active exchange of charge between nucleons, as one would expect on the basis of an interaction which is produced at least in part by charged mesons.

The second regularity concerns the sign of the quadrupole moment. Nuclei that contain apart from filled levels one loose particle (neutron or

* Private communication from Prof. M. H. L. Pryce: the lowest states of Pb^{207} in order of energy are $p_{\frac{1}{2}}(0)$, $f_{\frac{5}{2}}(565\text{ kev})$, $p_{\frac{3}{2}}(860\text{ kev})$, $f_{\frac{7}{2}}(1165\text{ kev})$ and $i_{\frac{13}{2}}(1630\text{ kev})$; with the exception of the missing $h_{\frac{9}{2}}$ level, these levels are in agreement with those of Fig. 8, bearing in mind that a single neutron "hole" would have energy levels in the reverse order to those of a single neutron.

proton) have negative quadrupole moments; those that require only one particle to complete a level (i.e. that have one hole) have positive quadrupole moments. Of the thirty or so measured examples, only Li^7 breaks the rule. A particularly beautiful example is afforded by the sulphur isotopes: S^{33} has one neutron in the $d_{\frac{3}{2}}$ level, and its quadrupole moment is negative, while S^{35} has one hole in this level and its quadrupole moment is positive. Qualitatively, the quadrupole moments behave in this respect as if they were primarily due to the motion of a single positive charge, or a single hole, in an otherwise closed distribution of positive charges. A proton of angular momentum l moving in a central field gives rise to a quadrupole moment

$$Q = -\frac{2l}{2l+3}\langle r^2\rangle_{\mathrm{av}},$$

where $\langle r^2\rangle_{\mathrm{av}}$ is the mean square radius vector of the orbit considered; for a hole we simply have to change the sign of this expression.

The third feature concerns the absolute magnitudes of the quadrupole moments. For masses up to about 100, and for the two heaviest nuclei yet measured, Hg^{201} and Bi^{209}, the absolute magnitudes are in very rough accord with the values obtained from the single particle expression above, when we put $\langle r^2\rangle_{\mathrm{av}}$ about equal to R^2, the square of the nucleus radius. Nuclei with masses in the range 100 to 200, however, have, with very few exceptions, moments abnormally large by a factor of about 10.

Now the quadrupole moment, even more than the magnetic moment, depends sensitively upon the model assumed; and in a shell model we must therefore take into account possible contributions which arise from the polarisation of the core by the odd particle. The core in its free state as an even-even nucleus would be spherically symmetric; but the addition of another particle will produce a deformation, and we may assume that is becomes slightly ellipsoidal. In a perturbation treatment such effects are taken care of in second order, the deformation being equivalent to a sum over intermediate states. However, we can form a simple estimate, following RAINWATER[52], on the basis of the semi-empirical mass formula, if we assume that the major contribution to the quadrupole moment again comes from the motion of a single particle; but this particle is now considered to be moving in a slightly ellipsoidal field, the effect of which is to remove partially the spatial degeneracy associated with the magnetic quantum number*.

The result of the calculation is to increase the simple one-particle value given above, by a factor which may, according to ROSENFELD, be written

$$\frac{4}{15}\frac{Z}{\sigma A^{\frac{1}{3}}}\frac{(\hbar^2/2Mr_0^2)\,k_{n,l}^2}{1-\gamma(Z^2/A)},$$

where it is assumed that the nuclear radius $R = r_0 A^{\frac{1}{3}}$; the $k_{n,l}$ are the successive zeros of the BESSEL function $J_{l+\frac{1}{2}}(z)$; and the constants $\sigma = 2{\cdot}74$ Mev and $\gamma = 0{\cdot}02$ are known from the semi-empirical formula. For Lu^{175}, with $n=1$ and $l=4$, this factor is about 5, which is at least of the right order

* See also the discussion by AAGE BOHR[52a].

of magnitude. Other forms of deformation, such as can be produced by noncentral forces, probably also contribute appreciably to the large quadrupole moments, but we shall not consider them here.

It appears, then, that the quadrupole moments afford us, within the framework of the single-particle model, a measure of the polarisation of the core by the odd particle; and we are entitled to enquire whether there is any relation between the quadrupole moments and the deviations of the observed magnetic moments from the ideal SCHMIDT values. There are several pairs of isotopes, differing by two neutrons, for which the quadrupole moments have also been reported. In Fig. 9, following KOPFERMANN *, are plotted the magnetic moments of some of these pairs against their quadrupole moments; and extrapolating linearly back to zero quadrupole moment, values of the magnetic moment are obtained in much closer accord with the SCHMIDT values, also indicated in the figure. The case of the Eu isotopes is of especial interest in that Eu^{153} was thought to be the only serious discrepancy amongst the magnetic moments; the extrapolation in this case, however, is so large that one should treat it with some reserve. Of course, there is no guarantee that the linear method of extrapolation is the correct one to use; more experimental evidence is required on this point; but at least it would seem that, qualitatively, the deviations of the magnetic moments from the ideal values can be attributed to polarisation effects. Accordingly, one feels more certain of the assignment of orbital momenta on the basis of the SCHMIDT model.

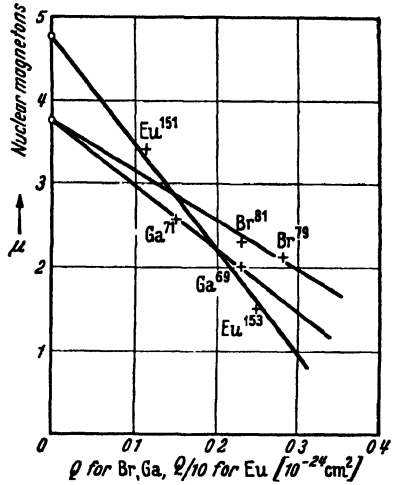


Fig. 9. Magnetic moments versus quadrupole moments.

7. ISOMERISM

We have seen that the single particle model holds remarkably well for the spins of the ground states of the odd-mass nuclei; and it can be expected that it may also hold good for their lowest excited states. On the basis of the proposed level assignment, which gives in addition to the spin values the parities of levels, it is therefore possible to reach some general conclusions regarding the low-lying excited states; in particular, we can predict where isomeric transitions can be expected; and to some extent we can classify the transitions according to their electric or magnetic multipolarity. Conversely, the known electromagnetic characters of some isomeric transitions enables us to verify any proposed level scheme.

The half-life against electromagnetic disintegration of a nucleus between two states differing by energy E has been represented by several approximate

* Reported at the Copenhagen Conference, 1951.

formulae of which the most recent, due to WEISSKOPF[53], seems to fit the experimental data most consistently. For an electric transition in which the spin change is ΔJ, WEISSKOPF's one-particle formula for the half-life in seconds is

$$\tau_{el.} = \frac{[1, 3 \ldots (2\Delta J + 1)]^2}{4(\Delta J + 1)} \frac{\lambda\!\!\!^{-}_e}{\varrho} \left(\frac{137}{E}\right)^{2\Delta J + 1}$$

where E is in units mc^2, $2\pi\lambda\!\!\!^{-}_e$ is the COMPTON wavelength of the electron, and ϱ is the nuclear radius in units of e^2/mc^2. For magnetic transitions in which the spin change is ΔJ the above expression must be multiplied by a factor $(R/\lambda\!\!\!^{-}_p)^2$, where R is the nuclear radius and $2\pi\lambda\!\!\!^{-}_p$ is the COMPTON wave-

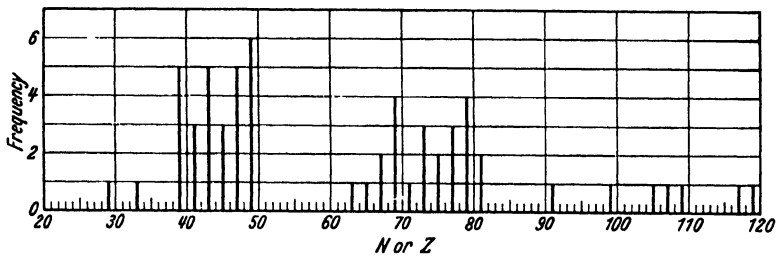


Fig. 10. Frequency of occurrence of odd-mass isomers.

length of the proton, times a constant numerical factor of about 0.1. The corresponding multipolarities, electric 2^{Δ}-pole or magnetic $2^{\Delta-1}$-pole, are shown below.

Transition	E1	M1	E2	M2	E3	M3	E4	M4	E5
ΔJ	1	1	2	2	3	3	4	4	5
Parity change	yes	no	no	yes	yes	no	no	yes	yes
Multipolarity	1	2	2	3	3	4	4	5	5

On the basis of the WEISSKOPF formulae, and of the relativistic calculations of the internal conversion coefficients by ROSE *et al.*[53a], a full classification of all known nuclear isomers has recently been given by GOLDHABER and SUNYAR[54].

For the purposes of this review we shall consider as isomeric only transitions that have $\Delta J \geq 3$, although this is an entirely arbitrary classification. Isomerism in the odd-mass nuclei may thus be expected, according to the selection rules, where the ground state has a very large spin such as $\frac{9}{2}$, or where it has very small spin but belongs to a shell in which levels of large spin may reasonably be expected to occur near to ground. Fig. 10 is a histogram showing the frequency of occurrence of odd-mass isomers as a function of N or Z, whichever is odd; with a few exceptions, all isomers are found in two distinct regions—"the islands of isomerism"—the first lying between 39 and 49, the second between 63 and 81, inclusive. Referring to the level scheme, Fig. 8, we see that these are respectively the regions where the $g_{\frac{9}{2}}$ competes with the $p_{\frac{1}{2}}$ level for lowest place, and where the $h_{\frac{11}{2}}$ level competes with the $s_{\frac{1}{2}}$ and $d_{\frac{3}{2}}$ levels. All transitions involving the $g_{\frac{9}{2}}$ and $h_{\frac{11}{2}}$ levels as

initial or final states require a change or parity, so that only odd A-values are expected in both these regions. In the first region where one is concerned only with the transition $g_{\frac{9}{2}} \rightarrow p_{\frac{1}{2}}$, $\Delta J = 4$, only M 4 transitions should occur.

Considering only the two main islands of isomerism, the great majority of isomeric transitions are indeed found to be M 4 in agreement with the shell model predictions. In addition, however, there are a number of E 3 transitions that do not fit the simple single-particle picture. Most of these occur in the first island and seem to involve the $g_{\frac{7}{2}}$ level. While the SCHMIDT interpretation of the magnetic moments is that in the ground state an odd number of particles, each with angular momentum j, combine to form a resultant $J = j$, there are in general several other states allowed by the exclusion principle, some of which may occur near to the ground state. These states are allowed in the more general *individual* particle model, although not in the single-particle model. The E 3 isomer Tc^{99}, which appears in the first island, seems to be of this kind: the ground state is $g_{\frac{9}{2}}$; but the isomeric transition takes place between two excited states the upper of which is thought to be $p_{\frac{1}{2}}$, while the lower is given as $\frac{7}{2}(+)$, and may be interpreted as one of the states of the configuration $(g_{\frac{9}{2}})^3$. According to GOLDHABER and SUNYAR, nearly all the E 3 transitions can be explained in terms of a $\frac{7}{2}(+)$ state of one of the configurations $(g_{\frac{7}{2}})^{3,5,7}$; the $g_{\frac{9}{2}}$ and $\frac{7}{2}(+)$ levels appear to be rather close in energy. These transitions were previously thought to have[55] $A = 4$, on the basis of inaccurate life-time formulae and non-relativistic calculations of the conversion coefficients, and as such constituted one of the chief difficulties of the shell model in its early days.

The evidence strongly supports the existence of $h_{\frac{11}{2}}$ levels as excited states of the 50–82 shell. For example, Ba^{137} with 81 neutrons has a $d_{\frac{3}{2}}$ ground state, and the isomeric transition is M 4. A spin change of 4 is required, and a parity change, so that the isomeric level must be of odd parity and spin $\frac{11}{2}$. From Fig. 10, we see that there may be a third island of isomerism for $N \gtrsim 90$; this is probably associated with the $i_{\frac{13}{2}}$-level.

8. β-DECAY

Any discussion of β-radioactivity is necessarily complicated by the fact that the exact nature of the interaction between electrons and neutrinos on the one hand, and neutrons and protons on the other, is not properly understood[56]. Of the five simple interactions which are allowed by conditions of invariance and which do not involve derivatives of the field, the evidence regarding the shapes of certain forbidden spectra[57] favours the tensor theory for which GAMOW-TELLER selection rules apply. It cannot be ruled out that the actual interaction consists of a linear combination of the simple types amongst which the tensor term has a dominant role; however, for the very brief discussion that follows it is sufficient to assume simply that the selection rules have the GAMOW-TELLER form.

For an allowed transition, the G–T rules are

$$\Delta J = 0,\ 1;\ \text{no parity change};\ 0 \rightarrow 0,\ \text{forbidden};$$

and for the first forbidden transitions

$$\Delta J = 0,\ 1,\ 2;\ \text{parity change};\ 0 \rightarrow 0,\ \text{forbidden}.$$

The degree of forbiddeness of a transition is often determined (somewhat arbitrarily) by its comparative lifetime, or ft value. In Fig. 11 we show a histogram, after FEENBERG and TRIGG[58], on which is plotted the frequency of occurrence of odd-mass β-emitters as a function of $\log_{10} ft$, where, however, first forbidden transitions with $\Delta J = 2$ have been omitted. These latter transitions are the ones which show the forbidden type of spectrum, and their ft values, when corrected by the "shape factor", are all about 10^{10}, as shown by SHULL and FEENBERG[59].

It is seen that the ft values, in spite of considerable straggling, fall into certain discernible groups. The first, quite distinct, group centred on $\log ft = 3{\cdot}5$ corresponds to the superallowed, or allowed and favoured, transitions that take place between the ground states of mirror nuclei, and for which, consequently, the spatial wave function remains unchanged in the transition, apart from a small change due to the Coulomb difference.

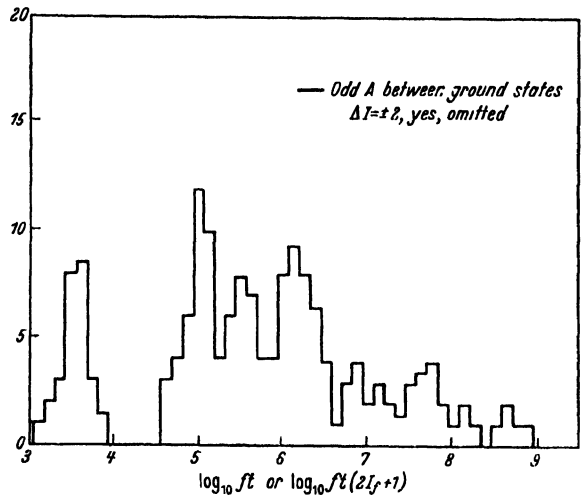


Fig. 11. Histogram of ft values for β-decay.

According to a shell model it is possible, as we have seen, to assign definite orbital momenta and parities to low-lying levels and in particular to the ground states. One may then, following NORDHEIM[60], reframe the above selection rules according to the changes in the orbital momentum L, or in intrinsic spin S, in addition to the total spin J. The normal allowed transitions are then those for which $\Delta L = 0, \Delta S = 0, 1$; these appear in a group in Fig. 11 centred on $\log ft = 5{\cdot}0$. The normal first forbidden transitions occur around $\log ft = 6{\cdot}2$; and these are interpreted as $\Delta L = 1$ (i.e. parity change), together with $\Delta J = 0, 1$. The group that appears in between these two in the histogram may be due to the allowed transitions in which the orbital angular momentum changes by two: $\Delta L = 2, \Delta S = 1, \Delta J = 1$, no parity change; the ft values one would expect to be larger than for the normal allowed transitions in which there is no change in L. The first forbidden transitions, $\Delta L = 1$, $\Delta J = 2$, with the forbidden shape of spectrum, have uncorrected values of $\log ft$ between 8 and 9; while higher forbidden transitions have values above 9. With this new and more extensive classification, NORDHEIM reports

that there is no discernible trend towards increasing *ft* values with increasing atomic weight as was formerly believed*.

More definite information regarding the spins and parities of nuclear levels may be obtained by studying the β–γ and γ–γ angular correlations and the internal conversion coefficients. Several examples of level schemes have been discovered, some quite complex, which are consistent with the one-particle interpretation; but a detailed discussion of this subject would take us too far afield. As in the case of isomerism, it is often found that levels occur which cannot be reconciled with the one-particle model, but which nevertheless are not inconsistent with the individual particle model. There is little doubt that the study of β- and γ-spectra provides the surest test of any shell theory.

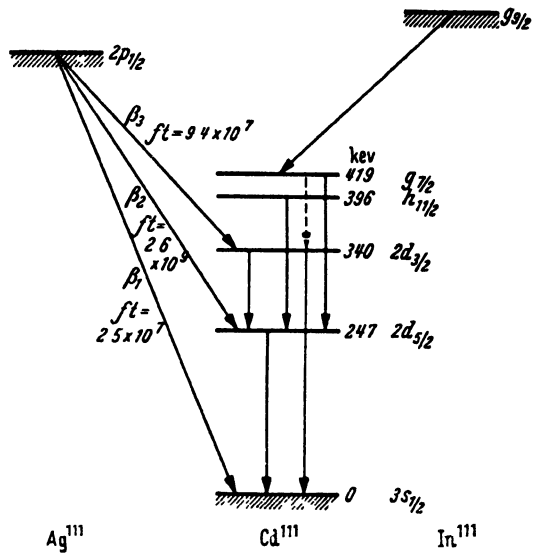


Fig. 12. Levels of Cd^{111}.

A single example must suffice; we choose Cd^{111}, obtained in the β^--decay of Ag^{111}, and in K-capture from In^{111}, studied recently by McGinnis[61]. In Fig. 12 the level scheme is shown. The ground state of Cd^{111} is known to be $\frac{1}{2}$, even; from the β-spectrum of Ag^{111} the conversion coefficients of the 340 and 247 kev gamma-rays are both found to be consistent with electric quadrupole, or a mixture of electric quadrupole and magnetic dipole, radiation; so that the spins must be $\frac{5}{2}$ or $\frac{3}{2}$ with no parity change. The *ft* values are also shown in Fig. 12; according to the selection rules the transitions β_1 and β_3 are first forbidden with $\Delta L = 1$ and $\Delta J = 0, 1$; so that the ground state of Ag^{111} must be $\frac{1}{2}$ or $\frac{3}{2}$, odd. The *ft* value of β_2 suggests first forbidden with $\Delta L = 1$ and $\Delta J = 2$; but the intensity of the transition is too small to allow this to be checked by the shape of the spectrum. On this basis, the lowest three levels of Cd^{111} are determined. The conversion coefficients for the 172 kev gamma-ray between the 419 and 247 kev levels indicate magnetic dipole, so that the 419 kev level must be $\frac{7}{2}$, even, and it is probably $g_{\frac{7}{2}}$. The *ft* value of the In^{111} transition suggests a normal first forbidden transition; no β-rays seem to go to the 247 kev level, so the ground state of In^{111} is fixed as $\frac{9}{2}$, even, and probably $g_{\frac{9}{2}}$. The remaining 396 kev level of Cd^{111} is metastable, and the single particle model suggests $\frac{11}{2}$ and odd parity, so that the 149 kev transition to the 247 kev level would be E 3. The half-life and the conversion

* A full discussion of β-decay and shell structure will be found in the papers by Mayer, Moszkowski and Nordheim[84], and by Nordheim[85].

data confirm this assignment according to GOLDHABER and SUNYAR[54]. All the levels are seen to be in accordance with the spin-orbit shell model, although, as is not surprising, the order of levels differs somewhat from that proposed in Fig. 8 which is based upon the ground states only. A further conclusion concerns the magnitude of the spin-orbit splitting; the splitting of the $2d$ levels is seen to be 93 kev.

Many further examples of level schemes may be found in the literature. In particular, the reader is referred to Prof. BURCHAM'S article for a detailed discussion of the energy levels of the lighter nuclei.

9. THE MANY-BODY PROBLEM

We turn now to consider some of the calculations that may be performed on the basis of the individual particle model. A fundamental difficulty immediately arises in that our knowledge of nuclear forces is very limited. The low-energy two-particle data is consistent with a force which, apart from the Coulomb interaction between protons, is symmetrical between neutrons and protons; it is of short but finite range, and probably in large part central; and it has a strong Majorana space exchange component which becomes more evident at high energies. In order to account for the properties of the deuteron, it is also necessary to assume a spin-exchange term and a non-central tensor force. At very high energies, $\gtrsim 50$ Mev, there is some evidence[62] that p–p and n–p forces are no longer identical, and that spin-orbit forces may have to be introduced; but this need not concern us since kinetic energies within a nucleus are probably less than about 30 Mev[51].

The general two-body central exchange force may be written $V = Q\,V(r)$, where the operator

$$Q = w + m\,P_x + h\,P_\tau + b\,P_\sigma$$

defines the exchange nature of the force whose radial dependence is given by $V(r)$. Here P_x exchanges the spatial coordinates, P_τ the charge coordinates, P_σ the spin coordinates. All theories agree that the leading term is P_x; for a symmetrical meson theory giving saturation and the correct triplet-singlet splitting of the deuteron we have[51] $w \approx 0{\cdot}13$, $m \approx -0{\cdot}93$, $h \approx -0{\cdot}26$, and $b \approx -0{\cdot}46$. For lack of other information it is usually assumed that the major part of the force is of this kind; and if only a central exchange force is considered, saturation requirements demand a symmetrical force: but the non-central forces are known to be present (and must be quite strong according to the spin-orbit coupling shell model); and the possibility of many-body interactions predicted by meson theory cannot be ignored.

Most work on the nuclear many-body problem has been based in the first instance upon the so-called WIGNER approximation[14], in which only the terms w and m are retained, all forces depending explicitly upon spin and charge being allowed for at a later stage. With this assumption, we may ask what properties are reflected in the nuclear wave function, irrespective of detailed structure, by the symmetry of the Hamiltonian. The Hamiltonian

is invariant with respect to certain groups of transformations: and the eigenfunctions are characterised by corresponding quantum numbers that arise from the representations of the groups. The powerful methods of group theory may thus be used to label states of the nuclear system, and to make at least semi-quantitative predictions regarding the energies of these states. The particular value of the group theoretical method in the problem of nuclear structure lies, as we have already remarked, in the fact that the effect of the Majorana exchange force strongly depends upon the properties of the wave function with respect to permutation of particles.

From the symmetry of the nuclear Hamiltonian with respect to spatial rotations, it follows that the total angular momentum vector $\boldsymbol{J}$ is quantized in such a way that $\mathbf{J}^2$ takes on the values $J(J+1)$, where J is integral if A is even, half-integral if A is odd. If in addition the coupling between spin and orbital motion is ignored, nuclear states may be grouped into degenerate spin multiplets, just as in atomic spectroscopy, characterised by the quantum numbers L and S; the multiplicity is $2S+1$, and the total angular momentum takes values between $|L-S|$ and $L+S$. This spin degeneracy is removed by the introduction of coupling forces.

A further quantum number that is always valid is the total charge of the nucleus. Just as one ascribes to a nucleon a spin vector σ having a z-component ± 1, so that the total intrinsic spin is $S = \frac{1}{2}\sum_i \sigma^{(i)}$, one may formally ascribe a charge vector τ with components ± 1 in the ζ-direction of a purely formal isotopic space[63], $+1$ denoting a neutron, -1 a proton, such that the total isotopic spin $T = \frac{1}{2}\sum_i \tau^{(i)}$. Clearly $2T_\zeta = N-Z$, the usual isotopic number. As long as charge dependent forces, including Coulomb forces, are ignored, the Hamiltonian will be invariant with respect to "rotations" in isotopic space; and it follows that not only T_ζ but also $\boldsymbol{T}$ will be quantized, in such a way that $\mathbf{T}^2$ takes on the values $T(T+1)$ with integral or half-integral T. The $2T+1$ degenerate terms for given T then define a charge multiplet: the terms correspond to isobaric nuclei of different isotopic number. The Coulomb interaction of the protons, and other forces dependent non-linearly upon charge, remove the degeneracy of the charge multiplet.

Now, in the WIGNER approximation, a number of these spin and charge multiplets will coincide in energy, forming a "supermultiplet"; and at least one further quantum number will be required to label this new degeneracy. The wave functions of a degenerate supermultiplet have the general form

$$\Psi(r^{(i)}, \sigma_z^{(i)}, \tau_\zeta^{(i)}) = \frac{1}{\sqrt{f}} \sum_{k=1}^{f} \Gamma_k(\sigma_z^{(i)}, \tau_\zeta^{(i)}) \Phi_k(r^{(i)})$$

where the linear combination of f terms is such as to make the total function Ψ completely antisymmetric as required by the exclusion principle. The supermultiplet is then completely characterised by the symmetry properties of the Φ_k with respect to permutation of particles.

The symmetry properties of a wave function of A particles with respect to permutations may be characterised by a partition of A into four positive integers

$$A = \lambda_1 + \lambda_2 + \lambda_3 + \lambda_4,$$

where

$$\lambda_1 \geq \lambda_2 \geq \lambda_3 \geq \lambda_4,$$

expressing the fact that Γ can be made symmetric with respect to groups of at most $\lambda_1 \ldots \lambda_4$ nucleons. The partitions of A are said to characterise the irreducible representations of the group of all permutations on A particles; but we consider only partitions into 4 parts because Γ cannot be made antisymmetric in more than 4 nucleons ($\sigma_z = \pm 1$, $\tau_\zeta = \pm 1$). We may regard λ_1 as the number, for example, of neutrons with $\sigma_z = +1$, λ_2 as the number of neutrons with $\sigma_z = -1$, and so on. It turns out that a supermultiplet may be characterised completely by three numbers, in addition to A, two of which are the maximum values which S and T may take, while the third is defined as having a z-component given by $Y_z = \frac{1}{2}\sum_i \sigma_z^{(i)} \tau_\zeta^{(i)}$.

The ordering in energy of supermultiplets on the WIGNER approximation is then determined by the values of the quantity[51]

$$\Xi = \tfrac{1}{2}\left[(P+2)^2 + (P'+1)^2 + P''^2\right],$$

where P, P', P'' are the numbers S, T, Y arranged so that $P \geq P' \geq P''$. In terms of the partitions it is clear that

$$P = \tfrac{1}{2}(\lambda_1 + \lambda_2 - \lambda_3 - \lambda_4)$$
$$P' = \tfrac{1}{2}(\lambda_1 - \lambda_2 + \lambda_3 - \lambda_4)$$
$$P'' = \tfrac{1}{2}(\lambda_1 - \lambda_2 - \lambda_3 + \lambda_4).$$

Since the values of P, P', P'', and therefore Ξ, do not change if each λ is increased by the same amount, it follows that an α-particle periodicity will arise quite naturally and without *ad hoc* assumptions.

The supermultiplet lowest in energy is that which has the lowest values of S, T, Y consistent with the inequality relations. The ground state of a nucleus in the WIGNER approximation is therefore the one having maximum spatial symmetry consistent with its known isotopic number, i.e. that with $P = T_\zeta = T = \frac{1}{2}(N-Z)$, while P' and P'' take their smallest possible values. The symmetry of Γ fixes uniquely the symmetry of Φ; for in order that Ψ should be completely antisymmetric it is required that Γ and Φ have dual symmetry. Thus not only Γ, but also Φ and Ψ, are characterised by the numbers S, T, Y.

The symmetry theory of WIGNER, although more general than an individual particle theory, forms a valuable starting point for a first-order perturbation treatment of a shell model similar to the SLATER treatment of atomic configurations. We consider, then, a nucleus which contains, apart from closed shells, n particles having orbital angular momentum l. The energy required to break up closed shells we suppose so large that the lowest states will be solely those of the configuration l^n. We neglect for the time being config-

urations in which particles are in different orbits; and we enquire what are the lowest states, in the WIGNER approximation, of the configuration l^n.

It is well known in group theory[64] that the partitions of n characterise also the irreducible representations of the group of linear unitary transformations U_{2l+1}, in $2l+1$ dimensions, applied to the wave functions Φ of n particles considered as tensors of rank n in the space spanned by the states of a single particle ($m=-l, \ldots, l-1, l$). If we now restrict ourselves to those unitary transformations which are in addition transformations of the ordinary rotation group in 3 dimensions, each of the representations of U_{2l+1} breaks down into irreducible representations $\mathfrak{D}_L$ of the rotation group R_3, characterised by the quantum number L. Thus a procedure exists for finding what possible L values correspond to a given supermultiplet. A further classification of states is possible if a group G exists such that G is a subgroup of U containing R_3 as a subgroup ($U \supset G \supset R_3$). For $l>1$, a suitable group is always furnished by the group R_{2l+1} of proper rotations in $2l+1$ dimensions, obtained by restricting our initial unitary transformations to those which are also orthogonal. The representations of R_{2l+1} provide fresh quantum numbers to label the nuclear states. The characterisation of states according to the representations of R_{2l+1} was first introduced into spectroscopy by RACAH[65].

The new classification has physical significance, strictly speaking, only if forces are of infinitely short range: in this case, all states which transform according to a given representation of R_{2l+1} are almost degenerate, so that the numbers characterising the representation are "good" quantum numbers. It is pointed out by JAHN[66] that, with conventional short-range forces, one is quite close to this fictitious limit*. The energy of a nuclear state in first order may in fact be written in the following manner:

$$E = e_0 E^{(0)} + e_1 E^{(1)} + e_2 E^{(2)} + \cdots + e_l E^{(l)}$$

where the $E^{(i)}$ are suitable combinations of the usual SLATER integrals (see CONDON and SHORTLEY[13]), and the e_i have a special significance. The coefficient $e_0 = \frac{1}{2} n(n-1)$ gives the interaction energy of the configuration independent of symmetry; the coefficient e_1 involves, in addition to n, the quantum numbers S, T, Y, and those characterising the representation of R_{2l+1} to which the state in question belongs, but not L. The remaining coefficients involve also the L values in a more or less complicated fashion. In the fictitious limit when all $E^{(i)}$ vanish except $E^{(0)}$ and $E^{(1)}$, all states belonging to a given supermultiplet and to a given representation of R_{2l+1} become degenerate. This is the "LAPORTE-PLATT[67] degeneracy" of atomic spectroscopy. The degeneracy is equivalent to the introduction of $l-1$ independent linear relationships among the SLATER integrals. Assuming wave functions of a harmonic oscillator or of a spherical well potential, SWIATECKI[68] has shown that $E^{(1)} \gg E^{(2)}, E^{(3)}, \cdots$, with forces of conventional non-zero range.

Assuming, then, that forces are mainly of the short-range WIGNER plus MAJORANA type, it is now possible to state the following conclusions regarding

* The degeneracy with a δ-function interaction is exact only for the d-shell.

the ground states of nuclei in RUSSELL-SAUNDERS coupling. Even-even nuclei should be in ^1S states; and odd-mass nuclei should be doublets with maximum orbital symmetry having $L=l$. These latter states are precisely those obtained by the addition of a single particle to a spherically symmetrical, even-even core: *the assumption of a* MAJORANA *force of short-range leads to a single-particle model for the ground state of an odd-mass configuration.* If we now assume further that a spin-orbit coupling term is added to the Hamiltonian, the doublet states split to give states with $J=l\pm\frac{1}{2}$; if the splitting is "inverted," i.e. if the coupling term has the right sign, the state with $J=l+\frac{1}{2}$ is the lower at the commencement of a shell, and that with $J=l-\frac{1}{2}$ at its closure. These results are in complete accordance with the requirements of the JENSEN-MAYER shell model, at least for light nuclei where the spin-orbit coupling is not large enough to invalidate the assumption of RUSSELL-SAUNDERS coupling.

Table 3—Spin of odd-odd nuclei in LS-coupling

Nucleus	*Predicted state*	*Observed spin*
H^2	$^3S_1$	1
Li^6	$^3S_1$	1
B^{10}	$^3S_1$	3
N^{14}	$^3S_1$	1
Na^{22}	$^3S_1$	3
Na^{24}	$^3F_1$	4
Cl^{36}	$^3F_1$	2
K^{40}	?	4
Sc^{44}	$^3H_6$?	?

The complete classification of states of the nuclear configurations s^n and p^n has been given by FEENBERG and WIGNER[12], and by HUND[69]; of the configurations d^n by JAHN[66]; and of the f^n configurations by FLOWERS[70].

The predicted spins of the odd-odd nuclei are less certain in that they depend more sensitively upon the exact nature of the force. There is firstly a choice between singlet and triplet states, of which the triplet would be the lower with symmetrical forces, as for instance in the deuteron. If there are equal numbers of neutrons and protons, $A=2Z$, the ground state should then be ^3S. If $A\neq 2Z$, the ground state depends also upon the range of the force as well as upon its exchange nature, though rather insensitively: with forces of conventional range, the lowest states in the p-shell would be $^3P_{0,1,2}$; and in the d-shell, $^3F_{2,3,4}$. With inverted spin-orbit coupling the usual choice of J may then be made according as the shell contains more or less than $l+1$ nucleons. Table 3 shows the observed and predicted spins as far as they are known for the odd-odd nuclei: the agreement is not striking. The reason for disagreement may lie in the more detailed dependence upon the nature of the force, and particularly upon the tensor force which we have neglected completely. The magnetic moments of Li^6, B^{10}, and N^{14}, certainly suggest that the tensor force is of increasing importance for heavier nuclei; and in B^{10} it seems that the $^3D_3$ state is actually depressed below the "mixed" state $^3S_1+^3D_1$. The disagreement in the cases of Na^{22} and Cl^{36} may be due to mixed configurations, for the $2d$ and $2s$ levels are very close in energy, while K^{40} is uncertain theoretically in that it contains a mixed configuration. The prediction of the high spin values of Table 3 suggests that isomerism can possibly be expected in these regions, particularly at th beginning of

the *f*-shell; and it is significant that the odd-odd nuclei Sc^{44} and Sc^{46} are both reported[54] as having isomeric states.

10. *jj*-COUPLING

According to the JENSEN-MAYER shell model, strong spin-orbit forces must be invoked to explain the regularities observed amongst the heavy nuclei, so that the extreme RUSSELL-SAUNDERS coupling approximation discussed in the last section may become a poor one. In extreme *jj*-coupling, states of a single particle are characterised by j in addition to l and the principal quantum number. States of systems of many particles, on account of the strong coupling, may no longer be characterised by L and S, but the total resultant angular momentum J must still remain a good quantum number. Provided, moreover, that forces depending in a non-linear manner upon charge are ruled out, the isotopic spin T in addition to its ζ-component will remain a good quantum number. This will certainly be so, for example, with symmetric forces; but the Coulomb interaction will eventually give rise to a mixing of T values in heavier nuclei.

Although the *jj*-coupling approximation is more restrictive than the *LS*-coupling approximation (since an additional quantity, j, must now be specified for each particle), similar group theoretical methods may nevertheless be applied. The classification of states of a configuration $(l_j)^n$ according to charge multiplets (i.e. according to T) is again equivalent to a classification according to the irreducible representations of the groups of unitary transformations U_{2j+1} in the $2j+1$-dimensional space spanned by the states of a single particle of momentum j; and corresponding to each representation of U it is possible to find the set of allowed J values. The role of the rotation groups R_{2l+1} is, however, taken by the groups of symplectic[64] transformations Sp_{2j+1}: again, if certain fictitious linear relationships exist between the SLATER integrals, all states belonging to a given representation of Sp, and of a given charge multiplicity, will be degenerate. Thus an analogue of the LAPORTE-PLATT degeneracy exists in *jj*-coupling; and calculation indicates that one is again not far from the ideal limit with conventional forces.

Results of the *jj*-coupling theory are as yet meagre. The complete classification of states of the configurations j^n, with $j = \frac{1}{2}, \frac{3}{2}, \frac{5}{2}$, and $\frac{7}{2}$, has been given by FLOWERS[71]; while a few special cases of the energy matrix for a MAJORANA interaction have been considered by MAYER[72], by KURATH[73] and by TALMI[73a]. These preliminary calculations are of some interest, however, and we state some of the conclusions below.

Mrs. MAYER has taken wave functions appropriate to *jj*-coupling, and has calculated for several configurations the effect of a central force of infinitesimal range (contact interaction), treated as a perturbation. Under these circumstances, she has been able to verify that a configuration containing an even number of neutrons or of protons would have $J=0$, while a configuration containing an odd number of particles of one kind or the other would have $J=j$, in the ground state. Thus, in both RUSSELL-SAUNDERS and *jj*-coupling, it appears to be possible to derive the single-particle model

from the more general individual particle model, provided that forces are of sufficiently short range. This result is encouraging; for the spin-orbit splitting, though large, is comparable with the "ordinary" level spacing. The coupling scheme in nuclei is probably intermediate between the two extremes. Further, Mrs. MAYER has shown that the "pairing energy", i.e. the interaction energy between pairs of equivalent particles, does increase with increasing j, as required in the JENSEN-MAYER model*.

The ordering of levels in jj-coupling, however, depends rather more sensitively upon the range of the central force assumed as interaction. A calculation of the ordering of levels of the $(d_{\frac{5}{2}})^3$ and $(f_{\frac{7}{2}})^3$ configurations as a function of range has been made by KURATH; these configurations are of especial interest in that they are the shell model assignments for the two nuclei Na^{23} and Mn^{55} which show the spin discrepancies, the former having spin $\frac{3}{2}$ instead of the expected $\frac{5}{2}$, the latter $\frac{5}{2}$ instead of $\frac{7}{2}$. The calculations show how the levels of $(d_{\frac{5}{2}})^3$ with $J=\frac{5}{2}, \frac{3}{2}$, and those of $(f_{\frac{7}{2}})^3$ with $J=\frac{7}{2}, \frac{5}{2}, \frac{3}{2}$, change order from that stated at very short range to the reverse at very long range; and in the latter case there is a small region about the crossover point where the $\frac{5}{2}$ level is actually the lowest. The transition occurs at a range bearing a definite ratio to the extension of the nuclear wave function: for heavier nuclei this corresponds to a range so great as to be unacceptable for nuclear interactions; but for light nuclei the crossover takes place at a point of the correct order of magnitude, though still somewhat too large. It has been emphasised by ROSENFELD[50] that the only possible spin discrepancies of this type are, then, Ne^{21} and Na^{23}, both with $(d_{\frac{5}{2}})^3$ configurations, and Ca^{43}, Ti^{47}, V^{51}, and Mn^{55}, with $(f_{\frac{7}{2}})^3$ configurations. The spin of Ne^{21} is undecided between $\frac{3}{2}$ and $\frac{5}{2}$, but Na^{23} is definitely anomalous; the spins of Ca^{43} and Ti^{47} are unknown, while V^{51} is normal, and Mn^{55} has the anomaly. These anomalies are to be expected in the above nuclei, but nowhere else. A similar problem arises, however, in the $g_{\frac{9}{2}}$ shell, as we have mentioned, where the $\frac{9}{2}$ and $\frac{7}{2}$ states appear to compete. A recent calculation by the present author has shown that the $\frac{7}{2}$ level is never the lowest with central forces of any range, but it lies very low in energy at significant ranges. It is most satisfactory that anomalies actually occur at the places where theory can account for them.

Regarding the odd-odd nuclei, the position is not yet clear. On the basis of the JENSEN-MAYER level assignment, and taking the observed spins as given, FEENBERG[74] has shown that the magnetic moments are in excellent agreement with theory, as shown in Table 4, if they are treated according to a two-particle model in which the odd neutron and the odd proton move independently. The spin predictions in extreme jj-coupling for Li^6 and B^{10} are both 3, while in LS-coupling they are both 1: in fact Li^6 has spin 1, while B^{10} has spin 3. This disagreement remains unexplained, although RACAH and ZELDES[75] report encouraging results in the more general intermediate

* All these results have recently been derived in a more general way (for forces of finite range) by FLOWERS and EDMONDS[82, 83]. (See also FLOWERS[83] for a brief summary.) In these papers it is shown that the symplectic group plays an important part in determining the energies of nuclear states in jj-coupling.

Table 4—Magnetic moments of odd-odd nuclei

Nucleus	*Neutron*	*Proton*	*Observed spin*	μ_{Exp}	μ_{calc}
Li^6	$p_{\frac{1}{2}}$	$p_{\frac{1}{2}}$	1	0·82	0·63
B^{10}	$p_{\frac{3}{2}}$	$p_{\frac{1}{2}}$	3	1·80	1·88
N^{14}	$p_{\frac{1}{2}}$	$p_{\frac{1}{2}}$	1	0·40	0·37
Na^{22}	$d_{\frac{5}{2}}$	$d_{\frac{3}{2}}$	3	1·75	1·73
K^{40}	$f_{\frac{7}{2}}$	$d_{\frac{3}{2}}$	4	—1·29	—1·70

coupling. It seems that the odd-odd nuclei constitute an important class which may lead to a better understanding of the nature of nuclear forces.

11. Higher Approximations

It has been shown how the individual particle model can be made to yield, as a result of a first-order perturbation treatment, in both *LS*- and *jj*-coupling, the observed single-particle model for the lowest states of nuclei. No *a priori* justification for the validity of the individual particle model, however, has been given; on the contrary, reasons have been stated why the model might not be expected to hold—the strength of the nuclear interaction and its short range, the correlation energy, and the likelihood of many-body forces, all lead one to expect a behaviour more akin to a liquid drop. If it could be shown that the perturbation treatment does in fact converge fairly quickly, at least for the low-lying states, one could feel considerably happier about the internal consistency of the model; but no such proof has yet been given. A step in this direction would be furnished by considering the second-order perturbation terms, including the effects of interconfigurational mixing. A few calculations along these lines have been performed, and we shall end this review by giving a brief account of them.

Euler[76], using a Gaussian potential, and more recently, Huby[77], with a Yukawa potential and a symmetrical exchange force mixture, have calculated the binding energy per nucleon of an infinitely heavy nucleus (no surface effect), neglecting the Coulomb repulsion, and taking as zero-approximation a Fermi gas confined within the nuclear volume. To second order, the total energy per nucleon may be written

$$E = T + V' + V'',$$

where T, the zero-order energy, is simply the expectation value of the kinetic energy, and V' is the expectation value of the potential energy in the ground state. The last term is the second-order term, summed over all intermediate states:

$$V'' = \sum_{i \neq 0} \frac{|V_{0i}|^2}{T_0 - T_i},$$

where V_{0i} is the matrix element of the interaction between the ground state and the state i. This term may be regarded as arising from interconfigurational mixing. The results of Huby's calculations are not encouraging: in arbitrary units of energy, the terms T, V', and V'', for a nuclear radius that minimises the total energy, are found to be 1·35, —1·41, and —0·35, respectively: and

the total, $T'+V'+V''$, amounts to some 40% of the observed energy per particle. As far as can be seen from three terms, the perturbation method converges only slowly, if at all, and the configurational mixing is quite large.

This calculation is open to objection from the point of view of the individual particle model, however: for it has been shown that the most important characteristic of a nuclear wave function is its symmetry property with respect to permutation of particles. The FERMI degenerate gas model, while preserving total antisymmetry with respect to all coordinates, does not reflect the maximum orbital symmetry required, according to WIGNER, for at least the lighter nuclei in their low-lying states. It may be, although this is speculation, that if the symmetries could properly be taken into account, a second-order perturbation treatment would show better convergence; for certainly there would be considerably fewer low-lying states available for interconfigurational mixing. For higher excitation energies, where the effects of symmetry, due to close level spacing, are no longer so pronounced, the calculation might be expected to hold rather better: the degenerate gas model and BOHR'S liquid drop model are in this respect similar and may even be reconcilable at sufficiently high excitation energies.

A calculation of the effects of interconfigurational mixing in a specific case, with due regard to symmetries, has recently been published by PRESENT[78]. Here the object is to find whether the observed positive quadrupole moment of Li^7 can be explained in terms of mixtures of states on the basis of central exchange forces, taking into account only the states of maximum orbital symmetry for each configuration. The shell model predicts for Li^7 the configuration $1s^4\,1p^3$, which gives rise to a negative quadrupole moment. The completed s-shell has no effect upon the symmetry (or upon the quadrupole moment) so the wave functions of Li^7 are characterised by the partitions [3], [2+1], and [1+1+1], of which the first is symmetrical in the spatial coordinates of all three particles and is lowest in energy in the WIGNER approximation (maximum orbital symmetry). The configurations considered by PRESENT are $1p^3$, $1p^2 2p$, and $1p^2 1f$, of which the $1p^2 2p$ configuration gives rise to two linearly independent ^2P states, labelled (a) and (b). The maximum quadrupole moment obtained, while not large, is positive, and is obtained with the following ratios of wave functions: $1p^3$, $2p^2 1f$, $1p^2 2p$(a), and $1p^2 2p$(b) = 0·344, 0·630, 0·670, −0·190. (This wave function does not affect the value of the magnetic moment.) Since the $1p^3$ function is only present to 12%, the interconfigurational mixing is very large. Present also shows that the inclusion of D states, produced by spin-orbit coupling, increases considerably the quadrupole moment, but the magnetic moment becomes further removed from the experimental value.

This work again is not encouraging; but a great deal more needs to be done before any firm conclusions can be reached about the importance of configurational interaction. The spheroidal well treatment of RAINWATER, introduced to account for the quadrupole moments, is further confirmation that considerable mixing takes place, but of a type which nevertheless allows the single-particle behaviour to remain dominant.

It may be that the solution to the problem lies much deeper, and that a proper account of nuclear phenomena will require the full formalism of a meson field theory, taking proper account of many-body forces[79]; and in this respect at least, the theory is closely connected with the saturation properties of nuclear forces. At present all that can be said is that the evidence presented here is overwhelmingly in favour of a shell model. At its worst the shell model is a valuable mnemonic which can give, in a wide variety of circumstances, useful guidance in the investigation of nuclear properties: why it should work so well we do not yet know.

The author would like to thank Professor PEIERLS, Professor PRYCE, Professor BURCHAM, and Dr. DALITZ for reading this article, and for their helpful comments.

REFERENCES

[1] BARTLETT, T. H.; *Phys. Rev.* 41 (1932) 370.
[2] — *Phys. Rev.* 42 (1932) 145.
[3] — *Nature, Lond.* 30 (1932) 165.
[4] ELSASSER, W.; *J. de Phys.* 4 (1933) 549.
[5] — *J. de Phys.* 5 (1934) 389.
[6] — *J de Phys.* 5 (1934) 635.
[7] GUGGENHEIMER, K.; *J. de Phys.* 5 (1934) 253.
[8] — *J. de Phys.* 5 (1934) 475.
[9] WHEELER, J. A.; *Phys. Rev.* 52 (1937) 1107.
[10] SCHMIDT, T.; *Z. Physik* 106 (1937) 358.
[11] SCHULER, H.; *Z. Physik* 107 (1937) 12.
[12] FEENBERG, E. and WIGNER, E., *Phys. Rev.* 51 (1937) 95.
[13] CONDON, E. U. and SHORTLEY, G. H.; *Theory of atomic spectra.* Cambridge University Press, 1935.
[14] WIGNER, E.; *Phys. Rev.* 51 (1937) 106.
[15] WIGNER, E.; *Phys. Rev.* 51 (1937) 947.
[16] BARKAS, W. H.; *Phys. Rev.* 55 (1939) 691.
[17] BOHR, N.; *Nature, Lond.* 137 (1936) 344.
[18] BOHR, N. and KALCKAR, F.; *Kgl. Dansk. Acad.* (1939).
[19] BREIT, G. and WIGNER, E.; *Phys. Rev.* 51 (1937) 593.
[20] KAPUR, P. L. and PEIERLS, R. E.; *Proc. Roy. Soc.* A. 166 (1938) 277.
[21] HARKINS, W. D.; see e.g. *Phys. Rev.* 79 (1950) 724 for list of references.
[22] MAYER, M. G.; *Phys. Rev.* 74 (1948) 235.
[23] BROWN, H.; *Rev. Med. Phys.* 21 (1949) 625.
[24] GAMOW, G. and CRITCHFIELD, C. L.; *Theory of atomic nucleus and nuclear energy sources.* Oxford University Press, 1949.
[25] GORDY, W.; *Phys. Rev.* 76 (1949) 139.
[26] GRIFFITHS, J. H. E.; *Proc. Roy. Soc.* 170 (1939) 513.
[27] MESCHERYAKOV, C. R.; *C. R. U.S.S.R.* 48 (1945) 555.
[28] HUGHES, D. T., SPATZ, W. D. B. and GOLDSTEIN, N.; *Phys. Rev.* 75 (1949) 1781.
[29] FLOWERS, B. H.; *A.E.R.E.* T/R 437, Nov. 1949.
[29a] MEITNER, L.; *Nature Lond.* 165 (1950) 561.
[30] SWIATECKI, W.; *Phys. Rev.* 83 (1951) 178.
[31] KOWARSKI, L.; *Phys. Rev.* 78 (1950) 477.
[32] BERTHELOT, A.; *J. de Phys.* 3 (1942) 17.
[33] GLÜCKAUF, E.; *Proc. Phys. Soc.* 61 (1948) 25.
[34] PRYCE, M. H. L.; *Proc. Phys. Soc.* 63 (1950) 692.
[35] BETHE, H. A. and BACHER, R. F.; *Rev. Mod. Phys.* 8 (1936) 165.
[36] THOMPSON, S. G., GHIORSO, A., RASMUSSEN, J. O. and SEABORG, G. T.; *Phys. Rev.* 76 (1949) 1406.

[37] DUCKWORTH, H. E. and PRESTON, R. S.; *Phys. Rev.* 82 (1951) 468.
[38] KINSEY, B. B., BARTHOLOMEW, G. A. and WALKER, W. H.; *Phys. Rev.* 83 (1951) 519.
[39] HARVEY, J. A.; *Phys. Rev.* 81 (1951) 353.
[40] SUESS, H. E. and JENSEN, H. (prepublication paper).
[41] FEENBERG, E.; *Phys. Rev.* 77 (1950) 771.
[42] NORDHEIM, L. W.; *Phys. Rev.* 75 (1949) 1894.
[43] MAYER, M. G.; *Phys. Rev.* 75 (1949) 1969.
[44] — *Phys. Rev.* 78 (1950) 16.
[45] HAXEL, O., JENSEN, J. H. D. and SUESS, H. E.; *Z. Physik* 128 (1950) 295.
[46] FEENBERG, E. and HAMMACK, K. C.; *Phys. Rev.* 75 (1949) 1877.
[47] SWIATECKI, W. J.; *Proc. Phys. Soc.* A. 63 (1950) 1208.
[47a] KEILSON, J.; *Phys. Rev.* 82 (1951) 759.
[48] CASE, K. M. and PAIS, A.; *Phys. Rev.* 80 (1950) 203.
[49] HUGHES, J. and LE COUTEUR, K.; *Proc. Phys. Soc.* A. 63 (1950) 1219.
[50] ROSENFELD, L.; *Physica* 17 (1951) 461.
[51] — *Nuclear Forces.* North Holland Publishing Co., 1948.
[52] RAINWATER, J.; *Phys. Rev.* 79 (1950) 432.
[52a] BOHR, A.; *Phys. Rev.* 81 (1951) 134.
[53] WEISSKOPF, V. F. and BLATT, J.; privately circulated chapter from forthcoming book "Nuclear Theory".
[53a] ROSE, M. E., GOERTZEL, G. H., SPINRAD, B. I., HARR, J. and STRONG, P.; *Phys. Rev.* 83 (1951) 79.
[54] GOLDHABER, M. and SUNYAR, A. W.; *Phys. Rev.* 83 (1951) 906.
[55] AXEL, P. and DANCOFF, S.; *Phys. Rev.* 76 (1949) 892.
[56] SKYRME, T. H. R.; *Progress in Nuclear Physics, Vol I.* London, 1951.
[57] WU, C. S.; *Rev. Med. Phys.* 22 (1950) 386.
[58] FEENBERG, E. and TRIGG, G.; *Rev. Med. Phys.* 22 (1950) 399.
[59] SHULL, H. and FEENBERG, E.; *Phys. Rev.* 75 (1949) 1768.
[60] NORDHEIM, L. W.; *Phys. Rev.* 78 (1950) 294.
[61] MCGINNIS, C. L.; *Phys. Rev.* 81 (1951) 734.
[62] CHRISTIAN, R. S. and NOYES, H. P.; *Phys. Rev.* 79 (1950) 85.
[63] HEISENBERG, W.; *Z. Physik* 77 (1932) 1.
[64] WEYL, H.; *Classical groups.* Princeton University Press, 1946.
[65] RACAH, G.; *Phys. Rev.* 76 (1949) 1352.
[66] JAHN, H.; *Proc. Roy. Soc.* A. 201 (1950) 516.
[67] LAPORTE, O. and PLATT, J. R.; *Phys. Rev.* 61 (1942) 305.
[68] SWIATECKI, W. J.; *Proc. Roy. Soc.* A. 205 (1951) 238.
[69] HUND, F.; *Z. Phys.* 105 (1937) 202.
[70] FLOWERS, B. H.; *A.E.R.E.* T/R 679 Feb. 1951; *Proc. Roy. Soc.* A 210 (1951) 497.
[71] FLOWERS, B. H.; *A.E.R.E.* T/R 713 May 1951; *Proc. Roy. Soc.* A 212 (1952) 248.
[72] MAYER, M. G.; *Phys. Rev.* 78 (1950) 22.
[73] KURATH, D.; *Phys. Rev.* 80 (1950) 98.
[73a] TALMI, I.; *Phys. Rev.* 82 (1951) 101.
[74] FEENBERG, E.; *Phys. Rev.* 76 (1949) 1275.
[75] RACAH, G. and ZELDES, N.; *Phys. Rev.* 79 (1950) 1012.
[76] EULER, H.; *Z. Phys.* 105 (1937) 553.
[77] HUBY, R.; *Proc. Phys. Soc.* 62 (1949) 62.
[78] PRESENT, R. D.; *Phys. Rev.* 80 (1950) 43.
[79] SCHIFF, L. I.; *Phys Rev.* 84 (1951) 1.
[80] BUTLER, S. T.; *Proc. Roy. Soc.* A. 208 (1951) 559.
[81] FLOWERS, B. H. and EDMONDS, A. R.; *A.E.R.E.* T/R 875 March 1952.
[82] FLOWERS, B. H. and EDMONDS, A. R.; *A.E.R.E.* T/R 917 May 1952.
[83] FLOWERS, B. H.; *Phys. Rev.* 86 (1952) 254.
[84] MAYER, M. G., MOSKOWSKI, S. A., and NORDHEIM, L. W.; *Rev. Med. Phys.* 23 (1951) 315.
[85] NORDHEIM, L. W.; *Rev. Med. Phys.* 23 (1951) 322.

IONISATION BY FAST PARTICLES

T. E. Cranshaw

1. Introduction 271
2. Theory of ionisation 271
3. Statistics of ionisation losses 273
(i) Small energy loss 273
(ii) Large energy loss 274
(iii) Loss of entire energy 275
4. The behaviour of W, the energy loss per ion pair 276
5. The determination of Δ_0 from experimental results 277
6. Comparison with experiment 279
7. The behaviour in liquids and solids 280
8. The behaviour of scintillators 281
9. Photographic plates 281
10. The logarithmic increase in energy loss with energy 282

1. Introduction

When charged particles pass through matter, they lose energy by making collisions with the atoms present, exciting or ionising them. If the energy transferred is large enough, the electron liberated in the collision may in turn make collisions, producing further excitation or ionisation. There exist several ways in which quantities related to the energy transfers in these collisions can be measured. For instance, in gases [1, 2], and some liquids [3, 4, 5, 6] and solids [7, 8, 9], the ions can be collected by an electric field and measured by the change of potential they produce in an electrometer or at the input of an amplifier. Under suitable conditions, the ions produced can be counted directly in cloud chamber photographs [10]. Scintillations produced in some materials by the collision processes were used in the earliest experiments on radioactivity for counting particles, and recently the development of photomultipliers has enabled measurements of the quantity of light produced by individual particles [11]. Finally the passage of charged particles through photographic plates renders some of the grains developable, and the number of such grains is related to the ionisation produced [12]. In this paper, we review the theory of energy loss, and its influence on experiments of these types.

2. Theory of Ionisation

When a fast (but non-relativistic) particle passes through matter, the probability per cm of transferring an amount of energy between ε and $\varepsilon + d\varepsilon$ to an electron (considered as free) is given classically by the well known formula [13]

$$W(\varepsilon)\,d\varepsilon = \frac{2\pi N e^4 \varrho}{m v^2} \frac{\Sigma Z}{\Sigma A} \frac{1}{\varepsilon^2}\, d\varepsilon \qquad (1)$$

where N is Avogadro's number, m the mass of the electron, e the electronic charge, v the velocity of the particle, ϱ the density of the substance, ΣZ the

sum of the atomic numbers in a molecule of the substance, and ΣA the sum of the atomic weights. This equation is assumed to be true for values of ε between $\varepsilon_{\min}$ and $\varepsilon_{\max}$ where $\varepsilon_{\min}$ is some ionisation potential of the atom, and $\varepsilon_{\max}$ is given by

$\varepsilon_{\max} = E_0$ for electrons

$\varepsilon_{\max} = \frac{4E_0}{\mu}$ for particles of mass μ electron masses, and $\mu \gg 1$

where E_0 is the energy of the incident particle.

To obtain the energy loss per cm of the particle, equation 1 may be integrated from $\varepsilon_{\min}$ to $\varepsilon_{\max}$. By a quantum mechanical treatment, and using relativistic equations, BETHE[14] obtained the expression

$$\frac{\partial E}{\partial x} = \frac{4\pi N e^4 \varrho \Sigma Z}{m v^2 \Sigma A}\left\{ln \frac{2mv^2}{I} - ln(1-\beta^2) - \beta^2\right\} \qquad (2)$$

I in this formula is an "effective excitation energy" which is best determined empirically. Values obtained for H[15], He[16], Air[13] and Al[17] show that $I \approx I_0 Z$, with $I_0 = 13{\cdot}5$ ev[18]. The energy loss is shown to be dependent on the velocity only, and is usually plotted as a function of $\beta/(1-\beta^2)^{\frac{1}{2}}$, which is the momentum of the particle in units of mc. The relation is plotted in Fig. 1. It will be seen that the curve has a minimum, for which the value of β is about 0·96. Above this value, the energy loss rises logarithmically with the momentum.

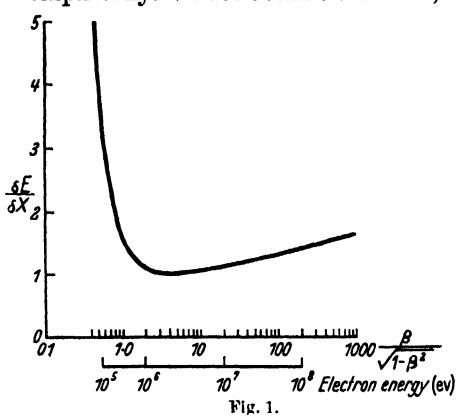


Fig. 1.

It has been pointed out by SWANN[19] that the state of condensation of the matter must have an effect on the energy loss, especially when β is nearly unity. FERMI[20] showed under certain simplifying assumptions that when the velocity of the particle exceeds a certain value, the energy loss should tend to a constant value. A more detailed calculation by HALPERN and HALL[21] and WICK[22] shows that the energy loss curve falls gradually below the value given by equation 2, and earlier than calculated by FERMI.

It has been shown by FRANK and TAMM[23], and others, that when the particle velocity exceeds the velocity of propagation of an electro-magnetic disturbance in the medium, part of the radiation field of the particle does not fall off exponentially with distance, but becomes a wave analogous to the bow wave produced by a ship. This radiation is called the CERENKOV[24] radiation after its discoverer. A comprehensive treatment of ionisation, including the radiation phenomena, has been given by SCHÖNBERG[25].

3. The Statistics of Ionisation Losses

(i) *Small energy loss*

To determine the energy loss of fast particles, the ionisation in a section of track is often measured. The amount of ionisation in equal lengths of track is, however, subject to fluctuations, partly because the number of collisions in a given length of track is governed by Poisson's Law, and partly because the energy transferred at each collision follows a distribution law similar to eq. (1). The resulting distribution has been discussed by Bohr[26, 27], Williams[28], Landau[29], and Blunck and Leisegang[30].

Following the treatment by Bohr, which gives a clear physical picture of the processes involved, we divide the collisions into two groups according as the energy transferred is greater or less than ξ, where ξ is chosen so that on the average just one collision transferring more energy than ξ occurs in the path length considered. Then the collisions transferring less energy than ξ are numerous and give a total energy loss with an approximately Gaussian distribution, whereas those rare collisions which transfer more than ξ form a distribution such that the probability of transferring ε falls off inversely as ε^2. The width of the distribution is caused mainly by collisions transferring quantities of energy in the neighbourhood of ξ, since the smaller energy transfers occur so frequently that their fluctuation is small, whereas the larger transfers occur so infrequently that they contribute to the distribution a long but low tail. In this region, the excess over the most probable value is mainly the result of one collision transferring the whole of the excess energy.

From eq. (1), we have

$$\xi = \frac{2\pi N e^4 \varrho}{m v^2} \cdot \frac{\Sigma Z}{\Sigma A} x, \tag{3}$$

where x is the length of track considered.

The value of ξ being proportional to x, it is clear from the foregoing discussion that the *relative* width of the distribution will be nearly independent of x. In fact, the whole distribution changes only slowly with x, and provided that x is already large enough for a substantial number of collisions to have taken place, no appreciable increase of accuracy of the determination of the most probable value of the ionisation results from an increase of x. This result remains true as long as $\xi < \varepsilon_{max}$, the maximum transferable energy. The case for $\xi > \varepsilon_{max}$ is discussed later.

This result was obtained more quantitatively by Landau, who by a Laplace transformation was able to deduce an expression for the whole distribution of energy losses. If Δ is the observed energy loss and Δ_0 the most probable energy loss, Landau gives the distribution of the quantity $(\Delta - \Delta_0)/\xi$, as a computed curve, shown in Fig. 2. For Δ_0, Landau obtains the expression

$$\Delta_0 = \xi \left[ln \frac{3 \cdot 10^3 \xi \beta^2}{Z^2 (1-\beta^2)} + 1 - \beta^2 \right] \tag{4}$$

where I has been put equal to $I_0 Z$ with $I_0 = 13{\cdot}5$ ev.

This expression differs slightly from the formula eq. (2) which gives the mean energy loss, notably in that x, contained in ξ appears in the logarithmic

term. This is a consequence of the law of energy transfer, eq.(1), as pointed out by WILLIAMS[28].

A number of experiments are reported (see § 6) in which the widths of the energy loss distributions have been measured. In most cases, the width is considerably greater than that calculated by LANDAU. A possible cause of this extra width has been investigated by BLUNCK and LEISEGANG[30], who point out that when ε is near the atomic binding energies, resonance effects take place. BLUNCK and LEISEGANG show how a knowledge of the binding energies can be used to correct LANDAU's theory. They find that the correction is small when Z is small, but may be large for large Z. Thus we may expect the LANDAU theory to be adequate when $Z < 10$, but the width is nearly doubled for Argon.

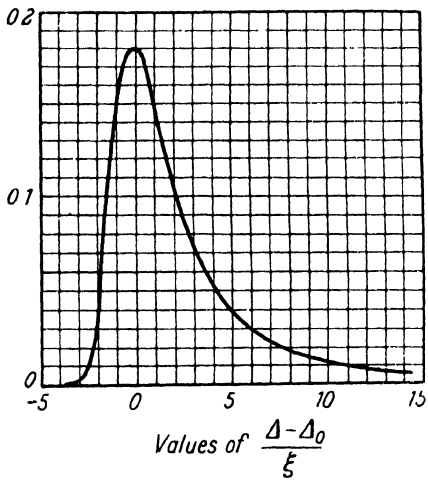


Fig. 2.

(ii) *Large energy loss*

When the path length x is made sufficiently large, the value of ξ as taken from eq.(3) becomes larger than $\varepsilon_{\max}$. There are then no rare, large energy transfers, and the distribution of energy losses becomes Gaussian. The width can then be obtained more directly. Using the classical law, eq. (1), we may write the probability of transfer of energy between ε and $\varepsilon + d\varepsilon$ in a single collision as

$$W(\varepsilon)\, d\varepsilon = \frac{\varepsilon_{\min}\, \varepsilon_{\max}}{\varepsilon_{\max} - \varepsilon_{\min}} \frac{d\varepsilon}{\varepsilon^2}\,. \tag{2a}$$

The mean energy loss for n collisions is then

$$\overline{\varepsilon_n} = n \frac{\varepsilon_{\min}\, \varepsilon_{\max}}{\varepsilon_{\max} - \varepsilon_{\min}} ln \frac{\varepsilon_{\max}}{\varepsilon_{\min}} = n\, C\,.$$

and the mean square deviation is

$$\overline{\delta_n^2} = n\, (\varepsilon_{\max}\, \varepsilon_{\min} - C^2) = n\, D\,.$$

If λ is the most probable number of collisions in the length of track considered, and λ is large, we may write the probability of n collisions occurring as

$$p_\lambda(n) = \frac{1}{\sqrt{2\pi\lambda}}\, e^{-\frac{(n-\lambda)^2}{2\lambda}}\,.$$

Then $\Delta_0 = \overline{\varepsilon_\lambda} = \lambda\, C$, and

$$\overline{\delta_\lambda^2} = \int_{-\infty}^{\infty} \frac{nD + (n-\lambda)^2\, C^2}{\sqrt{2\pi\lambda}}\, e^{-\frac{(n-\lambda)^2}{2\lambda}}\, dn$$

$$= \lambda\, \varepsilon_{\max}\, \varepsilon_{\min}\,.$$

The relative standard deviation is thus given by

$$\sigma = \sqrt{\frac{\varepsilon_{max}}{\Delta_0 \ln (\varepsilon_{max}/\varepsilon_{min})}} \tag{5}$$

and the total relative width at half height is

$$2{\cdot}6 \sqrt{\frac{\varepsilon_{max}}{\Delta_0 \ln (\varepsilon_{max}/\varepsilon_{min})}}.$$

This result holds if $(\delta_\lambda^2)^{\frac{1}{2}} > \varepsilon_{max}$, i.e. if $\Delta_0 > \varepsilon_{max} \ln (\varepsilon_{max}/\varepsilon_{min})$ or $\xi > \varepsilon_{max}$, where ξ has the meaning given by eq. (3).

This case may arise when the incident particle is heavy and of moderate energy. For instance, for 150 Mev protons, $\varepsilon_{max} \sim 0{\cdot}3$ Mev. If the protons pass through a proportional counter of usual dimensions, ξ will be much smaller than ε_{max}, and, if the gas is composed of light elements the width given by the LANDAU formulae will hold. If, on the other hand, the particles pass through a thickness of a scintillator, the inequality above may hold, and the width is then smaller. In Fig. 3, the width of the distribution to be expected for different values of Δ_0 is plotted for 150 Mev protons. The dotted region is drawn to join as smoothly as possible the two regions where the analyses hold. In this calculation, we have of course neglected the influence of nuclear collisions.

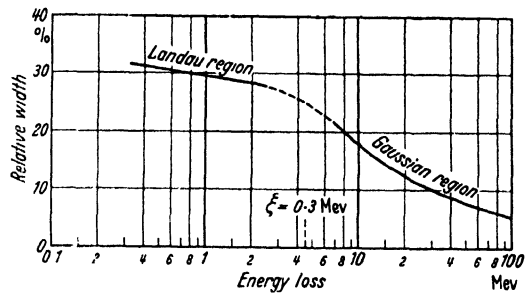


Fig. 3. Width (at half. maximum) of the energy-loss distribution curve, in % of the most probable energy loss.

(iii) *Loss of entire energy*

If in eq. (5), we put $\Delta_0 = E$, the initial energy of the particle, the expression gives the standard deviation of the energy distribution of those primary particles which lose all their energy in just the given track length. By using the range-energy relation, the straggling in range can be deduced. If the range is proportional to the $n'th$ power of the energy, (n is about $\frac{3}{2}$ for natural α-particles) we obtain the result that the standard relative deviation from the mean range is $n\sqrt{m/2ML}$, where M is the mass of the particle, m the mass of the electron, and L the term in curly brackets from eq. (2).

In the preceding sections, we have assumed that W, the energy loss per ion pair is a constant, that is to say that a measurement of the ionisation produced is a measure of the energy loss of the particle. When the entire range of the particle is contained in the material, the total ionisation produced is then a measure of the initial energy of the particle. FANO[31] has considered the fluctuation in the number of ions produced by particles of constant

energy. It is clear that if particles could only lose energy by ionizing atoms, there would be no fluctuation in the total number of ions produced. However, energy is also lost by collisions which excite the atom without ionising it, and also some energy is carried away by the electrons removed from the atom, and some of this energy may excite atoms without ionising them. By considering the probabilities of excitation and ionisation, FANO finds that the standard deviation of the number of ions is $F\sqrt{n}$ where n is the mean number of ions produced, and F a factor which is difficult to estimate but should lie between 0·3 and 0·5. Experimentally, it is usually found impossible to separate these fluctuations from other instrumental fluctuations, but this result seems to be in agreement with the work of HANNA *et al.*[32], and CURRAN *et al.*[33].

4. THE BEHAVIOUR OF W, THE ENERGY LOSS PER ION PAIR

The energy loss per ion pair is found, for all kinds of matter, to be in the neighbourhood of 30 ev. If values are substituted in the expression for the standard deviation of the number of ion pairs given in the last paragraph, it will be seen that the total number of ion pairs produced is a good measure of the energy of the particle, better in fact, in most cases than the range of the particle. With modern electronic techniques rapid accurate measurements of the size of pulses from ionisation chambers can be made. When we consider that ionisation chambers allow large areas of source, and large solid angles, to be used, it is clear that this is an important method of measuring the energy of particles. It can only give accurate values however, if the behaviour of W is known, and this has been frequently neglected.

The value of W may vary with (i) the gas, (ii) the mass and charge of the ionising particle, (iii) the velocity of the particle. Accurate absolute determinations of W are very difficult, and in general the experiments give the mean value of W over a range of velocities from the maximum to zero. Early work has shown that W varies surprisingly little with any of the above parameters. An explanation of the lack of correlation between W and the ionisation potential has been given by FANO[34] in terms of a compensating number of exciting collisions which "waste" energy when the ionisation potential is low.

The experimental evidence on the variation of W with the mass and charge of the particle, and with its velocity is at present conflicting, and little more than qualitative results are obtainable from theory. The variation with mass seems to be very small, as would be expected. CRENSHAW[35] has measured the loss of energy of protons and deuterons in hydrogen and deuterium, and finds it to be the same for both particles if their velocities are the same.

In air, the failure of the HOLLOWAY-LIVINGSTON[36] range-energy relations for α-particles, which depend on the assumption of constant W value, indicates that the assumption is not valid, and this is confirmed by JESSE, FORSTAT and SADAUSKIS[37]. These workers however report strict proportionality between the energy loss of α-particles and their total ionisation in argon. It is to be expected that W will be nearly constant when the ionisation potential is high, as it is for argon, because as FANO points out, in such gases relatively little of the energy loss is "wasted" in excitation, and therefore variations in excitation

probability have only a small effect on W. Nevertheless, CRANSHAW and HARVEY[38] measuring the total ionisation of natural α-emitters in argon found evidence of a variation of W, and proposed the empirical relation

$$W = 27{\cdot}5 + 1{\cdot}9\,E^{-\frac{1}{2}} \tag{6}$$

where W is in electron volts per ion pair, and E in Mev. The results of HANNA[39] on the disintegration of Boron by slow neutrons show that W is not the same for the α-particle and the Li fragment, the ratio W_{Li}/W_α being greater than unity by about 5%. The results are concordant with the assumption that eq. (6) holds for α-particles, and that W for the Li fragment is the same as for an α-particle of the same velocity. On the other hand TUNNICLIFFE and WARD[40] have measured the ionisation of recoil protons, deuterons, and α-particles in various gases. They find a variation in W for different particles which is roughly described by the above assumptions, but there remain contradictions which cannot be explained as the result of experimental error.

HANNA[39] has described the variation of $W^* = dE/dI$, the instantaneous value of W at energy E, in the following terms:

> At high energy, greater than 4 Mev say, W^* is constant, i.e. $E = W^* I + \varepsilon_0$ where ε_0 is a constant of integration. At intermediate energies, where W^* is not constant, we can still write $E = W^* I + \varepsilon_\alpha$, where ε_α is a small energy (less than 100 kev) which diminishes as E gets less. This has a physical interpretation. Below a certain minimum energy the α-particle will produce no ionisation, expending its energy in elastic collisions, so that $I = 0$ and $\varepsilon_\alpha = E$. At higher energies ionisation becomes a progressively more probable event (ε_α increasing with, but not as fast as, E) until finally, at a sufficiently high energy which is here taken as 4 Mev, the fraction of energy absorbed in ionisation attains a constant value, and ε_α also reaches its maximum and constant value, ε_0.

The value of ε_0 in the case of α-particles appears to be about 80 kev from the work of CRANSHAW and HARVEY, $\varepsilon_\alpha = 47$ kev for the α-particles, and $\varepsilon_{Li} = 65$ kev for the Li fragment from the B disintegration from the work of HANNA. Present experimental data are too scarce to permit any more definite statement.

5. THE DETERMINATION OF Δ_0 FROM EXPERIMENTAL RESULTS

A procedure for determining the most probable value of the ionisation from a limited number of observations has been given by BEHRENS[41]. It consists, briefly, in finding the best fit with the experimental data of a curve with two variable parameters, one governing the most probable value, and one the width of the curve. If only light elements are present (see § 6) the LANDAU curve itself may be taken. The distribution of energy losses of 2 Mev electrons in argon and krypton has been measured by Miss ROTHWELL[42], who used many particles so that statistical fluctuations were small. For experiments with these gases, it is reasonable to assume that these curves represent the probability distribution underlying any experiment with fewer particles. This procedure has been used in calculating the most probable value of energy loss in argon for the experiments of DUNLAP and CRANSHAW given in § 6, and the experiment of BECKER mentioned in § 10.

This procedure might also be applied to cloud chamber results. In such a case, the track would be divided into n cells, and the number of drops x in each cell counted. Then x should be distributed according to the probability distribution already discussed, and the most probable value of the ionisation can be determined by the curve-fitting procedure. It is usual to divide the track into cells and then to reject those in which x exceeds some chosen value x_1, in the neighbourhood of twice the most probable value. The mean of those values for which $x < x_1$ is then taken.

If x is distributed according to some function $f(x)$, then the mean of the values up to x_1 is given by

$$\bar{x} = \frac{\int_{-\infty}^{x_1} x f(x)\, dx}{\int_{-\infty}^{x_1} f(x)\, dx}.$$

(In the present case, the integrals will go from 0 to x_1 only.)

The object of the experiment is usually to determine some change in $\bar{x}$. Then

$$\frac{\partial \bar{x}}{\partial x_1} = \frac{f(x_1)}{\int_{-\infty}^{x} f(x)\, dx} (x_1 - \bar{x}).$$

By inspection of LANDAU's curve $\partial \bar{x}/\partial x_1 \sim 5\%$ for values of x_1 about twice the most probable value of x. Thus if the scale of x changes but x_1 remains constant, the change of scale will be underestimated by a few percent. The error is made smaller by making x_1 larger, but in that case the mean $\bar{x}$ is found to be unreasonably influenced by rare large values of x. The curve fitting procedure avoids these difficulties. Moreover the standard deviation of the most probable value so obtained can be determined from the curve fitting, whereas estimates of the error of $\bar{x}$ for all $x < x_1$ cannot be made on the data after rejection of those $x > x_0$, and estimates based on internal consistency are likely to overstimate the accuracy.

Another objection to the use of mean values is pointed out by PODGORETSKI[43]. He considers the contribution to the ionisation in an experiment by the large energy transfers. His assumptions are: the law given by eq. (1) for the distribution of energy transfers; that the angle of emission of the δ-rays is given by

$$\theta(\varepsilon) = \sqrt{\frac{2mc^2}{\varepsilon}};$$

that the loss of energy of δ-rays is the same as the primary particle; and that scattering is negligible. PODGORETSKI then shows that the distance r between the points at which the particle and a δ-ray emerge from a wall is distributed according to

$$n(r)\, dr = \frac{2\pi N e^4 \varrho}{mv^2} \frac{\Sigma Z}{\Sigma A} \left\{ \sqrt{\frac{2mc^2}{\Delta}} - \frac{sr}{\varepsilon_{\max} - \Delta} \right\}$$

where Δ is the energy loss in the wall, s is the ionisation loss per cm, and the other quantities refer to the gas outside the wall. With practical values for high energy particles and thin walls, the values of r can be of the order of 10 m, and

all these δ-rays will miss the counter. PODGORETSKI shows that the loss due to these missed rays is

$$\frac{\Delta I}{I} = \frac{ln\,(\varepsilon_{max}/\Delta) - (\varepsilon_{max} - \Delta/\varepsilon_{max})}{ln\,(\varepsilon_{max}/\varepsilon_{min})}.$$

If $\Delta \geq \varepsilon_{max}$, there is no loss of ionisation, but if the walls are thin, the loss may be large. For instance, if a meson of energy 5×10^8 ev passes through a chamber with Al walls 1 mm thick, $\Delta I/I \sim 20\%$. This reduction of the mean value is caused by the loss of the few highly energetic δ-rays, whereas the most probable value is scarcely affected.

6. COMPARISON WITH EXPERIMENT

In most of the published experimental work, insufficient attention has been paid to the foregoing considerations. When experimental determinations of a

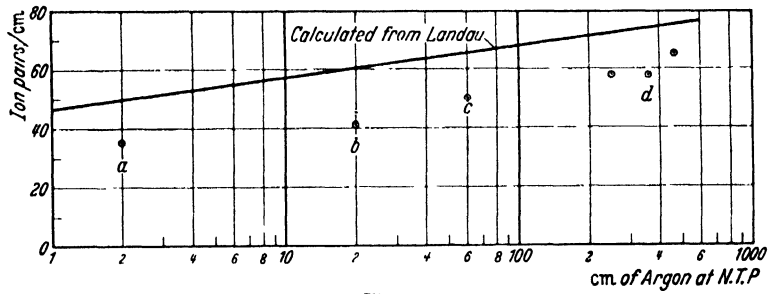


Fig. 4.

(*a*) STUHLINGER, E.; *Z. Physik* 44 (1942) 208. (*c*) SWANN, W. F. G.; *Phys. Rev.* 43 (1933) 775.
(*b*) CRANSHAW, T. E.; *Thesis* Cambridge University 1951. (*d*) DUNLAP, C.; *Phys. Rev.* 67 (1945) 67.

quantity are distributed according to some law such as the LANDAU distribution, it immediately appears unreasonable to give the *mean* value as the result, because it is found that the inclusion of a few rare observations a long way along the tail of the distribution affect the mean value to a large extent. It seems undesirable to weight these observations so highly. It is therefore safe to assume that published values of the specific ionisation refer to values near the *most probable* value. On this assumption, we may check the agreement of the experiments with eq.(4). In Fig. 4 are shown values of the specific ionisation for cosmic ray mesons in argon. All the data refer to the normal cosmic ray spectrum except the point due to CRANSHAW where the value refers to minimally ionising particles. Accordingly another point is shown dotted above this point to allow for the increase of energy loss with energy which may occur for mesons (see § 10). The data are rather meagre, but fortunately cover a wide range of energy loss. Although all the points fall below LANDAU's calculated value, the upward trend is clearly shown.

Several experiments have also been made recently which enable us to compare the widths of experimental distributions with the widths predicted by LANDAU, and by BLUNCK and LEISEGANG. The results are summarised in the accompanying table, where the widths given are total widths at half-height. The energy losses concerned are all in the region $\xi < \varepsilon_{max}$. In this region, as

already pointed out, the width changes only slowly with Δ_0, and only one calculated value is given although the experimental values refer to different values of Δ_0. Results obtained by workers with photomultipliers and scintillators are included in the table. The two experiments on mica and Al were made by measuring the energy of originally monokinetic electrons after passing through the layer of matter. Another experiment[44] in which the original electrons had a relatively wide distribution of energies is not included, but is discussed by BLUNCK and LEISEGANG. It should be pointed out that the experimental values are total widths, and include any spreading of the distribution which may be caused by instrumental factors. The quoted values are thus upper limits of the values due to the statistical processes of ionisation. In the proportional counter and ion chamber results, instrumental factors should be small compared with the quoted values. This may not be true for the scintillator results, where it is rather difficult to ensure that the photomultiplier receives the same fraction of the light generated when the light is generated at different parts of the crystal.

It will be seen that in general the agreement with the theory of BLUNCK and LEISEGANG is quite good, and that for light elements, the theory of BLUNCK and LEISEGANG does not differ significantly from that of LANDAU. In particular, the distributions in solids seem to obey the same law as in gases.

Table 1—Width (at half-maximum) of the energy-loss distribution curve, in % of the most probable energy loss

Substance / *Particles*	*Argon*	*Krypton*	*Mica*	*Anthracene*	*Pyrene Xylene*	*Al.*
Electrons	50[1]	65[1]	90[2]			>100[7]
Mesons	55[6] 65[8]	75[5]		50[3]	37[4]	
Calculated LANDAU .	37	39	45[2]	32[3]	32[4]	39[7]
Calculated BLUNCK, LEISEGANG	60		80	35	35	56[7]

[1] ROTHWELL, P.; *Proc. Phys. Soc.* B 64 (1951) 1911.
[2] WHITE, P. and MILLINGTON, G.; *Proc. Roy. Soc.* 120 (1928) 701.
[3] ROSER, F. X. and BOWEN, T.; *Phys. Rev.* 82 (1951) 284.
[4] NEY, E. P. and THON, D. M.; *Phys. Rev.* 81 (1951) 1068.
[5] BECKER, et al; *Proc. Phys. Soc* A 65 (1952) 437.
[6] CRANSHAW, T. E.; *Thesis*, Cambridge University 1951.
[7] BIRKHOFF, R. D.; *Phys. Rev.* 82 (1951) 448.
[8] DUNLAP, C.; *Phys. Rev.* 67 (1945) 67.

7. THE BEHAVIOUR IN LIQUIDS AND SOLIDS

In liquids, such as liquid argon[3,4,5], or helium[45], or solids such as diamonds[7,8,9], the collection of electrons has been demonstrated. The course of the phenomena is expected to be the same in these substances as in gases, but there are two features which may be expected to affect the details. Firstly, the density of ionisation is so much higher, that some recombination is almost unavoidable. Secondly, the energy required to make an ion pair may be much less than in

gases. For instance, FREEMAN and VAN DER VELDEN[9], AHEARN[8], and McKAY[7] agree that in diamonds, the energy loss per ion pair is about 8 ev. SEITZ[46], by a theoretical argument deduces a value even lower than this, and suggests 3 ev per ion pair in liquid argon. HUTCHINSON[4], however, obtains about 25 ev per ion pair.

Both these features will have some effect on the statistics of the ionisation process. If the energy required for the formation of an ion pair is much smaller than in gases, there will be a narrowing of the distribution. However, this effect depends only on the logarithm of the ionisation energies, and the effect is therefore small. The effect of recombination is to make the ionisation collected a non-linear function of the energy loss of the particle. HUTCHINSON[4] finds that for α-particles the number of ion pairs collected is much smaller than expected. If the non-linearity is appreciable in the energy region ξ for δ-rays, then the distribution in the region of the most probable value may be considerably narrowed by this effect, although the long tail will remain.

8. THE BEHAVIOUR OF SCINTILLATORS

Two groups of substances have come into use recently as scintillators. These are organic such as naphthalene, or inorganic, such as potassium iodide. The inorganic crystals are found to give a light output proportional to the energy of the particle when the whole range of the particle is contained in the crystal. From this it follows that the light yield is proportional to the ionisation, and all the previous theory for gases, or solids applies directly. The organic crystals, however, show marked deviations from linearity, the light output falling as the ionisation density increases. In this case, the same considerations as for the recombination in solids and liquids apply, and the distribution will be narrowed. JENTSCHKE[47] and HOPKINS[48] have given curves of light output against electron energy, which show that for many scintillators, the non-linearity is considerable in the energy region near 20 kev. For a total energy loss of about 200 kev, the effect of this non-linearity may be appreciable.

9. PHOTOGRAPHIC PLATES

The passage of ionising particles through photographic plates renders some of the grains developable. The number of grains per unit length is a monotonic function of the ionisation, or energy loss, but the function is not yet well known. LATTES *et al.*[12] have shown how the grain density can be used to make deductions without knowing the law exactly.

BLAU[49] has made the interesting assumption that the ionisation in the photographic grains can be treated by analogy with strong electrolytes. On this assumption, the probability of a grain becoming developable may be written

$$P = C\left\{1 - e^{-b\,(dE/dR)^{\frac{1}{2}}}\right\}$$

where dE/dR is the loss of energy per unit length of the particle, b and c are constants which can be chosen so that the formula fits the empirical data.

The number of grains per unit length for a constant energy of particle is found to be distributed very nearly according to the POISSON Law, as is to be expected, since there is a constant small probability that grains on the path of the particle should become developable.

10. THE LOGARITHMIC INCREASE IN ENERGY LOSS WITH ENERGY

Experiments have been made to observe the relativistic increase in energy loss with energy which is predicted by eq. (2), using nearly all the methods of observing ionisation which are mentioned in the introduction.

For electrons, the cloud-chamber experiments of HAZEN[50], CORSON and BRODE[51], and SEN GUPTA[52] show a close agreement with the BETHE theory. For mesons, the evidence is not yet very convincing. The points obtained by SEN GUPTA up to 5 Bev do not show the predicted increase, and points obtained by GOODMAN, NICHOLSON and RATHGEBER[53] with a proportional counter up to 50 Bev confirm these results. On the other hand, experiments by BECKER *et al.*[54] with proportional counters, and by GHOSH *et al.*[55] with a cloud chamber show satisfactory agreement with the BETHE theory, and not with the constant value found by other workers.

In scintillators, solid or liquid ion chambers, and photographic plates, the density effect sets in at quite low velocities, and limits the expected rise. PICKUP and VOYVODIC[56], measuring the energies and ionisation of cosmic ray particles by Coulomb scattering and grain counts respectively find a small increase of ionisation up to a limiting plateau, in agreement with the theories of WICK, and HALPERN and HALL. WHITTEMORE and STREET[57] using a crystal of silver chloride as an ionisation chamber found a small increase in ionisation, and conclude that the rise is limited by the density effect. BOWEN and ROSER[58] using anthracene with a photomultiplier find that the ionisation is almost independent of energy, and draw the same conclusion. It is clear that these experiments could be explained if the μ-meson ionisation does not show the relativistic rise, as suggested by the experiments of SEN GUPTA, and GOODMAN, NICHOLSON and RATHGEBER. Until more evidence is found confirming the relativistic rise for μ-mesons in gases, it is perhaps premature to consider that the HALPERN and HALL cut-off has been demonstrated.

In conclusion, the CERENKOV radiation for μ-mesons has been detected by JELLEY[59].

REFERENCES

[1] WILKINSON, D. H.; *Ionization Chambers and Counters*, Cambridge University Press, 1950.
[2] ROSSI, B. and STAUB, H.; *Ionization Chambers and Counters*, McGraw Hill, 1949.
[3] GERRITSEN, A. N.; *Physica* 14 (1948) 381.
[4] HUTCHINSON, G. W.; *Nature, Lond.* 162 (1948) 610.
[5] DAVIDSON, N. and LARSH, A. E.; *Phys. Rev.* 74 (1949) 220.
[6] MALKIN, M. S. and SCHULTZ, H. L.; *Phys. Rev.* 83 (1951) 1051.
[7] AHEARN, A. J.; *Phys. Rev.* 73 (1948) 1113.
[8] MCKAY, K. G.; *Phys. Rev.* 77 (1950) 816.
[9] FREEMAN, G. P. and VAN DER VELDEN, H. H.; *Physica* 17 (1951) 567.
[10] DAS GUPTA, N. N. and GHOSH, S. K.; *Rev. Mod. Phys.* 18 (1946) 225.

[11] KALLMANN, H.; *Phys. Rev.* 75 (1949) 623.
[12] LATTES, C. M. G., OCCHIALINI, G. P. S. and POWELL, C. F.; *Proc. Phys. Soc.* 61 (1948) 173.
[13] LIVINGSTON, M. S. and BETHE, H.; *Rev. Mod. Phys.* 9 (1937) 245.
[14] BETHE, H. A.; *Handbuch der Physik* 2nd. ed. 24/1, 518.
[15] —*Ann. Physik* 5 (1930) 325.
[16] WILLIAMS, E. J.; *Proc. Camb. Phil. Soc.* 33 (1937) 179.
[17] WILSON, R. R.; *Phys. Rev.* 60 (1941) 749.
[18] MONTGOMERY, D. J. X.; *Cosmic Ray Physics*, p.30, Princeton University Press, 1949.
[19] SWANN, W. F. G.; *J. Franklin Institute* 226 (1938) 598.
[20] FERMI, E.; *Phys. Rev.* 56 (1939) 1242.
[21] HALPERN, O. and HALL, H.; *Phys. Rev.* 57 (1940) 459.
[22] WICK, G. C.; *Ric. Scient.* 11 (1940) 273.
[23] FRANK, I. and TAMM, IG.; *Compt. Rend. Acad. Sci. U.S.S.R.* 14 (1937) 109.
[24] CERENKOV, P. A.; *Phys. Rev.* 52 (1937) 378.
[25] SCHÖNBERG, M.; *Bull. du Centre de Phys. Nucl. Bruxelles* No. 20, Aug. 1950.
[26] BOHR, N.; *Phil. Mag.* 30 (1915) 581.
[27] — *Math-fysiske Vedansk.* 18 (1948) 8.
[28] WILLIAMS, E. J.; *Proc. Roy. Soc.* 125 (1929) 420.
[29] LANDAU, L.; *J. Phys. U.S.S.R.* 8, 4 (1944) 201.
[30] BLUNCK, O. and LEISEGANG, S.; *Z. Physik* 128 (1950) 500.
[31] FANO, U.; *Phys. Rev.* 72 (1947) 26.
[32] HANNA, G. C., KIRKWOOD, D. H. W. and PONTECORVO, B.; *Phys. Rev.* 75 (1949) 985.
[33] CURRAN, S. C., SOCKROFT, A. L. and ANGUS, J.; *Phil. Mag.* 40 (1949) 929.
[34] FANO, U.; *Phys. Rev.* 70 (1946) 44.
[35] CRENSHAW, C. N.; *Phys. Rev.* 62 (1942) 54.
[36] HOLLOWAY, M. G. and LIVINGSTON, M. S.; *Phys. Rev.* 54 (1938) 18 and BETHE, H. A.; *Rev. Mod. Phys.* 22 (1950) 213.
[37] JESSE, W. P., FORSTAT, H. and SADAUSKIS, J.; *Phys. Rev.* 77 (1950) 782.
[38] CRANSHAW, T. E. and HARVEY, J. A.; *Can. J. Research* A 26 (1948) 243.
[39] HANNA, G. C.; *Phys. Rev.* 80 (1950) 530.
[40] TUNNICLIFFE, P. and WARD, A. G.; to be published.
[41] BEHRENS, D. J.; *A.E.R.E.* report T/M. 50, 1951.
[42] ROTHWELL, P.; *Proc. Phys. Soc.* B. 64 (1951) 911.
[43] PODGORETSKI, M. I; *Dok. Akad. Nank, S.S.S.R.* LXVII (1949) 4.
[44] PAUL, W. and REICH, H.; *Z. Physik*, 127 (1950) 429.
[45] MALKIN, M. S. and SCHULTZ, H. L.; *Phys. Rev.* 83 (1951) 1051.
[46] SEITZ, F.; *Phys. Rev.* 76 (1949) 1376.
[47] JENTSCHKE, W. K.; *Phys. Rev.* 83 (1951) 170.
[48] HOPKINS, J. I.; *Rev. Sci. Inst.* 22 (1951) 29.
[49] BLAU, M.; *Phys. Rev.* 75 (1949) 279.
[50] HAZEN, W. E.; *Phys. Rev.* 67 (1945) 269.
[51] CORSON, D. and BRODE, R. B.; *Phys. Rev.* 53 (1938) 773.
[52] SEN GUPTA, R. L.; *Proc. Nat. Inst. Sci. India* 9 (1943) 295.
[53] GOODMAN, P., NICHOLSON, K. P. and RATHGEBER, H. D.; *Proc. Phys. Soc.* A. 64 (1951) 96.
[54] BECKER, J., CHANSON, P., NAGEOTTE, E., TREILLE, P., PRICE, B. T., and ROTHWELL, P.; *Proc. Phys. Soc.* A 65 (1952) 437.
[55] GHOSH, S. K., JONES, G. M. D. B., and WILSON, J. G., *Proc. Phys. Soc.* A 65 (1952) 68.
[56] PICKUP, E. and VOYVODIC, L.; *Phys. Rev.* 80 (1950) 90.
[57] WHITTEMORE, W. L. and STREET, J. C.; *Phys. Rev.* 76 (1949) 1786.
[58] BOWEN, T. and ROSER, F. X.; *Phys. Rev.* 83 (1951) 689.
[59] JELLEY, J. V.; *Proc. Phys. Soc.* A. 64 (1951) 82.

NAME INDEX

Adair, R. K. 193, 194, 213, 221, 231, 233
Adamson, R. E. 229, 234
Ageno, M. 61
Agnew, H. M. 213, 233
Ahearn, A. J. 281, 282
Ajzenberg, F. 218, 228, 233, 234
Alburger, D. E. 226, 227, 229, 234
Alden, E. D. 69, 70, 87
Alder, F. 49, 218, 233
Allan, H. R. 185, 230
Allen, A. J. 87, 172
Allen, K. W. 159, 160, 161, 162, 172, 234
Allen, W. D. 189, 231
Allred, J. C. 220, 233
Almqvist, E. 234
Al-Salem, S. G. 168, 173
Alvarez, L. W. 158, 220, 222, 224, 225, 234
Anderson, H. L. 36, 48, 122
Anderson, R. A. 227, 234
Andrew, E. R. 41, 49
Angus, J. 199, 203, 232
Arakatsu, B. 170
Arfken, G. B. 207, 223, 232
Argo, H. V. 220, 233
Arnold, J. T. 38, 49
Arnold, W. R. 209, 232
Arrøe, O. H. 147, 171
Austern, N. 108, 119
Axel, P. 270

Bacher, R. F. 102, 119, 230, 243, 269
Bailey, C. L. 103, 119
Baker, W. 52, 86
Baldwin, G. C. 127, 130, 132, 133, 170
Barclay, F. R. 155, 172
Barkas, W. H. 119, 237, 269
Barker, E. C. 119
Barnes, C. A. 119, 209, 232
Barschall, H. H. 191, 231
Bartholomew, G. A. 217, 224, 232, 233, 234, 270
Bartlett, T. H. 235, 238, 269
Bashkin, S. 214, 233
Batchelor, R. 87
Batzel, R. E. 167, 173
Baxter, A. S. 220, 233
Bechsel, H. 214, 233
Becker, G. 50
Becker, J. 277, 280, 282, 283
Beghian, L. E. 111, 113, 114, 119, 226, 234
Behrens, D. J. 277, 283
Beiduk, F. M. 6, 19
Belcher, E. A. 75, 76, 88
Bell, P. R. 52, 53, 60, 70, 75, 86, 200, 203, 211, 232
Bell, R. E. 99, 119, 232
Bender, R. S. 184, 192, 230, 231
Benedetti, S. de 151, 172
Bennett, W. E. 184, 216, 230, 233
Benzie, R. J. 49
Bersohn, R. 41, 49
Berthelot, A. 242, 269
Bethe, H. A. 90, 91, 98, 102, 105, 107, 108, 109, 116, 117, 118, 119, 179, 180, 183, 230, 243, 269, 272, 283
Biedenharn, L. C. 223, 232
Birkhoff, R. D. 280
Birks, J. B. 86, 87
Birnbaum, W. 119
Bishop, G. R. 111, 113, 114, 119, 226, 234
Biswas, S. 129, 170
Blackmore, L. 87
Blatt, J. M. 91, 97, 98, 114, 115, 118, 119, 270
Blau, M. 52, 86, 281, 283
Bleuler, E. 191, 231
Bloch, F. 21, 22, 24, 25, 28, 48, 78, 88, 171
Bloch, I. 183, 230
Bloembergen, N. 32, 39, 40, 48, 49, 50
Blunck, O. 273, 274, 279, 280, 283
Blundell, M. 217, 233
Bockelman, G. K. 218, 233
Bøggild, J. K. 147, 171
Bohr, A. 254, 270
Bohr, N. 123, 124, 129, 142, 145, 152, 163, 170, 171, 237, 269, 273, 283
Bonner, T. W. 151, 171, 172, 194, 195, 230, 231
Bothe, W. 20, 217, 233

Bouricius, G. M. B. 231
Bowden, B. V. 185, 230
Bowen, E. J. 60, 76, 81, 82, 83, 87, 88
Bowen, T. 72, 88, 280, 282, 283
Bower, J. G. 232
Bowker, J. K. 168, 173
Boyer, K. 148, 171, 185, 230
Bradner, H. 168, 173
Brady, E. L. 200, 205, 207, 226, 232
Breit, G. 89, 118, 182, 237, 269
Bretscher, E. 122, 172
Briggs, G. H. 231
Brinkley, T. A. 159, 162, 172, 213, 232, 233
Brode, R. B. 282, 283
Broser, I. 52, 56, 64, 72, 81, 86, 88, 170
Brostrøm, K. J. 195, 231
Brown, A. B. 214, 215, 233
Brown, H. 219, 233, 238, 269
Browne, C. P. 186, 215, 227, 231, 233
Brunton, D. C. 127, 136, 137, 138, 140, 141, 171.
Buckley, H. E. 63, 87
Buecher, W. N. 217, 225, 226, 234
Buechner, W. W. 185, 186, 187, 230, 231, 233, 234
Bull, C. B. 88
Bunemann, O. 127, 170
Bunyan, D. E. 211, 233
Burcham, W. E. 184, 186, 220, 221, 230, 231, 233, 234, 251, 260, 269
Burgy, M. T. 100, 119
Burrows, H. B. 185, 187, 188, 210, 218, 230, 231, 232
Busch, H. 20
Bush, R. R. 190, 231
Butler, S. T. 210, 218, 232, 251, 270
Buyle, M. 48

Cahn, A. 149, 171
Cameron, A. G. N. 211, 220, 231, 232
Campbell, E. C. 147, 171
Carver, J. H. 119, 199, 225, 229, 231
Case, K. M. 117, 119, 248, 270
Cassels, J. M. 119, 159, 161, 162, 172
Cavanagh, P. E. 73, 88, 199, 203, 226, 231, 234
Cerenkov, P. A. 272, 282, 283
Chadwick, J. 184, 235
Chamberlain, O. 119, 153
Chambers, W. H. 49
Chanson, P. 283
Chao, C. Y. 187, 197, 200, 206, 224, 225, 231
Chappie, R. A. 172
Charbonnier, G. 170
Charpak, G. 226, 234
Chastel, R. 159, 172
Chilton, L. U. 231
Chiozzotto, M. 61
Christian, R. S. 116, 117, 119, 270
Christy, R. E. 183, 230
Class, C. M. 214, 233
Cockcroft, J. 184
Cockroft, A. L. 199, 203, 232
Cohen, E. R. 221, 234
Collinge, B. 61, 87
Collins, C. B. 135, 158, 171
Collins, E. R. 185, 186, 231
Condon, E. U. 118, 207, 232, 236, 263, 269
Cooke, A. H. 49
Cook, G. B. 122, 143, 144, 171, 172
Cook, C. S. Sharp 7, 19
Coltman, J. W. 52, 86
Cork, B. 119
Corson, D. 282, 283
Coryell, C. D. 134, 142, 171
Couteur, K. le 248, 270
Craig, D. S. 231, 233
Cranshaw, T. E. 127, 170, 277, 279, 280, 283
Crenshaw, C. N. 276, 283
Creveling, L. G. 172
Critchfield, C. L. 175, 213, 230, 233, 238, 269
Crookes, W. 52
Cuer, P. 185, 230
Cunningham, B. B. 129, 170
Curling, C. D. 201, 215, 232
Curran, S. C. 52, 86, 119, 203, 230, 276, 283
Curtis, B. R. 185, 230
Cusano, D. A. 64, 86
Czyzak, S. J. 56, 64, 86

Dabbs, J. 149, 171
Dainty, J. 159, 172
Dancoff, S. 270
Darby, F. S. 49
Das Gupta, N. N. 282
Davidson, N. 282
Davidson, W. L. 119
Day, R. B. 229, 234
Dee, D. I. 220, 234
Dehmelt, H. G. 47, 50
Demers, P. 148, 160, 161, 163, 172
Dennison, O. M. 7, 19
Deutsch, M. 11, 20, 52, 60, 86, 136, 171, 200, 205, 206, 207, 209, 226, 230, 232

Devons, S. 175, 184, 192, 196, 197, 202, 205, 206, 209, 211, 221, 223, 230, 231, 232, 234
Dewan, J. T. 159, 160, 161, 162, 172, 234
Dharmatti, S. S. 38, 49
Dickinson, W. C. 38, 39, 48, 49
Dismuke, N. 134, 143, 158, 170
Dodder, D. C. 213, 233
Dodé, M. 122
Donahue, D. J. 233
Dougherty, C. B. 202, 232
Dreyfuss, B. 52, 86
Driscoll, R. L. 48, 185, 231
Duckworth, H. E. 243, 270
Dudley, A. 171
Dumond, J. W. 13, 14, 17, 20
Dunbar, D. N. F. 232
Dunlap, C. 277, 279, 280

Eby, F. S. 87
Edmonds, A. R. 266, 270
Edwards, R. R. 142, 171
Ehrman, J. B. 217, 233
Eisenbud, L. 118, 183, 230
Elliot, J. O. 87
Elliott, L. G. 11, 20, 99, 119, 211, 232
Elsasser, W. 235, 236, 242, 246, 269
Enge, H. 234
Eppstein, J. S. 68, 87
Euler, H. 267, 270
Evans, J. E. 194, 195, 231
Evans, R. D. 11, 20

Facchini, U. 128, 170
Falk, C. E. 87
Falkoff, D. L. 206, 209, 232
Fano, U. 275, 276 283
Farmer, E. C. 56, 70, 86, 87
Farwell, G. 153, 158, 159, 160, 172
Fatehally, R. 86, 87
Feather, N. 159, 161, 169, 172, 173, 203, 232
Feenberg, E. 144, 171, 176, 179, 180, 202, 203, 215, 225, 230, 232, 233, 236, 245, 246, 247, 258, 264, 266, 269, 270
Feingold, A. M. 203, 212, 232
Feld, B. T. 130, 150, 170, 172
Fenning, F. W. 128, 169, 170, 173
Fermi, E. 93, 118, 119, 121, 122, 128, 154, 170, 272, 283
Fillmore, F. L. 119
Fishback, H. 170
Flammersfeld, A. 136, 171
Flerov, G. N. 122, 152, 172
Flowers, B. H. 68, 87, 179, 241, 264, 265, 266, 269, 270
Fock, V. 236
Forstat, H. 276, 283
Fortescue, R. L. 184, 230
Fowler, J. L. 136, 171, 230
Fowler, P. H. 185, 230.
Fowler, W. A. 119, 175, 185, 187, 194, 197, 199, 211, 214, 215, 230, 231, 233.
Fox, R. 119
Francis, J. E. 151, 172
Frank, I. 272, 283
Frankel, S. 20, 133, 170
Franzen, W. 69, 87
Fraser, J. S. 151, 172
Freedman, M. S. 134, 171
Freeman, G. P. 281, 282
Freeman, J. M. 186, 187, 188, 200, 221, 231, 234
Freier, D. 103, 104, 119, 213, 233
French, A. P. 185, 209, 230, 213, 222, 225, 232, 234
Frenkel, J. 123, 124, 125, 170
Frerichs, R. 55, 63, 87
Frey, H. B. 87
Friedland, S. S. 165, 173
Frisch, D. H. 103, 119
Frisch, O. R. 122, 123, 126, 150, 169
Fulbright, H. V. 190, 231
Furst, M. 56, 62, 83, 84, 86, 87

Galbraith, W. 155, 156, 168, 172, 173
Gamow, G. 175, 230, 238, 269
Garlick G. F. 86, 88, 200
Gasteiger, E. L. 133, 170
Gatti, E. 128, 170
Gentner, W. 136, 171
Gerritsen, A. N. 282
Gerjuoy, E. 228, 234
Ghiorso, A. 129, 170, 269
Ghosh, S. K. 282, 283
Gibson W. M. 189, 199, 210, 217, 218, 231, 232, 233
Gilbert C. W. 220, 234
Gittings H. T. 61, 87
Glaser W. 11, 20
Glendenin L. E. 135, 142, 143, 144, 157, 171
Glicksman, M 231
Glückauf, E. 242, 243, 269
Goeckermann, R. H. 164, 165, 166, 173
Goertzel, G. 206, 232, 270
Gofman, J. W. 170
Goldberg, M. L. 170
Goldhaber, M. 193, 216, 231, 256, 257, 260, 270
Goldstein, A. 171

GOLDSTEIN, H. 170, 213, 233
GOLDSTEIN, N. 269
GOOD, W. M. 147, 171
GOODMAN, C. 56, 70, 86
GOODMAN, P. 282, 283
GORDY, W. 240, 269
GOVE, H. E. 214, 227, 230, 233
GOWARD, F. K. 133, 159, 163, 170, 172, 205, 211, 220, 232
GRACE, M. A. 226, 234
GRAHAM, G. 158, 170
GRAHAM, R. L. 128, 135, 171
GRAY, T. S. 87
GREEN, J. L. 159, 172
GREEN, L. L. 159, 160, 162, 172
GREENLESS, G. W. 190, 226, 231
GRIFFITHS, J. H. E. 241, 269
GRIM, W. M. 87
GRIVET, P. 48
GROSS, W. E. 20
GROTDAL, T. 231
GRUMMIT, W. E. 171
GUGGENHEIMER, K. 181, 230, 235, 239, 269
GUTH, E. 215, 233
GUTOWSKY, H. S. 49

HADLEY, J. 116, 119
HAFNER, E. M. 226, 227, 229, 234
HAFSTAD, L. R. 181, 230
HAHN, E. L. 25, 30, 36, 38, 48, 121
HALBAN, H. 111, 113, 114, 119, 122, 226, 232, 234
HALG, W. 233
HALL, D. 149, 171
HALL, H. 272, 282, 283
HALLIDAY, D. 11, 20
HALPERN, I. 111, 113, 119
HALPERN, O. 272, 282, 283
HAMILTON, D. R. 206, 232
HAMMACK, K. C. 179, 203, 225, 230, 245, 246, 247, 270
HANNA, G. C. 127, 136, 138, 140, 141, 150, 156, 170, 171, 172, 192, 214, 231, 276, 277, 283
HANNA, S. S. 233
HANLE, W. 53, 86
HANSEN, W. W. 21, 48
HANSON, A. O. 190, 231
HANSSON, I. F. E. 114, 118, 119
HANSTEIN, H. B. 122
HARDING, G. N. 68, 70, 87
HARKINS, W. D. 237, 269
HARR, J. 270
HARRISON, F. B. 63, 87
HART, E. W. 116, 117, 119
HARTREE, D. R. 236
HARVEY, B. G. 127, 156, 170, 172
HARVEY, J. A. 170, 187, 214, 221, 227, 230, 231, 233, 244, 270, 277, 283.
HATTON, J. 40, 42, 49
HAXBY, R. O. 170
HAXEL, O. 180, 230, 246, 270
HAYDEN, R. J. 135, 171
HAZEN, W. E. 282, 283
HEBERT, G. 49
HEDGRAN, A. 7, 20
HEISENBERG, W. 270
HEITLER, W. 50, 207, 232
HELLINGMAN, J. E. 88.
HELMHOLZ A. C. 199, 202, 210, 231
HENDERSON, M. C. 141, 171
HENRI, V. F. 72, 88
HERB, R. G. 184, 230
HEREWARD, H. G. 211, 223, 232
HERRING, C. 50
HESS, D. C. 135, 158, 171
HEYDENBURG, N. P. 185, 205, 223, 225, 230, 232, 234
HILDEBRAND, R. H. 119
HILL, D. L. 170, 171
HILL, J. E. 130, 170
HILLIER, J. 20
HINE, M. G. N. 196, 197, 205, 206, 221, 223, 225, 231, 234
HIPPEL, A. VON 76, 88
HIPPLE, J. A. 48, 185, 231
HIRST, F. 232
HO, Z. W. 159, 172
HOFFMAN, C. J. 49
HOFFMAN, F. DE 150, 172
HOFSTADTER, R. 52, 61, 69, 73, 75, 86, 87, 88, 200, 231, 232
HOLLAND, S. S. 234
HOLLANDER, J. M. 131, 170
HOLLOWAY, M. G. 276, 283
HOLMES 76
HOLT, F. R. 169, 173
HOOD, J. R. 172
HOPKINS, J. I. 69, 87, 281, 283
HORNYAK, W. F. 14, 20. 119, 175, 199, 211, 222, 230, 231, 232, 234.
HORTON, G. K. 202, 232
HOWLAND, J. J. 164, 173
HUBY, R. 267, 270
HUBER, P. 233
HUDSON, A. M. 163, 172
HUDSON, C. M. 232
HUGHES, D. J. 100, 101, 118, 119, 149, 171
HUGHES, D. T. 241, 269
HUGHES, J. 248, 270

Hulthén, L. 114, 118, 119
Hund, F. 264, 270
Hutchinson, G. W. 186, 231, 281, 282
Huus, T. 195, 231

Imber, O, 87
Inghram, M. G. 135, 158, 171
Inglis, D. R. 185, 206, 215, 230, 232, 233

Jackson, J. D. 91, 97, 98, 114, 115, 118, 119
Jacobsohn, B. A. 33, 48
Jahn, H. 263, 264, 270
James, D. B. 186, 200, 222, 231
Jastrow, R. 117, 119
Jelley, J. V. 282, 283
Jennings, B. 172, 188, 231
Jensen, H. 243, 244, 246, 247, 270
Jensen, J. H. D. 180, 230
Jensen, P. 136, 171
Jentschke, W. K. 87, 122, 136, 171, 281, 283
Jesse, W. P. 276, 283
Johnson, C. H. 191, 216, 217, 231, 233
Johnson, L. R. 78, 87
Johnson, V. R. 233
Johnston, L. 119
Jones, E. J. 170
Jones, G. M. D. B. 222, 283
Jones, R. C. 76, 88
Joliot, F. 122
Jordan, W. H. 53, 86, 200, 203, 232
Jungerman, J. 130, 131, 153, 164, 165, 170, 173
Juren, J. de 119

Kalckar, F. 237, 269
Kallmann, H. 52, 54, 55, 56, 59, 60, 62, 72, 75, 83, 84, 86, 87, 88, 170, 283
Katkoff, S. 138, 147, 171
Kapur, P. L. 237, 269
Kaufman, S. G. 231
Keilson, J. 248, 270
Keister, G. L. 20
Kelly, E. L. 130, 170
Kempton, A. E. 190, 226, 231
Kennedy, J. W. 170
Kimura, K. 170
Kingsley, B. B. 233
Kinsey, B. B. 150, 172, 200, 201, 217, 224, 232, 234, 270
Kistiakowsky, G. B. 49
Klaiber, G. S. 127, 130, 132, 133, 170
Klema, E. D. 170, 185, 231
Knight, W. D. 48, 50
Knipp, J. K. 123, 163, 170
Koch, H. W. 133, 170
Koechlin, V. 63, 87
Koester, L. J. 233
Kofoed-Hansen, O. 8, 20
Kohn, W. 50
Koller, L. R. 69, 70, 87
Konopinski, E. S. 6, 19, 203, 204, 226, 232
Kopfermann, H. 255
Koski, W. S. 63, 86, 87
Kowarski, L. 122, 269
Kraushaar, W. L. 72, 88
Kroger, F. A. 79, 86, 88
Krüger, H. 47, 50
Kruger, P. G. 87
Kruse, U. E. 119
Kurath, D. 265, 266, 270
Kurie, F. N. D. 8, 19
Kyropoulos, S. 64, 87

Lamb, W. E. 38, 48
Lampi, E. E. 103, 104, 119, 213, 233
Landau, L. 90, 118, 273, 274, 275, 277, 278, 279, 280, 283
Langer, L. M. 7, 19
Laporte, O. 263, 265, 270
Larsh, A. E. 282
Lassen, N. O. 145, 146, 171
Latter, R. 183, 230
Lattes, C. M. G. 185, 230, 281, 283
Laubenstein, M. J. W. 219, 233
Laubenstein, R. A. 99, 119, 233
Lauritsen, C. C. 184, 187, 194, 197, 199, 214, 215, 230, 231, 232, 233
Lauritsen, T. 20, 119, 184, 194, 197, 199, 211, 222, 230, 231, 232, 234
Leachman, R. B. 139, 140, 141, 144, 171
Lees, D. J. 170
Leisegang, S. 273, 274, 279, 280, 283
Leith, C. E. 119
Leland, W. T. 213, 233
Leverenz, H. W. 86
Lewis, W. B. 185, 230
Li, C. W. 220, 234
Liebson, S. M. 87
Lindenfeld, D. 218, 233
Lindhard, J. 20
Lindsey, G. R. 202, 211, 221, 223, 232, 234
Lindström, G. 48
Littauer, R. M. 225, 234
Littler, D. J. 155, 172
Livesey, D. L. 159, 160, 162, 172, 217, 231, 233
Livingston, M. S. 230, 276, 283

LIVINGSTON, R. 49, 50
LONGINI, R. L. 86
LONGMIRE, C. 91, 107, 108, 109, 116, 117, 118
LUNBY, A. 87
LUNDBY, A. 233

MACK, J. E. 39, 49, 109, 119, 212
MACKINTOSH, C. E. 171
MACNAMARA, J. 135, 155, 158, 171, 172
MAGNUSSON, L. B. 170
MALKIN, M. S. 282, 283
MALM, R. 186, 187, 217, 231, 233
MANDEVILLE, C. E. 56, 86, 226, 230, 234
MARSHAL, J. 128, 170
MARSHAL, L. 118, 128, 160, 162, 170, 172
MARSHALL, H. 52, 86
MARTIN, G. R. 172
MARTIN, L. H. 205, 206, 232
MARTINS, U. M. 86
MASSEY, H. S. W. 118, 175, 216, 230
MAYER, M. G. 126, 157, 170, 179, 180, 219, 230, 237, 243, 244, 245, 246, 247, 251, 259, 265, 266, 269, 270
MCCLURE, R. E. 49
MCDANIEL, B. D. 200, 220, 221, 232, 233, 234
MCELHINNEY, J. 133, 170
MCGINNIS, C. L. 259, 270
MCINTYRE, J. A. 73, 88, 200, 232
MCINTYRE, W. J. 56, 63, 86
MCKAY, K. G. 281, 282
MCKENZIE, C. D. 185, 186, 231
MEITNER, L. 122, 123, 126, 157, 169, 170, 242, 269
MELKONIAN, E. 100, 119.
MENZIES, A. C. 65, 87
MERRISON, A. W. 193, 231
MESCHERYAKOV, C. R. 241, 269
METROPOLIS, N. 123, 124, 133, 170
METZGER, F. 209, 232
MEYER, D. I. 20, 122
MEYER, P. 225, 234
MEYERHOF, W. E. 75, 87
MICHAELIS, E. G. 87
MICKIEWICZ, E. 82, 87
MILLAR, C. H. 199, 211, 220, 224, 231, 232, 234
MILLER, L. C. 171
MILLER, W. C. 87
MIMS, H. 202, 226, 232
MINNHAGEN, L. 147, 171
MISKELL, J. A. 138, 147, 171
MITCHELL, A. C. G. 203, 204, 226, 232
MIYATAKE, O. 170
MOAK, C. D. 172, 217, 233

MOBLEY, R. C. 99, 119, 233
MONTGOMERY, D. D. 88
MONTGOMERY, D. J. X. 283
MONTGOMERY, C. G. 88
MOON, R. J. 87
MOON, P. B. 205, 232
MOORE, H. B. 56, 70, 86
MORRISON, P. 119, 175, 211, 230
MORTON, G. A. 20, 119
MOSS, N. 156, 170, 172
MOSZKOWSKI, S. A. 259, 270
MOTT, N. F. 118, 175, 216, 230
MOTTELSON, B. R. 215, 233
MOULTON, W. G. 87
MOYER, B. J. 119
MUELLER, D. W. 73, 88
MULLIN, C. J. 215, 233
MURAOKA, K. 170

NABHOLZ, H. 199, 231
NAGEL, B. 114, 119
NAGEOTTE, E. 283
NECHAJ, J. F. 172
NEILER, J. H. 87
NERESON, N. 171
NEWMAN, R. 42, 50
NEWTON, A. S. 164, 165, 173
NEWTON, J. O. 201, 209, 214, 215, 232, 233
NEY, E. P. 72, 88, 280
NICHOLSON, K. P. 282, 283
NIDAY, J. B. 134, 171
NIELSEN, O. B. 20, 147, 171
NIER, A. O. 119
NORDHEIM, L. W. 179, 230, 245, 246, 247, 258, 259, 270
NOYES, H. P. 117, 119, 270

OCCHIALINI, G. P. S. 231, 283
O'CONNOR, P. R. 164, 173
OGLE, W. E. 133, 170
ORLIN, J. J. 231
OSABA, J. S. 19
OSBORNE, D. W. 170
OWEN, G. E. 87
OXLEY, C. L. 119

PACKARD, M. E. 21, 38, 48, 49
PAIS, A. 117, 119, 248, 270
PAKE, G. E. 45, 46, 49, 50
PANOFSKY, W. K. H. 119
PAPPAS, A. C. 171
PATRO, A. P. 129, 170
PATTER, D. VAN 150, 172, 215, 231, 233, 234
PAUL, E. B. 220, 233

Paul, W. 283
Pecjak, F. A. 172
Peelle, R. W. 69, 87
Peierls, R. E. 105, 119, 151, 172, 237, 247, 269
Pepper, T. 227, 234
Perez-Mendez, V. 218, 219, 233
Perlman, I. 164, 165, 166, 173
Perry, J. E. 229, 234
Persico, E. 13, 14, 20
Peterson, S. 170
Petrzhak, K. A. 122, 152, 172
Phillips, G. C. 185, 223, 225, 231, 234
Phillips, M. 180, 230
Pichat, L. 63, 87
Pickavance, T. G. 119, 184, 230
Pickup, E. 282, 283
Platt, J. R. 263, 265, 270
Podgoretski, M. I. 278, 283
Pontecorvo, B. 172, 199, 203, 232
Pool, M. L. 172
Poole, M. J. 172
Pose, H. 155, 172
Poss, H. L. 87
Post, R. F. 61, 62, 87
Poulis, N. J. 50
Pound, R. V. 21, 32, 48, 49, 50
Powell, C. F. 185, 186, 187, 217, 230, 231, 283
Powell, J. L. 184, 230
Prankl, F. 122
Preiswerk, P. 181, 230
Present, R. D. 118, 123, 142, 144, 163, 170, 171, 172, 268, 270
Preston, G. 226, 234
Preston, R. S. 270
Preston, W. P. 191, 231
Preston, W. M. 87, 151, 172
Price, B. T. 283
Pringle, R. W. 53, 86, 200, 203, 232
Pringsheim, P. 86, 88
Proctor, W. G. 48, 49
Pryce, M. H. L. 172, 243, 253, 269
Purcell, E. M. 21, 32, 42, 48, 49, 50

Quade, E. A. 11, 20
Querzoli, B. 61

Rabi, I. I. 21
Racah, G. 263, 266, 270
Rae, E. R. 200, 202, 215, 225, 232, 233
Rainwater, J. 254, 268, 270
Rall, W. 87
Ramberg, E. G. 20, 86
Ramm, C. A. 185, 186, 231
Ramsay, M. 136, 171
Ramsey, N. F. 38, 49, 50, 119
Randall, J. T. 88
Randle, T. C. 119
Rarita, W. 117, 119
Rasmussen, J. O. 269
Rasmussen, V. K. 20, 199, 200, 224, 231, 232
Rathgeber, H. D. 282, 283
Ravilious, C. F. 87
Rechl, N. 78, 88
Redman, N. C. 172
Reich, H. 283
Reiffel, L. 72, 88
Reines, R. D. 123, 170
Remley, M. E. 87
Renwick, F. F. 87
Rest, F. G. 72, 88
Reynolds, D. C. 52, 56, 64, 86
Reynolds, G. T. 61, 86, 87
Reynolds, J. H. 135, 171
Rhoderick, E. H. 185, 190, 215, 226, 230, 231
Richardson, H. O. W. 15, 20, 232
Richards, J. A. 214, 215, 233
Richman, C. 119
Ringo, G. R. 100, 119
Robbins, E. J. 61, 87
Roberts, J. H. 122, 172
Roberts, T. R. 119
Robinson, G. P. 203, 217, 233
Robinson, H. 3, 19
Rochlin, R. S. 220, 233
Rollin, B. V. 40, 42, 49
Rose, B. 150, 152, 172
Rose, M. E. 180, 202, 207, 223, 230, 232, 256, 270
Rosen, L. 136, 163, 171, 172, 230
Rosenfeld, L. 175, 180, 212, 230, 248, 253, 254, 266, 270
Rosenblum, E. S. 19
Roser, F. X. 72, 88, 280, 282, 283
Rossel, J. 191, 231
Rossi, B. 282
Rotblat, J. 170, 185, 187, 210, 217, 218, 230, 231, 232, 233
Rothwell, P. 277, 280, 283
Roy, R. R. 218, 229, 233
Roys, P. A. 216, 233
Rubin, S. 230
Rutherford, E. 3, 19, 52
Rutherford, Lord 184, 185, 230
Rutherglen, J. C. 200, 215, 225, 232, 233

Sachs, R. G. 108, 119
Sachs, 42
Sadauskis, J. 276, 283
Salpeter, E. E. 104, 109, 119
Salvini, G. 86
Sawyer, R. B. 172
Saxon, D. 172
Scarrott, G. G. 186, 231
Schamberger, R. D. 119
Scherrer, P. 170
Schiff, L. I. 270
Schillinger, E. J. 61, 87
Schmidt, F. H. 14, 20
Schmidt, T. 236, 249, 269
Schön, M. 78, 79, 81, 88
Schönberg, M. 272, 283
Schorr, M. G. 63, 87
Schüler, H. 236, 269
Schultz, H. L. 282, 283
Schuster, N. A. 45, 46, 48, 50
Schwinger, J. 90, 115, 116, 117, 118, 119
Scott, J. M. C. 169, 173
Seaborg, G. T. 164, 170, 172, 173, 269
Seagrave, J. D. 229, 234
Seed, J. 224
Segrè, E. 119, 147, 153, 154, 155, 158, 159, 160, 170, 171, 172, 199, 202, 210, 231
Seiler, J. A. 171
Seitz, F. 73, 76, 77, 80, 88, 281, 283
Seligman, H. 128, 170
Sen Gupta, R. L. 282, 283
Sheer, R. 69, 87
Sherwin, C. W. 87
Shimizu, S. 170
Shinohara 119
Shirer, N. S. 61, 87
Shoemaker, F. C. 184, 230, 231
Shortley, G. H. 207, 232, 236, 263, 269
Shoupp, W. E. 87, 130, 170, 188, 231
Shull, C. G. 100, 101, 119
Shull, F. B. 7, 8, 19
Shull, H. 258, 270
Shurcliff, W. A. 76, 88
Siegbahn, K. 7, 11, 12, 14, 15, 17, 19, 20, 186, 190, 203, 204, 226, 231, 232
Siegert, A. J. F. 108, 119
Sigurgeirrsson, T. 147, 171
Skinner, J. 65, 87
Skyrme, T. H. R. 202, 232, 270
Slack, L. 19
Slater, 236, 262, 265
Slätis, H. 14, 15, 17, 20, 190, 231
Sleator, W. 213, 233
Smaller, B. 48
Smith, C. P. 87
Smith, F. M. 119
Smith, F. W. 82, 87
Smith, J. W. 87
Smith, K. F. 226, 234
Smith, R. D. 200, 215, 225, 227, 232, 233, 234
Smorodinsky, J. 90, 118
Snell, A. H. 119, 171
Snyder, T. M. 150, 172
Snyder, C. W. 185, 186, 214, 215, 230, 233
Sonoda, M. 170
Soutif, M. 48
Spatz, W. D. B. 269
Spence, R. W. 173
Sperduto, A. 229, 230, 231, 233, 234
Spinrad, B. 270
Squires, G. L. 100, 119
Stafford, G. H. 119, 194, 231
Stanley, C. W. 138, 147, 171
Staub, H. 171, 282
Stearns, M. B. 220, 221, 234
Stebler, A. 233
Stein, P. R. 150, 172
Steinberg, E. P. 134, 135, 158, 171
Stergiopoulos, C. G. 230
Sternberg, R. L. 119
Stetter, W. 217, 233
Stevens, W. E. 170
Stewart, A. T. 100, 119
Stöber, F. 67, 87
Stockbarger, D. C. 65, 67, 87
Stoll, P. 199, 231
Stowe, C. A. 72, 88
Stoughton, R. W. 170
Strait, E. N. 187, 230, 231
Strassmann, F. 121
Strauser, W. A. 147, 171
Street, J. C. 282, 283
Street, K. 129, 170
Strong, P. 270
Studer, F. J. 56, 64, 86
Stuhlinger, E. 279
Suess, H. E. 180, 230, 244, 246, 270
Sugarman, N. 134, 171, 172
Sun, K. H. 87, 172, 188, 231
Sunyar, A. W. 256, 257, 260, 270
Sutton, R. B. 100, 101, 119
Suzor, F. 147, 171, 226, 234
Svartholm, N. 7, 19, 20, 186, 231
Swann, W. F. G. 272, 279, 283
Swiatecki, W. J. 170, 242, 247, 263, 269, 270

Talmi, I. 265, 270
Tamm, Ig. 272, 283

TANGEN, R. 195, 231
TASCHEK, R. E. 190, 231
TASKER, H. S. 87
TAYLOR, A. E. 119, 171
TAYLOR, C. J. 69, 87
TEAZEL, C. E. 87
TELEGDI, V. 205, 221, 232, 234
TELLER, E. 50, 181, 230
TEMPLETON, D. H. 164, 173
THAXTON, H. M. 118
THIRION, J. 214, 216, 218, 221, 233
THODE, H. G. 135, 155, 158, 171, 172
THOMAS, C. O. 87
THOMAS, H. A. 48, 49, 185, 231
THOMAS, J. E. 72, 88
THOMAS, R. G. 217, 233
THOMPSON, S. G. 127, 136, 170, 243, 269
THOMPSON, W. B. 129, 171
THOMSON, 222
THON, D. M. 72, 88, 280
TIOMNO, J. 173
TITTERTON, E. W. 159, 160, 161, 162, 163, 169, 172, 173, 213, 232, 233
TITTLE, C. W. 148, 171
TOLLESTRUP, A. V. 181, 231
TOPPEL, B. J. 216, 233
TORNEY, F. L. 63, 87
TORREY, H. C. 21, 25, 30, 48
TOWNES, C. H. 50
TREACY, P. B. 185, 186, 200, 213, 225, 230, 231, 234
TREILLE, P. 283
TRIGG, G. L. 202, 232, 258, 270
TRUMPY, B. 231
TSIEN, S. T. 159, 161, 162, 163, 172
TUCKER, E. B. 222, 234
TUNNICLIFFE, P. 156, 170, 172, 277, 283
TURKEVITCH, A. 134, 171
TURNER, J. F. 42, 226, 234
TURNER, L. A. 121, 169

UEMURA, Y. 170
UHLENBECK, G. E. 206, 209, 232

VANCE, A. W. 20
VELDEN, H. H. VAN DER 281, 282
VENDRYES, G. 222, 234
VENDRYES, G. 222, 234
VERNEUIL, A. 65, 87
VERSTER, N. F. 19, 20
VIGNERON, L. 148, 159, 171, 172
VLECK, J. H. VAN 34, 48
VOGELS, H. 88
VOYVODIC, L. 282, 283

WÄFFLER, H. 170, 199, 231
WAHL, A. C. 170
WALCHLI, H. 49
WALDMAN, B. 87
WALKER, D. 233
WALKER, W. H. 217, 232, 233, 270
WALKER, R. L. 200, 216, 232
WALLER, I. 39, 43, 49
WALTON, E. T. S. 184
WANG, C. S. 122
WANGNESS, R. K. 33, 48
WARD, A. G. 277, 283
WARD, A. H. 233
WARMINSKY, R. 56, 81, 88
WARREN, R. E. 184, 230
WARSHAW, S. D. 228, 234
WATKINS, G. D. 29, 48
WATSON, W. H. H. 170
WATT, B. E. 171, 230
WAWILOV, S. 88
WAY, K. 133, 134, 142, 143, 158, 170, 171
WEISSKOPF, V. F. 170, 181, 230, 256
WEIZSÄCKER, C. F. VON 243
WELLS, W. A. 170
WEST, D. 172
WEST, H. I. 75, 87
WEYL, H. 270
WHALING, W. 220, 234
WHEELER, J. A. 123, 124, 125, 129, 142, 152, 163, 168, 170, 173, 181, 220, 230, 234, 236, 269
WHITE, P. 280
WHITEHEAD, W. D. 232
WHITEHOUSE, W. J. 155, 156, 168, 172, 173
WHITTEMORE, W. L. 282, 283
WIBLIN, E. R. 193, 231
WICK, G. C. 169, 272, 282, 283
WIEGAND, C. 119, 130, 147, 153, 158, 159, 160, 170, 171, 172
WIGNER, E. 142, 171, 176, 177, 180, 182, 183, 230, 236, 237, 262, 264, 268, 269
WILKINS, J. J. 163, 172, 205, 211, 220, 232
WILKINS, M. H. F. 88
WILKINSON, C. A. 185, 225, 230
WILKINSON, D. H. 114, 118, 119, 199, 229, 232, 282
WILKINSON, G. 171
WILKINSON, R. G. 87
WILLARD, H. B. 191, 231
WILLIAMS, D. 30, 48, 49
WILLIAMS, E. J. 273, 274, 283

Williams, J. H. 103, 104, 119, 190, 213, 231, 233
Williams, R. W. 150, 172
Williamson, R. M. 193, 214, 216, 231, 233
Wilson, A. R. W. 150, 152, 172
Wilson, J. G. 283
Wilson, R. R. 151, 169, 172, 173, 232, 283
Witcher, C. M. 13, 20
Woodward, W. M. 111, 113, 119
Woollan, E. O. 119, 172
Wright, S. C. 130, 164, 165, 166, 167, 170, 173
Wu, C. S. 20, 49, 232, 270
Wynn-Williams, C. E. 185, 230

Yaffe, L. 171
Yamaguchi, Y. 166, 173
Yang, C. N. 206, 208, 232
Yasaki, T. 170
Yasitas, E. 48
Young, A. H. 64, 86
Yu, F. C. 48, 49, 218, 233
Yuan, L. C. L. 87

Zeldes, N. 266, 270
Zerfoss, S. 87
Zimmerman, J. R. 48
Zünti, W. 14, 20, 221, 234
Zworykin, V. K. 20, 86

SUBJECT INDEX

Aberration 4
Alignment of nuclei 47
Alpha particle model 180
Angular distribution and correlation 205
Anthracene 52, 59

Beta decay and shell model 257
Beta decay, selection rules 203
Beta ray spectrometers, annular focussing 12
— — — double focussing 7
— — — intermediate image 14
— — — lens type 9
— — — line width 5
— — — prismatic 5
— — — semi-circular 3
— — — transmission 5

Capture, radiative 194, 197
Cloud chamber 282
Conjugated double bonds 81
Critical shape 124
Crystal growing 63

Deuteron binding energy 99
— photo-disintegration 105

Diamagnetic shift 38
Diamond 57
Dipole-dipole coupling 30

Effective range 90
Effective excitation energy 272
Electrostatic generator 184
Energy transfer in phosphors 78, 82
Energy loss per ion pair 276
— — relativistic 282
Exchange forces 236
Exciton 82

Fission and the shell model 157
— angular correlations 151
— asymmetry 124, 242
— at very high energy 164
— by mesons 167
— charge distribution 141
— cross-sections 128
— emission of light nuclei 158
Fission, energy distribution 135
— mass distribution 133
— negative proton emission 169
— neutrons and gamma rays 148
— ranges of fragments 144
— spontaneous 124, 152
— thresholds 129
— ternary 163
— velocity distribution 139

Guillotine 149
Gyromagnetic ratio 21

Independent particle model 178
Interconfigurational mixing 247, 268
Internal conversion 202
Intrinsic range 94
Ionisation chamber, gridded 127
Isobaric pairs 177
Isomerism 255
Isotopic spin 176, 261

Lifetimes of nuclear states 210
Liquid-drop model 122
Luminescence centres 76
— organic molecules 81
— rise and decay 79

Magic numbers 238
Many-body problem 260
Mirror nuclei 177
Multipolarity 198

Naphthalene 52, 59
Neutron capture by protons 109
Neutrons cross sections 241
Neutron-proton scattering 89, 99, 116
Nuclear g-factors 37
— induction 21
— magnetic susceptibility 21
— levels, width 182
— quadrupole moments 44, 240, 253
— resonance, in gases 36
— — in zero field 47
— — viscosity effect 35

Orientation of proton-proton lines 40
Ortho- and parahydrogen 100

Packing fraction 243
Pairing energy 251
Paramagnetic impurities 40
— ions 36
— resonance 21
Parity 180
Photofission 131
Photographic plates 185, 281
Photo-magnetic effect 106
Photomultiplier 54
Positive holes 79
Precession 25
Proton-proton scattering 114
Proton resonance, ammonium halides 41
— — gaseous hydrogen 36
— — hydrated crystals 40
— — solid hydrogen 42
— — water, oil, alcohol 38
Pulse analyser 186

Quenching 84
Quadrupole moments 44, 240, 253

Rabbit 149
Relaxation time 32, 43

Sapphire 65
Scattering, elastic 192
— inelastic 189
— length 93
— resonant 192
Scintillation, cosmic rays 71
— energy measurement 67
— gamma rays 72
— neutrons 70
Scintillators 281
— inorganic 55
— liquid 61
— organic 58
— plastic 63
Shielded isotopes 143
Spin echoes 36
Spin-lattice coupling 24
Spin-orbit coupling 180, 246
Spinthariscope 52
Supermultiplet 261
Super-regenerative oscillator 29

Tensor forces 116
Thallium activated alkali iodide 52
Tripartition 163
Tungstate phosphors 56, 65

Well-depth parameter 94
Wiggles 32